



HAL
open science

Development of new approaches for the synthesis of flavaglines

Christine Basmadjian

► **To cite this version:**

Christine Basmadjian. Development of new approaches for the synthesis of flavaglines. Other. Université de Strasbourg, 2015. English. NNT : 2015STRAF019 . tel-01270176v2

HAL Id: tel-01270176

<https://theses.hal.science/tel-01270176v2>

Submitted on 9 Jun 2016

HAL is a multi-disciplinary open access archive for the deposit and dissemination of scientific research documents, whether they are published or not. The documents may come from teaching and research institutions in France or abroad, or from public or private research centers.

L'archive ouverte pluridisciplinaire **HAL**, est destinée au dépôt et à la diffusion de documents scientifiques de niveau recherche, publiés ou non, émanant des établissements d'enseignement et de recherche français ou étrangers, des laboratoires publics ou privés.

GRADUATE SCHOOL of CHEMICAL SCIENCES - ED 222

Laboratory of Therapeutic Innovation - UMR 7200

THESIS

presented by:

Christine BASMADJIAN

defended on: **June 12th, 2015**

to obtain the grade of: **Doctor of the University of Strasbourg**

Discipline / Specialty: Chemistry

Development of new approaches for the synthesis of flavaglines

PhD supervisor:

M. DESAUBRY Laurent

Research director, University of Strasbourg

BOARD OF EXAMINERS:

M. CONSTANTIEUX Thierry

Professor, University of Aix-Marseille

M. FENSTERBANK Louis

Professor, University Pierre and Marie Curie

OTHER EXAMINERS:

M. DE GRAMONT Armand

Doctor, University of Lausanne

M. UNCITI-BROCETA Asier

Professor, University of Edinburgh

M. WEIBEL Jean-Marc

Professor, University of Strasbourg

ÉCOLE DOCTORALE des SCIENCES CHIMIQUES - ED 222

Laboratoire d'Innovation Thérapeutique - UMR 7200

THÈSE

présentée par :

Christine BASMADJIAN

soutenue le : **12 juin 2015**

pour obtenir le grade de : **Docteur de l'université de Strasbourg**

Discipline/ Spécialité : Chimie

Développement de nouvelles approches pour la synthèse des flavaglines

THÈSE dirigée par :

M. DESAUBRY Laurent

Directeur de recherche, Université de Strasbourg

RAPPORTEURS :

M. CONSTANTIEUX Thierry

Professeur, Université d'Aix-Marseille

M. FENSTERBANK Louis

Professeur, Université Pierre et Marie Curie

AUTRES MEMBRES DU JURY :

M. DE GRAMONT Armand

Docteur, Université de Lausanne

M. UNCITI-BROCETA Asier

Professeur, Université d'Edimbourg

M. WEIBEL Jean-Marc

Professeur, Université de Strasbourg

“Success consists of going from failure to failure without loss of enthusiasm.”

Winston Churchill

ACKNOWLEDGEMENTS

First and foremost, I would like to thank my PhD supervisor, Doctor Laurent Desaubry. I am extremely thankful for his dedicated involvement in my research project, for his support and trust over these past three and a half years.

I would also like to thank Professor Marcel Hibert for welcoming me in the Laboratory of Therapeutic Innovation (LIT) at the University of Strasbourg.

I would like to show my gratitude to the board of examiners, including Professor Thierry Constantieux (University of Aix-Marseille), Professor Louis Fensterbank (University Pierre et Marie Curie), Doctor Armand de Gramont (University of Lausanne), Professor Asier Unciti-Broceta (University of Edinburg) and Professor Jean-Marc Weibel (University of Strasbourg). Thank you for taking time to evaluate this PhD research.

This research was supported by the ANRT (Association Nationale de la Recherche et de la Technologie) with a CIFRE fellowship in collaboration with the company AAREC Filia Research represented by Doctor Armand de Gramont and Professor Eric Raymond. I would like to thank them for trusting me with this project.

I take this opportunity to show my appreciation to the members of Désaubry's group with whom I worked for 3 years, for assisting with the chemistry and contributing to a good work environment. Thank you Thierry, Laura, Amel, Qian and Fan. Specially, I would like to sincerely thank Doctor Nigel Ribeiro for his advices, support and guidance through my PhD.

Moreover, I want to thank all the members of the SOMP (Synthèse Organique Métallocalysée et Pharmacochimie) with whom I spent nice moments during these three years. More specifically, I would like to thank Doctor Nicolas Girard, Doctor Morgan Donnard and Doctor Mihaela Guela for taking time to discuss about my chemistry and for sharing their knowledge.

Also, thank you to all the members of the LIT (Laboratory of Therapeutic Innovation), to Emilie and Jessie and especially to Maud who shared this journey with me.

I would like to address my gratitude to Professor Mikiko Sodeoka and her group at RIKEN, Japan. I am really grateful for the great opportunity to work during six months in her laboratory as an IPA (International Program Associate) fellow during my PhD.

Most importantly, I would like to express my thanks and gratitude to my family. Ձեր բացարձակ վստահության և օգնության շնորհիվ է այս աշխատանքը: Մասնաւորապէս, շնորհակալութիւն կը հայտնեմ քեզի մամ: Նույնիսկ հազարաւոր գիլոմէրներ հեռուէն, միշտ ինձի ուժ տուած ևս որ հետեւիմ իմ նպատակներս: Շատ շնորհակալ եմ:

ABBREVIATIONS

A	Å	Ångström
	Ac	Acetyl
	AIBN	Azobisisobutyronitrile
	AIF	Apoptosis Inducing Factor
	Alloc	Allyloxycarbonyl
	An	Anisyl
	APCI	Atmospheric-pressure chemical ionization
	Ar	Aryl
ATM	Ataxia telangiectasia mutated	
B	Bcl-2	B-cell lymphoma 2
	BMF	Bcl-2 modifying factor
	Bn	Benzyl
	Boc	Di-tert-butyl dicarbonate
	brsm	Based on recovered starting material
	Bu	Butyl
	BuLi	Butyllithium
C	CamK	Calmodulin-dependent protein kinase
	CAN	Ceric ammonium nitrate
	CDK	Cyclin-dependent kinase
	CHIKV	Chikungunya virus
	Chk	Checkpoint kinase
	COSY	Homonuclear correlation spectroscopy
	Cy	Cyclohexyl
D	DBDMH	1,3-Dibromo-5,5-dimethylhydantoin
	DBU	1,8-Diazabicyclo[5.4.0]-undec-7-ene
	DCC	<i>N,N'</i> -Dicyclohexyl-carbodiimide
	DCE	1,2-Dichloroethane
	DDQ	2,3-Dichloro-5,6-dicyano-1,4-benzoquinone
	DEPBT	3-(Diethoxyphosphoryloxy)-1,2,3-benzotriazin-4(3H)-one
	DEPT	Distortionless enhancement by polarization transfer
	DIAD	Diisopropyl azodicarboxylate
	DIBAL-H	Diisobutylaluminium hydride
	DIPEA	<i>N,N</i> -Diisopropylethylamine
	DMAP	4-Dimethylaminopyridine
	DMF	Dimethylformamide
	DMSO	Dimethyl sulfoxide
	DNA	Deoxyribonucleic acid
E	EGF	Endothelial growth factor
	eIF4	Eukaryotic initiation factors
	eq	Equivalent
	ERK	Extracellular-signal-regulated kinase

	ESI	Electrospray ionisation
	Et	Ethyl
	EtOAc	Ethyl acetate
F	FL	Flavagline
G	GC-MS	Gaz chromatography-mass spectrometry
	Grp	Gastrin-releasing peptide
H	HMBC	Heteronuclear multiple-bond correlation spectroscopy
	HR-MS	High resolution-mass spectrometry
	HSF	Heat shock factor
	Hsp	Heat shock protein
	HSQC	Heteronuclear single-quantum correlation spectroscopy
	HUVEC	Human umbilical vein endothelial cells
I	IGF1	Insulin-like growth factor
	IgM	Immunoglobulin M
J	JNK	c-Jun <i>N</i> -terminal kinases
K	KHMDS	Potassium bis(trimethyl-silyl)amide
L	LC-MS	Liquid chromatography-mass spectrometry
	LDA	Lithium Diisopropylamide
	L-selectride®	Lithium tri-sec-butyl-borohydride
M	Mcl-1	Myeloid cell leukemia protein 1
	<i>m</i> -CPBA	<i>meta</i> -Chloroperoxybenzoic acid
	Me	Methyl
	MEK	Mitogen-activated protein kinase
	MMP9	Matrix metalloproteinase 9
	MS	Molecular sieve
N	NAP	2-Naphthylmethyl
	NBS	<i>N</i> -bromosuccinimide
	NMP	<i>N</i> -Methylpyrrolidone
	NMR	Nuclear magnetic resonance
	NOESY	Nuclear Overhauser effect spectroscopy
	NaCl	4-Nitrobenzenesulfonyl chloride
P	Pd/C	Palladium on carbon
	PDAC	Pancreatic ductal adenocarcinoma
	Ph	Phenyl
	PHB	Prohibitin
	PhMe	Toluene
	Pr	Propyl
	<i>p</i> -TsOH	<i>para</i> -Toluenesulfonic acid
	Py.SO ₃	Sulfur trioxide pyridine complex

Q	Q-Tof	Quadrupole time-of-flight mass spectrometer
R	Raf	Rapidly accelerated fibrosarcoma
	Red-Al®	Sodium bis(2-methoxy-ethoxy) aluminumhydride
	RNA	Ribonucleic acid
	rt	Room temperature
S	SAR	Structure–activity relationships
	Shp	Src homology region 2 domain-containing phosphatase
T	TADDOL	$\alpha,\alpha,\alpha,\alpha$ -Tetraaryl-1,3-dioxolane-4,5-dimethanol
	TBAF	Tetra- <i>n</i> -butylammonium fluoride
	TBS	Tert-butyldimethylsilyl
	TBSOTf	Trimethylsilyl trifluoromethanesulfonate
	TCICA	Trichloroisocyanuric acid
	TES	Triethylsilyl
	Tf	Trifluoromethanesulfonyl
	Tf ₂ O	Trifluoromethanesulfonic anhydride
	TFA	Trifluoroacetic acid
	TGF- β	Transforming growth factor
	THF	Tetrahydrofurane
	TMS	Trimethylsilyl
	TMSNCO	Trimethylisocyanate
	TMSOTf	Trimethylsilyl trifluoromethanesulfonate
	TRPM6	Transient receptor potential ion channel 6
	Ts	Tosyl
TsNCO	Tosylisocyanate	
V	VEGF	Vascular endothelial growth factor

SUMMARY IN FRENCH

1. Introduction

Les flavaglines, composés naturels extraits de plantes, possèdent un squelette cyclopentan[*b*]benzofurane unique. Leur premier représentant, le rocaglamide **1**, a été découvert en 1982 par King et collaborateurs pour son activité antileucémique (Figure 1).¹ Depuis, environ 50 autres flavaglines ont été isolées de plantes du genre *Aglaia*.

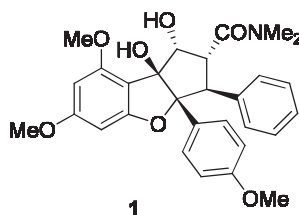


Figure 1 : Structure du rocaglamide (**1**).

Les flavaglines présentent un profil d'activité biologique unique notamment aux niveaux de leurs propriétés anticancéreuses, ces dernières étant les plus étudiées jusqu'à présent.² Les flavaglines sont très intéressantes de par leur squelette compact, comportant 2 centres chiraux quaternaires adjacents et 2 cycles aromatiques en position *cis* sur un cyclopentyle très fonctionnalisé. Les flavaglines représentent un défi intéressant en chimie organique.

2. Objectifs

Notre objectif principal était d'élaborer une nouvelle voie de synthèse originale des flavaglines qui permette d'introduire diverses substitutions afin d'établir les requis structuraux nécessaires pour leurs activités anticancéreuses. Un second objectif était de synthétiser une sonde de fluorescence des flavaglines afin de déterminer le mécanisme de chimiorésistance impliquant la prohibitine-1. Enfin, un dernier objectif était de préparer un isostère pyrazolique des flavaglines.

¹ Lu King, M.; Chiang, C.-C.; Ling, H.-C.; Fujita, E.; Ochiai, M.; McPhail, A. T. *Journal of the Chemical Society, Chemical Communications* **1982**, (20), 1150-1151.

² Basmadjian, C.; Thuaud, F.; Ribeiro, N.; Désaubry, L. *Future Medicinal Chemistry* **2013**, 5 (18), 2185-2197.

3. Première voie de synthèse selon l'approche de Ragot

Nous avons dans un premier temps mis en place la synthèse de l'intermédiaire clé, la cyclopenténone **188** selon la voie de synthèse décrite dans le schéma 1. Cette approche combine une étherification de l'alcool allylic **182a** catalysée par du molybdène(VI) avec une cyclisation intramoléculaire catalysée par un complexe d'or(I).^{3,4} Ces travaux ont conduit à un article publié dans *Tetrahedron Letters*.⁵

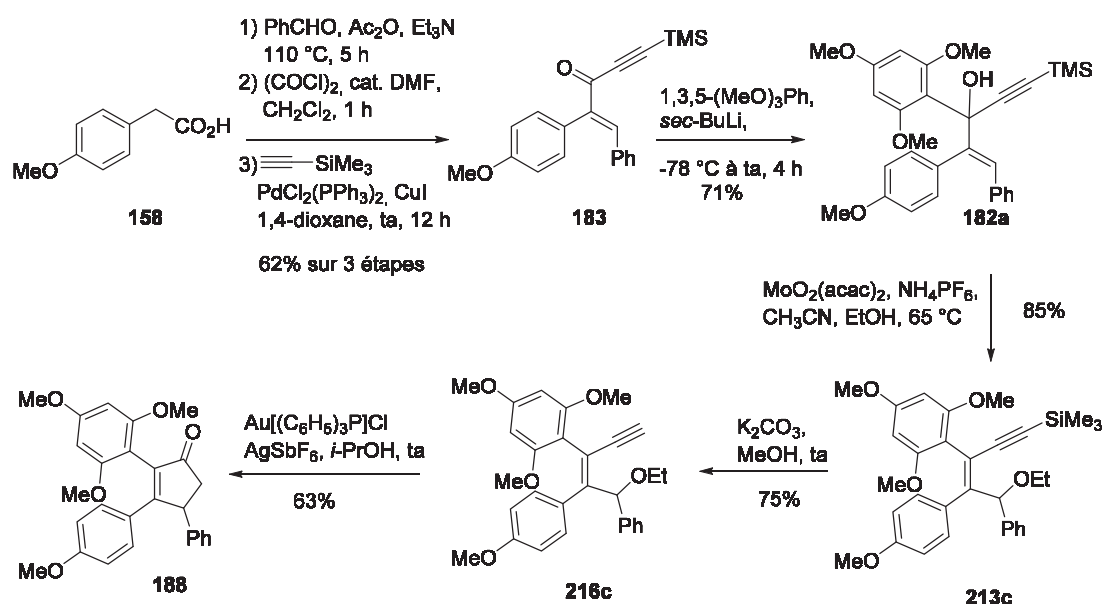


Schéma 1 : Synthèse de la cyclopenténone **188**.

Lors de notre travail d'optimisation de cette synthèse de cyclopenténones, nous avons examiné plusieurs catalyseurs pour transformer l'alcool allylique **182a** en éther **213c**, dont l'oxyde de rhénium Re₂O₇, qui a été décrit pour catalyser efficacement ce type de transformation. De manière inattendue, au lieu d'obtenir l'éther **213c**, nous avons observé la formation de la cyclopenténone **188** avec un rendement de 32% (Schéma 2). Le remplacement du groupement TMS par un TBS nous a permis d'améliorer le rendement à 44% (ce qui est supérieur au rendement global de la synthèse précédente en trois étapes).

³ An, S. E.; Jeong, J.; Baskar, B.; Lee, J.; Seo, J.; Rhee, Y. H. *Chemistry – A European Journal* **2009**, *15* (44), 11837-11841.

⁴ Yang, H.; Fang, L.; Zhang, M.; Zhu, C. *European Journal of Organic Chemistry* **2009**, *2009* (5), 666-672.

⁵ Basmadjian, C.; Zhao, Q.; Désaubry, L. *Tetrahedron Letters* **2015**, *56* (5), 727-730

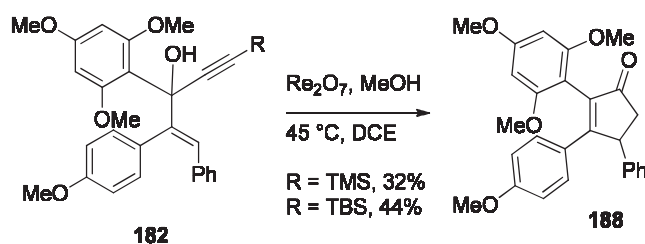


Schéma 2 : Synthèse de la cyclopenténone **188** catalysée à l'oxyde de rhénium.

Nous pouvons comparer l'efficacité de notre stratégie de synthèse de la cyclopenténone aux données de la littérature (Tableau 1). En seulement 5 étapes, nous obtenons notre intermédiaire clé de la synthèse de flavaglines avec un rendement global de 13%.

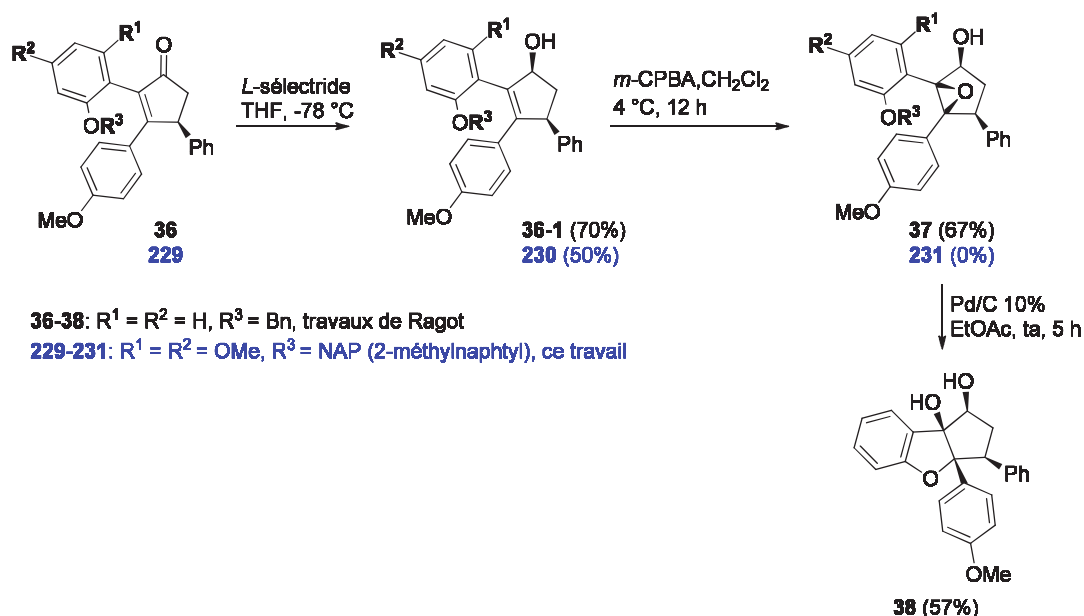
Tableau 1 : Comparaison de notre stratégie de synthèse de cyclopenténones à la littérature.

	Ragot <i>et al.</i> ⁶	Trost <i>et al.</i> ⁷	Ce travail
Intermédiaires			
Nombre d'étapes	6	8	5
Rendement global	6%	21%	13%

Ragot et coll. avaient décrit une synthèse de la flavagline **38** pharmacologiquement inactive (Schéma 3).⁶ Malgré de nombreuses tentatives, nous n'avons jamais réussi à appliquer cette stratégie à la synthèse de composés substitués par des méthoxys nécessaires à l'activité anticancéreuse. En remplaçant le phénol protégé **36-1** (Schéma 3) par le 3,5-diméthoxyphénol protégé par un groupement 2-méthylnaphtyl, l'époxydation n'a pas lieu malgré les nombreuses conditions essayées. L'impossibilité d'obtenir l'époxyde nous conduit à émettre des doutes quant à la validité de la stratégie de Ragot pour préparer des dérivés de flavaglines avec les groupes fonctionnels nécessaires à l'activité pharmacologique.

⁶ Thede, K.; Diedrichs, N.; Ragot, J. P. *Organic Letters* **2004**, 6 (24), 4595-4597.

⁷ Trost, B. M.; Greenspan, P. D.; Yang, B. V.; Saulnier, M. G. *Journal of the American Chemical Society* **1990**, 112 (24), 9022-9024.

Schéma 3 : Synthèse de flavaglines par la méthode de Ragot.⁶

4. Réarrangements d'alcools 1-styryl propargyles catalysés par des acides

Les résultats obtenus par la découverte de la réaction catalysée à l'oxyde de rhénium ont été exploités. Un travail d'optimisation et d'étude d'applicabilité à différents substrats a été réalisé. Pour cela différents ényols ont été préparés selon les méthodes décrites dans le schéma 4.

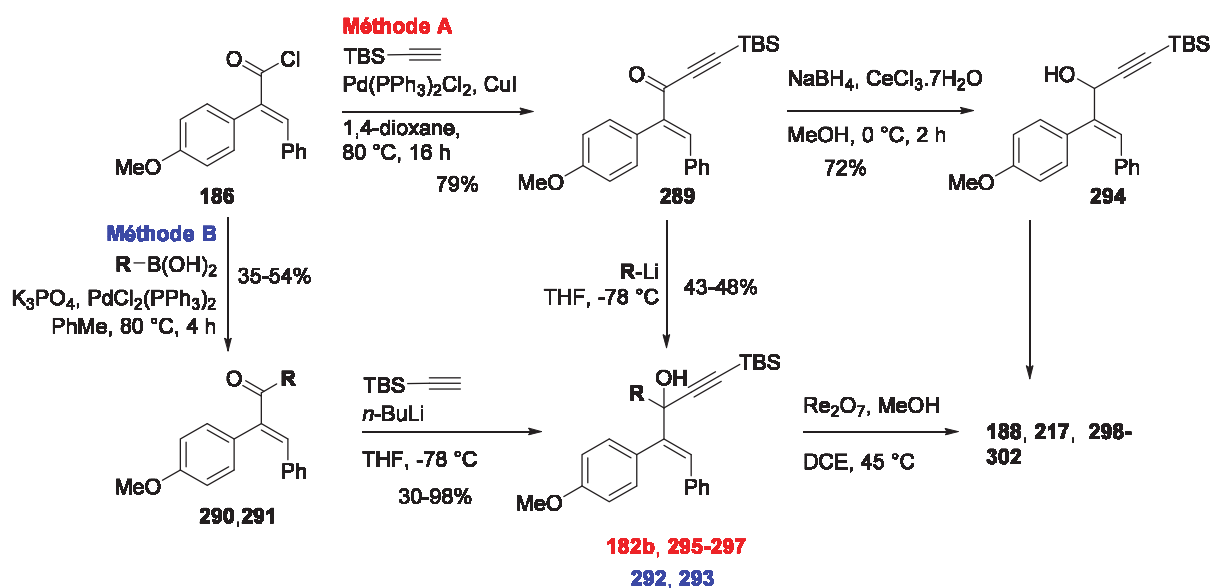


Schéma 4 : Préparations d'alcools 1-styryl propargyliques.

Lorsque R = 2,4,6-triméthoxyphényle, 2 produits sont obtenus, la cyclopenténone **188** et le méthylfuran **217** avec respectivement des rendements de 44 et 27%. Le mécanisme proposé pour cette réaction est représenté dans le schéma 7. Les produits **188** et **217** seraient tout deux issus de la formation du même carbocation stabilisé **303**. Cet intermédiaire pourrait, soit subir une fermeture de cycle en raison du caractère nucléophile de l'alcyne silylé (voie A) soit réagir avec une espèce nucléophile oxygénée, tel que l'anion perhénate, pour générer l'intermédiaire **305**. Ce dernier pourrait alors subir une oxo-cyclisation pour donner un oxonium qui après réarrangement conduirait au furane **217** (voie B). Alternativement, l'intermédiaire **305** pourrait résulter de la transposition allylique [1,3] de l'ester perhénique.

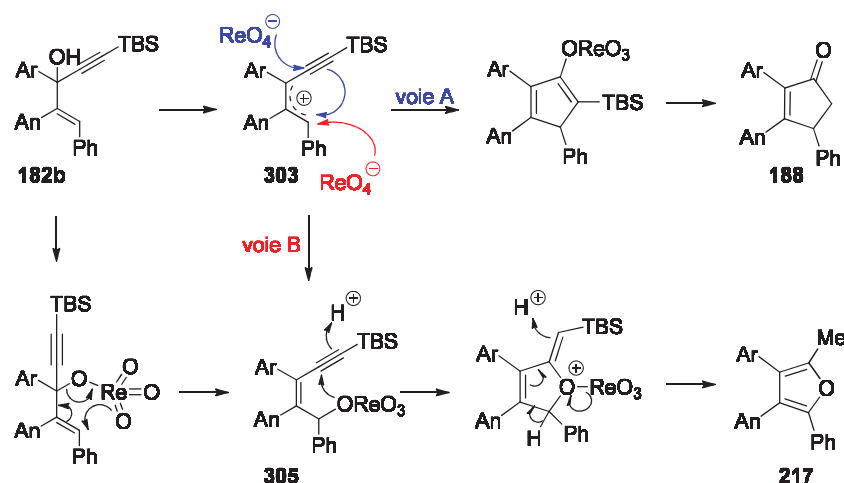


Schéma 5 : Mécanismes proposés pour la formation de la cyclopenténone **188** et du furane **217**.

Cependant, lorsque nous étudions le scope de la réaction, nous observons qu'un changement mineur dans le substrat conduit à des produits de natures différentes. Ainsi, ce réarrangement donne accès à différents composés tels que des cyclopenténones ou des furanes (Schéma 6). Nous émettons l'hypothèse d'un équilibre délicat entre plusieurs voies mécanistiques où un changement mineur de substrat peut se répercuter sur la nature des produits de réarrangements.⁸

⁸ Basmadjian, C., Zhang, F., Désaubry, L. Novel carbocationic rearrangements of 1-styryl propargyl alcohols, *Beilstein. J. Org. Chem.* **2015**, *11*, 1017-1022.

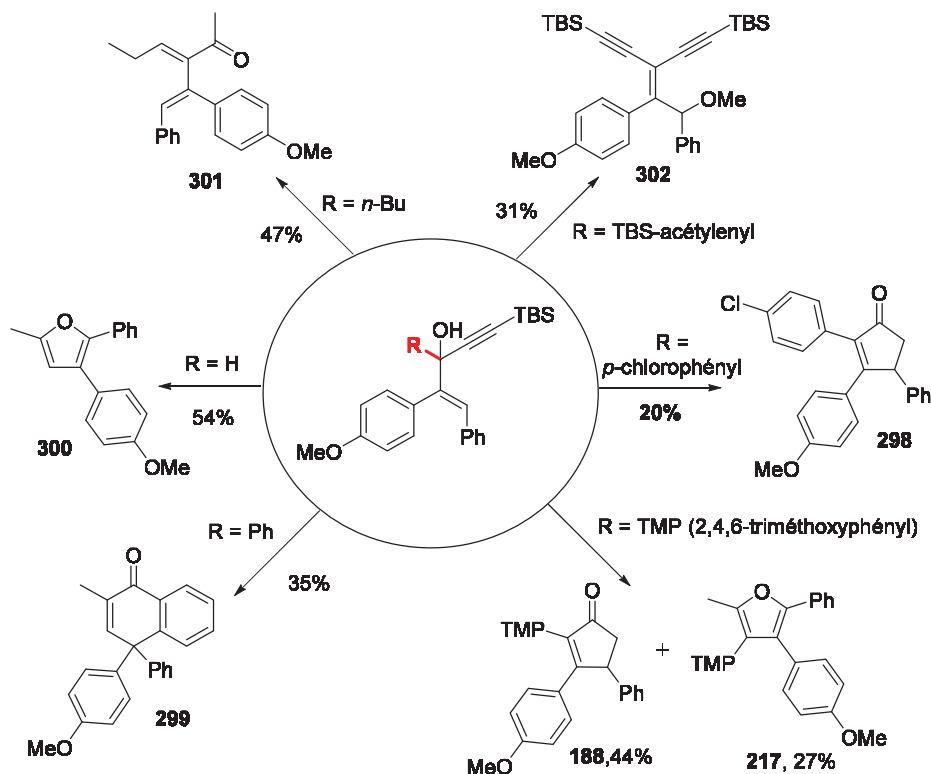


Schéma 6 : Réarrangements d'alcools 1-styryl propargyliques catalysés à l'oxyde de rhénium.⁸

5. Deuxième voie de synthèse selon l'approche de Magnus

La première voie de synthèse n'ayant pas abouti, une seconde voie inspirée des travaux de Magnus et collaborateurs a été considérée.⁹ L'étape clé de leur approche repose sur une réaction de Nazarov avec l'utilisation de bromure d'acétyle pour activer la cétone **40**.

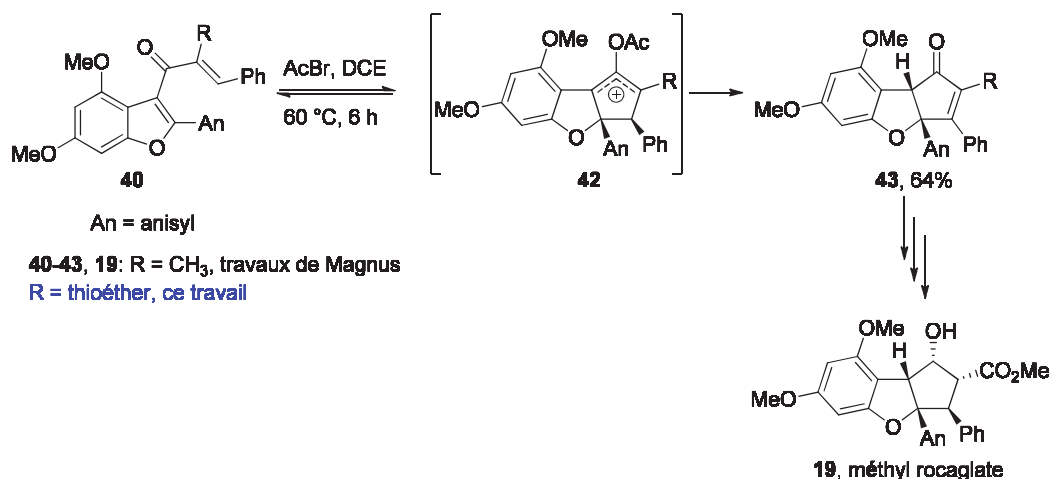


Schéma 7 : Réaction de Nazarov avec l'assistance de bromure d'acétyle.⁹

⁹ Magnus, P.; Freund, W. A.; Moorhead, E. J.; Rainey, T. *Journal of the American Chemical Society* **2012**, *134* (14), 6140-6142.

Lors de la formation de la cyclopenténone **43** un groupement (R = Me) en position α du carbonyle est nécessaire pour stabiliser l'intermédiaire **42** de la réaction de Nazarov (Schéma 7). De plus, Cavalli et coll. ont récemment décrit l'utilisation d'un thioéther en α du carbonyle pour la synthèse de cyclopenténones via une cyclisation de Nazarov.¹⁰ Ainsi, nous avons supposé que si l'on remplace le groupement méthyle du composé **40** par un thioéther, cela permettrait d'accélérer la fermeture du cycle en stabilisant l'intermédiaire carbocationique. De plus, *in fine*, le thioéther pourrait être utilisé pour introduire d'autres fonctionnalités.

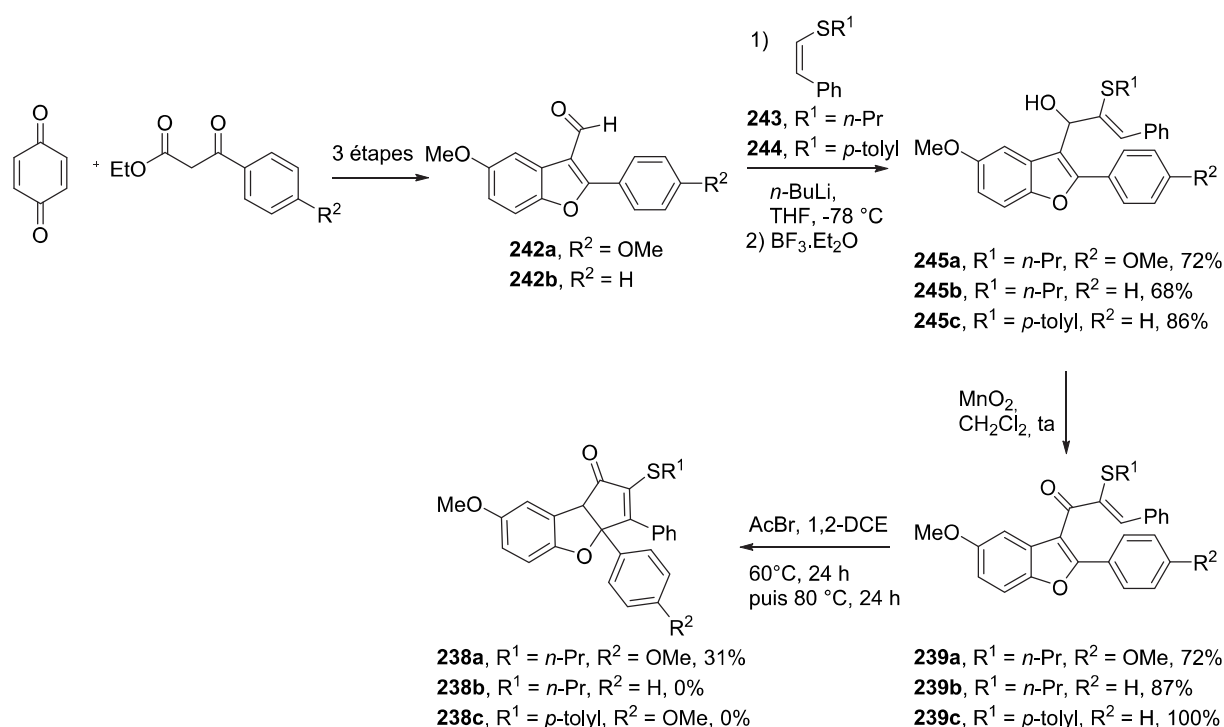


Schéma 8: Synthèse des cyclopenténones **238a**, **238b** et **238c**.

Le schéma 8 décrit la synthèse utilisée après optimisation. Les aldéhydes **242** sont préparés selon le protocole décrit par Chan et coll.¹¹ Ces derniers sont ensuite alkylés par les thiovinyléthers **243** et **244** lithiés. Les divinylalcools **245** ainsi obtenus sont par la suite oxydés en présence de MnO_2 conduisant à l'obtention des précurseurs de la réaction de Nazarov. La cyclopenténone **238** n'a pu être isolée seulement lorsque R¹ = *n*-Pr avec un rendement de 31%.

¹⁰ Cavalli, A.; Pacetti, A.; Recanatini, M.; Prandi, C.; Scarpi, D.; Occhiato, E. G. *Chemistry – A European Journal* **2008**, *14* (30), 9292-9304.

¹¹ Mothe, S. R.; Susanti, D.; Chan, P. W. H. *Tetrahedron Letters* **2010**, *51* (16), 2136-2140.

Avec cette deuxième voie de synthèse, nous avons réalisé en 9 étapes la première synthèse d'un analogue des flavaglines **238a** substituée par un thioéther. L'étape clé, basée sur une réaction de Nazarov a été réalisée avec un rendement non reproductible compris entre 0 et 31%, ce qui nous a conduit à abandonner cette approche.

6. Synthèse d'outils pharmacochimiques

Dans le cadre de cette thèse, la sonde de fluorescence **179** a été synthétisée (Figure 2). Celle-ci est actuellement utilisée dans l'équipe du Pr. Bruce Zetter à l'Université Harvard pour déchiffrer la signalisation des prohibitines (PHBs) impliquées dans les mécanismes de résistance aux chimiothérapies.

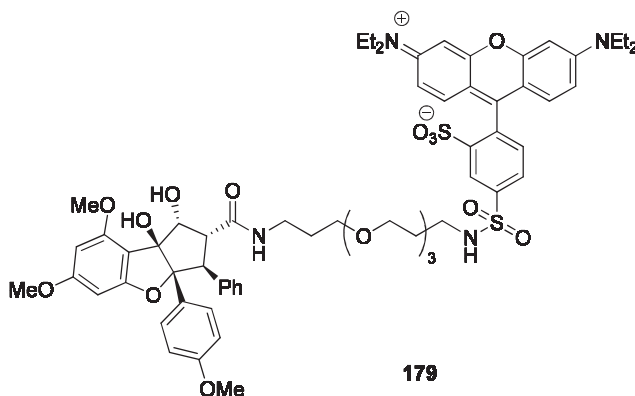


Figure 2 : Sonde de fluorescence **179**.

Aussi, au cours de cette thèse, d'autres composés dont le FL3 originellement développé au laboratoire ont été (re)synthétisés (Figure 3) puis testés pour l'inhibition d'eIF4A (Facteur d'Initiation Eucaryotique de la Traduction 4A) et leurs effets anticancéreux dans le mélanome métastatique chimiorésistant. Ces résultats ont donné lieu à une publication dans *Nature* et un article sous presse.¹²

¹² (i) Boussebart, L.; Malka-Mahieu, H.; Girault, I.; Allard, D.; Hemmingsson, O.; Tomasic, G.; Thomas, M.; Basmadjian, C.; Ribeiro, N.; Thuaud, F.; Mateus, C.; Routier, E.; Kamsu-Kom, N.; Agoussi, S.; Eggermont, A. M.; Desaubry, L.; Robert, C.; Vagner, S. *Nature* **2014**, *513* (7516), 105-109. (ii) Basmadjian, C.; Desaubry, L.; Malka-Mahieub H. *Anti-Cancer Agents in Medicinal Chemistry*, **2015**, in press.

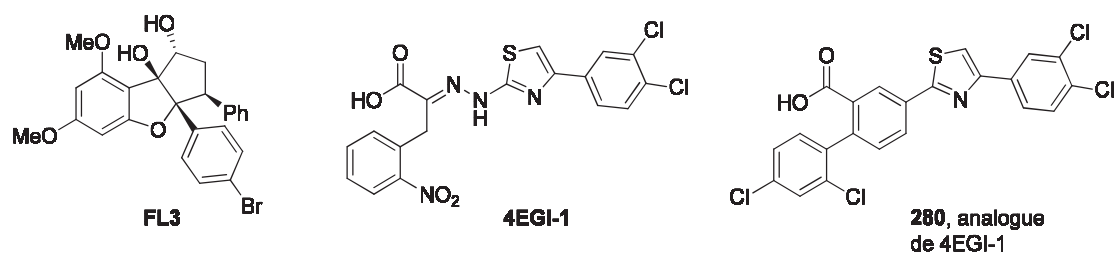


Figure 3 : Inhibiteurs d'eIF4A.¹²

De plus, avec nos collaborateurs, nous avons montré que les flavaglines en agissant sur les prohibitines, pouvaient avoir des actions originales et prometteuses dans des domaines sans lien direct avec l'oncologie. Ainsi, le Pr. Duncan Smith de l'Université Mahidol en Thaïlande avait montré que le virus du Chikungunya (CHIKV) utilise la PHB1 comme co-récepteur pour pénétrer à l'intérieur des cellules. Cette équipe a récemment démontré que des flavaglines que j'ai resynthétisées, diminuent de manière significative l'internalisation de ce récepteur. Ces travaux ont été publiés dans *Microbiology and Immunology*.¹³

Par ailleurs, l'équipe du Pr. Joost Hoenderop à l'Université Radboud à Nimègue (Pays-Bas) avec qui nous collaborons concentre son activité sur les canaux au magnésium TRPM6 et TRPM7. Cette équipe qui avait trouvé que la PHB2 inhibe l'activité du canal TRPM6, a récemment montré que des flavaglines que j'ai resynthétisées lèvent cette inhibition (manuscrit publié dans *Plos One*).¹⁴ Aucun autre composé testé dans ce laboratoire ne présente d'effet aussi prononcé. Cette étude a permis de mieux comprendre les mécanismes de régulation de ce canal en confirmant l'implication de la signalisation de l'insuline.

7. Synthèse d'un isostère

La synthèse de l'isostère pyrazolique des flavaglines est basée sur la cyclocondensation de l'énaminone **287** avec l'hydrazine (Schéma 9).

¹³ Wintachai, P.; Thuaud, F.; Basmadjian, C.; Roytrakul, S.; Ubol, S.; Désaubry, L.; Smith, D. R. *Microbiology and Immunology* **2015**, *59* (3), 129-141.

¹⁴ Blanchard, M. G.; de Baaij, J. H. F.; Verkaart, S. A. J.; Lameris, A. L.; Basmadjian, C.; Zhao, Q.; Désaubry, L.; Bindels, R. J. M.; Hoenderop, J. G. J. Activity. *PLoS ONE* **2015**, *10* (3), e0119028.

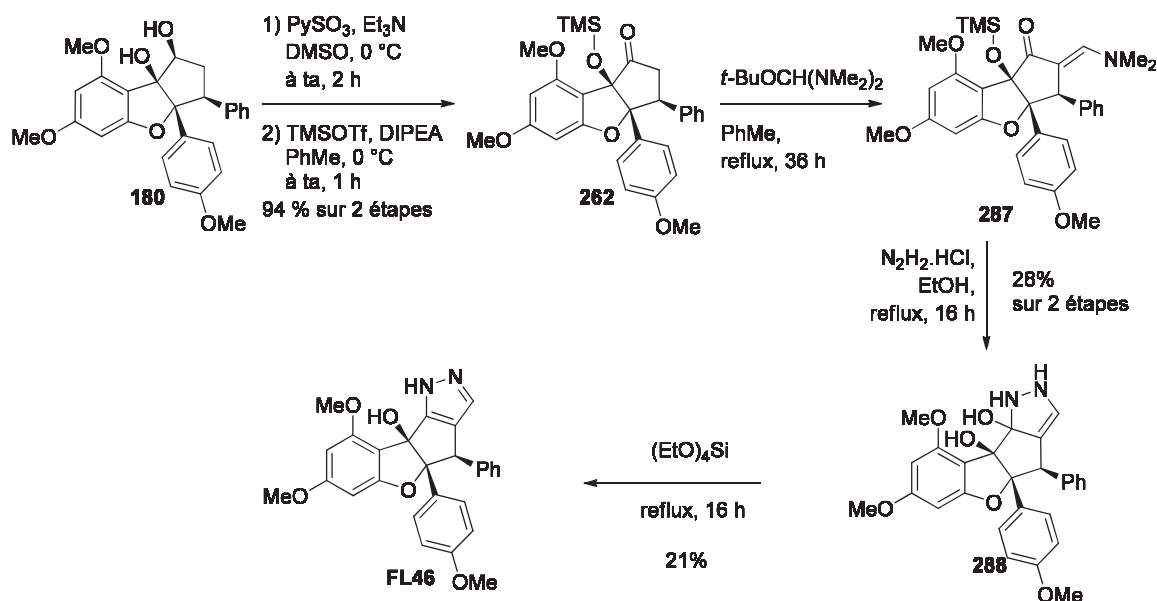


Schéma 9: Synthèse de l'isostère **FL46**.

Une oxydation de Parikh-Doering du rocaglaol **180** et la protection de l'alcool tertiaire avec un groupe triméthylsilyle permet la modification en position 2 de la cyclopenténone **262** avec un rendement de 94% sur deux étapes (Schéma 9). Le produit obtenu est alors converti en l'énaminone en utilisant le réactif de Bredereck (*tert*-BuOCH(NMe₂)₂). La condensation avec de l'hydrazine donne de manière inattendue l'hydrate **288**. Enfin, la déshydratation de l'hétérocycle avec du tétraméthoxysilane conduit à l'isostère (**FL46**).

Malheureusement, les tests biologiques ont montré que **FL46** possède une faible cytotoxicité sur deux lignées cellulaires (HEP2 et 789-0) par rapport à **FL23** utilisé comme référence. En raison de cette perte inattendue d'activité pharmacologique, nous n'avons pas essayé de préparer d'autres analogues de cette série.

8. Conclusion

Nous avons développé deux méthodes originales de synthèse de cyclopenténone fonctionnalisées et découvert de nouveaux réarrangements d'alcools 1-styryl propargyliques catalysés par des acides.

Ce travail de thèse a aussi permis d'expliquer pourquoi une méthode de synthèse des flavaglines par des chercheurs de Bayer n'avait jamais été utilisée pour préparer des composés présentant les substituants nécessaires à l'activité anticancéreuse.

De plus la resynthèse de certaines flavaglines et la synthèse d'une sonde de fluorescence originale ont permis de faire des avancées dans l'élucidation du mode d'action des flavaglines pour leurs effets anticancéreux mais également de découvrir d'autres effets sans lien direct avec leur activité anticancéreuse (régulation du canal TRPM6 et infection par le virus du Chikungunya).

TABLE OF CONTENTS

<i>Acknowledgments</i>	11
<i>Abbreviations</i>	13
<i>Summary in French</i>	19
1. Introduction	39
1.1 Avant-propos.....	39
1.2 Natural products in oncology.....	39
1.3 Discovery and pharmacological properties of flavaglines	42
1.3.1 Discovery of flavaglines	42
1.3.2 Pharmacological properties of flavaglines.....	42
1.3.3 Molecular targets of flavaglines and their mode of action	43
1.3.4 Structure-activity relationships of flavaglines	47
1.4 Synthesis of flavaglines	48
1.4.1 First total synthesis of rocaglamide	48
1.4.2 Synthesis of rocaglamide <i>via</i> benzofuranone intermediate.....	49
1.4.3 Other approaches to synthesis rocaglamide	50
1.4.4 Ragot's synthesis of rocaglaol derivative.....	53
1.4.5 Magnus' formal synthesis of (\pm)-methyl rocaglate.....	54
1.5 Rearrangements of vinyl propargyl alcohols and their esters	57
1.5.1 Discovery of the Rautenstrauch rearrangement	57
1.5.2 Transition-metal-catalyzed Rautenstrauch reaction	58
1.5.3 Rautenstrauch related reactions initiated by 1,2-acyloxy migration	64
1.5.4 Other vinyl propargyl alcohol rearrangement.....	66
1.5.5 Rearrangement of propargyl acetate in the synthesis a natural product.....	67
1.6 Overview of the Nazarov reaction	68
1.6.1 Introduction on the Nazarov reaction	68

1.6.2	Catalytic Nazarov reaction	69
1.6.3	Interrupted Nazarov reaction	71
1.6.4	Heteroatomic Nazarov reaction	75
1.6.5	Natural products synthesized <i>via</i> Nazarov electrocyclization	78
2.	Objectives	83
3.	Results	87
3.1	Synthesis of flavaglines based on Ragot's approach.....	87
3.1.1	Retrosynthetic strategy	87
3.1.2	Synthesis of cyclopentenone intermediate	87
3.1.3	Attempts to generate flavaglines from the cyclopentenone intermediate	101
3.2	Synthesis of flavaglines based on Magnus' approach.....	108
3.2.1	Retrosynthetic strategy	108
3.2.2	Synthesis of the scaffold of flavaglines via Nazarov reaction.....	108
3.2.3	Synthesis of a second class of substrates for the Nazarov reaction.....	114
3.2.4	Unexpected Friedel-Crafts reaction.....	116
3.3	Synthesis of pharmacochemical tools.....	118
3.3.1	Synthesis of a fluorescence probe of a flavagline	118
3.3.2	Synthesis of inhibitors of elf4A	120
3.3.3	Synthesis of flavagline FL3	124
3.4	Synthesis of an isostere of flavaglines	128
3.5	Rearrangements of 1-styryl propargyl alcohols	130
3.5.1	Preparation of 1-styryl propargyl alcohols	130
3.5.2	Study of the scope and limitations	131
3.5.3	Optimization of the reaction	137
4.	Conclusion	143

5. Experimental procedures	147
5.1 Generalities	147
5.2 Procedures for chapter 3.1.	149
5.3 Procedures for chapter 3.2.	176
5.4 Procedures for chapter 3.3.	195
5.5 Procedures for chapter 3.4.	211
5.6 Procedures for chapter 3.5.	213
6. Publications	231
6.1 Publication n°1	233
6.2 Publication n°2	253
6.3 Book chapter	269
6.4 Publication n°3	299
6.5 Publication n°4	305
6.6 Publication n°5	311
6.7 Publication n°6	331
6.8 Publication n°7	347
6.9 Publication n°8	361

1. INTRODUCTION

1. INTRODUCTION

1.1 Avant-propos

Cancer is defined by the National Cancer Institute as: “a collection of related diseases. In all types of cancer, some of the body’s cells begin to divide without stopping and spread into surrounding tissues.”¹⁵ Indeed, cancer is characterized by the fast growth of abnormal cells beyond their normal limit and the invasion of neighboring parts of the body that can induce metastases by spreading to other organs. The latter are the major cause for death in cancer patient.

According to the World Health Organization, cancers are one of the top causes of mortality around the world with approximately 14 million new cases and 8.2 million cancer related deaths in 2012.¹⁶ Despite the advances that are made in the treatment of cancer, with surgeries, radiotherapies, chemotherapies and targeted therapies, the number of new cancer patient is expected to increase by 70% in the next 20 years. This demonstrates the constant need to develop new anticancer drug.

1.2 Natural products in oncology

Natural products can be defined as small molecules produced by a biological source.¹⁷ Based on Albrecht Kossel’s proposal in 1891, natural products can be divided as primary or secondary metabolites.¹⁸ While primary metabolites govern the intrinsic functions that are vital for the survival of an organism, secondary metabolites have extrinsic function that can modulate biological pathways. In medicinal chemistry, natural products are often restricted to secondary metabolites. Concerning their structure, they usually have more chiral centers, more varied ring systems, a higher ratio of Csp³/Csp², less nitrogen, and more oxygen atoms than synthetic drugs.¹⁹ This structural diversity and the potential

¹⁵ <http://www.cancer.gov/cancertopics/what-is-cancer>

¹⁶ <http://www.who.int/mediacentre/factsheets/fs297/en/>

¹⁷ Editorial, All natural. *Nat Chem Biol* **2007**, *3*, 351-351.

¹⁸ Kossel, A. *Archiv für Physiologie*, **1892**, 181-186

¹⁹ Henkel, T.; Brunne, R. M.; Müller, H.; Reichel, F., *Angewandte Chemie International Edition* **1999**, *38* (5), 643-647.

pharmacological or biological activities of natural products make them therapeutically interesting for the treatment of diseases.

Therefore, natural products are an important source for the discovery of new drugs. Indeed, it has been estimated that about 40% of all medicines derive either directly from natural products or from their semi-synthetic derivatives.²⁰

However, since the emergence of targeted therapies in the 90s, the interest in natural products decreased with no new approved anticancer drugs between 1997 and 2006 (Figure 1) Indeed, some pharmaceutical companies even closed their natural product department to focus on targeted therapies which are fully synthetic molecules or antibodies that target specific proteins in tumor growth and progression.

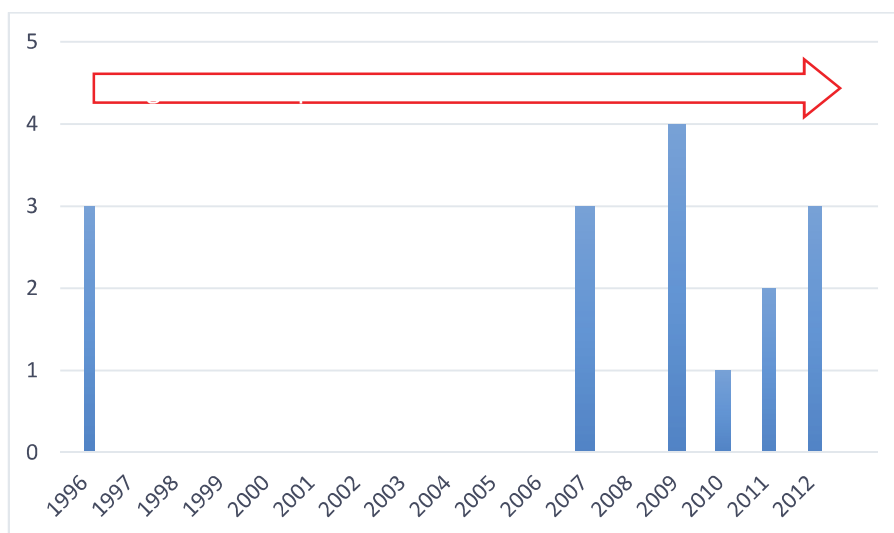


Figure 1 | Number of natural products approved for treatment of cancer between 1996 and 2012²¹

Nevertheless, in 2007, natural products made their come-back due to some drawbacks in targeted therapies. Indeed, for most of patients that are treated with targeted therapies using fully synthetic drugs or antibodies, mechanisms of resistance occurs after few months or a couple of years and the treatment lose their efficacies, especially for solid tumors.

²⁰ (i) Kahlou, M. *Pharmacology & Pharmacy* **2013**, 4, 17-31. (ii) Jacob, E.J. *Current science* **2009**, 96 (6), 753-754

²¹ Basmadjian, C.; Zhao, Q.; Djehal, A.; Bentouhami, E.; Nebigil, C. G.; Johnson, R. A.; Serova, M.; De Gramont, A.; Faivre, S.; Raymond, E.; Désaubry, L. G. *Frontiers in Chemistry* **2014**, 2, article 20.

Since the approval of rapamycin in 2007, 14 novel natural product derivatives (Figure 2) have been brought to market which proves the return of the natural products for the discovery and development of new anticancer drugs. We recently examined these developments in a review entitle “Cancer wars: natural products strike back” (see publication n°1, page 233).²¹

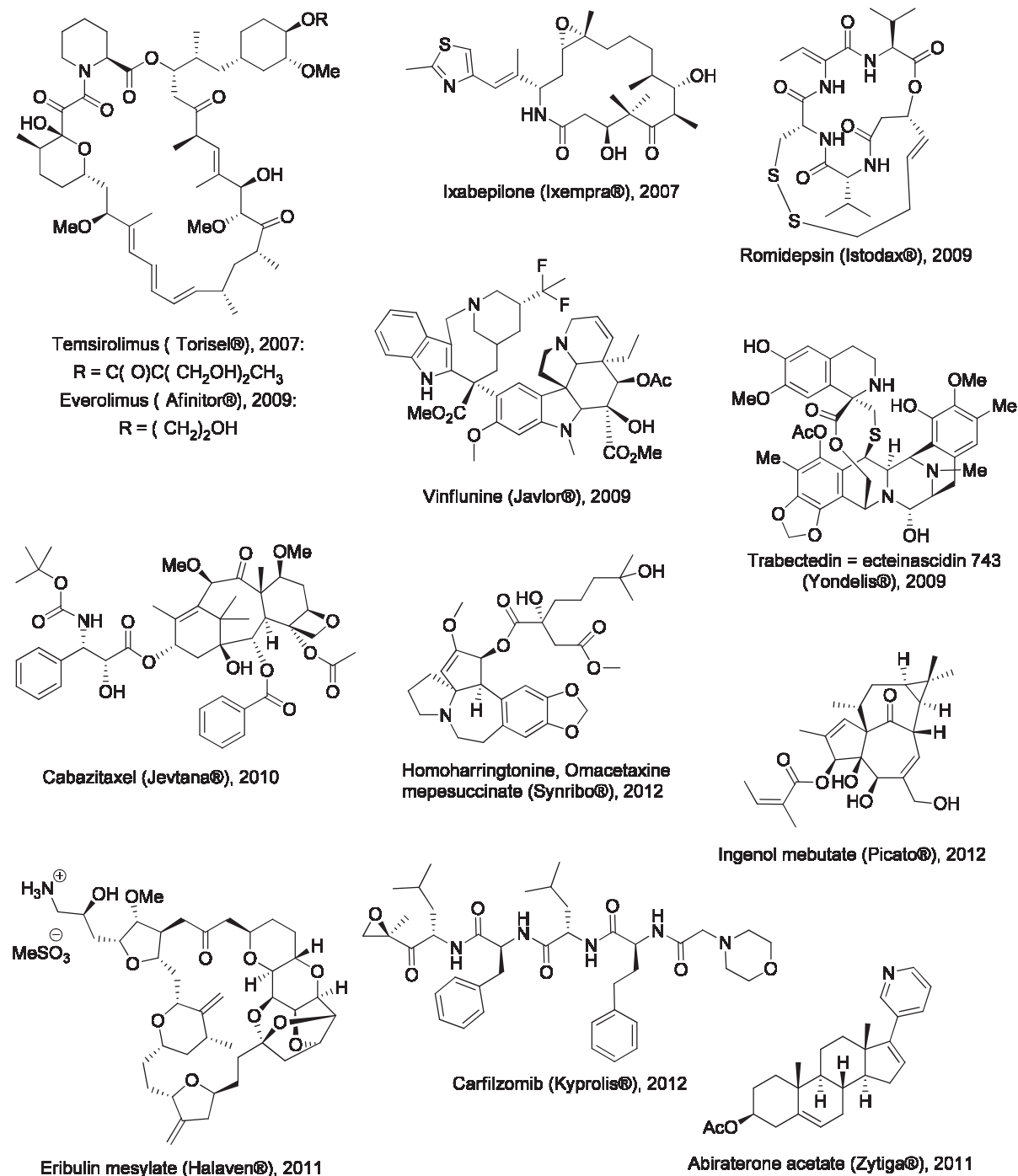


Figure 2 | Selected novel anticancer medicines based on natural products since 2007.²¹

1.3 Discovery and pharmacological properties of flavaglines

1.3.1 Discovery of flavaglines

First identified in 1982 by King and colleagues at the Taiwan National Defense Medical Center, flavaglines are a family of plant-derived natural products.²² These secondary metabolites are extracted from the plants of the genus *Aglaia* (Meliaceae) found in the Southeast Asia. The first representative of this class of compounds is rocaglamide (**1**, Figure 3), which was reported for its anti-leukemic activity. Traditionally, these compounds are used to treat respiratory diseases such as asthma or skin inflammation diseases. Concerning their structure, flavaglines are characterized by a unique cyclopenta[*b*]benzofuran skeleton. Up to date, more than 100 other natural flavaglines have been identified such as rocaglaol (**2**) or silvestrol (**3**). The latter has the particularity of having a complex pseudo-sugar substituent.²³

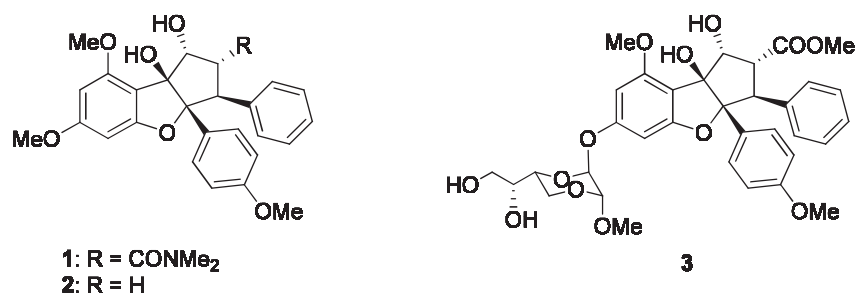


Figure 3 | Representative examples of natural flavaglines: rocaglamide (**1**), rocaglaol (**2**) and silvestrol (**3**).

1.3.2 Pharmacological properties of flavaglines

Due to their unique biological activity profile, flavaglines have attracted the attention of numerous biologists. Indeed, these compounds possess insecticidal, antifungal, anti-inflammatory and neuroprotective activities. But the most interesting biological property is by far the selective cytotoxicity toward cancer cells.²³ Indeed, it has been demonstrated that flavaglines inhibit the proliferation of tumor cells at low nanomolar concentrations without showing any significant toxicity on normal cells, such as endothelial cells of umbilical vein (HUVEC), normal intestinal epithelial cells, peripheral blood

²² Lu King, M.; Chiang, C.-C.; Ling, H.-C.; Fujita, E.; Ochiai, M.; McPhail, A. T., *Journal of the Chemical Society, Chemical Communications* **1982**, 20, 1150-1151.

²³ Basmadjian, C.; Thuaud, F.; Ribeiro, N.; Désaubry, L., *Future Medicinal Chemistry* **2013**, 5 (18), 2185-2197.

lymphocytes, bone marrow stem cells and cardiomyocytes. As far as we know, Hausott and coll. were the first one to show that normal cells (in that case intestinal epithelial IEC18 cells) are 1,000 times less sensitive ($IC_{50} > 10 \mu M$) than malignant (SW480 and HT29/HI I) or premalignant (VACO235 and LT97) adenoma cells.²⁴ⁱ Furthermore, these compounds show no signs of toxicity in mice. However, only in the case of silvestrol, which has the particular pseudo-sugar substituent, a toxicity to several normal hematopoietic cells has been shown which was not the case for rocaglamide and its derivatives.²⁴ⁱⁱ

Additionally to their selective cytotoxicity, flavaglines also promote the survival of neurons and cardiac cells when these cells are exposed to various stressors. This unique feature and their promising anticancer activities increased the number of pharmacological investigation on flavaglines in the past few years, especially with the identification of their molecular targets.

1.3.3 Molecular targets of flavaglines and their mode of action

As we recently described in a review (see publication n°2 page 253) and a book chapter (see page 269), the developments in the identification of the molecular targets of flavaglines and their modes of action, this chapter will only summarizes few key features.

1.3.3.1 Prohibitins as molecular targets of flavaglines

In 2012, Li-Weber's group at the German Cancer Research Center (DKFZ) identified prohibitins as the molecular target of flavaglines using an affinity ligand synthesized in the laboratory.²⁵ Prohibitins, PHB1 and PHB2, are scaffold proteins that can associate together as a dimer or with other proteins to regulate numerous signaling pathways. PHBs functions are regulated by post-translational modifications by different signaling pathways such as IGF1 (insulin-like growth factor), EGF (endothelial growth factor), TGF- β (transforming growth factor), and IgM (immunoglobulin M) receptors and also by the kinases Akt, CamK

²⁴ (i) Hausott, B., Greger, H., Marian, B., **2004**, *109* (6), 933-940 (ii) Lindqvist, L. M.; Vikstrom, I.; Chambers, J. M.; McArthur, K.; Ann Anderson, M.; Henley, K. J.; Hoppo, L.; Cluse, L.; Johnstone, R. W.; Roberts, A. W.; Kile, B. T.; Croker, B. A.; Burns, C. J.; Rizzacasa, M. A.; Strasser, A.; Huang, D. S. *Cell Death Dis* **2012**, *3*, e409.

²⁵ Polier, G.; Neumann, J.; Thuaud, F.; Ribeiro, N.; Gelhaus, C.; Schmidt, H.; Giaisi, M.; Köhler, R.; Müller, Wolfgang W.; Proksch, P.; Leippe, M.; Janssen, O.; Désaubry, L.; Krammer, Peter H.; Li-Weber, M., *Chemistry & Biology* **2012**, *19* (9), 1093-1104.

(calmodulin-dependent protein kinase) IV, and PKC- δ . This different modifications dictate in which cellular compartment the PHB will be localized; in the nucleus, the cytoplasm, the mitochondria, the endoplasmic reticulum or the plasma membrane.

In mitochondria, PHBs are essential to maintain structural and functional integrity such as respiration, protein metabolism, and possibly, resistance to oxidative stress. In the nucleus, PHBs control transcription and DNA synthesis by interacting with many transcription factors such as histone deacetylases, histone methyltransferases, transcriptional corepressors and minichromosome maintenance proteins. In the cytoplasm, PHBs has also important role in regulating the activity of numerous signaling proteins such as the kinases c-Raf, Akt and MLK2, the phosphatase Shp1/2, the chaperones Hsp70 and mortalin/Grp75, the phospholipase Cy2, and the magnesium channel TRPM6.

PHBs are required for the activation of the kinase c-Raf. This interaction can be disrupted by flavaglines (Figure 5). Thus, the inhibition of c-Raf-MEK-ERK (extracellular-signal-regulated kinase) signaling, which results from the interaction of flavaglines with PHBs could partially explain their anticancer activities as this pathway is activated in many human cancers.²⁶ Recently, Chen, He, and collaborators, in the context of pancreatic ductal adenocarcinoma (PDAC), confirmed the observation that the binding of flavaglines to PHBs prevents their interaction with c-Raf.²⁷

²⁶ Matallanas, D.; Birtwistle, M.; Romano, D.; Zebisch, A.; Rauch, J.; von Kriegsheim, A.; Kolch, W. *Genes & Cancer* **2011**, 2 (3), 232-260.

²⁷ Luan, Z.; He, Y.; Alattar, M.; Chen, Z.; He, F. *Molecular Cancer* **2014**, 13 (1), 38.

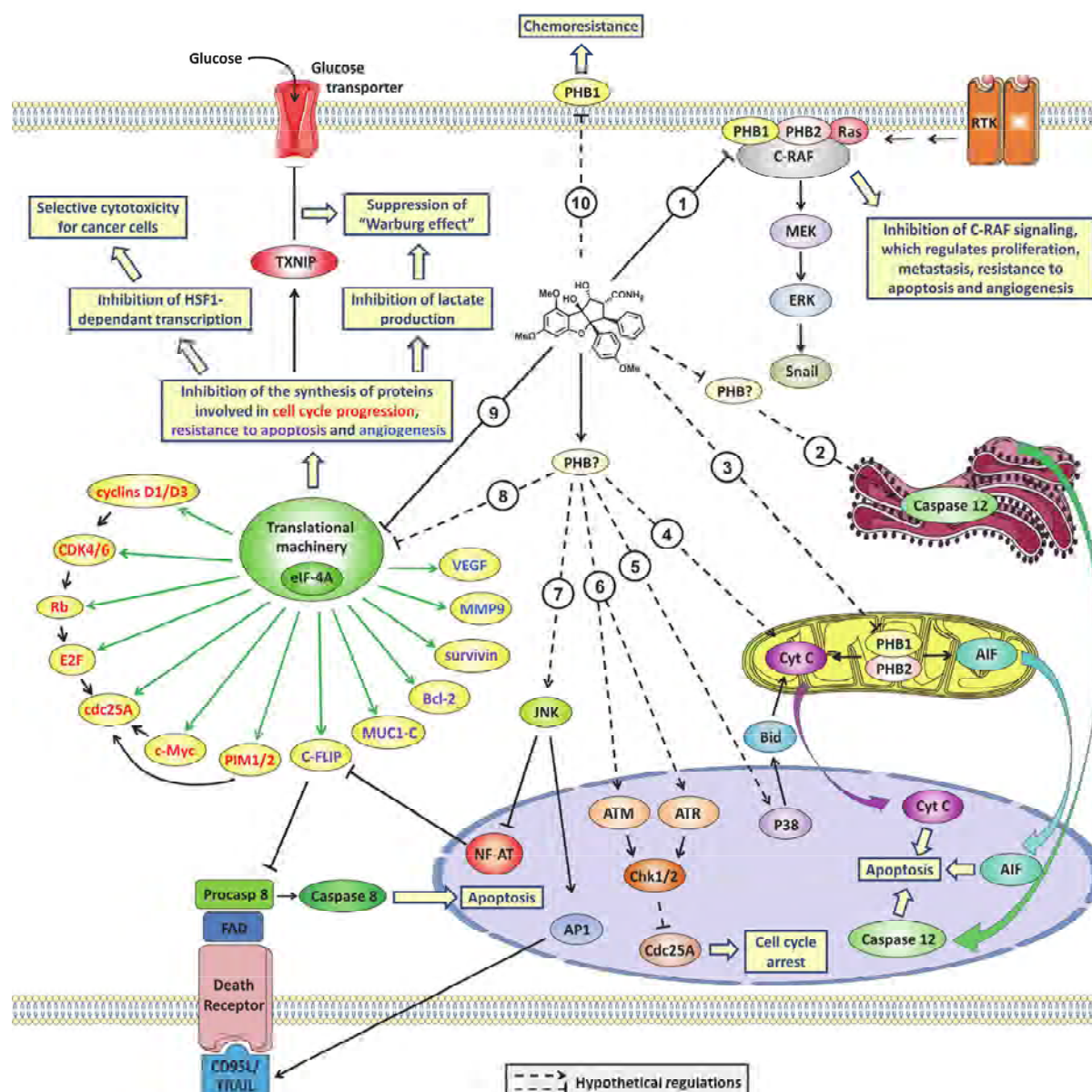


Figure 4 | Anticancer mechanisms of flavaglines.²⁸

1. Inhibition of the Ras-dependent C-Raf activation. 2, 3. Translocation of caspase-12 and AIF to the nucleus to induce apoptosis. 4. Translocation of cytochrome C to the nucleus to induce the intrinsic apoptotic pathway. 5. Activation of p38-mediated transcription of the pro-apoptotic Bcl-2 family. 6. Induction of the ATM/ATR-Chk1/2-Cdc25A pathway leading to cell cycle arrest. 7. Activation of JNK-dependent transcription of the pro-apoptotic proteins CD95 ligand and c-FLIP. 8. Hypothetical PHB-dependent inhibition of the translational machinery. 9. Inhibition of eIF4A leading to a down-regulation of expression of proteins involved in cell cycle progression, resistance to apoptosis and angiogenesis. This inhibition of protein synthesis leads to suppression of the activity of the transcription factor HSF1 and an up-regulation of the tumor suppressor TXNIP. TXNIP blocks glucose uptake and consequently prevents the "Warburg effect". 10. Hypothetical inhibition of cell surface PHB1-mediated chemo-resistance. Adapted from reference 28.

²⁸ Basmadjian, C.; Thuaud, F.; Ribeiro, N.; Désaubry, L. *Future Medicinal Chemistry* **2013**, 5 (18), 2185-2197.

1.3.3.2 eIF4A as a molecular target of flavaglines

In eukaryotic cells, translation of mRNA is a key step for the synthesis of few proteins. eIF4F, cap-binding complex, facilitates the cap-dependent translation of mRNAs. eIF4A is one of the three key proteins composing this complex. It is an ATP-dependent RNA helicase that unwind double-stranded RNA during the initiation of protein synthesis. In 2013, using affinity chromatography, Rizzacasa and colleagues demonstrated that some flavaglines directly bind to eIF4A (Eukaryotic Initiation Factor 4A).²⁹

Following Rizzacasa *et al.* report, Sadlish and colleagues, used chemogenomic profiling to validate eIF4A as the main target of flavaglines in yeast.³⁰ Indeed, they identified the binding site of flavaglines and proposed a model that could explain the enhancement of eIF4A binding to mRNAs promoted by flavaglines. This action inhibits the recycling of eIF4A leading to an inhibition of cap-dependent translation. This observation has already been published by Pelletier and colleagues.³¹

The helicase eIF4A is necessary for the translation of a very small number of mRNA having G-quadruplexes.³² Most of these mRNAs harbors G quadruplexes and code for factors controlling oncogenesis, angiogenesis, and chemoresistance. Importantly, housekeeping genes do not necessitate eIF4A for their translation, which explains, at least partially why flavaglines are selectively cytotoxic to cancer cells. Accordingly, flavaglines have been reported to inhibit the translation of mRNAs encoding CDK4 (cyclin-dependent kinase), CDK6, cyclins D1 and D3, cdc25A, Bcl-2 (B-cell lymphoma 2), survivin, Mcl-1 (myeloid cell leukemia protein 1), the PIM1/2 kinases, c-Myc, VEGF (vascular endothelial growth factor), matrix metalloproteinase 9 (MMP9), and MUC1-C.²⁸

²⁹ Chambers, J. M.; Lindqvist, L. M.; Webb, A.; Huang, D. C. S.; Savage, G. P.; Rizzacasa, M. A. *Organic Letters* **2013**, *15* (6), 1406-1409.

³⁰ Sadlish, H.; Galicia-Vazquez, G.; Paris, C. G.; Aust, T.; Bhullar, B.; Chang, L.; Helliwell, S. B.; Hoepfner, D.; Knapp, B.; Riedl, R.; Roggo, S.; Schuierer, S.; Studer, C.; Porco, J. A.; Pelletier, J.; Movva, N. R. *ACS Chemical Biology* **2013**, *8* (7), 1519-1527

³¹ Cencic, R.; Carrier, M.; Galicia-Vázquez, G.; Bordeleau, M.-E.; Sukarieh, R.; Bourdeau, A.; Brem, B.; Teodoro, J. G.; Greger, H.; Tremblay, M. L.; Porco, J. A., Jr.; Pelletier, J. *PLoS ONE* **2009**, *4* (4), e5223.

³² Wolfe, A. L.; Singh, K.; Zhong, Y.; Drewe, P.; Rajasekhar, V. K.; Sanghvi, V. R.; Mavrakis, K. J.; Jiang, M.; Roderick, J. E.; Van der Meulen, J.; Schatz, J. H.; Rodrigo, C. M.; Zhao, C.; Rondou, P.; de Stanchina, E.; Teruya-Feldstein, J.; Kelliher, M. A.; Speleman, F.; Porco, J. A.; Pelletier, J.; Ratsch, G.; Wendel, H.-G. *Nature* **2014**, *513* (7516), 65-70

1.3.4 Structure-activity relationships of flavaglines

Although the study of structure-activity relationships as previously been reviewed,²⁸ the key features will be presented in this section. Replacing the methoxy group in position 4' of rocaglaol by an electron-withdrawing group such as bromine ($R^8 = \text{Br}$) enhances cytotoxicity, whereas deletion ($R^8 = \text{H}$) decreases the cytotoxicity by 3 orders of magnitude, suggesting a preference for a hydrophobic substituent in the para position (Figure 5). The introduction of a methoxy group in position 4'' ($R^7 = \text{OMe}$) on the other phenyl is detrimental for cytotoxicity. The substitution in position 2 with an amide or an ester results in a significant reduction of the cytotoxicity to cancer cells that have developed chemotherapy resistance by overexpressing P-glycoprotein (P-gp), a protein to the plasma membrane encoded by the gene multi-drug resistant (MDR1). Similarly, the introduction of a pseudo-sugar dioxanyl in position 6 as in silvestrol appears to increase the cytotoxicity *in vitro*, but makes it very sensitive to multidrug resistance. 8-Demethoxy compounds are significantly less active than related compounds, showing a preference but not an absolute requirement of a methoxy group in position 8 for cytotoxicity.

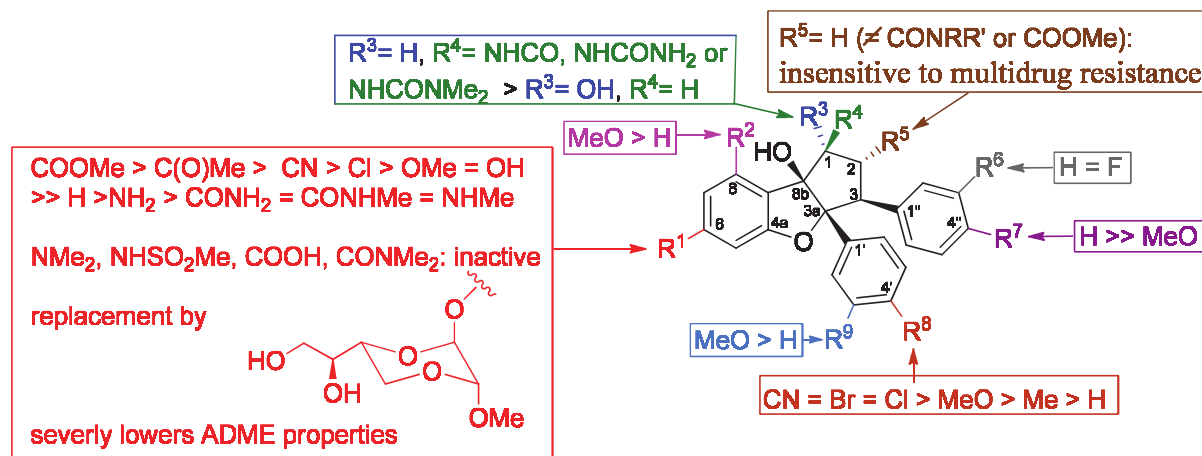
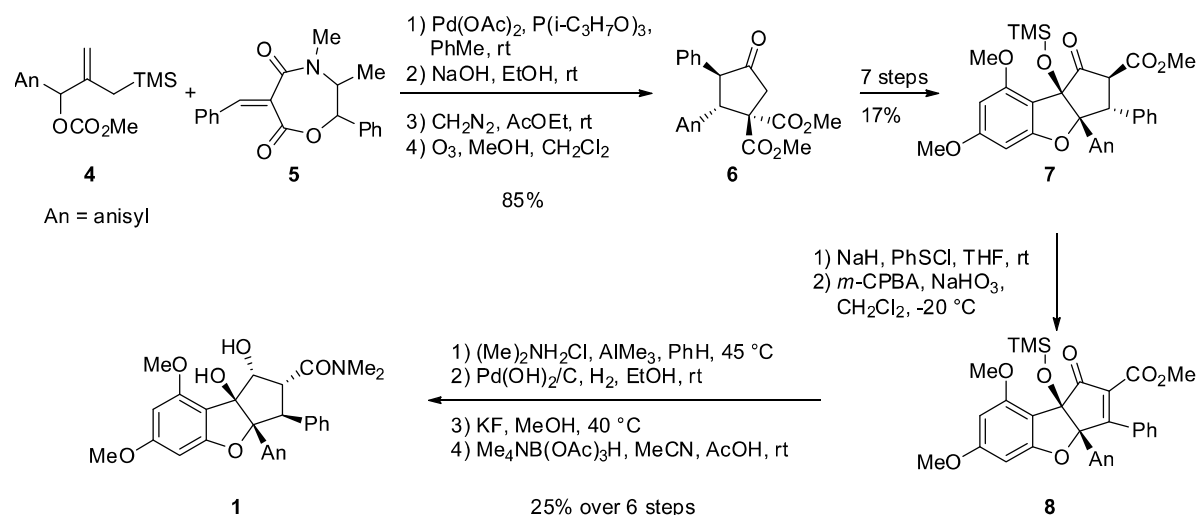


Figure 5 | Key SAR data for cytotoxic activities of flavaglines.²⁸

1.4 Synthesis of flavaglines

1.4.1 First total synthesis of rocaglamide

Since 1990, with Trost's first total synthesis of rocaglamide³³ (Scheme 1), flavaglines have received considerable attention from multiple laboratories due to the synthetic challenge of their complex structure. Indeed, the flavaglines core is a compact and functionalized heterocycle with two contiguous quaternary chiral centers and *cis* aryl groups on adjacent carbons on the cyclopentane ring. Up to date, more than a dozen of different synthetic approaches have been reported. In this section, a summary of the significant syntheses is presented. We recently reviewed more extensively this topic in a book chapter.³⁴



Scheme 1 | Trost's enantioselective synthesis of rocaglamide.³³

Trost's approach is based on the enantioselective [3+2]-cycloaddition of a trimethylenemethane derivatives generated from **4** with the oxazepinedione **5** to give access in 4 steps to cyclopentenone **6** in good yield (85%, Scheme 1). From there, 7 additional transformations were needed to reach the flavaglines skeleton, but with an incorrect configuration compared to the natural product. The stereochemistry could be

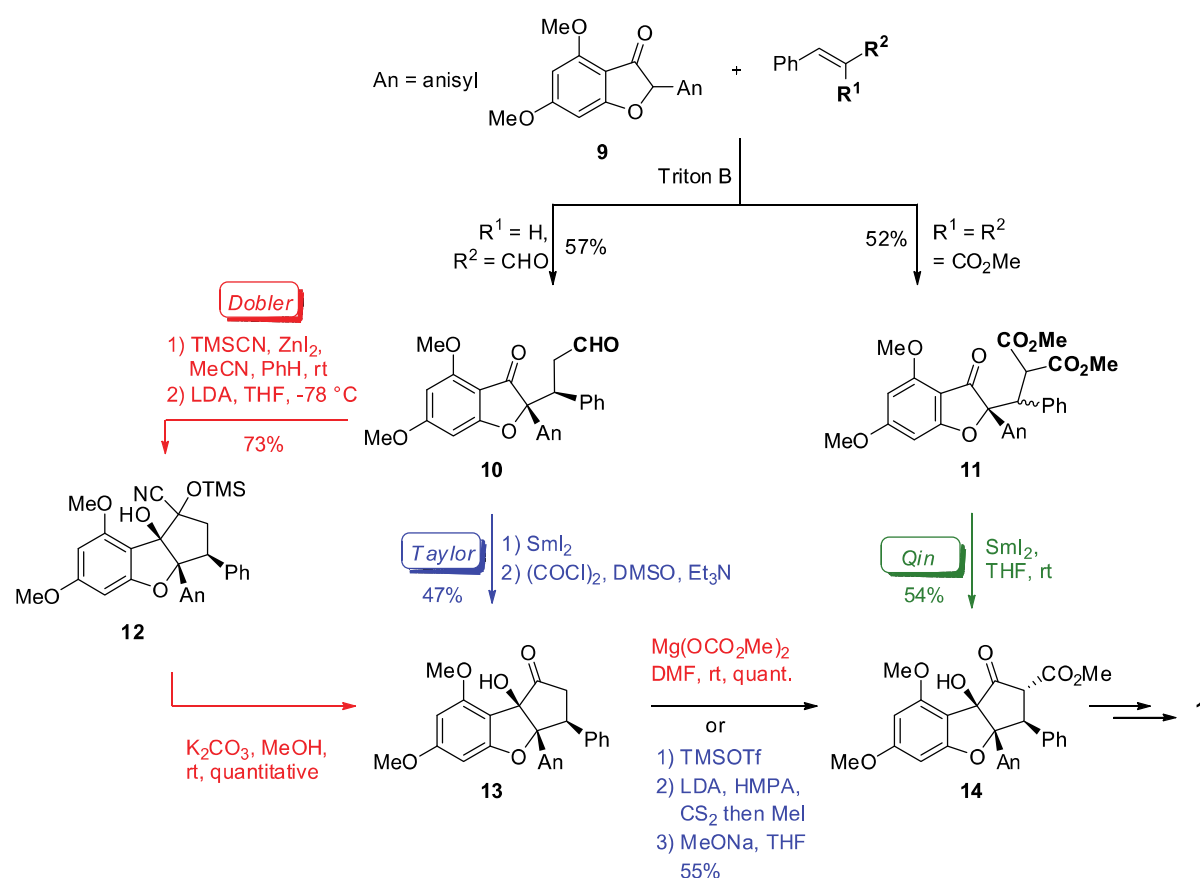
³³ Trost, B. M.; Greenspan, P. D.; Yang, B. V.; Saulnier, M. G. *Journal of the American Chemical Society* **1990**, *112* (24), 9022-9024.

³⁴ Synthesis and pharmacology of flavaglines, Basmadjian, C., Zhao, Q., De Gramont, A., Serova, M., Raymond, E., Vagner, S., Robert, C., Nebigil, C. G., Désaubry, L., *Bioactive Natural Products: Chemistry & Biology*, Brahmachari, G., Ed. John Wiley & Sons, **2015**.

corrected by additional six steps to afford rocaglamide (**1**) with the desired stereochemistry via dehydro-intermediate **8**. Although this approach relies on multiple reactions, it remains the only enantiospecific one to date.

1.4.2 Synthesis of rocaglamide *via* benzofuranone intermediate

The strategies developed by Taylor,³⁵ Dobler,³⁶ and Qin³⁷ are all based on a common intermediate, the benzofuranone **9** which is prepared via an intermolecular Michael addition and that leads to the rocaglamide tricyclic core through an intramolecular cyclization (Scheme 2).



Scheme 2 | Taylor's, Dobler's and Qin's synthesis of rocaglamide.³⁵⁻³⁷

³⁵ Davey, A. E.; Schaeffer, M. J.; Taylor, R. J. K. *Journal of the Chemical Society, Perkin Transactions 1* **1992**, (20), 2657-2666.

³⁶ Dobler, M. R.; Bruce, I.; Cederbaum, F.; Cooke, N. G.; Diorazio, L. J.; Hall, R. G.; Irving, E. *Tetrahedron Letters* **2001**, 42 (47), 8281-8284.

³⁷ Li, H.; Fu, B.; Wang, M. A.; Li, N.; Liu, W. J.; Xie, Z. Q.; Ma, Y. Q.; Qin, Z. *European Journal of Organic Chemistry* **2008**, 2008 (10), 1753-1758.

Taylor's and co-workers did the pioneer work on this approach.³⁵ Indeed, in 1992 they reported a synthesis based on an intermolecular Michael addition associated with a SmI_2 -catalyzed intramolecular reductive cyclization to construct the tricyclic core of rocaglamide (Scheme 2). Thereby, aldehyde **10** was prepared by Michael addition of trans-cinnamaldehyde to benzofuranone **9**, and was then converted to cyclopentanone **13** upon cyclization and Swern oxidation. Additional 3 steps led to β -ketoester **14** which was converted to rocaglamide (**1**) in the next two final steps.

Dobler and colleagues improved this synthesis.³⁶ They utilized the same intermolecular Michael addition to form aldehyde **10** but they modified the cyclization step. Indeed, instead of a SmI_2 -catalyzed cyclization, cyanohydrin **12** was used in an umpolung reaction to generate after deprotection the cyclopentanone **13** (Scheme 2). The carboxylation of the ketone was also modified by using Stiles' reagent to give ester **14**. The latter was then converted into rocaglamide (**1**) in three steps.

In 2008, Qin *et al.* made additional changes in Taylor's approach by introducing the methoxycarbonyl group earlier in the synthesis onto the Michael acceptor, therefore making Stiles' carboxylation unnecessary.³⁷ Condensation of benzofuranone **9** with dimethyl 2-benzylidenemalonate afforded adduct **11**, which underwent a SmI_2 -promoted pinacol coupling reaction giving access to the rocaglamide skeleton **14** (Scheme 2).

In 2005, Ragot's team used Taylor's approach to introduce variation on the benzofuran ring.³⁸ The only difference in this pathway lies on the preparation of the benzofuran intermediate **10**, which was obtained by Suzuki-type reaction.

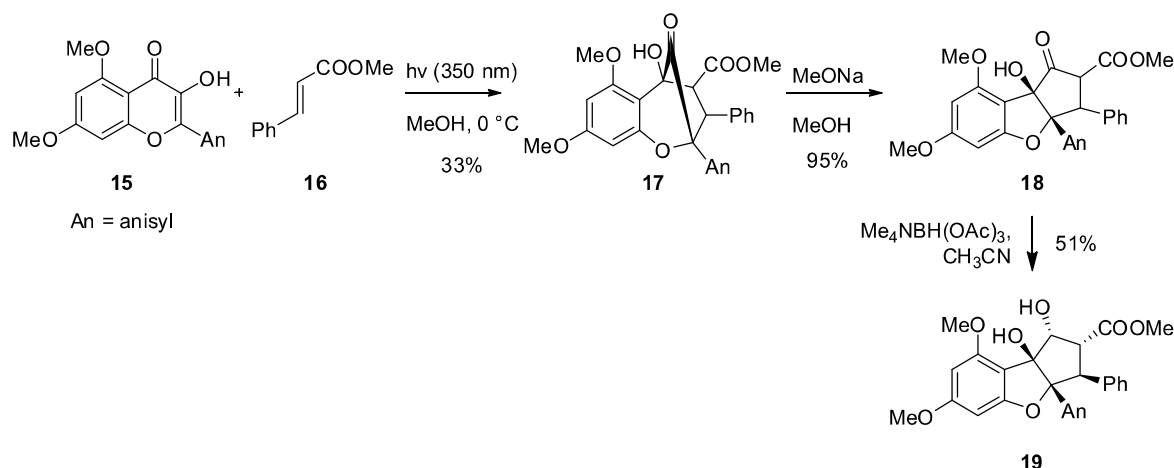
1.4.3 Other approaches to synthesis rocaglamide

1.4.3.1 Synthesis of flavaglines using photoirradiation

Based on an earlier proposal of Proksch's group for the biosynthesis of flavaglines³⁹ Porco reported in 2004 a biomimetic approach to prepare methyl rocaglate **19** using

³⁸ Diedrichs, N.; Ragot, J. P.; Thede, K. *European Journal of Organic Chemistry* **2005**, 2005 (9), 1731-1735

photochemistry (Scheme 3).⁴⁰ Thereby, irradiation of 3-hydroxyflavone **15** with cinnamic ester **16** gave the tricyclic adduct **17** via a [3+2]-cycloaddition reaction. β -Acyloln rearrangement of this intermediate in basic conditions followed by diastereoselective reduction gave methyl rocaglate **19**. In 2012, the same group developed a chiral version using TADDOL derivative to prepare photocycloaddition product **17** in 69% yield and 85.5:14.5 enantiomeric ratio.⁴¹



Scheme 3 | Porco's biomimetic synthesis of rocaglamide.⁴⁰

1.4.3.2 Synthesis of flavaglines using a Nazarov reaction

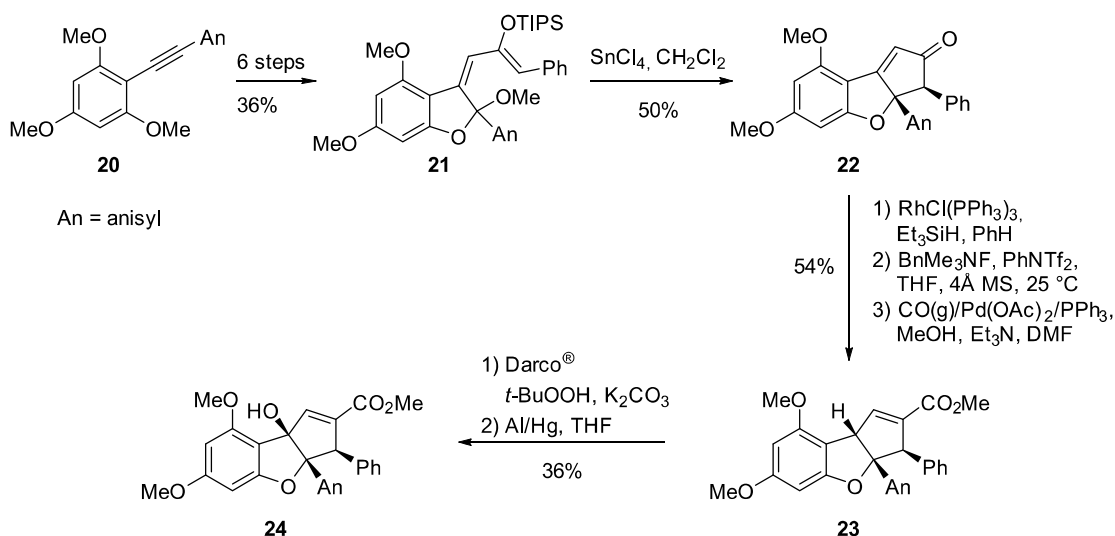
Magnus' group was the first to report the use of a conrotatory Nazarov cyclization, also known as Isler-Mukaiyama aldol reaction, as a key step to prepare the tricyclic flavagline core.⁴² Nazarov precursor **21** was prepared in 6 steps from the alkyne **20** (Scheme 4). Upon treatment with SnCl_4 , substrate **21** cyclized to afford cyclopentenone **22**. Following hydrosilylation, palladium-mediated introduction of the carboxymethyl group and hydroxylation led to the methyl rocaglate **24**.

³⁹ Proksch, P.; Edrada, R.; Ebel, R.; Bohnenstengel, F. I.; Nugroho, B. W. *Current Organic Chemistry* **2001**, 5 (9), 923-938.

⁴⁰ Gerard, B.; Jones, G.; Porco, J. A. *Journal of the American Chemical Society* **2004**, 126 (42), 13620-13621.

⁴¹ Lajkiewicz, N. J.; Roche, S. P.; Gerard, B.; Porco, J. A. *Journal of the American Chemical Society* **2012**, 134 (31), 13108-13113.

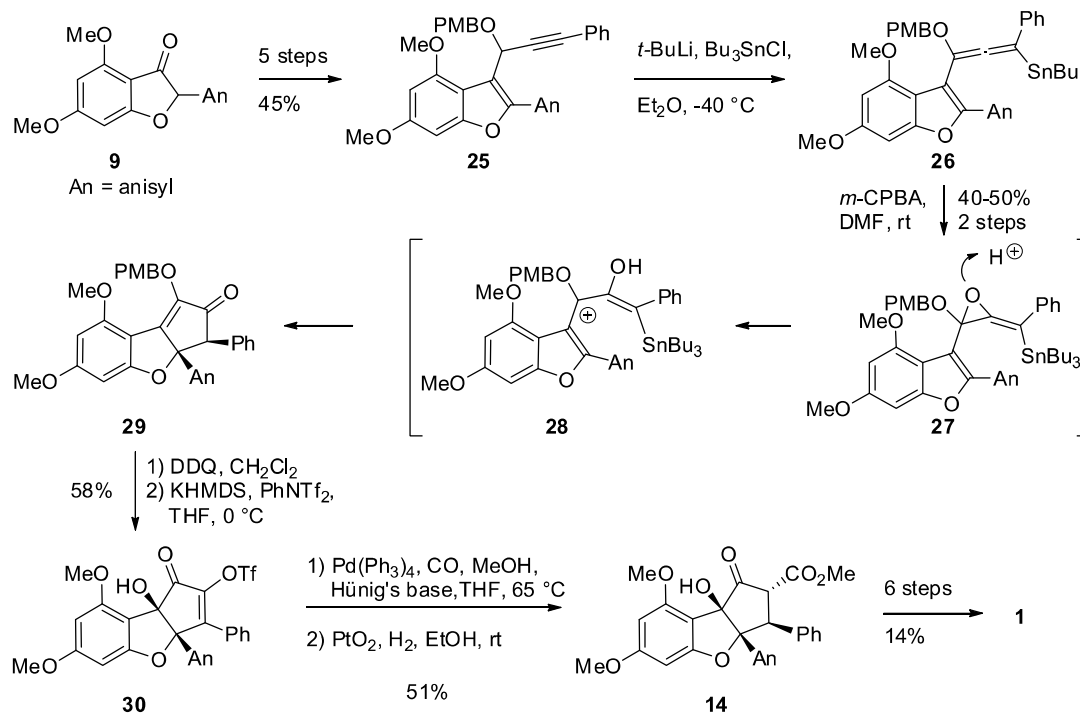
⁴² Magnus, P.; Stent, M. A. H. *Organic Letters* **2005**, 7 (18), 3853-3855.



Scheme 4 | Magnus' synthesis to access flavaglines.⁴²
DARCO[®], activated charcoal

A few years later, Frontier's group also used a Nazarov cyclization in their synthesis of flavaglines. Indeed, in 2009, they established a new synthetic route based on an oxidation-initiated Nazarov-type reaction to successfully synthesize rocaglamide **1** (Scheme 5).⁴³ Starting from benzofuranone **9**, a similar intermediate to Taylor and Dobler approaches, they prepared substrate **25** in 5 steps. The latter was then transformed into a highly functionalized alkoxyallene **26**, precursor of the Nazarov-type reaction. The cyclopentenone ring was obtained from highly reactive allenyl oxide **28** generated *in situ* by oxidation with *m*-CPBA. Thus, the flavagline core was obtained with the desired configuration at the carbons bearing the phenyl and anisyl groups. Subsequent steps including palladium-mediated carbonylation gave access to ketoester **14**, which was converted into rocaglamide **1**. This synthesis validates Magnus' initial Nazarov strategy as an original and direct approach to construct the flavagline core.

⁴³ Malona, J. A.; Cariou, K.; Frontier, A. J. *Journal of the American Chemical Society* **2009**, *131* (22), 7560-7561.



Scheme 5 | Frontier's synthesis of rocaglamide based on a Nazarov reaction.⁴³

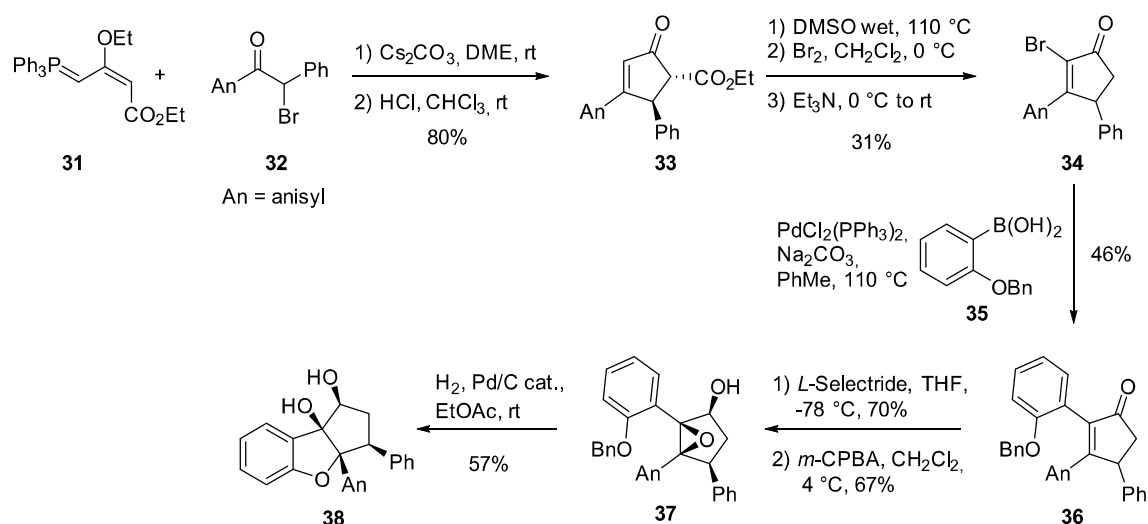
1.4.4 Ragot's synthesis of rocaglaol derivative

In 2004, Ragot's group at Bayer published a synthesis of flavaglines based on an intramolecular hydroxy epoxide opening.⁴⁴ They first constructed the eastern part of the molecule by preparing cyclopentenone **34** (Scheme 6). Although *symmetrical* 3,4-diaryl-cyclopent-2-enones are known to be easily accessible *via* cyclization of α,β -diketones⁴⁵ *unsymmetrical* ones are harder to prepare. Using Schoop's methodology⁴⁶ cyclopentenone **33** could be obtained on a multigrams scale in two steps from bromoketone **32** and triphenylphosphorane **31**. β -Ketoester **33** was decarboxylated upon heating at 110 °C in wet DMSO. Overheating at 140 °C led to an inseparable mixture of the desired product and its regioisomer due to a migration of the double bond. The next step was the α -bromination which was tedious as poly-bromination could not be avoided. The selected method here was the use of Br₂ followed by addition of triethylamine leading to the elimination of HBr. Thus, desired α -bromoenone **34** could be obtained with 35% yield.

⁴⁴ Thede, K.; Diedrichs, N.; Ragot, J. P. *Organic Letters* **2004**, 6 (24), 4595-4597.

⁴⁵ Polo, E.; Barbieri, A.; Traverso, O. *European Journal of Inorganic Chemistry* **2003**, 2003 (2), 324-330.

⁴⁶ Schoop, A.; Greiving, H.; Göhr, A. *Tetrahedron Letters* **2000**, 41 (12), 1913-1916.



Scheme 6 | Ragot's synthesis of flavaglines skeleton.⁴⁴

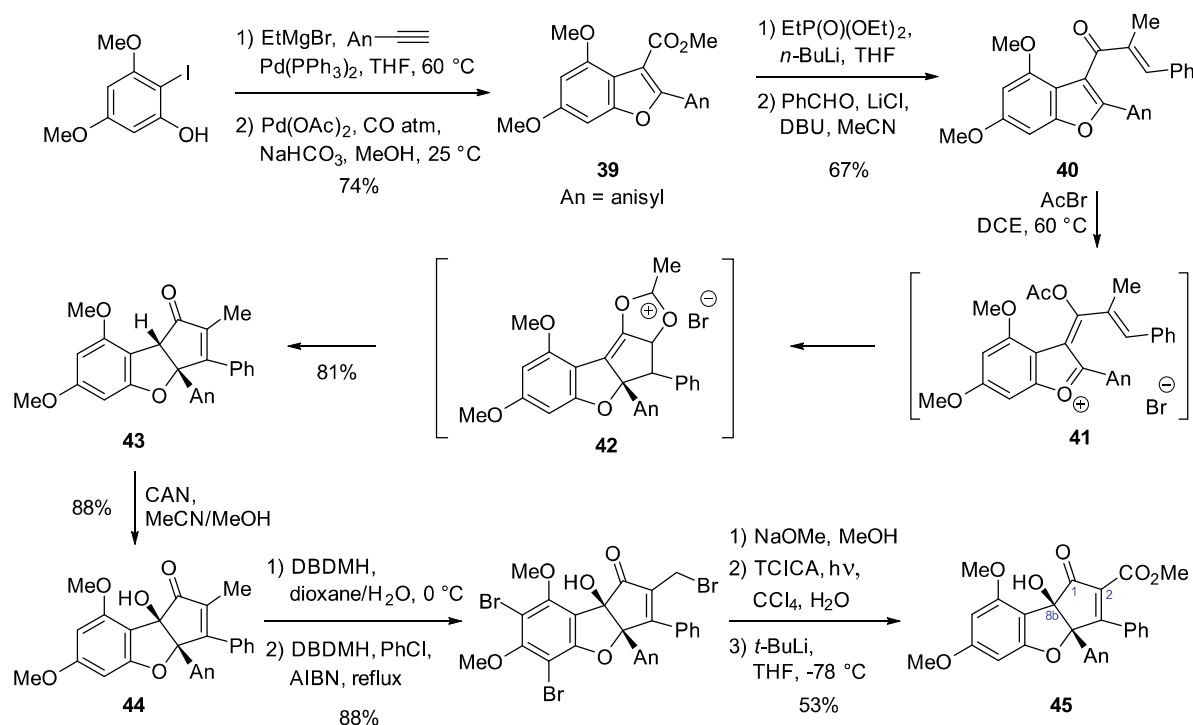
Ragot and collaborators then focus their attention on building the western side of the molecule. The first step is a Suzuki coupling reaction using palladium catalyst with boronate **35** (Scheme 6). This leads to the formation of trisubstituted cyclopentenone **36** which is then reduced. The use of NaBH_4 or DIBAL-H gave no selectivity at all. Low selectivity was observed under Luche conditions ($\text{NaBH}_4/\text{CeCl}_3$). However, using *L*-selectride gave the desired *syn*-alcohol (confirmed by NOESY experiments) with complete diastereoselectivity and 70% yield. With the allylic alcohol in hand, the two final stereocenters were installed by stereoselective epoxidation. Indeed, the use of *m*-CPBA gave complete control of the stereochemistry thanks to the assistance of the hydroxyl group (Henbest's rule).⁴⁷ Upon deprotection of the phenolic group under hydrogenation conditions (Pd/C 10% in EtOAc), the cyclization occurred spontaneously to afford didemethoxy-rocaglaol **38** with the desired stereochemistry.

1.4.5 Magnus' formal synthesis of (±)-methyl rocaglate

As showed previously in this chapter (section 1.4.3), Magnus' former approach did not give access to rocaglamide but only to (±)-1,2-anhydro-rocaglamide (**24**). This was due to heavy changes in the oxidation state of carbons 1, 2 and 8b. Therefore, a few years later, this laboratory improved their synthesis of methyl rocaglate using an unprecedented

⁴⁷ Henbest, H. B.; Wilson, R. A. L., *Journal of the Chemical Society (Resumed)* **1957**, (0), 1958-1965.

Nazarov reaction promoted by acetyl bromide (Scheme 7).⁴⁸ Starting material, benzofuran **39**, was easily prepared from 2-iodo-3,5-dimethoxyphenol via a Kumada cross-coupling reaction⁴⁹ with 4-methoxyphenylacetylene followed by treatment Pd(OAc)₂/CO in the presence of CBr₄/NaHCO₃. Exposure to diethyl ethylphosphonate/*n*-BuLi followed by treatment with benzaldehyde under Masamune-Roush conditions⁵⁰ afforded dienone **40** in 67% yield over 2 steps.



Scheme 7 | Magnus' synthesis of methyl rocaglate by acetyl bromide mediated Nazarov reaction.⁴⁸ DBDMH is 5,5-dimethyl-1,3-dibromohydantoin and TCICA is trichloroisocyanuric acid.

The next step is the key Nazarov reaction. First, dienone **40** was exposed to different Lewis acids including SnCl₄, AlCl₃, TiCl₄ and Sc(OTf)₃ (Scheme 7). All attempts only resulted in the isolation of retro Friedel-Crafts reaction product. They then turned their attention into Brønsted acids. Using concentrated HCl gave desired cyclopentenone **43** after 48 h at 100 °C but with low yield (12%) whereas using HBr only led to demethylation of ethers. Ultimately,

⁴⁸ Magnus, P.; Freund, W. A.; Moorhead, E. J.; Rainey, T. *Journal of the American Chemical Society* **2012**, *134* (14), 6140-6142.

⁴⁹ Tamao, K.; Kiso, Y.; Sumitani, K.; Kumada, M. *Journal of the American Chemical Society* **1972**, *94* (26), 9268-9269.

⁵⁰ Blanchette, M. A.; Choy, W.; Davis, J. T.; Essinfeld, A. P.; Masamune, S.; Roush, W. R.; Sakai, T. *Tetrahedron Letters* **1984**, *25* (21), 2183-2186.

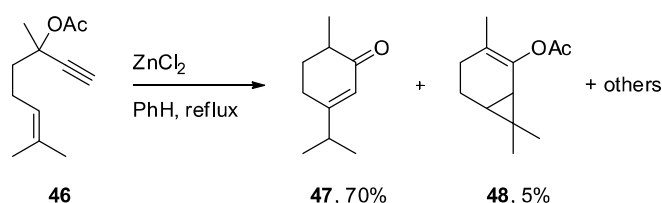
acetyl bromide was found to lead to product **43** with good yield (81%). Replacing it by acetyl chloride only resulted in recovery of starting material even after heating at 150 °C in a sealed tube. This could be explained by the fact that AcBr is much more reactive than AcCl.⁵¹ The authors proposed the following mechanism: oxonium ion **41** is obtained upon acetylation of ketone **40** (Scheme 7). This intermediate cyclized into acetoxonium ion **42**. Loss of a proton followed by aqueous workup leads to cyclopentenone **43**. It can be noted here that replacing the vinylic methyl group by hydrogen decreased the yield to 12% whereas with a cyano substituent, no cyclized product was observed. Cyclopentenone **43** could now be transformed into dehydroflavagline (**45**) in six steps with 41% yield. Only two extra steps are needed following Trost's synthesis to achieve the synthesis of methyl rocaglate.

⁵¹ Briody, J. M.; Satchell, D. P. N. *Journal of the Chemical Society (Resumed)* **1964**, (0), 3724-3728.

1.5 Rearrangements of vinyl propargyl alcohols and their esters

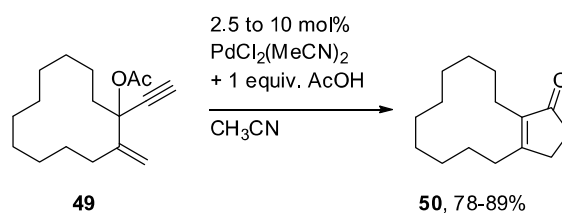
1.5.1 Discovery of the Rautenstrauch rearrangement

In 1976, Ohloff *et al.* at Firmenich reported the serendipitous discovery of the formation of carvenone (**47**) from propargyl acetate **46** catalyzed by zinc chloride (Scheme 8).⁵² Cycloisomerization with concomitant 1,2-acetyl shift afforded carvenone (**47**) as the major product (70% yield) along with small amount of 2-acetoxy-2-carene **48** (5%). Ohloff *et al.* postulated that the rearrangement is triggered by coordination of the zinc cation to the double bond.



Scheme 8 | Ohloff synthesis of carvenone (**47**).⁵²

In 1984, Rautenstrauch and collaborators, also at Firmenich, discovered a similar reaction but using palladium (II) instead of zinc catalyst (Scheme 9).⁵³ They described a new approach to access 2-cyclopentenones from 1-ethynyl-2-propenyl acetates in a Pd-catalyzed variant of the Nazarov cyclization.



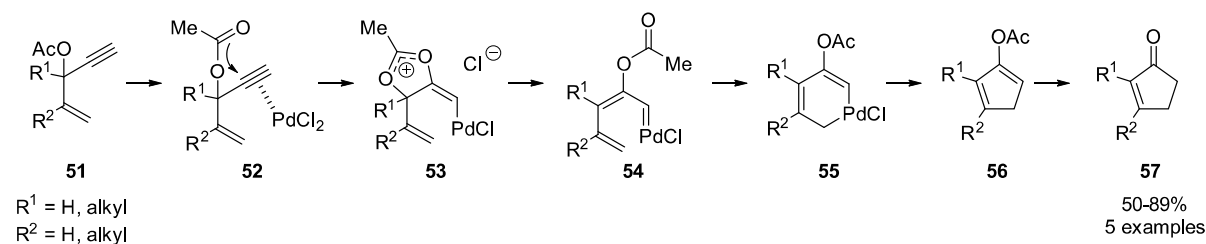
Scheme 9 | Rautenstrauch rearrangement of propargyl acetate **49**.⁵³

The common point between these two transformations is the 1,2-*O*-migration. The mechanism postulated by Rautenstrauch is depicted in Scheme 10. The cyclization was proposed to start with the formation of π -complex **52**. Then, 1,2-acetate migration could give acetoxonium species **53** which could be transformed into butadienylcarbene complex

⁵² Strickler, H.; Davis, J. B.; Ohloff, G. *Helvetica Chimica Acta* **1976**, *59* (4), 1328-1332.

⁵³ Rautenstrauch, V. *The Journal of Organic Chemistry* **1984**, *49* (5), 950-952.

54. Oxidative cyclization could give palladiacyclohexadiene **55**, which would reductively eliminate **56**. The reported scope of this reaction is limited to terminal alkyne and to R^1 and R^2 groups equivalent to a hydrogen or an alkyl chain.



Scheme 10 | Postulated mechanism of the Rautenstrauch rearrangement.⁵³

1.5.2 Transition-metal-catalyzed Rautenstrauch reaction

Since Rautenstrauch's report, other transition metals have been studied for this rearrangement. Hereafter, selected examples will be discussed using platinum-, ruthenium-, gold- and mercury-catalysts.

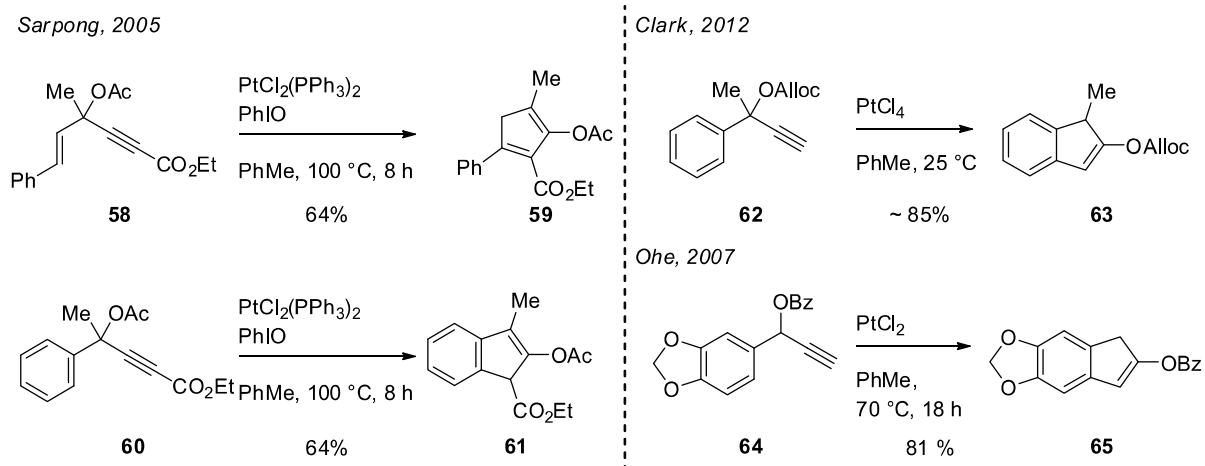
1.5.2.1 Platinum-catalyzed Rautenstrauch reactions

The Pt-catalyzed Rautenstrauch reaction was mainly reported by the groups of Sarpong,⁵⁴ Ohe⁵⁵ and Clark.⁵⁶ They could prepare functionalized indene derivatives **61**, **63** and **65** utilizing propargylic esters **60** and **62** or propargyl carbonates **64** via Pt-catalyzed Rautenstrauch reaction with different regioselectivities (Scheme 11). Moreover, Sarpong's group explored non-aromatic-based substrates such as propargylic acetate **58** that forms cyclopentadiene **59** as the sole product.

⁵⁴ Bhanu Prasad, B. A.; Yoshimoto, F. K.; Sarpong, R. *Journal of the American Chemical Society* **2005**, *127* (36), 12468-12469.

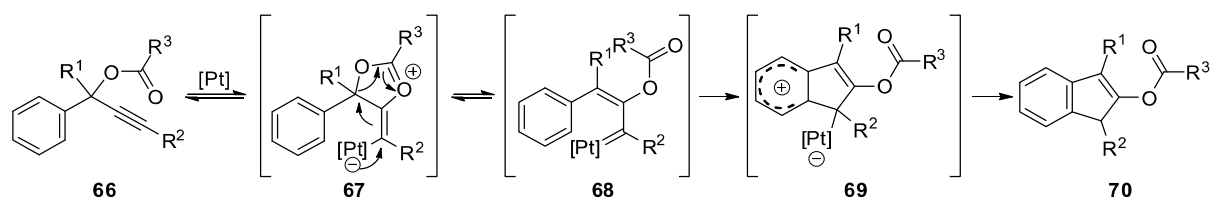
⁵⁵ Nakanishi, Y.; Miki, K.; Ohe, K. *Tetrahedron* **2007**, *63* (49), 12138-12148.

⁵⁶ Zhao, J.; Clark, D. A. *Organic Letters* **2012**, *14* (7), 1668-1671.



Scheme 11 | Platinum-Catalyzed Rautenstrauch-type reaction.⁵⁴⁻⁵⁶

They proposed that the pentannulation can be accounted for an *in situ* generated Pt-carbenoid intermediate **68** (Scheme 12). Compound **66** could undergo a potentially reversible Pt-catalyzed 5-*exo*-dig cyclization with the 1,2-acyloxy shift. A C-O bond cleavage would afford the metal-carbenoid **68**. Then, preferential irreversible C-H insertion into the phenyl group would provide indene derivative **70**.

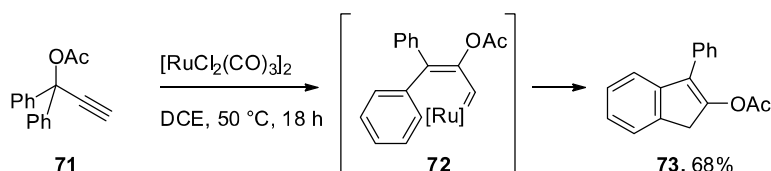


Scheme 12 | Proposed mechanism for the formation of indene derivatives.⁵⁴⁻⁵⁶

1.5.2.2 Ruthenium-catalyzed Rautenstrauch reaction

Uemura's group has also shown that formation of indene derivatives is possible utilizing a ruthenium-catalyst (Scheme 13).⁵⁷ Indeed, treatment of alkyne **71** in the presence of a catalytic amount of $[\text{RuCl}_2(\text{CO})_3]_2$ yielded to indene **73** in 68% yield. Similarly to platinum, the authors attributed the formation of **73** to the formal insertion of a vinylcarbene species to the C-H bond at the *ortho* position of one of the phenyl ring.

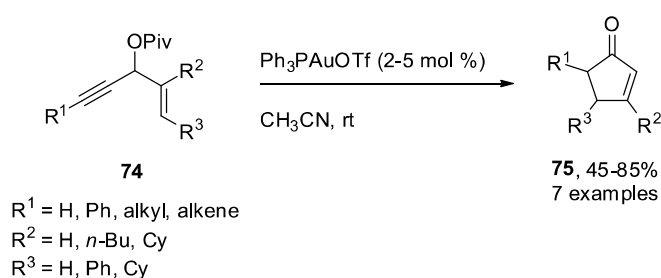
⁵⁷ Miki, K.; Ohe, K.; Uemura, S. *The Journal of Organic Chemistry* **2003**, *68* (22), 8505-8513.



Scheme 13 | Ru-Catalyzed Rautenstrauch reaction.⁵⁷

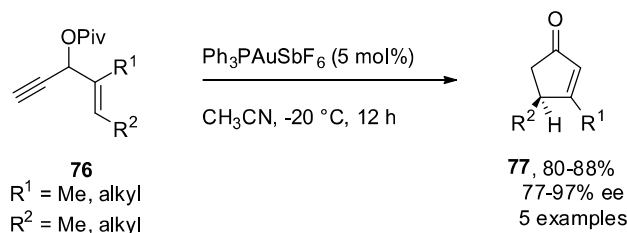
1.5.2.3 Gold-catalyzed Rautenstrauch reaction

In 2005, Toste group described a synthesis of 2-cyclopentenones **75** based on Rautenstrauch rearrangement using gold(I) as a catalyst instead of palladium (Scheme 14).⁵⁸



Scheme 14 | Gold(I)-catalyzed cyclopentenone synthesis.⁵⁸

The gold(I)-catalyzed reactions are tolerant to substitution at the acetylenic and olefinic positions (except for Z-olefins), thus providing access to a wide range of cyclopentenones under exceptionally mild conditions. Additionally, enantioenriched cyclopentenones can be prepared by the cyclization of propargylic alcohols using $\text{Ph}_3\text{AuSbF}_6$ as the catalyst (Scheme 15).

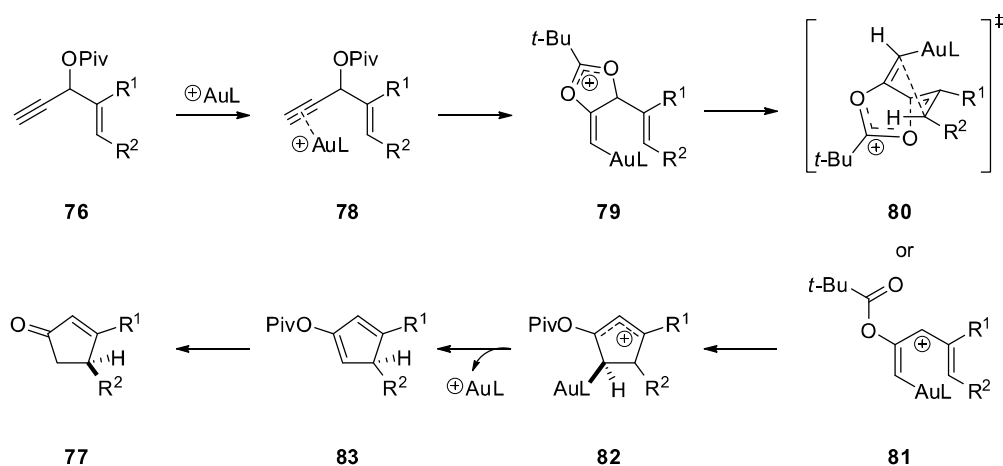


Scheme 15 | Enantioselective cyclopentenone synthesis.⁵⁸

The proposed mechanism that accounts for the stereochemical course of the Au(I)-catalyzed cyclopentenone synthesis is depicted in Scheme 16. Intramolecular 1,2-addition of the ester

⁵⁸ Shi, X.; Gorin, D. J.; Toste, F. D. *Journal of the American Chemical Society* **2005**, *127* (16), 5802-5803.

onto the alkyne, induced by coordination of the alkyne to the cationic gold(I) complex, affords vinyl gold species **79**. The stereoselectivity can be explained by either an intramolecular cyclization that proceeds through a transition state (**80**) in which the leaving group is in an orthogonal position to the plane of the olefin or by a helically chiral intermediate **81**. The cyclization produced cationic intermediate **82**, which upon elimination of cationic gold (I) and hydrolysis affords cyclopentenone **77**.



Scheme 16 | Mechanism of the gold-catalyzed Rautenstrauch rearrangement.^{58,59}

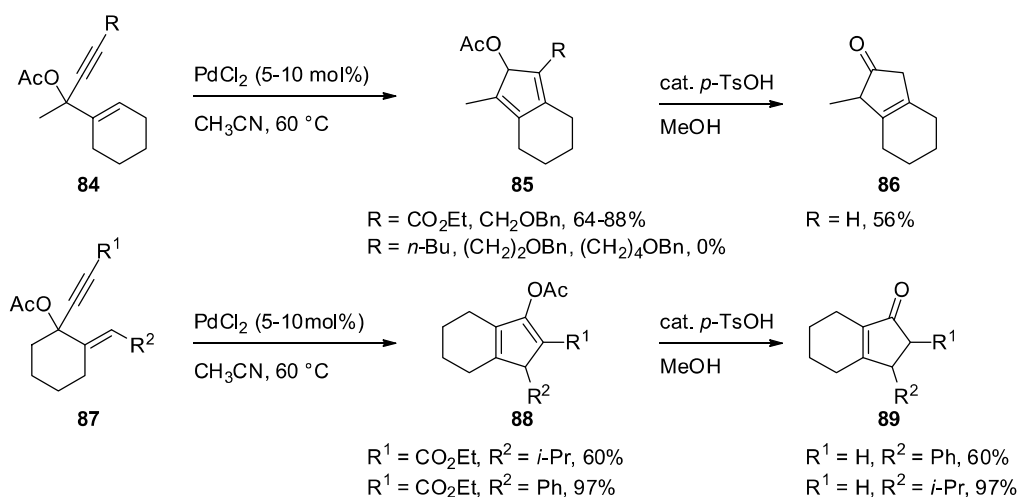
Although the metal carbenoid intermediate is widely proposed as an intermediate in the metal-catalyzed Rautenstrauch reaction with Pd, Pt or Ru, here it cannot explain the chirality transfer. Indeed, computational studies based on Toste's work indicate that the reaction proceeds through helical pentadienyl cationic intermediate.

1.5.2.4 Palladium-catalyzed Rautenstrauch reaction

In 2007, Frontier's group at the University of Rochester reported an expanded study of the Rautenstrauch metal-catalyzed rearrangement of propargyl acetates **84** and **87** utilizing palladium (Scheme 17).⁶⁰

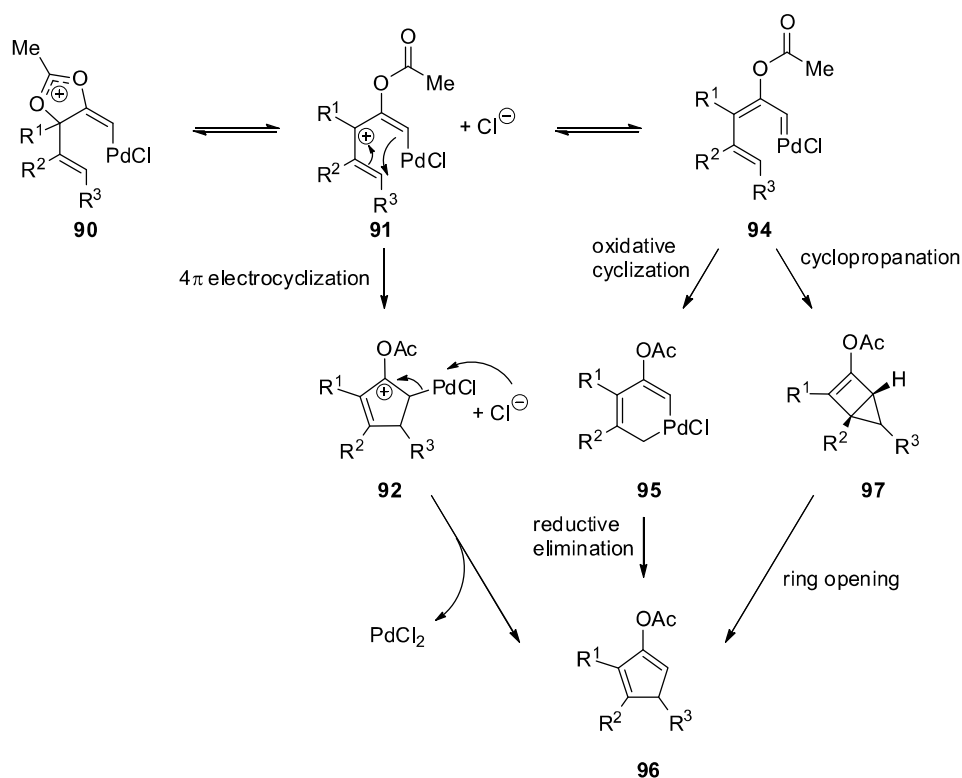
⁵⁹ Faza, O. N.; López, C. S.; Álvarez, R.; de Lera, A. R. *Journal of the American Chemical Society* **2006**, *128* (7), 2434-2437.

⁶⁰ Caruana, P. A.; Frontier, A. J. *Tetrahedron* **2007**, *63* (43), 10646-10656.



Scheme 17 | Rearrangement of propargyl acetates **84** and **87**.⁶⁰

The authors showed that substituents at the terminal positions of both the alkyne and the alkene have a strong impact on the outcome of the reaction. Substrates with ester substituents at the alkyne terminal (**87**, R¹ = CO₂Et) rearranged smoothly to give relatively stable enol acetate products **88**, as compared to those with alkyl substituents, which exhibited poor reactivity. Aryl substituents at the alkene terminus gave better results than alkyl substituents. Electron-withdrawing substituents at the propargylic position seem to improve the reactivity (**84**→**85**). They observed that this type of rearrangement could also be conducted using mercury(II) catalyst on the same substrate **87**.

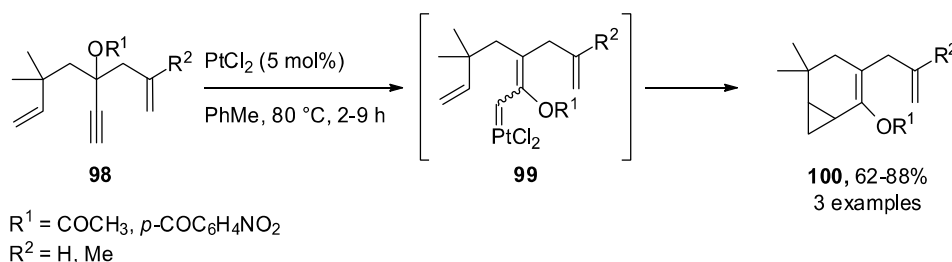


Scheme 18 | Mechanism for the formation of enol acetate **96** postulated by Frontier and coll.⁶⁰

Taking into account Toste's group developments on the mechanism of the Rautenstrauch rearrangement, Frontier proposed a more detailed mechanism focusing on the formation of enol acetate **96** (Scheme 18). 4π -Conrotatory electrocyclicization of polarized pentadienyl cation **91** was proposed to give stabilized allylic cation **92**, which upon elimination of the palladium moiety would afford the desired product **96** and the regenerated palladium (II) catalyst. If palladium carbene **94** is the reactive intermediate, then a few different pathways to enol acetate **96** exist. Oxidative cyclization of **94** to give palladium(IV) intermediate **95** followed by reductive elimination would lead to desired species, as originally proposed by Rautenstrauch. Another feasible pathway involves intramolecular cyclopropanation of carbene **94** to give fused [2.1.0]-bicyclic intermediate **97**, which upon ring opening would yield enol acetate **96**. Since both the carbene-based route to enol acetate **96** involve high-energy intermediate **95** and **97**, the 4π -electrocyclic mechanism is widely accepted.⁵⁹

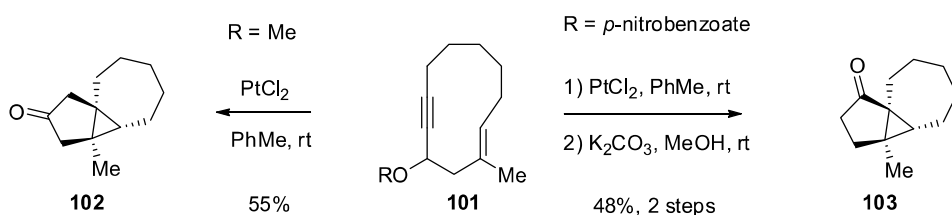
1.5.3 Rautenstrauch related reactions initiated by 1,2-acyloxy migration

In 2002, Fensterbank and co-workers reported the tandem rearrangement-cyclopropanation of dienynes **98** to give fused bicyclic cyclopropanes **100** catalyzed by platinum chloride (Scheme 19).⁶¹ The reaction mechanism proposed involves a metal carbene intermediate **99** generated through 1,2-acyloxy migration, similar to the reaction pathway proposed by Rautenstrauch for palladium(II).



Scheme 19 | PtCl_2 -catalyzed cyclization of dienynes **98**.⁶¹

Two years later, Fensterbank, Malacria and collaborators published a new application of their PtCl_2 -catalyzed transformation.⁶² They showed that tricyclic derivatives such as compound **102** (Scheme 20) could be obtained in an efficient *regio*- and *stereo*-controlled manner via a PtCl_2 -catalyzed transannular cycloisomerization of 1,5-enynes. Ketones **102** or **103** were efficiently prepared from the same cycloundec-5-en-1-yne precursor **101**, depending on the substituent at the propargylic position (either benzoate or methoxyl).

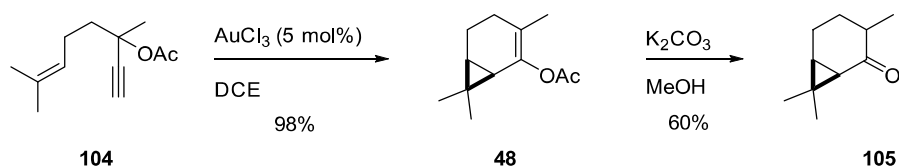


Scheme 20 | Synthesis of ketones **102** and **103** from the transannular cycloisomerization of macrocyclic 1,5-enynes **101**.⁶²

⁶¹ Mainetti, E.; Mouriès, V.; Fensterbank, L.; Malacria, M.; Marco-Contelles, J. *Angewandte Chemie International Edition* **2002**, *41* (12), 2132-2135.

⁶² Blaszykowski, C.; Harrak, Y.; Gonçalves, M.-H.; Cloarec, J.-M.; Dhimane, A.-L.; Fensterbank, L.; Malacria, M. *Organic Letters* **2004**, *6* (21), 3771-3774.

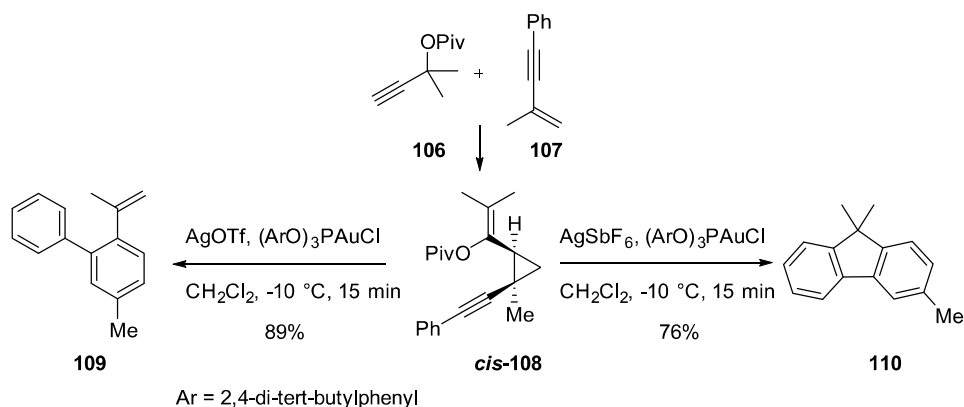
In 2006, Fürstner *et al.* showed that this type of rearrangement could also be performed with a gold(III) catalyst (Scheme 21).⁶³



Scheme 21 | Gold(III) catalyzed synthesis of ketone **105**.⁶³

All the reactions outlined above highlight the remarkable catalytic reactivity of late transition metal cations such as Pt(II) or Au(III) for fully atom economical and complexity-inducing cycloisomerization reactions.

Gold(I)-catalysts could also be utilized in the annulation of enynes and alkynes as reported by Toste group in 2008.⁶⁴ Indeed reaction of *cis*-**108** with an Au(I)-complex provides fluorenes and styrenes derivatives (Scheme 22). The outcome of this novel cycloisomerization reaction may be controlled simply through the choice of the catalyst's counterion (TfO⁻ vs. SbF₆⁻).



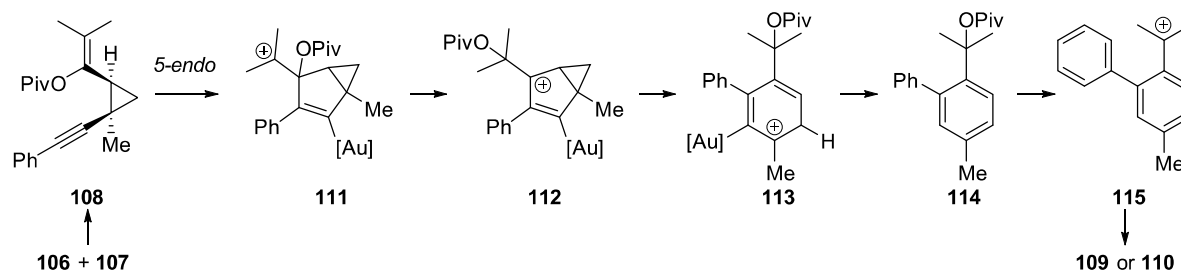
Scheme 22 | Gold(I)-catalyzed synthesis of fluorenes and styrenes derivatives.⁶⁴

Cyclopropanation of enyne **107** with propargyl ester **106** leads to the formation of product **108**. The latter could undergo 5-*endo*-dig cyclization thanks to the coordination of the cationic gold catalyst to the alkyne (Scheme 23). This cyclization generates the tertiary

⁶³ Fürstner, A.; Hannen, P. *Chemistry – A European Journal* **2006**, *12* (11), 3006-3019.

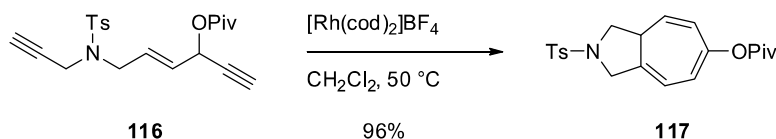
⁶⁴ Gorin, D. J.; Watson, I. D. G.; Toste, F. D. *Journal of the American Chemical Society* **2008**, *130* (12), 3736-3737.

carbocation **111**. Subsequent migration of the pivaloyloxy group gives allylic cation **112** that undergoes cyclopropyl ring opening to afford hexadienyl cation **113**. This final intermediate **115** is likely to be converted to products **109** or **110** by respectively E_1 and S_N1 mechanisms.



Scheme 23 | Proposed mechanism for the formation of product **109** and **110**.⁶⁴

The last example shown here is the interception of a Rautenstrauch intermediate by alkynes. Thus, Tong and coworkers reported a [5+2]-cycloaddition via a rhodium-catalyzed cycloisomerization of 3-acyloxy-4-ene-1,9-diyne.⁶⁵ This novel intramolecular [5+2]-cycloaddition with a 1,2-acyloxy migration gives access to highly functionalized seven-membered rings compounds such as **117** (Scheme 24). An interesting future of this bicyclic product is the possibility of further functionalization of three well-differentiated double bonds.



Scheme 24 | Rhodium-catalyzed cycloisomerization of 3-acyloxy-4-ene-1,9-diyne **116**.⁶⁵

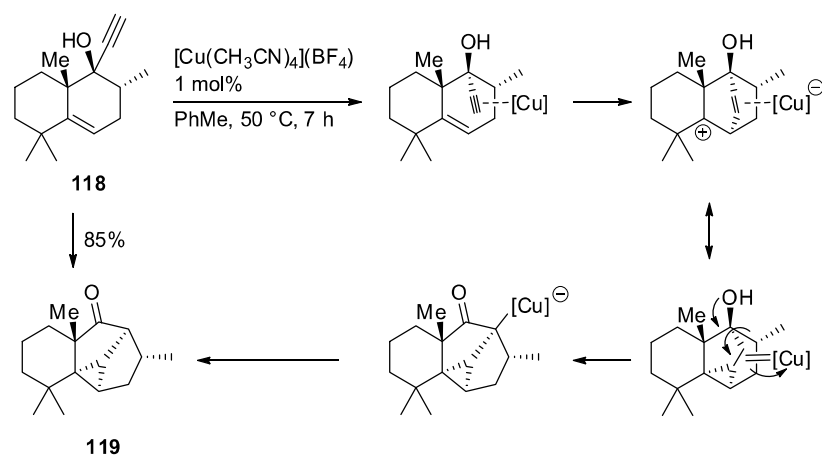
1.5.4 Other vinyl propargyl alcohol rearrangement

In 2006, Fehr's group showed that cycloisomerization of 5-en-1-yn-3-ols could also be achieved with a copper-catalyst (Scheme 25).⁶⁶ This 1,2-alkyl shift of tertiary 5-en-1-yn-3-ol **118** afford stereoselectively tetracyclic compound **119** of high molecular complexity. The authors postulated a mechanism in which the cyclopropanation precedes the skeletal

⁶⁵ Shu, X.-z.; Huang, S.; Shu, D.; Guzei, I. A.; Tang, W. *Angewandte Chemie International Edition* **2011**, *50* (35), 8153-8156.

⁶⁶ Fehr, C.; Farris, I.; Sommer, H. *Organic Letters* **2006**, *8* (9), 1839-1841.

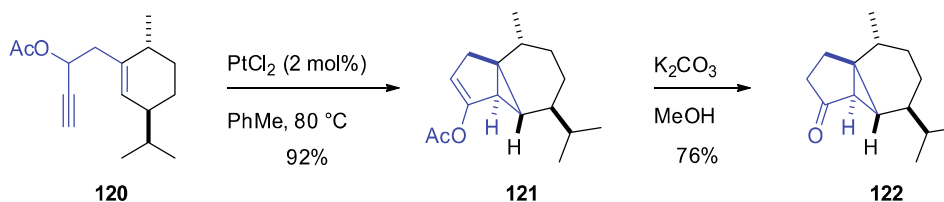
rearrangement with a perfect stereocontrol with respect to the orientation of the acetylene unit.



Scheme 25 | Copper-catalyzed cycloisomerization of 5-en-1-yn-3-ol **118**.⁶⁷

1.5.5 Rearrangement of propargyl acetate in the synthesis a natural product

In 2006, Fürstner *et al.* used this platinum-catalyzed rearrangement of propargyl acetates in the total synthesis of terpenes natural products (Scheme 26).⁶⁸



Scheme 26 | Synthesis of the cubeban skeleton (**122**).⁶⁸

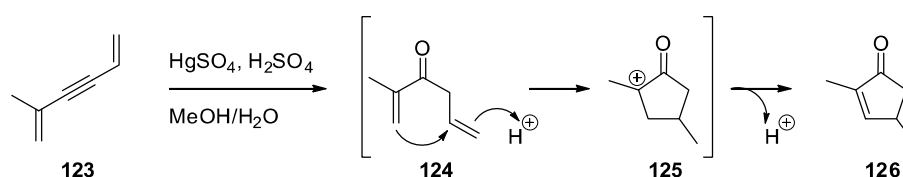
⁶⁷ Fehr, C.; Vuagnoux, M.; Sommer, H. *Chemistry – A European Journal* **2011**, *17* (14), 3832-3836.

⁶⁸ Fürstner, A.; Hannen, P. *Chemistry – A European Journal* **2006**, *12* (11), 3006-3019.

1.6 Overview of the Nazarov reaction

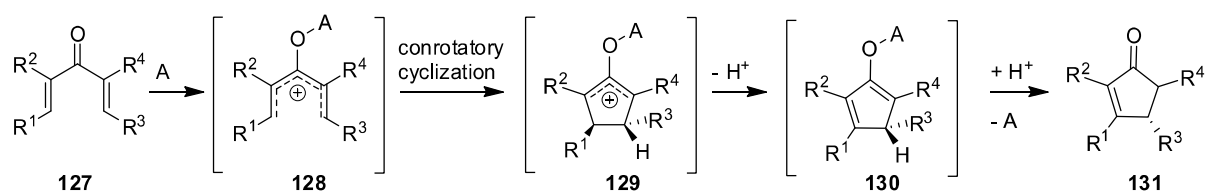
1.6.1 Introduction on the Nazarov reaction

The Nazarov reaction is an established method for the formation of cyclopentenones, based on the stereospecific construction of a new carbon-carbon bond by simple orbital reorganization. It was first reported by Ivan N. Nazarov in 1941 (Scheme 27).⁶⁹ While attempting to hydrate dienyne **123**, he observed the spontaneous cyclization of vinyl ketone intermediate **124** into 2-cyclopentenone **126** under acidic conditions.



Scheme 27 | Original Nazarov's observation.⁶⁹

Since then, this transformation has received tremendous attention due to its ability to form synthetically versatile cyclopentenones via a 4π -electrocyclization of a 1,4-pentadienyl cation, generated from cross-conjugated divinyl ketones (Scheme 28).⁷⁰ With suitable substitutions on dienones, the orbital reorganization creates new stereocenters in the oxyallyl cation **129**, which are retained in the pentacyclic product **131**.



A = Lewis acid or Brønsted acid

Scheme 28 | The Nazarov reaction mechanism.⁷⁰

The mechanism of this cyclization is depicted in Scheme 28.⁷¹ Coordination of a Brønsted or a Lewis acid to the ketone induces the electrocyclization of the pentadienyl cation **128**. A

⁶⁹ (i) Nazarov IN, Zaretskaya II. *Izv. Akad. Nauk SSSR, Ser. Khim* **1941**, 211–224. (ii) Nazarov IN, Zaretskaya II. *Zh. Obshch. Khim.* **1957**, 27, 693–713. (iii) Nazarov IN, Zaretskaya II, Sorkina TI. *Zh. Obshch. Khim.* **1960**, 30, 746–754.

⁷⁰ (i) Santelli-Rouvier, C.; Santelli, M. *Synthesis* **1983**, 1983 (06), 429–442. (ii) Habermas, K. L.; Denmark, S. E.; Jones, T. K., *Org. React. (N.Y.)* **1994**, 45, 1.

⁷¹ Denmark, S. E.; Jones, T. K. *Journal of the American Chemical Society* **1982**, 104 (9), 2642–2645.

conrotatory 4π -electron ring closure proceeds to form an oxyallyl cation intermediate **129**, having substituents R^1 and R^3 in an *anti* relationship. This intermediate can undergo diverse reaction pathways such as carbocationic rearrangements or interception from **129** with external nucleophiles. Commonly, E_1 elimination of a proton occurs to generate enolate **130** leading to 2-cyclopentenone **131** upon reprotonation

Although this reaction has been extensively developed and expanded, in this chapter, only selected examples will be discussed separated in three classes: the catalytic Nazarov reaction, the interrupted Nazarov reaction and the heteroatomic Nazarov reaction.

1.6.2 Catalytic Nazarov reaction

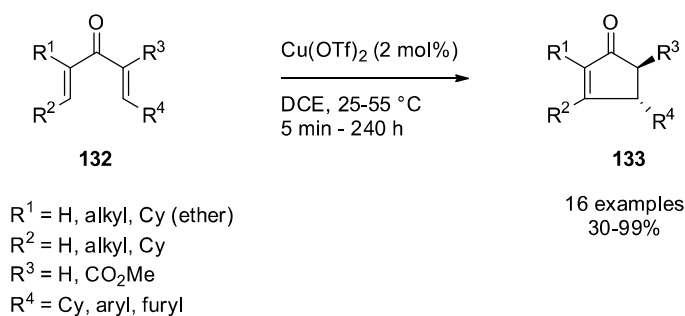
Until recently, optimal Nazarov cyclization conditions required the use of stoichiometric amount of Lewis acid such as BF_3 , $SnCl_4$, $TiCl_4$ or $AlCl_3$ to promote the reaction. This suggests that the Lewis acid-complexed enolate **130** (Scheme 28) is too stable to undergo protonation required for efficient release of the Lewis acid, preventing catalytic turnover. To overcome this issue, highly reactive divinyl ketones were established in combination with mild Lewis acids to catalyzed electrocyclizations. Based on these improvements, the focus was made on the development of catalytic asymmetric Nazarov cyclizations. However, so far, an efficient and general enantioselective cyclization has not been reported, but promising advances have been made toward this goal.⁷²

The catalytic Nazarov cyclization was mostly studied with polarized substrates by the groups of Frontier, Trauner, Tius and Belfield.

In 2003, Frontier and collaborators studied the effect of vinylic substituents on the reactivity of the polarized Nazarov reaction. They screened various substituents in α and β positions of the electrophile as well as in the α -position of the nucleophile (Scheme 29).⁷³

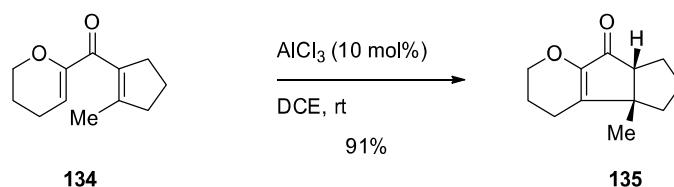
⁷² Frontier, A. J.; Collison, C. *Tetrahedron* **2005**, 61 (32), 7577-7606.

⁷³ He, W.; Sun, X.; Frontier, A. J. *Journal of the American Chemical Society* **2003**, 125 (47), 14278-14279.

**Scheme 29** | Effect of substituents in the polarized Nazarov reaction of divinyl ketone **132**.⁷³

With R¹ as an ether and R³ an ester, electron-rich aromatic substituents (R⁴) increased reaction rates, especially when substituted by an electron-donating group that contributes to the resonance system of the enone. When replacing R¹ and R² by a cyclic, acyclic or aromatic group, vinyl nucleophiles cyclized smoothly. In this case, reactions were slower compared to when R¹, R² is a dihydropyran. Finally, substrates with carbomethoxyl substitution at R³ cyclized more efficiently.

Trauner's group described the same year, an expeditious and high-yielding Nazarov cyclization of 2-alkoxy-1,4-pentadien-3-ones such as **134** (Scheme 30).⁷⁴ They were able to synthesize highly functionalized heterobicyclic and -tricyclic compounds such as **135** using aluminum chloride as a catalyst.

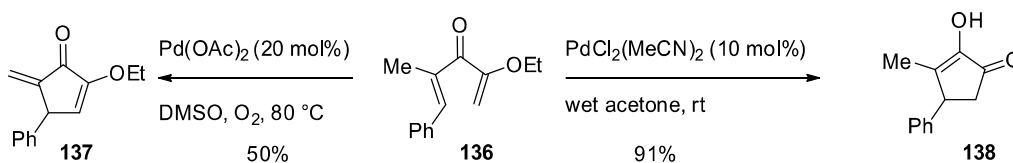
**Scheme 30** | AlCl₃-catalyzed synthesis of heterotricycle **135**.⁷⁴

The same year, Tius and co-workers described a catalyzed Nazarov reaction using palladium(II) catalyst (Scheme 31).⁷⁵ α -Alkoxy dienones **136** were converted to **137** or **138** depending on the counter anion of the metal catalyst. While PdCl₂ leads to 2-hydroxycyclopentenones such as **138**, Pd(OAc)₂ gives cross-conjugated cyclopentenones **137**

⁷⁴ Liang, G.; Gradl, S. N.; Trauner, D. *Organic Letters* **2003**, 5 (26), 4931-4934.

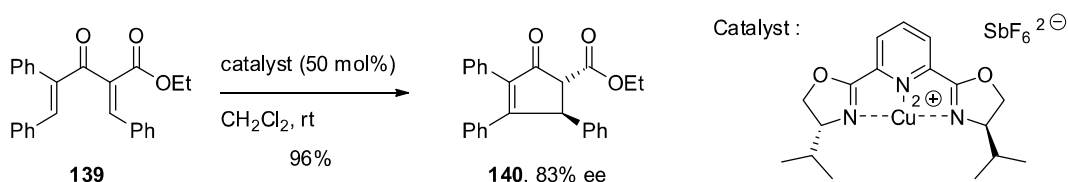
⁷⁵ Bee, C.; Leclerc, E.; Tius, M. A. *Organic Letters* **2003**, 5 (26), 4927-4930.

via an oxidative process. The reaction takes place under mild conditions and, in the case of the PdCl₂-catalyzed process, with high efficiency (91% yield).



Scheme 31 | Palladium(II)-catalyzed cyclization of ketone **136**.⁷⁵

Finally, Belfield's group worked on a catalytic asymmetric Nazarov reaction promoted by chiral Lewis acid complexes (Scheme 32).⁷⁶ Divinyl ketones bearing α -ester such as substrate **139** or α -amide groups underwent Nazarov cyclization with moderate to good enantiomeric excesses. This is an example of external asymmetric induction.



Scheme 32 | Nazarov cyclization of ketone **139** using a copper–bisoxazoline Lewis acid complex.⁷⁶

1.6.3 Interrupted Nazarov reaction

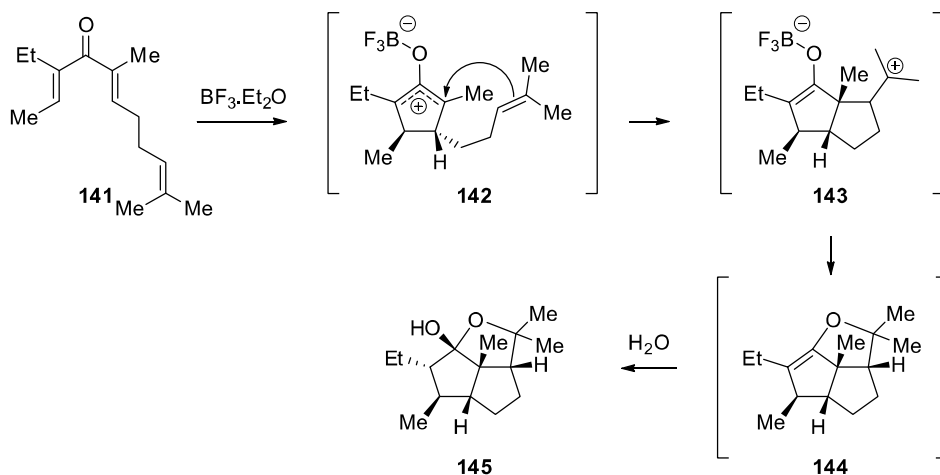
The key intermediate of the Nazarov reaction is the oxyallyl cation **129** (Scheme 28). It is stable enough to be intercepted with nucleophilic species. West has termed this the 'interrupted' Nazarov cyclization pathway, and has reported a number of different methods for trapping of the cationic intermediate.⁷⁷ In this section, trapping with alkenes and arenes, 1,3-dienes resulting in C-C bond forming and reduction of the oxyallyl cation with hydride are presented. Usually, this trapping changes the course of the reaction away from the formation of 2-cyclopentenones towards polycyclic compounds.

⁷⁶ Aggarwal, V. K.; Belfield, A. J. *Organic Letters* **2003**, 5 (26), 5075-5078.

⁷⁷ Grant, T. N.; Rieder, C. J.; West, F. G. *Chemical Communications* **2009**, (38), 5676-5688.

1.6.3.1 Intramolecular cyclization

The first example of interrupted Nazarov cyclization was reported by West and co-workers in 1998. It involves the trapping of oxyallyl cations **142** with a tethered alkene (Scheme 33).⁷⁸ In this example, a single hemiketal product **145** is obtained via the formation of two new carbon-carbon bonds and 6 stereocenters upon treatment of achiral trienone **141** to $\text{BF}_3 \cdot \text{Et}_2\text{O}$.



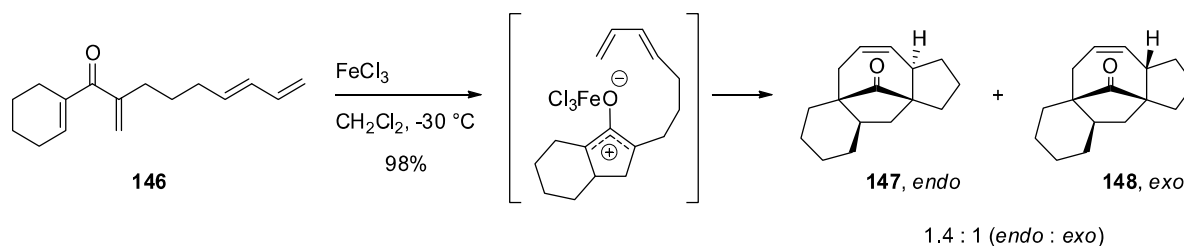
Scheme 33 | Interrupted Nazarov cyclization of ketone **141** with intramolecular alkene trapping.⁷⁸

Activation of the carbonyl by $\text{BF}_3 \cdot \text{Et}_2\text{O}$ promotes the 4π -conrotatory electrocyclicization that generates the cyclic oxyallyl cationic intermediate **142**. The latter is captured in a 5-*exo* intramolecular cyclization by the alkene, generating intermediate **143** as a boron enolate and a tertiary carbocation. Finally, the oxygen of the enolate attacks the carbocation to give **144**, which upon hydrolysis results in product **145** with exclusive protonation from the convex face. This reaction is possible only if the starting material has two carbon tethers between the alkene and the dienone and if both α positions of ketone are substituted.

Alternative trapping modes have also been described by the same group. They reported a tandem reaction involving an initial Nazarov type ring closure of 1,4-diene-3-one followed by intramolecular concerted [4+3]-cycloaddition. The oxyallyl intermediate generated by the electrocyclicization can be used as a dienophile in the [4+3]-cycloaddition

⁷⁸ Bender, J. A.; Blize, A. E.; Browder, C. C.; Giese, S.; West, F. G. *The Journal of Organic Chemistry* **1998**, *63* (8), 2430-2431.

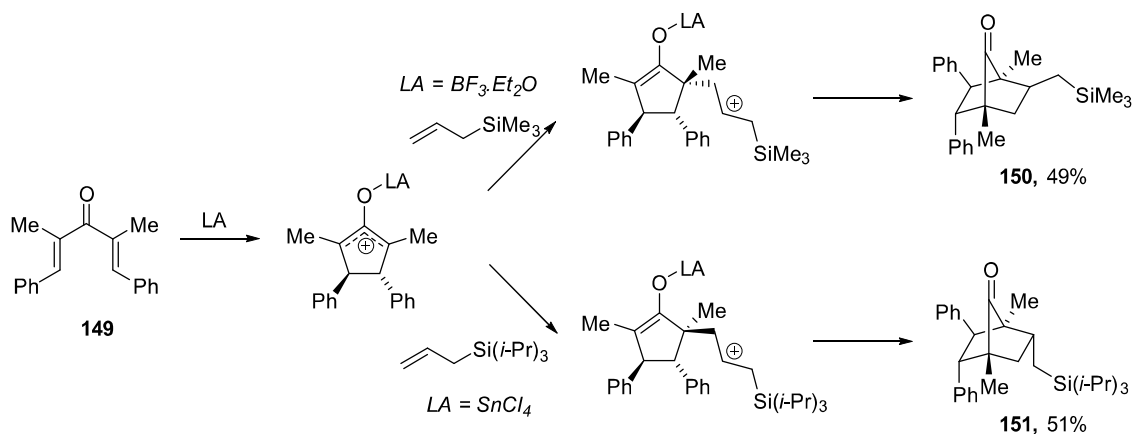
reaction.⁷⁹ Thus, tetraenone **146** was subjected to FeCl₃ at -30 °C providing tetracyclic cycloadduct in almost quantitative yield as a mixture of diastereomers **147** and **148** (Scheme 34). Both products result from the approach of the 1,3-diene to the less hindered face of the intermediate fused bicyclic cation followed by [4+3]-cycloaddition through either *endo* or *exo* transition states. This reaction leads to the formation of three new C-C bonds and 4 new stereocenters.



Scheme 34 | Intramolecular [4+3]-cycloaddition using FeCl₃.⁷⁹

1.6.3.2 Intermolecular cyclization

This type of interrupted Nazarov was also reported with an intermolecular olefin trapping. For example, West *et al.* examined the trapping of divinyl ketone **149** with allylsilanes (Scheme 35).⁸⁰ It can be noted here that SnCl₄ and BF₃·Et₂O provide complementary diastereoselectivity.

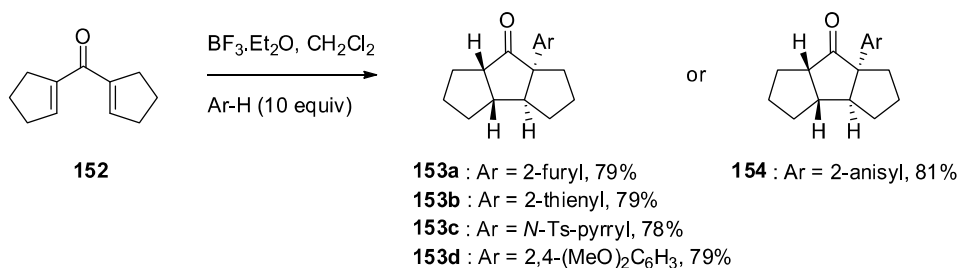


Scheme 35 | Interrupted Nazarov cyclization of ketone **149** with allyltriisopropylsilane.⁸⁰

⁷⁹ Wang, Y.; Arif, A. M.; West, F. G. *Journal of the American Chemical Society* **1999**, 121 (4), 876-877.

⁸⁰ Giese, S.; Kastrup, L.; Stiens, D.; West, F. G. *Angewandte Chemie International Edition* **2000**, 39 (11), 1970-1973.

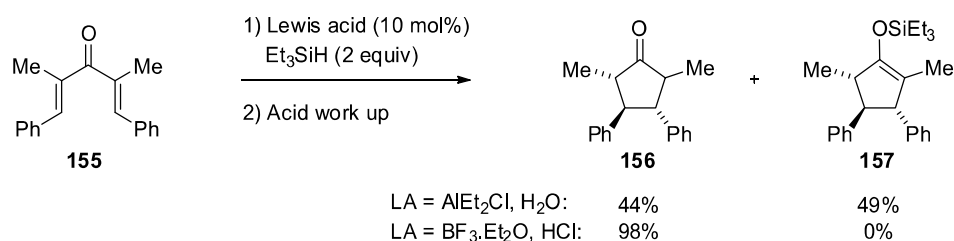
In 2008, a similar reaction was observed when dienones with constrained C=C bonds within rings were treated with Lewis acid in the presence of an electron-rich aromatic compounds (Scheme 36).⁸¹ This reaction furnished unique arylated tricyclic products **153** or **154** derived from electrophilic aromatic substitution of ketone **152**.



Scheme 36 | Interrupted Nazarov cyclization of ketone **153** with arenes.⁸¹

1.6.3.3 Reductive cyclization

Another option consists in intercepting the cationic intermediate with a hydride in a reductive Nazarov cyclization. Thereby, Giese and West were able to reduce the oxyallyl cation with trialkylsilane to give ketone product **156** (Scheme 37).⁸² This is an example of interrupted Nazarov cyclization with a trapping step involving hydride rather than the π -system of an alkene or arene. Upon acidic workup, ketone **156** could be isolated in good yield from this process, even with just 10 mol% of Lewis acid. The regioselective reduction occurs at the less-substituted position of the oxyallyl cation.



Scheme 37 | Reductive Nazarov cyclization of ketone **155**.⁸²

The interrupted Nazarov reaction is not limited to C-C bond formation. Indeed, the trapping can be broadened to heteroatomic nucleophiles such as oxygen, nitrogen and

⁸¹ Rieder, C. J.; Fradette, R. J.; West, F. G. *Chemical Communications* **2008**, (13), 1572-1574.

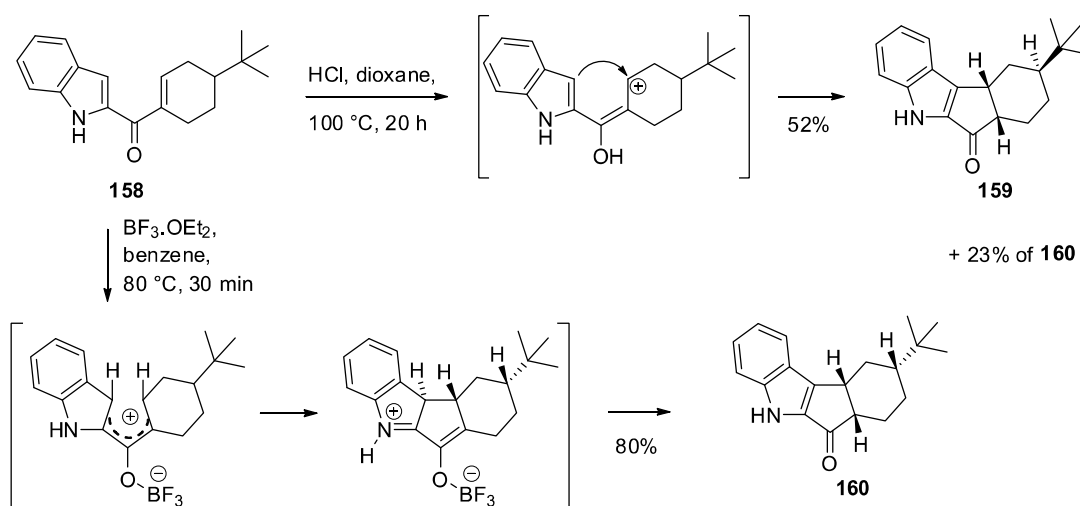
⁸² (i) Giese, S.; West, F. G. *Tetrahedron Letters* **1998**, 39 (46), 8393-8396. (ii) Giese, S.; West, F. G. *Tetrahedron* **2000**, 56 (52), 10221-10228.

halide nucleophiles. Also, trapping with electrophiles have also been reported with electrophilic halogens sources or Michael acceptors.

1.6.4 Heteroatomic Nazarov reaction

In the past ten years, the Nazarov reaction has been extended to heterocyclic systems with *N*-, *O*- and *S*-heterocyclic divinyl ketones to form cyclopentan-fused heterocyclic compounds. This increased interest arises from the presence of such heterocyclic core in several natural and biologically active compounds.

Based on Bergman's work⁸³, Ishikura and collaborators reported the synthesis of cyclopent[*b*]indolones **159** and **160** *via* intramolecular ring closure of α,β -unsaturated acylindoles such as **158** (Scheme 38).⁸⁴



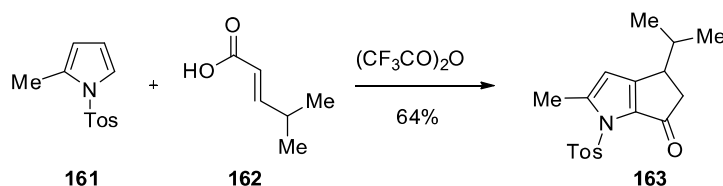
Scheme 38 | Cyclization of indole substrates **158** via Nazarov reaction.⁸³

The stereochemistry of the resulting product was controlled by the nature of the acid. Indeed, using HCl provided a mixture of **159** and **160** whereas $\text{BF}_3 \cdot \text{OEt}_2$ led only to **160** in 80% yield. The protic acid-promoted ring closure of **158** could be obtained by an intramolecular Michael addition. However, this cannot explain the exclusive formation of **160** utilizing $\text{BF}_3 \cdot \text{OEt}_2$. Instead, an electrocyclic Nazarov reaction through dienyl cation intermediate could account for the exclusive formation of **160**.

⁸³ Bergman, J.; Venemalm, L.; Gogoll, A. *Tetrahedron* **1990**, *46* (17), 6067-6084.

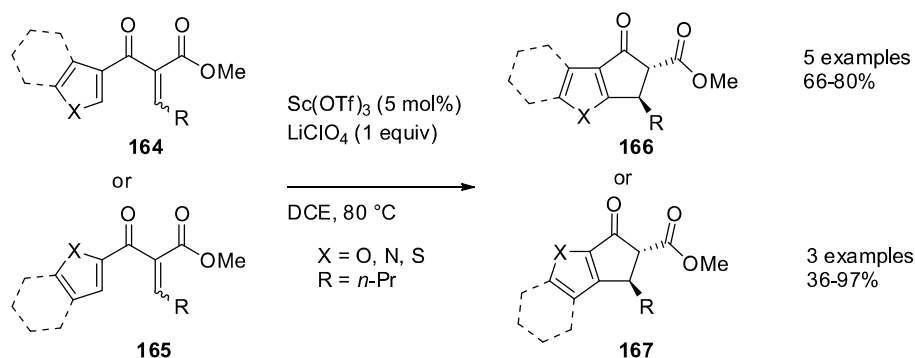
⁸⁴ Ishikura, M.; Imaizumi, K.; Katagiri, N. *Heterocycles* **2000**, *53* (10), 2201-2220.

In 2006, Whatton and colleagues published the first examples of Nazarov cyclizations leading to annulated pyrroles.⁸⁵ Reactions between α -substituted unsaturated carboxylic acids such as **162** and *N*-tosylpyrroles like compound **161** in the presence of trifluoroacetic anhydride result in α -acylation of the pyrrole, followed by Nazarov cyclization to give cyclopenta[*b*]pyrroles **163** with moderate to good yields (Scheme 39). The presence of an α -substituent in the α,β -unsaturated carboxylic acid appears to be essential.



Scheme 39 | Synthesis of annulated pyrrole **163** via a Nazarov reaction.⁸⁵

The same year, Frontier *et al.* established a general catalytic method for efficient Nazarov cyclization of systems containing heteroaromatic components (Scheme 40).⁸⁶ Scandium triflate was shown to be more efficient than copper triflate, indinium triflate, iridium(III) and iron chloride. They showed that the addition of lithium perchlorate was necessary to catalyze this cyclization. This method was utilized to synthesize a range of cyclopentanone-fused heteroaromatic systems such as **166** and **167** in moderate to good yields.



Scheme 40 | Heteroaromatic Nazarov cyclization.⁸⁶

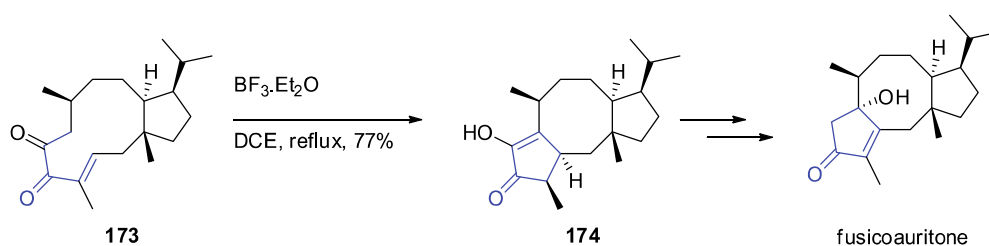
⁸⁵ Song, C.; Knight, D. W.; Whatton, M. A. *Organic Letters* **2006**, *8* (1), 163-166.

⁸⁶ Malona, J. A.; Colbourne, J. M.; Frontier, A. J. *Organic Letters* **2006**, *8* (24), 5661-5664.

1.6.5 Natural products synthesized *via* Nazarov electrocyclization

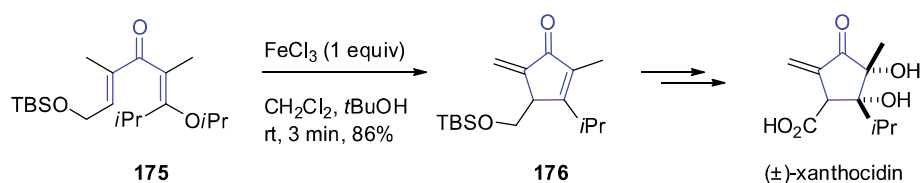
The Nazarov reaction and has been widely used in the synthesis of several natural product. Selected examples are described thereafter.

In 2007, Williams and coll. reported the total synthesis of fusicoauritone by a Nazarov reaction of endiketone **173**. Treatment of this macrobicyclic with catalytic amount of BF₃ etherate gave the desired tricyclic product **174** with an all-*syn* stereochemistry (Scheme 43).⁸⁹



Scheme 43 | Synthesis of fusicoauritone via Nazarov reaction.⁸⁹

In 2010, Shindo's group described the total synthesis of the antibiotic, (+/-)-xanthocidin (Scheme 44).⁹⁰ The key step of this approach was the FeCl₃-promoted fast Nazarov reaction of the β -alkoxy divinyl ketone **175** in the presence of *t*-BuOH. This reaction gives access to α -*exo*-methylene cyclopentenone **176**, which is the core skeleton of this natural product.



Scheme 44 | Synthesis of (±)-xanthocidin via Nazarov reaction.⁹⁰

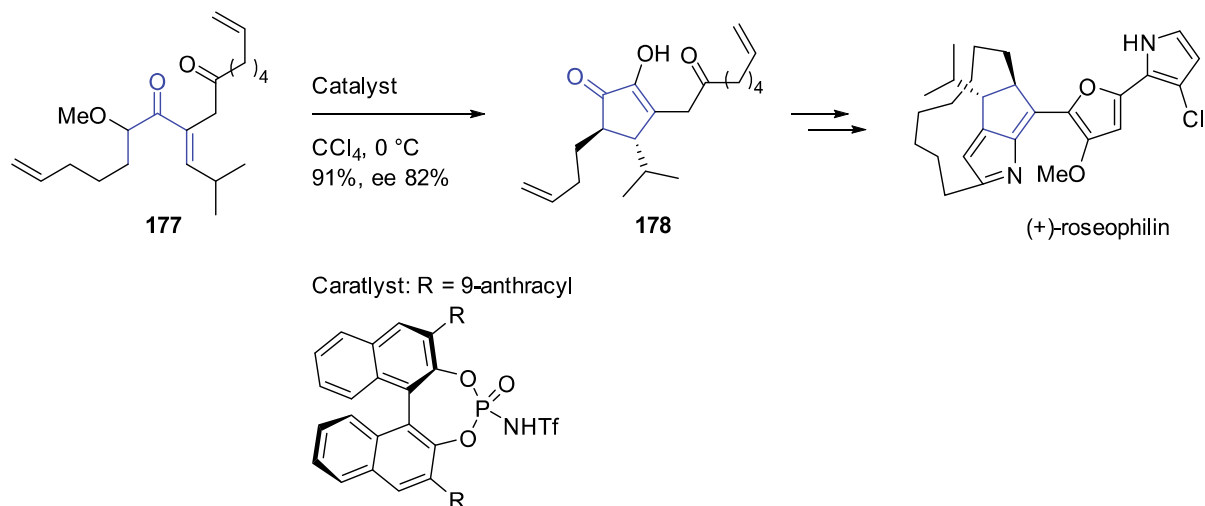
More recently, Flynn and coworkers reported the enantioselective formal synthesis of (+)-roseophilin, an anticancer natural product (Scheme 45).⁹¹ The key point of this synthesis is

⁸⁹ Williams, D. R.; Robinson, L. A.; Nevill, C. R.; Reddy, J. P. *Angewandte Chemie International Edition* **2007**, *46* (6), 915-918.

⁹⁰ Yaji, K.; Shindo, M. *Tetrahedron* **2010**, *66* (52), 9808-9813.

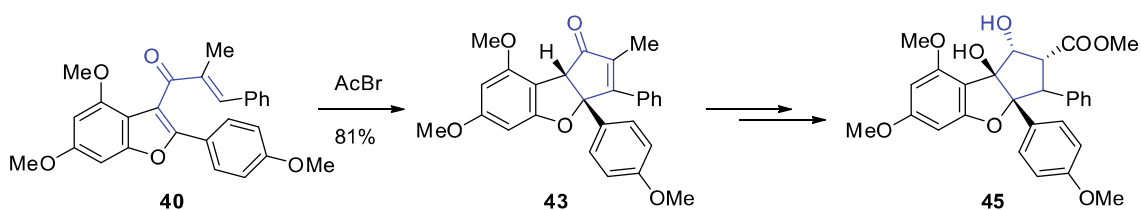
⁹¹ Kerr, D. J.; Flynn, B. L. *Organic Letters* **2012**, *14* (7), 1740-1743.

the combination of reductive coupling and chiral Brønsted acid catalyzed Nazarov cyclization. This two-step approach gives access to highly substituted cyclopentanoids **178** containing several stereocenters.



Scheme 45 | Synthesis of of (+)-roseophilin via Nazarov reaction.⁹¹

As it was described it the previous chapter, the Nazarov electrocyclization was also used in the total synthesis of flavaglines by Frontier⁹² and Magnus⁹³ groups (Scheme 46, see section 1.4.5 for more details).



Scheme 46 | Magnus's synthesis of methyl rocaglate **45** via Nazarov reaction.⁹³ⁱ

⁹² Malona, J. A.; Cariou, K.; Frontier, A. J. *Journal of the American Chemical Society* **2009**, *131* (22), 7560-7561.

⁹³ (i) Magnus, P.; Freund, W. A.; Moorhead, E. J.; Rainey, T. *Journal of the American Chemical Society* **2012**, *134* (14), 6140-6142. (ii) Magnus, P.; Stent, M. A. H. *Organic Letters* **2005**, *7* (18), 3853-3855.

2. OBJECTIVES

2. OBJECTIVES

The principal objective of this thesis was to develop a flexible synthesis of flavaglines to access original and patentable derivatives that cannot be prepared by methods described in the literature.

A second objective was to synthesize a flavagline conjugated via a spacer group to a polar fluorescent dye that cannot easily cross the plasma membrane by mere diffusion, in order to characterize the mechanism of chemoresistance involving prohibitin-1 (Figure 6).

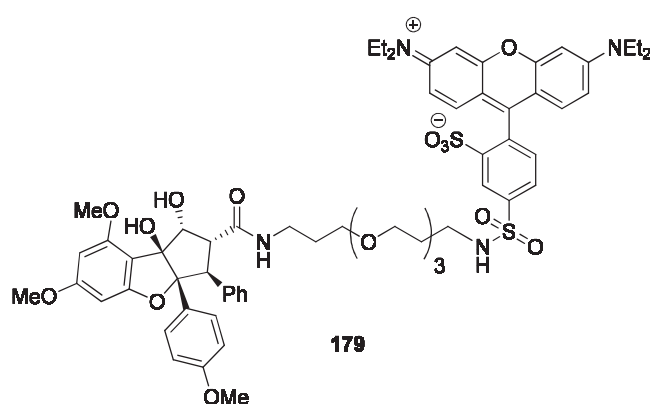


Figure 6 | Fluorescence probe **179**.

A third objective was to synthesize a pyrazole isostere of flavaglines (Figure 7). We hypothesized that this compound harbors the functionalities that are required for the anticancer and cytoprotective activities of flavaglines.

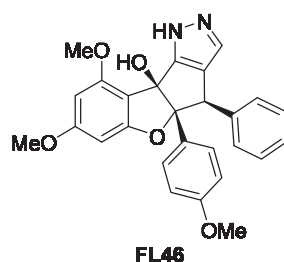


Figure 7 | Pyrazolic isostere of flavaglines.

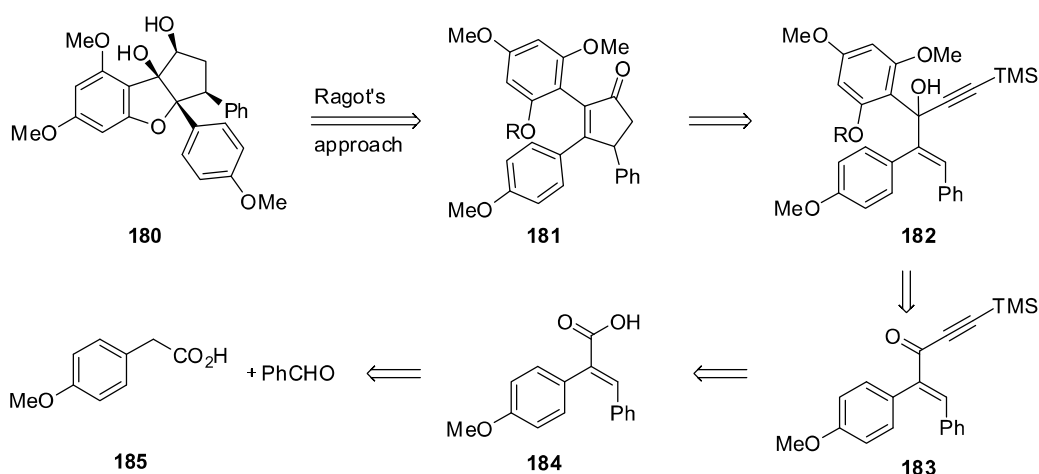
3. RESULTS

3. RESULTS

3.1 Synthesis of flavaglines based on Ragot's approach

3.1.1 Retrosynthetic strategy

To synthesize novel flavaglines, a new synthetic route was proposed based on key intermediate **181** using Ragot's approach⁹⁴ for the final steps as described in section 1.4.4 (Scheme 47). This cyclopentenone could be accessed via a Rautenstrauch rearrangement starting from the acetate of alcohol **182**. Propargyl alcohol **182** would be synthesized via a Sonogashira reaction followed by C-alkylation with lithiated trimethoxybenzene. Acid **184** could be prepared from a Perkin condensation of carboxylic acid **185** and benzaldehyde.

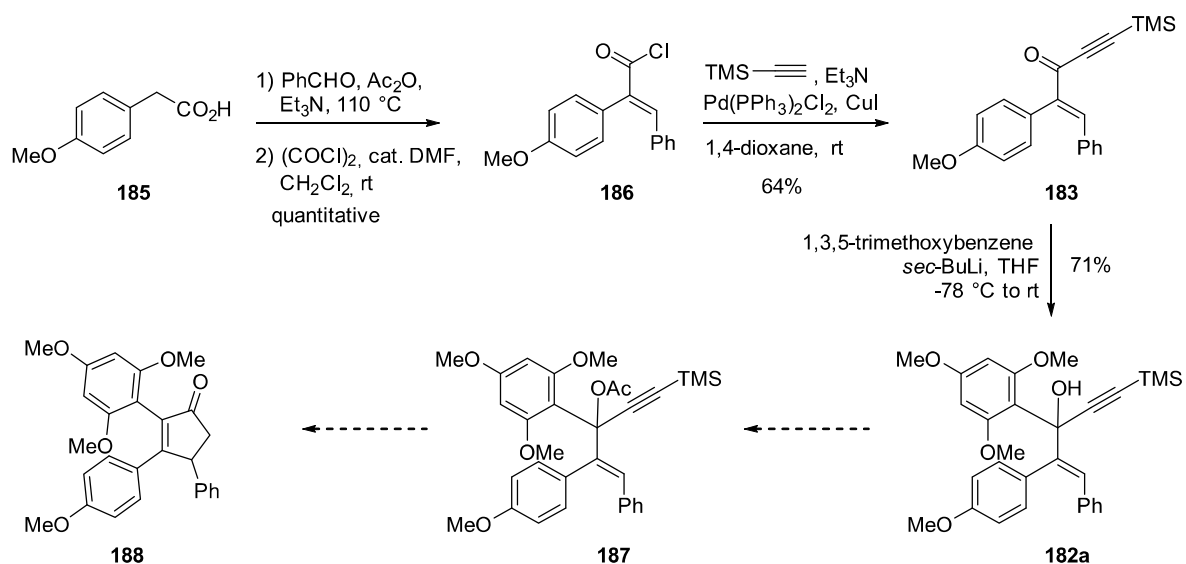


Scheme 47 | Initial retrosynthetic strategy for the synthesis of rocglaol **180**.

3.1.2 Synthesis of cyclopentenone intermediate

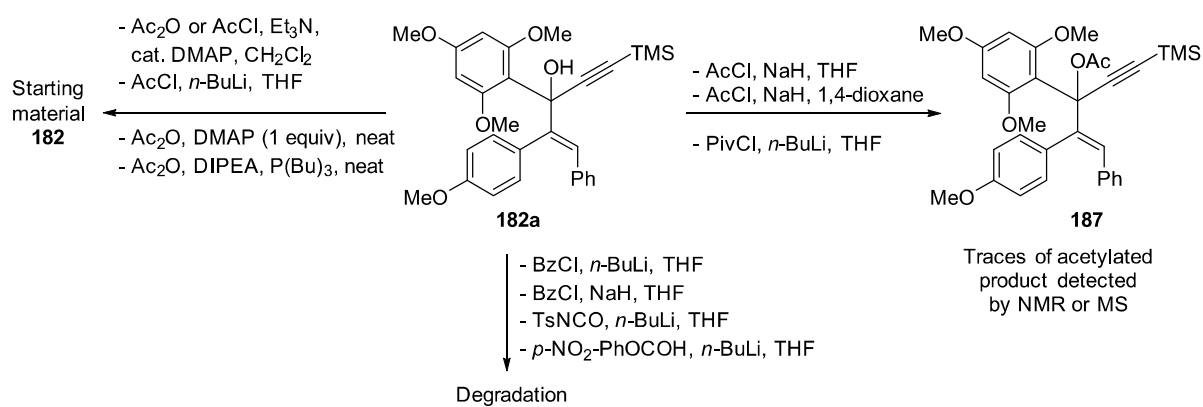
Acid chloride **186** was generated quantitatively from the corresponding carboxylic acid which was obtained stereoselectively by a Perkin reaction. A major advantage of the Perkin reaction is the production of a single adduct that harbors two aryl moieties in a *Z*-fashion. Introduction of trimethylsilylacetylene by a Sonogashira coupling (64%) and alkylation with lithiated trimethoxybenzene afforded propargyl alcohol **182a** in 71% yield.

⁹⁴ Thede, K.; Diedrichs, N.; Ragot, J. P. *Organic Letters* **2004**, *6* (24), 4595-4597.



Scheme 48 | Attempted synthesis of cyclopentenone **188**.

In order to achieve the Rautenstrauch rearrangement, propargyl alcohol **182a** must be acylated. All our attempts on the esterification of compound **182a** are depicted in Table 1 and Scheme 49.



Scheme 49 | Summary of attempts of acylation of **182**.

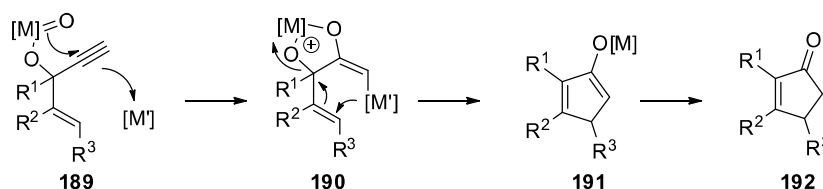
Table 1 | Representative examples of attempts to acylate propargyl alcohol **182**.

Entry	Reagent	Base	Catalyst	Solvent	T(°C)	182 ^a	187 ^a
1	AcCl	<i>n</i> -BuLi	-	THF	rt	100	0
2	AcCl	Et ₃ N	DMAP	DCM	50	100	0
3	AcCl	NaH	-	THF	reflux	85	15
4	AcCl	NaH	-	1,4-dioxane	reflux	0	traces
5	Ac ₂ O	-	DMAP	neat	rt	100	0
6	Ac ₂ O	DIPEA	P(Bu) ₃	neat	rt	100	0
7	PivCl	<i>n</i> -BuLi	-	THF	rt	0	traces
8	BzCl	<i>n</i> -BuLi	-	THF	rt		degradation
9	BzCl	NaH	-	THF	rt		degradation

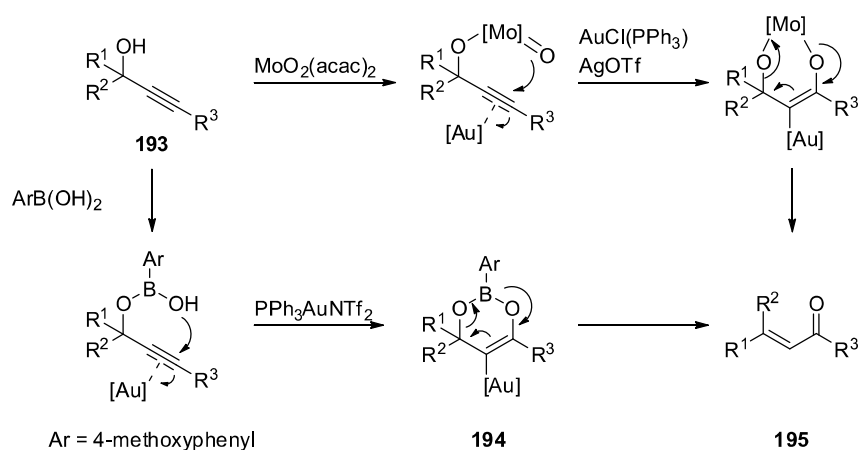
^aYields are based on ¹H NMR.

Using acetic anhydride or acetyl chloride, almost no reaction occurred (entries 1-6, Table 1). Indeed, only the starting material was observed, despite the wide range of bases used to form the alkoxide. Even heating at reflux did not promote the reaction in favor of the acetylated product. Best results were obtained using sodium hydride with acetyl chloride with 15% yield based on ¹H NMR (entry 3). We then changed the reagent of acylation to benzoyl chloride, tosyl isocyanate and *p*-nitrobenzyl formate. In all cases, degradation of the product was observed (entries 7 and 9). In some assays (entries 3 and 4), we could observe traces of acylated product by ¹H NMR or in mass spectrometry. Thereby, all our attempts were unsuccessful due to lack of reactivity or high instability of the expected ester **187**.

We then considered replacing the ester function by a labile inorganic ester in the Rautenstrauch reaction (Scheme 50). As far as we know, this type of approach has never been reported.

**Scheme 50** | Considered mechanism with an inorganic ester.

Two reagents were considered to form the inorganic ester: $\text{MoO}_2(\text{acac})_2$ and 4-MeO- $\text{PhB}(\text{OH})_2$. However, we needed to take into consideration the possibility of a competition with the Meyer-Schuster reaction. Indeed, in 2008, Akai *et al.* showed that the use of molybdenum in combination with a gold(I) catalyst leads to a 1,3-rearrangement of propargyl alcohols **193** in α,β -unsaturated ketones **195** (Scheme 51).⁹⁵ In the same manner, the group of T.D. Sheppard prepared enones **195** starting from propargyl alcohols **193** via the formation of boron enolate **194** catalyzed with gold(I) (Scheme 51).⁹⁶



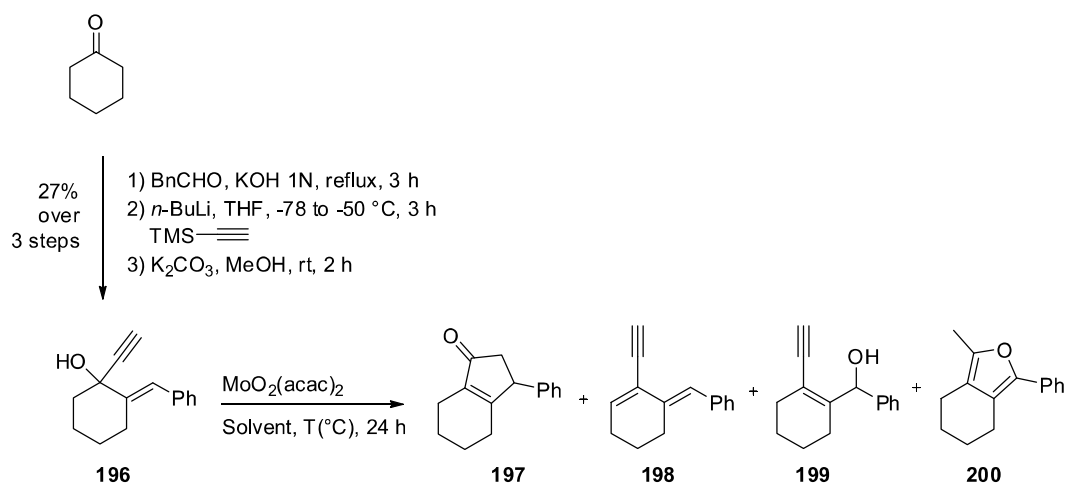
Scheme 51 | Meyer-Schuster's reaction using a combination of Mo-Au catalyst or boronic acid.^{95,96}

We examined this reaction on a model substrate (compound **196**, Scheme 52) which was well studied by Frontier's team in the Rautenstrauch rearrangement.⁹⁷ It was synthesized in 3 steps from cyclohexanone and benzaldehyde. Using molybdenum(VI) oxide, we did not observe any formation of the cyclopentenone **197** despite the various conditions tested (Table 2). When using acetone or nitromethane as a solvent, no reaction was observed (entries 1 and 2). Switching the solvent to dichloromethane at reflux, gave access to product **198** from dehydration of starting alcohol (entry 5). On the other hand, if the reaction is conducted at room temperature in dichloromethane or toluene, allylic rearrangement product **199** was generated (entries 3 and 4).

⁹⁵ Egi, M.; Yamaguchi, Y.; Fujiwara, N.; Akai, S. *Organic Letters* **2008**, 10 (9), 1867-1870.

⁹⁶ Pennell, M. N.; Unthank, M. G.; Turner, P.; Sheppard, T. D. *The Journal of Organic Chemistry* **2011**, 76 (5), 1479-1482.

⁹⁷ Caruana, P. A.; Frontier, A. J. *Tetrahedron* **2007**, 63 (43), 10646-10656.



Scheme 52 | Attempts for the formation of cyclopentenone **197** in the presence of $\text{MoO}_2(\text{acac})_2$.

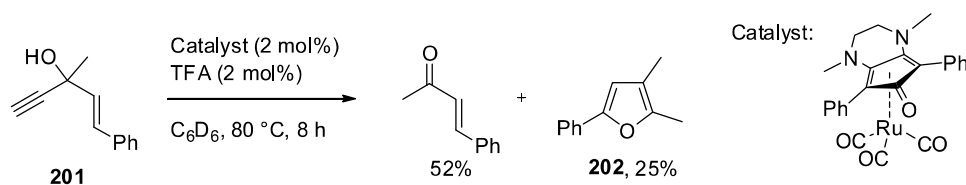
Table 2 | Attempts of cyclization of the model substrate **196**.

Entry	Solvent	T(°C)	196 (%) ^a	197 (%) ^a	198 (%) ^a	199 (%) ^a	200 (%) ^a
1	Acetone	rt	> 90	-	-	-	-
2	CH_3NO_2	rt	> 90	-	-	-	-
3	DCE	rt	-	-	-	> 90	-
4	PhMe	rt	-	-	-	> 90	-
5	DCE	reflux	-	-	> 90	-	-
6 ^b	DCE	rt	-	-	-	-	25

^a yield based on GC-MS ^b HgCl_2 was added as a co-catalyst.

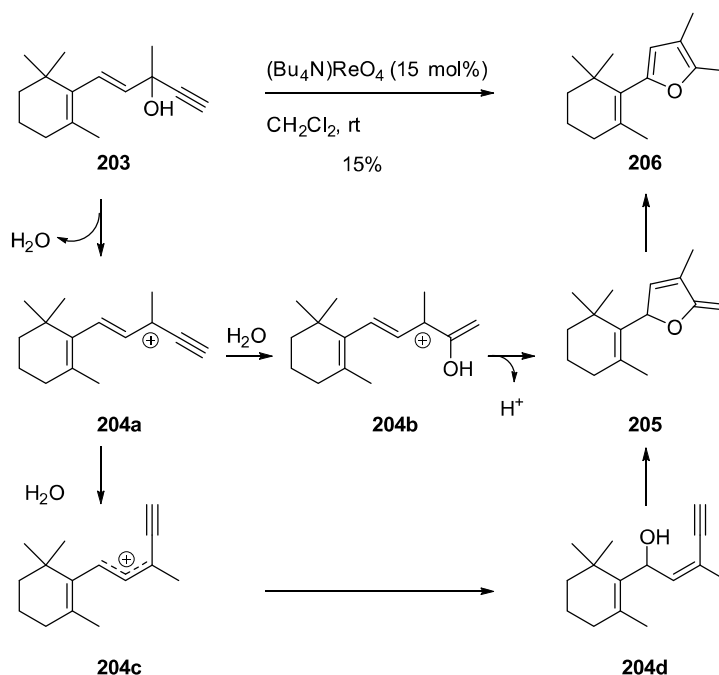
It can also be noted that using mercury chloride in addition to the molybdenum-catalyst, unexpectedly led to the formation of methylfuran **200** (Table 2, entry 6). Similar rearrangements using other catalytic systems have been reported in the literature. Indeed, in 2012, Haak and coworkers observed a ruthenium-catalyzed rearrangement of 1-vinyl propargyl alcohol into furan **202** (Scheme 53).⁹⁸ The starting enynol **201** could undergo oxo-cyclization in the presence of the ruthenium catalyst and trifluoroacetic acid. The authors attributed the formation of furan **202** to a transformation that may involve an allenylidene intermediate.

⁹⁸ (i) Thies, N.; Hrib, C. G.; Haak, E. *Chemistry – A European Journal* **2012**, *18* (20), 6302-6308 (ii) Jonek, A.; Berger, S.; Haak, E. *Chemistry – A European Journal* **2012**, *18* (48), 15504-15511.



Scheme 53 | Formation of furan **202** from 1-vinyl propargyl alcohol **201**.⁹⁸

In a similar manner, Thum's group observed, in a small amount, the formation of such furan using a perrhenate catalyst (Scheme 54).⁹⁹ They proposed that the mechanism could start with a dehydration forming carbocation **204a** which could be re-hydrated into intermediate **204b** and cyclize to give cyclic intermediate **205**. Aromatization could lead to furan product **206**. However, as intermediate **204b** is atypical, we propose an alternative pathway involving conformer **204c**, which could react with water to generate alcohol **204d** en route to intermediate **205**.

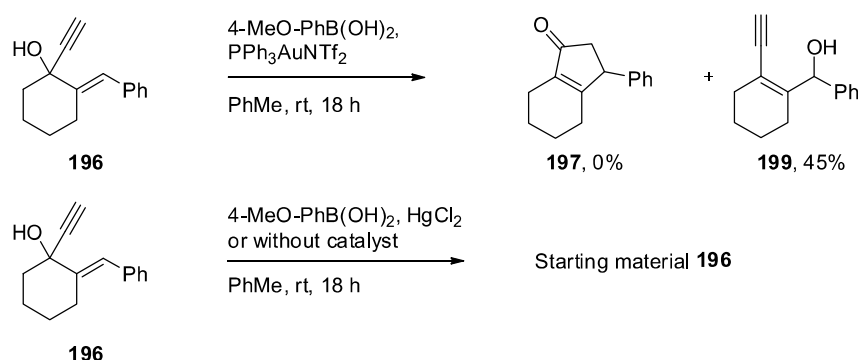


Scheme 54 | Rhenium-catalyzed rearrangements of enynol **203**.⁹⁹

On the same model substrate **196**, we also examined Sheppard's conditions using 4-methoxyboronic acid and gold catalyst PPh_3AuNTf_2 (Scheme 55). In these conditions, we did not observe any formation of the cyclopentenone. We only isolated the product of allylic

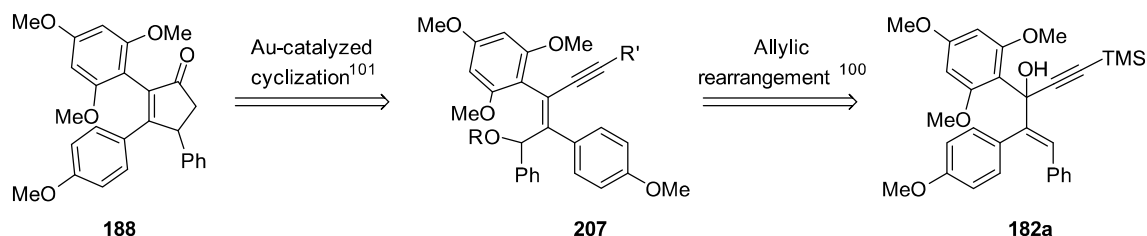
⁹⁹ Arnold, W.; Bonrath, W.; Pernin, R.; Thum, A. *Helvetica Chimica Acta* **1996**, 79 (3), 646-650.

rearrangement **199** with 45% yield. When the catalyst was switched to mercury chloride or deleted, no reaction was observed.



Scheme 55 | Attempts to perform an Rautenstrauch-like reaction catalyzed by a boronic acid and Au(I) or Hg(II) salts.

As all our attempts of acylation of propargyl alcohol **182a** were unsuccessful, we considered a new route to access cyclopentenone starting from the same propargyl alcohol (Scheme 56). This approach combines a molybdenum(VI)-catalyzed etherification of allylic alcohol with a gold(I)-catalyzed intramolecular cyclization process based respectively on Zhu's and Rhee's groups' work.¹⁰⁰⁻¹⁰¹

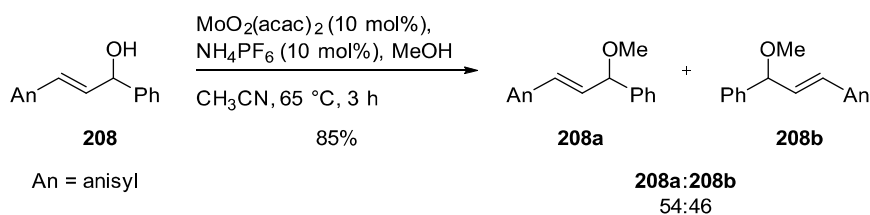


Scheme 56 | New strategy for the preparation of cyclopentenone **188**.

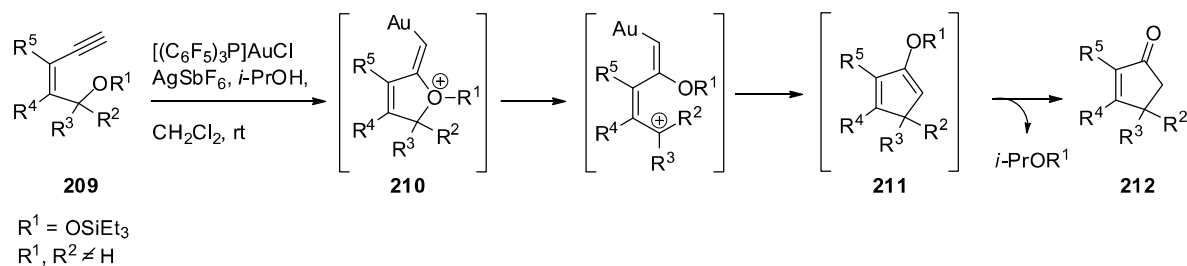
Zhu *et al.* developed a substitution of allylic alcohol **208** with various nucleophiles including alcohols, catalyzed by molybdenum(VI) (Scheme 57).¹⁰⁰

¹⁰⁰ Yang, H.; Fang, L.; Zhang, M.; Zhu, C. *European Journal of Organic Chemistry* **2009**, 2009 (5), 666-672.

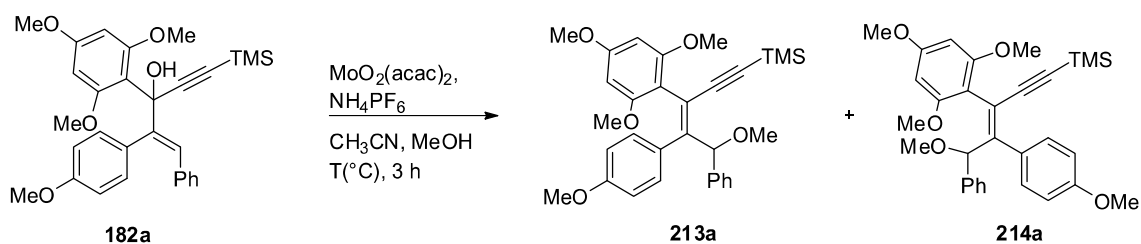
¹⁰¹ An, S. E.; Jeong, J.; Baskar, B.; Lee, J.; Seo, J.; Rhee, Y. H. *Chemistry – A European Journal* **2009**, 15 (44), 11837-11841.


Scheme 57 | Rearrangement and nucleophilic substitution of allylic alcohols **208**.¹⁰⁰

Rhee *et al.* prepared substituted 2-cyclopentenones starting from 5-siloxy-pent-3-en-1-yne **209** using gold(I) catalyst (Scheme 58).¹⁰¹ The authors proposed that, in the presence of highly electrophilic cationic gold(I) complex, oxonium intermediate **210** could arise from the attack of the siloxy group to the alkyne. With the assistance of *i*PrOH, cyclized intermediate **211** could lead to cyclopentenone **212**.


Scheme 58 | Gold(I)-catalyzed cyclopentanone formation developed by Rhee and coll.¹⁰¹

Although this reaction was described exclusively with tertiary silyl ethers (**209**, Scheme 58), we considered that the phenyl and the trimethoxyphenyl groups of substrate **182a** should sufficiently stabilize the carbocationic intermediate to allow the reaction to proceed (Scheme 59). The silyl ether was replaced by a methoxy due to its easier preparation. Indeed, the direct molybdenum (VI)-catalyzed transposition and etherification of allylic alcohol **182a** at 50 °C afforded a 1:1 mixture of ethers **213a** and **214a** in a 26% yield (Table 3, entry 2). Increasing the temperature to 65 °C improved the ratio to 3:1 in favor of the desired ether **213a** in a 40% yield (entry 4). Increasing the temperature further promoted the decomposition of this product (entry 7).



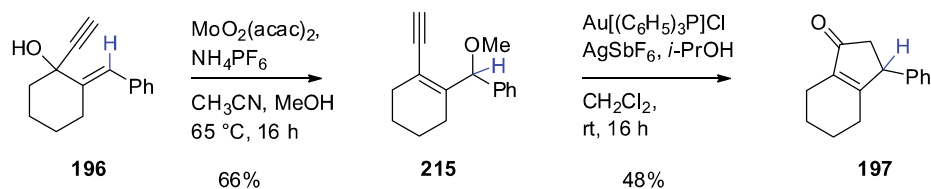
Scheme 59 | Rearrangement and nucleophilic substitution of allylic alcohols **182**.

Table 3 | Optimization of the temperature for the molybdenum-catalyzed rearrangement.

Entry	T ($^{\circ}\text{C}$)	ratio 213a/214a ^a	213a/214a (%) ^b	213a (%) ^b	214a (%) ^b
1	r.t.	1/1	n/a	25	n/a
2	50	1/1	55	26	n/a
3	60	3/1	85	40	16
4 ^c	65	3/1	n/a	38	n/a
5	70	3/1	n/a	38	n/a
6	80	3/1	n/a	39	n/a
7	100		degradation		

^a based on ^1H NMR ^b isolated yields.

Before examining the synthesis of cyclopentenone **188** from rearranged product **213a**, we validated Rhee's approach on a substrate similar to the one explored by Frontier and collaborators. Alcohol **196** was rearranged and etherified to the desired isomer **215** with 66% yield (Scheme 60). We can conclude based on the various experiments reported in Table 4 that the presence of isopropanol and AgSbF_6 is required to completely convert the starting material. More importantly, we demonstrated that this reaction can be performed with a methyl ether instead of a silyl ether that is present on a quaternary carbon.



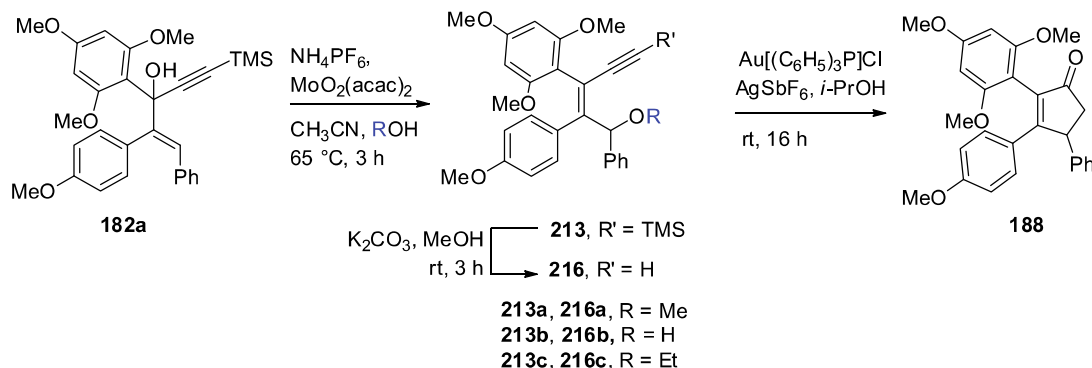
Scheme 60 | Synthesis of cyclopentenone **197**.

Table 4 | Optimization of the gold-catalyzed cyclization.

Entry	Catalysts	Co-catalyst	<i>i</i> -PrOH	215 (%) ^{a,b}	197 (%) ^a
1	AuPPh ₃ .Tf ₂ N	-	+	60	32
2	Au[(C ₆ H ₅) ₃ P]Cl	-	+	90	0
3	Au[(C ₆ H ₅) ₃ P]Cl	AgSbF ₆	-	75	16
4	Au[(C ₆ H ₅) ₃ P]Cl	AgSbF ₆	+	52	48

^a yield based on ¹H NMR; ^b recovered starting material.

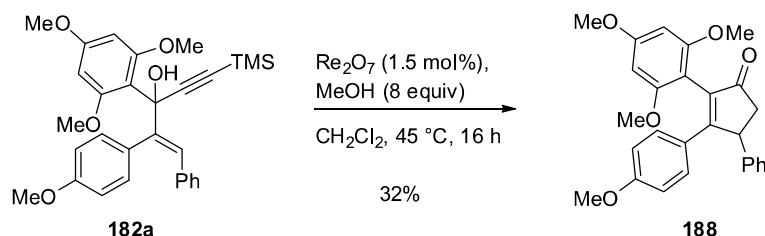
These conditions were then used on compound **182a**, which had been deprotected using K₂CO₃ (Scheme 61). The results are reported in Table 5. In the absence of an alcohol (entry 1), rearranged alcohol **213b** was obtained with a low yield (11%). Furthermore, it did not cyclize after deprotection. Using MeOH or EtOH gave the same yield for the allylic rearrangement and in both cases afforded compound **216b** and **216c** with excellent yields (entries 2 and 3). However, when R = Et, cyclopentenone **188** was obtained with a slightly better yield (63% vs. 55% for R = Me). Gratifyingly, the attempt to perform this reaction on silylated alkyne **213a** also afforded **188** with 58% yield (entry 4).

**Scheme 61** | Synthesis of cyclopentenone **188**.**Table 5** | Yields of the different steps for the synthesis of cyclopentenone **24**.

Entry	R	213 (%)	216 (%) from 213	188 (%) from 216	188 (%) from 182
1	-	213b , 11	216b , 96	0	0
2	Me	213a , 64	216a , 100	55	35
3	Et	213c , 64	213c , 93	63	30
4	Me	213a , 64	-	58 ^a	37

^a Compound **213a** was used as the substrate.

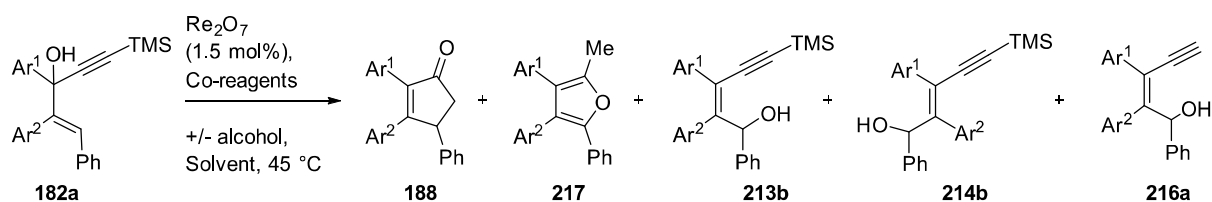
During the optimization process of this synthesis, we examined Re_2O_7 as a catalyst to transform allylic alcohol **182a** into the ether **213a**. Indeed, rhenium oxide is described to efficiently catalyze this type of transformation.¹⁰² Unexpectedly, instead of obtaining ether **213a**, we observed the formation of cyclopentenone **188** in a 32% yield (Scheme 62).



Scheme 62 | Re_2O_7 -catalyzed synthesis of cyclopentenone **188**.

To increase the yield of this cyclization, we changed several parameters such as the catalyst, the alcohol, the solvent and the temperature of the reaction (Tables 6 and 7). Despite numerous attempts, we failed to significantly improve the synthesis of the cyclopentenone. In most of the cases, either the reaction did not occur or a mixture of products was obtained such as rearranged allylic alcohols **213b** and **214b**, deprotected starting material **216a** or methylfuran **217**.

¹⁰² Herrmann, A. T.; Saito, T.; Stivala, C. E.; Tom, J.; Zakarian, A. *Journal of the American Chemical Society* **2010**, *132* (17), 5962-5963.



Ar^1 = 2,4,6-trimethoxybenzene

Ar^2 = anisyl

Table 6 | Attempts of formation of cyclopentenone **188** using different co-reagents. (Conditions: Re_2O_7 (1.5 mol%), MeOH (3 eq.), DCM, 45 °C, 16 h).

Entry	Co-reagents (eq)	Alcohol	182a	188	217	213b	214b	216a
1	$\text{Au}(\text{Ph}_3\text{P})\text{Cl}$ (0,05)	MeOH	-	-	-	-	-	+
2	$\text{Au}(\text{Ph}_3\text{P})\text{NTf}_2$ (0,05)	MeOH	-	+	-	-	-	+
3	$\text{NaAuCl}_4 \cdot 2\text{H}_2\text{O}$ (0,05)	MeOH	-	+	-	-	-	-
4	$\text{Cu}^+(\text{CNCH}_3)_4\text{BF}_3^-$ (0,05)	MeOH	-	+	-	-	-	-
5 ^a	$\text{CH}_3\text{CO}_2\text{H}$ (3)	-	+	-	-	-	-	-
6	1,3-propan-diol (3)	-	-	+	-	-	-	+
7	-	MeOH ^b	-	+	-	-	-	-

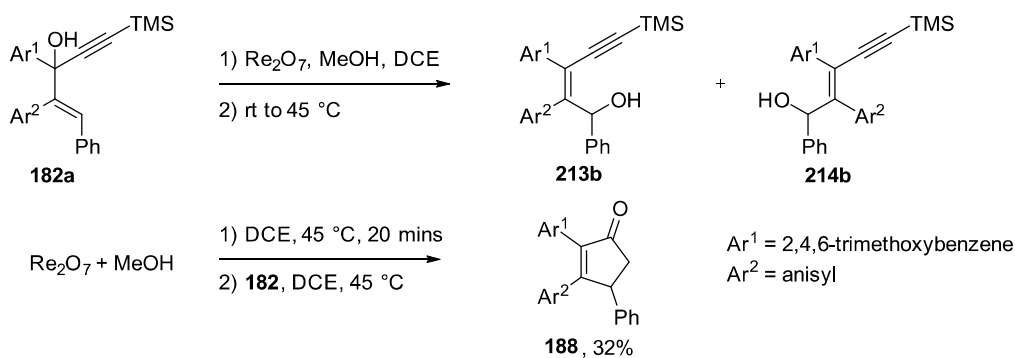
+ : compounds formed in substantial quantities, characterized by NMR. ^a reaction was carried at rt ^b 6 equivalents of MeOH were used.

Table 7 | Attempts of formation of cyclopentenone **188** using different alcohols. (Conditions: Re_2O_7 (1.5 mol%), DCE, 45 °C, 16 h)

Entry	Alcohol (eq)	182a	188	217	213b	214b	216a
1	MeOH (3)	-	-	-	+	+	-
2	<i>t</i> -BuOH (6)	-	-	+	+	-	-
3	<i>n</i> -BuOH (6)	-	+	-	-	-	-
4	Phenylethylalcohol (3)	+	-	-	-	-	-
5 ^a	MeOH (3)	-	-	-	+	+	-
6	MeOH (3)	-	-	+	+	+	-
7	MeOH (6)	-	+	-	-	-	-
8	<i>t</i> -BuOH (6)	-	+	-	-	-	-

+ : Compounds formed in substantial quantities, characterized by NMR. ^a 3 equivalents of formamide were added to the reaction mixture.

Examining closely the procedures, we realized that it is essential that the rhenium oxide reacts with methanol in 1,2-dichloroethane for 20 minutes at 45 °C prior to the addition of propargyl alcohol at 45 °C (Scheme 63). This data therefore suggests that the rhenium oxide Re_2O_7 works as a precatalyst which has to be activated by treatment with MeOH at 45 °C.



Scheme 63 | Reaction conditions to obtain cyclopentenone **188** with Re_2O_7 as a catalyst.

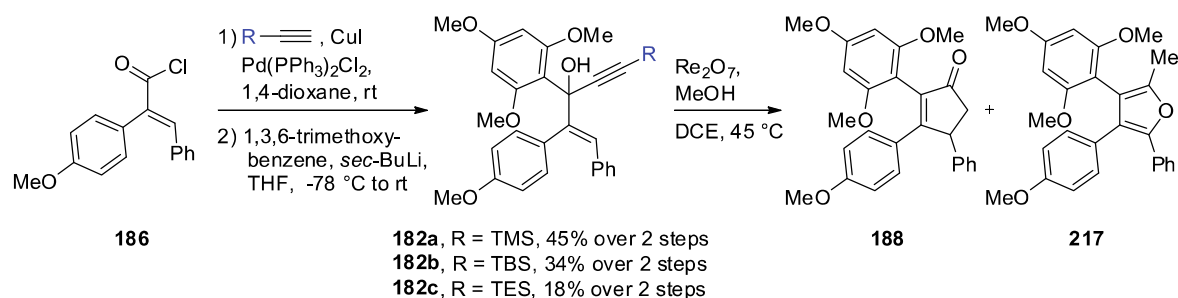
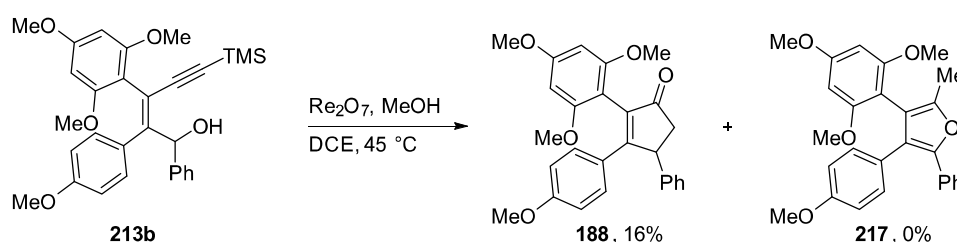


Table 8 | Modulation of the silyl group for the formation of cyclopentenone **24**.

Entry	R	182	Re_2O_7 (mol%)	188 (%)	217 (%)
1	TMS	182a	1.5	32	18
2	TMS	182a	20	30	N/A
3	TBS	182b	1.5	44	27
4	TES	182c	1.5	22	19

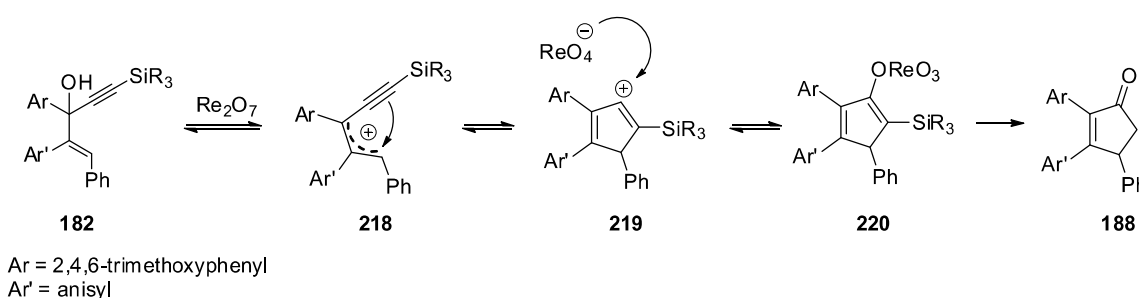
Along with cyclopentenone **188**, a second product was formed in the rhenium-catalyzed cyclization with a lower yield, the methylfuran **217**.

To further optimize this reaction, we modified the silyl group. Replacing trimethylsilyl group with a more bulky *tert*-butyldimethylsilyl group improved the reaction allowing the formation of 44% of cyclopentenone **188** along with 27% of methylfuran **217** (Table 8, entry 3). On the contrary, replacing it with the triethylsilyl group reduced the reactivity of the starting material. The TBDMS group stabilizes the carbocation intermediate slightly better than the TMS group, probably due to the higher inductive effect of the *t*-butyl group, leading to an increase in yield. We could also observe that the cyclopentenone **188** could be formed starting from rearranged alcohol **213b** but with lower yield (16%, Scheme 64). In this case, no formation of the methylfuran **217** was obtained.



Scheme 64 | Formation of cyclopentenone **188** from rearranged alcohol **217**.

In order to improve the yields of these reactions and to gain insight in the reaction mechanism, we explored different reaction conditions starting from carbinol **182**. The detailed optimization will be presented in chapter 3.6. The key information is that this rearrangement can be catalyzed by a strong Brønsted acid such as triflic acid. This led us to postulate the following mechanism for the formation of cyclopentenone **188** (Scheme 65):

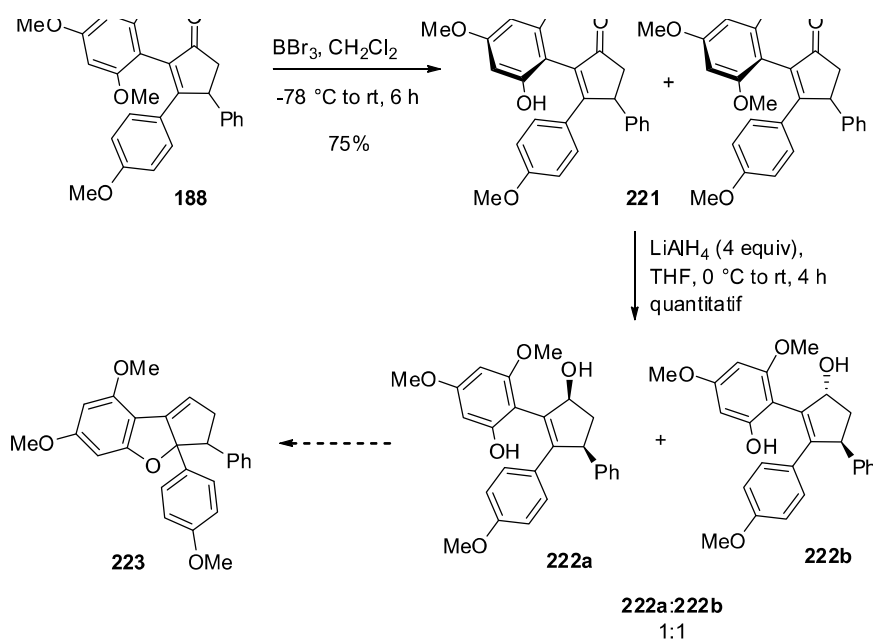


Scheme 65 | Postulated mechanism for the formation of cyclopentenone **188**.

Cyclopentenone **188** is expected to arise through the formation of a stabilized carbocation **218**. This intermediate may undergo a ring closure due to the nucleophilic character of the silylated alkyne to form carbocation **219**. Rearrangement and cleavage of the silyl group gives cyclopentenone **188**.

3.1.3 Attempts to generate flavaglines from the cyclopentenone intermediate

With cyclopentenone **188** in hand, we continued our synthesis by performing the regioselective demethylation using tribromoborane (75% yield). Thus, coordination of the borane to the ketone facilitates the selective mono-demethylation (Scheme 66). Ketone **221** was then reduced.



Scheme 66 | Partial synthesis of benzofuran **223**.

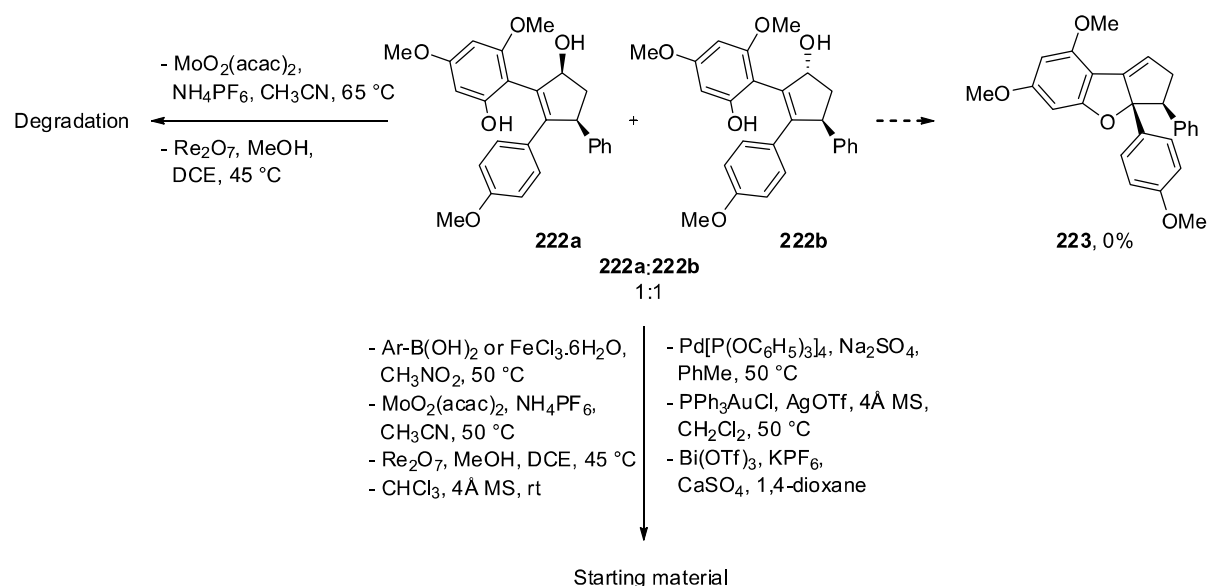
Table 9 | Optimization of the reduction of cyclopentenone **221**.

Entry	Reagents (eq)	Solvents	T(°C)	221 (%)	dr ^a 222a:222b	222a/222b (%) ^b
1	<i>L</i> -selectride (1.1)	THF	-78 to rt	+	1.5:1	15
2	Red-Al (1.5)	THF	-20 to rt	+	2:1	38
3	Red-Al (1.5)	THF	0 to rt	+	2:1	50
4	Red-Al (1.5)	THF	0 to rt	-	0.8:1	90 ^c
5	NaBH ₄ (2)	CH ₂ Cl ₂ /MeOH, 1/1	rt	40	-	< 10
6	NaBH ₄ (10)	MeOH	rt	40	-	< 10
7	NaBH ₄ (2), CeCl ₃ ·7H ₂ O (2)	CH ₂ Cl ₂ /MeOH		26	1.2:1	37
8	NaBH ₄ (2), CeCl ₃ ·7H ₂ O (2)	H ₂ O, sonication	rt	80	-	< 10
9	LiAlH ₄ (4)	THF	0 to rt	-	1:1	100 ^c

^a based on ¹H NMR ^b isolated yields ^c no purification on SiO₂ ; +: product was not isolated.

Attempts of diastereoselective reductions are described in Table 9. Despite the various reagents used, we consistently obtained a mixture of isomers **222a**/**222b** with the hydroxy group either in *cis* or *trans* position relative to the phenyl group. However, the reaction is quantitative with lithium aluminum hydride (Table 9, entry 9). It should be noted that the isomerization is observed in deuterated chloroform, and degradation occurs if the product is heated or if it is in presence of silica gel.

With **222a** and **222b** obtained, we tried to convert these reactive allylic alcohols into the flavagline precursor **223** using many methods of activation of allylic alcohols (Scheme 67, Table 10). Despite the variety of conditions used, we never observed any cyclized product **223**. The different reactions lead either to the degradation or the recovery of starting material. In some cases, as with $\text{MoO}_2(\text{acac})_2$ or Re_2O_7 (entries 2 and 4), we noticed a change in the diastereomeric ratio in the starting material on ^1H NMR. Unfortunately, all of these assays were unsuccessful. Even though compounds with similar structures to **223** have been described in the literature,¹⁰³ in our case, all assays of such cyclization were unsuccessful probably due to the inherent ring strain of this product and the kinetic lability of the carbocationic intermediate.



Scheme 67 | Summary of the assays of formation of benzofuran **223**.

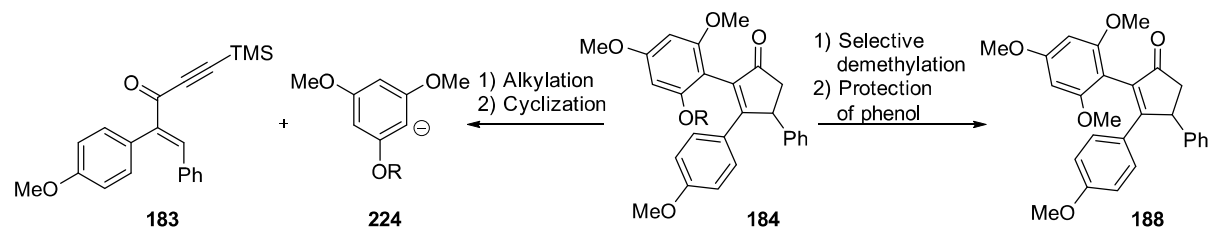
¹⁰³ (i) Giese, M. W.; Moser, W. H. *Organic Letters* **2008**, *10* (19), 4215-4218. (ii) Magnus, P.; Stent, M. A. H. *Organic Letters* **2005**, *7* (18), 3853-3855. (iii) Malona, J. A.; Cariou, K.; Frontier, A. J. *Journal of the American Chemical Society* **2009**, *131* (22), 7560-7561. (iv) Malona, J. A.; Cariou, K.; Spencer, W. T.; Frontier, A. J. *The Journal of Organic Chemistry* **2012**, *77* (4), 1891-1908. (v) Trost, B. M.; Greenspan, P. D.; Yang, B. V.; Saulnier, M. G. *Journal of the American Chemical Society* **1990**, *112* (24), 9022-9024.

Table 10 | Attempts of formation of benzofuran **223**.

Entry	Reagents	Solvent	T(°C)	Observations
1	MoO ₂ (acac) ₂ , NH ₄ PF ₆	CH ₃ CN	65	degradation
2	MoO ₂ (acac) ₂ , NH ₄ PF ₆	CH ₃ CN	0 to 50	222a/222b
3	Re ₂ O ₇ , MeOH	DCE	45	degradation
4	Re ₂ O ₇ , MeOH	DCE	0 to 50	222a/222b
5	Re ₂ O ₇ , MeOH	DCE diluted	30	degradation
6	4Å MS	CHCl ₃	rt	222a/222b ^a
7	Pd(OAc) ₂ , PPh ₃ , Ti(O <i>i</i> -Pr) ₄ , 4Å MS	PhH	50	3 uncharacterized products
8	Pd[P(OC ₆ H ₅) ₃] ₄ , Na ₂ SO ₄	PhMe	rt to 50	222a/222b
9	SiO ₂	CH ₂ Cl ₂	rt	222a/222b and traces of dehydration
10	Al ₂ O ₃	CH ₂ Cl ₂	rt	222a/222b
11	Bi(OTf) ₃ , KPF ₆ , CaSO ₄	1,4-dioxane	rt to 35	222a/222b
12	AuCl ₃ , 4Å MS	DCE		222a/222b and 1 uncharacterized product
13	<i>p</i> -TSA, 4Å MS	CHCl ₃	rt to 35	222a/222b and 2 uncharacterized products
14	PPh ₃ AuCl, AgOTf, 4Å MS	CH ₂ Cl ₂	rt to 50	222a/222b
15	Ar-B(OH) ₂ ^b	CH ₃ NO ₂	rt to 50	222a/222b
16	FeCl ₃ .6H ₂ O	CH ₃ NO ₂	rt to 50	222a/222b
17	BF ₃ .Et ₂ O	CH ₂ Cl ₂	-30 to 0	222a/222b and 2 uncharacterized products

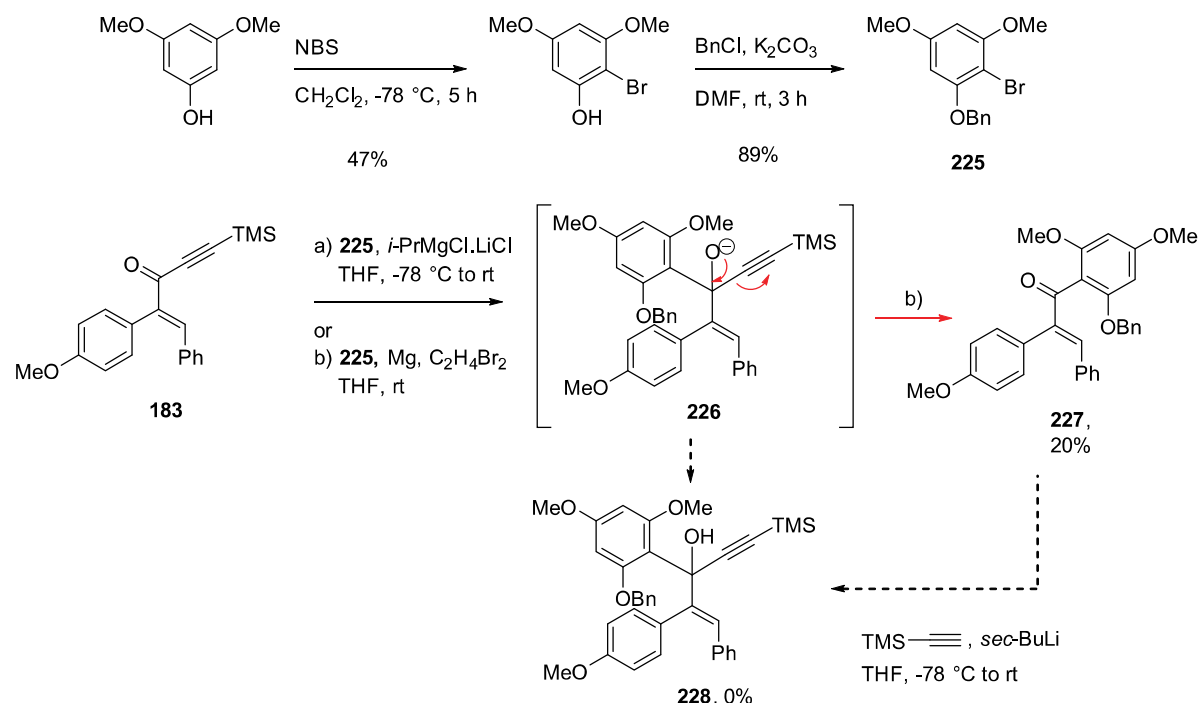
^a A change in the ratio of isomer **222a/222b** was observed on ¹H NMR from 50:50 to 80:20 ^b ArB(OH)₂ = (2,3,4,5-tetrafluorophenyl)boronic acid.

As all cyclization attempts were inconclusive, we choose to continue the synthesis by introducing a protecting group on the phenol in a similar manner to that employed by Ragot. To protect the phenol with a benzyl, two approaches are possible (Scheme 68). The first possibility is to introduce the benzyl group from the beginning of the synthesis, by preparing reactant **224** instead of using 1,3,6-trimethoxybenzene. The second way consists of starting directly from cyclopentenone **188**, selectively demethylating one methoxy group and then protecting with a benzyl group.



Scheme 68 | Alternatives for the formation of cyclopentenone **184**.

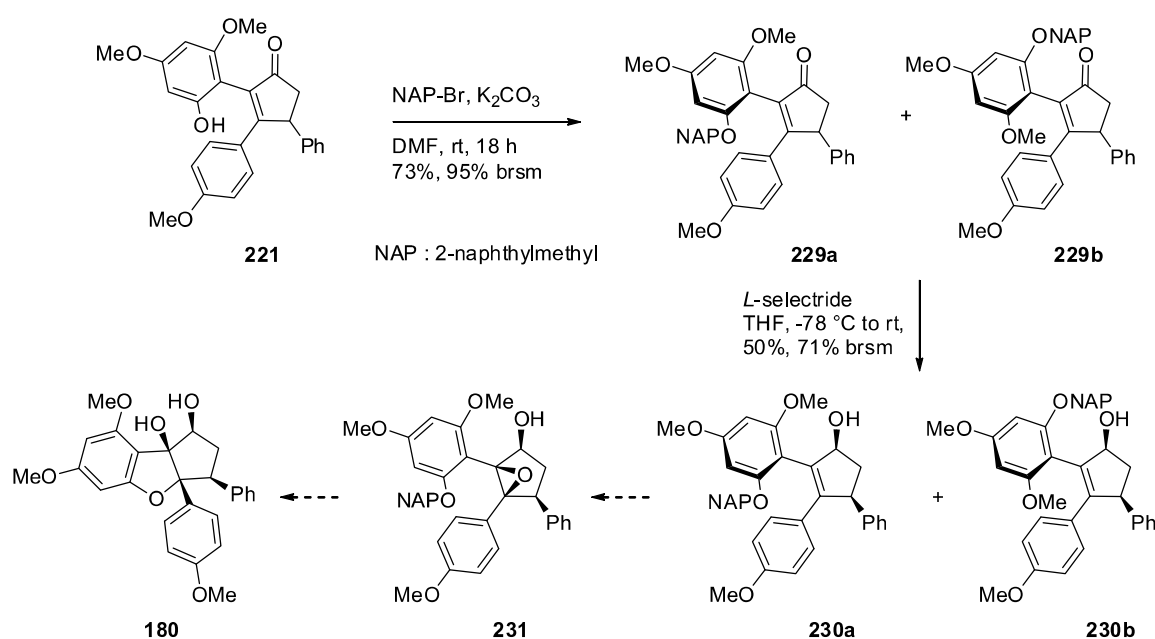
To achieve the alkylation of ketone **183**, we performed first a Grignard reaction prepared from the bromide derivative **225** (synthesized in 2 steps from 2,4-dimethoxyphenol, Scheme 69). This assay did not lead to the desired propargyl alcohol (Scheme 69). However, we can note the presence of enone **227** with 20% yield obtained from intermediate **226**. We can note here that we did not observe this reaction when using lithium instead of magnesium (section 3.1.2, Scheme 48). We then tried to alkylate the latter by lithiated trimethylsilylacetylene. No reaction was observed and the starting material was completely recovered. A second attempt at the Grignard reaction was achieved but this time in the presence of *i*-PrMgCl.LiCl.¹⁰⁴ The reaction was not conclusive since we only recovered the starting material.



Scheme 69 | Attempts of formation of propargyl alcohol **228**.

¹⁰⁴ León, B.; Fong, J. C. N.; Peach, K. C.; Wong, W. R.; Yildiz, F. H.; Lington, R. G. *Organic Letters* **2013**, *15* (6), 1234-1237.

As the first approach to obtain protected phenol **228** was unsuccessful, we considered the second method which consists to re-protect phenol **221**. Here we choose a 2-naphthylmethyl group which is known to be more labile in the catalytic hydrogenation conditions (Scheme 70).¹⁰⁵ Phenol **221** was alkylated with 2-(bromomethyl)naphthalene in the presence of potassium carbonate which gave better conversion compared to cesium carbonate. From there, we applied Ragot's strategy. Using LiAlH_4 gave a mixture of diastereoisomer 85:15 with 68% yield. Gratefully, *L*-selectride provided diastereoselective reduction to desired alcohol **230** as 1:1 mixture of atropoisomers. Epoxidation of cyclopentenol **230a/230b** was unsuccessful in two different conditions (Table 11, entries 9-10).

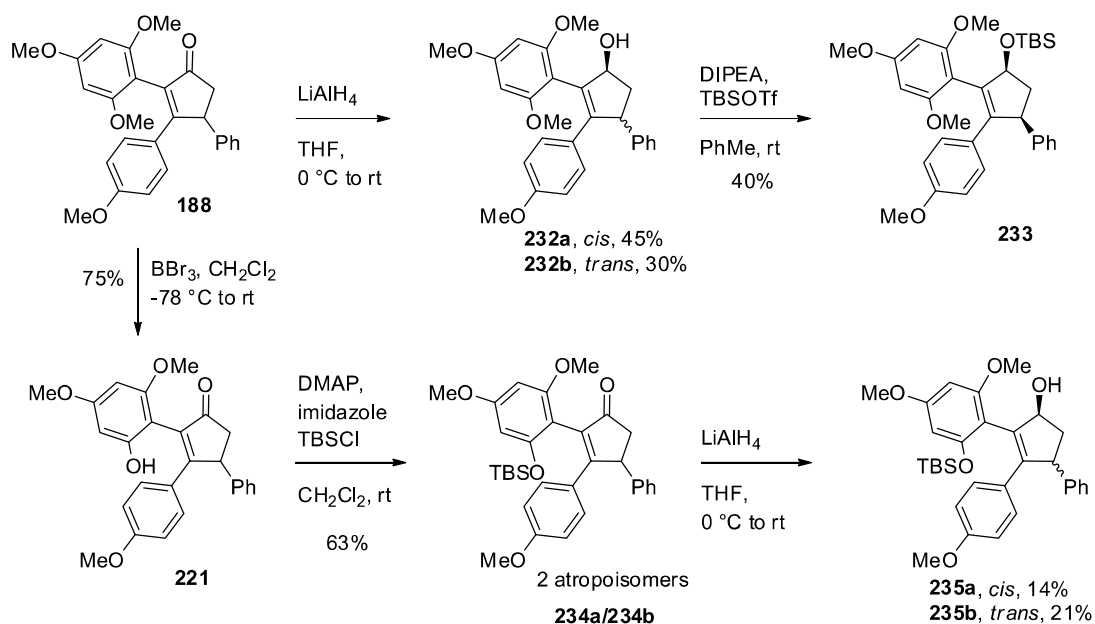


Scheme 70 | Partial synthesis of flavagline **180**.

To further attempt the epoxidation, two more substrates were prepared: protected cyclopentenol **233** and protected phenol **235a/235b** (Scheme 71). Cyclopentenone **188** was reduced in the presence of LiAlH_4 to afford 45% of the *cis* diastereoisomer **232a** and 30% of the *trans* **232b**. Isomer **232a** was then protected using *tert*-butyldimethylsilyl triflate and diisopropylethyl amine to afford product **233**. In a similar way, phenol **221** was protected with *tert*-butyldimethylsilyl chloride giving a 1:1 mixture of atropoisomers **234a/234b** with

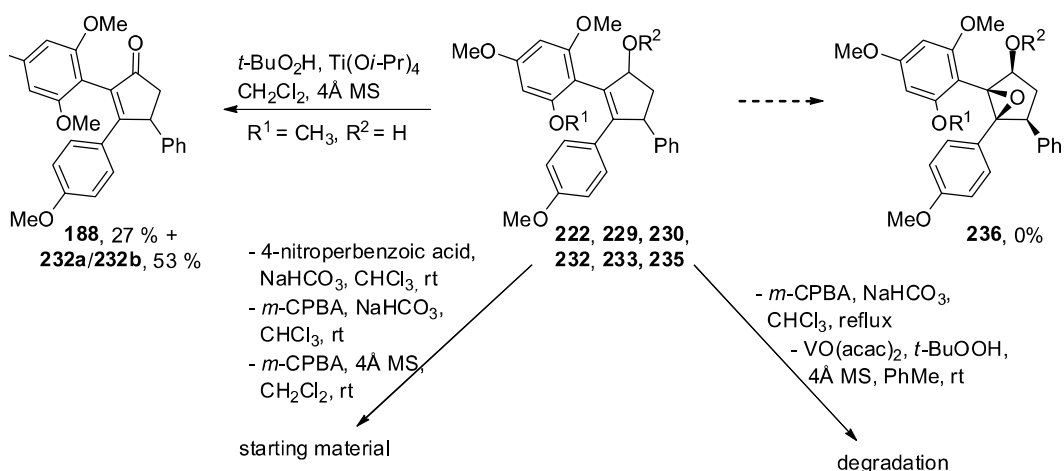
¹⁰⁵ Gaunt, M. J.; Yu, J.; Spencer, J. B. *The Journal of Organic Chemistry* **1998**, 63 (13), 4172-4173.

63% yield. After reduction protected phenol **235a** was obtained along with its diastereoisomer **235b**.



Scheme 71 | Preparation of cyclopentenols **233**, **235a** and **235b**.

Various conditions (*m*-CPBA, NaHCO_3 ; $\text{VO}(\text{acac})_2$, *t*-BuOOH; H_2O_2 , NaOH; 4-nitroperbenzoic acid, NaHCO_3) with various starting alkenes provided none of the desired product probably due to the low reactivity of the sterically hindered alkene and instability of the product (Table 11). In Sharpless type conditions (entry 1), starting from alkene **232a/232b**, formation of the ketone **188** was observed, probably due to ring strain release.



Scheme 72 | Summary of the assays of epoxidation of various alkenes.

Table 11 | Attempts of epoxidation of alkenes **222**, **229**, **230**, **232**, **233** and **235**.

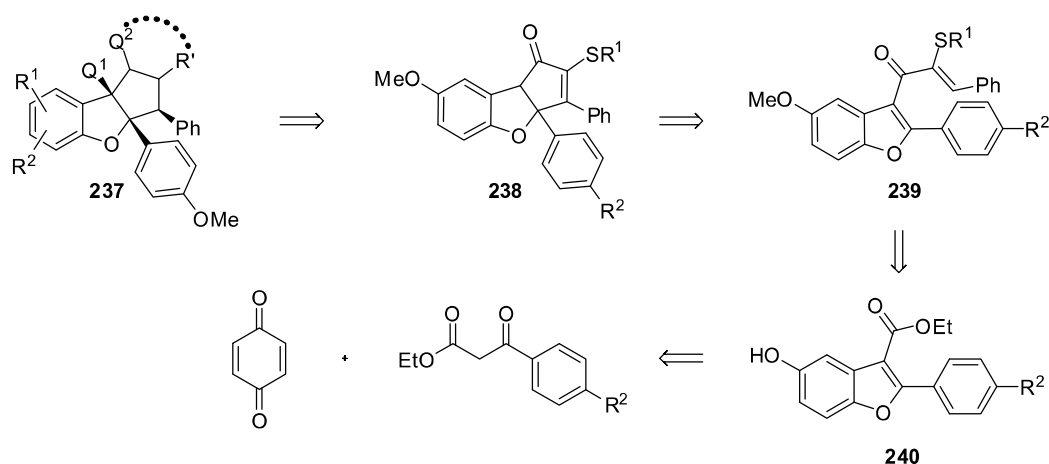
Entry	Alkenes	R ¹	R ²	Reagents	Solvents, T(°C)	Results
1	232a/232b	MeO	H	<i>t</i> -BuOOH, Ti(<i>Oi</i> -Pr) ₄ , 4Å MS	CH ₂ Cl ₂ , 0	188 , 27% + 232a/232b , 53%
2	232a/232b	MeO	H	4-nitroperbenzoic acid, NaHCO ₃	CHCl ₃ , rt	232a/232b
3	233	MeO	TBS	<i>t</i> -BuOOH, VO(acac) ₂ , 4Å MS	PhMe, rt	degradation
4	233	MeO	TBS	<i>m</i> -CPBA, 4Å MS	CH ₂ Cl ₂ , rt	233
5	233	MeO	TBS	<i>m</i> -CPBA, NaHCO ₃	CHCl ₃ , r.t.	233
6	233	MeO	TBS	<i>m</i> -CPBA, NaHCO ₃	CHCl ₃ , reflux	degradation
7	235a/235b	TBS	H	<i>t</i> -BuOOH, Ti(<i>Oi</i> -Pr) ₄ , 4Å MS	CHCl ₃ , rt	235a/235b
8	235a/235b	TBS	H	<i>t</i> -BuOOH, Ti(<i>Oi</i> -Pr) ₄ , 4Å MS	CHCl ₃ , 50	degradation
9	230a/230b	NAP	H	<i>t</i> -BuOOH, VO(acac) ₂ , 4Å MS	PhMe, rt	degradation
10	230a/230b	NAP	H	<i>m</i> -CPBA, 4Å MS	CH ₂ Cl ₂ , 0	degradation
11	230a/230b	NAP	H	H ₂ O ₂ , NaOH	CH ₂ Cl ₂ , 0	230a/230b
12	230a/230b	NAP	H	H ₂ O ₂ , NaOH	CH ₂ Cl ₂ , rt	degradation
13	229a/229b	NAP	C=O	<i>m</i> -CPBA, 4Å MS	CH ₂ Cl ₂ , 0	degradation
14	222a/222b	H	H	<i>m</i> -CPBA, 4Å MS	CH ₂ Cl ₂ , 0	3 unidentified products
15	222a/222b	H	H	<i>t</i> -BuOOH, VO(acac) ₂ , 4Å MS	PhMe, rt	3 unidentified products

The inability to obtain the epoxidation product **236** suggests that the method reported by Bayer scientist is restricted to the synthesis of flavaglines that are not substituted by functional groups on the benzofuran moiety. Indeed, none of the required decorations for pharmacological activity such as the two methoxy groups proposed here were described in Bayer patents. This work was published in *Tetrahedron lett.* **2015**, *56*, 727–730 (see publication n°3, page 299).

3.2 Synthesis of flavaglines based on Magnus' approach

3.2.1 Retrosynthetic strategy

As it was described in the first chapter, Magnus and coll. obtained flavaglines via an acetyl bromide-mediated Nazarov reaction.¹⁰⁶ In this reaction, a methyl group was necessary to stabilize the carbocationic intermediate in α position of the carbonyl group.¹⁰⁷ We considered that replacing the methyl group with a thioether could also favor the cyclization by stabilizing the carbocation intermediate. Indeed, as we presented in section 1.6.4, Cavalli and colleagues demonstrated that a thioether in α position of the ketone promotes Nazarov reactions.¹⁰⁸ Another advantage of the thioethers lies on their use to introduce various functionalities (Scheme 73). Therefore, a retrosynthetic route was proposed to synthesize the cyclopentenone **238**. The divinyllic ketone **239** could be prepared from easily accessible benzofuran **240**.



Scheme 73 | Retrosynthetic route to flavaglines **237**.

3.2.2 Synthesis of the scaffold of flavaglines via Nazarov reaction

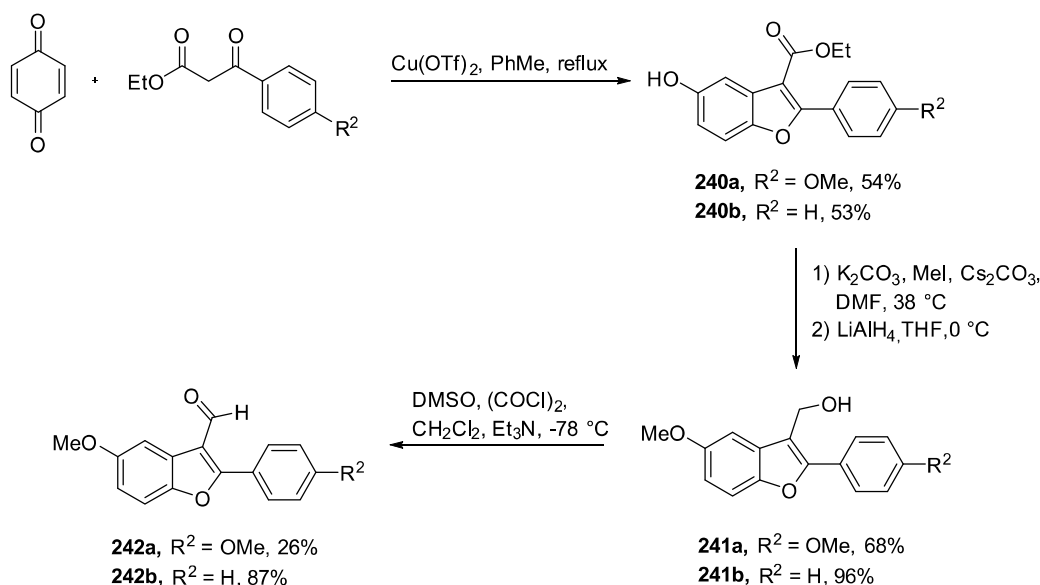
Copper(II)-catalyzed condensation of benzoquinone with oxopropionate afforded benzofurans **240a** and **240b** in 54% and 53% yield respectively (Scheme 74). These products were chosen because there are easy to access according to a procedure described by Chan

¹⁰⁶ Magnus, P.; Freund, W. A.; Moorhead, E. J.; Rainey, T. *Journal of the American Chemical Society* **2012**, *134* (14), 6140-6142.

¹⁰⁷ Vaidya, T.; Eisenberg, R.; Frontier, A. J. *ChemCatChem* **2011**, *3* (10), 1531-1548.

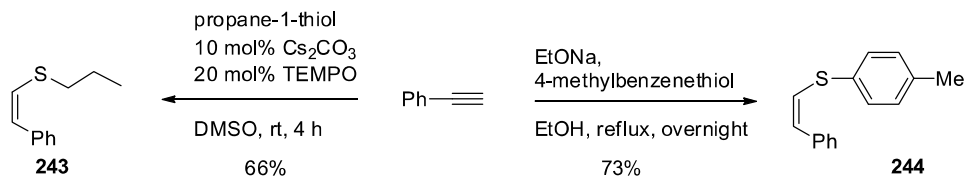
¹⁰⁸ Cavalli, A.; Pacetti, A.; Recanatini, M.; Prandi, C.; Scarpi, D.; Occhiato, E. G. *Chemistry – A European Journal* **2008**, *14* (30), 9292-9304.

*et al.*¹⁰⁹ After methylation with iodomethane, reduction of ester to aldehyde **241b** using DIBAL-H at low temperature was not successful. Therefore, the ester was first reduced to the alcohol using aluminum hydride afforded compounds **241a** and **241b**. While oxidation with MnO₂ was incomplete, Swern oxidation afforded aldehydes **242a** and **242b**. The synthesis of these aldehydes was performed jointly with another PhD student, Qian Zhao.



Scheme 74 | Synthesis of benzofurans **242a** and **242b**.

With the aldehydes in hand, the thioethers **243** and **244** were then prepared starting from phenylacetylene (Scheme 75). Compound **243** was synthesized from propane-1-thiol following Oshima and coll. procedure, in the presence TEMPO.¹¹⁰ Compound **244** was selectively prepared from 4-methylbenzenethiol in the presence of sodium and ethanol with 73% yield.



Scheme 75 | Synthesis of thioethers **243** and **244**.

¹⁰⁹ Mothe, S. R.; Susanti, D.; Chan, P. W. H. *Tetrahedron Letters* **2010**, 51 (16), 2136-2140.

¹¹⁰ Kondoh, A.; Takami, K.; Yorimitsu, H.; Oshima, K. *The Journal of Organic Chemistry* **2005**, 70 (16), 6468-6473.

The next step was the alkylation of aldehydes **242a** with lithiated thiovinylether **244**. Several conditions were examined using different ratio of starting materials and two Lewis acids: $\text{LaCl}_3 \cdot 2\text{LiCl}$ and $\text{BF}_3 \cdot \text{Et}_2\text{O}$ (Table 12). Paul Knochel and coll. showed that $\text{LaCl}_3 \cdot 2\text{LiCl}$ attenuates the basicity of Grignard reagents, preventing competitive enolization side reactions while leading to a selective 1,2-addition of Grignard reagents to ketones.¹¹¹ $\text{BF}_3 \cdot \text{Et}_2\text{O}$ is a strong oxophilic Lewis acid known to enhance the electrophilicity of carbonyls. Best results were obtained with $\text{BF}_3 \cdot \text{Et}_2\text{O}$, with a quasi-quantitative conversion (97%) and a good yield (86%). An excess of thiovinylether was needed to complete the reaction (Table 12, entry 4). These conditions were selected to synthesize substrates **245b**, **245c** and **245d** (Scheme 76).

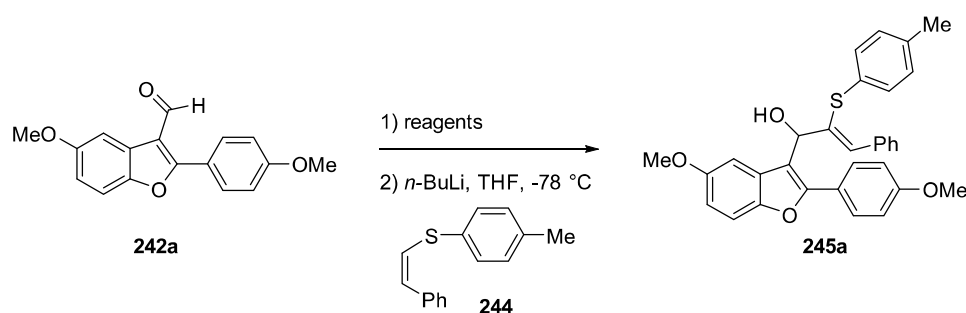
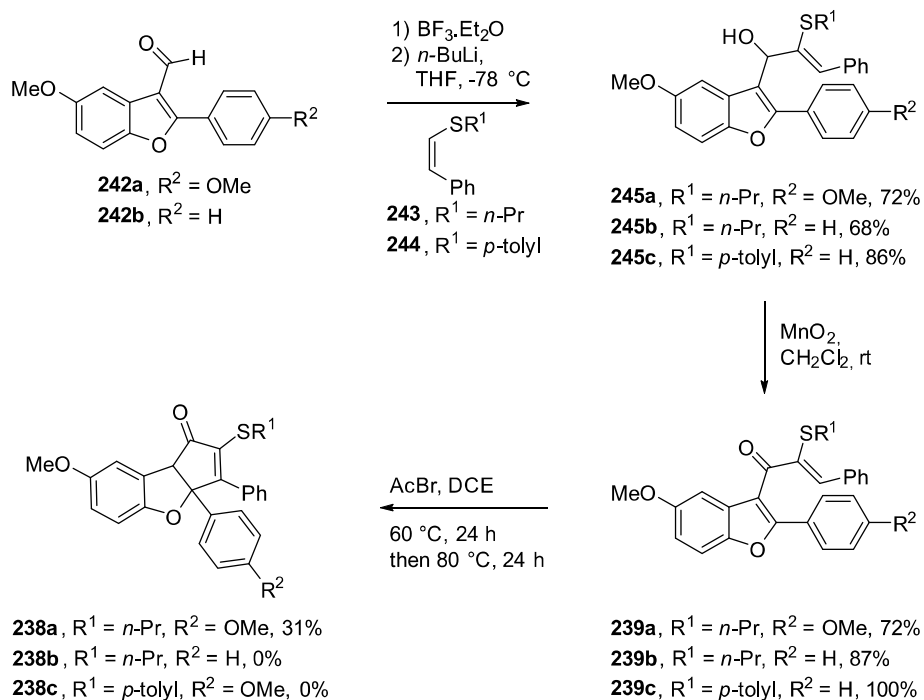


Table 12 | Optimization of the addition of thiovinylether **244** to aldehyde **245a**.

Entry	242a:244	Reagent (eq)	Conversion of 242a (%)	245a (%) ^a
1	1.1:1	TMEDA (1.2)	62	21
2	1:1	$\text{LaCl}_3 \cdot 2\text{LiCl}$ (1)	79	40
3	2:1	$\text{BF}_3 \cdot \text{Et}_2\text{O}$ (1)	73	46
4	1:1.5	$\text{BF}_3 \cdot \text{Et}_2\text{O}$ (1)	97	86

^a isolated yields

¹¹¹ (ii) Metzger, A.; Gavryushin, A.; Knochel, P. *Synlett* **2009**, 2009 (09), 1433-1436. (ii) Krasovskiy, A.; Kopp, F.; Knochel, P.. *Angewandte Chemie International Edition* **2006**, 45 (3), 497-500.



Scheme 76 | Synthesis of cyclopentenone **238**.

Divinylalcohols **239** were then oxidized with MnO₂ to afford the precursors of the acyl bromide-mediated Nazarov reaction (Scheme 76). These divinylketone intermediates **239** were prepared jointly with Qian Zhao, another PhD student.

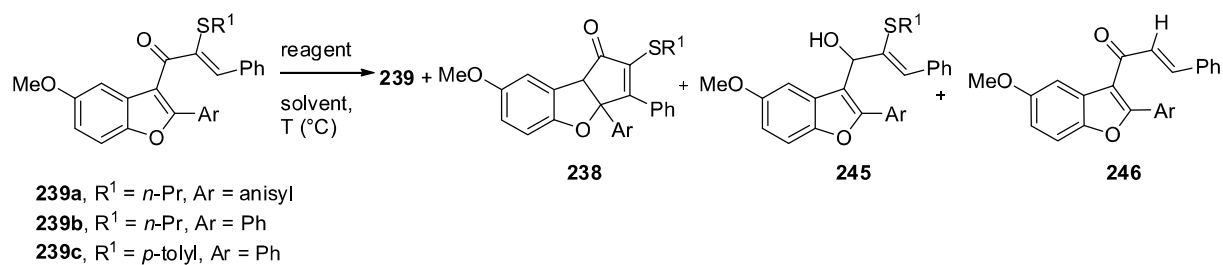


Table 13 | Optimization of the AcBr-mediated Nazarov reaction.
(Conditions: AcBr (1.5 eq), 80 °C, overnight)

Entry	R ¹	Ar	Solvent	239 (%) ^a	238 (%) ^a	245 (%) ^a
1	<i>n</i> -Pr	Ph	DCE	+ ^b	31	-
2	<i>n</i> -Pr	Ph	DCE	86 ^c	14 ^c	-
3 ^d	<i>n</i> -Pr	Ph	DCE	+	13	-
4 ^e	<i>n</i> -Pr	Ph	DCE	traces	traces	-
5 ^f	<i>n</i> -Pr	Ph	DCE	+	-	-
6	<i>n</i> -Pr	Ph	CH ₃ NO ₂	-	traces	-
14	<i>n</i> -Pr	anisyl	DCE	85 ^c	15 ^c	-
19 ^g	<i>p</i> -tolyl	anisyl	DCE	100 ^f	-	-

^a yields are based on the crude, unless indicated otherwise. ^b +: compounds found in substantial quantities, characterized by ¹H NMR ^c yield based on ¹H NMR ^d 16 equivalents of AcBr were used ^e reaction carried in a sealed tube ^f 2,6-Di-*tert*-butylphenol (1.5 eq) was added to the reaction mixture ^g 6.5 equivalents of AcBr were used.

With enones **239** in hand, different conditions were examined for the Nazarov cyclization (Table 13). Based on all these experiments, the cyclopentenone **238** could only be obtained when R¹ = *n*-Pr. The best results were obtained when the reaction was promoted with 1.5 equivalents of AcBr with 31% yield after purification on silica gel (entry 1). However this result could not be reproduced; when repeating this reaction, the yield dropped to 14% (entry 2). When the amount of AcBr was increased to 16 equivalents, the yield also dropped to 13 % (entry 3). Some attempts were made to improve the yield by adding a base, 2-6-di-*tert*-butyl pyridine (entry 5) or changing the solvent to nitromethane (entry 6) but in both cases, nearly no formation of cyclopentenone was observed.

Table 14 | Screening of reagent for the Nazarov reaction.

Entry	R ¹	Ar	Reagents (eq)	Solvent, T(°C)	239 (%) ^a	238 (%) ^a	245 (%) ^a	246 (%) ^a
7	<i>n</i> -Pr	Ph	EtC(O)Br (1.5)	DCE, 90	+ ^b	degradation		
8	<i>n</i> -Pr	Ph	EtC(O)Br (1.5)	DCE, 75	25	-	-	30
9	<i>n</i> -Pr	Ph	TIBAL (2), 4Å MS	DCE, r.t.	60	-	23	-
10	<i>n</i> -Pr	Ph	NsCl, 2,6-DTBP (1.3)	DCE, 50	100	-	-	-
11	<i>n</i> -Pr	Ph	NsCl (1.3)	DCE, 50	80	-	-	-
12	<i>n</i> -Pr	Ph	Tf ₂ O (3), 2,6-DTBP (6)	CH ₃ NO ₂ , 80	-	-	-	-
13	<i>n</i> -Pr	Ph	Tf ₂ O (3)	CH ₃ NO ₂ , 80	25 ^c	degradation		
13b	<i>n</i> -Pr	Ph	TFAA (1.2), FeCl ₃ (0.3)	DCE, 70	100 ^d	-	-	-
15	<i>p</i> -tolyl	anisyl	phosphomolybdic acid (0.02)	CH ₃ CN, r.t.	100 ^d	-	-	-
16	<i>p</i> -tolyl	anisyl	-	H ₂ O, r.t.	100 ^d	-	-	-
17	<i>p</i> -tolyl	anisyl	Cu(OTf) ₂ (0.4)	DCE, 50	100 ^d	-	-	-
18	<i>p</i> -tolyl	anisyl	Cu(OTf) ₂ (0.4)	DCE, 85	degradation			

^a yields are based on the crude, unless indicated otherwise. ^b +: compounds found in substantial quantities, characterized by ¹H NMR ^c yield based on ¹H NMR ^d based on TLC.

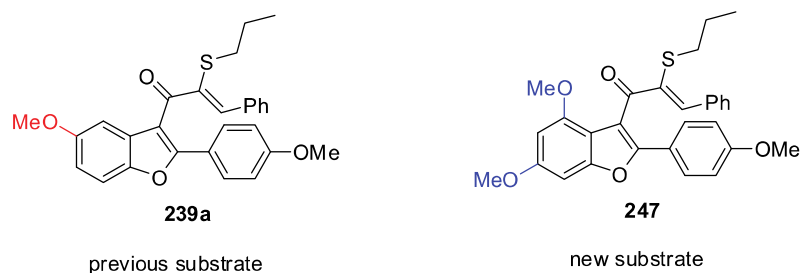
Some efforts were then made to increase the conversion by changing the reagent. Surprisingly, using propionyl bromide that has a higher boiling point than acetyl bromide, compound **246** was formed with 30% yield instead of the cyclopentenone (entry 8). When switching to reductive Nazarov conditions with triisobutylaluminium,¹¹² the only product isolated besides the starting material **239** was the reduced product **245** with 23% yield (entry 9). When NsCl, Tf₂O, phosphomolybdic acid or copper triflate were used, either no reaction happened or the reaction mixture degraded (entries 10-13 and 15-18).

We achieved here the synthesis of a flavaglines-type product substituted with a thioether group. However, the low reproducibility of the AcBr-mediated Nazarov reaction led us to explore a new class of substrates.

¹¹² Kwon, Y.; McDonald, R.; West, F. G. *Angewandte Chemie International Edition* **2013**, 52 (33), 8616-8619.

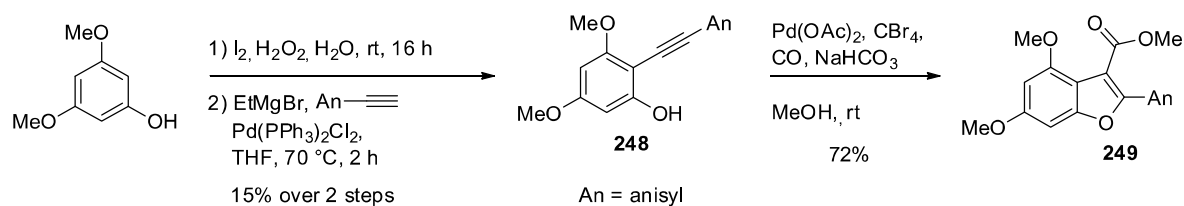
3.2.3 Synthesis of a second class of substrates for the Nazarov reaction

Considering that substrate **239a** reacted poorly in our assays of Nazarov reactions, we examined another substrate, **247**, hoping that it would give better results (Scheme 77). To synthesize this compound, we considered a different approach to prepare the benzofuran ring (Scheme 78).



Scheme 77 | Classes of substrate for the Nazarov reaction.

Benzofuran **249** could be prepared based on Magnus and coll. approach (Scheme 78).¹¹³ The first step was the iodation of dimethoxyphenol in *ortho* position. The yield was low (29%) due to the formation of para substituted and di-substituted products. Then, the addition of a Grignard catalyzed by palladium(II) allowed the formation of tolane **248** which was cyclized in the presence of a palladium catalyst under CO atmosphere to obtain benzofuran **249** in 72% yield. The synthesis of this intermediate was performed jointly with another PhD student, Qian Zhao.

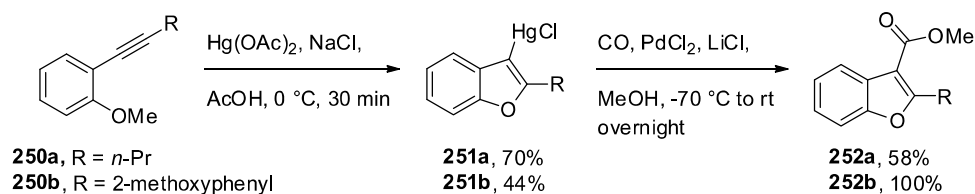


Scheme 78 | Synthesis of benzofuran **249**.

As the yield for the first step of this synthesis was low, we looked into a more efficient method based on a reaction discovered by Larock (Scheme 79).¹¹⁴ With this approach, alkynes **250** were activated by mercury, which could promote the heterocyclization to afford benzofurans **251**. Insertion of CO catalyzed by PdCl₂ gave esters **252**.

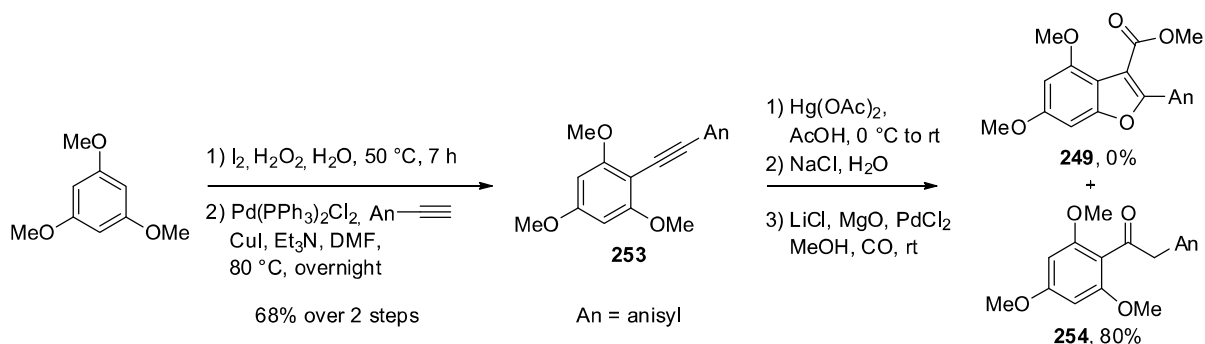
¹¹³ Magnus, P.; Freund, W. A.; Moorhead, E. J.; Rainey, T. *Journal of the American Chemical Society* **2012**, *134* (14), 6140-6142.

¹¹⁴ Larock, R. C.; Harrison, L. W. *Journal of the American Chemical Society* **1984**, *106* (15), 4218-4227.



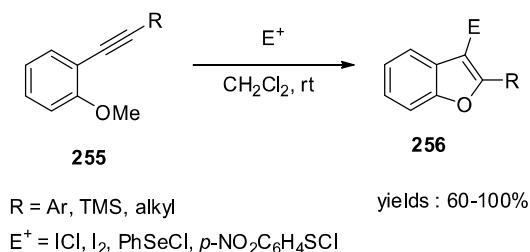
Scheme 79 | Synthesis of benzofuran **252** described by Larock and coll.¹¹⁴

Our attempt to synthesize benzofuran **249** following Larock's method is depicted in Scheme 80. Iodation of trimethoxybenzene underwent smoothly with a very good yield (94%) compared to the earlier iodation of dimethoxyphenol (29%). This resolved the regioselectivity issue that we had before as the molecule is now symmetrical. Sonogashira coupling with 4-methoxyphenyl acetylene afforded alkyne **253** with 70% yield. Cyclization promoted by mercury did not lead to the desired product. Instead, we isolated ketone **254** with 80% yield, resulting from the hydration of alkyne **253**.



Scheme 80 | Attempt to synthesize benzofuran **249** following Larock's method.

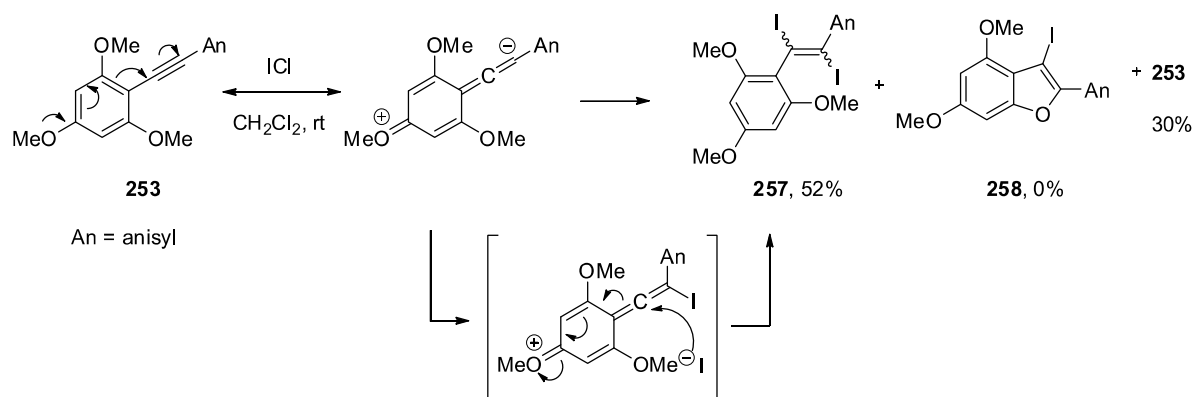
Larock's group also described in 2005 the use of different electrophiles such as I_2 or $PhSeCl$ to access 2,3-disubstituted benzo[*b*]furans by electrophilic cyclization.¹¹⁵



Scheme 81 | Synthesis of 2,3-disubstituted benzo[*b*]furans **256** by electrophilic cyclization.¹¹⁵

¹¹⁵ Yue, D.; Yao, T.; Larock, R. C. *The Journal of Organic Chemistry* **2005**, *70* (25), 10292-10296.

Based on this work, we attempted to use an iodine source such as I_2 or ICl instead of mercury. In both conditions, we did not observe any iodocyclization product. Indeed, with iodine, the product degraded and with ICl we could only observe the formation of compound **257**. This could be explained by the presence of the methoxy group in para which could increase the electron density on the distal end of the triple bond and favor the electrophilic attack at that position, disfavoring a 5-*endo*-dig cyclization. This leads to addition of the electrophile to the triple bond rather than cyclization. This reaction was observed by Larock's team in couple of similar substrates.

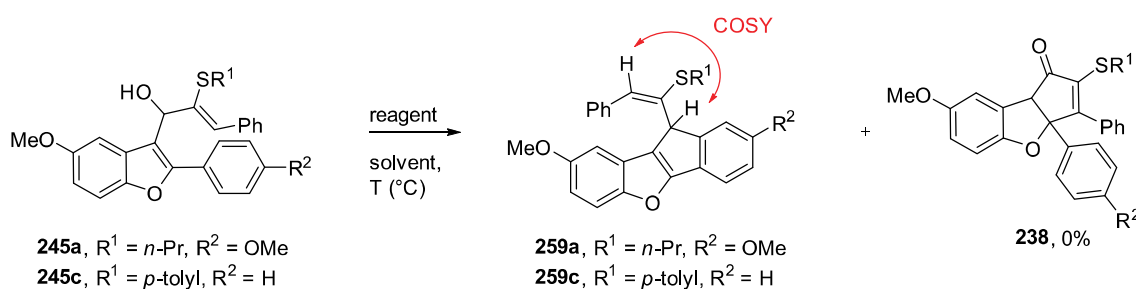


Scheme 82 | Attempt of iodocyclization of compound **258**.

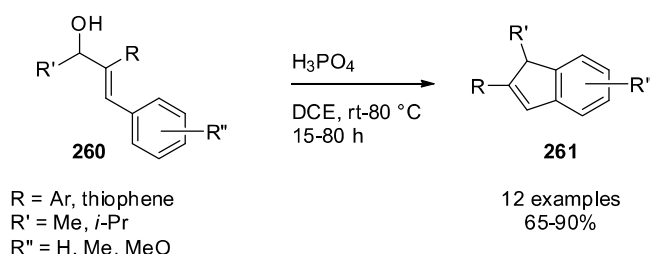
Unsuccessful iodocyclization and low yields of the first approach did not allow us to continue the synthesis of the new class of substrate for the Nazarov reaction. Moreover, as indicated in section 3.2.2 that Nazarov reaction mediated with acetyl bromide was not promising, therefore we decided not to pursue this approach.

3.2.4 Unexpected Friedel-Crafts reaction

While working on the Nazarov reaction, we also examined the cyclization starting from alcohols **245** (Scheme 83). Unexpectedly, instead of obtaining the cyclopentenone **238**, we were able to isolate the tetracyclic product **259**.


Scheme 83 | Unexpected Friedel-Crafts reaction on benzofurans **245**.

Such compounds are poorly described in the literature. This type of intramolecular Friedel-Crafts reaction was described by Lautens *et al.* starting from benzylidene alcohol **260** to form indenenes **261** in the presence of a Lewis or Brønsted acids (Scheme 84).¹¹⁶


Scheme 84 | Lautens' synthesis of indenenes **261**.¹¹⁶

The formation of the tetracyclic product was observed in three different conditions: Re₂O₇/MeOH or Ar-B(OH)₂ in 1,2-dichloroethane¹¹⁷ or (COCl)₂, Et₃N in DMSO (Table 15). The reaction gave better yield starting from alcohol **245c** substituted by the *p*-tolyl group.

Table 15 | Optimization of the Friedel-Crafts reaction.

Entry	245	Reagents	Solvent	T (°C)	259 (%) ^a
1	245a	Re ₂ O ₇ , MeOH	DCE	45	259a , 46
2	245a	Ar-B(OH) ₂	DCE	50	259a , 57
3	245c	Ar-B(OH) ₂	DCE	50	259c , 68
4	245c	DMSO, Et ₃ N	CH ₂ Cl ₂	-78	259c , 69

Ar-B(OH)₂ = (2,3,4,5-tetrafluorophenyl)boronic acid, ^a isolated yields.

As far as we know, such a reaction was never reported for the synthesis of dihydrobenzindeno furan.

¹¹⁶ Panteleev, J.; Huang, R. Y.; Lui, E. K. J.; Lautens, M. *Organic Letters* **2011**, 13 (19), 5314-5317.

¹¹⁷ Zheng, H.; Lejkowski, M.; Hall, D. G. *Tetrahedron Letters* **2013**, 54 (1), 91-94.

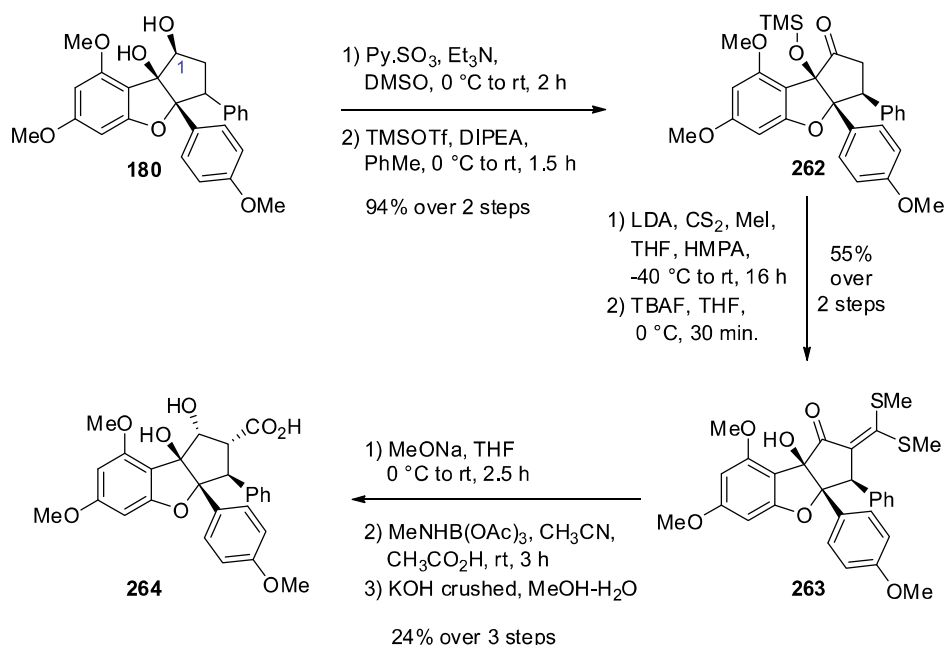
3.3 Synthesis of pharmacochemical tools

3.3.1 Synthesis of a fluorescence probe of a flavagline

The team of Prof. Bruce Zetter at Harvard recently identified a mechanism of chemoresistance involving prohibitin-1.¹¹⁸ To further characterize the mechanism, we synthesized a flavagline combined to a fluorophore via a polar spacer group that cannot rapidly penetrate into the cells. This new probe was designed to selectively target the overexpression of PHB1 on the surface of cells resistant to taxotere.

Several probes are described in the literature. We chose the sulforhodamine B which has been extensively used for conjugation with biomolecules because of its excellent fluorescence properties and high solubility in water to prevent its passive diffusion across the plasma membrane. Sulforhodamine B is a red fluorescent dye (excitation/emission maxima \approx 565/586 nm). Such red emission dyes generate a minimum of phototoxicity and are not sensitive to cell autofluorescence due to biological molecules.

We synthesized rocaglaic acid (**264**) starting from rocaglaol (**180**) based on Taylor synthesis (Scheme 85).¹¹⁹

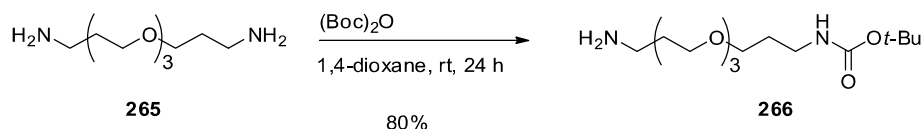


Scheme 85 | Synthesis of rocaglaic acid (**264**).

¹¹⁸ Patel, N.; Chatterjee, S. K.; Vrbanac, V.; Chung, I.; Mu, C. J.; Olsen, R. R.; Waghorne, C.; Zetter, B. R. *Proceedings of the National Academy of Sciences* **2010**, *107* (6), 2503-2508.

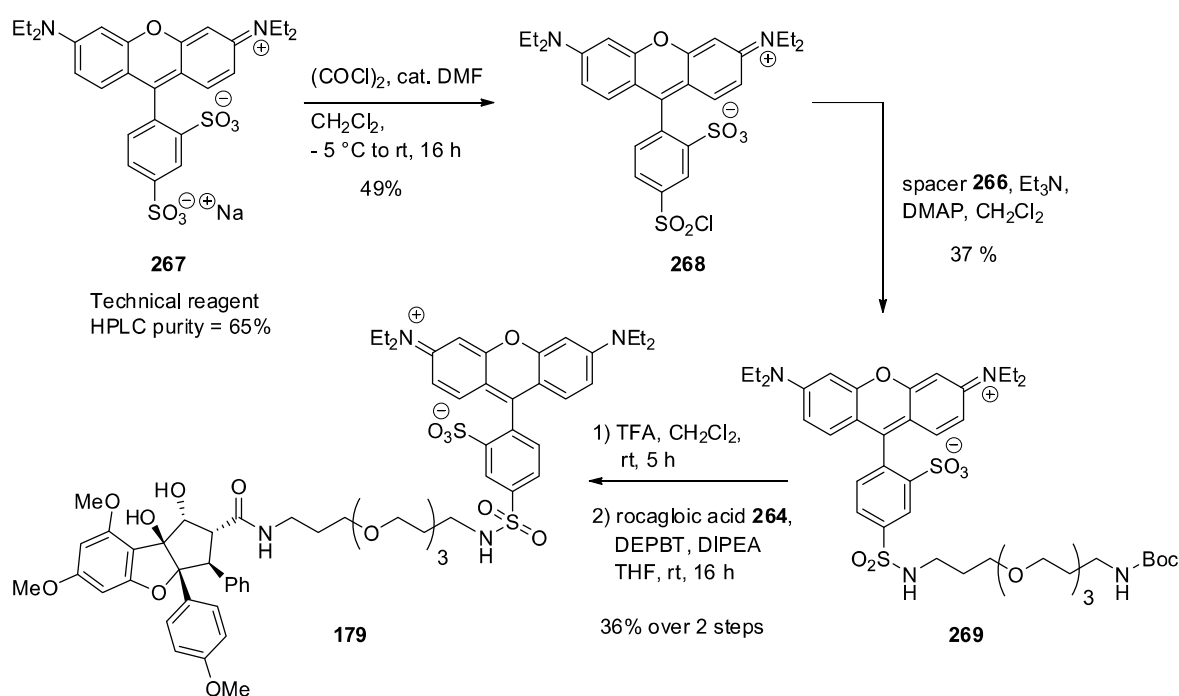
¹¹⁹ Davey, A. E.; Schaeffer, M. J.; Taylor, R. J. K. *Journal of the Chemical Society, Perkin Transactions 1* **1992**, (20), 2657-2666.

The alcohol in position 1 was oxidized with $\text{Py}\cdot\text{SO}_3$, Et_3N in DMSO and the second alcohol was protected by a trimethylsilyl group with 94% yield over 2 steps (Scheme 85). The successive addition of disulfide and iodomethane, followed by deprotection of the silyl group afforded the intermediate **263**. Treatment with sodium methoxide gave access to β -keto ester which was then converted to the rocaglaic acid (**264**) in 2 steps with 24% yield.



Scheme 86 | Protection of the spacer **266**.

We then used a polyethyleneoxy spacer (PEO, **265**), which was first monoprotected. While carboxybenzyl group gave a mixture of mono- and di-protected product, *tert*-butyloxycarbonyl group gave desired compound **266** with 80% yield (Scheme 86). Then, the fluorophore **267** was activated by oxalyl chloride to give the rhodamine sulfonyl chloride **268** in 49% yield (Scheme 87). The average yield is due to the concomitant formation of the product activated in the ortho position (7%), the deactivated product (5%) and the hydrolyzed product (5%) along with some other compounds which may come from the impurities present in the commercial product (HPLC purity 65%).



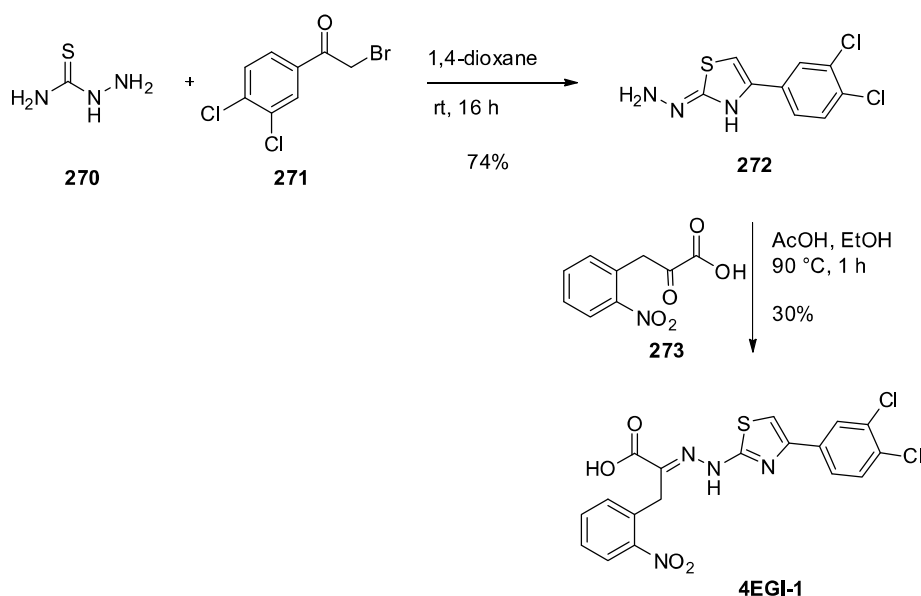
Scheme 87 | Synthesis of fluorescence probe **179**.

To finalize the synthesis of the probe, the activated sulforhodamine **268** was coupled to the spacer **266** with 37% yield. After deprotection with TFA, the over extremity of the spacer was coupled to the rocaglaic acid (**264**) using DEPBT as a coupling agent¹²⁰ to afford the fluorescent probe **179** with 36% yield after semi-preparative HPLC purification.

This fluorescence probe is currently used by Prof. Bruce Zetter group to decipher the signaling of prohibitins (PHB). Preliminary results have already helped to highlight a new mechanism by which flavaglines selectively induce cytotoxicity in cancer cells.

3.3.2 Synthesis of inhibitors of eIF4A

In their study of the effect of flavaglines on the inhibition of eIF4A in chemoresistant melanoma, our collaborators wanted to compare the effects of different classes of eIF4A inhibitors. Therefore, we prepared 4EGI-1, a synthetic molecule, developed by Wagner G. and coll. from Harvard University that modulates the growth of certain type of cancers by inhibiting eIF4E (eukaryotic translation initiation factor 4E). We synthesized this inhibitor based on the literature (Scheme 88).¹²¹



Scheme 88 | Synthesis of **4EGI-1**.

¹²⁰ Ye, Y.-h.; Li, H.; Jiang, X. *Peptide Science* **2005**, *80* (2-3), 172-178.

¹²¹ Aktas, H.; Chorev, M.; Halperin, J.; Moerke, N.J.; Wagner, G. *WO2006078942 A3*

The thiosemicarbazide **270** reacted with the phenylacetyl bromide **271** to give the thiazol-2-yl-hydrazine **272** with 74% yield (Scheme 1) which after condensation with the oxopropionic acid **273** afforded the desired hydrazone **4EGI-1**.

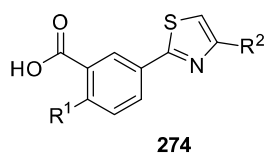
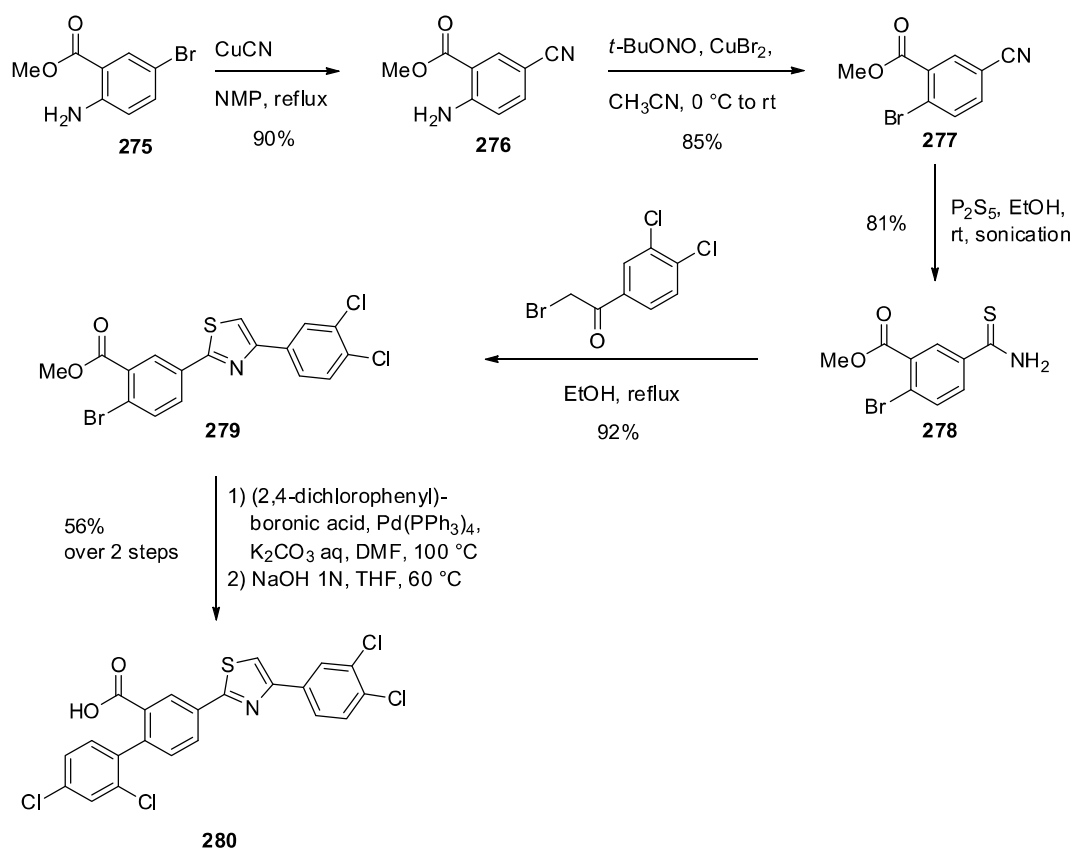


Figure 9 | General structure of benzoic acid derivatives **274** developed by Hoffman-LaRoche.

In this class of inhibitors, we also prepared a benzoic acid derivative of general structure **274** (Figure 9). Such a new series of eIF4E inhibitors was described in Hoffman-LaRoche patent in 2013.¹²¹ We chose **280** because of its low IC₅₀ (1.4 μM) and the fairly good overall yield of its synthesis (Scheme 89).



Scheme 89 | Improved synthesis of inhibitor **280**.

The first step is the substitution of the bromine of compound **275** by a cyano group (Scheme 89). We first attempted to use the conditions described in the patent, *i.e.* the use of CuCN(I) as the cyanation reagent, but we only isolated 5% of the cyano derivative **276** (entry 1, Table 16) instead of the 73% announced. We then replaced the cyanation reagent by Zn(CN)₂ in the presence of a catalytic amount of palladium(0) triphenylphosphine tetrakis. These conditions yielded to a mixture of starting material and desired product **276** in a 40/60 ratio based on ¹H NMR (entry 2). Neither increasing the amount of reactants, the reaction time or temperature led to a total conversion of the starting material. Using CuCN and changing the work up by warming the reaction mixture to 60 °C for 1.5 h in an aqueous solution of FeCl₃ and concentrated HCl increased the yield to 90% (entry 3). Indeed, ferric chloride has been shown by Friedman and Shechter to destroy the reaction complexes formed in dimethylformamide during the reaction.¹²²

Table 16 | Optimization of the cyanation of compound **275**.

Entry	Reagent	Work up	275 (%) ^a	276 (%) ^a
1	CuCN	Ethylenediamine, H ₂ O	2	5
2	Zn(CN) ₂ , Pd(PPh ₃) ₄	H ₂ O	40 ^a	60 ^a
3	CuCN	FeCl ₃ / HCl conc., H ₂ O	0	90

^a Isolated yields, ^b yields based on ¹H NMR.

After the substitution of the amine by a bromine group via a diazonium, the cyano derivative **277** was converted into a thioamide with phosphorous pentasulfide using the conditions described in the patent. However, we noticed an inconsistency between the amount of P₂S₅ expressed in grams or in moles. Based on the literature, we started with 0.5 equivalent of P₂S₅, and then we continued adding the reagent by portions until total conversion of the starting material, which took a total of 2.5 equivalents. We isolated the thioamide with 81% yield. Alkylation with bromoacetophenone afforded compound **279** with 92% yield.

¹²² Friedman, L.; Shechter, H. *The Journal of Organic Chemistry* **1961**, 26 (7), 2522-2524.

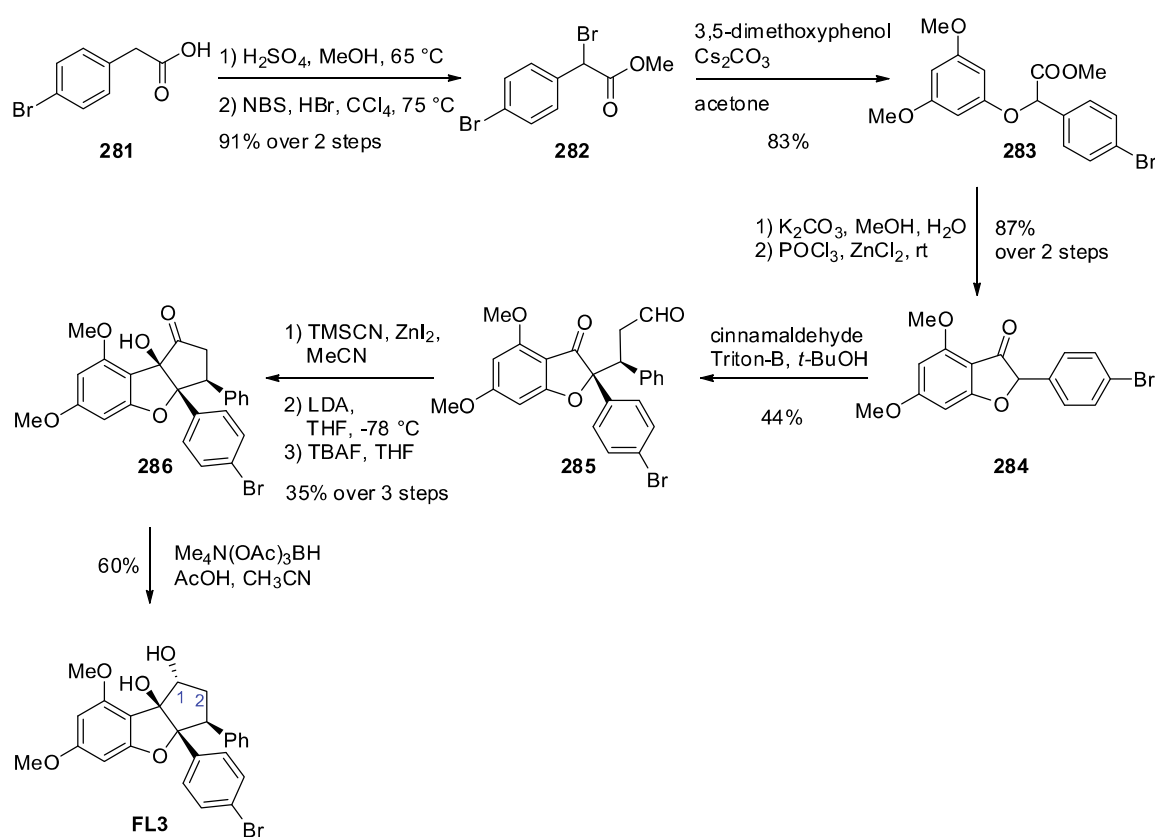
The last steps are the Suzuki coupling and the hydrolysis. In the patent, these two reactions were realized in one-pot. To make sure that all the traces of palladium were removed, we decided to isolate the product of the Suzuki coupling prior to saponification. The product of the Suzuki coupling, obtained with 70% yield after a silica gel chromatography was hydrolyzed with an aqueous solution of NaOH 1N to afford the carboxylic acid **280** with 77% yield. The latter was recrystallized in CH₂Cl₂ prior to being used for biological tests.

Using a bicistronic luciferase reporter construct (pR-HepC-L) assay, compound **280** did not display any inhibition of cap-dependent translation. This observation is in contrast with the reported activity of **280** in Hoffmann-La Roche patent. This work was published in *Anticancer Agents in Medicinal Chemistry*, **2015**, *15*, in press (see publication n°4, page 305).

3.3.3 Synthesis of flavagline FL3

In order to examine the anticancer effects of **FL3** in a mouse model of chemoresistant melanoma, a stock of **FL3** was synthesized in a sufficient amount to perform these *in vivo* assays.

FL3 was synthesized by Dobler's approach¹²³ which is the most convenient to prepare flavaglines unsubstituted in position 2 (Scheme 90) with benzofuranone **284** as a key intermediate.



Scheme 90 | Synthesis of **FL3** based on Dobler's procedure.¹²³

The synthesis of **FL3** starts with an esterification of carboxylic acid **281** followed by bromination using NBS. Nucleophilic substitution with 3,5-dimethoxyphenol followed by saponification and intramolecular Fiedel-Crafts cyclization afforded benzofuranone **284** with 72% over 3 steps. A Michael addition between benzofuranone **284** and cinnamaldehyde in

¹²³ Dobler, M. R.; Bruce, I.; Cederbaum, F.; Cooke, N. G.; Diorazio, L. J.; Hall, R. G.; Irving, E. *Tetrahedron Letters* **2001**, 42 (47), 8281-8284.

the presence of Triton B gave aldehyde **285**. Cyanosilylation of aldehyde **285** with trimethylsilyl cyanide afforded protected cyanohydrin which was then engaged in the cyclization with LDA. After deprotection with TBAF, ketone **286** was isolated with 35% yield over 3 steps. The latter is then diastereoselectively reduced with tetramethylammonium triacetoxyborohydride to afford desired **FL3**.

About half of the patients that suffer from metastatic melanoma harbor a mutation of the kinase BRAF V600 that leads to its constitutive activation. Vemurafenib which is now in clinical use and PLX 4720 (currently in clinical trial) specifically inhibit this mutated kinase. Unfortunately for most patients, a resistance to these treatments rapidly occurs before one year. Our collaborators, Dr. Caroline Robert, Dr. Stephan Vagner and colleagues at Gustave Roussy Institute, analyzed how this resistance occurs. They identified three major mechanisms: overactivation of C-Ras, activation of the ERK-independent PI(3)K–AKT–mTOR pathway, and down-regulation of BMF (BCL2-modifying factor) leading to down-regulation of caspases, which degrade the eIF4F complex (Figure 10).¹²⁴ These three different pathways all converge towards an up-regulation of eIF4F.¹²⁵

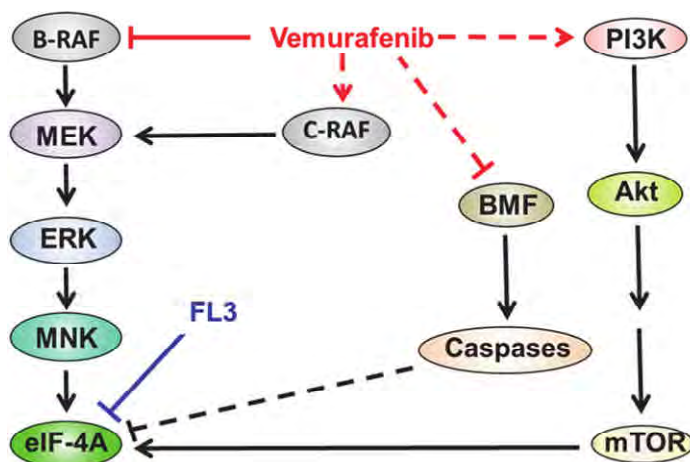


Figure 10 | The three major mechanisms for resistance to anti-BRAF treatment converge to the overactivation of eIF4A.¹²⁴

¹²⁴ (i) Boussemaert L., Malka-Mahieu H., Girault I., Hemmingsson O., Allard D., Tomasic G., Thomas M., Ribeiro N., Thuaud F., Basmadjian C., Mateus C., Routier E., Kamsu-Kom N., Agoussi S., Eggermont A., Désaubry L., Robert C., Vagner S. *Nature* **2014**, *513*, 105-109. (ii) Lito, P.; Rosen, N.; Solit, D. B. *Nat Med* **2013**, *19* (11), 1401-1409. (iii) Levy, J. M. M.; Thompson, J. C.; Griesinger, A. M.; Amani, V.; Donson, A. M.; Birks, D. K.; Morgan, M. J.; Mirsky, D. M.; Handler, M. H.; Foreman, N. K.; Thorburn, A. *Cancer Discovery* **2014**, *4* (7), 773-780. (iv) Tentori, L.; Lacal, P. M.; Graziani, G. *Trends in Pharmacological Sciences* **2013**, *34*, 656-666.

¹²⁵ (i) Blagden, S. P.; Willis, A. E. *Nat Rev Clin Oncol* **2011**, *8* (5), 280-291. (ii) Silvera, D.; Formenti, S. C.; Schneider, R. J. *Nat Rev Cancer* **2010**, *10* (4), 254-266.

Using the inhibitor 4EGI-1, our collaborators showed that the formation of the eIF4F complex is directly involved in sensitivity to vemurafenib. Therefore, it was hypothesized that inhibiting eIF4F could relieve the resistance to anti-BRAF and/or anti-MEK therapies. For this purpose, a series of synthetic flavaglines were evaluated for their capacity to inhibit eIF4A activity. The results showed that an eIF4A inhibitor, such as FL3, in combination with vemurafenib has a synergistic effect on the proliferation of Mel624 cells. Moreover, experiments in xenograft mice were performed with FL3, and showed that this compound could relieve the resistance to anti-BRAF treatments (Figure 11 and publication n°5, page 311 for more details).¹²⁴ⁱ

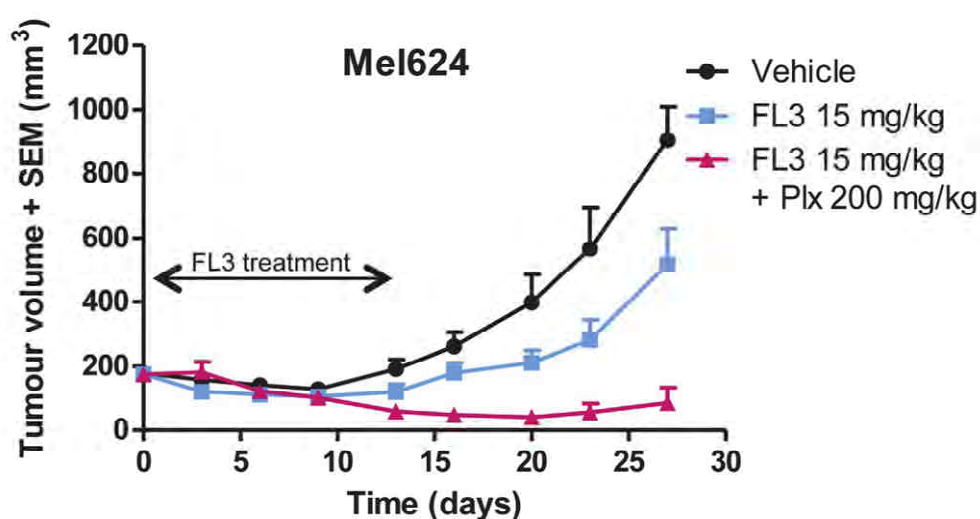


Figure 11 | Growth of Mel624 xenografts in mice treated with vehicle, FL3 and/or PLX 4720 (vehicle and PLX 4720 displayed identical effects).¹²⁴ⁱ

In addition, the synthesized flavagline **FL3** was used by other collaborators to show its action on prohibitines in areas not directly related to oncology. Indeed, Professor Duncan Smith at Mahidol University in Thailand showed that the Chikungunya virus (CHIKV) uses PHB1 as a co-receptor to enter the interior of the cells. This team has recently shown that flavaglines such as **FL3** significantly decrease the internalization of the receptor (see publication n°6, page 331).¹²⁶

¹²⁶ Wintachai, P.; Thuaud, F.; Basmadjian, C.; Roytrakul, S.; Ubol, S.; Désaubry, L.; Smith, D. R. *Microbiology and Immunology* **2015**, 59 (3), 129-141.

Moreover, the team of Prof. Joost GJ Hoenderop at Radboud University in Nijmegen (Netherlands) with whom we collaborate focuses his work on magnesium channels TRPM6 and TRPM7. This team recently showed that the PHB2 inhibits the activity of TRPM6 channel and that flavaglines such as **FL3** relieve this inhibition.¹²⁷ No other compound tested in this laboratory presents such pronounced effect. This study has provided insight into the mechanisms of regulation of this receptor, confirming the involvement of insulin signaling (see publication n°7, page 347).

¹²⁷ Blanchard, M. G.; de Baaij, J. H. F.; Verkaart, S. A. J.; Lameris, A. L.; Basmadjian, C.; Zhao, Q.; Désaubry, L.; Bindels, R. J. M.; Hoenderop, J. G. J. *PLoS ONE* **2015**, *10* (3), e0119028.

3.4 Synthesis of an isostere of flavaglines

Instead of having an OH in position 1, pharmacologically active **FL23** and aglaiformosanin have a formylamino or an sp^2 nitrogen, which implies that the hydroxyl found in most of the flavaglines could be replaced by another polar group (Figure 10). We have made the hypothesis that **FL46** (Scheme 91), which displays these structural features, should also be active. Such compounds which are called isosteres could potentially display enhanced bioavailability and pharmacodynamic properties.

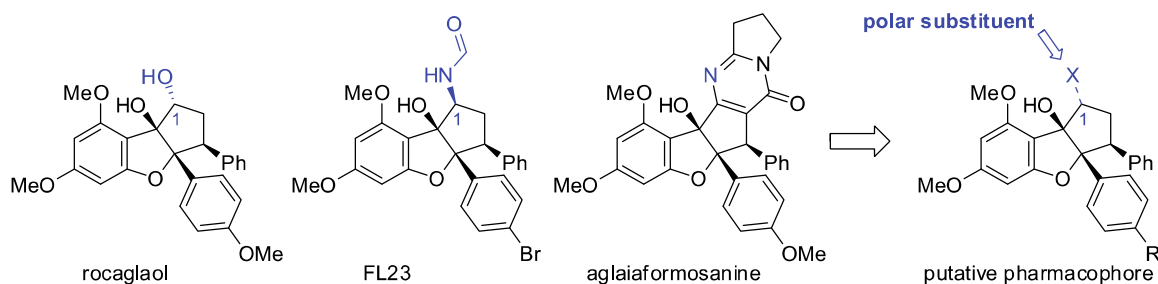
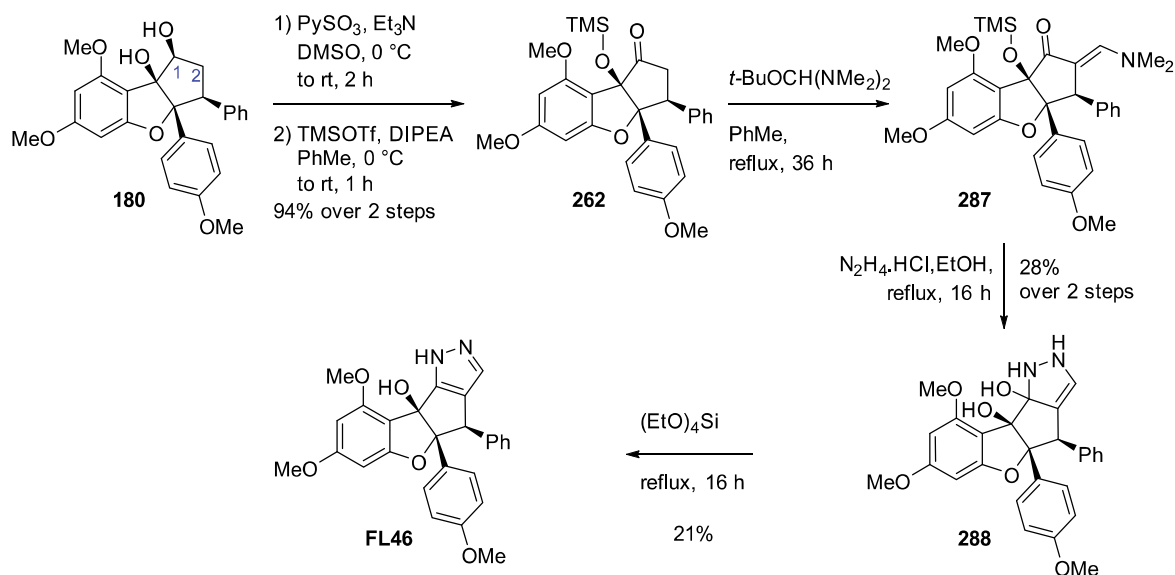


Figure 12 | Flavaglines and their putative pharmacophore.

The strategy to synthesize the pyrazoline isostere of flavaglines is based on the cyclocondensation of enaminone **287** with hydrazine (Scheme 91).



Scheme 91 | Synthesis of pyrazoline isostere **FL46**.

Parikh-Doering oxidation of rocaglaol **180** and protection of the tertiary alcohol with a trimethylsilyl group permitted the modification at the position 2 of the cyclopentenone **262** with 94% yield over 2 steps (Scheme 91). The latter was converted to the enaminone using Brederick's reagent ($t\text{-BuOCH}(\text{NMe}_2)_2$). Condensation with hydrazine surprisingly afforded the hydrate of **288**. Dehydration of the heterocycle was achieved with tetramethoxysilane in only 21% yield.

Unfortunately, **FL46** displayed a poor cytotoxicity on two cell lines (HEP2 and 789-0) compared to **FL23** used as a reference (Figure 13). Due to this unexpected loss of pharmacological activity, we did not try to synthesize other analogs of this series.

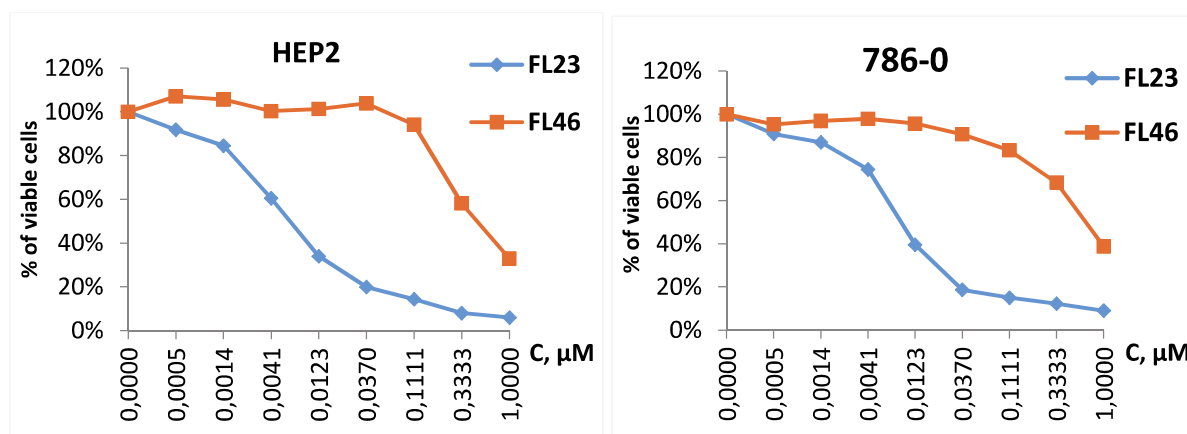
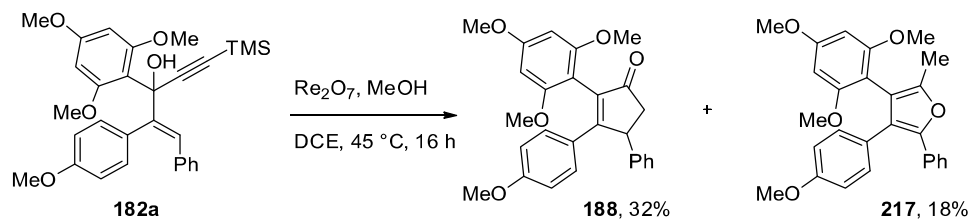


Figure 13 | Cytotoxicity of **FL23** and **FL46** in HEP2 and 789-0 cell lines.

3.5 Rearrangements of 1-styryl propargyl alcohols

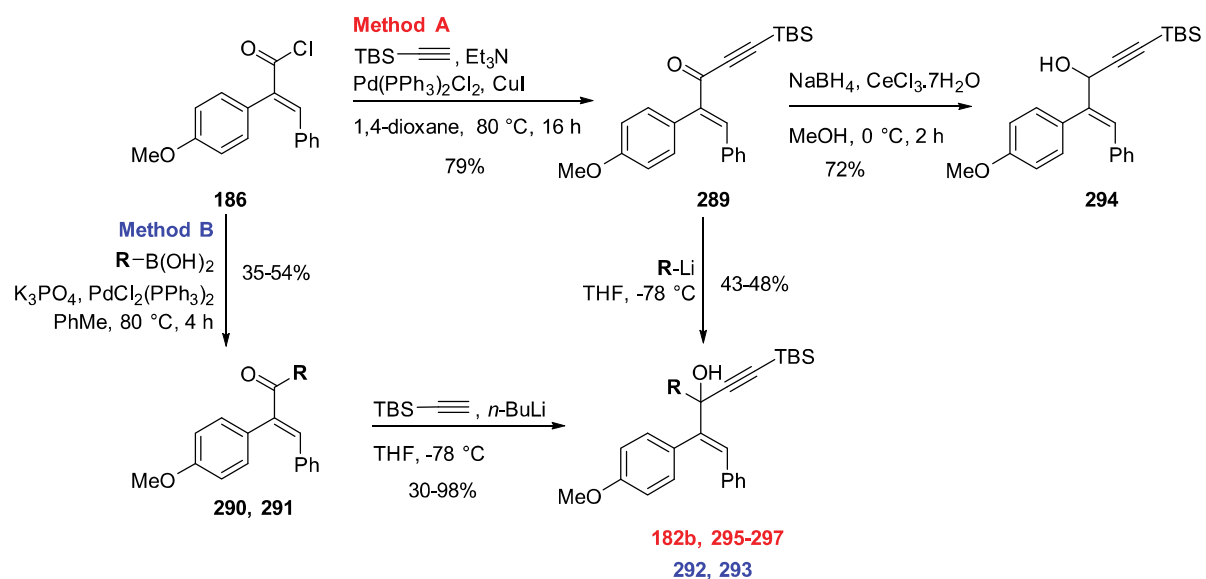
3.5.1 Preparation of 1-styryl propargyl alcohols

In the course of our research, as seen in section 3.1.2, we serendipitously discovered novel rhenium-catalyzed rearrangements starting from enynol **182a** and giving access to a mixture of cyclopentenone **188** and methylfuran **217** (Scheme 92).



Scheme 92 | Discovered novel rhenium-catalyzed rearrangements of enynol **182a**.

In order to study the scope and limitations of this rearrangement, various 1-styryl propargyl alcohols were prepared following two methods. As seen in the beginning of this chapter, acyl chloride **186** was prepared quantitatively from the corresponding carboxylic acid which was obtained stereoselectively by Perkin reaction. Following method A, acyl chloride **186** reacted with *tert*butyldimethylsilyl acetylene by Sonogashira coupling to afford propargyl ketone **289** in 79% yield (Scheme 93). Alkylation via a lithiated derivative gave access to propargyl alcohols **182b**, **295-297**. This method could not give access to carbinol **292** and **293** as the first alkylation step was unsuccessful. Therefore, a second method was used starting with a Suzuki coupling of the acyl chloride **186** with different boronic acids to obtain allylic ketone **290** and **291**. Alkylation with lithiated *tert*butyldimethylsilyl acetylene afforded propargyl alcohols **292** and **293**. Finally, carbinol **294** was obtained via reduction of ketone **289** with 72% yields in Luche conditions.



Scheme 93 | Methods to prepare various propargyl alcohols **182b**, **192-197**.

3.5.2 Study of the scope and limitations

As presented in section 3.1.2, starting from propargyl alcohol **20**, we were able to isolate cyclopentenone **2** (44%) along with methylfuran **27** (27%, Table 17, entry 1).

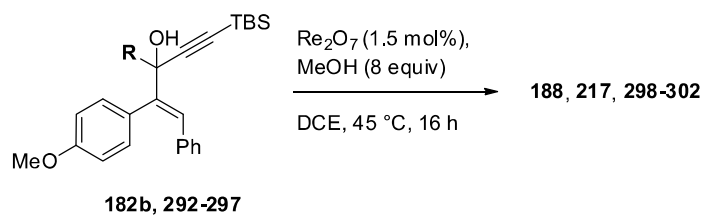


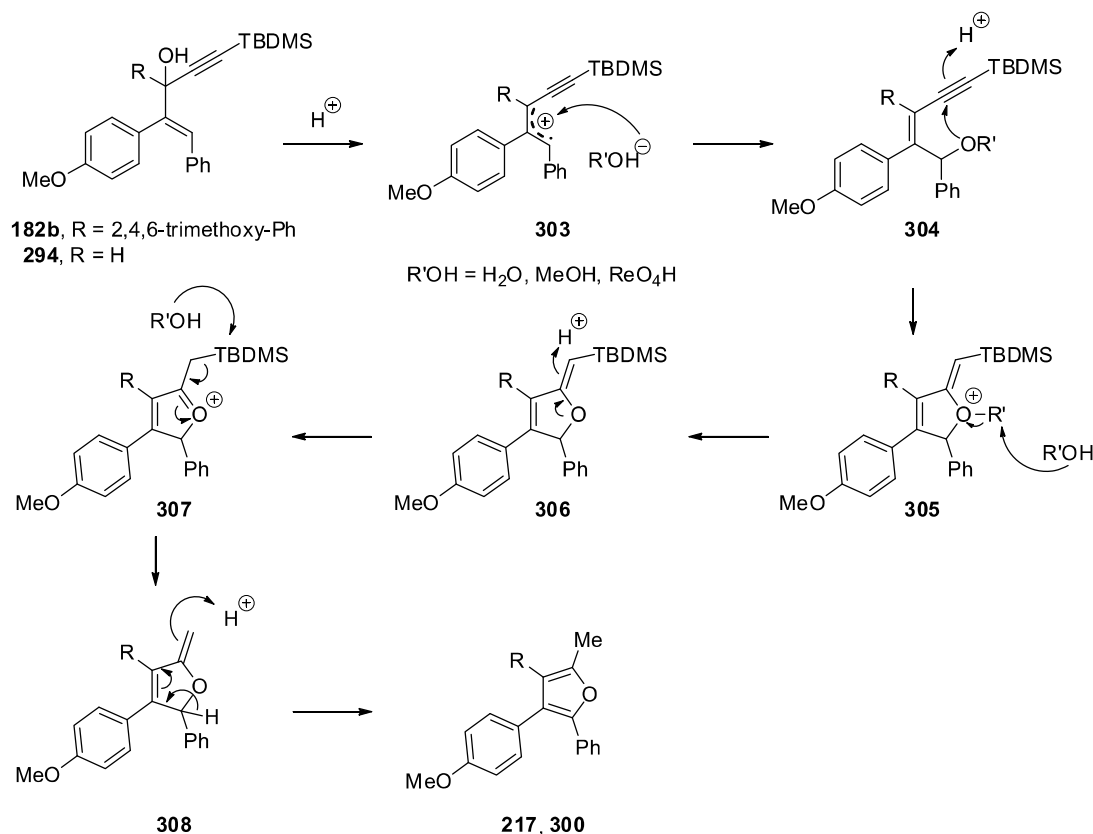
Table 17 | Rhenium oxide-mediated rearrangement of 1-styryl propargyl alcohols **182b**, **292-297**.

Entry	R	Method	Products	Yield (%) ^a
1	182b	A	188	44
			217	27
2	292	B	298	20
3	293	B	299	35
4	H	294	300	54
5	295	A	301	47
6	296	A	302	31
7	297	A	Mixture of uncharacterized products	

An = anisyl, ^a isolated yields.

The proposed mechanism for the formation of the cyclopentenone **188** was already depicted in Scheme 65 (chapter 3.1.2). We hypothesized here a mechanism for the

formation of the methylfuran **217** through the same stabilized carbocation intermediate which reacts with an oxygenated nucleophile to form the intermediate **304**. Oxo-cyclization generates oxonium **305**. Nucleophilic attack of ROH cleaves the *R*-O bond giving intermediate **306** converted to oxonium **307**. This intermediate was desilylated with the assistance of ROH giving alkene **308** which rearranged to form furan **217**. In this case ($R = H$), a similar product was isolated with formation of methylfuran **300** with 54% yield (Table 17, entry 4).



Scheme 94 | Postulated mechanism for the formation of furan **217** and **300**.

Replacing the highly electron-donating 2,4,6-trimethoxy groups by a 4-chloro group reduced the yield of cyclopentenone formation to 20% (entry 2, Table 17). No furan or other compound could be isolated. Next, we turned to the examination of substrate **293**, whose unsubstituted phenyl group stabilizes even less the carbocationic intermediate. Unsurprisingly, we could not detect any cyclopentenone. Instead, we were amazed to isolate ketone **299**. Indeed, 4,4-diarylnaphthalen-1-ones are highly unusual compounds,

whose synthesis is poorly described.¹²⁸ The structure of **299** was confirmed by NOE and key HMBC correlations (Figure 14). There is indeed a NOE correlation between H² (δ 4.91 ppm) and H³ (δ 7.18 ppm) and HMBC correlations between C¹ (δ 206.7 ppm) and H¹ (δ 1.65 ppm), and between H² (δ 4.91 ppm) and C² (δ 1.65 ppm).

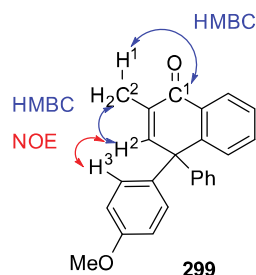
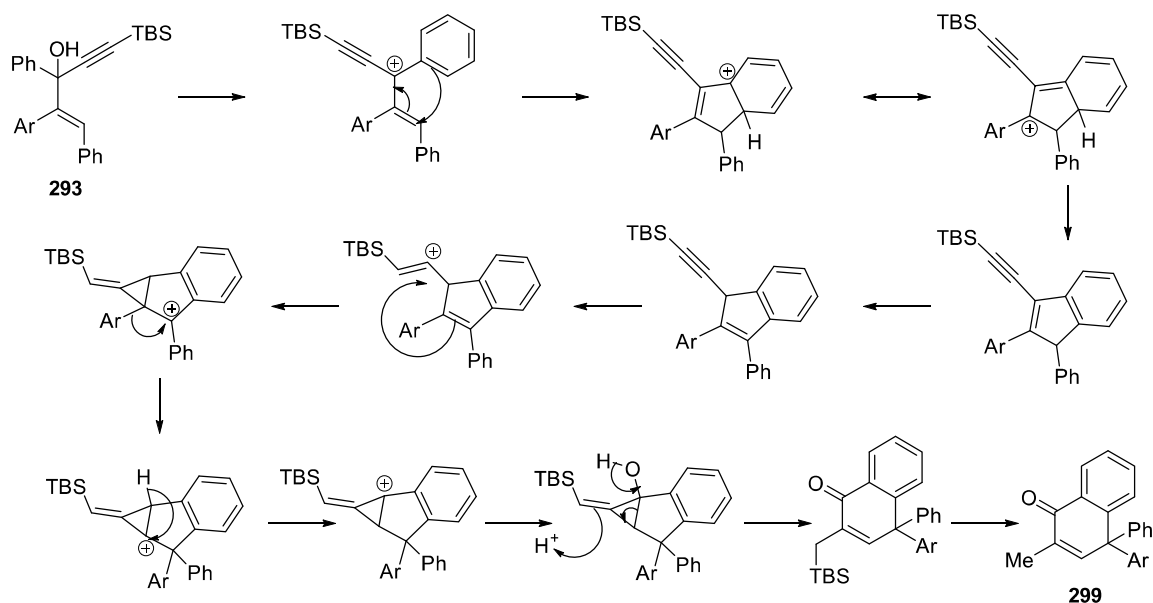


Figure 14 | HMBC and NOESY correlation of methylnaphthalenone **299**.

We hypothesized without any experimental support, a highly speculative mechanism for the formation of this unexpected methylnaphthalenone **299** depicted in Scheme 95.

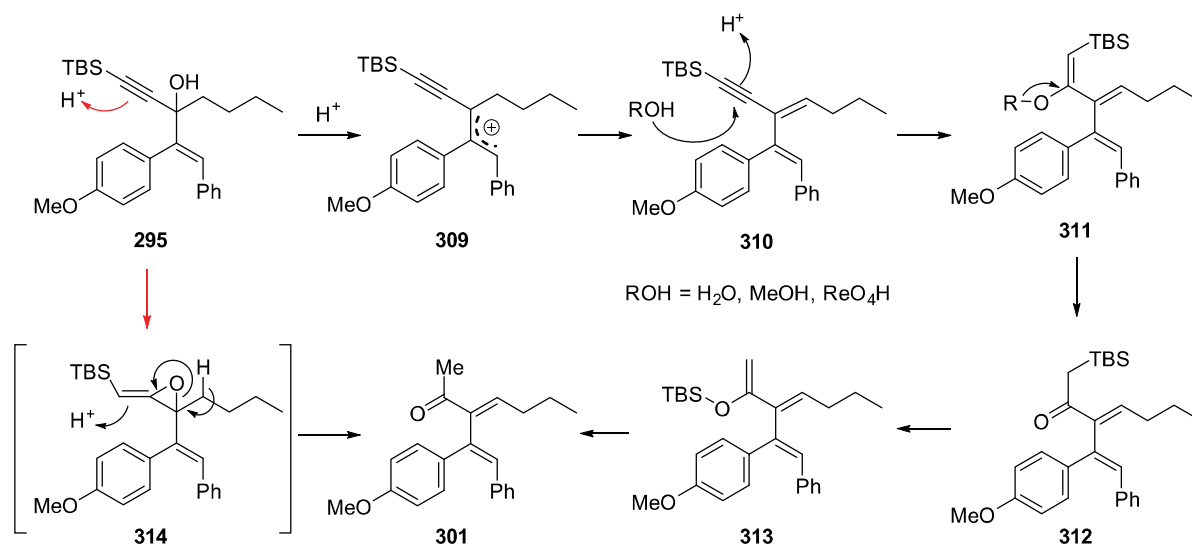


Scheme 95 | Speculation on the mechanism of formation of methylnaphthalenone **299**.

When the substrate is substituted by *n*-butyl group, interestingly, acyclic enone **301** was obtained with 47% yield (Table 17, entry 5). The postulated mechanism is described below (Scheme 96). After formation of the stabilized carbocation **309**, attack of a nucleophilic

¹²⁸ Terao, Y.; Kametani, Y.; Wakui, H.; Satoh, T.; Miura, M.; Nomura, M. *Tetrahedron* **2001**, *57* (28), 5967-5974.

species gives intermediate **311**. Cleavage of the R-O bond leads to enone **313**. Finally Brook's rearrangement followed by desilylation affords enone **301**. It could also be envisioned that compound **311** could arise from the rearrangement of an allene oxide intermediate **314**.



Scheme 96 | Postulated mechanism for the formation of acyclic enone **301**.

The structure of ketone **301** was confirmed by NMR 2D experiment (Figure 15). NOESY correlations were observed between H¹ (δ 6,832 ppm) and H² (δ 2,163 ppm), and also between H³ (δ 2,381 ppm) and H⁴ (δ 6,422 ppm).

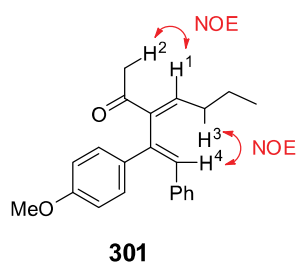
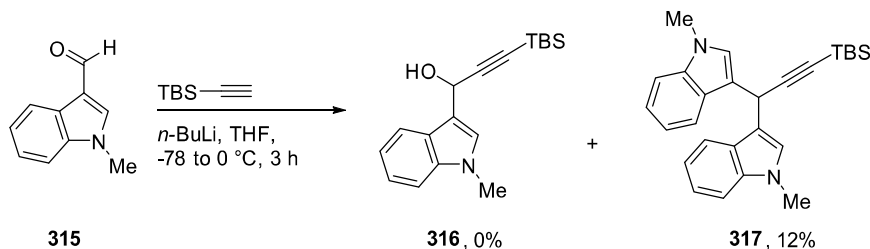


Figure 15 | HMBC and NOESY correlation of acyclic enone **301**.

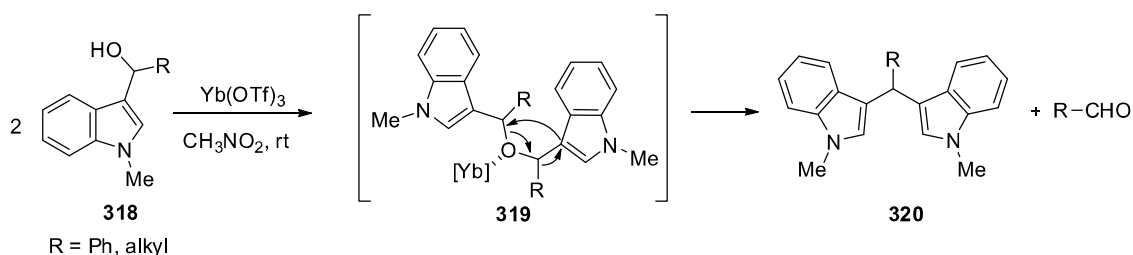
When propargyl alcohol **296** was substituted by *tert*-butyldimethylsilyl acetylenide, no cyclization was observed. The only isolated compound was the product of allyl rearrangement **302** obtained with 31% yield (Table 17, entry 6). With a 2-furyl substituted substrate **297**, only a mixture of unidentified products was obtained (entry 7).

We then decided to change the substituents in the vinylic position. In the first example (Scheme 97), we aimed to prepare propargyl alcohol **316** by alkylation of aldehyde **315** with lithiated *tert*-butyldimethylsilyl acetylenide. However, the only product isolated was the diadduct **317** with 12% yield. As we did not obtain the desired alcohol **316**, we have not been able to examine its reactivity with Re_2O_7 .



Scheme 97 | Attempt to synthesis carbinol **316**.

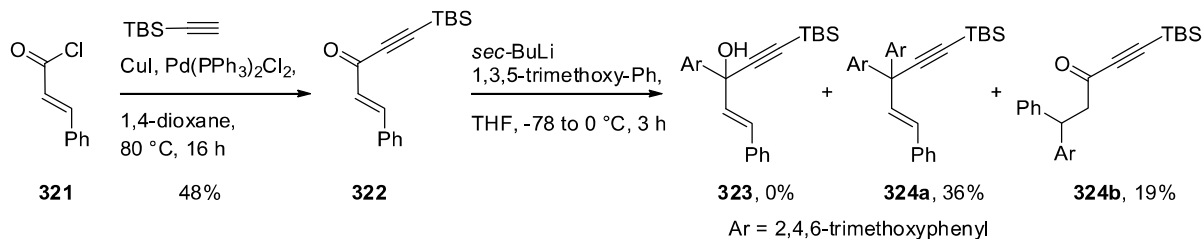
This type of reaction has been recently described by Ramasastry *et al.*, but in the presence of $\text{Yb}(\text{OTf})_3$ as a catalyst.¹²⁹ As depicted in Scheme 98, the mechanism involves the formation of symmetric ether intermediate **319** promoted by a Lewis acid. Allylic migration of indole gives access to diheteroarylalkane **320**.



Scheme 98 | Synthesis of diheteroarylalkane **320** described by Ramasastry *et al.*¹²⁹

In the second example (Scheme 99), cinnamoyl chloride **321** underwent a Sonogashira coupling reaction followed by an alkylation with lithiated trimethoxybenzene. Unfortunately, we did not get the expected alcohol **323**, but instead diadduct **324** was isolated with 36% yield. The mechanism of this reaction may be similar to the one involved in the formation of compound **317** (Scheme 97).

¹²⁹ Dhiman, S.; Ramasastry, S. S. V. *Organic & Biomolecular Chemistry* **2013**, *11* (46), 8030-8035.

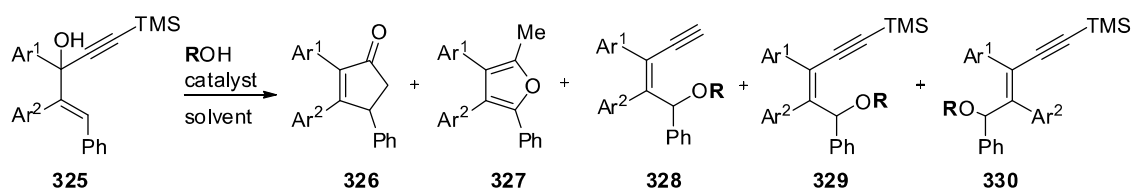


Scheme 99 | Attempt to synthesis carbinol **323**.

Out of the seven substrates tested for their reactivity in the presence of rhenium oxide, only two led to the formation of a cyclopentenone as originally expected. Other substrates were generated such as furan **300**, enone **301**, allyl ether **302**, and methylnaphthalenone **299**. These unexpected results illustrate the versatility of the mechanisms involved after activation of propargyl alcohols by rhenium oxide. The formation of the naphthalenone **299** is the most troubling, because it suggests a cascade of reactions, which to our knowledge has not been described yet. In the absence of any experimental evidence, any rationalization mechanism would be highly speculative.

3.5.3 Optimization of the reaction

In order to improve the yields of these reactions and to gain insight in the reaction mechanisms, we explored different reaction conditions starting from alcohol **325** (Table 1). Carbinol **325** was prepared in 4 steps with 37% yields from 2-(4-chlorophenyl)acetic acid following previously described method (Scheme 48, section 3.1.2). Using Re_2O_7 (0.015 eq.), we first examined the effect of the solvent on the reaction (Table 18). Compared to THF and CH_2Cl_2 , 1,2-dichloroethane gave better yields with 31% for cyclopentenone **326** and 16% for methylfuran **327** (entry 1). Increasing the quantity of catalyst to 0.2 eq. did not lead to higher conversion. In effort to understand the role of Re_2O_7 , the catalyst was changed to $\text{ReO}_4\text{SiPh}_3$ (entry 4) and ReO_4H (entry 5). In both cases, the results are similar to those of Re_2O_7 . To confirm that the reaction is catalyzed by an acid, we used two Brønsted acids. With triflic acid (entry 7), we obtained similar yields with 36% of cyclopentenone **326** and 12% of furan **327**. When using a weaker acid such as acetic acid (entry 12) the two acyclic isomers **329** and **330** were isolated.

Ar¹ = 2,4,6-trimethoxy-PhAr² = 4-Cl-Ph**Table 18** | Optimization of the acid catalyzed rearrangements of enynol **325**.

Entry	R	Catalyst	Solvent, T(°C)	326 (%)	327 (%)	328 (%)	329 (%)	330 (%)
1	CH ₃	Re ₂ O ₇	DCE, 45	31	16	0	0	0
2	CH ₃	Re ₂ O ₇	THF, 45	11	9	0	12	0
3	CH ₃	Re ₂ O ₇	THF, rt	12	0	0	4	0
4	CH ₃	ReO ₄ SiPh ₃	DCE, 45	28	17	6	0	0
5	CH ₃	ReO ₄ H	DCE, 45	30	17	0	0	0
6	-	ReO ₄ H	DCE, 45	0	5	0	5	0
7	CH ₃	F ₃ CSO ₃ H	DCE, 45	36	12	0	0	0
8	CF ₃ CH ₃	F ₃ CSO ₃ H	DCE, 45			degradation		
9	-	F ₃ CSO ₃ H	DCE, 45			degradation		
10	CH ₃	F ₃ CSO ₃ H	CH ₃ NO ₂ , 45	30	0	0	0	0
11 ^a	CH ₃	F ₃ CSO ₃ H	CH ₃ NO ₂ , rt			degradation		
12	CH ₃	AcOH	DCE, 45	0	0	0	51	47

In the absence of methanol (entries 6 and 9), no cyclized products were isolated. Replacing methanol with trifluoroethanol only led to products of degradation. Thus, the presence of methanol seems important for the cyclization to occur, perhaps by stabilizing an intermediate. Finally, the best yield was obtained with triflic acid in 1,2-dichloroethane in the presence of methanol with 80% HPLC purity towards cyclopentenone **326** prior to purification. In these conditions, there were no traces of furan **327**. However, after silica gel chromatography, the yield dropped to 30% (entry 10). We then challenged the stability of the compound over SiO₂ but after 5 hours in saturated SiO₂, the pure cyclopentenone **326** seemed to be stable.

To better understand why the yield is so low, each step of the reaction was followed by ^1H NMR with 4,4'-di-*tert*-butylbiphenyle as an internal reference. The results are shown in Table 19.

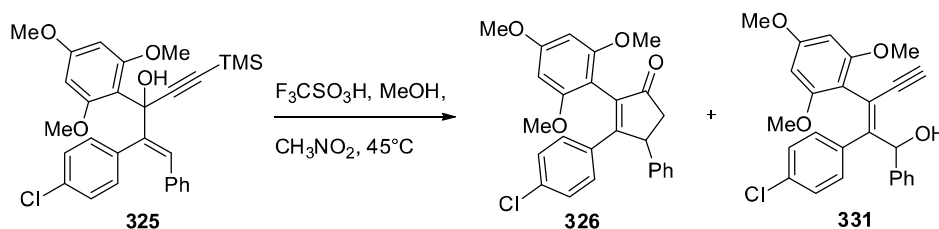


Table 19 | NMR and HPLC monitoring of the rearrangement of carbinol **325**.

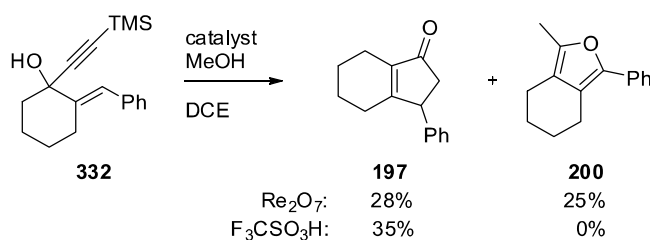
Entry	Time (h)	Sample	326 (%) ^a [%] ^b	331 (%) ^a [%] ^b
1	2	reaction mixture	20 [41]	10 [49]
		crude product	6 [41]	4 [51]
2 ^c	16	reaction mixture	12 [37]	6 [49]
		crude product	4 [40]	- [53]
3	16	crude product	10 [38]	3 [51]
		isolated product	15 ^d	7 ^d

^a yield based on ^1H NMR using 4,4'-di-*tert*-butylbiphenyle as an internal standard ^b yields based on HPLC ^c crude of entry 1 was reintroduced in the same conditions ^d isolated yield.

The reaction was first carried out in the same conditions. After 2 hours, the starting material was consumed (entry 1, Table 19). After work up, both NMR and HPLC showed the formation of the cyclopentenone as expected but also a byproduct. To be sure that the byproduct is not an intermediate of the reaction, the crude was reintroduced in the same reaction conditions (entry 2) but after 16 h at 45 °C, the ratio between **326** and the byproduct did not change. The reaction was reproduced starting from **325**. After one night, the observations were the same. These experiments show that the low yield did not come from the purification on silica gel as the percentage of the cyclopentenone **326** is already low in both the reaction mixture and the crude. A rational explanation accounting for these observations still remains unknown.

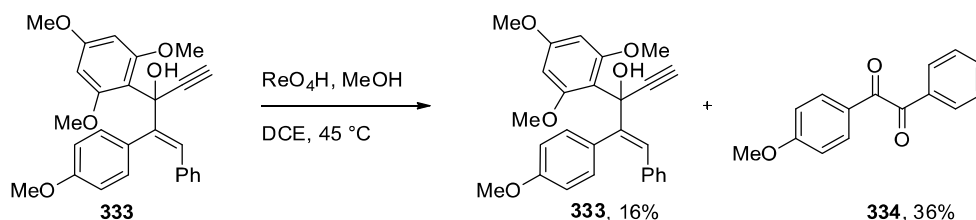
Next we examined his reaction with a very different substrate. Starting from enynol **332**, we were able to isolate 28% of cyclopentenone **197** and 25% of furan **200** in the presence of a catalytic amount of Re_2O_7 (Scheme 100). As with the previous substrate, the reaction could be performed with triflic acid promoting the obtaining of cyclopentenone **197**, which seems

to be the major product in the ^1H NMR of the crude reaction mixture. As before, after purification the yield dropped to 35%.



Scheme 100 | Rearrangement of carbinol **332**.

We then decided to see whether the presence of the silyl substituent on the alkyne was necessary. On the terminal alkyne **333**, in the presence of perrhenic acid, 16% of the starting material was recovered along with 36% of the diketone **334** (Scheme 101). No cyclization product was isolated. This observation strengthened the hypothesis that the silyl group is necessary for the cyclization.



Scheme 101 | Rearrangement of carbinol **333** with a terminal alkyne.

This optimization work showed that this rearrangement is catalyzed by a Brønsted acid such as triflic acid. We hypothesized a delicate balance among several mechanistic pathways due to a minor change of substrate in acid-catalyzed rearrangements of 1-styrylpropargyl alcohols. This work was published in *Beilstein. J. Org. Chem.* **2015**, *11*, 1017–1022 (see publication n°8, page 361).

4. CONCLUSION

4. CONCLUSION

The main objective of this research was to develop a new synthesis of flavaglines to prepare original analogs. Pursuing this goal, we established two novel methods to access advanced intermediates of flavaglines. On one hand, a tri-substituted cyclopentenone intermediate was obtained *via* an acid catalyzed-rearrangement of 1-styryl propargylic alcohol. Thus, in only 5 steps, the cyclopentenone was obtained with 13% overall yield. This approach compare favorably to reported ones (Ragot's synthesis: 6 steps, 6% yield; Trost's synthesis: 8 steps, 21% yields). The inability to apply Ragot's synthesis of flavaglines to our cyclopentenone intermediate could explain why this strategy was never reported to prepare pharmacologically active compounds. On the other hand, our second synthetic pathway gave access to the tricyclic core of the flavaglines via a key Nazarov reaction. We were able to achieve the first synthesis of a flavaglines-type product substituted with a thioether group. As the final step of this route was not reproducible, some efforts are currently made in the laboratory to explore new strategies.

During this work, different pharmacochemical tools were prepared. Thus, we synthesized a new fluorescence probe of a flavagline that is currently under study and has already shown promising results in the elucidation of prohibitin signaling pathway in cancer. Also, a flavagline originally developed in the laboratory (FL3) was re-synthesized and tested for the inhibition of eIF4A and its anticancer activities in chemoresistant metastatic melanoma. FL3 was also shown to display other pharmacological effects unrelated to cancer (regulation of TRPM6 canal and infection with the Chikungunya virus).

Another objective was to synthesis an original pyrazole isostere of flavaglines. This goal was successfully reached but unfortunately, this compound displayed a poor cytotoxicity compare to pharmacologically active FL23.

Finally, an unexpected of 1-styryl propargylic alcohol acid-catalyzed rearrangement was discovered in the course of our research. Preliminary results concerning the scope and limitations of this reaction demonstrated the delicate balance among several mechanistic pathways by a minor change of substrate leading to different compounds such as cyclopentenones, furans, an enone or even a naphthalenone.

5. *EXPERIMENTAL PROCEDURES*

5. EXPERIMENTAL PROCEDURES

5.1 Generalities

All commercial reagents and reactants were used without further purification except from benzaldehyde and cyclohexanone which were distilled prior to being used. Dry solvents were purchase anhydrous or over molecular sieve in sealed bottles. All reactions sensitive to moisture or oxygen were carried out under argon atmosphere in oven-dried glassware (110 °C).

The progress of reactions was followed by thin layer chromatography on Silica Gel 60 F254 precoated aluminum sheets. The revelation of the plates was achieved by ultraviolet irradiation at 254 or 360 nm, and if needed by immersion in a stain (ninhydrin or phosphomolybdic acid), followed by heating.

The crudes of reaction were purified by column chromatography on silica gel Merck 60; 0,040-0,065 mm (230-400 mesh). The product is loaded onto the column either diluted in a minimum starting solvent or adsorbed on a minimal amount of silica 0.063-0.200 mm (Merck). The chromatography was eluted with a suitable eluent under medium air pressure.

^1H and ^{13}C NMRs were recorded on either RMN Bruker Avance DPX - 300 MHz spectrometer or RMN Bruker Avance III - 400 MHz spectrometer at 25 °C. The multiplicities of the signals are depicted as follow: s, singlet; br, broad signal; d, doublet; t, triplet; quad., quadruplet; quint., quintuplet; sex., sextuplet; m, multiplet; dd, doublet of doublet; dt, doublet of triplet. The residual peak of deuterated solvents is used as a reference (CDCl_3 , 7.26 ppm, 77.16 ppm; $\text{DMSO-}d_6$, 2.5 ppm, 39.52 ppm). The coupling constants J are expressed in hertz and the chemical shifts in ppm (part per million). The assignments of the spectra signals were carried out, compared with literature data whenever possible, or with comparison to neighboring structures or thanks to additional experiments such as DEPT, COSY, NOESY, HSQC, and HMBC.

Mass spectrums were carried out by the PACSI (Plateforme d'Analyse Chimique de Strasbourg Illkirch) using Agilent 1200: source, MM ESI/APCI; analyzer, quadrupole-Agilent 5973B) for low resolution (referred to as LC-MS). High resolution mass spectrometry (HR-MS) was executed using Agilent 1200: sources, ESI or APCI; analyzer, Q-ToF in tandem - Agilent Accurate Mass QToF 6520). Thermo trace GC/DSQ II apparatus was used for GC-MS experiments.

The names of the compounds are generated using ChemDraw software from CambridgeSoft.

→ *The compounds are described in order of appearance in the manuscript.*

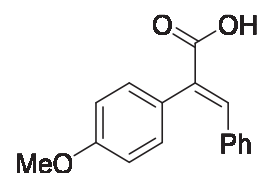
5.2 Procedures for chapter 3.1.

General procedure I: Perkin reaction

To a mixture containing aryl acetic acid (1 eq), benzaldehyde (1.1 eq) and triethylamine (1 eq) was added dropwise at 0 °C acetic anhydride. The resulting mixture was stirred at 50°C for 2 hours. The temperature was then raised to 100 °C for an additional 5 hours. The mixture was cooled down at room temperature and a NaOH solution was added until pH reached 14. The resulting mixture was stirred 0.5 hour then extracted with diethylether. The resulting aqueous layer was acidified with a solution of HCl 3 M. The product was extracted with Et₂O. The organic layer was dried over anhydrous MgSO₄. Filtration and evaporation under reduced pressure gave quantitatively the desired product.

Compound 184:

(E)-2-(4-Methoxyphenyl)-3-phenylacrylic acid



Compound **184** was obtained following general procedure I starting from compound 4-methoxyphenyl acetic acid (33 g, 0.2 mol), benzaldehyde (22 mL, 0.22 mol) and triethylamine (27.4 mL, 0.2 mol). Product **184** was obtained quantitatively (50 g).

¹H NMR (CDCl₃, 400 MHz) δ 3.85 (s, 3H), 6.92 (d, 2H, J = 8.7 Hz), 7.18 (d, 2H, J = 8.9 Hz), 7.11-7.47 (m, 5H), 7.94 (s, 1H) ppm;

¹³C NMR (CDCl₃, 400 MHz) δ 55.4, 114.4 (2C), 128.2, 128.5 (2C), 128.5, 128.7, 129.5, 130.9 (2C), 131.2 (2C), 142.4, 159.5, 173.5 ppm;

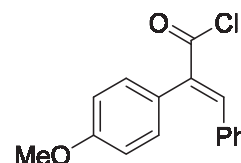
HR-MS calculated for C₁₆H₁₄O₃: 254.0943, found: 255.1013 (M+H)⁺.

General procedure II: Preparation of acyl chlorides

The carboxylic acid (1 eq) was dissolved in CH₂Cl₂ containing catalytic amount of DMF (0.025 eq). The mixture was cooled down at 0 °C and oxalyl chloride (1.15 eq) was added dropwise. The resulting mixture was stirred at room temperature overnight. The obtained mixture was concentrated to dryness, washed 3 times with toluene and concentrated again to give quantitatively the desired product.

Compound 186:

(E)-2-(4-Methoxyphenyl)-3-phenylacryloyl chloride



Compound **186** was obtained following general procedure II starting from compound acetic acid **184** (30.75 g, 0.121 mol) in CH₂Cl₂ (160 mL) with DMF (235 μL, 3 mmol) and oxalyl chloride (11.76 mL, 0.139 mol). Product **186** was obtained quantitatively (33 g).

¹H NMR (CDCl₃, 400 MHz) δ 3.85 (s, 3H), 6.75 (d, 2H, J = 8.9 Hz), 7.12-7.30 (m, 7H), 8.08 (s, 1H) ppm;

¹³C NMR (CDCl₃, 400 MHz) δ 54.4, 114.7 (2C), 126.9, 128.4, 128.6 (2C), 130.6, 131.2 (2C), 131.5 (2C), 136.0, 147.6, 160.0, 169.8 ppm.

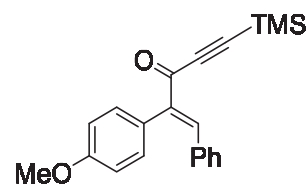
HR-MS calculated for C₁₆H₁₃ClO₂: 272.0604, found 272.0604 [C₁₆H₁₃ClO₂]⁺.

General procedure III: Sonogashira reaction

Acyl chloride (1 eq), Pd(PPh₃)₂Cl₂ (0.02 eq) and CuI (0.04 eq) were added to a solution of silylacetylene (1.4 eq) in 1,4-dioxane under argon atmosphere. At 0 °C, triethylamine (3 eq) was added dropwise. The mixture was warmed up at room temperature and stirred overnight at 80 °C. The reaction mixture was filtered and the resulting filtrate was concentrated. The crude was purified on silica column to give desired product.

Compound 183:

(E)-2-(4-Methoxyphenyl)-1-phenyl-5-(trimethylsilyl)pent-1-en-4-yn-3-one



Compound **183** was obtained following general procedure III starting from compound **186** (26 g, 0.095 mol) in 1,4-dioxane (500 mL) with trimethylsilylacetylene (13.16 g, 0.134 mol), Pd(PPh₃)₂Cl₂ (1.33 g, 1.9 mmol), CuI (720 mg, 3.8 mmol) and Et₃N (39.8 mL, 0.3 mol). Product **183** was obtained with 64% yield (20.36 g).

¹H NMR (CDCl₃, 400 MHz) δ 0.29 (s, 9H), 3.84 (s, 3H), 6.93 (d, 2H, J = 8.7 Hz), 7.08 (d, 2H, J = 8.7 Hz), 7.15 (d, 2H, J = 7.1 Hz), 7.20-7.27 (m, 3H), 8.10 (s, 1H) ppm;

¹³C NMR (CDCl₃, 400 MHz) δ -0.6 (3C), 55.3, 100.4, 101.1, 114.4 (2C), 126.6, 128.3 (2C), 129.9, 131.1 (2C), 131.2 (2C), 134.7, 141.2, 145.6, 159.7, 179.4 ppm;

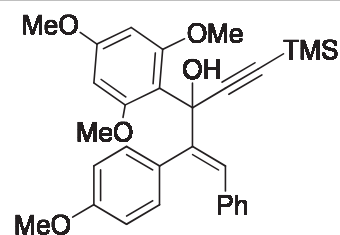
HR-MS calculated for C₂₁H₂₂O₂Si: 334.1389, found: 335.1469 (M+H)⁺.

General procedure IV: Alkylation of ketones

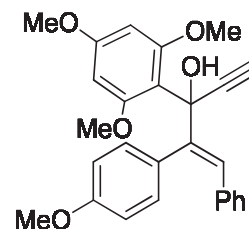
Alkylation agent (1-2 eq) was dissolved in anhydrous THF under argon atmosphere. At -78 °C, *sec*- or *n*-BuLi (1-2 eq) was added dropwise and the mixture was stirred at 0 °C for 1 hour. The obtained lithiated product was added dropwise à -78 °C to a solution of ketone (1 eq) in anhydrous THF. The obtained mixture was stirred at 0 °C for 3 hours. The mixture was washed with water then with a saturated solution of NH₄Cl. After extraction with EtOAc, the organic layer was dried over MgSO₄, filtered and concentrated. The crude was purified on silica column to give desired product.

Compound 182a:

(E)-2-(4-Methoxyphenyl)-1-phenyl-3-(2,4,6-trimethoxyphenyl)-5-(trimethylsilyl) pent-1-en-4-yn-3-ol

**Compound 333:**

(E)-2-(4-Methoxyphenyl)-1-phenyl-3-(2,4,6-trimethoxyphenyl) -pent-1-en-4-yn-3-ol



Compound **182a** was obtained following general procedure IV starting from compound **183** (25.2 g, 0.075 mol) in THF (500 mL) with trimethoxybenzene (18.9 g, 0.113 mol) and *sec*-BuLi (1.4 M, 80.6 mL, 0.113 mol). Product **182a** was obtained with 71% yield (26.6 g) along with deprotected alkyne **333** (1.1 g, 14%)

Compound 182a:

¹H NMR (CDCl₃, 400 MHz) δ 0.21 (s, 9H), 3.63 (s, 6H), 3.77 (s, 3H), 3.78 (s, 3H), 6.07 (s, 2H), 6.50 (s, 1H), 6.72 (d, 2H, J = 8.7 Hz), 6.90-6.93 (m, 4H), 7.04-7.09 (m, 3H), 7.21 (s, 1H) ppm;

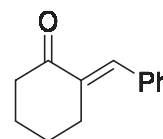
¹³C NMR (CDCl₃, 400 MHz) δ 0.3 (3C), 55.3, 55.4, 56.3 (2C), 76.9, 88.7, 92.8 (2C), 107.8, 111.4, 113.2 (2C), 126.5, 127.0, 127.9 (2C), 129.5 (2C), 130.2, 131.8 (2C), 137.4, 143.6, 158.7, 159.0 (2C), 160.4 ppm;

HR-MS calculated for C₃₀H₃₄O₅Si: 502.2176, found: 525.2077 (M+Na)⁺.

Compound 333:

¹H NMR (CDCl₃, 400 MHz) δ 3.65 (s, 6H), 3.75 (s, 3H), 3.77 (s, 3H), 5.83 (s, 1H), 6.05 (s, 2H), 6.75 (d, 2H, J = 8.8 Hz), 7.18-7.29 (m, 6H), 7.75 (d, 2H, J = 8.8 Hz) ppm;

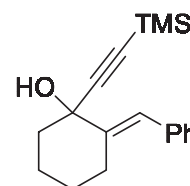
¹³C NMR (CDCl₃, 400 MHz) δ 55.4 (2C), 55.9 (2C), 91.3 (2C), 111.3, 113.2 (2C), 126.4, 128.0 (2C), 129.8 (2C), 130.1 (2C), 130.6, 139.5, 158.1 (2C), 160.7, 162.4, 198.2 ppm.

Compound 196-1:**(E)-2-Benzylidenecyclohexanone**

Cyclohexanone (15.8 mL, 0.153 mol) and benzaldehyde (16.96 mL, 0.168 mol) were mixed together. A solution of 1 N KOH (150 mL) was added. The resulting mixture was heated at reflux for 3 hours. It was then diluted in Et₂O and washed with water. The obtained organic layer was dried over MgSO₄, filtered and concentrated. The obtained crude was purified on a silica column to give 12.15 g (42%) of product **196-1**.

¹H NMR (CDCl₃, 400 MHz) δ 1.74-1.80 (m, 2H), 1.90-1.96 (m, 2H), 2.54 (t, 2H, J = 6.7 Hz), 2.84 (td, 2H, J = 2.3 and 6.5 Hz), 7.31-7.40 (m, 5H), 7.50 (t, 1H, J = 2.3 Hz) ppm;

¹³C NMR (CDCl₃, 400 MHz) δ 23.4, 23.9, 28.9, 40.3, 128.3 (2C), 128.3, 128.5, 130.3 (2C), 135.6, 136.9, 201.7 ppm.

Compound 196-2:**(E)-2-Benzylidene-1-((trimethylsilyl)ethynyl)cyclohexanol**

Compound **196-2** was obtained following general procedure IV starting from compound **196-1** (3.5 g, 0.019 mol) in THF (40 mL) with ethynyltrimethylsilane (5.41 mL, 0.038 mol) and *n*-BuLi (1.6 M, 24 mL, 0.038 mol). Product **196-2** was obtained with 65% yield (3.7 g) after recrystallization in TBDME.

¹H NMR (CDCl₃, 400 MHz) δ 0.20 (s, 9H), 1.42-1.54 (m, 1H), 1.72-1.93 (m, 4H), 2.00-2.09 (m, 1H), 2.17 (br, s, 1H), 2.37-2.47 (m, 1H), 2.61-2.75 (m, 1H), 6.90 (s, 1H), 7.20-7.27 (m, 3H), 7.32 (d, 2H, J = 7.2 Hz) ppm;

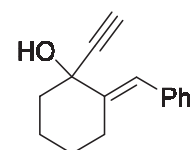
¹³C NMR (CDCl₃, 400 MHz) δ 0.1 (3C), 23.1, 26.3, 27.4, 42.6, 72.0, 90.5, 108.0, 122.0, 126.5, 128.2 (2C), 129.1 (2C), 137.8, 143.1 ppm.

General procedure V: Deprotection of alkynes

Alkynes (1 eq) were dissolved in anhydrous MeOH under argon atmosphere. Anhydrous K_2CO_3 (2 eq) was added and the mixture was stirred at room temperature. After 2 hours, the reaction mixture was filtered. The obtained filtrate was diluted in Et_2O and washed with water and brine. The organic layer was dried over $MgSO_4$, filtered and concentrated. The obtained crude was purified on silica column to give terminal alkynes.

Compound 196:

(E)-2-Benzylidene-1-ethynylcyclohexanol



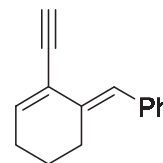
Compound **196** was obtained following general procedure V starting from compound **196-2** (6 g, 0.02 mol) in MeOH (70 mL) with K_2CO_3 (5.5 g, 0.04 mol). Product **196** was obtained with 94% yield (4 g).

1H NMR ($CDCl_3$, 400 MHz) δ 1.45-1.7 (m, 1H), 1.76-1.98 (m, 4H), 2.06-2.14 (m, 1H), 2.2 (br, s, 1H), 2.40-2.50 (m, 1H), 2.65-2.74 (m, 1H), 2.68 (s, 1H), 6.94 (s, 1H), 7.23-7.28 (m, 3H), 7.34 (d, 2H, $J = 7.2$ Hz) ppm;

^{13}C NMR ($CDCl_3$, 400 MHz) δ 23.0, 26.2, 27.3, 42.45, 71.69, 74.0, 86.4, 122.3, 126.6, 128.2 (2C), 129.1 (2C), 137.6, 142.7 ppm.

General procedure VI: Molybdenum-catalyzed allylic rearrangements

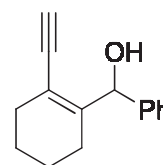
$MoO_2(acac)_2$ (0.05 eq) and propargyl alcohol (1 eq) were dissolved in DCE. The mixture was stirred between room temperature and reflux overnight. The reaction mixture was cooled down at room temperature and filtered on celite to afford product.

Compound 198:**(E)-((2-Ethynylcyclohex-2-en-1-ylidene)methyl)benzene**

Compound **198** was obtained following general procedure VI starting from compound **196** (50 mg, 0.234 mmol) in DCE (500 μ L) with $\text{MoO}_2(\text{acac})_2$ (3.8 mg, 0.018 mmol) at reflux. Product **198** was obtained with 90% yield (45 mg) based on GC-MS of the crude.

$^1\text{H NMR}$ (CDCl_3 , 400 MHz) δ 1.66-1.74 (m, 2H), 2.24-2.31 (m, 2H), 2.62-2.67 (m, 2H), 3.04 (s, 1H), 6.47 (t, 1H, $J = 4.7$ Hz), 7.01 (s, 1H), 7.17-7.40 (m, 5H) ppm;

$^{13}\text{C NMR}$ (CDCl_3 , 400 MHz) δ 22.0, 26.3, 26.4, 77.8, 80.1, 125.8, 126.0, 126.5, 126.9, 127.9, 128.0 (2C), 129.3 (2C), 139.2 ppm.

Compound 199:**(2-Ethynylcyclohex-1-en-1-yl)(phenyl)methanol**

Compound **199** was obtained following general procedure VI starting from compound **196** (50 mg, 0.234 mmol) in DCE (500 μ L) with $\text{MoO}_2(\text{acac})_2$ (3.8 mg, 0.018 mmol) at room temperature. Product **199** was obtained with 90% yield (45 mg) based on GC-MS of the crude.

$^1\text{H NMR}$ (CDCl_3 , 400 MHz) δ 1.49-1.81 (m, 4H), 2.00 (br, s, 1H), 2.21-2.30 (m, 4H), 3.17 (s, 1H), 6.13 (s, 1H), 7.25 (t, 1H, $J = 7.2$ Hz), 7.34 (t, 2H, $J = 7.3$ Hz), 7.44 (d, 2H, $J = 7.2$ Hz) ppm;

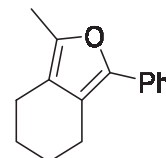
$^{13}\text{C NMR}$ (CDCl_3 , 400 MHz) δ 22.0, 22.3, 22.8, 30.3, 74.4, 80.7, 125.6 (2C), 125.9, 126.1, 127.2, 128.3 (2C), 128.5, 130.5 ppm.

Compound 199 was also be obtained with the following procedure:

Alcohol **196** (80 mg, 0.377 mmol) was dissolved in toluene (500 μ L) under argon atmosphere. 4-Methoxyphenylboronic acid (10.3 mg, 0.0754 mmol) and the reaction mixture was stirred at room temperature overnight. After filtration over celite, the mixture

was diluted in Et₂O and washed with water. The organic layer was separated, dried over MgSO₄, filtered and concentrated. After purification on silica gel, product **199** was obtained with 45% yield (36 mg).

Compound 200:



1-Methyl-3-phenyl-4,5,6,7-tetrahydroisobenzofuran

Compound **200** was obtained following general procedure VI starting from compound **196** (50 mg, 0.234 mmol) in DCE (500 μ L) with MoO₂(acac)₂ (3.8 mg, 0.018 mmol) and HgCl₂ (3.2 mg, 0.018 mmol) at room temperature. Product **200** was obtained with 25% yield (12 mg) based on GC-MS of the crude.

¹H NMR (CDCl₃, 400 MHz) δ 1.71-1.79 (m, 4H), 2.26 (s, 3H), 2.46 (t, 2H, J = 6.0 Hz), 2.77 (t, 2H, J = 5.8 Hz), 7.17 (t, 1H, J = 7.4 Hz), 7.37 (t, 2H, J = 7.5 Hz), 7.60 (d, 2H, J = 7.3 Hz) ppm;

¹³C NMR (CDCl₃, 400 MHz) δ 11.8, 20.8, 23.1, 23.2, 23.7, 118.4, 119.4, 124.0 (2C), 125.7, 128.8 (2C), 132.5, 144.7, 145.1 ppm.

General procedure VII: Molybdenum-catalyzed reactions

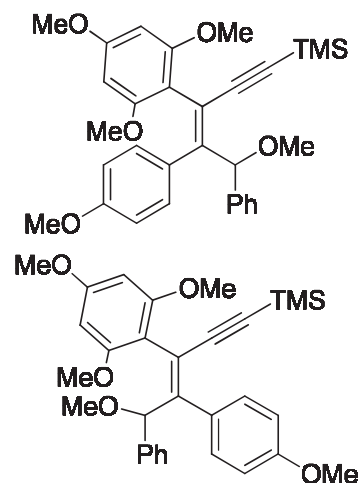
MoO₂(acac)₂ (0.1 eq), NH₄PF₆ (0.1 eq) and ROH (3 eq) were dissolved in acetonitrile. The mixture was stirred at 60-65 °C and after 10 minutes, propargylic alcohol (1 eq) was added. After stirring at 60-65 °C for 3 hours, the reaction mixture was cooled down at room temperature and filtered on celite to afford rearranged products.

Compound 213a:

(Z)-(5-Methoxy-4-(4-methoxyphenyl)-5-phenyl-3-(2,4,6-trimethoxyphenyl)pent-3-en-1-yn-1-yl)trimethylsilane

Compound 214a:

(E)-(5-Methoxy-4-(4-methoxyphenyl)-5-phenyl-3-(2,4,6-trimethoxyphenyl)pent-3-en-1-yn-1-yl)trimethylsilane



Compound **213a/214a** was obtained following general procedure VII starting from compound **182a** (500 mg, 1 mmol) in CH₃CN (5 mL) with MoO₂(acac)₂ (32 mg, 0.1 mmol), NH₄PF₆ (16 mg, 0.1 mmol) and MeOH (120 μL, 3 mmol). Desired product was obtained with 85% yield (414 mg) in a 3/1 ratio of **213a/214a**.

Compound 213a:

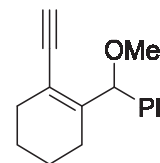
¹H NMR (CDCl₃, 400 MHz) δ 0.18 (s, 9H), 3.58 (s, 3H), 3.60 (s, 3H), 3.63 (s, 3H), 3.71 (s, 3H), 3.72 (s, 3H), 5.90 (d, 1H, J = 2.1 Hz), 5.95 (d, 1H, J = 2.0 Hz), 6.19 (s, 1H), 6.44 (s, 2H, J = 8.8 Hz), 6.62 (d, 2H, J = 8.8 Hz), 7.12-7.30 (m, 3H), 7.46 (d, 2H, J = 7.7 Hz) ppm;

¹³C NMR (CDCl₃, 400 MHz) δ -0.7 (3C), 54.0, 54.3, 54.8, 55.0, 55.7, 81.0, 82.4, 90.0, 90.1, 96.3, 111.1 (2C), 111.6, 125.4 (2C), 125.7, 125.8, 126.0, 126.6, 126.9 (2C), 128.9 (2C), 130.5, 140.0, 157.2, 159.8, 167.2 ppm.

Compound 214a:

¹H NMR (CDCl₃, 400 MHz) δ -0.04 (s, 9H), 3.37 (s, 3H), 3.75 (s, 3H), 3.80 (s, 3H), 3.48 (s, 3H), 3.85 (s, 3H), 4.98 (s, 1H), 6.18 (d, 1H, J = 2.1 Hz), 6.20 (d, 1H, J = 2.3 Hz), 6.72 (d, 2H, J = 8.8 Hz), 7.12-7.30 (m, 7 H) ppm;

¹³C NMR (CDCl₃, 400 MHz) δ -1.0 (3C), 54.3, 54.5, 54.7, 54.9, 55.8, 81.0, 90.1, 90.2, 111.1 (2C), 111.6, 125.4 (2C), 125.7, 125.8, 126.0, 126.6, 126.8 (2C), 128.9 (2C), 130.5, 139.9, 149.4, 149.9, 157.2, 157.3, 160.3 ppm.

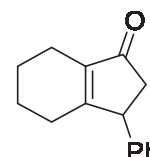
Compound 215:**((2-Ethynylcyclohex-1-en-1-yl)(methoxy)methyl)benzene**

Compound **215** was obtained following general procedure VII starting from compound **196** (300 mg, 1.41 mmol) in CH₃CN (7 mL) with MoO₂(acac)₂ (46 mg, 0.141 mmol), NH₄PF₆ (23 mg, 0.141 mmol) and MeOH (171 μL, 4.23 mmol). Product **215** was obtained with 66% yield (211 mg).

¹H NMR (CDCl₃, 400 MHz) δ 1.50-1.78 (m, 5H), 2.08-2.18 (m, 1H), 2.18-2.30 (m, 2H), 3.18 (s, 1H), 3.38 (s, 3H), 5.63 (s, 1H), 7.23 (t, 1H, J = 7.2 Hz), 7.31 (t, 2H, J = 7.5 Hz), 7.41 (d, 2H, J = 7.5 Hz) ppm.

General procedure VIII: Gold-catalyzed cyclization

Gold catalyst Au[(C₆H₅)₃P]Cl (0.05 eq) and AgSbF₆ (0.025 eq) were dissolved in CH₂Cl₂. After 15 minutes at room temperature, the mixture was cooled at -15 °C and a solution allylic ether (1 eq) in CH₂Cl₂ was added followed by isopropanol (1.1 eq). After stirring at room temperature overnight, the reaction mixture was filtered through celite and purified by silica gel chromatography to give cyclized product.

Compound 197:**3-Phenyl-2,3,4,5,6,7-hexahydro-1H-inden-1-one**

Compound **197** was obtained following general procedure VIII starting from compound **215** (40 mg, 0.177 mmol) in CH₂Cl₂ (1.5 mL) with Au[(C₆H₅)₃P]Cl (4.3 mg, 0.0088 mmol), AgSbF₆ (1.5 mg, 0.0044 mmol) and *i*-PrOH (13 μL, 0.170 mmol). Product **197** was obtained with 48% yield (18 mg).

¹H NMR (CDCl₃, 400 MHz) δ 1.62-1.65 (m, 4H), 2.02-2.06 (m, 5H), 2.89 (dd, 1H J = 6.9 and 18.9 Hz), 3.81 (m, 1H), 7.05-7.08 (m, 2H), 7.22-7.30 (m, 3H) ppm;

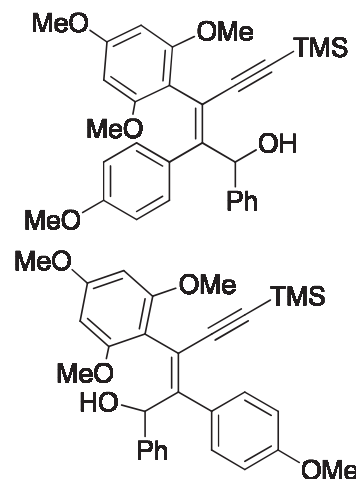
¹³C NMR (CDCl₃, 400 MHz) δ 20.3, 21.7, 22.3, 26.6, 45.1, 48.2, 127.1, 127.4 (2C), 129.0 (2C), 139.4, 142.0, 175.3, 208.4 ppm.

Compound 213b:

(Z)-2-(4-Methoxyphenyl)-1-phenyl-3-(2,4,6-trimethoxyphenyl)-5-(trimethylsilyl)pent-2-en-4-yn-1-ol

Compound 214b:

(E)-2-(4-Methoxyphenyl)-1-phenyl-3-(2,4,6-trimethoxyphenyl)-5-(trimethylsilyl)pent-2-en-4-yn-1-ol



Compound **213b** was obtained following general procedure VI starting from compound **182a** (3.5 g, 6.97 mmol) in CH₃CN (15 mL) with MoO₂(acac)₂ (224 mg, 0.697 mmol). Product **213b** was obtained with 11% yield (400 mg). Its isomer **214b** was isolated with 6%.

Compound 213b:

¹H NMR (CDCl₃, 400 MHz) δ 0.13 (s, 9H), 2.26 (d, 1H, J = 7.4 Hz), 3.49 (s, 3H), 3.64 (s, 3H), 3.72 (s, 3H), 3.82 (s, 3H), 5.85 (d, 1H, J = 2.1 Hz), 6.02 (d, 1H, J = 2.1 Hz), 6.49 (d, 2H, J = 8.9 Hz), 6.54 (d, 1H, J = 6.9 Hz), 6.64 (d, 2H, J = 8.8 Hz), 7.30 (t, 1H, J = 7.5 Hz), 7.37 (t, 2H, J = 7.3 Hz), 7.67 (d, 2H, J = 8.0 Hz) ppm;

¹³C NMR (CDCl₃, 400 MHz) δ 0.2 (3C), 55.2, 55.4, 55.7, 56.1, 74.8, 91.0, 98.0, 105.0, 112.7 (2C), 115.0, 126.4 (2C), 127.0, 128.2 (2C), 129.4, 130.1 (2C), 142.5, 153.4, 157.8, 128.8, 158.9, 161.0 ppm.

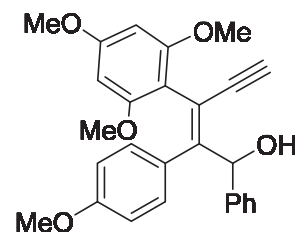
Isomer of 214b:

¹H NMR (CDCl₃, 400 MHz) δ 0.02 (s, 9H), 2.73 (d, 1H, J = 3.4 Hz), 3.74 (s, 3H), 3.84 (s, 3H), 3.90 (s, 3H), 3.90 (s, 3H), 5.55 (d, 1H, J = 3.0 Hz), 6.21 (d, 1H, J = 2.0 Hz), 6.24 (d, 1H, J = 2.1 Hz), 6.70 (d, 2H, 8.8 Hz), 7.06 (m, 1H), 7.16 (d, 4H, J = 4.3 Hz), 7.30 (d, 2H) ppm;

¹³C NMR (CDCl₃, 400 MHz) δ -0.0 (3C), 55.3, 55.6, 56.2, 56.7, 73.8, 86.4, 91.7, 92.2, 96.1, 105.8, 112.7 (2C), 116.0, 125.9 (2C), 126.4, 127.8 (2C), 130.2, 131.4 (2C), 141.5, 152.3, 127.8, 158.9, 159.3, 161.3 ppm.

Compound 216b:

(E)-2-(4-Methoxyphenyl)-1-phenyl-3-(2,4,6-trimethoxyphenyl)pent-2-en-4-yn-1-ol



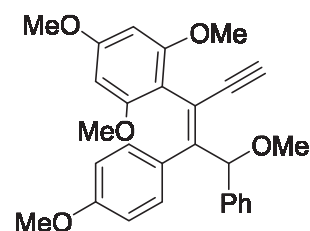
Compound **216b** was obtained general procedure V starting from compound **213b** (400 mg, 0.795 mmol) in MeOH (3 mL) with K_2CO_3 (222 mg, 1.59 mmol). Product **216b** was obtained with 96% yield (330 mg).

1H NMR ($CDCl_3$, 400 MHz) δ 3.53 (s, 6H), 3.68 (s, 1H), 3.77 (s, 3H), 3.82 (s, 3H), 6.08 (s, 2H), 6.74 (d, 2H, $J = 8.7$ Hz), 6.88 (d, 1H, $J = 1.5$ Hz), 6.92 (d, 1H, $J = 1.5$ Hz), 7.03 (d, 2H, $J = 8.7$ Hz), 7.13 (t, 1H, $J = 7.4$ Hz), 7.21 (t, 2H, $J = 7.3$ Hz), 7.48 (d, 2H, $J = 7.3$ Hz) ppm;

^{13}C NMR ($CDCl_3$, 400 MHz) δ 22.1, 22.2, 25.6 (2C), 90.6, 90.7, 112.5, 113.3 (2C), 125.5 (2C), 125.8, 126.1, 126.3, 128.0 (2C), 129.7, 130.3 (2C), 130.8, 130.9 ppm.

Compound 216a:

(E)-1,3,5-Trimethoxy-2-(5-methoxy-4-(4-methoxyphenyl)-5-phenylpent-3-en-1-yn-3-yl)benzene



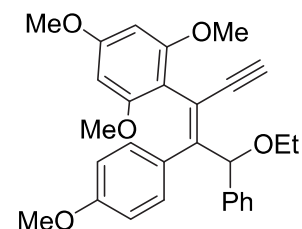
Compound **216a** was obtained following general procedure V starting from compound **213a** (200 mg, 0.398 mmol) in MeOH (2 mL) with K_2CO_3 (111 mg, 0.795 mmol). Product **216a** was obtained quantitatively (176.9 mg).

1H NMR ($CDCl_3$, 400 MHz) δ 2.79 (s, 1H), 3.39 (s, 3H), 3.77 (s, 3H), 3.83 (s, 3H), 3.86 (s, 3H), 3.87 (s, 3H), 4.99 (s, 1H), 6.21 (d, 1H, $J = 2.2$ Hz), 6.23 (d, 1H, $J = 2.2$ Hz), 6.77 (d, 2H, $J = 8.6$ Hz), 7.14-7.23 (m, 7H) ppm;

^{13}C NMR ($CDCl_3$, 400 MHz) δ 55.0, 55.3, 55.8, 56.0, 56.7, 80.4, 83.4, 83.7, 90.8, 90.9, 112.2 (2C), 126.4 (2C), 126.9, 127.9 (2C), 129.6, 129.7 (2C), 140.7, 151.7, 157.9, 158.1, 158.4, 161.0 ppm.

Compound 216c:

(E)-2-(5-Ethoxy-4-(4-methoxyphenyl)-5-phenylpent-3-en-1-yn-3-yl)-1,3,5-trimethoxy-benzene



Compound **216c** was obtained following general procedure V starting from compound **213c** (210 mg, 0.396 mmol) in MeOH (500 μ L) with K_2CO_3 (110 mg, 0.08 mmol). Product **216c** was obtained with 93% yield (169 mg).

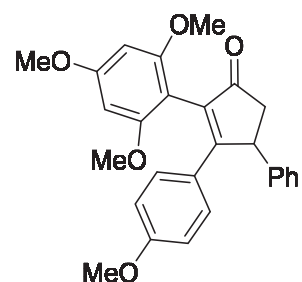
1H NMR ($CDCl_3$, 400 MHz) δ 1.31 (t, 3H, $J = 6.9$ Hz), 3.2 (s, 1H), 3.63 (s, 3H), 3.65 (s, 3H), 3.72 (s, 3H), 3.75 (s, 3H), 3.77-3.82 (m, 1H), 3.93-3.99 (m, 1H), 5.94 (dd, 2H, $J = 19.3$ and 2.1 Hz), 6.28 (s, 1H), 6.46 (dd, 2H, $J = 8.9$ and 2.1 Hz), 6.66 (dd, 2H, $J = 9.0$ and 2.1 Hz), 7.20-7.24 (m, 1H), 7.28-7.32 (m, 2H), 7.54 (d, 2H, $J = 8.0$ Hz) ppm;

^{13}C NMR ($CDCl_3$, 400 MHz) δ 15.4, 54.9, 55.3, 55.8, 55.9, 64.1, 80.2, 81.3, 83.7, 90.7, 90.8, 109.7, 112.1 (2C), 115.9, 126.4 (2C), 126.7, 127.8 (2C), 129.7, 129.7 (2C), 141.0, 152.2, 157.9, 158.0, 158.2, 160.9 ppm;

HR-MS calculated for $C_{29}H_{30}O_5$: 458.2093, found 459.2171(M+H) $^+$.

Compound 188:

3-(4-Methoxyphenyl)-4-phenyl-2-(2,4,6-trimethoxyphenyl)-cyclopent-2-enone



Compound **188** was obtained following general procedure VIII starting from compound **213c** ((170 mg, 0.37 mmol) in CH_2Cl_2 (4 mL) with $Au[(C_6H_5)_3P]Cl$ (9 mg, 0.019 mmol), $AgSbF_6$ (3.2 mg, 0.0093 mmol) and *i*-PrOH (31 μ L, 0.4 mmol). Product **188** was obtained with 63% yield (100 mg).

1H NMR ($CDCl_3$, 400 MHz) δ 2.48 (dd, 1H, $J = 18.3$ and 1.9 Hz), 3.17 (dd, 1H, $J = 18.1$ and 7.6 Hz), 3.57 (s, 3H), 3.70 (s, 3H), 3.76 (s, 3H), 3.85 (s, 3H), 4.63 (dd, 1H, $J = 7.4$ and 1.9 Hz), 6.17

(d, 1H, J = 2.1 Hz), 6.24 (d, 1H, J = 2.1 Hz), 6.62 (d, 2H, J = 9.0 Hz), 7.16 (m, 1H), 7.24-7.27 (m, 4H), 7.32 (d, 2H, J = 8.1 Hz) ppm;

^{13}C NMR (CDCl_3 , 400 MHz) δ 45.9, 47.2, 55.1, 55.4, 55.9, 55.7, 91.4, 91.6, 113.4 (2C), 126.6, 127.4 (2C), 128.9 (2C), 129.4, 129.9 (2C), 132.1, 144.3, 151.4, 156.9, 158.6, 160.3, 161.8, 168.6, 206.9 ppm.

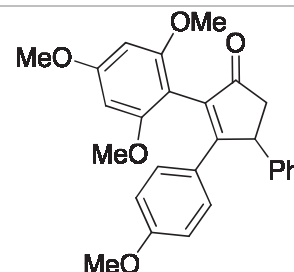
HR-MS calculated for $\text{C}_{27}\text{H}_{26}\text{O}_5$: 430.1780, found: 431.2071 ($\text{M}+\text{H}$) $^+$.

General procedure IX: Rhenium-catalyzed cyclization

Re_2O_7 (0.015 eq) and MeOH (7.7 eq) were dissolved in DCE under argon atmosphere, and the mixture was stirred at 45 °C for 15 minutes. At 45 °C, a solution of propargylic alcohol (1 eq) was added and the mixture was stirred at the same temperature overnight. The reaction was then filtered on celite and concentrated to dryness. The obtained crude was purified on silica gel to afford rearranged products.

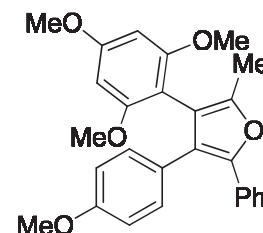
Compound 188:

3-(4-Methoxyphenyl)-4-phenyl-2-(2,4,6-trimethoxyphenyl)cyclopent-2-en-1-one



Compound 217:

3-(4-Methoxyphenyl)-5-methyl-2-phenyl-4-(2,4,6-trimethoxyphenyl)furan



Compounds **188** and **217** were obtained following general procedure IX starting from compound **182a** (9.3 g, 0.019 mol) in DCE (60 mL) with Re_2O_7 (134 mg, 0.278 mmol) and MeOH (5 mL, 0.146 mol). Cyclopentenone **188** (2.46 g, 31%) was obtained along with methylfuran **217** (1.43 g, 18 %). Cyclopentenone **188** was already described page 162 following another method.

Methylfurane **217**:

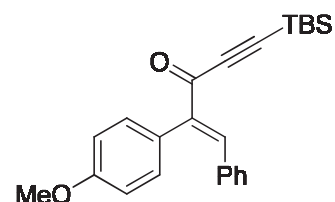
$^1\text{H NMR}$ (CDCl_3 , 400 MHz) δ 2.23 (s, 3H), 3.53 (s, 6H), 3.77 (s, 3H), 3.81 (s, 3H), 6.08 (s, 2H), 6.74 (d, 2H, $J = 8.8$ Hz), 7.03 (d, 2H, $J = 8.8$ Hz), 7.13 (t, 1H, $J = 7.3$ Hz), 7.21 (t, 2H, $J = 7.8$ Hz), 7.47 (d, 2H, $J = 7.3$ Hz) ppm;

$^{13}\text{C NMR}$ (CDCl_3 , 400 MHz) δ 11.9, 54.2, 54.4, 54.7 (2C), 89.8 (2C), 102.3, 112.4 (2C), 114.7, 123.3, 124.6 (2C), 125.9, 126.6, 127.2 (2C), 129.4 (2C), 131.0, 145.4, 148.3, 157.2, 158.1, 160.0 ppm;

HR-MS calculated for $\text{C}_{27}\text{H}_{26}\text{O}_5$: 430.1780, found: 431.1854 ($\text{M}+\text{H}$) $^+$.

Compound 182b-1:

(E)-5-(*tert*-Butyldimethylsilyl)-2-(4-methoxyphenyl)-1-phenylpent-1-en-4-yn-3-one



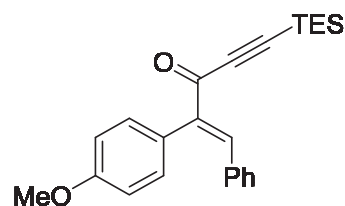
Compound **182b-1** was obtained following [general procedure III](#) starting from compound **186** (6.9 g, 25 mmol) in 1,4-dioxane (125 mL) with *tert*-butyldimethylsilylacetylene (5 g, 36 mmol), $\text{Pd}(\text{PPh}_3)_2\text{Cl}_2$ (350 mg, 0.5 mmol), CuI (190 mg, 1 mmol) and Et_3N (10 mL, 75 mmol). Product **182b-1** was obtained with 79% yield (7.5 g).

$^1\text{H NMR}$ (CDCl_3 , 400 MHz) δ 0.21 (s, 6H), 1.00 (s, 9H), 3.84 (s, 3H), 6.92 (d, 2 H, $J = 8.8$ Hz), 7.08 (d, 2 H, $J = 8.8$ Hz), 7.12-7.38 (m, 5H), 8.11 (s, 1 H) ppm.

$^{13}\text{C NMR}$ (CDCl_3 , 400 MHz) δ -4.9 (2C), 16.8, 26.2 (3C), 55.3, 99.1, 101.8, 114.4 (2C), 126.5, 128.5 (2C), 129.9, 131.1 (3C), 134.6, 141.1, 145.4, 159.6, 179.3 ppm.

Compound 182c-1:

(E)-2-(4-Methoxyphenyl)-1-phenyl-5-(triethylsilyl)pent-1-en-4-yn-3-one



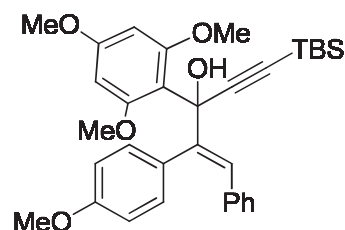
Compound **182c-1** was obtained following general procedure III starting from compound **186** (1.8 g, 6.6 mmol) in 1,4-dioxane (35 mL) with triethylsilylacetylene (1.66 mL, 9.25 mmol), Pd(PPh₃)₂Cl₂ (93 mg, 0.132 mmol), CuI (50 mg, 0.264 mmol) and Et₃N (2.8 mL, 0.02 mol). Product **182c-1** was obtained with 38% yield (963 mg).

¹H NMR (CDCl₃, 400 MHz) δ 0.71 (quad., 6H, J = 7.6 and 15.5 Hz), 1.05 (t, 9H, J = 7.9 Hz), 3.84 (s, 3H), 6.92 (d, 2H, J = 8.8 Hz), 7.08 (d, 2H, J = 8.7 Hz), 7.12-7.13 (m, 2H), 7.188-7.24 (m, 3H), 8.13 (s, 1H) ppm;

¹³C NMR (CDCl₃, 400 MHz) δ 4.0 (3C), 7.4 (3C), 55.2, 114.3 (2C), 102.2, 114.3 (2C), 126.5, 128.4 (2C), 129.8, 131.0 (2C), 131.1 (2C), 134.6, 141.1, 145.4 ppm.

Compound 182b:

(E)-5-(tert-Butyldimethylsilyl)-2-(4-methoxyphenyl)-1-phenyl-3-(2,4,6-trimethoxyphenyl)pent-1-en-4-yn-3-ol



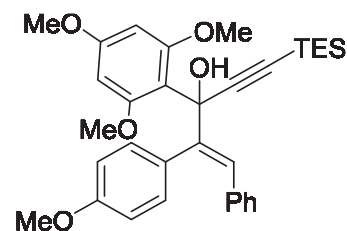
Compound **182b** was obtained following general procedure IV starting from compound **182b-1** (1 g, 2.66 mmol) in THF (20 mL) with trimethoxybenzene (670 mg, 3.99 mmol) and *sec*-BuLi (1.4 M, 2.85 mL, 3.99 mmol). Product **182b** was obtained with 43% yield (629 mg).

¹H NMR (CDCl₃, 400 MHz) δ 0.12 (s, 3H), 0.16 (s, 3H), 1.00 (s, 9H), 3.63 (s, 6H), 3.76 (s, 3H), 3.78 (s, 3H), 6.05 (s, 2H), 6.65 (s, 1H), 6.70 (d, 2H, J = 8.7 Hz), 6.90-6.93 (m, 4H), 7.05-7.72 (m, 3H), 7.31 (s, 1H) ppm;

¹³C NMR (CDCl₃, 400 MHz, DEPT 45°) δ -4.4, -4.4, 26.3 (3C), 55.1, 55.2, 56.6 (2C), 92.4 (2C), 113.1 (2C), 126.4, 130.0, 127.8 (2C), 129.3 (2C), 131.6 (2C) ppm;

Compound 182c:

(E)-2-(4-Methoxyphenyl)-1-phenyl-5-(triethylsilyl)-3-(2,4,6-trimethoxyphenyl)pent-1-en-4-yn-3-ol



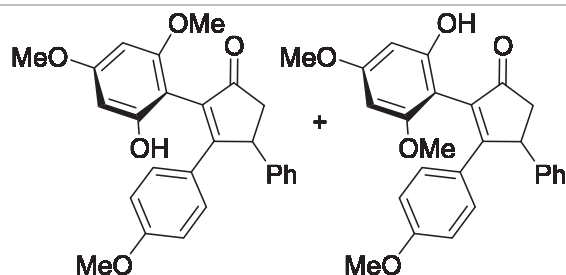
Compound **182c** was obtained following general procedure IV starting from compound **182c-1** (900 mg, 2.39 mmol) in THF (20 mL) with trimethoxybenzene (603 mg, 3.59 mmol) and *sec*-BuLi (1.4 M, 2.56 mL, 3.59 mmol). Product **182c** was obtained with 48% yield (624 mg).

$^1\text{H NMR}$ (CDCl_3 , 400 MHz) δ 0.65 (quad., 6H, $J = 8.2$ and 16.2 Hz), 1.03 (t, 9H, $J = 7.9$ Hz), 3.63 (s, 6H), 3.76 (s, 3H), 3.78 (s, 3H), 6.05 (s, 2H), 6.60 (s, 2H), 6.70 (d, 2H, $J = 8.8$ Hz), 6.90-6.93 (m, 3H), 7.04-7.08 (m, 3H), 7.31 (s, 1H) ppm;

$^{13}\text{C NMR}$ (CDCl_3 , 400 MHz, DEPT 45°) δ 4.6 (2C), 7.6 (2C), 55.1, 55.2, 56.2 (2C), 92.5 (2C), 113.1 (2C), 126.3, 127.7 (2C), 129.3 (2C), 129.9, 131.7 (2C) ppm.

Compound 221:

2-(2-Hydroxy-4,6-dimethoxyphenyl)-3-(4-methoxyphenyl)-4-phenylcyclopent-2-en-1-one



Compound **188** (4.5 g, 0.010 mol) was dissolved in anhydrous CH_2Cl_2 (450 mL) under argon atmosphere. At -78°C , BBr_3 (10.5 mL, 0.010 mol) was added dropwise and the mixture was stirred at this temperature for 10 minutes then at 0°C for 20 minutes and finally at room temperature for 6,5 hours. The reaction mixture was then quenched with a solution of HCl 1N. The product was extracted with CH_2Cl_2 and the organic layer was washed with water, dried over MgSO_4 , filtered and concentrated under vacuum. The obtained crude was purified with chromatography column to afford product **221** as a 1/1 mixture of atropoisomers (3.13 g, 75%).

$^1\text{H NMR}$ (CDCl_3 , 400 MHz) δ 2.51 (dd, 0.5H, $J = 1.8$ and 16.7 Hz), 2.56 (dd, 0.5H, $J = 1.6$ and 16.7 Hz), 3.15 (dd, 0.5H, $J = 7.3$ and 18.9 Hz), 3.19 (s, 1.5H), 3.27 (dd, 0.5H, $J = 7.4$ and 18.9 Hz), 3.53 (s, 1.5H), 3.70 (s, 1.5H), 3.70 (s, 1.5H), 3.80 (s, 3H), 4.56 (dd, 0.5H, $J = 1.6$ and 7.2 Hz), 4.73 (dd, 0.5H, $J = 1.4$ and 7.3 Hz), 5.97 (d, 0.5H, $J = 2.4$ Hz), 6.11 (d, 0.5H, $J = 2.3$ Hz), 6.20 (d, 0.5H, $J = 2.4$ Hz), 6.27 (d, 0.5H, $J = 2.3$ Hz), 6.62 (d, 1H, $J = 9.0$ Hz), 6.64 (d, 1H, $J = 8.9$ Hz), 7.10-7.24 (m, 5H), 7.29-7.37 (m, 4H) ppm;

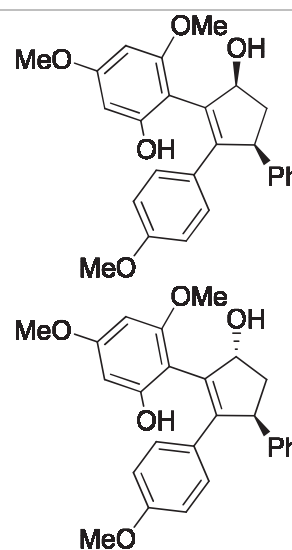
LC-MS calculated for $\text{C}_{26}\text{H}_{24}\text{O}_5$: 416.2, found: 417.2 ($\text{M}+\text{H}$) $^+$.

Compound 222a:

2-((3*S*,5*S*)-5-Hydroxy-2-(4-methoxyphenyl)-3-phenylcyclopent-1-en-1-yl)-3,5-dimethoxyphenol

Compound 222b:

2-((3*S*,5*R*)-5-Hydroxy-2-(4-methoxyphenyl)-3-phenyl-cyclopent-1-en-1-yl)-3,5-dimethoxyphenol



LiAlH_4 (364 mg, 9.6 mmol) was dissolved in anhydrous THF (12.5 mL) under argon atmosphere. At 0°C , a solution of compound **221** (1 g, 2.4 mmol) in anhydrous THF (37.5 mL) was added to the reaction mixture which was afterwards stirred at room temperature for 2 hours. Water (364 μL) was added dropwise at 0°C followed by a solution of NaOH 15% (364 μL) and water again (728 μL). The salts precipitated and were filtered off. The filtrate was concentrated under vacuum to afford compound **222a** and **222b** as a 1/1 mixture of the 2 diastereoisomers (1.03 g, quantitative).

Compound 222a:

$^1\text{H NMR}$ (CDCl_3 , 400 MHz) δ 1.67 (dt, 1H, $J = 3.6$ and 13.9 Hz), 2.85-2.91 (m, 1H), 3.28 (s, 3H), 3.59 (s, 3H), 3.71 (s, 3H), 4.41 (dd, 1H, $J = 3.9$ and 9.0 Hz), 4.82 (m, 1H), 5.96 (d, 1H, $J = 2.4$ Hz), 6.12 (d, 1H, $J = 2.4$ Hz), 6.25 (d, 1H, $J = 4.9$ Hz), 6.58 (d, 2H, $J = 9.0$ Hz), 6.97 (d, 2H, $J = 9.0$ Hz), 7.06 (t, 1H, $J = 7.4$ Hz), 7.19 (t, 2H, $J = 7.6$ Hz), 7.32 (d, 2H, $J = 7.1$ Hz), 9.83 (s, 1H) ppm;

^{13}C NMR (CDCl_3 , 400 MHz) δ 42.7, 51.7, 54.8, 55.0, 55.3, 79.4, 91.1, 94.4, 106.6, 112.9 (2C), 125.8, 128.1 (2C), 128.2 (2C), 128.8 (2C), 129.0, 132.5, 144.6, 145.8, 157.6, 157.8, 157.9, 160.3 ppm.

Compound **222b**:

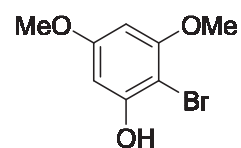
^1H NMR (CDCl_3 , 400 MHz) δ 2.01-2.10 (m, 1H), 2.29-2.35 (m, 1H), 3.59 (s, 3H), 3.72 (s, 3H), 3.73 (s, 3H), 4.49-4.53 (m, 1H), 4.98-5.02 (m, 1H), 6.04 (d, 1H, 2.4 Hz), 6.15 (d, 1H, $J = 2.4$ Hz), 6.59 (d, 2H, $J = 6.8$ Hz), 6.97 (d, 2H, $J = 9.1$ Hz), 7.18 (t, 1H, $J = 7.6$ Hz), 7.24 (t, 2H, $J = 7.6$ Hz), 7.30 (d, 2H, $J = 8.4$ Hz) ppm;

^{13}C NMR (CDCl_3 , 400 MHz) δ 44.1, 51.6, 54.8, 54.9, 55.7, 78.7, 90.5, 94.2, 106.1, 113.0 (2C), 125.8, 127.3 (2C), 128.3, 128.4 (2C), 128.5 (2C), 134.7, 141.9, 145.9, 156.4, 157.8, 158.5, 160.1 ppm;

LC-MS calculated for $\text{C}_{26}\text{H}_{26}\text{O}_5$: 418.2, found: 401.2 ($\text{M}-\text{H}_2\text{O}+\text{H}$) $^+$.

Compound 225-1:

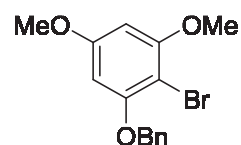
2-Bromo-3,5-dimethoxyphenol



3,5-Dimethoxyphenol (30 g, 0.194 mol) was dissolved in CH_2Cl_2 (1.3 L) under argon atmosphere. At -78 °C was added NBS (34.6 g, 0.194 mol) and the mixture was stirred at this temperature for 5 hours. The reaction mixture was quenched with a 10% solution of K_2CO_3 in water. The organic layer was separated, dried over MgSO_4 , filtered and concentrated. Purification on silica gel afforded product **225-1** (21.1 g, 47%).

^1H NMR (CDCl_3 , 400 MHz) δ 3.78 (s, 3H), 3.85 (s, 3H), 5.64 (br, s, 1H), 6.11 (d, 1H, $J = 2.6$ Hz), 6.26 (d, 1H, $J = 2.8$ Hz) ppm.

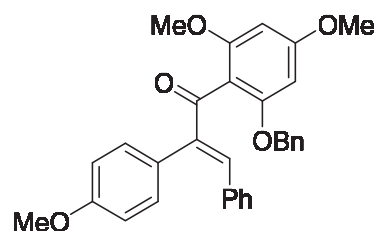
^{13}C NMR (CDCl_3 , 400 MHz) δ 55.7, 56.4, 91.2, 92.7, 93.4, 154.0, 156.9, 160.8 ppm.

Compound 225:**1-(Benzyloxy)-2-bromo-3,5-dimethoxybenzene**

Compound **225-1** (21.1 g, 0.091 mol) was dissolved in DMF (220 mL) under argon atmosphere. K_2CO_3 (13.1 g, 0.095 mol) was added followed by (bromomethyl)benzene (17 g, 0.01 mol). After stirring for 3 hours at room temperature the reaction mixture was washed with water and the product was extracted with CH_2Cl_2 . The organic layer was dried over $MgSO_4$, filtered and concentrated under vacuum to afford product **225** (19.78 g, 89%).

1H NMR ($CDCl_3$, 400 MHz) δ 3.77 (s, 3H), 3.88 (s, 3H), 5.14 (s, 2H), 6.20 (d, 2H, $J = 2.5$ and 13.2 Hz), 7.32 (t, 1H, $J = 7.2$ Hz), 7.39 (t, 2H, $J = 7.0$ Hz), 7.49 (d, 2H, $J = 7.3$ Hz) ppm;

^{13}C NMR ($CDCl_3$, 400 MHz) δ 55.6, 56.5, 71.1, 92.3, 92.8, 93.5, 127.1 (2C), 128.0, 128.7 (2C), 136.7, 156.7, 157.7, 160.4 ppm.

Compound 227:**(E)-1-(2-(Benzyloxy)-4,6-dimethoxyphenyl)-2-(4-methoxyphenyl)-3-phenylprop-2-en-1-one**

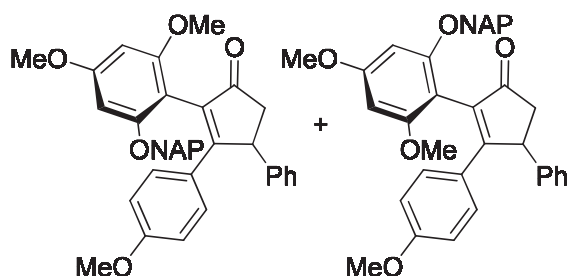
To a suspension of flame dried Mg turnings (23 mg, 0.958 mmol) in THF (500 μ L) was added a solution of compound **225** (39 mg, 0.12 mmol) in THF (05 μ L) and dibromoethane (20 μ L) to initiate the reaction. Once bubbling had ceased, the remaining brominated derivative **225** (232 mg, 0.72 mmol) in THF (450 μ L) was added. The resulting mixture was stirred at room temperature for 30 minutes and refluxed for 10 min. The solution was diluted with THF (2.5 mL), cooled to -78 $^{\circ}C$ and a solution of ketone **183** (200 mg, 0.60 mmol) in THF (500 μ L) was added. The solution was stirred at -78 $^{\circ}C$ for 45 minutes then warmed at room temperature. The reaction mixture was quenched with a saturated aqueous solution of NH_4Cl . The resulting aqueous layer was extracted with EtOAc (x 3). The combined organic layers were dried over $MgSO_4$, filtered and concentrated. After purification on silica gel, compound **227** was obtained with 20% yield (48 mg)

$^1\text{H NMR}$ (CDCl_3 , 400 MHz) δ 3.62 (s, 3H), 3.72 (s, 3H), 3.79 (s, 3H), 4.93 (d, 1H, $J = 12.2$ Hz), 5.05 (d, 1H, $J = 12.0$ Hz), 5.89 (s, 1H), 6.05 (d, 1H, $J = 2.3$ Hz), 6.13 (d, 1H, $J = 2.3$ Hz), 6.74 (d, 2H, $J = 9.0$ Hz), 7.20-7.361 (m, 10H), 7.73 (d, 2H, $J = 8.9$ Hz) ppm;

$^{13}\text{C NMR}$ (CDCl_3 , 400 MHz) δ 55.3, 55.4, 55.7, 70.6, 91.5, 92.5, 111.6, 113.2 (2C), 126.5 (2C), 127.3 (2C), 127.9 (2C), 128.0 (2C), 128.6 (2C), 129.9 (2C), 130.2 (2C), 130.6, 136.9, 139.6, 157.0, 158.3, 160.5, 162.4, 197.9 ppm.

Compound 229:

2-(2,4-Dimethoxy-6-(naphthalen-2-ylmethoxy)phenyl)-3-(4-methoxyphenyl)-4-phenyl-cyclopent-2-en-1-one



Compound **221** (570 mg, 1.37 mmol) was dissolved in anhydrous DMF (6 mL) under argon atmosphere. K_2CO_3 (199 mg, 1.44 mmol) was added followed by NAP-Br (333 mg, 1.51 mmol). After one night at room temperature, the reaction mixture was washed with water and extracted with Et_2O . The organic layer was dried over MgSO_4 , filtered and concentrated. Purification on silica gel afforded product **229** as a 1/1 mixture of atropoisomers (557 mg, 73%). Recovered starting material (125.4 mg, 22%).

First atropisomere of **229**:

$^1\text{H NMR}$ (CDCl_3 , 400 MHz) δ 2.42 (dd, 1H, $J = 1.6$ and 18.3 Hz), 3.16 (dd, 1H, $J = 7.5$ and 18.4 Hz), 3.61 (s, 3H), 3.71 (s, 3H), 3.84 (s, 3H), 4.57 (dd, 1H, $J = 1.5$ and 7.4 Hz), 5.13 (d, 1H, $J = 12.3$ Hz), 5.19 (d, 1H, $J = 11.3$ Hz), 6.21 (d, 1H, $J = 2.1$ Hz), 6.35 (d, 1H, $J = 2.1$ Hz), 6.64 (d, 2H, $J = 9.0$ Hz), 6.69 (t, 2H, $J = 7.7$ Hz), 6.83 (t, 1H, $J = 7.3$ Hz), 7.10 (d, 2H, $J = 7.6$ Hz), 7.23-7.30 (m, 4H), 7.41-7.45 (m, 2H), 7.65-7.67 (m, 2H), 7.77 (d, 1H, $J = 8.0$ Hz) ppm;

$^{13}\text{C NMR}$ (CDCl_3 , 400 MHz) δ 46.0, 47.2, 55.1, 55.4, 55.9, 70.7, 91.7, 92.4, 104.4, 113.4 (2C), 125.8, 126.0, 126.2, 126.74, 127.1, 127.6, 127.9, 128.0 (2C), 128.6 (2C), 130.1 (2C), 133.2, 134.2, 134.7, 144.1, 157.4, 158.0, 160.3, 168.5 ppm;

LC-MS calculated for $\text{C}_{37}\text{H}_{32}\text{O}_5$: 556.2, found: 557.2 ($\text{M}+\text{H}$) $^+$.

Second atropisomere of **229**:

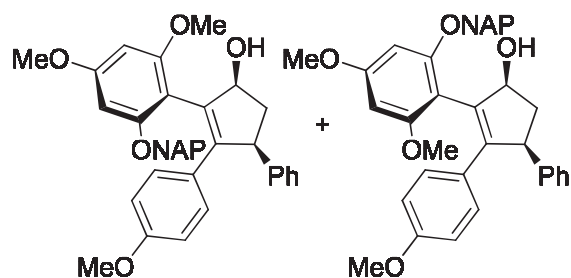
$^1\text{H NMR}$ (CDCl_3 , 400 MHz) δ 2.50 (dd, 1H, $J = 1.9$ and 18.4 Hz), 3.13 (dd, 1H, $J = 7.4$ and 18.4 Hz), 3.70 (s, 3H), 3.79 (s, 3H), 3.80 (s, 3H), 4.60 (dd, 1H, $J = 1.6$ and 7.4 Hz), 4.97 (d, 1H, $J = 12.3$ Hz), 5.10 (d, 1H, $J = 12.3$ Hz), 6.21 (d, 1H, $J = 2.1$ Hz), 6.26 (d, 1H, $J = 2.1$ Hz), 6.63 (d, 2H, $J = 8.9$ Hz), 7.05-7.17 (m, 2H), 7.23-7.31 (m, 5H), 7.43-7.47 (m, 2H), 7.52 (s, 1H), 7.65-7.71 (m, 3H), 7.78-7.80 (m, 1H) ppm;

$^{13}\text{C NMR}$ (CDCl_3 , 400 MHz) δ 45.8, 46.9, 55.1, 55.4, 56.1, 70.4, 91.6, 92.9, 101.5, 113.5 (2C), 125.8, 126.0, 126.2, 126.6, 127.4, 127.7, 128.1, 128.2 (2C), 128.9 (2C), 130.0 (2C), 133.1, 134.2, 134.3, 143.8, 157.8, 158.7, 161.6, 168.9 ppm;

LC-MS calculated for $\text{C}_{37}\text{H}_{32}\text{O}_5$: 556.2, found: 557.2 ($\text{M}+\text{H}$) $^+$.

Compound 230:

(1*S*,4*S*)-2-(2,4-Dimethoxy-6-(naphthalen-2-ylmethoxy)phenyl)-3-(4-methoxyphenyl)-4-phenylcyclopent-2-en-1-ol



Compound **229** (60 mg, 0.108 mmol) was dissolved in anhydrous THF (800 μL) under argon atmosphere. At -78 $^\circ\text{C}$, *L*-selectride $^\circ$ was added dropwise. After 30 minutes at -78 $^\circ\text{C}$, the mixture was stirred at 0 $^\circ\text{C}$ for 30 minutes then 4 hours at room temperature. The reaction mixture was quenched with a saturated aqueous solution of NH_4Cl , and extracted with Et_2O . The organic layer was dried over MgSO_4 , filtered and concentrated. Purification over silica gel afforded product **230** (30 mg, 50%) as a 1/1 mixture of atropisomers. Recovered starting material (18 mg, 30%).

$^1\text{H NMR}$ (CDCl_3 , 400 MHz) δ 1.80 (dt, 0.5H, $J = 3.5$ and 13.7 Hz), 1.88 (dt, 0.5H, $J = 4.3$ and 13.6 Hz), 2.42 (d, 0.5H, $J = 7.8$ Hz), 2.81 (d, 0.5H, $J = 7.2$ Hz), 2.90-3.02 (m, 1H), 3.65 (s, 1.5H), 3.66 (s, 1.5H), 3.68 (s, 1.5H), 3.77 (s, 1.5H), 3.82 (s, 1.5H), 3.88 (s, 1.5H), 4.27 (dd, 0.5H, $J = 3.9$ and 8.5 Hz), 4.35 (dd, 0.5H, $J = 4.8$ and 8.4 Hz), 4.91-4.98 (m, 1.5H), 5.10 (d, 0.5H, $J = 12.7$ Hz), 5.16 (d, 0.5H, $J = 11.3$ Hz), 5.25 (d, 0.5H, $J = 11.3$ Hz), 6.17 (s, 1H), 6.25 (d, 0.5H, $J = 1.6$ Hz), 6.35 (d, 0.5H, $J = 1.4$ Hz), 6.55 (d, 1H, $J = 8.4$ Hz), 6.56 (d, 1H, $J = 8.4$ Hz), 6.77 (t, 1H, $J =$

7.4 Hz), 6.88 (t, 0.5 H, $J = 7.3$ Hz), 6.99 (d, 1H, $J = 8.3$ Hz), 7.00 (d, 1H, $J = 8.5$ Hz), 7.10-7.24 (m, 3H), 7.31 (d, 1H, $J = 8.5$ Hz), 7.36 (d, 1H, $J = 7.3$ Hz), 7.44-7.50 (m, 2H), 7.59 (s, 0.5H), 7.71-7.76 (m, 2H), 7.82 (d, 1H, $J = 6.9$ Hz) ppm;

^{13}C NMR (CDCl_3 , 400 MHz) δ 43.9 (0.5C), 44.2 (0.5C), 52.4 (0.5C), 52.7 (0.5C), 55.0 (0.5C), 55.1 (0.5C), 55.4 (0.5C), 55.5 (0.5C), 56.0 (0.5C), 56.2 (0.5C), 70.3 (0.5C), 71.1 (0.5C), 80.8 (0.5C), 81.0 (0.5C), 91.5 (0.5C), 91.9 (0.5C), 92.3 (0.5C), 93.3 (0.5C), 113.1, 113.2, 124.2 (0.5C), 124.8 (0.5C), 125.5 (0.5C), 125.8 (0.5C), 125.9 (0.5C), 126.0, 126.2 (0.5C), 126.3, 127.1 (0.5C), 128.8, 128.0 (1.5C), 128.1, 128.2, 128.3 (0.5C), 128.4, 128.6 (0.5C), 128.7, 129.2, 129.3, 129.4 (0.5C), 143.1 (0.5C), 144.0 (0.5C), 146.2 (0.5C), 146.4, 158.2, 158.7 (0.5C), 159.5 (0.5C), 160.9 (0.5C), 161.0 (0.5C) ppm;

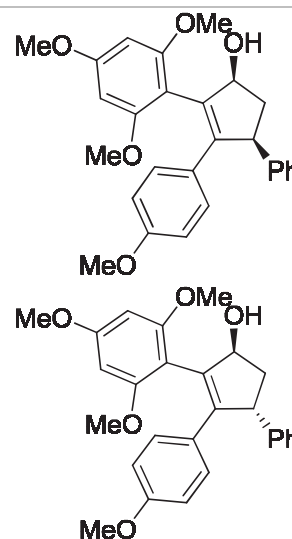
LC-MS calculated for $\text{C}_{37}\text{H}_{34}\text{O}_5$: 558.2, found: 541.2 ($\text{M}-\text{H}_2\text{O}+\text{H}$) $^+$.

Compound 232a:

(1*S*,4*S*)-3-(4-Methoxyphenyl)-4-phenyl-2-(2,4,6-trimethoxyphenyl)cyclopent-2-en-1-ol

Compound 232b:

(1*S*,4*R*)-3-(4-Methoxyphenyl)-4-phenyl-2-(2,4,6-trimethoxyphenyl)cyclopent-2-en-1-ol



LiAlH_4 (106 mg, 2.79 mmol) was dissolved in anhydrous THF (1.5 mL) under argon atmosphere. At 0 °C, a solution of compound **188** (1 g, 2.32 mmol) in anhydrous THF (3 mL) was added to the reaction mixture which was afterwards stirred at room temperature for 2 hours. Water (106 μL) was added dropwise at 0 °C followed by a solution of NaOH 15% (106 μL) and water again (212 μL). The salts precipitated and were filtered off. The filtrate was concentrated under vacuum to afford compound **232a** (454 mg, 45%) and **232b** (300 mg, 30%).

Compound 232a:

$^1\text{H NMR}$ (CDCl_3 , 400 MHz) δ 1.87 (td, 1H, $J = 3.9$ and 13.7 Hz), 2.66 (d, 1H, $J = 6.0$ Hz), 2.93-3.00 (m, 1H), 3.59 (s, 3H), 3.65 (s, 3H), 3.82 (s, 3H), 3.83 (s, 3H), 4.32 (dd, 1H, $J = 4.1$ and 8.8 Hz), 4.90 (s, 1H), 6.13 (d, 1H, $J = 1.8$ Hz), 6.22 (d, 1H, $J = 1.8$ Hz), 6.53 (d, 2H, $J = 9.0$ Hz), 6.95 (d, 2H, $J = 8.9$ Hz), 7.13 (t, 1H, $J = 7.4$ Hz), 7.24 (t, 2H, $J = 7.8$ Hz), 7.38 (d, 2H, $J = 7.2$ Hz) ppm;

$^{13}\text{C NMR}$ (CDCl_3 , 400 MHz) δ 43.7, 52.5, 55.0, 55.1, 55.4, 55.9, 80.7, 112.9 (2C), 125.9, 128.0 (2C), 128.5 (2C), 129.0 (2C) ppm.

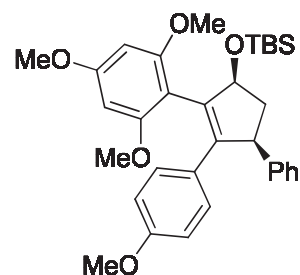
Compound 232b:

$^1\text{H NMR}$ (CDCl_3 , 400 MHz) δ 2.33-2.43 (m, 2H), 2.44-2.47 (m, 1H), 3.62 (s, 3H), 3.65 (s, 3H), 3.81 (s, 3H), 3.84 (s, 3H), 4.54 (d, 1H, $J = 7.0$ Hz), 5.10-5.14 (m, 1H), 6.17 (d, 1H, $J = 1.9$ Hz), 6.23 (d, 1H, $J = 1.8$ Hz), 6.56 (d, 2H, $J = 8.9$ Hz), 6.99 (d, 2H, $J = 8.9$ Hz), 7.14 (t, 1H, $J = 7.2$ Hz), 7.25 (t, 2H, $J = 7.7$ Hz), 7.34 (d, 2H, $J = 7.2$ Hz) ppm;

$^{13}\text{C NMR}$ (CDCl_3 , 400 MHz) δ 45.0, 52.5, 55.1, 55.5, 56.0, 56.1, 80.4, 91.5, 91.6, 107.7, 113.1 (2C), 126.0, 127.7 (2C), 128.6 (2C), 128.8 (2C), 129.4, 134.3, 143.0, 145.8, 158.3, 158.7, 159.0, 161.1 ppm.

Compound 233:

***tert*-Butyl(((1*S*,4*S*)-3-(4-methoxyphenyl)-4-phenyl-2-(2,4,6-trimethoxyphenyl)cyclopent-2-en-1-yl)oxy)dimethylsilane.**



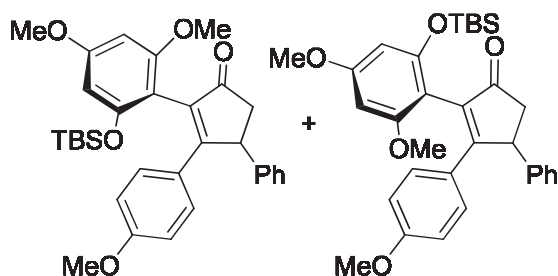
TBSOTf (120 μL , 0.0522 mmol) and DIPEA (153 μL , 0.878 mmol) were added at 0 $^\circ\text{C}$ to compound **232a** in solution in anhydrous toluene (12 mL) under argon atmosphere. After stirring at room temperature overnight, the reaction mixture was diluted in hexane. The precipitated salts were filtered off and the filtrate was concentrated. Purification over silica gel afforded protected alcohol **233** (75 mg, 40%).

$^1\text{H NMR}$ (CDCl_3 , 400 MHz) δ -0.38 (s, 3H), -0.19 (s, 3H), 0.70 (s, 9H), 1.76 (td, 1H, $J = 3.3$ and 13.3 Hz), 2.78-2.86 (m, 1H), 3.61 (s, 3H), 3.64 (s, 3H), 3.77 (s, 3H), 3.83 (s, 3H), 4.13 (dd, 1H, $J = 3.5$ and 8.5 Hz), 5.08 (dd, 1H, $J = 2.8$ and 7.2 Hz), 6.10 (d, 1H, $J = 2.1$ Hz), 6.14 (d, 1H, $J = 2.0$ Hz), 6.51 (d, 2H, $J = 8.9$ Hz), 6.96 (d, 2H, $J = 8.9$ Hz), 7.15 (t, 1H, $J = 7.4$ Hz), 7.26 (t, 2H, $J = 7.3$ Hz), 7.55 (s, 2H, $J = 7.2$ Hz) ppm;

$^{13}\text{C NMR}$ (CDCl_3 , 400 MHz) δ -3.8, 3.6, 26.1 (3C), 46.0, 46.9, 55.2, 55.4, 55.7, 66.0, 92.2, 97.5, 106.7, 113.5 (2C), 126.6, 127.5, 127.8 (2C), 128.2, 128.8 (2C), 121.0, 129.8 (2C), 130.2, 135.5, 143.7, 158.5, 160.2, 161.1, 169.4 ppm.

Compound 234:

2-(2-((*tert*-Butyldimethylsilyl)oxy)-4,6-dimethoxyphenyl)-3-(4-methoxyphenyl)-4-phenylcyclopent-2-en-1-one



TBS-Cl (380 mg, 2.52 mmol), imidazole (229 mg, 3.36 mmol) and DMAP (41 mg, 0.336 mmol) were added to phenol **221** in solution in anhydrous CH_2Cl_2 (20 mL) under argon atmosphere. After stirring at room temperature overnight, the reaction mixture was washed with water. The product was extracted and the organic layer was dried over MgSO_4 , filtered and concentrated. Purification over silica gel afforded protected phenol **234** (664 mg, 63%) as a 1:1 mixture of atropoisomers.

Isomer 234a:

$^1\text{H NMR}$ (CDCl_3 , 400 MHz) δ 0.26 (s, 6H), 0.96 (s, 9H), 2.45 (dd, 1H, $J = 2.8$ Hz and 18.6 Hz), 3.19 (dd, 1H, $J = 7.4$ Hz and 18.6 Hz), 3.41 (s, 3H), 3.69 (s, 3H), 3.80 (s, 3H), 4.69 (dd, 1H, $J = 2.6$ and 7.4 Hz), 6.07 (d, 1H, $J = 2.1$ Hz), 6.19 (d, 1H, $J = 2.1$ Hz), 6.63 (d, 2H, $J = 8.9$ Hz), 7.11-7.17 (m, 1H), 7.21-7.27 (m, 6H) ppm;

$^{13}\text{C NMR}$ (CDCl_3 , 400 MHz) δ -3.8, -3.6, 18.5, 26.1 (3C), 46.0, 46.9, 55.2, 55.4, 55.7, 92.2, 97.5, 106.7, 113.5 (2C), 126.6, 127.8 (2C), 128.2, 128.8 (2C), 129.8 (2C), 135.5, 143.7, 155.9, 128.5, 160.2, 161.1, 169.4, 206.7 ppm.

Isomer 234b:

$^1\text{H NMR}$ (CDCl_3 , 400 MHz) δ -0.03 (s, 6H), 0.09 (s, 6H), 0.78 (s, 3H), 2.5 (dd, 1H, J = 1.8 and 18.6 Hz), 3.09 (dd, 1H, J = 7.5 and 18.4 Hz), 3.69 (s, 3H), 3.79 (s, 3H), 3.81 (s, 3H), 4.58 (dd, 1H, J = 1.5 and 7.4 Hz), 6.07 (d, 1H, J = 2.3 Hz), 6.26 (d, 1H, J = 2.1 Hz), 6.63 (d, 2H, J = 9.0 Hz), 7.15 (t, 1H, J = 7.3 Hz), 7.22-7.31 (m, 6 H) ppm;

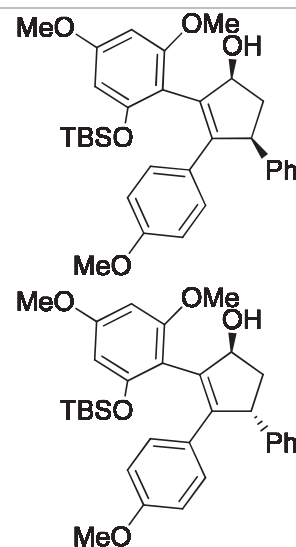
$^{13}\text{C NMR}$ (CDCl_3 , 400 MHz) δ -4.3, -4.2, 18.0, 25.6 (3C), 45.7, 46.9, 55.2, 55.4, 56.1, 92.2, 97.9, 107.2, 113.6 (2C), 126.7, 127.5 (2C), 127.8, 129.0 (2C), 130.2 (2C), 135.1, 144.2, 154.4, 159.5, 160.5, 161.2, 168.7, 204.3 ppm.

Compound 235a:

(1*S*,4*S*)-2-(2-((*tert*-Butyldimethylsilyl)oxy)-4,6-dimethoxyphenyl)-3-(4-methoxyphenyl)-4-phenylcyclopent-2-en-1-ol

Compound 235b:

(1*S*,4*R*)-2-(2-((*tert*-Butyldimethylsilyl)oxy)-4,6-dimethoxyphenyl)-3-(4-methoxyphenyl)-4-phenylcyclopent-2-en-1-ol



LiAlH_4 (29 mg, 0.75 mmol) was dissolved in anhydrous THF (1.2 mL) under argon atmosphere. At 0 °C, a solution of compound **234** (100 mg, 0.19 mol) in anhydrous THF (3.5 mL) was added to the reaction mixture which was afterwards stirred at room temperature for 2 hours. Water (29 μL) was added dropwise at 0 °C followed by a solution of NaOH 15% (29 μL) and water again (58 μL). The salts precipitated and were filtered off. The filtrate was concentrated under vacuum. The crude was then purified on silica gel to afford compound **235a** (14 mg, 14%) and **235b** (21 mg, 21%).

LC-MS calculated for $\text{C}_{32}\text{H}_{40}\text{O}_5\text{Si}$: 532.3, found: 515.2 ($\text{M}-\text{H}_2\text{O}+\text{H}$) $^+$.

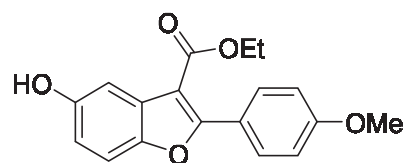
5.3 Procedures for chapter 3.2.

General procedure X: Condensation of benzoquinones

Benzoquinone (1 eq) in solution in toluene was added dropwise to a mixture of oxopropionate (2 eq) and $\text{Cu}(\text{OTf})_2$ (0.05 eq) in toluene. The reaction mixture was heated at reflux for 10 hours then quenched with a saturated aqueous solution of NH_4Cl . The product was extracted with EtOAc and washed with brine. The organic layer was dried over MgSO_4 , filtered and concentrated. After purification on silica gel and crystallization in Et_2O , benzofuran was obtained.

Compound 240a:

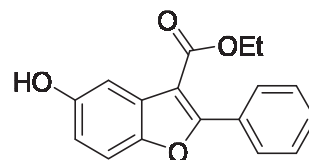
Ethyl 5-hydroxy-2-(4-methoxyphenyl)-benzofuran-3-carboxylate



Compound **240a** was obtained following general procedure X starting from oxopropionate **241** (82.2 g, 370 mmol) in toluene (500 mL) with benzoquinone (20.0 g, 185 mmol) and $\text{Cu}(\text{OTf})_2$ (3.05 g, 9.3 mmol). Product **240a** was obtained with 54% yield (30.92 g).

$^1\text{H NMR}$ (CDCl_3 , 400 MHz), δ 1.34 (t, 3H, $J = 7.2$ Hz), 3.83 (s, 3H), 4.34 (q, 2H, $J = 7.1$ Hz), 6.81 (dd, 1H, $J = 8.8$ and 2.5 Hz), 6.93 (d, 2H, $J = 9.1$ Hz), 7.29 (d, 1H, $J = 8.8$ Hz), 7.41 (d, 1H, $J = 2.3$ Hz), 7.93 (d, 2H, $J = 9.1$ Hz) ppm;

$^{13}\text{C NMR}$ (CDCl_3 , 400 MHz), δ 14.5, 55.5, 60.8, 107.7, 107.8, 111.7, 113.6, 113.7, 122.3, 128.5, 131.3, 148.8, 152.7, 161.4, 162.2, 164.5 ppm.

Compound 240b:**Ethyl 5-hydroxy-2-phenylbenzofuran-3-carboxylate**

Compound **240b** was obtained following general procedure X starting from oxopropionate (32.4 mL, 185 mmol) in toluene (250 mL) with benzoquinone (10.0 g, 92 mmol) and $\text{Cu}(\text{OTf})_2$ (1.53 g, 4.6 mmol). Product **X** was obtained with 53% yield (13.9 g).

$^1\text{H NMR}$ (CDCl_3 , 400 MHz) δ 1.39 (t, 3H, $J = 7.2$ Hz), 4.40 (quad., 2H, $J = 7.2$ Hz), 4.99 (s, 1H), 6.89 (dd, 1H, $J = 2.6$ and 8.8 Hz), 7.39 (d, 1H, 8.8 Hz), 7.47-7.50 (m, 3H), 7.52 (dd, 1H, $J = 0.4$ and 2.6 Hz), 7.97-8.00 (m, 2H) ppm;

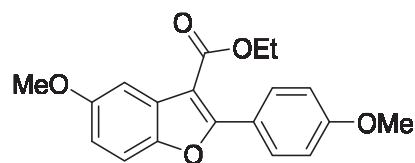
$^{13}\text{C NMR}$ (CDCl_3 , 400 MHz) δ 14.3, 60.7, 107.6, 108.8, 11.7, 113.9, 128.0 (2C), 128.2, 129.5 (2C), 129.7, 130.3, 148.9, 152.6, 161.8, 164.1 ppm.

General procedure XI: Methylation

MeI (1.5 eq), K_2CO_3 (2 eq) and Cs_2CO_3 (0.1 eq) were added to a solution of benzofuran in DMF. After stirring overnight at 65°C, the reaction mixture was concentrated to dryness, diluted in EtOAc and washed with water. The organic layer was separated, washed with brine, dried over MgSO_4 , filtered and concentrated. After purification on silica gel and crystallization in Et_2O , methylated product was obtained.

Compound 241a-1:

Ethyl 5-methoxy-2-(4-methoxyphenyl)-benzofuran-3-carboxylate



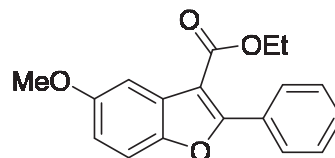
Compound **241a-1** was obtained following general procedure XI starting from benzofuran **240a** (30.92 g, 99 mmol) in DMF (370 mL) with MeI (9.25 mL, 149 mmol), K₂CO₃ (27.39 g, 198 mmol) and Cs₂CO₃ (3.23 g, 9.9 mmol). Product **241a-1** was obtained with 77% yield (24.88 g).

¹H NMR (CDCl₃, 400 MHz), δ 1.34 (t, 3H, J = 7.2 Hz), 3.83 (s, 3H), 3.89 (s, 3H), 4.34 (q, 2H, J = 7.1 Hz), 6.81 (dd, 1H, J = 8.8 and 2.5 Hz), 6.93 (d, 2H, J = 9.1 Hz), 7.29 (d, 1H, J = 8.8 Hz), 7.41 (d, 1H, J = 2.3 Hz), 7.93 (d, 2H, J = 9.1 Hz) ppm;

¹³C NMR (CDCl₃, 400 MHz), δ 14.5, 55.5, 56.0, 60.6, 77.2, 105.1, 108.0, 111.6, 113.7, 113.8, 122.4, 128.3, 131.3, 148.7, 156.9, 161.3, 161.8, 164.4 ppm.

Compound 241b-1:

Ethyl 5-methoxy-2-phenylbenzofuran-3-carboxylate



Compound **241b-1** was obtained following general procedure XI starting from benzofuran **240b** (10 g, 35.2 mmol) in DMF (120 mL) with MeI (3.3 mL, 52.8 mmol), K₂CO₃ (9.7 g, 70.4 mmol) and Cs₂CO₃ (1.14 g, 3.5 mmol). Product **241b-1** was obtained quantitatively (10.5 g).

¹H NMR (CDCl₃, 400 MHz) δ 1.41 (t, 3H, J = 7.2 Hz), 3.90 (s, 3H), 4.40 (quad., 2H, J = 7.2 Hz), 6.96 (dd, 1H, J = 2.8 and 9 Hz), 7.42 (d, 1H, J = 8.9 Hz), 7.47-7.50 (m, 3H), 7.57 (d, 1H, J = 2.6 Hz), 7.98-8.00 (m, 2H) ppm;

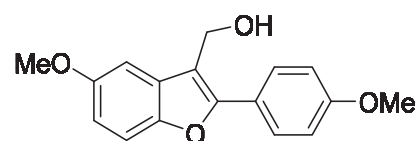
¹³C NMR (CDCl₃, 400 MHz) δ 14.4, 56.0, 60.7, 105.0, 109.1, 11.8, 114.3, 128.1, 128.1 (2C), 129.6 (2C), 129.9, 130.3, 149.0, 157.0, 161.5, 164.2 ppm.

General procedure XII: Reduction of esters

LiAlH₄ (5 eq) was dissolved in anhydrous THF under argon atmosphere at 0 °C. Ester (1 eq) in solution in anhydrous THF was added dropwise and the mixture was stirred at 0 °C. After 2 hours, the reaction mixture was quenched with water. Rochelle salt was added and the precipitated salts were filtered off. The filtrate was concentrated, dissolved in Et₂O and washed with water and brine. The organic layer was dried over MgSO₄, filtered and concentrated to afford reduced product.

Compound 241a:

(5-Methoxy-2-(4-methoxyphenyl)-benzofuran-3-yl)methanol



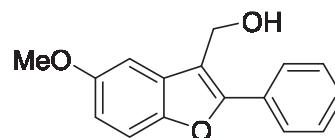
Compound **241a** was obtained following general procedure XII starting from ester **241a-1** (24.9 g, 78 mmol) in anhydrous THF (500 mL) with LiAlH₄ (14.7 g, 388 mmol). Product **241a** was obtained with 88% (19.32 g).

¹H NMR (CDCl₃, 400 MHz), δ 1.70 (t, 1H, J = 5.3 Hz), 3.87 (s, 6H), 4.91 (d, 2H, J = 5.3 Hz), 6.88 (dd, 1H, J = 2.6 and J = 8.9 Hz), 7.01 (d, 2H, J = 9.0 Hz), 7.12 (d, 1H, J = 2.6 Hz), 7.37 (d, 1H, J = 8.9 Hz), 7.76 (d, 2H, J = 9.0 Hz) ppm;

¹³C NMR (CDCl₃, 400 MHz) δ 55.5, 55.8, 56.1, 101.9, 111.7, 113.1, 113.7, 114.4 (2C), 123.1, 128.9 (2C), 130.1, 148.9, 154.7, 156.3, 160.3 ppm.

Compound 241b:

(5-Methoxy-2-phenylbenzofuran-3-yl)methanol



Compound **241b** was obtained following general procedure XII starting from ester **241b-1** (10.5 g, 35.2 mmol) in anhydrous THF (175 mL) with LiAlH₄ (7.3 g, 193.6 mmol). Product **241b** was obtained with 96% (8.7 g).

$^1\text{H NMR}$ (CDCl_3 , 400 MHz), δ 3.89 (s, 3H), 4.98 (d, 2H, $J = 5.4$ Hz), 6.93 (dd, 1H, $J = 2.6$ and 8.9 Hz), 7.16 (d, 1H, $J = 2.5$ Hz), 7.40-7.44 (m, 2H), 7.48-7.52 (m, 2H), 7.83-7.85 (m, 2H) ppm;

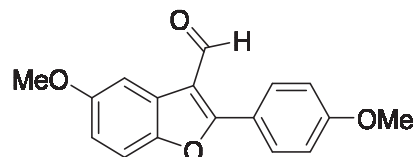
$^{13}\text{C NMR}$ (CDCl_3 , 400 MHz) δ 55.7, 56.0, 102.0, 111.8, 113.6, 115.0, 127.3 (2C), 128.8 (2C), 128.9, 129.8, 130.3, 149.0, 154.3, 156.2 ppm.

General procedure XIII: Oxidation of primary alcohols

To a solution of $(\text{COCl})_2$ (1.2 eq) in anhydrous CH_2Cl_2 was added dropwise at -78°C a solution of DMSO (2 eq) in anhydrous CH_2Cl_2 under argon atmosphere. Alcohol (1 eq) in solution in anhydrous CH_2Cl_2 was added followed by the dropwise addition of triethylamine (2.5 eq). The mixture was stirred for 2 hours and let warm up at room temperature. The reaction mixture was quenched with saturated aqueous solution of NH_4Cl until $\text{pH} = 7$. The organic layer was separated, washed with brine, dried over MgSO_4 , filtered and concentrated. Purification on silica gel let to desired aldehyde.

Compound 242a:

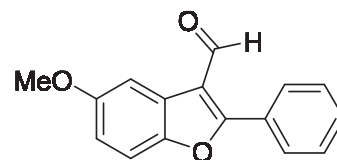
5-Methoxy-2-(4-methoxyphenyl)-benzofuran-3-carbaldehyde



Compound **242a** was obtained following general procedure XIII starting from alcohol **241a** (19.32 g, 68 mmol) in anhydrous CH_2Cl_2 (450 mL) with $(\text{COCl})_2$ (7 mL, 82 mmol), DMSO (9.66 mL, 136 mmol) and triethylamine (23,5 mL, 170 mmol). Product **242a** was obtained with 26% (5.5 g).

$^1\text{H NMR}$ (CDCl_3 , 400 MHz), δ 3.90 (s, 3H), 3.91 (s, 3H), 6.96 (dd, 1H, $J = 2.6$ and 9.0 Hz), 7.07 (d, 2H, $J = 8.9$ Hz), 7.41 (d, 1H, $J = 9.0$ Hz), 7.74 (d, 1H, $J = 2.6$ Hz), 7.80 (d, 2H, $J = 8.9$ Hz), 10.30 (s, 1H) ppm;

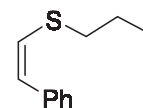
$^{13}\text{C NMR}$ (CDCl_3 , 400 MHz), δ 55.7, 56.1, 104.4, 111.7, 114.8 (2C), 115.1, 117.0, 121.4, 126.4 (2C), 130.8, 148.8, 157.6, 162.1, 166.4, 186.8 ppm.

Compound 242b:**5-Methoxy-2-phenylbenzofuran-3-carbaldehyde**

Compound **242b** was obtained following general procedure XIII starting from alcohol **241b** (5 g, 19.7 mmol) in anhydrous CH_2Cl_2 (130 mL) with $(\text{COCl})_2$ (2 mL, 23.6 mmol), DMSO (2.8 mL, 39.4 mmol) and triethylamine (7 mL, 49 mmol). Product **242b** was obtained with 87% (4.3 g).

$^1\text{H NMR}$ (CDCl_3 , 400 MHz) δ 3.91 (s, 3H), 8.00 (dd, 1H, $J = 2.8$ and 9.0 Hz), 7.45 (d, 1H, $J = 8.9$ Hz), 7.57 (m, 3H), 7.76 (d, 1H, $J = 2.6$ Hz), 7.85 (m, 2H), 10.34 (s, 1H) ppm;

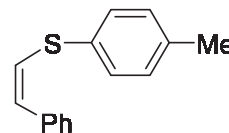
$^{13}\text{C NMR}$ (CDCl_3 , 400 MHz) δ 56.2, 104.4, 111.9, 115.6, 117.9, 126.2, 128.9, 129.2 (2C), 129.3 (2C), 131.2, 149.1, 157.7, 166.1, 186.9 ppm.

Compound 243:**(Z)-Propyl(styryl)sulfane**

To a solution of Cs_2CO_3 (3.19 g, 9.8 mmol) in DMSO (600 mL) was added 1-propanethiol (10.63 mL, 117.6 mmol). After stirring for 15 minutes, TEMPO (3.06 g, 19.5 mmol) was added and after another 15 minutes, phenylacetylene (10.75 mL, 98.0 mmol) was also added. After stirring at room temperature for 3 hours, the reaction mixture was quenched with water, and extracted with Et_2O . The organic layer was dried over MgSO_4 , filtered and concentrated. Purification on silica gel afforded thiovinylether **243** (11.46 g, 66%).

$^1\text{H NMR}$ (CDCl_3 , 400 MHz), δ 1.03 (t, 3H, $J = 7.4$ Hz), 1.73 (six., 2H, $J = 7.3$ Hz), 2.77 (t, 2H, $J = 7.2$ Hz, H_7), 6.25 (d, 1H, $J = 10.9$ Hz), 6.33 (d, 1H, $J = 10.9$ Hz), 7.21 (t, 1H, $J = 7.3$ Hz), 7.35 (t, 2H, $J = 7.5$ Hz), 7.49 (d, 2H, $J = 7.3$ Hz) ppm ;

$^{13}\text{C NMR}$ (CDCl_3 , 400 MHz), δ 13.3, 23.7, 38.1, 77.2, 125.4, 126.7, 127.8, 128.3, 128.7, 137.2 ppm.

Compound 244:**(Z)-Styryl(*p*-tolyl)sulfane**

Na (2.37 g, 0.103 mol) was dissolved in absolute EtOH (100 mL) at 0 °C. 4-Methylbenzenethiol (12.75 g, 0.103 mol) was added followed by phenylacetylene (10.8 mL, 0.098 mol) at room temperature. After on night at reflux, the reaction mixture was cooled down at 0 °C and poured in iced cold water. The obtained precipitate was filtered and dried under vacuum to afford product **244** (16.1 g, 73%).

¹H NMR (CDCl₃, 400 MHz) δ 2.36 (s, 3H), 6.48 (d, 1H, J = 10.8 Hz), 6.56 (d, 1H, J = 10.8 Hz), 7.17 (d, 2H, J = 7.9 Hz), 7.25-7.29 (m, 1H), 7.36-7.42 (m, 4H), 7.55 (d, 2H, J = 8.5 Hz) ppm;

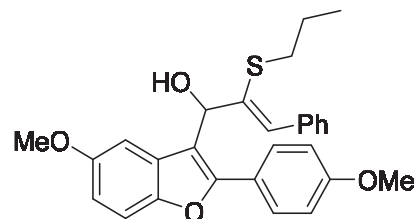
¹³C NMR (CDCl₃, 400 MHz) δ 21.2, 126.6, 127.1, 127.1, 128.4 (2C), 128.8 (2C), 130.0 (2C), 130.6 (2C), 132.8, 136.7, 137.5 ppm.

General procedure XIV: Formation of divinylalcohols

n-BuLi (1.6 M, 1.6 eq) was added dropwise at -78 °C to a solution of thiovinylether **22** (1.5 eq) in anhydrous THF under argon atmosphere and stirred at this temperature for 45 minutes. Simultaneously, BF₃·Et₂O (1.1 eq) was added to a solution of aldehyde (1 eq) in anhydrous THF under argon atmosphere at -78 °C and stirred at this temperature for 45 minutes. The activated aldehyde was added dropwise the lithiated thiovinylether. After 2 hours at -78 °C, the reaction mixture was quenched with water and a saturated aqueous solution of NaHCO₃. The product was extracted with Et₂O and the organic layer was washed with water and brine dried over MgSO₄, filtered and concentrated. Purification over silica gel afforded desired divinyl alcohol.

Compound 245a:

(Z)-1-(5-Methoxy-2-(4-methoxyphenyl)-benzofuran-3-yl)-3-phenyl-2-(propylthio)prop-2-en-1-ol



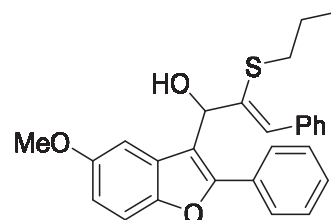
Compound **245a** was obtained following general procedure XIV starting from aldehyde **242a** (1.50 g, 5.3 mmol) and thiovinylether **243** (1.42 g, 8.0 mmol) in anhydrous THF (140 mL) with *n*-BuLi (5.3 mL, 8.5 mmol) and BF₃·Et₂O (0.73 mL, 5.8 mmol). Product **245a** was obtained with 72% (1.76 g).

¹H NMR (CDCl₃, 400 MHz), δ 0.80 (t, 3H, J = 7.4 Hz), 1.50 (six., 2H, J = 7.4 Hz), 2.53 (m, 2H), 2.84 (s, 1H), 3.76 (s, 3H), 3.97 (s, 3H), 5.74 (s, 1H), 6.88 (dd, 1H, J = 2.6 and 8.9 Hz), 6.90 (d, 2H, J = 8.9 Hz), 7.19 (s, 1H), 7.24 (d, 1H, J = 2.6 Hz), 7.25 (t, 1H, J = 7.4 Hz), 7.33 (t, 2H, J = 7.3 Hz), 7.39 (d, 1H, J = 8.9 Hz), 7.62 (d, 2H, J = 7.3 Hz), 7.73 (d, 2H, J = 8.9 Hz) ppm;

¹³C NMR (CDCl₃, 400 MHz), δ 13.4, 23.22, 34.8, 55.5, 56.0, 66.0, 70.2, 77.2, 104.0, 111.7, 113.3, 114.3, 114.5, 123.1, 127.7, 128.2, 128.6, 129.5, 129.6, 132.0, 136.3, 136.3, 149.4, 154.8, 155.9, 160.5 ppm.

Compound 245b:

(Z)-1-(5-Methoxy-2-phenylbenzofuran-3-yl)-3-phenyl-2-(propylthio)prop-2-en-1-ol



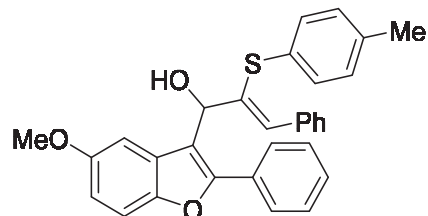
Compound **245b** was obtained following general procedure XIV starting from aldehyde **242b** (200 mg, 0.787 mmol) and thiovinylether **243** (210 mg, 1.18 mmol) in anhydrous THF (20 mL) with *n*-BuLi (1.6 M, 788 μL, 1.26 mmol) and BF₃·Et₂O (110 μL, 0.866 mmol). Product **245b** was obtained with 23% (77 mg). Recovered starting material: thiovinylether **243** (143 mg, 68%) and aldehyde **242b** (98 mg, 50%).

¹H NMR (CDCl₃, 400 MHz) δ 0.80 (t, 3H, J = 7.3 Hz), 1.49 (sex., 2H, J = 7.3 Hz), 2.48-2.62 (m, 2H), 2.86 (d, 1H, J = 3.4 Hz), 3.77 (s, 3H), 5.78 (dd, 1H, J = 1.6 and 3.4 Hz), 6.91 (dd, 1H, J = 2.5 and 8.9 Hz), 7.18 (s, 1H), 7.25 (m, 2H), 7.34 (t, 2H, J = 7.3 Hz), 7.42 (d, 1H, J = 8.5 Hz), 7.45-7.51 (m, 3H), 7.62 (d, 2H, J = 7.3 Hz), 7.85 (d, 2H, J = 8.4 Hz) ppm;

^{13}C NMR (CDCl_3 , 400 MHz) δ 13.2, 23.1, 34.6, 55.9, 69.9, 104.0, 111.7, 113.6, 115.5, 127.6, 127.9 (2C), 128.1 (2C), 128.3, 128.7 (2C), 129.1, 129.5 (2C), 130.4, 132.1, 136.0, 136.1, 149.5, 154.4, 155.8 ppm.

Compound 245c:

(Z)-1-(5-Methoxy-2-phenylbenzofuran-3-yl)-3-phenyl-2-(p-tolylthio)prop-2-en-1-ol



Compound **245c** was obtained following general procedure XIV starting from aldehyde **242b** (3 g, 0.0118 mol) and thiovinylether **244** (4 g, 0.0177 mol) in anhydrous THF (300 mL) with *n*-BuLi (1.6 M, 11.8 mL, 0.0189 mol) and $\text{BF}_3 \cdot \text{Et}_2\text{O}$ (1.64 mL, 0.013 mol). Product **245c** was obtained with 86% (4.83 g).

^1H NMR (CDCl_3 , 400 MHz) δ 2.24 (s, 3H), 2.60 (d, 1H, $J = 3.5$ Hz), 3.76 (s, 3H), 5.61 (dd, 1H, $J = 1.4$ and 3.5 Hz), 6.90 (dd, 1H, $J = 2.6$ and 8.9 Hz), 6.92 (d, 2H, $J = 7.8$ Hz), 7.13 (d, 2H, $J = 8.0$ Hz), 7.26-7.37 (m, 7H), 7.40 (d, 1H, $J = 8.9$ Hz), 7.45 (s, 1H), 7.55-7.58 (m, 2H), 7.65 (d, 2H, $J = 7.4$ Hz) ppm;

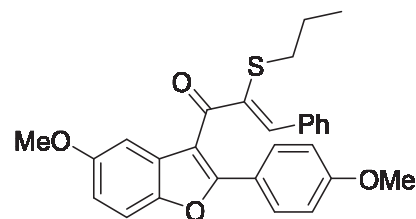
^{13}C NMR (CDCl_3 , 400 MHz) δ 21.1, 55.9, 69.1, 103.8, 111.7, 113.6, 115.2, 127.6 (2C), 128.0, 128.1 (2C), 128.3, 128.5 (2C), 128.7, 129.1, 129.6 (2C), 129.7 (2C), 130.3, 131.2 (2C), 133.3, 135.2, 135.7, 137.3, 149.4, 154.5, 155.8 ppm.

General procedure XV: Oxidation of secondary alcohols

MnO_2 (6 eq) was added to a solution of divinyl alcohol (1 eq) in CH_2Cl_2 . After 48 hours, the mixture was filtered through celite and purified on silica gel to afford desired divinyl ketone.

Compound 239a:

(Z)-1-(5-Methoxy-2-(4-methoxyphenyl)-benzofuran-3-yl)-3-phenyl-2-(propylthio)prop-2-en-1-one



Compound **239a** was obtained following general procedure XV starting from alcohol **245a** (1.5 g, 4.23 mmol) in CH₂Cl₂ (100 mL) with MnO₂ (2.21 g, 0.025 mol). Product **239a** was obtained with 72% (1.4 g).

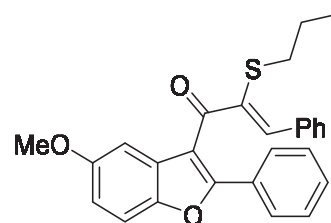
¹H NMR (CDCl₃, 400 MHz), δ 0.92 (t, 3H, J = 7.4 Hz), 1.58 (six., 2H, J = 7.3 Hz), 2.78 (t, 2H, J = 7.4 Hz), 3.79 (s, 3H), 3.82 (s, 3H), 6.92 (d, 2H, J = 8.9 Hz), 6.94 (dd, 1H, J = 2.6 and 8.9 Hz), 7.27 (d, 1H, J = 2.5 Hz), 7.31 (t, 1H, J = 7.3 Hz), 7.33 (t, 2H, J = 7.3 Hz), 7.43 (s, 1H), 7.44 (d, 1H, J = 8.9 Hz), 7.49 (d, 2H, J = 7.3 Hz), 7.79 (d, 2H, J = 8.9 Hz) ppm;

¹³C NMR (CDCl₃, 400 MHz), δ 13.4, 23.5, 35.2, 55.5, 56.0, 103.7, 111.9, 113.4, 114.2, 114.3, 115.4, 128.3, 128.9, 129.2, 130.47, 130.5, 131.4, 135.1, 137.5, 141.3, 148.7, 157.0, 160.3, 161.3, 190.5 ppm;

LC-MS calculated for C₂₈H₂₆O₄S: 458.2, found: 459.1 (M+H)⁺.

Compound 239b:

(Z)-1-(5-Methoxy-2-phenylbenzofuran-3-yl)-3-phenyl-2-(propylthio)prop-2-en-1-one



Compound **239b** was obtained following general procedure XV starting from alcohol **245b** (75 mg, 0.174 mmol) in CH₂Cl₂ (3 mL) with MnO₂ (91 mg, 1.5 mmol). Product **239b** was obtained with 87% (65 mg).

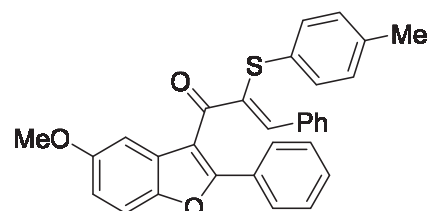
¹H NMR (CDCl₃, 400 MHz) δ 0.93 (t, 3H, J = 7.3 Hz), 1.60 (sex., 2H, J = 7.3 Hz), 2.80 (t, 2H, J = 7.4 Hz), 3.81 (s, 3H), 6.98 (dd, 1H, J = 2.6 and 9.0 Hz), 7.29-7.32 (m, 4H), 7.39-7.41 (m, 3H), 7.45-7.48 (m, 4H), 7.79-7.82 (m, 2H) ppm;

^{13}C NMR (CDCl_3 , 400 MHz) δ 13.5, 23.5, 35.2, 56.0, 103.6, 112.1, 114.9, 116.5, 128.3 (2C), 128.7 (2C), 128.8, 128.9 (2C), 129.3, 130.0, 130.2, 130.5 (2C), 135.0, 137.0, 142.3, 149.0, 157.0, 159.7, 190.5 ppm;

LC-MS calculated for $\text{C}_{27}\text{H}_{24}\text{O}_3\text{S}$: 428.1, found: 428.1 ($\text{M}+\text{H}$) $^+$.

Compound 239c:

(Z)-1-(5-Methoxy-2-phenylbenzofuran-3-yl)-3-phenyl-2-(p-tolylthio)prop-2-en-1-one



Compound **239c** was obtained following general procedure XV starting from alcohol **245c** (2 g, 4.18 mmol) in CH_2Cl_2 (65 mL) with MnO_2 (2.18 g, 0.0251 mol). Product **239c** was obtained quantitatively (2 g).

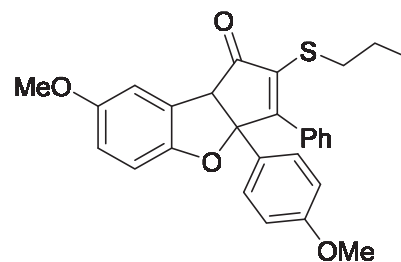
^1H NMR (CDCl_3 , 400 MHz) δ 2.11 (s, 3H), 3.78 (s, 3H), 6.80 (d, 2H, $J = 7.9$ Hz), 6.89 (dd, 1H, $J = 2.5$ and 8.9 Hz), 6.97 (d, 1H, $J = 2.5$ Hz), 7.02 (d, 2H, $J = 8.0$ Hz), 7.33-7.38 (m, 7H), 7.54-7.56 (m, 2H), 7.65-7.67 (m, 3H) ppm;

^{13}C NMR (CDCl_3 , 400 MHz) δ 21.0, 31.1, 56.0, 103.4, 111.6, 114.4, 116.8, 128.4 (2C), 128.5(2C), 128.5 (2C), 129.6, 129.7 (2C), 123.9, 128.0, 130.0, 130.1, 130.6 (2C), 131.9 (2C), 134.8, 137.6, 137.8, 139.6, 141.4, 148.5, 156.3 ppm;

LC-MS calculated for $\text{C}_{31}\text{H}_{24}\text{O}_3\text{S}$: 476.1, found: 477.1 ($\text{M}+\text{H}$) $^+$.

Compound 238a:

7-Methoxy-3a-(4-methoxyphenyl)-3-phenyl-2-(propylthio)-3a,8b-dihydro-1H-cyclopenta[*b*]benzofuran-1-one



AcBr (24 μ L, 0.33 mmol) was added to a solution of ketone **239a** (100 mg, 0.22 mmol) in DCE (3 mL) and the mixture was stirred at 65 $^{\circ}$ C for 24 hours then at 80 $^{\circ}$ C for another 24 hours. The reaction mixture was quenched at room temperature with a saturated aqueous solution of NaHCO₃ and the product was extracted with CH₂Cl₂. The organic layer was separated, washed with water, dried over MgSO₄, filtered and concentrated. Purification on silica gel afforded cyclopentenone **238a** (31 mg, 31%).

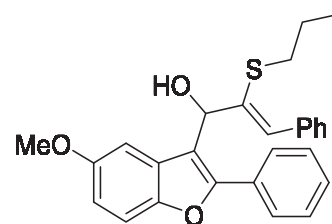
¹H NMR (CDCl₃, 400 MHz), δ 0.80 (t, 3H, J = 7.4 Hz), 1.40 (six., 2H, J = 7.4 Hz), 2.91 (t, 2H, J = 7.4 Hz), 3.76 (s, 3H), 3.77 (s, 3H), 4.05 (s, 1H), 6.80 (dd, 1H, J = 2.6 and 8.9 Hz), 6.80 (d, 2H, J = 8.9 Hz), 6.88 (d, 1H, J = 8.9 Hz), 6.97 (d, 1H, J = 2.5 Hz), 7.25 (d, 2H, J = 8.9 Hz), 7.33 (t, 2H, J = 7.3 Hz), 7.30 (t, 1H, J = 6.4 Hz), 7.53 (d, 2H, J = 7.3 Hz) ppm;

¹³C NMR (CDCl₃, 400 MHz), δ 13.1, 23.4, 33.1, 55.3, 56.1, 62.8, 95.7, 109.8, 110.8, 114.2, 116.1, 124.1, 126.2, 128.0, 129.6, 132.5, 133.2, 137.7, 152.8, 155.0, 159.2, 165.2 ppm;

LC-MS calculated for C₂₈H₂₆O₄S: 458.2, found: 459.9 (M+H)⁺.

Compound 245b:

(Z)-1-(5-Methoxy-2-phenylbenzofuran-3-yl)-3-phenyl-2-(propylthio)prop-2-en-1-one

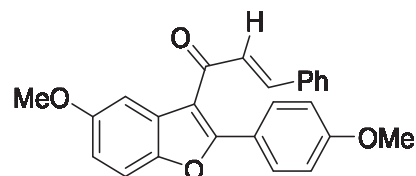


TIBAL (1 M, 436 μ L, 0.436 mmol) was added at -78 $^{\circ}$ C to compound **239b** (100 mg, 0.218 mmol) in solution in anhydrous DCE over 4 \AA MS, under argon atmosphere. The reaction mixture was let warming up at room temperature. After 16 hours at room temperature the reaction mixture was quenched with a 1 N solution of HCl until it reached basic pH. The product was extracted and washed with brine. The organic layer was dried over MgSO₄,

filtered and concentrated. Purification on silica gel gave compound **245b** (23 mg, 23%). Recovered starting material (60 mg, 60%). This product was already described page 183 following another method.

Compound 246:

(E)-1-(5-Methoxy-2-(4-methoxyphenyl)benzofuran-3-yl)-3-phenylprop-2-en-1-one



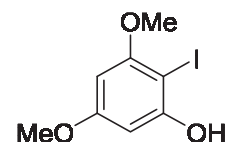
Compound **239b** (200 mg, 0.436 mmol) was dissolved in anhydrous DCE (6 mL) under argon atmosphere. Propionyl bromide (59 μ L, 0.65 mmol) was added and the mixture was stirred at 65 °C for 24 hours then at 75 °C for 48 hours. The reaction mixture was concentrated, dissolved in EtOAc and washed with a saturated aqueous solution of NaHCO₃ with few drops of NH₄OH. The product was extracted and washed with brine. The organic layer was dried over MgSO₄, filtered and concentrated. Purification on silica gel afforded product **246** (50.4 mg, 30%). Recovered starting material (49.2 mg, 25%).

¹H NMR (CDCl₃, 400 MHz) δ 3.87 (s, 3H), 3.892 (s, 3H), 6.96 (dd, 1H, J = 2.6 and 8.9 Hz), 6.97 (d, 1H, J = 15.8 Hz), 7.02 (d, 2H, J = 9.0 Hz), 7.32-7.34 (m, 5H), 7.42 (dd, 1H, J = 0.4 and 8.9 Hz), 7.62 (d, 1H, J = 2.5 Hz), 7.74 (d, 1H, 15.8 Hz), 7.76 (d, 2H, J = 8.9 Hz) ppm;

¹³C NMR (CDCl₃, 400 MHz) δ 55.6, 56.1, 107.2, 111.6, 114.3 (2C), 114.7, 117.9, 122.7, 125.9, 128.4 (2C), 128.5, 129.0 (2C), 130.4, 131.4 (2C), 135.0, 142.5, 149.0, 157.1, 160.6, 161.5, 187.8 ppm.

General procedure XVI: Iodation

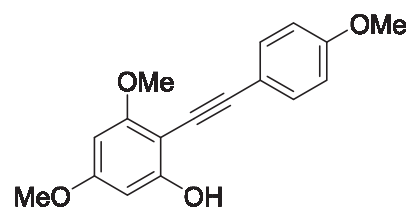
H₂O₂ (30% aq., 0.6-0.9 eq) and I₂ (0.7-0.4 eq) were added to a solution of aryl (1 eq) in water and the obtained suspension was stirred between room temperature and 50 °C for 7 to 16 hours. The reaction mixture was dissolved in CH₂Cl₂, washed with a solution of Na₂S₂O₃ then with water. The organic layer was dried over MgSO₄, filtered and concentrated to afford iodine derivatives.

Compound 248-1:**2-Iodo-3,5-dimethoxyphenol**

Compound **248-1** was obtained following general procedure XVI starting from 3,5-dimethoxyphenol (15 g, 97.4 mmol) in water (180 mL) with H₂O₂ (30% aq., 7.17 g, 63.3 mmol) and I₂ (12.4 g, 48.7 mmol) for 16 hours at room temperature. Product **248-1** was obtained with 29% yield (7.75 g).

¹H NMR (CDCl₃, 400 MHz) δ 3.79 (s, 3H), 3.84 (s, 3H), 5.47 (s, 1H), 6.06 (d, 1H, J = 2.6 Hz), 6.29 (d, 1H, J = 2.6 Hz) ppm;

¹³C NMR (CDCl₃, 400 MHz) δ 55.2, 56.1, 66.8, 91.7, 92.7, 156.2, 158.7, 161.9 ppm.

Compound 248:**3,5-Dimethoxy-2-((4-methoxyphenyl)ethynyl)phenol**

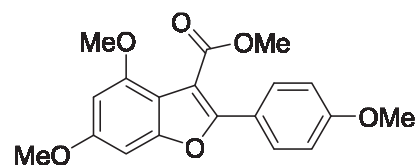
4-Methoxyphenyl acetylene (1.55 mL, 12.01 mmol) and iodophenol **248-1** (3.06 g, 10.92 mmol) were dissolved in anhydrous THF (25 mL) under argon atmosphere. At 0 °C, EtMgBr (22.93 mL, 22.93 mmol) was added dropwise and stirred 5 minutes at this temperature. At room temperature, Pd(PPh₃)₂Cl₂ (146 mg, 0.21 mmol) was added and the resulting mixture was heated at 70 °C for 2 hours. The reaction mixture was quenched with a 0.5 M solution of HCl and the product extracted with EtOAc. The organic layer was washed with water, dried over MgSO₄, filtered and concentrated to afford tolane **248** with 52% yield (1.6 g).

¹H NMR (CDCl₃, 400 MHz) δ 3.80 (s, 3H), 3.83 (s, 3H), 3.86 (s, 3H), 5.98 (s, 1H), 6.06 (d, 1H, J = 2.3 Hz), 6.19 (d, 1H, J = 2.3 Hz), 6.88 (d, 2H, J = 8.9 Hz), 7.48 (d, 2H, J = 8.9 Hz) ppm;

¹³C NMR (CDCl₃, 400 MHz) δ 55.3, 55.5, 56.0, 78.2, 91.4, 92.1, 92.4, 98.9, 113.9 (2C), 115.0, 133.1 (2C), 158.7, 159.7, 160.9, 161.8 ppm.

Compound 249:

Methyl 4,6-dimethoxy-2-(4-methoxyphenyl)-benzofuran-3-carboxylate



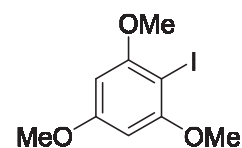
Pd(OAc)₂ (25 mg, 0.11 mmol), CBr₄ (3.85 g, 11.6 mmol) and NaHCO₃ (0.970 g, 11.6 mmol) were added to tolane **248** (1.5 g, 5.29 mmol) in solution in methanol (30 mL) under CO atmosphere. After overnight stirring at room temperature, the reaction mixture was filtered on celite, concentrated and dried under vacuum to afford ester **249** with 72% yield (1.3 g).

¹H NMR (CDCl₃, 400 MHz) δ 3.85 (s, 3H), 3.85 (s, 3H), 3.89 (s, 3H), 3.92 (s, 3H), 6.35 (d, 1H, J = 1.9 Hz), 6.65 (d, 1H, J = 2.0 Hz), 6.96 (d, 2H, J = 8.9 Hz), 7.75 (d, 2H, J = 9.0 Hz) ppm;

¹³C NMR (CDCl₃, 400 MHz) δ 55.4, 55.5, 55.9, 56.0, 88.1, 95.3, 107.9, 111.0, 114.1 (2C), 122.6, 128.7 (2C), 153.6, 153.8, 155.5, 159.6, 160.4, 166.3 ppm.

Compound 253-1:

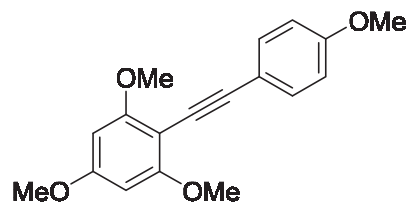
2-Iodo-1,3,5-trimethoxybenzene



Compound **253-1** was obtained following general procedure XVI starting from 3,5-dimethoxyphenol (15 g, 97.4 mmol) in water (180 mL) with H₂O₂ (30% aq., 4.50 mL, 40.0 mmol) and I₂ (5.08 g, 20.0 mmol) for 7 hours at 50°C. Product **253-1** was obtained with 94% yield (12.01 g).

¹H NMR (DMSO-*d*₆, 400 MHz), δ 3.80 (s, 9H), 6.28 (s, 2H) ppm;

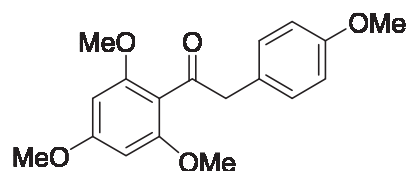
¹³C NMR (DMSO-*d*₆, 400 MHz), δ 55.5, 56.4, 66.3, 91.6, 159.3, 161.9 ppm.

Compound 253:**1,3,5-Trimethoxy-2-((4-methoxyphenyl)ethynyl)benzene**

Triethylamine (30 mL) was added dropwise to a solution of 2-iodo-1,2,3-trimethoxybenzene **253-1** (3.91 g 13.3 mmol), 4-methoxyphenylacetylene (3.5 g, 26.5 mmol), Pd(PPh₃)₂Cl₂ (280 mg, 0.40 mmol) and CuI (76 mg, 0.40 mmol) in DMF (30 mL) under argon atmosphere. After one night at 80 °C, the reaction mixture was cooled at room temperature, filtered over celite and the filtrate was concentrated. Purification silica gel afforded tolane **253** (2.73 g, 70%).

¹H NMR (CDCl₃, 400 MHz), δ 3.81 (s, 3H), 3.83 (s, 3H), 3.88 (s, 6H), 6.12 (s, 2H), 6.84 (d, 2H, J = 8.9 Hz), 7.49 (d, 2H, J = 8.9 Hz) ppm;

¹³C NMR (CDCl₃, 400 MHz), δ 55.4, 55.5, 56.2 (2C), 80.5, 90.7 (2C), 94.9 (2C), 96.3, 113.9 (2C), 116.6, 133.1 (2C), 159.3, 161.5, 162.2 ppm.

Compound 254:**2-(4-Methoxyphenyl)-1-(2,4,6-trimethoxyphenyl)ethan-1-one**

Hg(OAc)₂ (3.31 g, 10.4 mmol) was added to a solution of tolane **253** (2.40 g, 8.4 mmol) in glacial acetic acid (150 mL) at 0 °C and the mixture was stirred at this temperature for an hour and under sonication for an extra hour. The reaction mixture was poured into brine (150 mL) at 0°C and stirred vigorously under it warmed up at room temperature. It was then filtered, washed with water and pentane and dried under vacuum. The product was used in the next step after recrystallization in CHCl₃ (crude weight: 2.11 g).

Anhydrous LiCl (379 mg, 8.9 mmol), PdCl₂ (721 mg, 4.1 mmol), and MgO (327 mg, 8.2 mmol) were dissolved in MeOH (50 mL). The mixture was cooled at -78 °C for 20 min. The previously synthesized intermediate (2.11 g, 4.1 mmol) was added under carbon monoxide atmosphere. After 16 hours at room temperature, activated charcoal was added along with

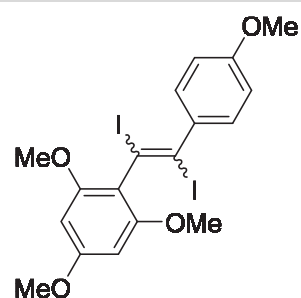
Et₂O. The reaction mixture was filtered through celite, washed with saturated aqueous solution of NH₄Cl. The organic layer was dried over MgSO₄, filtered and concentrated to afford ketone **254** (1.04 g, 80%).

¹H NMR (CDCl₃, 400 MHz), δ 3.74 (s, 6H), 3.78 (s, 3H), 3.81 (s, 3H), 3.97 (s, 2H), 6.01 (s, 2H), 6.81 (d, 2H, J = 8.7 Hz), 7.12 (d, 2H, J = 8.7 Hz) ppm;

¹³C NMR (CDCl₃, 400 MHz), δ 50.7, 55.3 (2C), 55.5, 55.9, 90.7 (2C), 113.7 (2C), 127.1, 130.9 (2C), 158.2, 158.4, 162.4 (2C), 201.9 ppm.

Compound 257:

2-(1,2-Diiodo-2-(4-methoxyphenyl)vinyl)-1,3,5-trimethoxybenzene



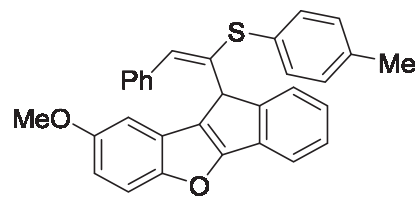
To a solution of alkyne **253** (150 mg, 0.503 mmol) in CH₂Cl₂ (2 mL) under argon atmosphere was added gradually ICl (122.5 mg, 0.755 mmol) dissolved CH₂Cl₂ (3 mL). The reaction mixture was allowed to stir at room temperature overnight. The excess ICl was removed by washing with a saturated aqueous solution of Na₂S₂O₃. The mixture was then extracted by EtOAc (2 × 10 mL). The combined organic layers were dried over anhydrous MgSO₄ and concentrated under a vacuum to yield the crude product, which was purified by chromatography on silica gel to yield 52% of product **257** (144 mg).

¹H NMR (400 Hz, CDCl₃), δ 3.83 (s, 3H), 3.85 (s, 3H), 3.90 (s, 6H), 6.17 (s, 2H), 6.87 (d, 2H, J = 8.7 Hz), 7.47 (d, 2H, J = 8.7 Hz) ppm;

LC-MS calculated for C₁₈H₁₈I₂O₄: 551.9, found: 551.2 (M+H)⁺.

Compound 259c:

(E)-8-Methoxy-10-(2-phenyl-1-(p-tolylthio)vinyl)-10H-indeno[1,2-b]benzofuran



(COCl)₂ (64 μ L, 0.752 mmol) was dissolved in anhydrous CH₂Cl₂ (6 mL) under argon atmosphere. At -78 °C was added dropwise a solution of DMSO (89 μ L, 1.25 mmol) in CH₂Cl₂ (1 mL) followed by a solution of compound **245c** (300 mg, 0.627 mmol) in CH₂Cl₂ (1 mL). After 30 minutes at -78 °C, Et₃N was added dropwise and the mixture was stirred at that temperature for 2 hours. The reaction mixture was then quenched with water and neutralized with a saturated solution of NaHCO₃ until pH = 1. The organic layer was separated, dried over MgSO₄, filtered and concentrated. Purification on silica gel afforded product **259c** (200 mg, 69%).

¹H NMR (CDCl₃, 400 MHz) δ 2.29 (s, 3H), 3.56 (s, 3H), 5.20 (s, 1H), 6.12 (d, 1H, J = 2.6 Hz), 6.68 (d, 1H, J = 1.9 Hz), 6.78 (dd, 1H, J = 2.6 and 8.9 Hz), 7.00 (d, 2H, J = 8.2 Hz), 7.04 (dd, 1H, J = 1.5 and 7.4 Hz), 7.16 (d, 1H, J = 7.4 Hz), 7.23-7.29 (m, 4H), 7.32 (d, 1H, J = 8.9 Hz), 7.41 (d, 1H, J = 6.9 Hz), 7.44 (d, 2H, J = 7.4 Hz), 7.80 (dd, 2H, J = 1.6 and 8.3 Hz) ppm;

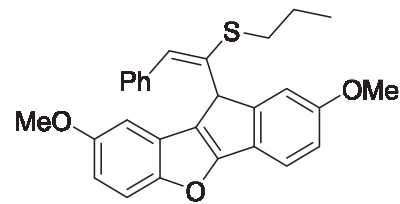
¹³C NMR (CDCl₃, 400 MHz) δ 21.3, 49.6, 55.8, 103.4, 111.4, 112.2, 112.7, 120.1, 123.7, 125.0, 127.6, 127.9 (2C), 128.7, 128.8 (2C), 129.2, 129.2, 130.0 (2C), 130.9, 133.4 (2C), 138.4, 143.7, 146.3, 148.0, 149.4, 155.0, 155.6 ppm.

Product 259c was also be obtained with the following procedure:

2,3,4,5-Tetrafluorophenyl boronic acid (8.1 mg, 0.0418 mmol) was added to compound **245c** (100 mg, 0.209 mmol) in solution in anhydrous DCE (2 mL) under argon atmosphere. After 3 hours at 50 °C, the reaction mixture was concentrated, diluted in Et₂O and washed with water and brine. The organic layer was separated, dried over MgSO₄, filtered and concentrated. Purification on silica gel afforded product **259c** (65 mg, 68%).

Compound 259a:

(E)-2,8-Dimethoxy-10-(2-phenyl-1-(propylthio)vinyl)-10H-indeno[1,2-b]benzofuran



Compound **259a** was obtained following general procedure IX starting from compound **245a** (100 mg, 0.232 mmol) in DCE (2 mL) with Re_2O_7 (1.7 mg, 0.0035 mmol) and MeOH (72 μL , 1.786 mmol). Tetracyclic compound **259a** was obtained (47 mg, 46%).

$^1\text{H NMR}$ (CDCl_3 , 400 MHz) δ 0.94 (t, 3H, $J = 7.3$ Hz), 1.68 (sex., 2H, $J = 7.3$ Hz), 2.83 (t, 2H, $J = 7.3$ Hz), 3.53 (s, 3H), 3.88 (s, 3H), 5.09 (s, 1H), 6.03 (d, 1H, $J = 2.6$ Hz), 6.64 (d, 1H, $J = 1.8$ Hz), 6.74 (dd, 1H, $J = 2.6$ and 8.9 Hz), 7.00 (td, 1H, $J = 1.3$ and 7.4 Hz), 7.65 (d, 2H, $J = 8.8$ Hz), 7.14 (d, 1H, $J = 7.4$ Hz), 7.23 (d, 1H, $J = 7.7$ Hz), 7.31 (d, 2H, $J = 9.0$ Hz), 7.91 (d, 2H, $J = 8.8$ Hz) ppm;

$^{13}\text{C NMR}$ (CDCl_3 , 400 MHz) δ 13.7, 22.1, 34.6, 50.1, 55.5, 55.7, 103.4, 111.2, 111.4, 112.2, 114.5 (2C), 119.2, 123.5, 123.6, 123.7, 124.3, 127.5, 128.8, 129.4 (2C), 144.3, 145.5, 148.7, 149.2, 155.0, 155.5, 160.2 ppm.

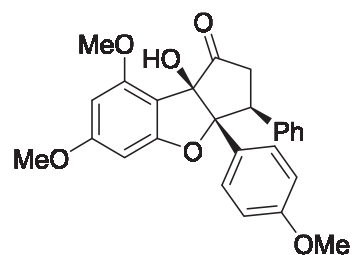
Product 259a was also be obtained with the following procedure:

2,3,4,5-Tetrafluorophenyl boronic acid (9 mg, 0.0464 mmol) was added to compound **245a** (100 mg, 0.232 mmol) in solution in anhydrous DCE (2 mL) under argon atmosphere. After 3 hours at 50 $^\circ\text{C}$, the reaction mixture was concentrated, diluted in Et_2O and washed with water and brine. The organic layer was separated, dried over MgSO_4 , filtered and concentrated. Purification on silica gel afforded product **259a** (59 mg, 57%).

5.4 Procedures for chapter 3.3.

Compound 262-1:

(3*S*,3*aR*,8*bR*)-8*b*-Hydroxy-6,8-dimethoxy-3*a*-(4-methoxyphenyl)-3-phenyl-2,3,3*a*,8*b*-tetrahydro-1*H*-cyclopenta[*b*]benzofuran-1-one



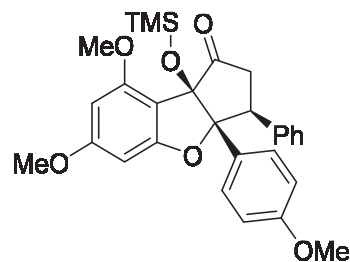
Alcohol **180** (1 g, 2.3 mmol) was dissolved in DMSO (20 mL) under argon atmosphere. At 0 °C, triethylamine (3.53 mL, 25.3 mmol) was added dropwise than PySO₃ complex (1.1 g, 6.9 mmol) dissolved in DMSO (10 mL). After 2.5 h at room temperature, the mixture was quenched with a solution of saturated aqueous NH₄Cl at 0 °C and stirred at this temperature for 30 minutes. The precipitated was filtered off and washed with a small amount of water. The product was purified by silica chromatography to afford **262-1** (935 mg, 94%).

¹H NMR (CDCl₃, 400 MHz) δ 2.94-3.09 (m, 3H), 3.14 (br, s, 1H), 3.71 (s, 3H), 3.83 (s, 3H), 3.85 (s, 3H), 6.10 (d, 1H, J = 2.1 Hz), 6.34 (d, 1H, J = 2.1 Hz), 6.67 (d, 2H, J = 8.8 Hz), 6.94-6.97 (m, 4H), 7.10-7.13 (m, 3H) ppm;

¹³C NMR (CDCl₃, 400 MHz) δ 40.0, 48.7, 55.2, 55.7, 55.9, 88.9, 89.8, 92.8, 101.4, 106.7, 113.3 (2C), 126.0, 126.9, 128.0 (2C), 128.0 (2C), 128.1 (2C), 137.4, 158.6, 158.9, 161.3, 164.9, 210.8 ppm.

Compound 262:

(3*S*,3*aR*,8*bR*)-6,8-Dimethoxy-3*a*-(4-methoxyphenyl)-3-phenyl-8*b*-((trimethylsilyl)oxy)-2,3,3*a*,8*b*-tetrahydro-1*H*-cyclopenta[*b*]benzofuran-1-one



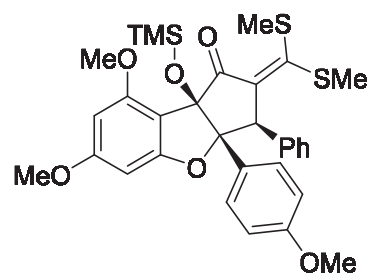
Alcohol **262-1** (100 mg, 0.23 mmol) was dissolved in anhydrous toluene (6 mL) under argon atmosphere. DIPEA (80 μ L, 0.46 mmol) was added dropwise to the mixture at 0 $^{\circ}$ C followed by TMSOTf (75 μ L, 0.416 mmol). The mixture was stirred at 0 $^{\circ}$ C for 30 minutes than at room temperature for another 45 minutes. The mixture was then diluted with hexane (60 mL). The precipitated salts were filtered out and the filtrate was evaporated under reduced pressure to afford **262** (117 mg, quantitative).

$^1\text{H NMR}$ (CDCl_3 , 400 MHz) δ -0.40 (s, 9H), 2.84-2.90 (m, 2H), 3.67-3.74 (m, 1H), 3.73 (s, 3H), 3.84 (s, 3H), 3.87 (s, 3H), 6.09 (d, 1H, $J = 2$ Hz), 6.33 (d, 1H, $J = 2$ Hz), 6.65 (d, 2H, $J = 8.5$ Hz), 6.82-6.83 (m, 2H), 6.94 (d, 2H, $J = 8.5$ Hz), 7.07-7.10 (m, 3H) ppm;

$^{13}\text{C NMR}$ (CDCl_3 , 400 MHz) δ -0.2 (3C), 39.2, 47.3, 54.3, 54.4, 54.8, 88.7, 89.3, 91.5, 101.0, 105.3, 111.7 (2C), 125.9, 125.8, 126.9 (2C), 127.2 (2C), 127.7 (2C), 136.7, 157.8, 158.4, 160.7, 164.1, 207.6 ppm.

Compound 263-1:

(3*R*,3*aR*,8*bR*)-2-(Bis(methylthio)methylene)-6,8-dimethoxy-3*a*-(4-methoxyphenyl)-3-phenyl-8*b*-((trimethylsilyl)oxy)-2,3,3*a*,8*b*-tetrahydro-1*H*-cyclopenta[*b*]benzofuran-1-one



Diisopropylamine (347 μ L, 2.47 mmol) was dissolved in anhydrous THF (15 mL) under argon atmosphere. At -40 $^{\circ}$ C, *n*-BuLi (1.6 M, 1.49 mL, 2.38 mmol) was added dropwise and the mixture was stirred at this temperature for 15 minutes. HMPA (2.44 mL, 0.014 mol) was then added rapidly and the mixture was stirred for another 30 minutes. Cyclopentenone **262** (300 mg, 0.595 mmol) was dissolved in anhydrous THF (5 mL) and added dropwise and the

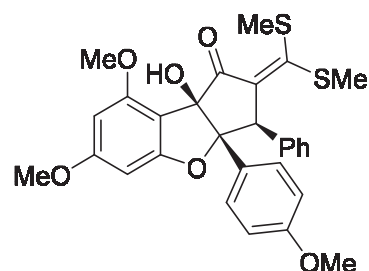
mixture was stirred for 1 h. Freshly distilled CS₂ (1.09 mL, 0.018 mol) was added rapidly and the mixture was stirred for 5 h. Finally, MeI (1.48 mL, 0.024 mol) was added rapidly and the mixture was stirred at room temperature for 16 hours. The mixture was diluted with hexane (60 mL) and the organic layer was washed with four times with water and once with brine. The organic layer was dried over MgSO₄, filtered and evaporated under reduced pressure. Chromatography on silica yield to **263-1** (266 mg, 73%).

¹H NMR (CDCl₃, 400 MHz) δ -0.41 (s, 9H), 2.04 (s, 3H), 2.53 (s, 3H), 3.66 (s, 3H), 3.79 (s, 3H), 3.86 (s, 3H), 4.31 (s, 1H), 6.05 (s, 1H), 6.31 (s, 1H), 6.52 (d, 2H, J = 8.9 Hz), 6.73-6.79 (m, 2H), 6.89 (d, 2H, J = 8.9 Hz), 6.94-6.96 (m, 3H) ppm;

¹³C NMR (CDCl₃, 400 MHz) δ -0.1 (3C), 17.3, 19.0, 54.3, 54.4, 54.8, 59.3, 88.4, 89.0, 91.5, 99.6, 106.5, 111.2 (2C), 125.1, 126.4 (2C), 127.2, 127.9 (2C), 128.1, 130.7, 137.0, 137.9, 155.3, 157.3, 157.9, 160.63, 163.7, 192.3 ppm.

Compound 263:

(3*R*,3*aR*,8*bR*)-2-(Bis(methylthio)methylene)-8*b*-hydroxy-6,8-dimethoxy-3*a*-(4-methoxyphenyl)-3-phenyl-2,3,3*a*,8*b*-tetrahydro-1*H*-cyclopenta[*b*]benzofuran-1-one

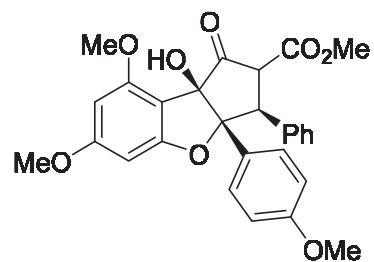


To a solution of **263-1** (246 mg, 0.40 mmol) in anhydrous THF (6 mL) under argon atmosphere was added TBAF (1 M, 889 μL, 0.889 mmol) dropwise at 0 °C. The mixture was stirred at this temperature for 30 minutes, washed with water and extracted with Et₂O. The organic layer was dried over MgSO₄, filtered and concentrated under reduced pressure to afford **263** (166 mg, 76%).

¹H NMR (CDCl₃, 400 MHz) δ 2.25 (s, 3H), 2.50 (s, 3H), 3.65 (s, 3H), 3.79 (s, 3H), 3.83 (s, 3H), 4.51 (s, 1H), 6.05 (s, 1H), 6.28 (s, 1H), 6.55 (d, 2H, J = 8.8 Hz), 6.84-6.05 (m, 2H), 6.91 (d, 2H, J = 8.8 Hz), 6.99-7.00 (m, 3H) ppm;

Compound 264-1:

Methyl(3*S*,3*aR*,8*bR*)-8*b*-hydroxy-6,8-dimethoxy-3*a*-(4-methoxyphenyl)-1-oxo-3-phenyl-2,3,3*a*,8*b*-tetrahydro-1*H*-cyclopenta[*b*]benzofuran-2-carboxylate

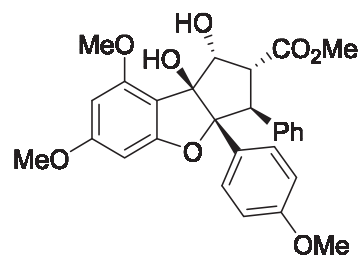


To a solution of **263** (100 mg, 0.164 mmol) in anhydrous THF (5 mL) under argon atmosphere was added MeOH (333 μ L, 0.825 mmol) dropwise at 0 °C followed by sodium (38 mg, 1.64 mmol). The mixture was stirred at this temperature for 30 minutes. After 2 hours at room temperature, the reaction was quenched with a 1 N aqueous solution of HCl and extracted with CH₂Cl₂. The organic layer was dried over MgSO₄, filtered and concentrated. The crude was purified on silica gel to yield **264-1** (166 mg, 79%) as a keto-enolique mixture, 35/65.

¹H NMR (CDCl₃, 400 MHz) δ 3.60 (s, 1H), 3.66 (s, 1H), 3.67 (s, 2H), 3.72 (s, 2H), 3.80 (s, 1H), 3.82 (s, 2H), 3.83 (s, 1H), 3.86 (s, 2H), 4.04 (s, 0.2H), 4.08 (s, 0.33H), 4.23 (s, 0.33H), 4.26 (s, 0.2H), 4.48 (s, 0.33H), 6.05 (d, 0.33H, J = 1.9 Hz), 6.11 (d, 0.66H, J = 1.9 Hz), 6.19 (d, 0.33H, J = 1.8 Hz), 6.35 (d, 0.66H, J = 1.9 Hz), 6.53 (d, 0.66H, J = 8.4 Hz), 6.68 (d, 1.33H, J = 8.4 Hz), 6.90-6.92 (m, 1.33H), 6.95 (d, 1.33H, J = 8.7 Hz), 7.02 (d, 0.66H, J = 8.7 Hz), 7.08-7.14 (m, 3H) ppm;

Compound 264-2:

Methyl(1*R*,2*R*,3*S*,3*aR*,8*bS*)-1,8*b*-dihydroxy-6,8-dimethoxy-3*a*-(4-methoxyphenyl)-3-phenyl-2,3,3*a*,8*b*-tetrahydro-1*H*-cyclopenta[*b*]benzofuran-2-carboxylate



Me₄NHB(OAc)₃ (322 mg, 1.22 mmol) and AcOH (117 μ L, 2.04 mmol) dissolved in CH₃CN (10 mL). The mixture was stirred at room temperature for 5 minutes. The cyclopentenone **264-1** (100 mg, 0.204 mmol) in solution in CH₃CN (5 mL) was added dropwise and the mixture was stirred at room temperature for 3 hours. The mixture was quenched with an aqueous saturated solution of NH₄Cl then with a solution of potassium tartrate 3M. After stirring for

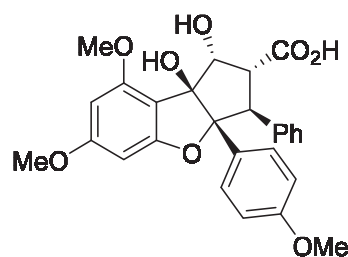
30 minutes, the product was extracted with CH₂Cl₂. The organic layer was dried over MgSO₄, filtered and concentrated under reduced pressure to afford **264-2** (79 mg, 79%).

¹H NMR (CDCl₃, 400 MHz) δ 3.65 (s, 3H), 3.71 (s, 3H), 3.72 (s, 3H), 3.83 (s, 3H), 3.90 (dd, 1H, J = 12.7 and 7.0 Hz), 4.31 (d, 1H, J = 14.2 Hz), 5.03 (d, 1H, J = 6.7 Hz), 6.12 (d, 1H, J = 1.9 Hz), 6.28 (d, 1H, J = 1.9 Hz), 6.67 (d, 2H, J = 9.0 Hz), 6.86-6.89 (m, 2H), 7.05-7.08 (m, 3H), 7.11 (d, 2H; J = 8.9 Hz) ppm;

¹³C NMR (CDCl₃, 400 MHz) δ 50.6, 52.1, 55.1, 55.3, 55.9, 55.9, 79.7, 89.6, 92.8, 93.8, 102.0, 107.8, 112.9 (2C), 126.6, 126.7, 127.8 (2C), 127.9 (2C), 129.1 (2C), 137.1, 157.1, 158.9, 161.0, 164.2, 170.7 ppm.

Compound 264:

(1*R*,2*R*,3*S*,3*aR*,8*bS*)-1,8*b*-Dihydroxy-6,8-dimethoxy-3*a*-(4-methoxyphenyl)-3-phenyl-2,3,3*a*,8*b*-tetrahydro-1*H*-cyclopenta[*b*]benzofuran-2-carboxylic acid



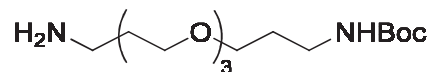
Crushed KOH (170 mg, 3.05 mmol) was added to **264-2** (75 mg, 0.15 mmol) in solution in MeOH:H₂O, 4:1. The mixture was stirred at 45 °C overnight, then cooled down to room temperature and quenched with an aqueous solution of HCl 1 N. The product was extracted twice with EtOAc and the combined organic layer was dried over MgSO₄, filtered and concentrated under reduced pressure to yield to compound **264** (28 mg, 38%).

¹H NMR (CDCl₃, 400 MHz) δ 3.68 (s, 3H), 3.80 (s, 3H), 3.95 (s, 3H), 3.9 (dd, 2H, J = 6.5 and 13.9 Hz) 4.24 (d, 1H, J = 14.1 Hz), 5.00 (d, 1H, J = 6.5 Hz), 6.10 (d, 1H, J = 1.9 Hz), 6.26 (d, 1H, J = 1.9 Hz), 6.65 (d, 2H, J = 8.9 Hz), 7.08 (d, 2H, J = 8.9), 6.87 (m, 2H), 7.05 (m, 3H) ppm;

¹³C NMR (CDCl₃, 400 MHz) δ 50.3, 55.1, 55.2, 55.9, 55.9, 60.6, 79.5, 89.6, 92.8, 93.8, 102.0, 107.6, 112.9 (2C), 126.4, 126.7, 127.9 (2C), 128.0 (2C), 129.1 (2C), 136.8, 157.1, 158.9, 161.0, 164.3 ppm.

Compound 266:

***tert*-Butyl (3-(2-(2-(3-aminopropoxy)ethoxy)ethoxy)-propyl)carbamate**



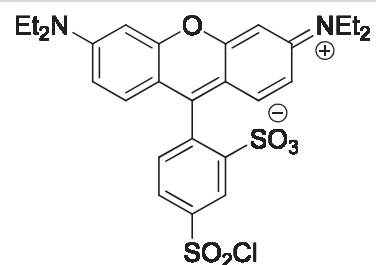
The diamine **265** (16.1 mL, 73.6 mmol) was dissolved in 1,4-dioxane (120 mL). (Boc)₂O (2.1 mL, 9.2 mmol) was dissolved in 1,4-dioxane (50 mL) and added dropwise to the mixture. After 24 hours at room temperature the mixture was concentrated, washed with water (100 mL) and extracted with EtOAc. The organic layer was dried over MgSO₄, filtered and concentrated under reduced pressure to yield **266** (2.3 g, 80%).

¹H NMR (CDCl₃, 400 MHz) δ 1.41 (s, 9H), 1.73 (quint., 4H, J = 6.3 and 12.7 Hz), 1.93 (br, s, 2H), 2.81 (t, 2H, J = 6.7 Hz), 3.20 (quad., 2H, J = 6.3 and 12.0 Hz), 3.50-3.63 (12H), 5.11 (br, s, 1H) ppm;

¹³C NMR (CDCl₃, 400 MHz) δ 28.6 (3C), 29.8, 32.8, 38.6, 39.7, 69.6, 69.7, 70.3, 70.3, 70.6, 70.7, 79.0, 156.2 ppm.

Compound 268:

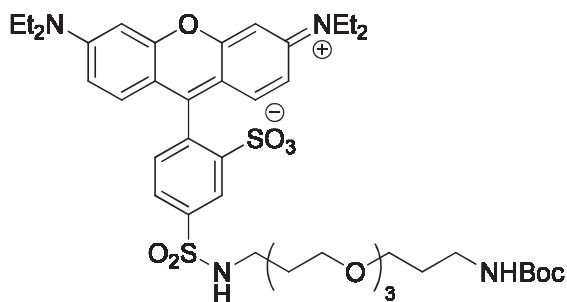
5-(Chlorosulfonyl)-2-(6-(diethylamino)-3-(diethyliminio)-3H-xanthen-9-yl)benzene-sulfonate



The lissamine **267** (3 g, 5.17 mmol) and DMF (0.1 mL, 1.29 mmol) were dissolved in anhydrous CH₂Cl₂ (250 mL) under argon atmosphere. At -10 °C, (COCl)₂ in solution in anhydrous CH₂Cl₂ (3 mL) was added dropwise over 3 hours. The mixture was cooled down to room temperature and stirred at this temperature overnight. The mixture was evaporated then washed 3 times with anhydrous toluene (40 mL) and concentrated. The obtained solid was filtered, washed with EtOAc (15 mL) then with Et₂O (100 mL) and dried under vacuum to afford desired product **268** with the concomitant formation of the product activated in the ortho position, the diactivated product and the hydrolyzed product. The mixture was used in the next step without purification.

Compound 269:

2-(6-(Diethylamino)-3-(diethyliminio)-3H-xanthen-9-yl)-5-(N-(2,2-dimethyl-4-oxo-3,9,12,15-tetraoxa-5-azaoctadecan-18-yl)sulfamoyl)benzenesulfonate



Et₃N (120.5 μL, 0.87 mmol) was added to a solution of **266** (308 mg, 0.90 mmol) in CH₂Cl₂ (5 mL) at 0 °C followed by DMAP (16 mg, 0.13 mmol). **268** (503 mg, 0.87 mmol) in solution in CH₂Cl₂ (5 mL) was added dropwise over 2 hours then the mixture was stirred at room temperature overnight. The mixture was evaporated and purified on silica gel chromatography to afford **269** (278 mg, HPLC purity 90%, 37% yield).

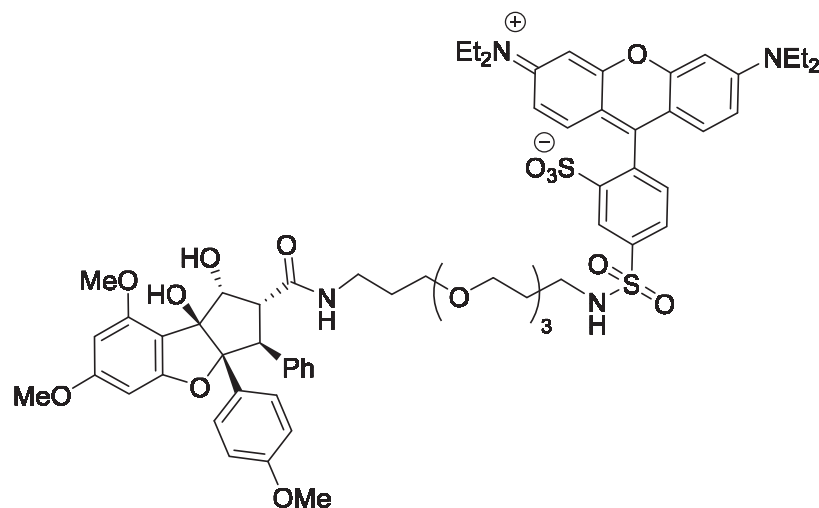
¹H NMR (CDCl₃, 400 MHz) δ 1.29 (t, 12H, J = 7.0 Hz), 1.42 (s, 9H), 1.75 (quint., 2H, J = 6.3 and 12.7 Hz), 1.84 (quint., 2H, J = 6.3 and 12.7 Hz), 2.70 (br, s, 1H), 3.03 (s, 2H), 3.19-3.24 (m, 4H), 3.45-3.72 (m, 18H), 6.64 (d, 2H, J = 2.4 Hz), 6.80 (dd, 2H, J = 2.4 and 9.5 Hz), 7.20 (d, 1H, J = 7.9 Hz), 7.28 (d, 2H, J = 9.4 Hz), 7.99 (dd, 1H, J = 1.9 and 9.5 Hz), 8.82 (d, 1H, J = 1.8 Hz) ppm;

¹³C NMR (CDCl₃, 400 MHz) δ 12.75 (4C), 28.63 (3C), 29.16, 29.84, 39.39, 42.31, 46.0 (4C), 69.6, 69.8, 70.3, 70.4, 70.7, 70.8, 77.4, 95.8 (2C), 113.6 (2C), 114.6 (2C), 127.2, 127.4, 129.8, 133.5, 133.7 (2C), 142.3, 148.4, 155.7 (2C), 156.2, 158.1 (2C), 159.3 ppm;

LC-MS calculated for C₄₂H₆₀N₄O₁₁S₂: 860.4, found: 883.2 (M+Na)⁺.

Compound 179:

2-(6-(Diethylamino)-3-(diethyliminio)-3H-xanthen-9-yl)-5-(N-(1-((1*S*,2*S*,3*R*,3*aS*,8*bR*)-1,8*b*-dihydroxy-6,8-dimethoxy-3*a*-(4-methoxyphenyl)-3-phenyl-2,3,3*a*,8*b*-tetrahydro-1H-cyclopenta[*b*]benzofuran-2-yl)-1-oxo-6,9,12-trioxa-2-azapentadecan-15-yl)sulfamoyl)benzenesulfonate



TFA (325 μ L, 4.38 mmol) was added dropwise to a solution of **269** (50 mg, 0.058 mmol) in CH_2Cl_2 (1.5 mL) and stirred at room temperature for 5 hours. The mixture was concentrated under vacuum and was used without further purification.

LC-MS calculated for $\text{C}_{37}\text{H}_{52}\text{N}_4\text{O}_9\text{S}_2$: 760.3, found: 761.2 ($\text{M}+\text{H}$)⁺.

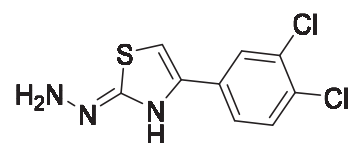
DEPBT (37 mg, 0.11 mmol) was added to solution of **264** (28 mg, 0.058 mmol) in anhydrous THF (600 μ L) at 0 $^\circ\text{C}$ followed by DIPEA (19 μ L, 0.11 mmol) under argon atmosphere. After 30 minutes at room temperature, a solution of deprotected amine (58 mg, 0.076 mmol) in anhydrous THF (600 μ L) at 0 $^\circ\text{C}$ and the mixture was stirred overnight at room temperature. The mixture was quenched with a saturated aqueous solution NH_4Cl , extracted with EtOAc. The organic layer was washed with a saturated aqueous solution of NaHCO_3 , dried over MgSO_4 , filtered and concentrated. The crude was purified by silica gel chromatography to yield compound **179** (25 mg, 36%).

$^1\text{H NMR}$ (CDCl_3 , 400 MHz) δ 1.25 (m, 22H), 3.24 (s, 3H), 3.44-3.55 (m, 8H), 3.61 (s, 3H), 3.64-3.75 (m, 10H), 3.79 (s, 3H), 3.81 (s, 3H), 3.97 (d, 1H, $J = 15.5$ Hz), 4.42 (d, 1H, $J = 14.2$ Hz), 4.75 (br, s, 1H), 6.05 (d, 1H, $J = 1.7$ Hz), 6.22 (d, 1H, $J = 1.7$ Hz), 6.49 (d, 2H, $J = 8.7$ Hz), 6.65 (s, 4H), 6.78 (d, 1H, $J = 9.4$ Hz), 6.94-6.98 (m, 1H), 7.04 (t, 2H, $J = 7.2$ Hz), 7.10-7.13 (m, 4H), 7.18 (d, 2H, $J = 9.3$ Hz), 7.63 (br, s, 1H), 8.09 (d, 1H, $J = 7.8$ Hz), 8.89 (s, 1H) ppm;

HR-MS calculated for $\text{C}_{64}\text{H}_{76}\text{N}_4\text{O}_{16}\text{S}_2$: 1220.4698, found: 1243.4573 ($\text{M}+\text{Na}$) $^+$.

Compound 272:

(Z)-4-(3,4-Dichlorophenyl)-2-hydrazono-2,3-dihydrothiazole



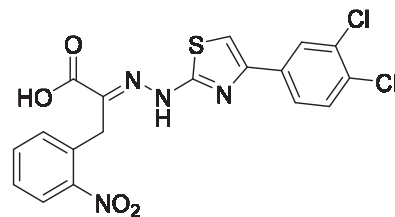
Compound **272** (0.910 g, 10 mmol) and compound **271** (2.68 g, 10 mmol) were dissolved in 1,4-dioxane (20 mL) and the resulting mixture was stirred at room temperature overnight. The formed precipitate was filtered, washed with 1,4-dioxane (3 x 10 mL), basified with a 2N solution of Na_2CO_3 , washed with water and dried under vacuum to afford product **272** with 74% yield (1.92 g).

$^1\text{H NMR}$ ($\text{DMSO}-d_6$, 400 MHz) δ 4.89 (br, s, 2H), 7.29 (s, 1H), 7.59 (d, 1H, $J = 8.4$ Hz), 7.77 (dd, 1H, $J = 2.0$ and 8.4 Hz), 8.01 (d, 1H, $J = 2.0$ Hz), 8.65 (br, s, 1H) ppm;

$^{13}\text{C NMR}$ ($\text{DMSO}-d_6$, 400 MHz) δ 108.8, 118.2, 127.8, 130.6, 132.2, 133.6, 133.5, 144.6, 161.6 ppm.

Compound 4EGI-1:

(E)-2-(2-(4-(3,4-Dichlorophenyl)thiazol-2-yl)hydrazono)-3-(2-nitrophenyl)propanoic acid



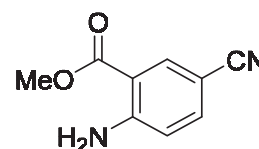
To a solution of hydrazine **272** (100 mg, 0.386 mmol) in ethanol (2 mL) was added carboxylic acid **273** (81 mg, 0.386 mmol) in solution in 5% acetic acid (1 mL). The resulting mixture was stirred at 90 °C for an hour, cooled down at 0 °C. The obtained precipitate was filtered, washed with water and dried under vacuum. Recrystallization in MeOH-H₂O afforded **4EGI-1** with 30% yield (52 mg).

¹H NMR (DMSO-*d*₆, 400 MHz) δ 4.30 (s, 2H), 7.08 (d, 1H, J = 7.6 Hz), 7.52 (t, 1H, J = 7.4 Hz), 7.63 – 7.72 (m, 3H), 7.81 (d, 1H, J = 8.5 Hz), 8.07 (s, 1H), 8.08 (d, 1H, J = 8.5 Hz), 12.10 (br, s, 1H), 12.90 (br, d, 1H) ppm;

¹³C NMR (DMSO-*d*₆, 400 MHz) δ 30.0, 108.8, 125.8, 126.2, 127.9, 128.5, 129.6, 130.6, 131.5, 131.8, 132.2, 134.6, 135.5, 138.3, 148.6, 149.7, 166.1, 169.3 ppm.

Compound 276:

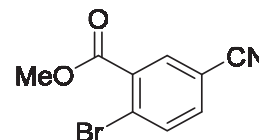
Methyl 2-amino-5-cyanobenzoate



Methyl 2-amino-5-bromobenzoate **275** (5 g, 0.0217 mol) and copper (I) cyanide (2.34 g, 0.0261 mol) were dissolved in N-methyl-2-pyrrolidone (25 mL). The reaction mixture was stirred at reflux for 6 hours then cooled at room temperature and added to a solution of FeCl₃ (9 g) and concentrated HCl (2.2 mL) in water (100 mL). After 1.5 h at 60 °C, the mixture was cooled at room temperature and extracted with EtOAc. The organic layer was washed with a solution of NaOH 1 N then with brine, dried over MgSO₄, filtered and concentrated. After trituration in Et₂O, compound **276** was obtained in 90% yield (3.57 g).

¹H NMR (DMSO-*d*₆, 400 MHz) δ 3.82 (s, 3H), 6.87 (d, 1H, J = 8.8 Hz), 7.46 (br, s, 2H), 7.57-7.60 (dd, 1H, J = 2.0 and 8.8 Hz), 8.05 (d, 1H, J = 2 Hz) ppm;

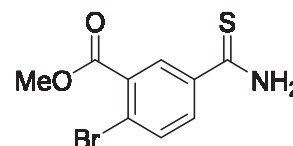
¹³C NMR (DMSO-*d*₆, 400 MHz) δ 51.1, 104.2, 109.6, 118.3, 131.7, 135.9, 149.8, 166.1 ppm.

Compound 277:**Methyl 2-bromo-5-cyanobenzoate**

Copper (II) bromide (3.56 g, 0.017 mol) was suspended in acetonitrile (50 mL). *Tert*-butyl nitrite (2.24 mL, 0.018 mol) was added dropwise at 0 °C then, after 5 minutes, **276** was added by portions. After 2 hours at 0 °C then 16 hours at room temperature, the reaction mixture was concentrated and acidified with a solution of HCl 1 N until pH = 2. The product was extracted 3 times with EtOAc and the organic layer was dried over MgSO₄, filtered and concentrated. After filtration over silica gel, compound **277** was obtained in 85% yield (4.1 g).

¹H NMR (DMSO-*d*₆, 400 MHz) δ 3.89 (s, 3H), 7.93 (dd, 1H, J = 2.1, 8.4 Hz), 7.99 (dd, 1H, J = 0.5 and 8.3 Hz), 8.23 (dd, 1H, J = 0.5 and 2.0 Hz) ppm;

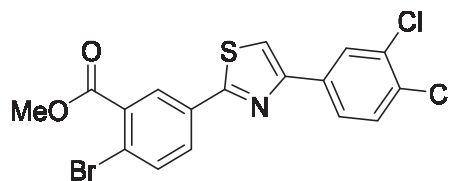
¹³C NMR (DMSO-*d*₆, 400 MHz) δ 52.5, 110.5, 116.8, 125.2, 133.2, 133.6, 134.7, 135.4, 164.3 ppm.

Compound 278:**Methyl 2-bromo-5-carbamothioylbenzoate**

Phosphorus pentasulfide (3.59 g, 8 mmol) was added to compound **277** (3.88 g, 0.016 mol) in suspension in absolute EtOH (40 mL) under argon atmosphere. 0.5 Equivalent of phosphorus pentasulfide were added after 6 hours then every hour until completion of the reaction. After stirring at room temperature for 16 hours and sonication for 1.5 h, the reaction mixture was diluted with EtOAc, washed 3 times with water then with a solution of saturated NaHCO₃. The organic layer was dried over MgSO₄, filtered and concentrated. After trituration in CH₂Cl₂, compound **278** was obtained in 81% yield (3.6 g).

¹H NMR (DMSO-*d*₆, 400 MHz) δ 3.90 (s, 3H), 7.82 (d, J = 8.4 Hz, 1H), 7.91 (dd, 1H, J = 2.4 and 8.4 Hz), 8.26 (d, 1H, J = 2.3 Hz), 9.72 (br, s, 1H), 10.10 (br, s, 1H) ppm;

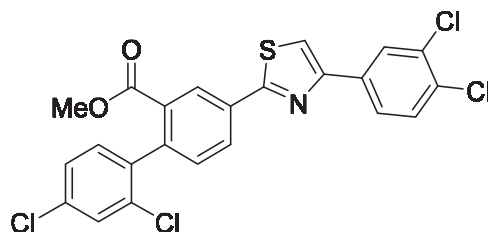
¹³C NMR (DMSO-*d*₆, 400 MHz) δ 52.7, 123.1, 129.7, 130.9, 131.7, 133.6, 165.6, 197.6 ppm.

Compound 279:**Methyl 2-bromo-5-(4-(3,4-dichlorophenyl)thiazol-2-yl)benzoate**

Compound **278** (3.5 g, 0.013 mol) and 2-bromo-1-(3,4-dichlorophenyl)ethan-1-one (3.46 g, 0.013 mol) were dissolved in absolute EtOH (50 mL) under argon atmosphere. After stirring at 70 °C for 16 hours, the reaction mixture was cooled at room temperature and the formed precipitate was filtered to yield **279** (5.28 g, 92%).

¹H NMR (DMSO-*d*₆, 400 MHz) δ 3.92 (s, 3H), 7.71 (d, 1H, J = 8.5 Hz), 7.88 (d, 1H, J = 8.4 Hz), 8.03 (dd, 1H, J = 2.0 and 8.4 Hz), 8.08 (dd, 1H, J = 2.3 and 8.3 Hz), 8.29 (d, 1H, J = 2.0 Hz), 8.35 (d, 1H, J = 2.1 Hz), 8.42 (s, 1H) ppm;

¹³C NMR (DMSO-*d*₆, 400 MHz) δ 52.7, 114.4, 123.5, 125.5, 128.4, 129.1, 130.0, 130.8, 132.4, 132.6, 133.0, 133.1, 134.0, 135.1, 154.3, 166.0, 166.1 ppm.

Compound 280-1:**2',4'-Dichloro-4-(4-(3,4-dichlorophenyl)thiazol-2-yl)-[1,1'-biphenyl]-2-carboxylic acid**

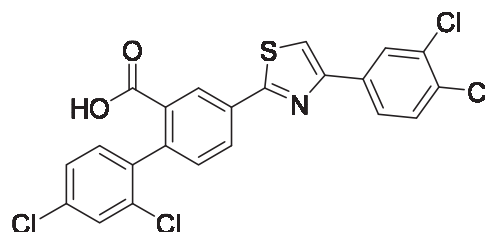
Compound **279** (500 mg, 1.13 mmol) and 2,4-dichlorophenyl boronic acid (431 mg, 2.26 mmol) were dissolved in DMF (12 mL) under argon atmosphere. Palladium (0) triphenylphosphine tetrakis (104 mg, 0.09 mmol) and a 3 M aqueous solution of K₂CO₃ were added and the mixture was stirred at 100 °C for 20 hours. The product was extracted with EtOAc and washed with water. The organic layer was dried over MgSO₄, filtered and concentrated. A chromatography on silica gel (pentane/CH₂Cl₂, 50/50) afforded the ester **280-1** (422 mg, 73%).

$^1\text{H NMR}$ (DMSO- d_6 , 400 MHz) δ 3.71 (s, 3H), 7.41 (d, 1H, $J = 8.3$ Hz), 7.51 (d, 1H, $J = 8.3$ Hz), 7.53 (dd, 1H, $J = 2.1$ and 8.3 Hz), 7.73 (d, 1H, $J = 2.1$ Hz), 7.78 (d, 1H, $J = 8.4$ Hz), 8.08 (dd, 1H, $J = 2.0$ and 8.4 Hz), 8.33 (d, 1H, $J = 2.0$ Hz), 8.34 (dd, 1H, $J = 1.0$ and 1.9 Hz), 8.51 (s, 1H), 8.55 (d, 1H, $J = 1.9$ Hz) ppm;

$^{13}\text{C NMR}$ (DMSO- d_6 , 400 MHz) δ 52.4, 114.4, 125.6, 127.0, 128.4, 128.4, 129.1, 129.7, 130.8, 130.8, 131.1, 132.0, 132.3, 133.1, 133.5, 133.5, 134.1, 134.2, 138.5, 141.0, 154.3, 166.5, 166.6 ppm.

Compound 280:

2',4'-Dichloro-4-(4-(3,4-dichlorophenyl)thiazol-2-yl)-[1,1'-biphenyl]-2-carboxylic acid



An aqueous solution of NaOH 1N (4 mL, 4 mmol) was added to ester **280-1** (320 mg, 6.28 mmol) in solution in THF (4 mL). After stirring overnight at 60 °C, 4 mL of NaOH 1N were added and the mixture was stirred at 80 °C. After 5 hours, 4 mL of NaOH 1N and 4 mL of THF were added and the mixture was stirred at 90 °C. After 16 hours, the reaction mixture was concentrated, dissolved in water and extracted with EtOAc. The aqueous layer was quenched with a solution HCl 1N until pH < 5, and then extracted with EtOAc. The organic layers were combined, dried over MgSO₄, filtered and concentrated to afford compound **280** (241 mg, 77%). The product is further purified by recrystallization in CH₂Cl₂ (**280**, 120 mg, 39%).

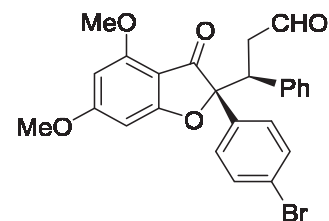
$^1\text{H NMR}$ (DMSO- d_6 , 400 MHz) δ 7.39 (d, 1H, $J = 8.3$ Hz), 7.45 (d, 1H, $J = 7.9$ Hz), 7.50 (dd, 1H, $J = 2.1$ and 8.2 Hz), 7.70 (d, 1H, $J = 2.1$ Hz), 7.77 (d, 1H, $J = 8.4$ Hz), 8.08 (d, 1H, $J = 2.0$ and 8.4 Hz), 8.28 (dd, 1H, $J = 2.0$ and 8.0 Hz), 8.33 (d, 1H, $J = 2.0$ Hz), 8.49 (s, 1H), 8.55 (d, 1H, $J = 2.0$ Hz), 13.15 (br, s, 1H);

$^{13}\text{C NMR}$ (DMSO- d_6 , 400 MHz) δ 35.9, 131.6, 131.6, 132.4, 132.7, 133.5, 133.6, 134.6, 135.9, 136.4, 136.8, 137.0, 137.4, 137.5, 137.9, 138.0, 138.1, 139.6, 144.1, 145.6, 158.1, 171.1, 172.1 ppm;

LC-MS calculated for C₂₂H₁₁Cl₄NO₂S: 495.2, found: 495.6 (M+H)⁺.

Compound 285

(S)-3-((R)-2-(4-Bromophenyl)-4,6-dimethoxy-3-oxo-2,3-dihydrobenzofuran-2-yl)-3-phenylpropanal



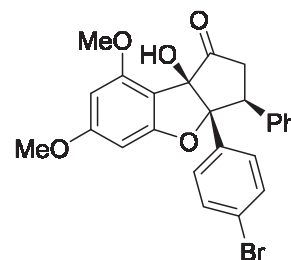
A solution of benzofuranone **284** (4.7 g, 13.5 mmol) in *t*-BuOH (300 mL) was heated at 50 °C under argon atmosphere. Benzyltrimethylammonium hydroxide (Triton B) in solution in MeOH (40%, 306 μ l, 0.73 mmol) was added immediately followed by cinnamaldehyde (3.40 ml, 27.0 mmol). The resulting mixture was stirred at 50 °C for 2 hours. After cooling down at room temperature, the reaction mixture was concentrated and a 1 N solution of HCl (30 ml) was added. The aqueous layer was extracted with CH₂Cl₂ and the organics were combined, dried over MgSO₄, filtered and concentrated. The crude was purified over silica gel to afford compound **285** in 44% yield (2.85 g).

¹H RMN (CDCl₃, 300 MHz): 2.61 (ddd, 1H, J = 0.9, 4.0 and 17.3 Hz), 3.07 (ddd, 1H, J = 2.3, 10.9 and 17.3 Hz), 3.70 (s, 3H), 3.85 (s, 3H), 4.19 (dd, 1H, J = 4.0 and 10.9 Hz), 5.81 (d, 1H, J = 1.8 Hz), 6.21 (d, 1H, J = 1.8 Hz), 7.08 - 7.17 (m, 3H), 7.29-7.32 (m, 2H), 7.49, 7.63 (m, 4H, J = 8.7 Hz), 9.41 (d, 1H, J = 1.1 Hz);

¹³C RMN (CDCl₃, 300 MHz): 44.0, 46.8, 55.9, 56.1, 88.4, 93.0, 103.7, 122.6, 126.9 (2C), 127.5 (2C), 128.2 (2C), 129.5, 131.8 (2C), 132.0, 135.6, 136.3, 159.1, 169.9, 174.1, 194.1, 200.0.

Compound 286:

(3*S*,3*aR*,8*bR*)-3*a*-(4-Bromophenyl)-8*b*-hydroxy-6,8-dimethoxy-3-phenyl-2,3,3*a*,8*b*-tetrahydro-1*H*-cyclopenta[*b*]benzofuran-1-one



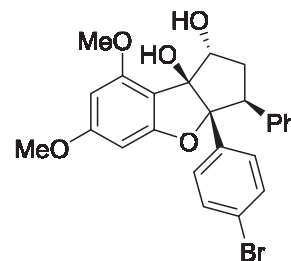
Trimethylsilyle cyanide (744 mg, 7.5 mmol) was added to a solution of aldehyde **285** (1.2 g, 2.5 mmol) in CH₃CN (12 ml) immediately followed by zinc iodine (10 mg, 0.025 mmol). After stirring for 1 hour, the reaction mixture was filtered, concentrated and gave cyanohydrin intermediate (1.74 g, 40%) used in the next step without further purification. A solution of LDA (2.7 mmol, 0.6 M) was added dropwise at -78 °C to a solution of de cyanohydrin (1.43 g, 2.46 mmol) in THF (12 mL). After 2 hours at -78 °C, the reaction mixture was warmed up at -50 °C for 30 minutes and quenched with a saturated aqueous solution of NH₄Cl (15 ml). The aqueous layer was extracted with CH₂Cl₂ and the obtained organic layer was washed with brine, dried over MgSO₄ and concentrated under reduced pressure to give 1.49 g of product. TBAF (2.7 ml, 1 M in THF) was added dropwise at room temperature to a solution of the crude in anhydrous THF (10 mL). After 4 hours, the reaction mixture was diluted in EtOAc, and the obtained organic layer was washed with brine, dried over MgSO₄, filtered and concentrated. Purification on silica gel afforded ketone **286** in 35 % yield (360 mg).

¹H RMN (CDCl₃, 300 MHz): 2.96-3.09 (m, 2H), 3.21 (s, 1H), 3.81 (s, 3H), 3.84 (s, 3H), 3.90 (dd, 1H, J = 10.2 and 12.1 Hz), 6.10 (d, 1H, J = 1.9 Hz), 6.33 (d, 1H, J = 1.9 Hz), 6.89-6.94 (m, 4H), 7.10-7.12 (m, 3H), 7.24-7.27 (m, 2H);

¹³C RMN (CDCl₃, 300 MHz): 39.6, 48.6, 55.6, 55.7, 88.6, 89.7, 92.8, 100.8, 106.2, 121.7, 127.1, 127.8 (2C), 128.0 (2C), 128.3 (2C), 130.7 (2C), 133.0, 136.6, 158.4, 160.9, 164.8, 210.3.

Compound FL3:

(1*R*,3*S*,3*aR*,8*bS*)-3*a*-(4-Bromophenyl)-6,8-dimethoxy-3-phenyl-1,2,3,3*a*-tetrahydro-8*bH*-cyclopenta[*b*]benzofuran-1,8*b*-diol



Me₄NBH(OAc)₃ (817 mg, 3.1 mmol) was dissolved in a solution of acetic acid (296 μL, 5.17 mmol) in CH₃CN (11 mL). After stirring for 5 minutes at room temperature, ketone **286** (250 mg, 0.517 mmol) in solution in CH₃CN (13 mL) was added dropwise and the resulting mixture was stirred at room temperature for 3 hours. The reaction mixture was quenched with a solution of saturated aqueous NH₄Cl (3 mL) then with a 3 M solution of Rochelle salt (2 mL) and stirred for one hour at room temperature. The product was extracted with EtOAc and the organic layer was dried over MgSO₄, filtered and concentrated under reduced pressure. Purification on silica gel column afforded **FL3** (123 mg, 49%).

¹H RMN (CDCl₃, 300 MHz): 1.89 (s, 1H), 2.14 (dd, 1H, J = 7.0 and 13.3 Hz), 2.67 (ddd, 1H, J = 6.4, 13.9 and 13.9 Hz), 3.27 (s, 1H), 3.83 (s, 3H), 3.86 (s, 3H), 3.99 (dd, 1H, J = 6.5 and 14.0 Hz), 4.77 (d, 1H, J = 7.0 Hz), 6.10 (d, 1H, J = 1.8 Hz), 6.28 (d, 1H, J = 1.8 Hz), 6.95-6.98 (m, 2H), 7.05-7.12 (m, 5H), 7.23-7.26 (m, 2H);

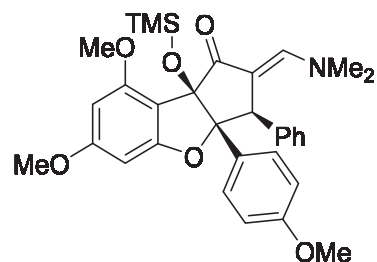
¹³C RMN (CDCl₃, 300 MHz): 36.1, 53.2, 55.6, 55.7, 79.0, 89.4, 92.5, 94.8, 103.1, 107.4, 121.4, 126.4, 127.7 (2C), 127.9 (2C), 129.4 (2C), 130.2 (2C), 134.1, 138.1, 156.8, 160.6, 163.9;

HR-MS calculated for C₂₅H₂₃BrK₁O₆: 521.0366, found: 521.0360.

5.5 Procedures for chapter 3.4.

Compound 287:

(3*R*,3*aR*,8*bR*,*E*)-2-((Dimethylamino)methylene)-6,8-dimethoxy-3*a*-(4-methoxyphenyl)-3-phenyl-8*b*-((trimethylsilyl)oxy)-2,3,3*a*,8*b*-tetrahydro-1*H*-cyclopenta[*b*]benzofuran-1-one



Compound **262** (120 mg, 0.238 mmol) was dissolved in anhydrous toluene (1.5 mL) under argon atmosphere. Bredereck's reagent (62 mg, 0.357 mmol) was added and the solution heated at reflux overnight. The reaction mixture was concentrated under reduced pressure to dryness and used without further purification.

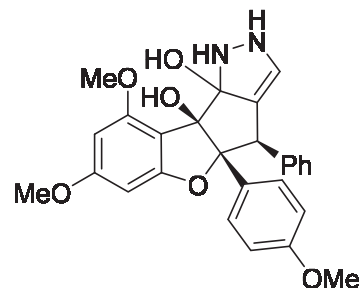
¹H NMR (CDCl₃, 400 MHz) δ -0.43 (s, 9H), 3.66 (s, 3H), 3.84 (s, 3H), 3.86 (s, 3H), 4.28 (s, 1H), 6.08 (d, 1H, J = 1.9 Hz), 6.31 (d, 1H, J = 1.9 Hz), 6.50 (d, 2H, J = 8.9 Hz), 6.62-6.87 (m, 2H), 6.95-6.97 (m, 5H), 7.62 (d, 1H, J = 1.5 Hz) ppm;

¹³C NMR (CDCl₃, 400 MHz) δ 1.0 (3C), 55.2, 55.6, 55.7, 56.7, 88.8, 89.2, 92.3, 101.4, 102.6, 108.5, 112.0 (2C), 126.2 (2C), 127.7 (2C), 128.6, 128.7, 129.0 (2C), 141.4, 148.9, 158.2, 159.1, 161.4, 164.1, 196.7 ppm;

LC-MS calculated for C₃₂H₃₇NO₆Si: 559.2, found: 582.2 (M+Na)⁺.

Compound 288:

(4*R*,4*aR*,9*bR*)-7,9-Dimethoxy-4*a*-(4-methoxyphenyl)-4-phenyl-1,2,4,4*a*-tetrahydrobenzofuro[2',3':4,5]cyclopenta[1,2-*c*]pyrazole-9*b*,9*c*-diol



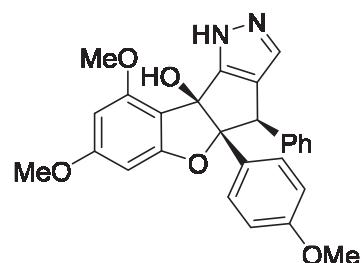
Compound **287** (120 mg, 0.225 mmol) was dissolved under argon atmosphere in EtOH (2 mL) beforehand dried over activated 4Å MS. Hydrazine monohydrate (22 µL, 0.45 mmol) and the mixture was stirred at reflux overnight. The reaction mixture was concentrated to dryness and the obtained crude was purified on silica gel to afford compound **288** in 28% yield (30 mg).

¹H NMR (CDCl₃, 400 MHz) δ 3.73 (s, 3H), 3.82 (s, 3H), 3.92 (s, 3H), 6.15 (d, 1H, J = 2.0 Hz), 6.24 (d, 1H, J = 1.9 Hz), 6.60 (s, 1H), 6.67 (d, 1H, J = 1.4 Hz), 6.73 (d, 2H, J = 8.9 Hz), 6.94-6.98 (m, 2H), 7.09-7.12 (m, 3H), 7.21 (d, 2H, J = 8.9 Hz) ppm;

LC-MS calculated for C₂₇H₂₆N₂O₆: 474.2, found: 475.0 (M+H)⁺.

Compound FL46:

(4*R*,4*aR*,9*bS*)-7,9-Dimethoxy-4*a*-(4-methoxyphenyl)-4-phenyl-4,4*a*-dihydrobenzofuro [2',3':4,5]cyclopenta[1,2-*c*]pyrazol-9*b*(1H)-ol



Compound **288** (10 mg, 0.0211 mmol) was dissolved in (EtO)₄Si (1 mL, 4.48 mmol) under argon atmosphere and the mixture was stirred at reflux overnight. The reaction mixture was concentrated under reduced pressure to dryness and the obtained crude was purified over silica gel to afford **FL46** (2 mg, 21%).

¹H NMR (CDCl₃, 400 MHz) δ 3.66 (s, 3H), 3.84 (s, 3H), 3.86 (s, 3H), 4.63 (s, 1H), 6.10 (d, 1H, J = 1.8 Hz), 6.32 (d, 1H, J = 1.9 Hz), 6.58 (d, 2H, J = 8.9 Hz), 7.06-7.14 (m, 5H), 7.21 (d, 2H, J = 7.3 Hz), 7.47 (s, 1H) ppm;

LC-MS calculated for C₂₇H₂₄N₂O₅: 456.2, found: 470.0 (M+Na)⁺.

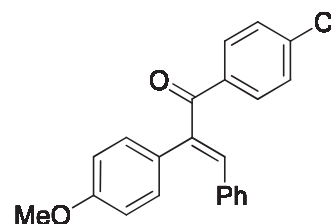
5.6 Procedures for chapter 3.5.

General procedure XVII: Suzuki reaction

Acyl chloride **14** (1 eq), boronic acid (1.2 eq), $K_3PO_4 \cdot 2H_2O$ (1.2 eq) and $PdCl_2(PPh_3)_2$ (0.02 eq) were dissolved in toluene under argon atmosphere. The reaction mixture was stirred at 80 °C for 4 hours, then cooled at room temperature, filtered through celite, washed with EtOAc and concentrated under vacuum. Purification on silica gel afforded desired product.

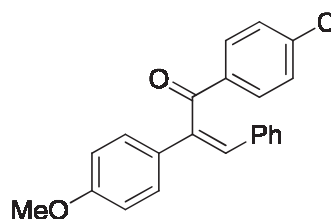
Compound 290:

(E)-1-(4-Chlorophenyl)-2-(4-methoxyphenyl)-3-phenylprop-2-en-1-one



Compound 290-1:

(Z)-1-(4-Chlorophenyl)-2-(4-methoxyphenyl)-3-phenylprop-2-en-1-one



Compound **290** was obtained following general procedure XVII starting from acyl chloride **186** (1 g, 3.67 mmol) and boronic acid (689 mg, 4.41 mmol) in solution toluene (16 mL) with $K_3PO_4 \cdot 2H_2O$ (1.095 g, 4.41 mmol) and $PdCl_2(PPh_3)_2$ (49.1 mg, 0.07 mmol). Product **290** was obtained with 26% yield (328 mg). Its isomer **290-1** was also isolated with 35% yield (451 mg).

Compound **290**:

1H NMR ($CDCl_3$, 400 MHz) δ 3.82 (s, 3H), 6.87 (dd, 2H, $J = 8.9$ and 2.0 Hz), 7.13 - 7.19 (m, 5H), 7.20 - 7.24 (m, 3H), 7.40 (dd, 2H, $J = 8.9$ and 2.0 Hz), 7.78 (dd, 2H, $J = 8.9$ and 2.0 Hz) ppm;

^{13}C NMR ($CDCl_3$, 400 MHz): 55.38, 114.52 (2C), 128.4 (2C), 128.5, 128.7 (2C), 129.1, 130.4 (2C), 131.0 (2C), 131.3 (2C), 135.1, 136.7, 138.6, 136.6, 140.3, 159.6, 196.8 ppm;

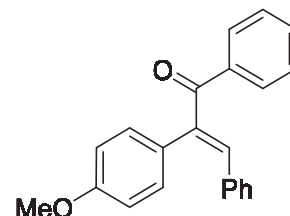
HR-MS calculated for $C_{22}H_{17}ClO_2$: 348.0917, found 349.0992 ($M+H$) $^+$.

Compound **290-1**:

$^1\text{H NMR}$ (DMSO, 400 MHz) δ 3.77 (s, 3H), 6.94 (d, 2H, $J = 8.8$ Hz), 7.15 (d, 4H, $J = 8.8$ Hz), 7.18 (s, 1H), 7.24 – 7.26 (m, 3H), 7.58 (d, 2H, $J = 8.7$ Hz), 7.82 (d, 2H, $J = 8.7$ Hz) ppm.

Compound 291:

(E)-2-(4-Methoxyphenyl)-1,3-diphenylprop-2-en-1-one



Compound **291** was obtained following general procedure XVII starting from acyl chloride **186** (1 g, 3.67 mmol) and boronic acid (540 mg, 4.41 mmol) in solution toluene (16 mL) with $\text{K}_3\text{PO}_4 \cdot 2\text{H}_2\text{O}$ (1.095 g, 4.41 mmol) and $\text{PdCl}_2(\text{PPh}_3)_2$ (49.1 mg, 0.07 mmol). Product **291** was obtained with 54% yield (626 mg).

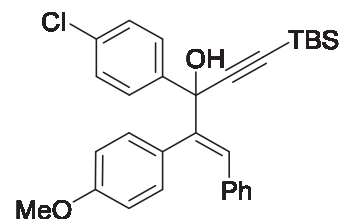
$^1\text{H NMR}$ (CDCl_3 , 400 MHz) δ 3.82 (s, 3H), 6.88 (d, 2H, $J = 8.8$ Hz), 7.12 (d, 1H, $J = 2.0$ Hz), 7.14 (d, 1H, $J = 1.4$ Hz), 7.18-7.23 (m, 5H), 7.42 - 7.46 (m, 2H), 7.52-7.56 (m, 1H), 7.86 (dd, 2H, $J = 8.3$ and 1.3 Hz) ppm;

$^{13}\text{C NMR}$ (CDCl_3 , 400 MHz): 55.3, 114.4 (2C), 128.4 (4C), 128.8, 128.9, 129.9 (2C), 130.4 (2C), 131.1 (2C), 132.2, 135.2, 138.4, 139.5, 140.6, 159.5, 198.1 ppm;

HR-MS calculated for $\text{C}_{22}\text{H}_{18}\text{O}_2$: 314.1307, found 315.1385 ($\text{M}+\text{H}$) $^+$.

Compound 292:

(E)-5-(tert-Butyldimethylsilyl)-3-(4-chlorophenyl)-2-(4-methoxyphenyl)-1-phenylpent-1-en-4-yn-3-ol



Compound **292** was obtained following general procedure IV starting from ketone **290** (290 mg, 0.83 mmol) in THF (5 mL) with tertbutyldimethylsilylacetylene (160 μ L, 0.83 mmol) and *n*-BuLi (1.6 M, 540 μ L, 0.87 mmol). Product **292** was obtained with 68% yield (275 mg).

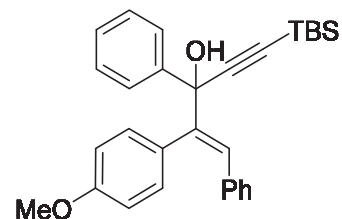
$^1\text{H NMR}$ (CDCl_3 , 400 MHz) δ 0.15 (d, 6H, $J = 6.5\text{Hz}$), 1.00 (s, 9H), 3.78 (s, 3H), 6.72 - 6.77 (m, 2H), 6.75 (d, 2H, $J = 3.9\text{ Hz}$), 6.88 - 6.90 (m, 2H), 7.08-7.10 (m, 3H), 7.24 (s, 1H), 7.27 (dd, 2H, $J = 8.8$ and 2.0 Hz), 7.49 (dd, 2H, $J = 8.7$ and 2.0 Hz) ppm;

$^{13}\text{C NMR}$ (CDCl_3 , 400 MHz): -4.6, -4.5, 16.8, 26.3 (3C), 55.3, 76.4, 92.3, 107.1, 113.8 (2C), 127.3, 127.8, 128.1 (2C), 128.2 (2C), 128.3 (2C), 128.8, 129.6 (2C), 131.8 (2C), 133.7, 136.3, 141.4, 143.3, 159.2 ppm;

HR-MS calculated for $\text{C}_{30}\text{H}_{33}\text{ClO}_2\text{Si}$: 488.1938, found 511.1840 ($\text{M}+\text{Na}$) $^+$.

Compound 293:

(E)-5-(tert-Butyldimethylsilyl)-2-(4-methoxyphenyl)-1,3-diphenylpent-1-en-4-yn-3-ol



Compound **293** was obtained following general procedure IV starting from ketone **291** (300 mg, 0.95 mmol) in THF (5 mL) with tertbutyldimethylsilylacetylene (160 μ L, 0.95 mmol) and *n*-BuLi (1.6 M, 540 μ L, 0.87 mmol). Product **293** was obtained with 68% yield (275 g).

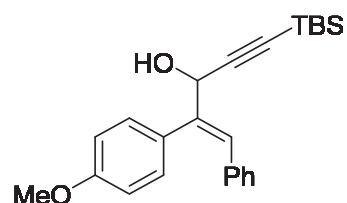
$^1\text{H NMR}$ (CDCl_3 , 400 MHz) δ 0.14 (s, 3H), 0.15 (s, 3H), 0.95 (s, 9H), 2.64 (s, 1H), 3.77 (s, 3H), 6.73 (dd, 4H, $J = 16.4$ and 9.0Hz), 6.88 - 6.90 (m, 2H), 7.07-7.09 (m, 3H), 7.20 (s, 1H), 7.29 (s, 1H), 7.28-7.31 (m, 2H), 7.56 (d, 1H, $J = 1.5\text{ Hz}$), 7.57 (d, 1H, $J = 1.9\text{ Hz}$) ppm;

^{13}C NMR (CDCl_3 , 400 MHz) : -4.4, -4.0, 16.8, 26.2 (3C), 55.2, 76.8, 91.8, 107.5, 113.6 (2C), 126.9 (2C), 127.1, 127.4, 127.9, 128.0 (2C), 128.0 (2C), 129.2, 129.6 (2C), 131.8 (2C), 136.5, 142.6, 143.7, 159.0 ppm;

HR-MS calculated for $\text{C}_{30}\text{H}_{34}\text{O}_2\text{Si}$: 454.2328, found: 454.2328 [$\text{C}_{30}\text{H}_{34}\text{O}_2\text{Si}^+$].

Compound 294:

(E)-5-(tert-Butyldimethylsilyl)-2-(4-methoxyphenyl)-1-phenylpent-1-en-4-yn-3-ol



NaBH_4 (36.3 mg, 0.96 mmol) and $\text{CeCl}_3 \cdot 2\text{H}_2\text{O}$ (209 mg, 0.56 mmol) were added to a solution of ketone **289** (300 mg, 0.8 mmol) in anhydrous MeOH (5 mL) at 0 °C. After 2 hours at 0 °C, the reaction mixture was quenched with water and the product was extracted with Et_2O . The separated organic layer was washed with brine, dried over MgSO_4 , filtered, concentrated and dried under vacuum to afford alcohol **294** (230 mg, 76%).

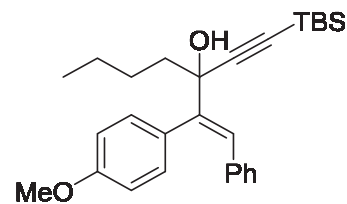
^1H NMR (CDCl_3 , 400 MHz) δ 0.11 (s, 3H), 0.12 (s, 3H), 0.92 (s, 9H), 2.01 (d, 1H, $J = 6.8$ Hz), 3.82 (s, 3H), 5.17 (d, 1H, $J = 6.8$ Hz), 6.57-6.89 (m, 3H), 6.99-7.01 (m, 2H), 7.11-7.13 (m, 3H), 7.23 (d, 2H, $J = 8.8$ Hz) ppm;

^{13}C NMR (CDCl_3 , 400 MHz) δ -4.5 (2C), 18.0, 26.2 (3C), 45.4, 68.6, 91.9, 111.3, 112.2, 114.3 (2C), 127.3 (2C), 128.1 (2C), 128.1, 129.5 (2C), 130.9 (2C), 131.0, 132.9 ppm;

HR-MS calculated for $\text{C}_{24}\text{H}_{30}\text{O}_2\text{Si}$: 378.2015, found: 401.1914 ($\text{M}+\text{Na}$) $^+$.

Compound 295:

(E)-3-((*tert*-Butyldimethylsilyl)ethynyl)-2-(4-methoxyphenyl)-1-phenylhept-1-en-3-ol



Compound **295** was obtained following general procedure IV starting from ketone **289** (300 mg, 0.8 mmol) in THF (5 mL) with *n*-BuLi (1.6 M, 750 μ L, 1.2 mmol). Product **295** was obtained with 48% yield (166 mg).

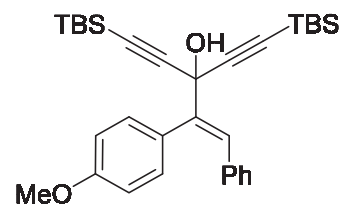
$^1\text{H NMR}$ (CDCl_3 , 400 MHz) δ 0.15 (s, 3H), 0.16 (s, 3H), 0.86 - 0.90 (m, 4H), 0.98 (s, 9H), 1.21-1.32 (m, 3H), 1.69-1.73 (m, 2H), 2.15 (s, 1H), 3.83 (s, 3H), 6.86 - 6.90 (m, 4H), 7.08-7.10 (m, 3H), 7.17 (d, 2H, 8.7 Hz), 7.19 (s, 1H) ppm;

$^{13}\text{C NMR}$ (CDCl_3 , 400 MHz) δ -4.5 (2C), 14.2, 16.8, 22.8, 26.3 (3C), 26.9, 40.6, 47.2, 55.3, 108.3, 114.0 (2C), 125.2, 127.0, 128.0 (2C), 128.6, 129.6 (2C), 131.7 (2C), 142.9, 159.2 ppm;

HR-MS calculated for $\text{C}_{28}\text{H}_{38}\text{O}_2\text{Si}$: 434.2641, found: 457.2537 ($\text{M}+\text{Na}$) $^+$.

Compound 296:

(E)-5-(*tert*-Butyldimethylsilyl)-3-((*tert*-butyldimethylsilyl)ethynyl)-2-(4-methoxyphenyl)-1-phenylpent-1-en-4-yn-3-ol



Compound **296** was obtained following general procedure IV starting from ketone **289** (290 mg, 0.83 mmol) in THF (5 mL) with *tert*-butyldimethylsilylacetylene (180 μ L, 0.95 mmol) and *n*-BuLi (1.6 M, 630 μ L, 1 mmol). Product **296** was obtained with 30% yield (128 g).

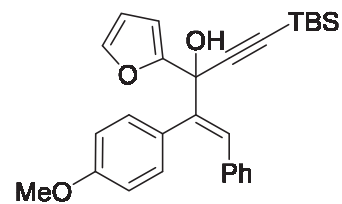
$^1\text{H NMR}$ (CDCl_3 , 400 MHz) δ 0.13 (s, 12H), 0.93 (s, 18H), 2.65 (s, 1H), 3.83 (s, 3H), 6.86 (d, 2H, $J = 8.9$ Hz), 6.93-7.12 (m, 5H), 7.29 (d, 2 H, $J = 8.9$ Hz), 7.34 (s, 1H) ppm;

$^{13}\text{C NMR}$ (CDCl_3 , 400 MHz) δ -4.7 (4C), 16.9 (2C), 26.2 (6C), 55.4, 67.9, 89.7, 104.7, 113.9 (2C), 127.4, 128.1 (2C), 128.5, 129.2, 129.7 (2C), 132.2 (2C), 136.2, 139.9, 159.5 ppm;

HR-MS calculated for $\text{C}_{32}\text{H}_{44}\text{O}_2\text{Si}$: 516.2880, found: 529.2782 ($\text{M}+\text{Na}$) $^+$.

Compound 297:

(E)-5-(tert-Butyldimethylsilyl)-3-(furan-2-yl)-2-(4-methoxyphenyl)-1-phenylpent-1-en-4-yn-3-ol



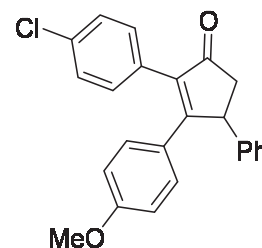
Compound **297** was obtained following general procedure IV starting from ketone **289** (300 mg, 0.8 mmol) in THF (5 mL) with furan (60 μ L, 0.8 mmol) and *n*-BuLi (1.6 M, 60 μ L, 0.86 mmol). Product **297** was obtained with 98% yield (350 mg).

$^1\text{H NMR}$ (CDCl_3 , 400 MHz) δ 0.13 (s, 6H), 0.92 (s, 9H), 2.80 (br, s, 1H), 3.79 (s, 3H), 6.32 (dd, 1H, $J = 1.9$ and 3.3 Hz), 6.39 (dd, 1H, $J = 0.9$ and 3.3 Hz), 6.77 (d, 2H $J = 8.8$ Hz), 6.90-6.94 (m, 4H), 7.08-7.10 (m, 3H), 7.13 (s, 1H), 7.43 (dd, 1H, $J = 0.9$ and 1.8 Hz) ppm;

$^{13}\text{C NMR}$ (CDCl_3 , 400 MHz) δ -5.6 (2C), 25.2 (3C), 25.4, 54.3, 89.7, 104.1, 108.2, 109.6, 112.8 (2C), 126.2, 126.6, 127.0 (2C), 127.3, 128.7 (2C), 130.5 (2C), 135.4, 140.0, 141.8, 153.1, 158.2, 199.0 ppm.

Compound 298:

2-(4-Chlorophenyl)-3-(4-methoxyphenyl)-4-phenylcyclopent-2-en-1-one

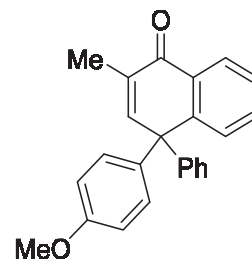


Compound **298** was obtained following general procedure IX starting from alcohol **292** (100 mg, 0.22 mmol) in DCE (2 mL) with Re_2O_7 (1.45 mg, 0.003 mmol) and MeOH (65 μ L, 1.58 mmol). Product **298** was obtained with 20% yield (15 mg).

$^1\text{H NMR}$ (CDCl_3 , 400 MHz) δ 2.59 (dd, 1H, $J = 18.8$ and 2.1 Hz), 3.22 (dd, 1H, $J = 18.9$ and 7.5 Hz), 3.72 (s, 3H), 4.56 (dd, 1H, $J = 7.4$ and 2.1 Hz), 6.66 (dd, 2H, $J = 8.9$ and 2.0 Hz), 7.12 (dd, 1H, $J = 9.0$ and 2.1 Hz), 7.15-7.19 (m, 3H), 7.23-7.27 (m, 3H), 7.33 (dd, 2H, $J = 8.5$ and 1.9 Hz) ppm;

$^{13}\text{C NMR}$ (CDCl_3 , 400 MHz) δ 46.1, 47.2, 55.3, 113.9 (2C), 126.8, 127.1, 127.5 (2C), 128.9 (2C), 129.1 (2C), 130.8 (2C), 131.0, 131.2 (2C), 134.0, 138.5, 142.7, 160.7, 170.2, 206.3 ppm;

HR-MS calculated for $\text{C}_{24}\text{H}_{19}\text{ClO}_2$: 374.1074, found 375.1155 ($\text{M}+\text{H}$) $^+$.

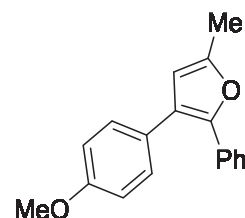
Compound 299:**4-(4-Methoxyphenyl)-2-methyl-4-phenylnaphthalen-1(4H)-one**

Compound **299** was obtained following general procedure IX starting from alcohol **293** (100 mg, 0.22 mmol) in DCE (2 mL) with Re_2O_7 (1.6 mg, 0.0033 mmol) and MeOH (70 μL , 1.77 mmol). Product **299** was obtained with 35% yield (26 mg).

$^1\text{H NMR}$ (CDCl_3 , 400 MHz) δ 1.65 (s, 3H), 3.77 (s, 3H), 4.91 (s, 1H), 6.74 (d, 2 H, $J = 9.0$ Hz), 7.18 (d, 2 H, $J = 9.0$ Hz), 7.23-7.49 (m, 9H) ppm;

$^{13}\text{C NMR}$ (CDCl_3 , 400 MHz) δ 24.3, 55.3, 67.2, 114.1 (2C), 120.8, 123.7, 126.1, 127.3, 128.0, 128.2, 129.2 (2C), 129.3 (2C), 130.0 (2C), 135.5, 139.6, 139.9, 141.6, 147.2, 159.2, 206.7 ppm;

HR-MS calculated for $\text{C}_{24}\text{H}_{20}\text{O}_2$: 340.1463, found: 341.1536 ($\text{M}+\text{H}$) $^+$.

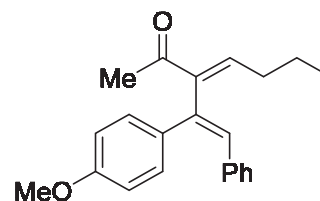
Compound 300:**3-(4-Methoxyphenyl)-5-methyl-2-phenylfuran**

Compound **300** was obtained following general procedure IX starting from alcohol **294** (100 mg, 0.26 mmol) in DCE (2 mL) with Re_2O_7 (1.92 mg, 0.004 mmol) and MeOH (80 μL , 2 mmol). Product **300** was obtained with 54% yield (37 mg).

$^1\text{H NMR}$ (CDCl_3 , 400 MHz) δ 2.38 (s, 3H), 3.83 (s, 3H), 6.12 (s, 1H), 6.88 (d, 2H, $J = 8.8$ Hz), 7.17-7.51 (m, 5H), 7.30 (d, 2H, $J = 8.8$ Hz) ppm;

$^{13}\text{C NMR}$ (CDCl_3 , 400 MHz) δ 13.7, 55.3, 110.3, 114.1 (2C), 122.2, 125.8 (2C), 126.9, 127.1, 128.4 (2C), 129.8 (2C), 131.7, 146.5, 151.2, 158.8 ppm;

HR-MS calculated for $\text{C}_{18}\text{H}_{16}\text{O}_2$: 264.1150, found: 265.1226 ($\text{M}+\text{H}$) $^+$.

Compound 301:**(E)-3-((E)-1-(4-Methoxyphenyl)-2-phenylvinyl)hept-3-en-2-one**

Compound **301** was obtained following general procedure IX starting from alcohol **295** (100 mg, 0.23 mmol) in DCE (2 mL) with Re_2O_7 (1.67 mg, 0.0035 mmol) and MeOH (70 μL , 1.77 mmol). Product **301** was obtained with 47% yield (35 mg).

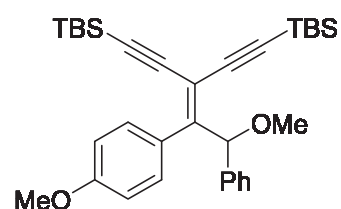
$^1\text{H NMR}$ (CDCl_3 , 400 MHz) δ 0.96 (t, 3H, $J = 7.3$ Hz), 1.54 (sex., 2H, $J = 7.3$ Hz), 2.16 (s, 3H), 2.38 (quad., 2H, $J = 7.4$ Hz), 3.78 (s, 3H), 6.42 (s, 1H), 6.75 (d, 2H, $J = 8.9$ Hz), 6.83 (t, 1H, $J = 7.5$ Hz), 7.09 (d, 2H, $J = 8.9$ Hz), 7.14-7.19 (m, 5H) ppm;

$^{13}\text{C NMR}$ (CDCl_3 , 400 MHz) δ 14.2, 22.5, 27.7, 31.8, 55.3, 113.9 (2C), 127.0, 128.2 (2C), 129.4 (2C), 130.6 (2C), 131.1, 136.7, 137.1, 143.6, 145.3, 159.1, 199.2 ppm;

HR-MS calculated for $\text{C}_{22}\text{H}_{24}\text{O}_2$: 320.1776, found: 321.1858 ($\text{M}+\text{H}$) $^+$.

Compound 302:

3-(2-Methoxy-1-(4-methoxyphenyl)-2-phenylethylidene)-penta-1,4-diyne-1,5-diylbis(tert-butyldimethylsilane)



Compound **302** was obtained following general procedure IX starting from alcohol **296** (100 mg, 0.19 mmol) in DCE (2 mL) with Re_2O_7 (1.4 mg, 0.0029 mmol) and MeOH (60 μL , 1.46 mmol). Product **302** was obtained with 31% yield (31 mg).

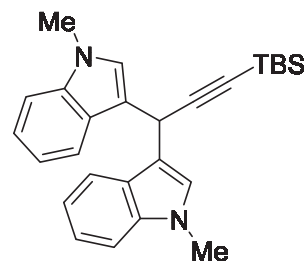
$^1\text{H NMR}$ (CDCl_3 , 400 MHz) δ -0.01 (s, 3H), 0.00 (s, 3H), 0.20 (s, 6H), 0.78 (s, 9H), 0.99 (s, 9H), 3.47 (s, 3H), 3.75 (s, 3H), 6.00 (s, 1H), 6.69 (d, 2H, $J = 8.8$ Hz), 7.04 (d, 2H, $J = 8.8$ Hz), 7.19-7.31 (m, 5H) ppm;

$^{13}\text{C NMR}$ (CDCl_3 , 400 MHz) δ -4.6 (2C), -4.8 (2C), 16.8, 17.0, 26.1 (3C), 26.3 (3C), 55.3, 57.1, 83.0, 96.4, 98.3, 102.2, 102.4, 106.4, 112.9 (2C), 126.2 (2C), 127.3, 128.2 (2C), 128.4, 130.9 (2C), 140.0, 157.5, 159.5 ppm;

HR-MS calculated for $\text{C}_{33}\text{H}_{46}\text{O}_2\text{Si}_2$: 530.3036, found: 553.2922 ($\text{M}+\text{Na}$) $^+$.

Compound 317:

3,3'-(3-(*tert*-Butyldimethylsilyl)prop-2-yne-1,1-diyl)bis(1-methyl-1H-indole)



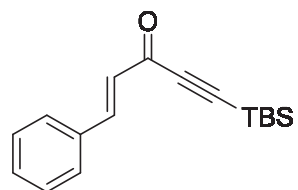
Compound **317** was obtained following general procedure IV starting from aldehyde **315** (2 g, 12.6 mmol) in THF (60 mL) with *tert*-butyldimethylsilylacetylene (2.59 mL, 13.8 mmol) and *n*-BuLi (1.6 M, 8.27 mL, 13.23 mmol). Product **317** was obtained with 12% yield (603 mg).

¹H NMR (CDCl₃, 400 MHz) δ 0.12 (s, 6H), 0.95 (s, 9H), 3.72 (s, 6H), 5.56 (s, 1H), 6.94 (s, 2H), 7.07 (td, 2H, J = 1.0 and 7.0 Hz), 7.22 (td, 2H, J = 1.0 and 7.0 Hz), 7.29 (d, 2H, J = 8.2 Hz), 7.72 (d, 2H, J = 8.0 Hz) ppm;

¹³C NMR (CDCl₃, 400 MHz) δ -4.2 (2C), 16.8, 26.4 (3C), 27.4, 32.6 (2C), 83.7, 108.2, 109.3 (2C), 114.8 (2C), 118.8 (2C), 120.1 (2C), 121.6 (2C), 126.9 (2C), 127.3 (2C), 137.5 (2C) ppm.

Compound 322:

(*E*)-5-(*tert*-Butyldimethylsilyl)-1-phenylpent-1-en-4-yn-3-one



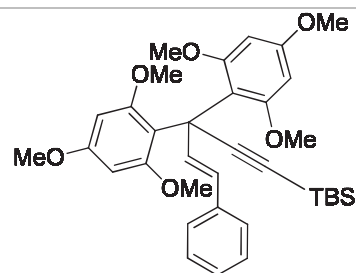
Compound **322** was obtained following general procedure III starting from compound **321** (573 mg, 3.44 mmol) in 1,4-dioxane (10 mL) with *tert*-butyldimethylsilylacetylene (900 μL, 4.82 mmol), Pd(PPh₃)₂Cl₂ (43 g, 0.07 mmol), CuI (26 mg, 0.138 mmol) and Et₃N (1.44 mL, 10.3 mol). Product **322** was obtained with 48% yield (930 mg).

¹H NMR (CDCl₃, 400 MHz) δ 0.25 (s, 6H), 1.04 (s, 9H), 6.79 (d, 1H, J = 16.2 Hz), 7.41-7.45 (m, 3H), 7.55-7.57 (m, 2H), 7.88 (d, 1H, J = 16.1 Hz) ppm.

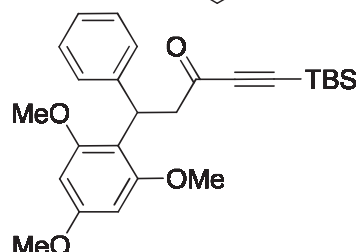
¹³C NMR (CDCl₃, 400 MHz) δ -4.9 (2C), 26.2 (3C), 97.7, 101.5, 128.3, 128.6, 128.9 (2C), 129.2 (2C), 131.3, 134.2, 149.1, 178.1 ppm.

Compound 224a:

(*E*)-*tert*-Butyldimethyl(5-phenyl-3,3-bis(2,4,6-trimethoxyphenyl)pent-4-en-1-yn-1-yl)-silane

**Compound 224b:**

1-(*tert*-Butyldimethylsilyl)-5-phenyl-5-(2,4,6-trimethoxyphenyl)pent-1-yn-3-one



Compound **324a** was obtained following general procedure IV starting from ketone **322** (444 mg, 1.64 mmol) in THF (12 mL) with 1,3,5-trimethoxybenzene (414 mg, 2.46 mmol) and *sec*-BuLi (1.4 M, 1.76 mL, 2.46 mmol). Product **324a** was obtained with 36% yield (350 mg) along with product **324b** (135 mg, 19%)

Product 324a:

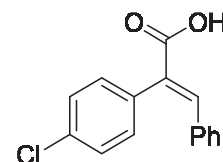
¹H NMR (CDCl₃, 400 MHz) δ 0.04 (s, 3H), 0.06 (s, 3H), 0.89 (s, 9H), 3.38 (s, 6H), 3.75 (s, 6H), 3.81 (s, 3H), 3.81 (s, 3H), 6.12 (d, 1H, J = 9.8 Hz), 6.13 (s, 2H), 6.15 (s, 2H), 6.70 (d, 1H, J = 9.9 Hz), 7.09 (t, 1H, J = 7.4 Hz), 7.20 (t, 2H, J = 7.8 Hz), 7.33 (d, 2H, J = 8.2 Hz) ppm.

¹³C NMR (CDCl₃, 400 MHz) δ -4.3 (2C), 16.9, 26.2 (3C), 41.2, 55.4, 55.4, 56.1 (2C), 56.2 (2C), 91.5 (2C), 91.8 (2C), 93.4, 105.1, 111.9, 112.9, 115.2, 125.1, 127.6 (2C), 127.7 (2C), 144.6, 145.7, 158.9 (2C), 159.5 (2C), 159.9, 160.4 ppm.

Product 324b:

¹H NMR (CDCl₃, 400 MHz) δ 0.15 (s, 3H), 0.16 (s, 3H), 0.96 (s, 9H), 3.37 (dd, 1H, J = 7.4 and 16.1 Hz), 3.53 (dd, 1H, J = 8.0 and 16.2 Hz), 3.75 (s, 6H), 3.78 (s, 3H), 5.32 (t, 1H, J = 7.7 Hz), 6.10 (s, 2H), 7.11 (t, 1H, J = 7.2 Hz), 7.20 (t, 2H, J = 7.8 Hz), 7.28 (d, 2H, J = 7.3 Hz) ppm;

¹³C NMR (CDCl₃, 400 MHz) δ -5.0 (2C), 16.7, 26.1 (3C), 35.4, 48.9, 55.4, 55.8 (2C), 91.4 (2C), 96.2, 103.3, 112.6, 125.7, 127.8 (2C), 128.0 (2C), 144.0, 159.1 (2C), 160.0, 187.5 ppm.

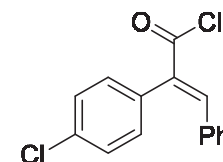
Compound 325-1:**(E)-2-(4-Chlorophenyl)-3-phenylacrylic acid**

Compound **325-1** was obtained following general procedure I starting from compound 4-chlorophenyl acetic acid (28 g, 0.163 mol) in acetic anhydride (62 mL) with benzaldehyde (18.4 mL, 0.182 mol) and triethylamine (22.3 mL, 0.2 mol). Product **325-1** was obtained quantitatively (50 g).

¹H NMR (CDCl₃, 400 MHz) δ 7.09 (d, 2H, J = 7.2 Hz), 7.17-7.27 (m, 5H), 7.36 (d, 2H, J = 8.5 Hz), 7.98 (s, 1H) ppm;

¹³C NMR (CDCl₃, 400 MHz) δ 128.6 (2C), 129.2 (2C), 129.9, 130.5, 130.9 (2C), 131.5 (2C), 133.8, 134.1, 134.3, 142.3, 172.7 ppm;

LC-MS calculated for C₁₅H₁₁ClO₂: 258.0, found: 258.0 (M+H)⁺.

Compound 325-2:**(E)-2-(4-Chlorophenyl)-3-phenylacryloyl chloride**

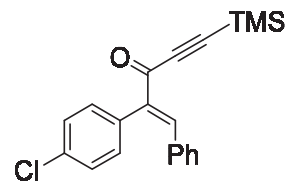
Compound **325-2** was obtained following general procedure II starting from compound acetic acid **325-1** (9.9 g, 0.039 mol) in CH₂Cl₂ (50 mL) with DMF (70 μL, 1 mmol) and oxalyl chloride (3.8 ml, 0.045 mol). Product **325-2** was obtained quantitatively (10 g).

¹H NMR (CDCl₃, 400 MHz) δ 7.72 (d, 2H, J = 7.5 Hz), 7.18 (d, 2H, J = 8.5 Hz), 7.25 (t, 2H, J = 7.9 Hz), 7.32-7.36 (m, 1H), 7.41 (d, 2H, J = 8.4 Hz) ppm;

¹³C NMR (CDCl₃, 400 MHz) δ 128.3, 128.5 (2C), 129.1 (2C), 129.9, 130.4, 130.9 (2C), 131.5 (2C), 133.7, 137.1, 143.3, 172.6 ppm.

Compound 325-3:

(E)-2-(4-Chlorophenyl)-1-phenyl-5-(trimethylsilyl)pent-1-en-4-yn-3-one



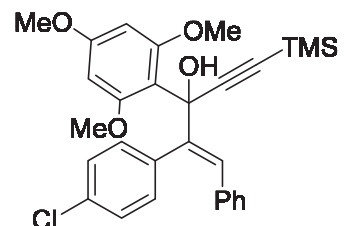
Compound **325-3** was obtained following general procedure III starting from compound **325-2** (10 g, 0.037 mol) in 1,4-dioxane (280 mL) with trimethylsilylacetylene (5.27 mL, 0.037 mol), Pd(PPh₃)₂Cl₂ (512 mg, 0.73 mmol), CuI (282 mg, 1.48 mmol) and Et₃N (15.5 mL, 0.111 mol). Product **325-3** was obtained with 80% yield (10 g).

¹H NMR (CDCl₃, 400 MHz) δ 0.287 (s, 9H), 7.09-7.13 (m, 4H), 7.22 - 7.30 (m, 3H), 7.37 (d, 2H, J = 8.7 Hz), 8.13 (s, 1H) ppm;

¹³C NMR (CDCl₃, 400 MHz) δ -0.6 (3C), 100.7, 101.0, 128.7 (2C), 129.2 (2C), 130.3, 131.2 (2C), 131.5 (2C), 133.0, 134.1, 134.4, 140.3, 146.4, 178.7 ppm.

Compound 325:

(E)-2-(4-Chlorophenyl)-1-phenyl-3-(2,4,6-trimethoxyphenyl)-5-(trimethylsilyl)pent-1-en-4-yn-3-ol



Compound **325** was obtained following general procedure IV starting from compound **325-3** (5 g, 0.015 mol) in THF (110 mL) with trimethoxybenzene (7.4 g, 0.044 mol) and *sec*-BuLi (1.3 M, 33.8 mL, 0.044 mol). Product **325** was obtained with 46% yield (3.5 g).

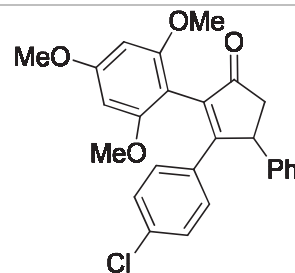
¹H NMR (CDCl₃, 400 MHz) δ 0.20 (s, 9H), 3.65 (s, 6H), 3.79 (s, 3H), 6.07 (s, 2H), 6.57 (s, 1H), 6.88-6.90 (m, 2H), 6.97 (d, 2H, J = 8.4 Hz), 7.06-7.10 (m, 3H), 7.15 (d, 2H, J = 8.5 Hz), 7.21 (s, 1H) ppm;

¹³C NMR (CDCl₃, 400 MHz) δ 0.1 (3C), 55.2, 56.1 (2C), 88.8, 92.6 (2C), 107.3, 110.7, 126.7, 127.2, 127.7 (2C), 127.8 (2C), 129.3 (2C), 132.1 (2C), 132.8, 136.6, 136.8, 142.7, 158.7, 160.5 ppm;

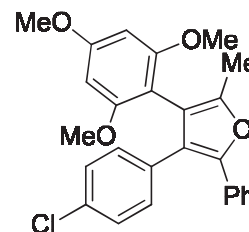
HR-MS calculated for C₂₉H₃₁ClO₄Si: 506.1651, found: 529.1573 (M+Na)⁺.

Compound 326:

3-(4-Chlorophenyl)-4-phenyl-2-(2,4,6-trimethoxyphenyl)cyclopent-2-en-1-one

**Compound 327:**

3-(4-Chlorophenyl)-5-methyl-2-phenyl-4-(2,4,6-trimethoxyphenyl)furan



Compounds **326** and **327** were obtained following general procedure IX starting from compound **325** (150 mg, 0.296 mmol) in DCE (2 mL) with Re_2O_7 (2.1 mg, 0.0044 mmol) and MeOH (92 μL , 2.28 mmol). Cyclopentenone **326** (40 mg, 31%) was obtained along with methylfuran **327** (21 mg, 16%).

Cyclopentenone 326:

$^1\text{H NMR}$ (CDCl_3 , 400 MHz) δ 2.45 (dd, 1H, $J = 1.9$ and 18.4 Hz), 3.19 (dd, 1H, $J = 7.4$ and 18.6 Hz), 3.53 (s, 3H), 3.77 (s, 3H), 3.84 (s, 3H), 4.60 (dd, 1H, $J = 2.0$ and 7.4 Hz), 6.12 (d, 1H, $J = 2.1$ Hz), 6.22 (d, 1H, $J = 2.1$ Hz), 7.07 (d, 2H, $J = 8.8$ Hz), 7.18-7.16 (m, 3H), 7.25 - 7.27 (m, 4 H) ppm;

$^{13}\text{C NMR}$ (CDCl_3 , 400 MHz) δ 45.9, 47.4, 55.5, 55.8, 56.1, 66.0, 91.4, 91.5, 127.0, 127.5 (2C), 128.3 (2C), 129.1 (2C), 129.3 (2C), 134.3, 135.0, 136.5, 143.3, 158.5, 159.1, 162.1, 168.3, 207.1 ppm;

HR-MS calculated for $\text{C}_{26}\text{H}_{23}\text{ClO}_4$: 434.1285, found: 435.1359 ($\text{M}+\text{H}$) $^+$.

Methylfuran 327:

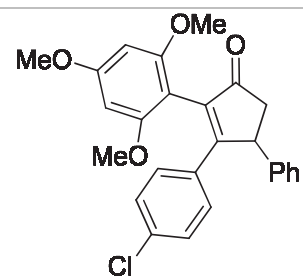
$^1\text{H NMR}$ (CDCl_3 , 400 MHz) δ 2.24 (s, 3H), 3.53 (s, 6H), 3.82 (s, 3H), 6.09 (s, 2H), 7.08 (d, 2H, $J = 8.7$ Hz), 7.15-7.18 (m, 3H), 7.22-7.24 (m, 2H), 7.45 (d, 2H, $J = 7.0$ Hz) ppm;

$^{13}\text{C NMR}$ (CDCl_3 , 400 MHz) δ 14.4, 54.4, 54.6 (2C), 65.0, 89.8 (2C), 101.7, 114.4, 122.3, 124.9 (2C), 125.8, 127.2 (2C), 127.3 (2C), 129.6 (2C), 130.6, 131.2, 132.9, 145.8, 148.7, 158.0, 160.2 ppm;

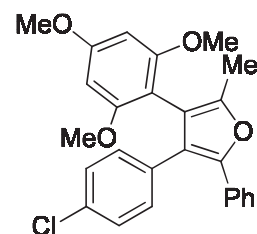
HR-MS calculated $\text{C}_{26}\text{H}_{23}\text{ClO}_4$: 434.1285, found: 435.1363 ($\text{M}+\text{H}$) $^+$.

Compound 326:

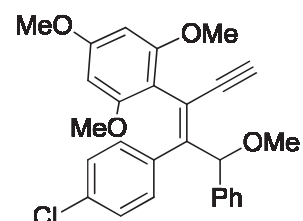
3-(4-Chlorophenyl)-4-phenyl-2-(2,4,6-trimethoxyphenyl)cyclopent-2-en-1-one

**Compound 327:**

3-(4-Chlorophenyl)-5-methyl-2-phenyl-4-(2,4,6-trimethoxyphenyl)furan

**Compound 328:**

(E)-2-(4-(4-Chlorophenyl)-5-methoxy-5-phenylpent-3-en-1-yn-3-yl)-1,3,5-trimethoxybenzene



Compounds **326-328** were obtained following general procedure IX starting from compound **325** (100 mg, 0.197 mmol) in DCE (2 mL) with $\text{ReO}_4\text{SiPh}_3$ (1.5 mg, 0.003 mmol) and MeOH (61 μL , 1.52 mmol). Cyclopentenone **326** (24 mg, 28%) was obtained along with methylfuran **327** (15 mg, 17%) and rearranged product **328** (5 mg, 6%). Cyclopentenone **326** and methylfuran **327** were already described on the previous page following another method.

Rearranged product **328**:

$^1\text{H NMR}$ (CDCl_3 , 400 MHz) δ 3.23 (s, 1H), 3.62 (s, 3H), 3.64 (s, 3H), 3.72 (s, 3H), 3.74 (s, 3H), 5.91 (d, 1H, $J = 2.1$ Hz), 5.95 (d, 1H, $J = 2.1$ Hz), 6.14 (s, 1H), 6.62 (d, 2H, $J = 8.5$ Hz), 6.87 (d, 2H, 8.5 Hz), 7.21-7.24 (m, 1H), 7.26-7.28 (m, 2H), 7.43 (d, 2H, $J = 8.0$ Hz) ppm;

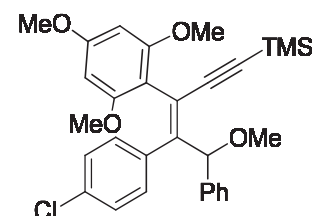
$^{13}\text{C NMR}$ (CDCl_3 , 400 MHz) δ 55.4, 55.9, 56.0, 56.5, 80.1, 84.1, 91.1 (2C), 106.3, 109.9, 121.3, 127.6 (2C), 128.6 (2C), 128.7, 129.8 (2C), 131.3 (2C), 132.5, 137.4, 141.5, 149.6, 157.2, 159.2, 163.4 ppm.

General procedure XVIII: Acid-catalyzed rearrangements

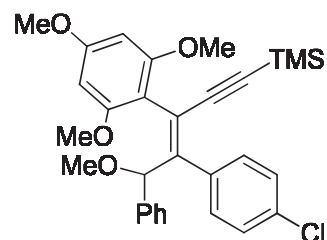
MeOH (7.7 eq) and acid (≈ 1.5 mol%) were added to a solution of compound **325** in anhydrous DCE (2 mL) under argon atmosphere. The reaction mixture was stirred overnight at 45 °C, concentrated and purified over silica gel to give product.

Compound 329:

(Z)-(4-(4-Chlorophenyl)-5-methoxy-5-phenyl-3-(2,4,6-trimethoxyphenyl)pent-3-en-1-yn-1-yl)trimethylsilane

**Compound 330:**

(E)-(4-(4-Chlorophenyl)-5-methoxy-5-phenyl-3-(2,4,6-trimethoxyphenyl)pent-3-en-1-yn-1-yl)trimethylsilane



Compounds **329** and **330** were obtained following general procedure XVIII starting from compound **325** (80 mg, 0.158 mmol) in anhydrous DCE (2 mL) with AcOH (3 μ L, 0.049 mmol) and MeOH (62 μ L, 1.52 mmol). Compound **329** (53 mg, 51%) was obtained along with compound **330** (48 mg, 47%).

Compound 329:

$^1\text{H NMR}$ (CDCl_3 , 400 MHz) δ 0.19 (s, 9H), 6.61 (s, 6H), 3.69 (s, 3H), 3.72 (s, 3H), 5.91 (d, 1H, $J = 2.1$ Hz), 5.93 (d, 1H, $J = 2.1$ Hz), 6.18 (s, 1H), 6.62 (d, 2H, $J = 8.5$ Hz), 6.86 (d, 2H, $J = 8.5$ Hz), 7.20 (t, 1H, $J = 7.2$ Hz), 7.27 (t, 2H, $J = 7.2$ Hz), 7.40 (d, 2H, $J = 7.9$ Hz) ppm;

$^{13}\text{C NMR}$ (CDCl_3 , 400 MHz) δ 0.1 (3C), 55.2, 55.7, 55.7, 56.6, 83.1, 90.8 (2C), 97.8, 104.3, 109.3, 118.2, 126.7 (2C), 126.7 (2C), 126.1, 127.8 (2C), 130.1 (2C), 132.4, 135.9, 140.5, 149.8, 157.9, 158.0, 161.0 ppm;

HR-MS calculated for $\text{C}_{30}\text{H}_{33}\text{ClO}_4\text{Si}$: 520.1837, found: 521.1907 ($\text{M}+\text{H}$) $^+$.

Compound **330**:

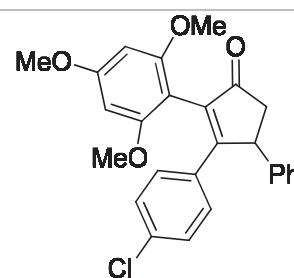
$^1\text{H NMR}$ (CDCl_3 , 400 MHz) δ -0.05 (s, 9H), 3.37 (s, 3H), 3.82 (s, 3H), 3.85 (s, 3H), 3.86 (s, 3H), 4.99 (s, 1H), 6.20 (d, 1H, $J = 2.3$ Hz), 6.21 (d, 1H, $J = 2.1$ Hz), 7.14-7.21 (m, 9H) ppm;

$^{13}\text{C NMR}$ (CDCl_3 , 400 MHz) δ -0.1 (3C), 55.5, 55.7, 55.9, 56.9, 81.8, 91.1, 91.2, 96.8, 105.4, 107.9, 118.5, 126.8 (2C), 126.9, 127.3 (2C), 127.7 (2C), 131.8 (2C), 132.9, 137.0, 140.4, 149.8, 158.2, 158.8, 161.5 ppm;

HR-MS calculated for $\text{C}_{30}\text{H}_{33}\text{ClO}_4\text{Si}$: 520.1837, found: 521.736 ($\text{M}+\text{H}$) $^+$.

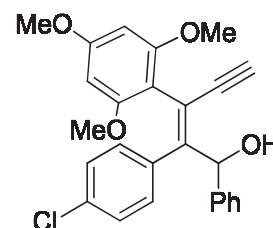
Compound 326:

3-(4-Chlorophenyl)-4-phenyl-2-(2,4,6-trimethoxyphenyl)cyclopent-2-en-1-one



Compound 331:

(E)-2-(4-Chlorophenyl)-1-phenyl-3-(2,4,6-trimethoxyphenyl)pent-2-en-4-yn-1-ol

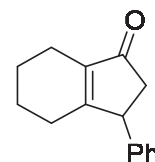


Compounds **326** and **331** were obtained following general procedure XVIII starting from compound **325** (80 mg, 0.158 mmol) in nitromethane (2 mL) with triflic acid (2.5 μL , 0.002 mmol) and MeOH (49 μL , 1.22 mmol). Cyclopentenone **326** (10 mg, 15%) was obtained along with rearranged product **331** (5 mg, 7%). Cyclopentenone **326** was already described page 225 following another method.

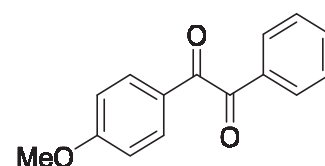
Rearranged product **331**:

$^1\text{H NMR}$ (CDCl_3 , 400 MHz) δ 3.67 (s, 6H), 3.76 (s, 3H), 5.81 (s, 1H), 6.05 (s, 2H), 7.20-7.31 (m, 7H), 7.70 (d, 2H, $J = 8.8$ Hz) ppm;

$^{13}\text{C NMR}$ (CDCl_3 , 400 MHz) δ 55.3, 56.2, 56.8, 74.1, 81.1, 91.1 (2C), 107.7, 110.8, 121.2, 128.3 (2C), 129.3 (2C), 129.7, 130.8 (2C), 131.3 (2C), 132.7, 138.5, 143.5, 150.3, 159.2, 160.1, 162.5 ppm.

Compound 197:**3-Phenyl-2,3,4,5,6,7-hexahydro-1H-inden-1-one**

Compound **197** was obtained following general procedure XVIII starting from compound **332** (100 mg, 0.35 mmol) in DCE (2 mL) with triflic acid (5 μ L, 0.005 mmol) and MeOH (114 μ L, 2.8 mmol). Cyclopentenone **197** was obtained with 35% yield (26.1 mg) and was already described page 158 following another method.

Compound 334:**1-(4-Methoxyphenyl)-2-phenylethane-1,2-dione**

MeOH (109 μ L, 2.68 mmol) and ReO₄H/H₂O (50/50, v/v, 2.6 μ L, 0.005 mmol) were added to a solution of compound **333** (150 mg, 0.35 mmol) in anhydrous DCE (2 mL) under argon atmosphere. The reaction mixture was stirred 48 hours at 45 °C, concentrated and purified over silica gel to give compound **334** (30 mg, 36%). Recovered starting material (24 mg, 16%).

¹H NMR (CDCl₃, 400 MHz) δ 3.89 (s, 3H), 6.98 (d, 2H, J = 8.9 Hz), 7.50 (t, 2H, J = 8.0 Hz), 7.65 (t, 1H, J = 7.4 Hz), 7.94-7.98 (m, 4 H) ppm;

¹³C NMR (CDCl₃, 400 MHz) δ 55.8, 114.5 (2C), 126.3, 129.1 (2C), 130.1 (2C), 132.5 (2C), 133.4, 134.8, 165.1, 193.3, 195.0 ppm.

6. PUBLICATIONS

Cancer wars: Natural products strike back.

Basmadjian, C.; Zhao, Q.; Djehal, A.; Bentouhami, E.; Nebigil, CG.; Johnson, RA., Serova, M.;
de Gramont, A.; Faivre, S.; Raymond, E.; Désaubry, L. *Frontiers Chem.* **2014**, 2, article 20



Cancer wars: natural products strike back

Christine Basmadjian^{1,2}, Qian Zhao^{1,2}, Embarek Bentouhami³, Amel Djehal^{1,3}, Canan G. Nebigil⁴, Roger A. Johnson⁵, Maria Serova², Armand de Gramont², Sandrine Faivre^{2,6}, Eric Raymond^{2,6} and Laurent G. Désaubry^{1*}

¹ Therapeutic Innovation Laboratory, UMR7200, CNRS/University of Strasbourg, Illkirch, France

² AAREC Filla Research, Clichy, France

³ L.C.I.M.N Laboratory, Department of Process Engineering, Faculty of Technology, University Ferhat Abbas, Sétif, Algeria

⁴ Biotechnology and Cell Signaling Laboratory, UMR 7242, CNRS/ University of Strasbourg, Illkirch, France

⁵ Department of Physiology and Biophysics, State University of New York, Stony Brook, NY, USA

⁶ Department of Medical Oncology, Beaujon University Hospital, INSERM U728/AP-HP, Clichy, France

Edited by:

Asier Unciti-Broceta, The University of Edinburgh, UK

Reviewed by:

Luis Álvarez De Cienfuegos Rodríguez, University of Granada, Spain

Francisco Franco-Montalbán, University of Granada, Spain

*Correspondence:

Laurent G. Désaubry, Therapeutic Innovation Laboratory (UMR 7200), Faculté de Pharmacie, 74 Route du Rhin, 67401 Illkirch, France
e-mail: desaubry@unistra.fr

Natural products have historically been a mainstay source of anticancer drugs, but in the 90's they fell out of favor in pharmaceutical companies with the emergence of targeted therapies, which rely on antibodies or small synthetic molecules identified by high throughput screening. Although targeted therapies greatly improved the treatment of a few cancers, the benefit has remained disappointing for many solid tumors, which revitalized the interest in natural products. With the approval of rapamycin in 2007, 12 novel natural product derivatives have been brought to market. The present review describes the discovery and development of these new anticancer drugs and highlights the peculiarities of natural product and new trends in this exciting field of drug discovery.

Keywords: natural products, cancer, drug discovery, pharmacognosy, molecular targets, privileged structures

INTRODUCTION

Recent analyses of tooth plaques showed that ~50,000 years ago Neanderthals already used medicinal plants to treat their ailments (Hardy et al., 2012). Currently, more than half of humanity does not have access to modern medicine and relies on traditional treatments (Cordell and Colvard, 2012). A recent analysis of the strategies used in the discovery of new medicines showed that 36% of the first-in-class small-molecules approved by U.S. Food and Drug Administration (FDA) between 1999 and 2008 were natural products or natural products derivatives (Swinney and Anthony, 2011).

Natural products are small-molecule secondary metabolites that contribute to organism survival. These substances display considerable structural diversity and “privileged scaffolds,” i.e., molecular architectures that are tailored to protein binding, as first coined by Evans in the late 1980s (Evans et al., 1988). Indeed natural products have evolved to bind biological targets and elicit biological effects as chemical weapons or to convey information from one organism to another. Steroid derivatives are often not considered as natural products because their design is not based on a research in pharmacognosy, however we subjectively decided to include them here due to their importance in drug discovery.

The synthesis of aspirin by Charles Gerhard at Strasbourg faculty of pharmacy in 1853 paved the road for the medicinal chemistry of natural products (Gerhardt, 1853). In 1964, actinomycin became the first natural product approved for an indication in oncology. Other natural products based medicines such as anthracyclines, *vinca* alkaloids, epipodophyllotoxin lignans, camptothecin derivatives, and taxoids that were launched before 1997, are still an essential part of the armament for treating cancers.

From 1997 to 2007 no new natural product was approved for the treatment of cancer (Bailly, 2009). With the imminent achievement of the genome project, the head of a pharmaceutical company declared that natural products were outdated. Their development was greatly reduced and many big pharmaceutical companies closed their departments of natural product chemistry (Bailly, 2009). The future was targeted therapies, which uses fully synthetic molecules or antibodies to target specific proteins in tumor growth and progression. In some forms of leukemia, gastrointestinal, prostate or breast cancers, targeted therapies greatly delayed tumor progression, and/or improved the life expectancy of the patients. Some tumors with specific oncogenic addictions (for example fusion proteins leading to ALK expression in lung cancer or Bcr-Abl in chronic myeloid leukemia, KIT expression or mutations in GIST or EGFR mutation in lung cancer, HER2 amplification in breast cancer or MET overexpression in liver tumors) greatly benefited from targeted agents. However, the vast majority of common tumors were found to be not dependent of a single “targetable” oncogenic activation. For instance altogether ALK activations and EGFR mutations account for less than 10% of lung adenocarcinoma and while those targeted agents are more efficient than chemotherapy in oncogenic tumors, antitumor effects are limited to few months. Importantly, most tumors were shown to activate multiple signaling pathway redundancies and adaptive mechanisms that either render tumors primarily resistant to targeted drugs or facilitate acquired resistance to cell signaling inhibition after only few months of treatments. As a result, the expected progression-free survival benefit from targeted therapy is often less than 6-months. For those later forming complex but rather frequent tumors, chemotherapy alone remains the cornerstone of treatment with

some limited add-on benefits by use of monoclonal antibodies in a limited proportion of patients. Combinations of several targeted agents have also been proposed to counteract potential adaptive mechanisms although one should notice that combining targeted agent together was more often associated with unacceptable toxicity than great clinical synergy. Then there is the additional influence of cost-to-benefit concerns. The financial cost of such targeted therapies, to patients or health insurance entities, can be considered enormous, e.g., thousands to tens of thousands of euros per day of extended life. However, the net financial benefit to pharmaceutical companies of those agents that are given only for few months (or years) in only a small proportion of patients in niche indications may lead to restricted investment by pharmaceutical industries; blockbuster indications usually provide higher revenues.

These drawbacks are at the origin of the re-emergence of natural products in oncology. Since 2007, with the approval of rapamycin and derivatives of it, 12 natural product derivatives have been approved for the treatment of cancers (Table 1).

Recently Stuart Schreiber, Paul Clemons and coworkers at the Broad Institute in Boston performed a bioinformatics analysis of natural product targets and demonstrated that natural products statically tend to target proteins with a high number of protein–protein interactions that are particularly essential to an organism (Dančik et al., 2010). This observation is consistent with the common role played by natural products as chemical weapons against predators or competitors.

Henkel et al. at Bayer AG in Germany offered a statistical analysis of the structural differences between natural products and fully synthetic drugs (Henkel et al., 1999). Compared with fully synthetic drugs, natural product tend to have more chiral centers, more oxygen atoms, less nitrogen atoms, and more varied ring systems. Complementary analyses of structural features of natural products have been reviewed (Lee and Schneider, 2001; Ortholand and Ganesan, 2004; Ganesan, 2008; Grabowski et al., 2008). A consequence of this structural complexity is that natural products tend to be more selective toward their targets than fully synthetic drugs, and consequently rarely display off-target—induced iatrogenicity.

Moreover, complex natural products tend to act through only one class of molecular target, even though there are some exceptions. Indeed, taxanes are known to target β -tubulin and interfere with microtubule dynamics; however they also bind to Bcl-2 to block its anti-apoptotic activity. Both β -tubulin and Bcl-2 interact with the orphan nuclear receptor Nur77 (NGFI-B, TR3, NR4A1). Ferlini et al. showed that in fact taxanes mimic the domain of Nur77 involved in the interaction with β -tubulin and Bcl-2 (Ferlini et al., 2009). Another example concerns flavaglines, an emerging family of natural compounds found in medicinal plants of South-East Asia, which display potent anticancer effects through their direct effects on the scaffold proteins prohibitins and the initiation factor of translation eIF4a (Basmadjian et al., 2013; Thuaud et al., 2013).

Modifying the structure of a drug may change the nature of its molecular target. A striking example concerns the not so rational development of the anticancer medicines etoposide and teniposide (Figure 1). Considering that cardiac glycosides

display enhanced pharmacological properties compared to the cognate aglycone, Sandoz scientists hypothesized that conjugating podophyllotoxin to a glucose moiety could improve the activity of this cytotoxic agent that binds tubulin and inhibits assembly of the mitotic spindle. Fortunately, this glycoconjugate named etoposide displayed a promising anticancer activity with reduced adverse effects compared with podophyllotoxin. Surprisingly, etoposide did not affect tubulin polymerization but inhibited another very important target in oncology: DNA topoisomerase II. This story illustrates well the importance in drug discovery of serendipity, which was likened to “looking for a needle in a haystack and discovering the farmer’s daughter” by Professor Pierre Potier, inventor of the anticancer drug taxotere (Zard, 2012).

Another non-rational issue regarding the SAR of derivatives of natural compounds concerns the relationship between the chemical structure of a drug and its therapeutic indication. Indeed, transforming the structure of a drug may modify the nature of the targeted cancer. This is well established for *vinca* alkaloids for instance (Table 2). If we could understand the influence of the molecular structure of a drug with its optimal therapeutic indication, then we might be able to adapt known medicines to treat cancers that are reluctant to current therapies.

In spite of the major achievements in systems biology and translational medicine over the last decade, there is still, at best, a presumptive relationship between the efficacy of a drug in preclinical assays and the likelihood of its value in clinic.

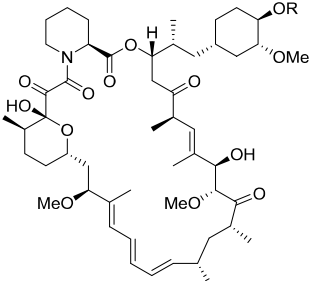
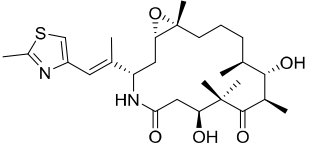
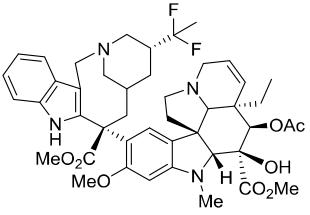
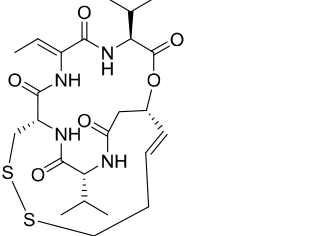
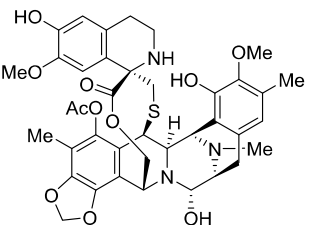
RAPALOGUES: TEMSIROLIMUS® AND EVEROLIMUS®

In 1975, researchers at Ayerst Laboratories (Canada) reported the isolation of rapamycin as a secondary metabolite from a strain of *Streptomyces hygroscopicus* based on its antifungal activity (Sehgal et al., 1975; Vezina et al., 1975). Its name comes from Rapa Nui (Easter Island) where its producer strain had been collected from a soil sample. Its richly adorned macrocyclic structure was fully elucidated a few years later (Swindells et al., 1978; Findlay and Radics, 1980; McAlpine et al., 1991). Rapamycin did not attract so much attention until the discovery in 1987 of the structurally related immunosuppressant FK506 (Kino et al., 1987a,b). Rapamycin was eventually developed without further structural modifications as the oral immunosuppressant drug sirolimus. It was approved for prevention of rejection in organ transplantation in 1999 (Calne et al., 1989; Kahan et al., 1991; Watson et al., 1999; Calne, 2003).

Determining the mode of action of rapamycin unraveled one of the most important signaling pathways in cell biology, which illustrates another important aspect of the pharmacology of natural products. Indeed a common caveat of developing an original natural product toward clinical application is the requirement to identify its molecular target and understand its mode of action (Krysiak and Breinbauer, 2012). However, when the target is identified, it may lead to major breakthroughs in cell biology (Pucheault, 2008). Gratefully, current technologies render this task increasingly easier (Ares et al., 2013).

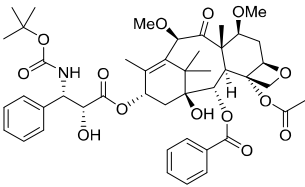
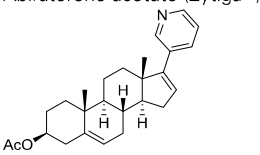
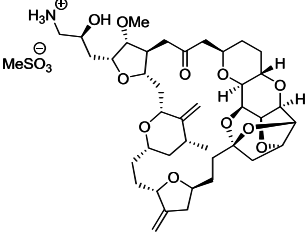
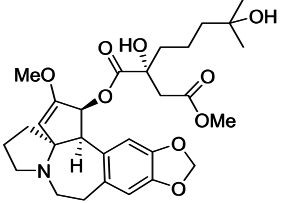
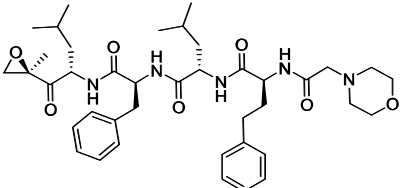
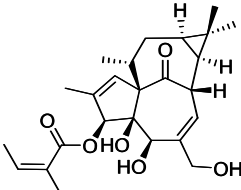
In 1991, Michael Hall et al. identified the molecular target of rapamycin in a gene complementation assay in yeast and named it TOR for “Target Of Rapamycin” (Hietman et al., 1991).

Table 1 | Novel anticancer medicines based on natural products.

Name (trade name), structure	Year of approval, company	Therapeutic indication, mode of action
Temsirolimus (Torisel®): R=R ¹ Everolimus (Afinitor®), R=R ²  $R^1 = C(O)C(CH_2OH)_2CH_3$ $R^2 = (CH_2)_2OH$	2007, Wyeth	Treatment of renal cell carcinoma (RCC), inhibition of mTOR
	2007, Bristol-Myers Squibb	Treatment of aggressive metastatic or locally advanced breast cancer no longer responding to currently available chemotherapies, stabilization of microtubules
Vinflunine (Javlor®) 	2009, Pierre Fabre	Treatment of bladder cancer, inhibition of tubulin polymerization
Romidepsin (Istodax®) 	2009, Celgene	Treatment of cutaneous T-cell lymphoma (CTCL), inhibition of the isoforms 1 and 2 of histone deacetylases
Trabectedin = ecteinascidin 743 (Yondelis®) 	2009, Zeltia and Johnson and Johnson	Treatment of advanced soft tissue sarcoma and ovarian cancer, induction of DNA damage

(Continued)

Table 1 | Continued

Name (trade name), structure	Year of approval, company	Therapeutic indication, mode of action
Cabazitaxel (Jevtana®) 	2010, Sanofi-Aventis	Treatment of hormone-refractory metastatic prostate cancer, microtubule stabilization
Abiraterone acetate (Zytiga®) 	2011, Janssen	Treatment of castration-resistant prostate cancer, inhibition of 17 α -hydroxylase/C17, 20 lyase (CYP17A1)
Eribulin mesylate (Halaven®) 	2011, Eisai Co.	Treatment of metastatic breast cancer, inhibition of microtubule dynamics
Homoharringtonine, Omacetaxine mepesuccinate (Synribo®) 	2012, Teva	Chronic myelogenous leukemia (CML), inhibition of protein synthesis
Carfilzomib (Kyprolis®) 	2012, Onyx	Treatment of multiple myeloma, inhibition of proteasome
Ingenol mebutate (Picato®) 	2012, LEO Pharma	Actinic keratosis, activation of PKC δ

Three years later, Stuart Shreiber et al. identified its mammalian homolog referred to today as the kinase mTOR (mammalian TOR) (Brown et al., 1994). The mode of action of rapamycin is unique: it binds to two proteins at the same time, mTOR and the immunophilin FKBP-12, to form a ternary complex devoid of any kinase activity. mTOR plays a central role integrating signals from growth factors, nutrients, stress, and hormones to regulate metabolism, proliferation, cell growth, and apoptosis. However, the exact mechanisms of action of rapamycin derivatives, called rapalogues, remain only moderately understood. Some recent evidence indicates that rapalogues may primarily display their anticancer effects through an inhibition of angiogenesis in patients (Faivre and Raymond, 2008). This hypothesis would explain why rapalogues are particularly effective in hyper-vascularized tumors.

Currently, two rapalogues, temsirolimus, and everolimus, have been developed for the treatment of renal, breast, and pancreas cancers, astrocytoma, and mantle cell lymphoma. These drugs

differ in their formulation, application, and dosing schemes, thereby yielding varying bioavailabilities. They are all prepared by semi-synthesis.

IXABEPILONE (IXEMPRA®)

Drugs that target microtubules, such as taxoids and *vinca* alkaloids, continue to represent an important class of chemotherapeutic agents (Jordan and Wilson, 2004). Over the last two decades other classes of naturally occurring nontaxoid compounds, the epothilones (Gerth et al., 1996; Höfle et al., 1996), discodermolides (Gunasekera et al., 1990), eleutherobins (Lindel et al., 1997), and laulimalides (Mooberry et al., 1999) that stabilize microtubule assemblies similarly to taxol, have been identified (Figure 2). Based upon extensive structure-activity data, a common pharmacophore for these different classes of compounds has been proposed (Ojima et al., 1999).

Not only is epothilone B more cytotoxic than taxol, but it is also much less sensitive toward the development of multidrug-resistance, a major concern in the clinic (Horwitz, 1994; Bollag et al., 1995; Kirikae et al., 1996). This impressive pharmacological profile coupled with the challenge of its total synthesis has attracted the attention of some of the most well-known organic chemists in the world, including Samuel Danishefsky (Balog et al., 1996; Su et al., 1997), followed by Nicolaou (Nicolaou et al., 1997; Yang et al., 1997), Schinzer (Schinzer et al., 1997), Mulzer (Mulzer et al., 2000) and Carreira (Bode and Carreira, 2001).

Early investigations indicated that natural epothilones display poor metabolic stability and unfavorable pharmacokinetic properties (Lee et al., 2000). Several synthetic and semi-synthetic analogs were then examined and evaluated in preclinical studies. Eventually, isosteric replacement of the lactone by a lactam afforded ixabepilone (also known as azaepothilone B) (Lee et al., 2008). Not only is this drug not susceptible to hydrolysis by esterases, conferring metabolic stability, but it also displays improved water solubility, which greatly alleviate galenic problems associated with hypersensitivity reaction in patients.

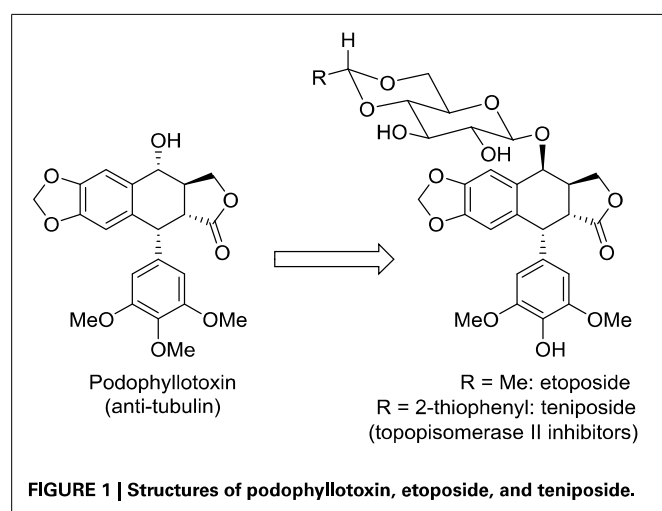
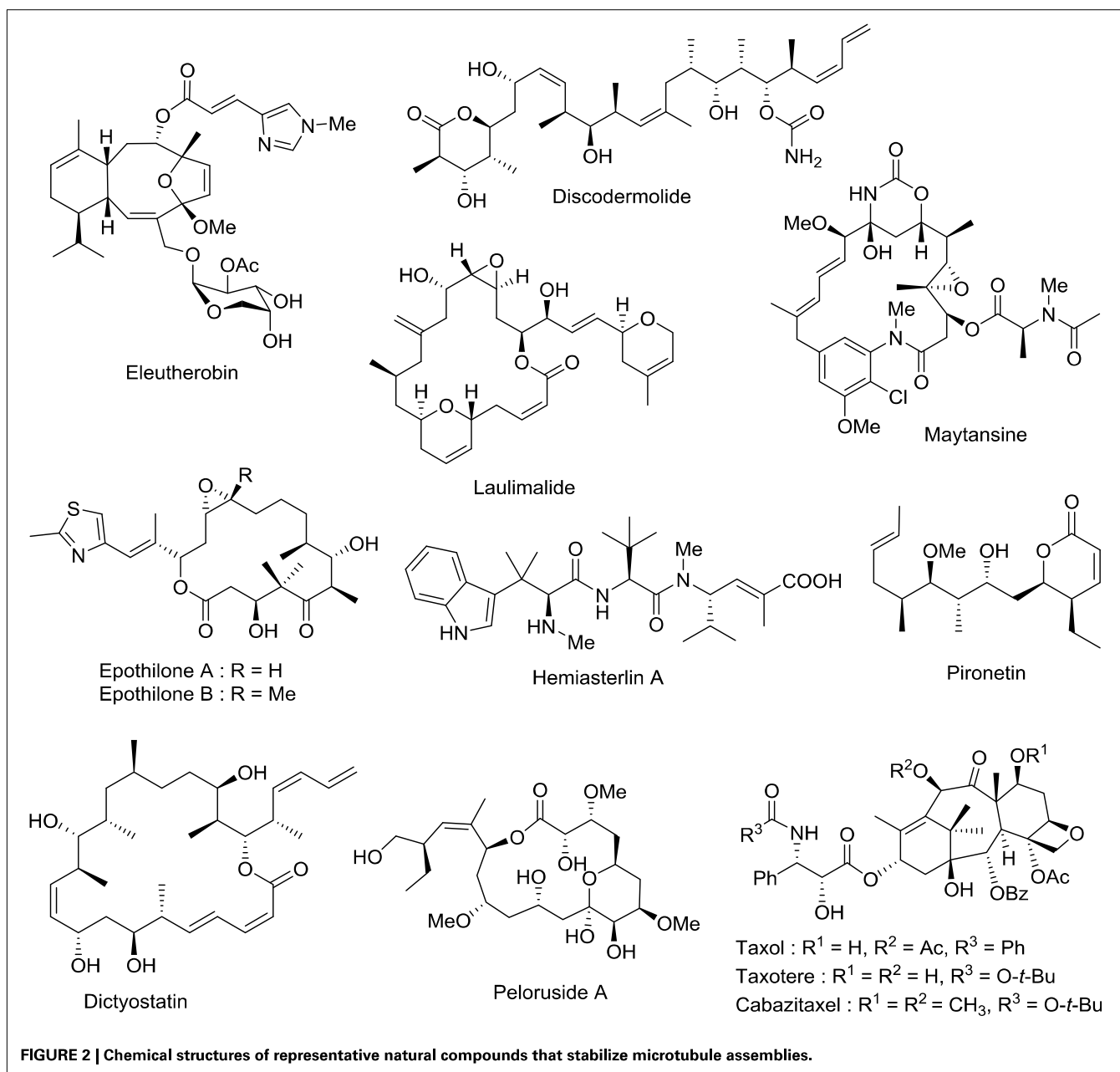


Table 2 | Structures and therapeutic indications of *vinca* alkaloids.

Name	n	Q	R ¹	R ²	R ³	R ⁴	R ⁵	Therapeutic indication
Vinblastine	2	OH	H	Et	OAc	Me	OMe	Lymphomas, germ cell tumors, breast, head and neck cancer and testicular cancers
Vinorelbine	1	Q=R ¹ =∅ (alkene)		Et	OAc	Me	OMe	Osteosarcoma, breast, and non-small cell lung cancers
Vincristine	2	OH	H	Et	OAc	CHO	OMe	Acute lymphoblastic leukemia, rhabdomyosarcoma, neuroblastoma, lymphomas, and nephroblastoma
Vindesine	2	OH	H	Et	OH	Me	NH ₂	Melanoma, lung, breast and uterine cancers, leukemia and lymphoma
Vinflunine	1	H	H	CF ₂ Me	OAc	Me	OMe	Bladder cancer



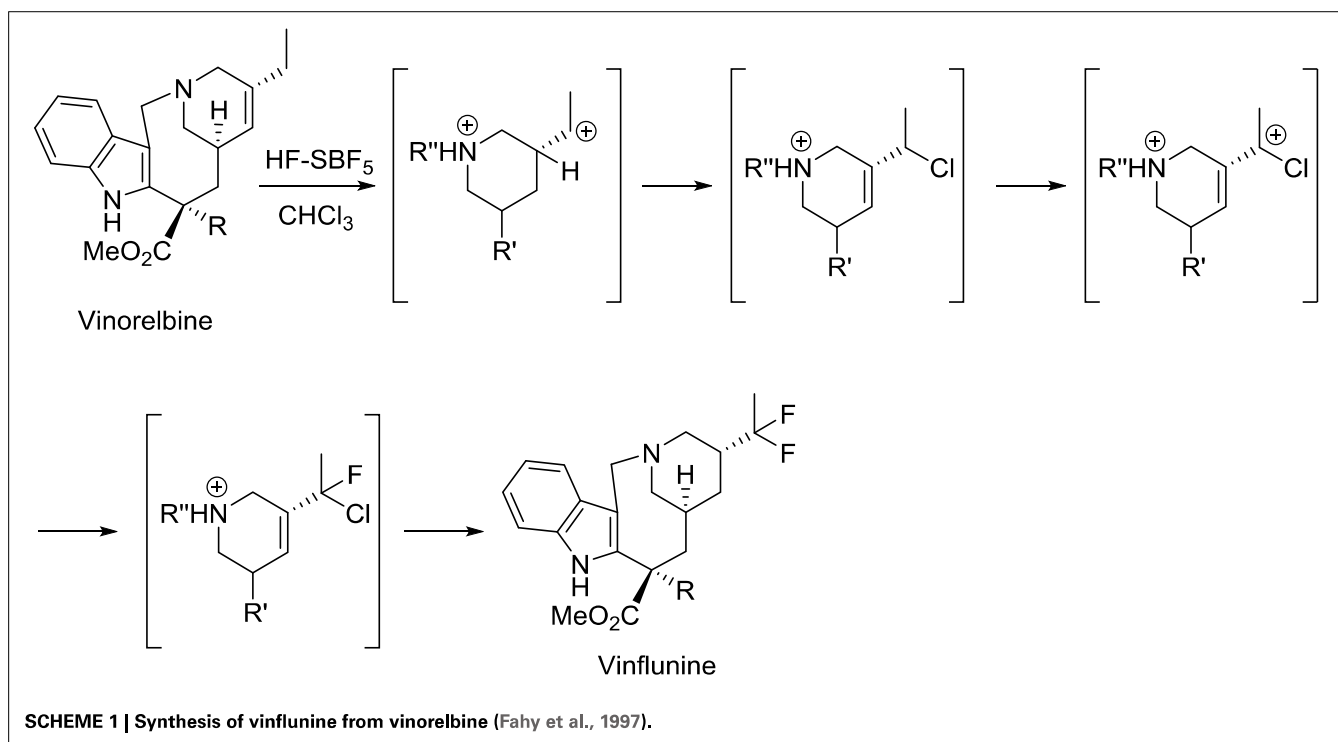
In 2007, the FDA (but not its European equivalent, European Medicines Agency or EMA) approved ixabepilone for the treatment of aggressive metastatic or locally advanced breast cancer no longer responding to currently available chemotherapies.

VINFLUNINE (JAVLOR®)

Vinca alkaloids were the first chemotherapeutic agents that target microtubules. The first member of this class, vinblastine, was isolated in 1958 (Noble et al., 1959). Later, some derivatives, vincristine, vinorelbine, and finally avelbine, were developed to treat hematological and solid malignancies in both adult and pediatric patients (Table 1). *Vinca* alkaloids block the polymerization of tubulin molecules into microtubules to prevent the formation of the mitotic spindle.

In the course of their study on the reactivity of functionalized molecules in superacid media, Jacquesy and collaborators found that the treatment of vinorelbine with a combination of HF and SbF₅ gave a difluoro analog, later called vinflunine (Scheme 1) (Fahy et al., 1997). Importantly, this new compound displayed an enhanced bioavailability compared to other *vinca* alkaloids. Indeed, its terminal half-life was calculated to be about 40 h and the terminal half-life for its active metabolite (4-*O*-deacetylvinflunine) was reported to be 4–6 days in several phase I trials (Bennouna et al., 2003, 2005; Johnson et al., 2006).

Resistance to vinflunine develops more slowly than with other *vinca* alkaloids. In addition, vinflunine *in vitro* neurotoxicity is lower than that of vincristine or vinorelbine (Etiévant et al., 1998, 2001; Estève et al., 2006). Further development by Pierre Fabre



and Bristol Myers Squibb laboratories ended with the approval of vinflunine for the treatment of bladder cancer by the European Medicines Agency (EMA) in 2009.

ROMIDEPSIN (ISTODAX®)

The cyclic depsi-pentapeptide romidepsin, also called FR901228, FK228, or NSC 630176, was isolated and identified by Ueda and colleagues at Fujisawa Pharmaceutical in Japan through a screening program of fermentation products able to revert the transformed morphology of a Ha-ras NIH3T3 cells to normal (Ueda et al., 1994). Indeed Ha-ras is an oncogene involved in tumorigenesis and consequently represents an important target in oncology. Importantly, romidepsin displayed potent antitumor activities against A549 and MCF-7 tumors in xenografted mice. These results attracted the attention of NCI scientists who continued to explore its anticancer properties under a Cooperative Research and Development Agreement with Fujisawa Corporation (now Astellas).

When romidepsin was discovered, histone deacetylases (HDAC) were emerging as important targets for the treatment of cancer (Thaler and Mercurio, 2014). Screening of microbial metabolites for their effects on transcription showed that romidepsin behaves similarly to trichostatin A, a known HDAC inhibitor (Nakajima et al., 1998). Romidepsin acts as a prodrug, which is reduced in cells to its active form by glutathione, yielding a monocyclic dithiol that preferentially inhibits the isoforms HDAC1 and HDAC2 (Furumai et al., 2002).

In 2002, when it became established that romidepsin holds a promising therapeutic potential, Fujisawa Corporation began clinical trials. Romidepsin was licensed to Gloucester Pharmaceuticals in 2004 (latter acquired by Celgene Co)

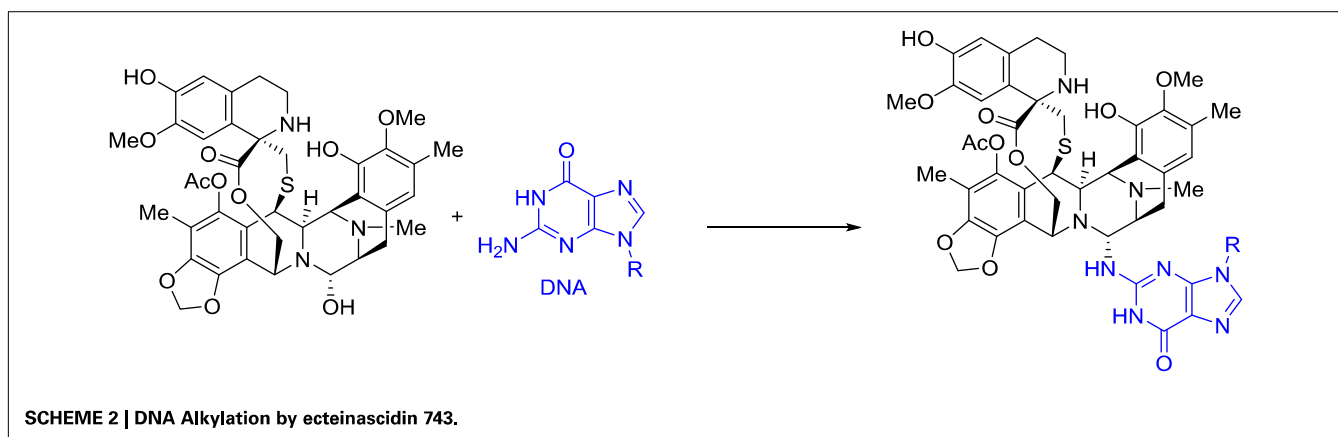
and was approved by the FDA in 2009 for the treatment of cutaneous T-cell lymphoma. The preclinical and clinical development has been described in an excellent review (Vandermolen et al., 2011).

ECTEINASCIDIN 743 = TRABECTEDIN (YONDELIS®)

In 1969, unidentified alkaloids from the Caribbean tunicate *Ecteinascidia turbinata* were shown to display some anticancer activities, but the structure of these complex alkaloids could not be determined because of their natural scarcity and the limitation of analytical chemistry at that time (Sigel et al., 1970). In 1990, Rinehart et al. from the University of Illinois at Urbana-Champaign elucidated the structure and reported the cytotoxicity of these tetrahydroisoquinoline alkaloids, the ecteinascidins (Rinehart et al., 1990). These compounds displayed greater *in vitro* and *in vivo* antitumor activity than those reported for the structurally related microbial metabolites saframycins and safracins.

Ecteinascidin 743, also called trabectedin and ET-743, was then selected for preclinical development based on its exceptional *in vitro* cytotoxicity. Pommier et al. at NCI demonstrated that this drug binds in the minor groove of DNA and alkylates the exocyclic amino group at position 2 of guanine in GC-rich regions (Scheme 2) (Pommier et al., 1996).

Ecteinascidin 743 was shown to block the DNA excision repair system (Takebayashi et al., 2001; Zewail-Foote et al., 2001), to cross-link DNA with topoisomerase I (Martinez et al., 1999; Takebayashi et al., 1999; Zewail-Foote and Hurley, 1999), and also to inhibit the binding of DNA to some transcription factors (Bonfanti et al., 1999; Jin et al., 2000; Minuzzo et al., 2000). However, the cascade of events that links DNA damage



to the resulting antitumor activity is far from being understood (D'Incalci and Galmarini, 2010).

When ecteinascidin 743 was licensed to PharmaMar; this company launched a very challenging program of aquaculture to produce sufficient quantities of tunicate biomass to feed clinical trials program. After several years of intensive development, the cumulative total biomass reached some 250 metric tons. However, isolation of ecteinascidin 743 required complex and costly steps of purification with final yields less than 1 g/ton (Cuevas and Francesch, 2009). Several total syntheses have been reported, but they cannot be translated into industrial production (Corey et al., 1996; Endo et al., 2002; Chen et al., 2006; Zheng et al., 2006; Fishlock and Williams, 2008; Imai et al., 2012; Kawagishi et al., 2013). Eventually, this supply problem was solved by use of a complex semi-synthesis from cyanosafraicin B, which is available in kilogram quantities by fermentation (Cuevas et al., 2000; Menchaca et al., 2003).

Preclinical studies did not reveal that soft tissue sarcoma is more sensitive to ecteinascidin 743 than other solid tumors. This response was unveiled first during phase I clinical trials and confirmed in phase II (Taamma et al., 2001; Villalona-Calero et al., 2002; D'Incalci and Jimeno, 2003). This drug was approved under the name of Yondelis in 2007 in the European Union for the treatment of patients with advanced soft tissue sarcoma. This compound was the first anticancer medicine of marine origin to be approved. It was followed by eribulin (*vide infra*), validating the concept that marine natural products should be considered important contenders in drug discovery.

CABAZITAXEL (JEVTANA®)

The taxane anticancer drug cabazitaxel is a semi-synthetic derivative of the natural taxoid 10-deacetylbaccatin III. It was approved in 2010 by the FDA, in combination with prednisone, for the treatment of patients with hormone-refractory metastatic prostate cancer who had already been administered a treatment containing the taxane docetaxel (Galsky et al., 2010). In 2013, Vrignaud et al. showed that *in vitro*, cabazitaxel stabilized microtubules as effectively as docetaxel but was also 10 times more potent than docetaxel in chemotherapy-resistant tumor cells. They also noted that cabazitaxel was active in docetaxal-resistant

tumors (Vrignaud et al., 2013). In addition, cabazitaxel penetrates the blood-brain barrier. Cabazitaxel was approved 20 years after taxol, illustrating that there is still room to improve well established anticancer medicines.

ABIRATERONE ACETATE (ZYTIGA®)

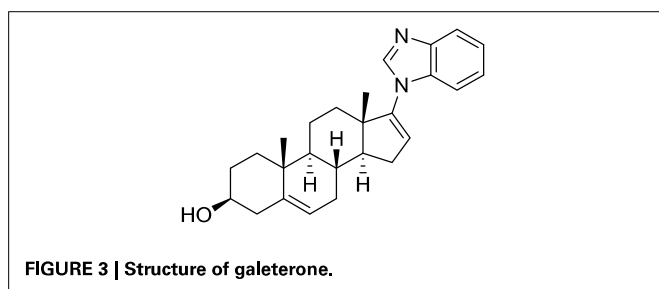
Abiraterone acetate is an oral inhibitor of androgen synthesis used since 2011 for the treatment of castration-resistant prostate cancer. Previous treatments of prostatic cancers prevented androgen production by the testes, but not by the adrenals. Abiraterone acetate is rapidly hydrolyzed *in vivo* to abiraterone, which is a selective, irreversible inhibitor of cytochrome P450 17 α (CYP17), an enzyme that catalyzes the conversion of pregnenolone and progesterone into DHEA or androstenedione, two precursors of testosterone. This drug was originally designed and synthesized by Jarman et al. at the Institute of Cancer Research in Sutton (UK) based on the hypothesis that the nitrogen lone pair of a pyridyl moiety linked to the steroid skeleton would coordinate with the iron atom of the heme cofactor in the active site of CYP17 (Potter et al., 1995; Jarman et al., 1998).

The inhibition of CYP17 by abiraterone acetate blocks androgen biosynthesis and significantly improves the therapy of castration-resistant prostate cancer, which remains a challenge to treat (Rehman and Rosenberg, 2012). Unfortunately, this CYP17 inhibition also decreases glucocorticoid and increases mineralocorticoid production, which results in the main source of adverse effects.

Since the invention of abiraterone, different steroids bearing a heteroaromatic substituent on the D ring continued to be developed as CYP17 inhibitors. Among those, galeterone (TOK-001 or VN/124-1) recently entered clinical trials for the treatment of chemotherapy-naïve, castration-resistant prostate cancer (Figure 3) (Vasaitis and Njar, 2010). Interestingly, this drug not only inhibits CYP17, but is also an androgen receptor antagonist (Handratta et al., 2005).

ERIBULIN MESYLATE (HALAVEN®)

In 1985, Uemura et al. isolated and identified norhalichondrin A from the marine sponge *Halichondria okadai* based on its potent *in vitro* toxicity (Uemura et al., 1985). Related polyether macrolides, including halichondrin B (Hirata and

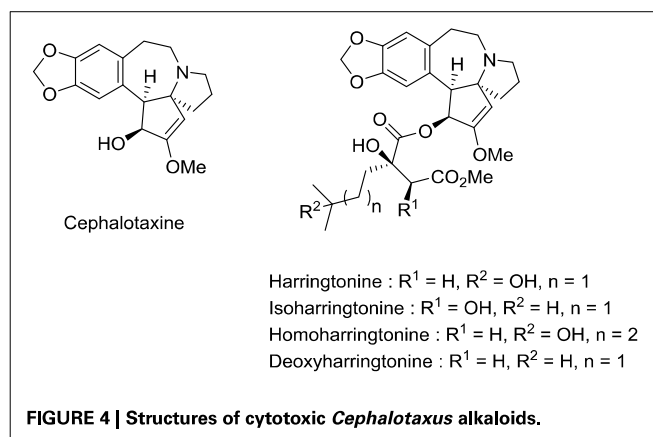


Uemura, 1986) were identified in the following years (Qi and Ma, 2011). Tests with NCI's 60-cell line screen suggested that halichondrin B affects tubulin polymerization. Further studies showed that this drug displays subtle differences in mechanism of action from those of other known antimetotics targeting tubulin. Although halichondrin B displayed promising activity, its preclinical investigation has been hampered by its scarcity from natural sources.

Due to its complexity, the total synthesis of halichondrin B was considered as an attractive objective by Kishi et al. at Harvard University. This team achieved this formidable challenge in 1992 (Aicher et al., 1992). Further collaborative studies from this group and Eisai Co. ultimately led to the development of the simplified and pharmaceutically improved analog eribulin (Jackson et al., 2009). Although it is less complex than natural halichondrins, eribulin contains 19 stereogenic centers, two exocyclic olefins, seven polyoxygenated pyrans and tetrahydrofurans, a 22-membered macrolactone ring, and a 36 carbon backbone. With its 35 steps, eribulin synthesis extended the limit of feasibility for industrial production. Indeed, eribulin is the single most complex molecule synthesized at an industrial scale and represents an awe-inspiring testimony to the current power of organic synthesis. Eribulin was approved by FDA in 2010 to treat patients with metastatic breast cancer who have received at least two prior chemotherapy regimens for late-stage disease.

HOMOHARRINGTONINE = OMACETAXINE MEPESUCCINATE (CEFLATONIN®)

Toxic seeds of the conifer *Cephalotaxus harringtonia* K. Koch var *harringtonia* belong to the traditional Chinese pharmacopeia. In observance with Mao Tse-tung's judgment that Chinese medicine and pharmacology represent a national treasure that needs to be valorized, Chinese investigators established that the total alkaloids from *Cephalotaxus fortunei* Hook.f possesses anti-tumor activity in preliminary clinical trials (Group, 1976). In the same period, National Cancer Institute (NCI) scientists found that *Cephalotaxus harringtonia* seed extracts displayed significant *in vivo* activity against L-1210 and P-388 leukemia tumors in mice. Powell et al. from the U.S. Department of Agriculture isolated and identified the structure of cytotoxic *Cephalotaxus* alkaloids: harringtonine, isoharringtonine, homoharringtonine, and deoxyharringtonine (Powell et al., 1970) (Figure 4). These compounds are esters of cephalotaxine, an inactive alkaloid first isolated by Paudler et al. in 1963 at Ohio University (Paudler et al., 1963). Homoharringtonine was found to be the most effective in



prolonging survival of P388 leukemic mice (Powell et al., 1972). Clinical trials performed in China demonstrated the efficacy of this agent against acute myeloid leukemia (AML), myelodysplastic syndrome (MDS), acute promyelocytic leukemia (APL), polycythemia vera, and central nervous system (CNS) leukemia (Kantarjian et al., 2013).

Homoharringtonine inhibits protein synthesis (Huang, 1975). More specifically, it blocks the aminoacyl-tRNA binding to free ribosomes and monosomes, but not to polyribosomes (Fresno et al., 1977). Tang et al. demonstrated that decreased expression of the antiapoptotic factor myeloid cell leukemia-1 (Mcl-1) is a key event in this antileukemic mechanism of action (Tang et al., 2006).

In 1998, a Texan biotech company developed the semisynthetic form of homoharringtonine, designated "omacetaxine mepesuccinate" (Synribo®), and provided a reliable source supply for clinical investigations by ChemGenex and the M.D. Anderson Cancer Center (Robin et al., 1999).

This preparation of homoharringtonine [Omacetaxine mepesuccinate (Synribo®)] has been granted orphan drug status in Europe and the U.S. to treat chronic myelogenous leukemia (CML). It was approved by the US FDA in October 2012 for the treatment of adult patients with CML after failure of two or more tyrosine kinase inhibitors (for a review on its clinical development, see Kantarjian et al., 2013). It is interesting to note that these approvals occurred more than 40 years after the initial discovery of this compound. Even though omacetaxine has a narrow indication in the U.S. and Europe, it has been part of standard acute myeloid leukemia (AML) therapy in China, which begs for extending its use for additional indications.

CARFILZOMIB (KYPROLIS®)

In 1992, Bristol-Myers Squibb scientists from Tokyo reported the structure of epoxomicin, a microbial tetrapeptide appended with an electrophilic epoxy ketone group. This compound displayed potent *in vivo* antitumor activity against murine B16 melanoma tumors. However, because the mechanism of action could not be established, its investigation was abandoned, thereby leading to the publication of the initial discovery. Eventually, BMS closed the research center in Tokyo. It was a common practice

during that period for big pharmaceutical companies to close their departments of natural product chemistry.

In 1999, the potent anticancer activity of epoxomicin attracted the attention of Craig Crews at Yale University, who designed the first synthesis of epoxomicin. In the course of this endeavor, he established the absolute configuration of the epoxide stereocenter and synthesized also a biotinylated probe, which was used to identify the proteasome as the molecular target of epoxomicin. The proteasome is a multiprotein complex that degrades unneeded or damaged proteins by proteolysis. Importantly, epoxomicin does not display any cross-inhibition with proteases, which is a major problem encountered with other anticancer proteasome inhibitors, such as bortezomib (Velcade®). The source of this selectivity was elucidated by a crystallographic approach (Groll et al., 2000). The crystal structure of the proteasome bound to epoxomicin revealed the formation of a morpholino ring between the amino terminal threonine of the proteasome and the electrophilic moiety of epoxomicin, probably through the mechanism displayed in **Scheme 3**.

The specificity of epoxomicin toward proteasome prompted Crews to associate with Caltech professor Raymond Deshaies to establish a start-up company, Proteolix, dedicated to the development of a clinical candidate. During this process, they identified YU-101, which had better inhibitory activity than bortezomib (**Figure 5**). Addition of a morpholine moiety to YU-101 improved its solubility, thereby creating carfilzomib, which rapidly entered Phase I and II clinical trials. Importantly, the peripheral neuropathy that was observed with bortezomib did not occur with carfilzomib. In 2009, Onyx Pharmaceuticals acquired Proteolix and this compound was approved for the treatment of multiple myeloma in 2012.

INGENOL MEBUTATE (PICATO®)

Phorbol diesters, such as 12-O-tetradecanoylphorbol-13-acetate (TPA), rank among the most potent tumor promoters identified so far (**Figure 6**) (Nishizuka, 1984). These compounds induce tumor formation by activating protein kinase C (PKC). Interestingly, a natural compound extracted from *Euphorbia peplus* plants, Ingenol mebutate, also activates PKC but with a different pharmacological profile. Indeed, this compound induces the death of precancerous skin lesions induced by sunlight, called actinic keratosis.

The sap of *Euphorbia peplus* (known commonly as petty spurge) is commonly used as an alternative therapy for skin

diseases in Australia (Weedon and Chick, 1976). In 1998, its efficacy was established for the self-treatment of skin cancers and actinic keratosis (Green and Beardmore, 1988).

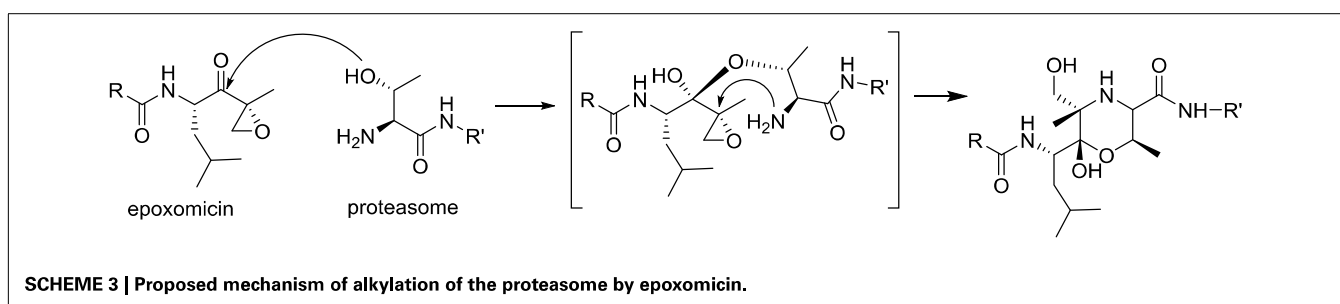
Ingenol mebutate was first identified in 1980 by Evans et al. from the National Research Center in Cairo (Egypt) (Sayed et al., 1980). These authors demonstrated also that this compound is cytotoxic to cancer cells. For more than 20 years, ingenol mebutate remained poorly investigated, until 2004, when the lab of Peter Blumberg at NCI showed that it activates PKC isoforms, but with a different pharmacological profile than that of TPA. Importantly, the activation of protein kinase C delta (PKC δ) was shown to promote the production and release of inflammatory cytokines contributing to the elimination of actinic keratosis.

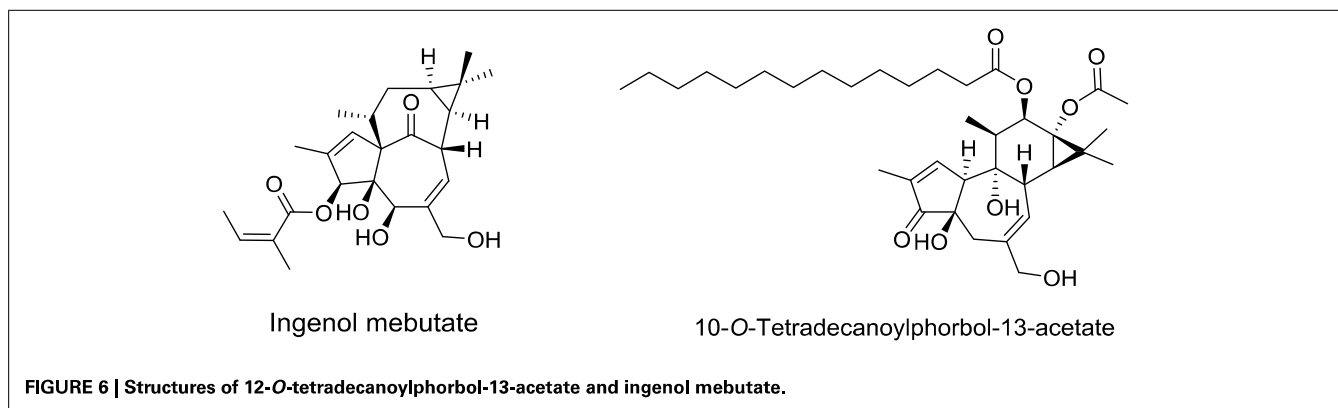
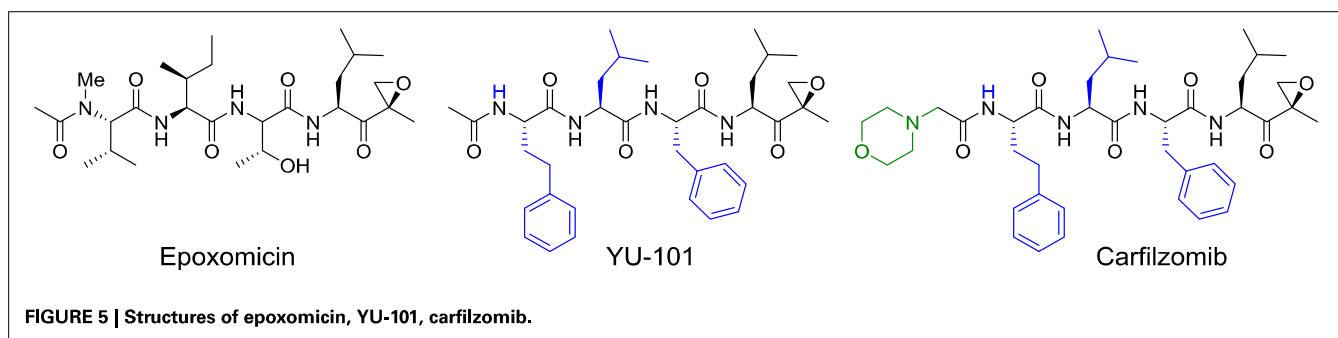
At the same time, Eric Raymond in Clichy (France) showed that ingenol mebutate-induced activation of PKC δ and reduced expression of PKC α lead to an activation of Ras/Raf/MAPK, an inhibition of the phosphatidylinositol 3-kinase/AKT signaling pathways, and ultimately to apoptosis of cancer cells (Benhadji et al., 2008; Serova et al., 2008; Ghoul et al., 2009).

After few years of preclinical investigations, ingenol mebutate entered clinical trials (Siller et al., 2009) and was eventually approved by FDA and EMA in 2012 for the topical treatment of actinic keratosis. This compound is produced by extraction from the petty spurge plant in low yield (1 g of pure compound/800 kg of plant). To improve the production of this molecule, Jakob Felding of LEO pharma associated with Phil Baran from Scripps Institute to develop an elegant synthesis of ingenol in only 14 steps from inexpensive (+)-3-carene (Jørgensen et al., 2013). This synthesis has been rapidly scaled-up to kilogram levels (Ritter, 2013).

CONJUGATION OF NATURAL PRODUCTS TO ANTIBODIES OR FOLIC ACID TO TARGET TUMORS

At the end of 19th century, Paul Ehrlich already considered the conjugation of a toxin to a compound that selectively targets a disease-causing organism to generate a “magic bullet” (“*magische kugel*”) that would destroy the origin of the disease without toxicity to healthy tissues in the body (Ehrlich, 1897). About 60 years later, Mathé et al. conjugated anti-tumor antibodies to the folic acid antagonist, methotrexate (Loc et al., 1958). Although the experiments in mice were encouraging, this approach did not attract interest in the scientific community and returned to limbo for two decades, until 1975, when Ghose et al. demonstrated the efficacy of an anticancer alkylating





agent, chloranbucil, conjugated to an antibody against a mouse lymphoma (Ghose et al., 1975). The advent of monoclonal antibodies the same year definitely boosted this field of research (Kohler and Milstein, 1975). Since then, almost every cytotoxic agent has been conjugated to antibodies following various strategies.

After two decades of endeavor, low cytotoxicity, and lack of specificity of antibodies for their targeted antigens, conjugate instability, immunogenicity, and heterogeneous product characteristics were identified as important sources of failure in the clinic (Scott et al., 2012; Ho and Chien, 2014). However, a significant step forward was made with the use of extremely highly toxic agents such as calicheamicin, maytansine, or auristatin (Figure 7). These drugs are so toxic that they cannot be used by themselves without a targeting agent.

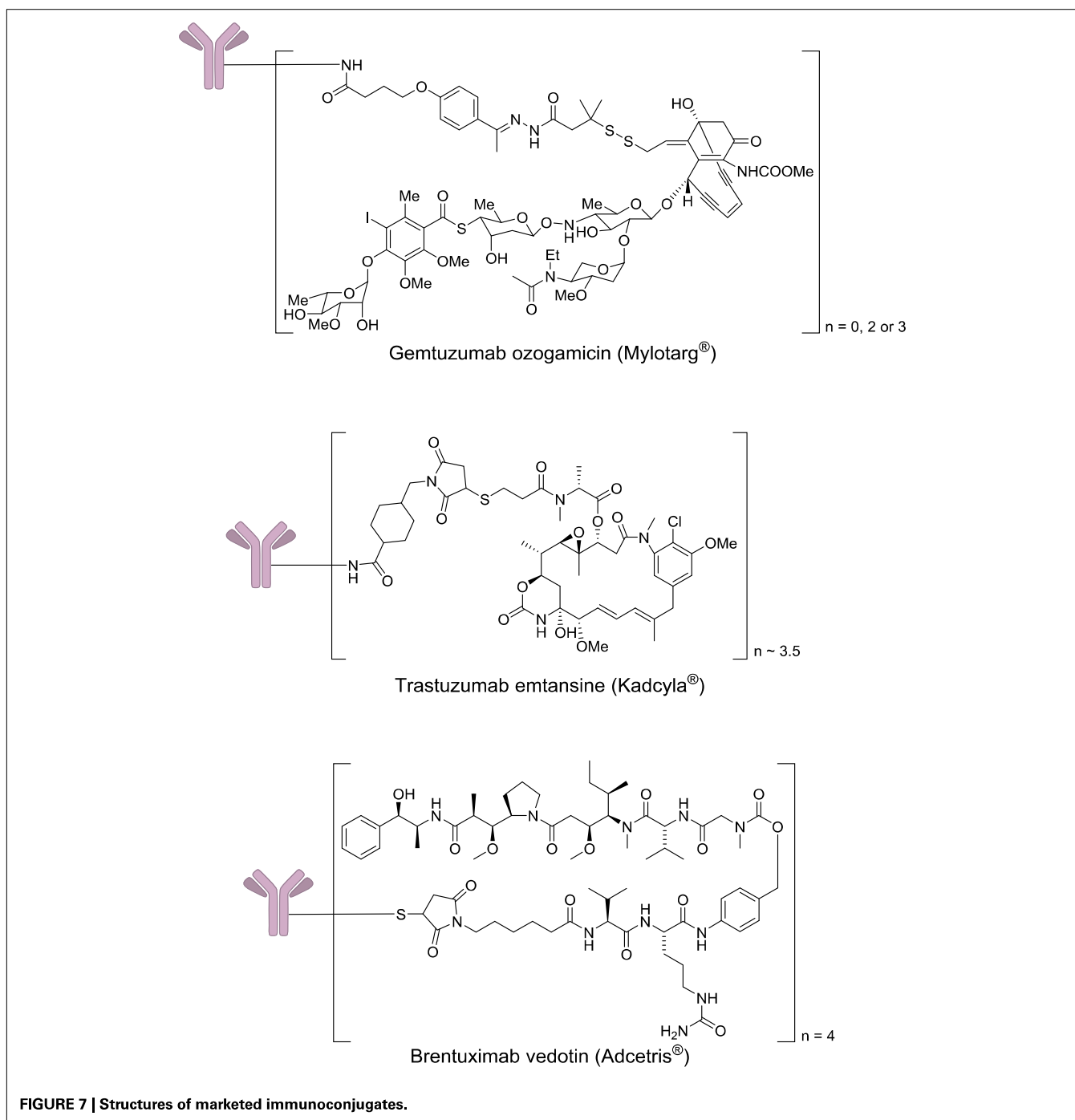
In 2000, four decades after Mathé's pioneering work and one century after Ehrlich's dream, Wyeth received approval to commercialize Gemtuzumab ozogamicin (Mylotarg®) which results from the conjugation of a monoclonal antibody targeting CD33 with a calicheamicin derivative. This drug was used for 10 years against acute myelogenous leukemia, before being withdrawn in 2010, when it was demonstrated that it does not provide any significant benefit over conventional cancer therapies. In 2011 and 2013, two other immunoconjugates were marketed: brentuximab vedotin (Adcetris®) and trastuzumab emtansine (Kadcyla®). The first one targets the protein CD30, which is expressed in classical Hodgkin lymphoma and systemic anaplastic large cell lymphoma. This antibody is conjugated to a fully synthetic analog of the antimetabolic agent dolastatin (Figure 7).

Trastuzumab emtansine results of the conjugation of a monoclonal antibody targeting the receptor HER2 (a receptor tyrosine-kinase erbB-2), which is overexpressed mainly in some forms of breast and gastric cancers to the highly cytotoxic natural product maytansine. The development of this class of agents requires a careful optimization of the monoclonal antibody, the cytotoxic payload, and the chemical linker (Ducry, 2012). The successful introduction of immunoconjugates has validated this approach to treat cancers, and currently as many as 415 antibody–drug conjugates are under clinical evaluation.

In addition to antibodies, alternative tumor-selective ligands have been conjugated to anticancer drugs. Based on observations that cells internalize vitamins, such as folate, by receptor-mediated endocytosis, Leamon, and Low from Purdue University demonstrated in 1991, that macromolecules conjugated to folic acid could be delivered into living cells (Leamon and Low, 1991). Following this seminal observation, hundreds of publications have improved upon this approach, which is currently being examined in clinical trials. The efficacy of this technology lies on the overexpression of the folate receptor in tumors, while it is quasi-absent in normal tissues. Very importantly also, folic acid retains a high affinity to its receptor when it is conjugated via its γ -carboxyl (Vlahov and Leamon, 2012).

Early attempts were limited by the release properties of the conjugates. After two decades of intensive research, some guiding rules were identified to lead compounds toward clinics:

1. anticancer agents must display a high cytotoxicity (similar to immunoconjugates);

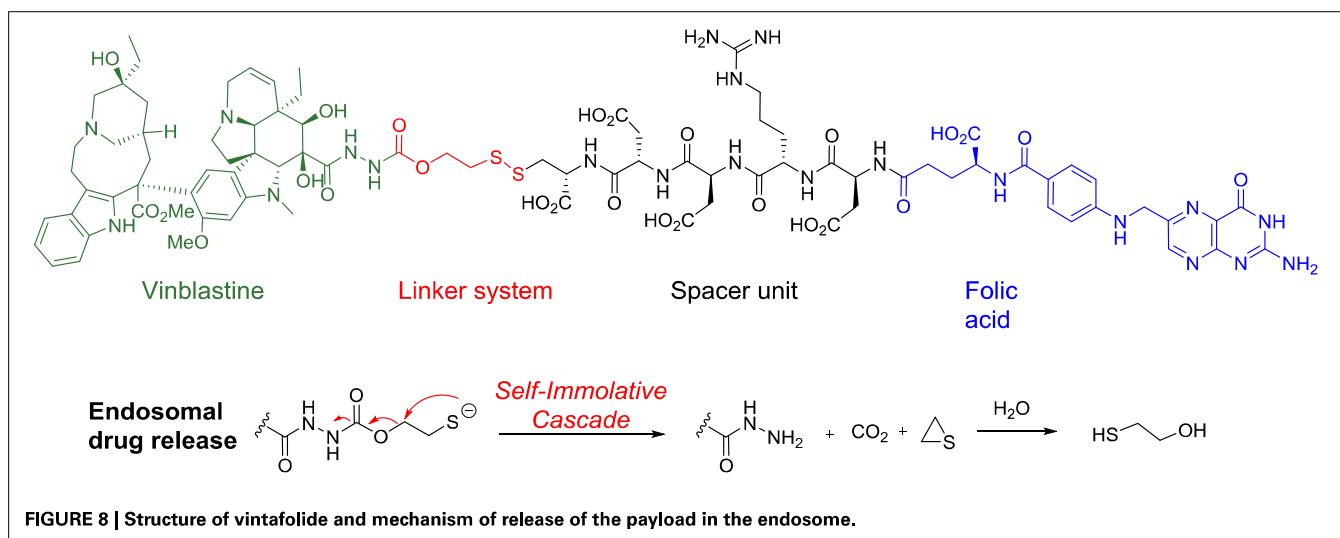


2. enhanced hydrophilicity, to prevent passive diffusion into normal tissue;
3. an efficient cleavable linker system that releases the anticancer drug at a reliable rate once inside the targeted cell;
4. a low molecular weight, to optimize the penetration into solid tumor tissue with concomitant rapid systemic clearance.

Following these guidelines, five folic acid conjugates have reached clinical trials, including the most advanced one, vintafolide

(EC145), which is currently in a phase 3 trial in women with cisplatin-resistant ovarian cancer.

In vintafolide, the highly cytotoxic vinblastine is connected to the folate moiety through a self-immolative linker and a peptidic spacer (**Figure 8**). To provide the desired hydrophilicity to the final drug-conjugate and prevent unspecific internalization, acidic, and basic amino acids such as aspartic acid and arginine were introduced in the peptide-based unit.



The self-destructive linker system is based on a 1,2-elimination mechanism by reduction of the disulfide bond between the cysteine of the spacer and the linker, which occurs in the endosome through a not fully understood mechanism (Figure 8) (Yang et al., 2006).

TRADITIONAL HERBAL REMEDIES

In addition to purified molecules, traditional herbal remedies are slowly emerging in modern Western medicine (Basu, 2004). An injectible form of an extract of the Chinese medicinal plant *Semen coicis* called Kanglaite® (Kang-Lai-Te) has been used in China as a lipid emulsion since the end of the 90's for the treatment of non-small cell lung, liver, stomach, and breast cancers. It has been marketed also in the Russian Federation since 2003 and is the first traditional Chinese herbal remedy to enter into clinical trials in the US. As with many other traditional Chinese medicines, Kanglaite activity probably results from the combined actions of multiple pharmacologically active ingredients that have not been yet identified (Xu, 2011). Over the last decade, other botanical drugs have entered clinical trials in the West to treat cancers or other ailments.

NANOPARTICLE DELIVERY OF ANTICANCER DRUGS

Tumor growth requires angiogenesis, i.e., the formation of new blood vessels. In contrast to normal angiogenesis, newly formed vessels in tumors display many structural and functional defects, which permit the leakage of macromolecules. This feature is referred to as the "enhanced permeability and retention (EPR) effect." Recent advances in the application of nanotechnology to medicine enabled the approval of five nanoparticle chemotherapeutics for cancer (Wang et al., 2012). Four liposomal formulations have been approved for clinical use in oncology: pegylated liposomal doxorubicin (DOXIL®, Caelyx®), nonpegylated liposomal doxorubicin (Myocet®), and liposomal cytarabine (DepoCyt®) (Hofheinz et al., 2005). Nab-paclitaxel (Abraxane®) is an albumin bound approved for the treatment of breast cancer and is undergoing clinical trials for other clinical indications. And finally, Genexol-PM is a polymeric micelle formulation of

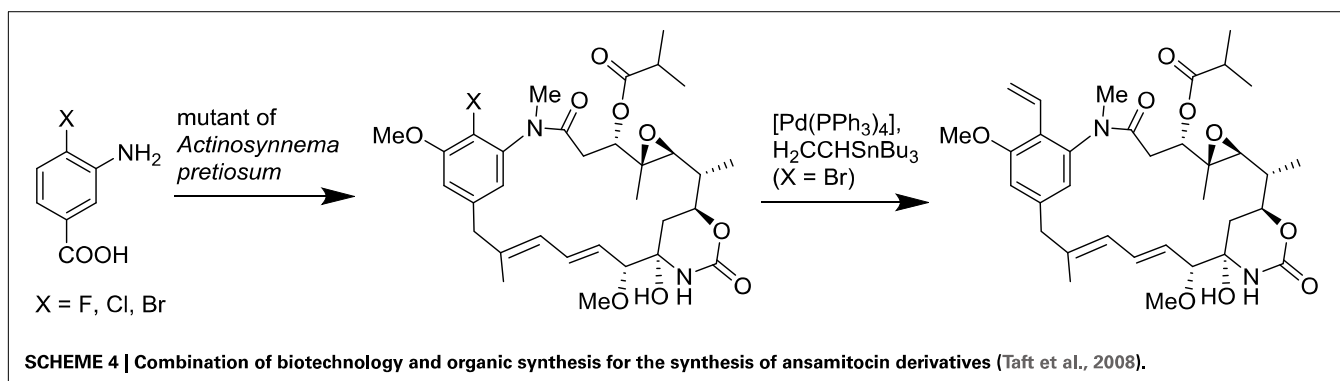
paclitaxel composed of block copolymers of PEG and poly-(D,L-lactic acid) (Kim et al., 2004).

Although nanomedicine is a new discipline, its translation into clinics has been rapid. A novel generation of nanoparticle chemotherapeutics is under development and expected to greatly improve cancer treatments. These new formulations may also offer novel opportunities for established anticancer drugs (Wang et al., 2012).

MISSED OPPORTUNITIES AND HOW TO RESCUE THEM

In 2010, Bristol-Myers Squibb stopped the phase III clinical trial of Tanespimycin, an inhibitor of heat shock protein 90, for the treatment of multiple myeloma, probably because of the expiration of the patent in 2014. In addition to drug developments that were terminated because of the shortness of patent life, there are many interesting drugs that did not reach clinical trial or that failed in clinical trial because the conceptual tools to correctly perform these assays were not available at that time. Indeed, "there are no bad anticancer agents, only bad clinical trial designs" as stated by Von Hoff (1998).

Flavaglines, such as rocaglamide, represent a striking example of natural products that are enjoying reinvigorated investigation after their original discovery by King et al. from the National Defense Medical Center of Taiwan (King et al., 1985). The recent identification of their molecular targets, the scaffold proteins prohibitins and the initiation factor of translation eIF4A, coupled with a description in *Science* about the origin of their selective cytotoxicity in cancer cells should promote further investigations to unveil their therapeutic usefulness (Basmadjian et al., 2013; Santagata et al., 2013). However, clinical trials with these compounds are unlikely unless some structurally original and patentable analogs are identified. Indeed, clinical trials of non-patentable compounds are still scarce (Roin, 2009; Cvek, 2012). For instance, a non-profit company, the Institute for OneWorld Health, developed in 2007 paromomycin, which is not patentable, as an effective treatment for visceral leishmaniasis. This was accomplished with financial support from the Bill and Melinda Gates Foundation, the Special Program for Research and Training



in Tropical Diseases of the United Nations Development Program, the World Bank, and the World Health Organization (Sundar et al., 2007). GlobalCures is another example of a non-profit medical research organization, which aims to develop novel and cost-effective treatments for cancers (Cvek, 2012). State agencies, such as the National Center for Advancing Translational Sciences are also deeply involved in the development of non-profitable drugs. Only a radical change in public or international policy could support the further development of clinically useful compounds that are currently fated to be traded as generics.

BIOTECHNOLOGY-BASED GENERATION OF NOVEL NATURAL PRODUCTS

Since the seminal synthesis of aspirin by Gerhardt (1853), all the natural product derivatives were prepared by total synthesis or semi-synthesis. Alternate approaches are currently emerging based on the progress in the deciphering of biosynthetic pathways and advances in biotechnologies. Currently, only a tiny fraction of microbes can be cultured with conventional approaches, yet uncultivated microorganisms represent an attractive source of novel natural products. It is now possible to isolate large fragments of microbial DNA directly from environmental samples and to express them in an easily cultured microorganism. This approach provides access to secondary metabolites that were originally produced by inaccessible microorganisms. Additionally, the manipulation of these biosynthetic pathways can lead to novel natural product derivatives. Metabolic engineering and synthetic biology are poised to revolutionize conventional chemical and pharmaceutical manufacturing in the coming decade (Yadav et al., 2012). Recently, methods and concepts of organic synthesis have begun to be integrated to synthetic biology to generate novel natural product derivatives. Such approaches that merge biotechnology with organic synthesis are rapidly blooming and are expected to efficiently generate novel natural product analogs in the near future (Goss et al., 2012; Kirschning and Hahn, 2012). A representative example of such an approach has been the use of an *Actinosynnema pretiosum* mutant that accepts 3-amino-4-bromobenzoic acid as a substrate to prepare pharmacologically active ansamitocin derivatives, which can then be transformed by classical organic reactions (Scheme 4; Taft et al., 2008).

CONCLUSION

The success of gleevec and herceptin in the 90's announced the obsolescence of natural products in therapeutics. A decade

later, many cancer patients continue to die and pharmaceutical companies have reconsidered their position on the potential of natural products in oncology. Indeed, for too many solid tumors of advanced grades, the only therapeutic options remain exclusively palliative. There is therefore an urgent need to develop original medicines.

Some of newly developed agents induce a strong cytotoxicity targeting conventional targets, DNA (for trabectedin) or microtubules (for ixabepilone, vinflunine, or eribulin), while other target specific biochemical events such as steroid biosynthesis (abiraterone acetate), histone remodeling (for romidepsin), protein translation (homoharringtonine), or degradation (carfilzomib). The case of rapamycin derivatives is atypical. These drugs are not cytotoxic, but can be considered as targeted therapy agents due to their inhibition of mTOR signaling.

In contrast with targeted therapeutics, which are designed for a specific type of cancer, the development of natural products is often more erratic and heavily relies on the skill of pharmacologists to unravel their mechanism of action and clinicians to identify the optimal indication in the clinic.

Over the last 15 years, natural products have been rehabilitated by pharmaceutical companies, even though some complementary approaches, such as molecular modeling based drug design are gaining in momentum. This latter methodology, which was pioneered by 2013 Nobel laureates, has successfully led to innovative medicines. When it is possible to predict the 3D structure of proteins, then it will probably overshadow other methods for identifying drug candidates. Until then, natural products should continue to play a major role in drug discovery, especially in the treatment of cancers and infectious diseases.

ACKNOWLEDGMENTS

We are grateful to the "Association pour la Recherche sur le Cancer" (ARC, grant numbers 3940 and SFI20111204054) for generous financial support. We also thank AAREC Filia Research for fellowships to Christine Basmadjian and Qian Zhao.

REFERENCES

- Aicher, T. D., Buszek, K. R., Fang, F. G., Forsyth, C. J., Jung, S. H., Kishi, Y., et al. (1992). Total synthesis of halichondrin B and norhalichondrin B. *J. Am. Chem. Soc.* 114, 3162–3164. doi: 10.1021/ja00034a086
- Ares, J., Durán-Peña, M. J., Hernández-Galán, R., and Collado, I. (2013). Chemical genetics strategies for identification of molecular targets. *Phytochem. Rev.* 12, 895–914. doi: 10.1007/s11101-013-9312-6

- Bailly, C. (2009). Ready for a comeback of natural products in oncology. *Biochem. Pharmacol.* 77, 1447–1457. doi: 10.1016/j.bcp.2008.12.013
- Balog, A., Meng, D., Kamenecka, T., Bertinato, P., Su, D.-S., Sorensen, E. J., et al. (1996). Totalsynthese von (-)-Epothilon A. *Angew. Chem.* 108, 2976–2978. doi: 10.1002/ange.19961082318
- Basmadjian, C., Thuaud, F., Ribeiro, N., and Désaubry, L. (2013). Flavaglines: potent anticancer drugs that target prohibitins and the helicase eIF4A. *Future Med. Chem.* 5, 2185–2197. doi: 10.4155/fmc.13.177
- Basu, P. (2004). Trading on traditional medicines. *Nat. Biotechnol.* 22, 263–265. doi: 10.1038/nbt0304-263
- Benhadji, K. A., Serova, M., Ghoul, A., Cvitkovic, E., Le Tourneau, C., Ogbourne, S. M., et al. (2008). Antiproliferative activity of PEP005, a novel ingenol angelate that modulates PKC functions, alone and in combination with cytotoxic agents in human colon cancer cells. *Br. J. Cancer* 99, 1808–1815. doi: 10.1038/sj.bjc.6604642
- Bennouna, J., Campone, M., Delord, J. P., and Pinel, M.-C. (2005). Vinflunine: a novel antitubulin agent in solid malignancies. *Expert Opin. Investig. Drugs* 14, 1259–1267. doi: 10.1517/13543784.14.10.1259
- Bennouna, J., Fumoleau, P., Armand, J.-P., Raymond, E., Campone, M., Delgado, F.-M., et al. (2003). Phase I and pharmacokinetic study of the new vinca alkaloid vinflunine administered as a 10-min infusion every 3 weeks in patients with advanced solid tumours. *Ann. Oncol.* 14, 630–637. doi: 10.1093/annonc/mdg174
- Bode, J. W., and Carreira, E. M. (2001). Stereoselective syntheses of epothilones A and B via directed nitrile oxide cycloaddition. *J. Am. Chem. Soc.* 123, 3611–3612. doi: 10.1021/ja0155635
- Bollag, D. M., McQueney, P. A., Zhu, J., Hensens, O., Koupal, L., Liesch, J., et al. (1995). Epothilones, a new class of microtubule-stabilizing agents with a taxol-like mechanism of action. *Cancer Res.* 55, 2325–2333.
- Bonfanti, M., La Valle, E., Fernandez Sousa Faro, J. M., Faircloth, G., Caretti, G., Mantovani, R., et al. (1999). Effect of ecteinascidin-743 on the interaction between DNA binding proteins and DNA. *Anticancer Drug Des.* 14, 179–186.
- Brown, E. J., Albers, M. W., Tae Bum, S., Ichikawa, K., Keith, C. T., Lane, W. S., et al. (1994). A mammalian protein targeted by G1-arresting rapamycin-receptor complex. *Nature* 369, 756–758. doi: 10.1038/369756a0
- Calne, R. Y. (2003). The development of immunosuppression: the rapamycin milestone. *Transplant. Proc.* 35, S15–S17. doi: 10.1016/S0041-1345(03)00209-4
- Calne, R. Y., Lim, S., Samaan, A., Collier, D. S. J., Pollard, S. G., White, D. J. G., et al. (1989). Rapamycin for immunosuppression in organ allografting. *The Lancet* 334, 227. doi: 10.1016/S0140-6736(89)90417-0
- Chen, J., Chen, X., Bois-Choussy, M. L., and Zhu, J. (2006). Total synthesis of ecteinascidin 743. *J. Am. Chem. Soc.* 128, 87–89. doi: 10.1021/ja0571794
- Cordell, G. A., and Colvard, M. D. (2012). Natural products and traditional medicine: turning on a paradigm. *J. Nat. Prod.* 75, 514–525. doi: 10.1021/np200803m
- Corey, E. J., Gin, D. Y., and Kania, R. S. (1996). Enantioselective total synthesis of ecteinascidin 743. *J. Am. Chem. Soc.* 118, 9202–9203. doi: 10.1021/ja962480t
- Cuevas, C., and Francesch, A. (2009). Development of Yondelis[registered sign] (trabectedin, ET-743). A semisynthetic process solves the supply problem. *Nat. Prod. Rep.* 26, 322–337. doi: 10.1039/b808331m
- Cuevas, C., Pérez, M., Martín, M. J., Chicharro, J. L., Fernandez-Rivas, C., Flores, M., et al. (2000). Synthesis of ecteinascidin ET-743 and phthalascidin Pt-650 from cyanosafrafrin B. *Org. Lett.* 2, 2545–2548. doi: 10.1021/ol0062502
- Cvek, B. (2012). Nonprofit drugs as the salvation of the world's healthcare systems: the case of antabuse (disulfiram). *Drug Discov. Today* 17, 409–412. doi: 10.1016/j.drudis.2011.12.010
- D'Incalci, M., and Jimeno, J. (2003). Preclinical and clinical results with the natural marine product ET-743. *Expert Opin. Investig. Drugs* 12, 1843–1853. doi: 10.1517/13543784.12.11.1843
- D'Incalci, M., and Galmarini, C. M. (2010). A review of trabectedin (ET-743): a unique mechanism of action. *Mol. Cancer Ther.* 9, 2157–2163. doi: 10.1158/1535-7163.mct-10-0263
- Dančik, V., Seiler, K. P., Young, D. W., Schreiber, S. L., and Clemons, P. A. (2010). Distinct biological network properties between the targets of natural products and disease genes. *J. Am. Chem. Soc.* 132, 9259–9261. doi: 10.1021/ja102798t
- Ducry, L. (2012). Challenges in the development and manufacturing of antibody-drug conjugates. *Methods Mol. Biol.* 899, 489–497. doi: 10.1007/978-1-61779-921-1_29
- Ehrlich, P. (1897). Zur kenntnis der antitoxinwirkung. *Fortschr. Med.* 15, 41–43.
- Endo, A., Yanagisawa, A., Abe, M., Tohma, S., Kan, T., and Fukuyama, T. (2002). Total synthesis of ecteinascidin 743. *J. Am. Chem. Soc.* 124, 6552–6554. doi: 10.1021/ja026216d
- Estève, M.-A., Carré, M., Bourgarel-Rey, V., Kruczyński, A., Raspaglio, G., Ferlini, C., et al. (2006). Bcl-2 down-regulation and tubulin subtype composition are involved in resistance of ovarian cancer cells to vinflunine. *Mol. Cancer Ther.* 5, 2824–2833. doi: 10.1158/1535-7163.mct-06-0277
- Etiévant, C., Barret, J.-M., Kruczyński, A., Perrin, D., and Hill, B. (1998). Vinflunine (20',20'-difluoro-3',4'-dihydrovinorelbine), a novel Vinca alkaloid, which participates in P-glycoprotein (Pgp)-mediated multidrug resistance *in vivo* and *in vitro*. *Invest. New Drugs* 16, 3–17. doi: 10.1023/A:1006022811895
- Etiévant, C., Kruczyński, A., Barret, J.-M., Tait, A., Kavallaris, M., and Hill, B. (2001). Markedly diminished drug resistance-inducing properties of vinflunine (20',20'-difluoro-3',4'-dihydrovinorelbine) relative to vinorelbine, identified in murine and human tumour cells *in vivo* and *in vitro*. *Cancer Chemother. Pharmacol.* 48, 62–70. doi: 10.1007/s002800100275
- Evans, B. E., Rittle, K. E., Bock, M. G., Dipardo, R. M., Freidinger, R. M., Whitter, W. L., et al. (1988). Methods for drug discovery: development of potent, selective, orally effective cholecystokinin antagonists. *J. Med. Chem.* 31, 2235–2246. doi: 10.1021/jm00120a002
- Fahy, J., Duflos, A., Ribet, J.-P., Jacquesy, J.-C., Berrier, C., Jouannetaud, M.-P., et al. (1997). Vinca alkaloids in superacidic media: a method for creating a new family of antitumor derivatives. *J. Am. Chem. Soc.* 119, 8576–8577. doi: 10.1021/ja971864w
- Faivre, S., and Raymond, E. (2008). Mechanism of action of rapalogues: the antiangiogenic hypothesis. *Expert Opin. Investig. Drugs* 17, 1619–1621. doi: 10.1517/13543784.17.11.1619
- Ferlini, C., Cicchillitti, L., Raspaglio, G., Bartollino, S., Cimitan, S., Bertucci, C., et al. (2009). Paclitaxel directly binds to Bcl-2 and functionally mimics activity of Nur77. *Cancer Res.* 69, 6906–6914. doi: 10.1158/0008-5472
- Findlay, J. A., and Radics, L. (1980). On the chemistry and high field nuclear magnetic resonance spectroscopy of rapamycin. *Can. J. Chem.* 58, 579–590. doi: 10.1139/v80-090
- Fishlock, D., and Williams, R. M. (2008). Synthetic studies on Et-743. Assembly of the pentacyclic core and a formal total synthesis. *J. Org. Chem.* 73, 9594–9600. doi: 10.1021/jo801159k
- Fresno, M., Jiménez, A., and Vázquez, D. (1977). Inhibition of translation in eukaryotic systems by harringtonine. *Eur. J. Biochem.* 72, 323–330. doi: 10.1111/j.1432-1033.1977.tb11256.x
- Furumai, R., Matsuyama, A., Kobashi, N., Lee, K. H., Nishiyama, M., Nakajima, H., et al. (2002). FK228 (depsipeptide) as a natural prodrug that inhibits class I histone deacetylases. *Cancer Res.* 62, 4916–4921
- Galsky, M. D., Dritselis, A., Kirkpatrick, P., and Oh, W. K. (2010). Cabazitaxel. *Nat. Rev. Drug Discov.* 9, 677–678. doi: 10.1038/nrd3254
- Ganesan, A. (2008). The impact of natural products upon modern drug discovery. *Curr. Opin. Chem. Biol.* 12, 306–317. doi: 10.1016/j.cbpa.2008.03.016
- Gerhardt, C. (1853). Untersuchungen über die wasserfreien organischen Säuren. *Justus Liebigs Ann. Chem.* 87, 57–84. doi: 10.1002/jlac.18530870107
- Gerth, K., Bedorf, N., Hofle, G., Irshchik, H., and Reichenbach, H. (1996). Epothilons A and B: antifungal and cytotoxic compounds from *Sorangium cellulosum* (Myxobacteria). Production, physico-chemical and biological properties. *J. Antibiot. (Tokyo)* 49, 560–563. doi: 10.7164/antibiotics.49.560
- Ghose, T., Guclu, A., and Tai, J. (1975). Suppression of an AKR Lymphoma by antibody and chlorambucil. *J. Natl. Cancer Inst.* 55, 1353–1357. doi: 10.1093/jnci/55.6.1353
- Ghoul, A. D., Serova, M., Astorgues-Xerri, L., Bieche, I., Bousquet, G., Varna, M., et al. (2009). Epithelial-to-mesenchymal transition and resistance to ingenol 3-angelate, a novel protein kinase C modulator, in colon cancer cells. *Cancer Res.* 69, 4260–4269. doi: 10.1158/0008-5472.can-08-2837
- Goss, R. J. M., Shankar, S., and Fayad, A. A. (2012). The generation of “unNatural” products: synthetic biology meets synthetic chemistry. *Nat. Prod. Rep.* 29, 870–889. doi: 10.1039/C2NP00001F
- Grabowski, K., Baringhaus, K.-H., and Schneider, G. (2008). Scaffold diversity of natural products: inspiration for combinatorial library design. *Nat. Prod. Rep.* 25, 892–904. doi: 10.1039/B715668P
- Green, A. C., and Beardmore, G. L. (1988). Home treatment of skin cancer and solar keratoses. *Australas. J. Dermatol.* 29, 127–130. doi: 10.1111/j.1440-0960.1988.tb00383.x

- Groll, M., Kim, K. B., Kairies, N., Huber, R., and Crews, C. M. (2000). Crystal structure of the 20s proteasome: TMC-95A complex: a non-covalent proteasome inhibitor. *J. Am. Chem. Soc.* 122, 1237–1238. doi: 10.1021/ja993588m
- Group, C. R. C. (1976). Cephalotaxine esters in the treatment of acute leukemia. A preliminary clinical assessment. *Chin. Med. J. (Engl.)* 2, 263–272.
- Gunasekera, S. P., Gunasekera, M., Longley, R. E., and Schulte, G. K. (1990). Discodermolide: a new bioactive polyhydroxylated lactone from the marine sponge *Discodermia dissoluta*. *J. Org. Chem.* 55, 4912–4915. doi: 10.1021/jo00303a029
- Handratta, V. D., Vasaitis, T. S., Njar, V. C. O., Gediya, L. K., Kataria, R., Chopra, P., et al. (2005). Novel C-17-heteroaryl steroidal CYP17 inhibitors/antiandrogens: synthesis, *in vitro* biological activity, pharmacokinetics, and antitumor activity in the LAPC4 human prostate cancer xenograft model. *J. Med. Chem.* 48, 2972–2984. doi: 10.1021/jm040202w
- Hardy, K., Buckley, S., Collins, M. J., Estalrich, A., Brothwell, D., Copeland, L., et al. (2012). Neanderthal medics? Evidence for food, cooking, and medicinal plants entrapped in dental calculus. *Naturwissenschaften* 99, 617–626. doi: 10.1007/s00114-012-0942-0
- Henkel, T., Brunne, R. M., Müller, H., and Reichel, F. (1999). Statistical investigation into the structural complementarity of natural products and synthetic compounds. *Angew. Chem. Int. Ed. Engl.* 38, 643–647. doi: 10.1002/(SICI)1521-3773(19990301)38:5<643::AID-ANIE643>3.0.CO;2-G
- Hietman, J., Movva, N. R., and Hall, M. N. (1991). Targets for cell cycle arrest by the immunosuppressant rapamycin in yeast. *Science* 253, 905–909. doi: 10.1126/science.1715094
- Hirata, Y., and Uemura, D. (1986). Halichondrins - antitumor polyether macrolides from a marine sponge. *Pure Appl. Chem.* 58, 701–710. doi: 10.1351/pac198658050701
- Ho, R. J. Y., and Chien, J. (2014). Trends in translational medicine and drug targeting and delivery: new insights on an old concept—targeted drug delivery with antibody–drug conjugates for cancers. *J. Pharm. Sci.* 103, 71–77. doi: 10.1002/jps.23761
- Hofheinz, R. D., Gnad-Vogt, S. U., Beyer, U., and Hochhaus, A. (2005). Liposomal encapsulated anti-cancer drugs. *Anticancer Drugs* 16, 691–707. doi: 10.1097/01.cad.0000167902.53039.5a
- Höfle, G., Bedorf, N., Steinmetz, H., Schomburg, D., Gerth, K., and Reichenbach, H. (1996). Epothilone A and B - novel 16-membered macrolides with cytotoxic activity: isolation, crystal structure, and conformation in solution. *Angew. Chem. Int. Ed. Engl.* 35, 1567–1569. doi: 10.1002/anie.199615671
- Horwitz, S. B. (1994). Taxol (paclitaxel): mechanisms of action. *Ann. Oncol.* 5(Suppl. 6), S3–S6.
- Huang, M. T. (1975). Harringtonine, an inhibitor of initiation of protein biosynthesis. *Mol. Pharmacol.* 11, 511–519.
- Imai, T., Nakata, H., Yokoshima, S., and Fukuyama, T. (2012). Synthetic studies toward ecteinascidin 743 (Trabectedin). *Synthesis* 44, 2743–2753. doi: 10.1055/s-0032-1316579
- Jackson, K. L., Henderson, J. A., and Phillips, A. J. (2009). The halichondrins and E7389. *Chem. Rev.* 109, 3044–3079. doi: 10.1021/cr900016w
- Jarman, M., Barrie, S. E., and Llera, J. M. (1998). The 16,17-double bond is needed for irreversible inhibition of human cytochrome P45017 α by abiraterone (17-(3-Pyridyl)androsta-5,16-dien-3 β -ol) and related steroidal inhibitors. *J. Med. Chem.* 41, 5375–5381. doi: 10.1021/jm981017j
- Jin, S., Gorfajin, B., Faircloth, G., and Scotto, K. W. (2000). Ecteinascidin 743, a transcription-targeted chemotherapeutic that inhibits MDR1 activation. *Proc. Natl. Acad. Sci. U.S.A.* 97, 6775–6779. doi: 10.1073/pnas.97.12.6775
- Johnson, P., Geldart, T., Fumoleau, P., Pinel, M.-C., Nguyen, L., and Judson, I. (2006). Phase I study of Vinflunine administered as a 10-minute infusion on days 1 and 8 every 3 weeks. *Invest. New Drugs* 24, 223–231. doi: 10.1007/s10637-005-3902-0
- Jordan, M. A., and Wilson, L. (2004). Microtubules as a target for anticancer drugs. *Nat. Rev. Cancer* 4, 253–265. doi: 10.1038/nrc1317
- Jørgensen, L., McKerrall, S. J., Kuttruff, C. A., Ungeheuer, F., Felding, J., and Baran, P. S. (2013). 14-step synthesis of (+)-ingenol from (+)-3-carene. *Science* 341, 878–882. doi: 10.1126/science.1241606
- Kahan, B. D., Chang, J. Y., and Sehgal, S. N. (1991). Preclinical evaluation of a new potent immunosuppressive agent, rapamycin. *Transplantation* 52, 185–191. doi: 10.1097/00007890-199108000-00001
- Kantarjian, H. M., O'Brien, S., and Cortes, J. (2013). Homoharringtonine/Omacetaxine mepesuccinate: the long and winding road to food and drug administration approval. *Clin. Lymphoma Myeloma Leuk.* 13, 530–533. doi: 10.1016/j.cml.2013.03.017
- Kawagishi, F., Toma, T., Inui, T., Yokoshima, S., and Fukuyama, T. (2013). Total synthesis of ecteinascidin 743. *J. Am. Chem. Soc.* 135, 13684–13687. doi: 10.1021/ja408034x
- Kim, T. Y., Kim, D. W., Chung, J. Y., Shin, S. G., Kim, S. C., Heo, D. S., et al. (2004). Phase I and pharmacokinetic study of Genexol-PM, a Cremophor-free, polymeric micelle-formulated paclitaxel, in patients with advanced malignancies. *Clin. Cancer Res.* 10, 3708–3716. doi: 10.1158/1078-0432.CCR-03-0655
- King, M. L., Chiang, C. C., Ling, H. C., Ochiai, M., Fujita, E., and Mcphail, A. T. (1985). X-Ray crystal structure of rocgamide, a novel antileukemic 1H-cyclopenta[b]benzofuran from *Aglaia elliptifolia*. *J. Chem. Soc. Chem. Commun.* 1982, 1150–1151. doi: 10.1039/C39820001150
- Kino, T., Hatanaka, H., Hashimoto, M., Nishiyama, M., Goto, T., Okuhara, M., et al. (1987a). FK-506, a novel immunosuppressant isolated from a Streptomyces. I. Fermentation, isolation, and physico-chemical and biological characteristics. *J. Antibiot. (Tokyo)* 40, 1249–1255.
- Kino, T., Hatanaka, H., Miyata, S., Inamura, N., Nishiyama, M., Yajima, T., et al. (1987b). FK-506, a novel immunosuppressant isolated from a Streptomyces. II. Immunosuppressive effect of FK-506 *in vitro*. *J. Antibiot. (Tokyo)* 40, 1256–1265.
- Kirikae, T., Ojima, I., Kirikae, F., Ma, Z., Kuduk, S. D., Slater, J. C., et al. (1996). Structural requirements of taxoids for nitric oxide and tumor necrosis factor production by murine macrophages. *Biochem. Biophys. Res. Commun.* 227, 227–235. doi: 10.1006/bbrc.1996.1494
- Kirschning, A., and Hahn, F. (2012). Merging chemical synthesis and biosynthesis: a new chapter in the total synthesis of natural products and natural product libraries. *Angew. Chem. Int. Ed. Engl.* 51, 4012–4022. doi: 10.1002/anie.201107386
- Kohler, G., and Milstein, C. (1975). Continuous cultures of fused cells secreting antibody of predefined specificity. *Nature* 256, 495–497. doi: 10.1038/256495a0
- Krysiak, J., and Breinbauer, R. (2012). Activity-based protein profiling for natural product target discovery. *Top. Curr. Chem.* 324, 43–84. doi: 10.1007/128_2011_289
- Leamon, C. P., and Low, P. S. (1991). Delivery of macromolecules into living cells: a method that exploits folate receptor endocytosis. *Proc. Natl. Acad. Sci. U.S.A.* 88, 5572–5576. doi: 10.1073/pnas.88.13.5572
- Lee, F. F., Borzilleri, R., Fairchild, C., Kamath, A., Smykla, R., Kramer, R., et al. (2008). Preclinical discovery of ixabepilone, a highly active antineoplastic agent. *Cancer Chemother. Pharmacol.* 63, 157–166. doi: 10.1007/s00280-008-0724-8
- Lee, F. Y. F., Vite, G., Borzilleri, R. M., Arico, M. A., Clark, J. L., Fager, K. L., et al. (2000). Preclinical pharmacology of the epothilone B analog BMS-247550—an epothilone analog possessing potent activity against paclitaxel sensitive and resistant human tumors. *Clin. Cancer Res.* 6:4580s.
- Lee, M.-L., and Schneider, G. (2001). Scaffold architecture and pharmacophoric properties of natural products and trade drugs: application in the design of natural product-based combinatorial libraries. *J. Comb. Chem.* 3, 284–289. doi: 10.1021/cc000097l
- Lindel, T., Jensen, P. R., Fenical, W., Long, B. H., Casazza, A. M., Carboni, J., et al. (1997). Eleutherobin, a new cytotoxin that mimics paclitaxel (Taxol) by stabilizing microtubules. *J. Am. Chem. Soc.* 119, 8744–8745. doi: 10.1021/ja9717828
- Loc, T. B., Mathé, G., and Bernard, J. (1958). Effet sur la leucémie 1210 de la souris d'une combinaison par diazotation d'A-méthoptérine et de γ -globulins de hamsters porteurs de cette leucémie par hétérogreffe. *C. R. Acad. Sci. Paris* 246, 1626–1628.
- Martinez, E. J., Owa, T., Schreiber, S. L., and Corey, E. J. (1999). Phthalascidin, a synthetic antitumor agent with potency and mode of action comparable to ecteinascidin 743. *Proc. Natl. Acad. Sci. U.S.A.* 96, 3496–3501. doi: 10.1073/pnas.96.7.3496
- McAlpine, J. B., Swanson, S. J., Jackson, M., and Whittern, D. N. (1991). Revised NMR assignments for rapamycin. *J. Antibiot. (Tokyo)* 44, 688–690. doi: 10.1164/antibiotics.44.688
- Menchaca, R., Martinez, V., Rodriguez, A., Rodriguez, N., Flores, M., Gallego, P., et al. (2003). Synthesis of natural ecteinascidins (ET-729, ET-745, ET-759B, ET-736, ET-637, ET-594) from cyanosafrafin B. *J. Org. Chem.* 68, 8859–8866. doi: 10.1021/jo034547i
- Minuzzo, M., Marchini, S., Brogini, M., Faircloth, G., D'Incalci, M., and Mantovani, R. (2000). Interference of transcriptional activation by the

- antineoplastic drug ecteinascidin-743. *Proc. Natl. Acad. Sci. U.S.A.* 97, 6780–6784. doi: 10.1073/pnas.97.12.6780
- Mooberry, S. L., Tien, G., Hernandez, A. H., Plubrukarn, A., and Davidson, B. S. (1999). Laulimalide and isolaulimalide, new paclitaxel-like microtubule-stabilizing agents. *Cancer Res.* 59, 653–660.
- Mulzer, J., Mantoulidis, A., and Öhler, E. (2000). Total syntheses of epothilones B and D. *J. Org. Chem.* 65, 7456–7467. doi: 10.1021/jo0007480
- Nakajima, H., Kim, Y. B., Terano, H., Yoshida, M., and Horinouchi, S. (1998). FR901228, a potent antitumor antibiotic, is a novel histone deacetylase inhibitor. *Exp. Cell Res.* 241, 126–133. doi: 10.1006/excr.1998.4027
- Nicolaou, K. C., Ninkovic, S., Sarabia, F., Vourloumis, D., He, Y., Vallberg, H., et al. (1997). Total syntheses of epothilones A and B via a macrolactonization-based strategy. *J. Am. Chem. Soc.* 119, 7974–7991. doi: 10.1021/ja971110h
- Nishizuka, Y. (1984). The role of protein kinase C in cell surface signal transduction and tumour promotion. *Nature* 308, 693–698. doi: 10.1038/308693a0
- Noble, R. L., Beer, C. T., and Cutts, J. H. (1959). Further biological activities of vincalcaleukoblastine - an alkaloid isolated from *Vinca rosea* (L.). *Biochem. Pharmacol.* 1, 347–348. doi: 10.1016/0006-2952(59)90123-6
- Ojima, I., Chakravarty, S., Inoue, T., Lin, S., He, L., Horwitz, S. B., et al. (1999). A common pharmacophore for cytotoxic natural products that stabilize microtubules. *Proc. Natl. Acad. Sci. U.S.A.* 96, 4256–4261. doi: 10.1073/pnas.96.8.4256
- Ortholand, J.-Y., and Ganesan, A. (2004). Natural products and combinatorial chemistry: back to the future. *Curr. Opin. Chem. Biol.* 8, 271–280. doi: 10.1016/j.cbpa.2004.04.011
- Paudler, W. W., Kerley, G. I., and McKay, J. (1963). The alkaloids of *Cephalotaxus drupacea* and *Cephalotaxus fortunei*. *J. Org. Chem.* 28, 2194–2197. doi: 10.1021/jo01044a010
- Pommier, Y., Kohlhagen, G., Bailly, C., Waring, M., Mazumder, A., and Kohn, K. W. (1996). DNA sequence- and structure-selective alkylation of guanine N2 in the DNA minor groove by ecteinascidin 743, a potent antitumor compound from the caribbean tunicate *Ecteinascidia turbinata*. *Biochemistry* 35, 13303–13309. doi: 10.1021/bi960306b
- Potter, G. A., Barrie, S. E., Jarman, M., and Rowlands, M. G. (1995). Novel steroidal inhibitors of human cytochrome P45017.alpha.-hydroxylase-C17.20-lyase): potential agents for the treatment of prostatic cancer. *J. Med. Chem.* 38, 2463–2471. doi: 10.1021/jm00013a022
- Powell, R. G., Weisleder, D., and Smith, C. R. (1972). Antitumor alkaloids from *Cephalotaxus harringtonia*: structure and activity. *J. Pharm. Sci.* 61, 1227–1230. doi: 10.1002/jps.2600610812
- Powell, R. G., Weisleder, D., Smith, C. R. Jr., and Rohwedder, W. K. (1970). Structures of harringtonine, isoharringtonine, and homoharringtonine. *Tetrahedron Lett.* 11, 815–818. doi: 10.1016/S0040-4039(01)97839-6
- Pucheault, M. (2008). Natural products: chemical instruments to apprehend biological symphony. *Org. Biomol. Chem.* 6, 424–432. doi: 10.1039/b713022h
- Qi, Y., and Ma, S. (2011). The medicinal potential of promising marine macrolides with anticancer activity. *ChemMedChem* 6, 399–409. doi: 10.1002/cmdc.201000534
- Rehman, Y., and Rosenberg, J. E. (2012). Abiraterone acetate: oral androgen biosynthesis inhibitor for treatment of castration-resistant prostate cancer. *Drug Des. Devel. Ther.* 6, 13–18. doi: 10.2147/DDDT.S15850
- Rinehart, K. L., Holt, T. G., Fregeau, N. L., Stroh, J. G., Keifer, P. A., Sun, F., et al. (1990). Ecteinascidins 729, 743, 745, 759A, 759B, and 770: potent antitumor agents from the Caribbean tunicate *Ecteinascidia turbinata*. *J. Org. Chem.* 55, 4512–4515. doi: 10.1021/jo00302a007
- Ritter, S. K. (2013). 2013's notable advances. *Chem. Eng. News* 91, 16–19.
- Robin, J.-P., Dhal, R., Dujardin, G., Girodier, L., Mevellec, L., and Poutot, S. (1999). The first semi-synthesis of enantiopure homoharringtonine via anhydrohomoharringtonine from a preformed chiral acyl moiety. *Tetrahedron Lett.* 40, 2931–2934. doi: 10.1016/S0040-4039(99)00327-5
- Roin, B. N. (2009). Unpatentable drugs and the standards of patentability. *Tex. Law Rev.* 87, 503–570.
- Santagata, S., Mendillo, M. L., Tang, Y.-C., Subramanian, A., Perley, C. C., Roche, S. P., et al. (2013). Tight coordination of protein translation and HSF1 activation supports the anabolic malignant state. *Science* 341, 1238303-1–1238303-10. doi: 10.1126/science.1238303
- Sayed, M. D., Risz, A., Hammouda, F. M., El-Missiry, M. M., Williamson, E. M., and Evans, F. J. (1980). Constituents of Egyptian Euphorbiaceae. IX. Irritant and cytotoxic ingenane esters from *Euphorbia paralias* L. *Experientia* 36, 1206–1207. doi: 10.1007/BF01976131
- Schinzer, D., Limberg, A., Bauer, A., Böhm, O. M., and Cordes, M. (1997). Total synthesis of (-)-epothilone A. *Angew. Chem. Int. Ed. Engl.* 36, 523–524. doi: 10.1002/anie.199705231
- Scott, A. M., Wolchok, J. D., and Old, L. J. (2012). Antibody therapy of cancer. *Nat. Rev. Cancer* 12, 278–287. doi: 10.1038/nrc3236
- Sehgal, S. N., Baker, H., and Vezina, C. (1975). Rapamycin (AY 22,989), a new antifungal antibiotic. II. Fermentation, isolation and characterization. *J. Antibiot. (Tokyo)* 28, 727–732.
- Serova, M., Ghoul, A. D., Benhadji, K. A., Faivre, S., Le Tourneau, C., Cvitkovic, E., et al. (2008). Effects of protein kinase C modulation by PEP005, a novel ingenol angelate, on mitogen-activated protein kinase and phosphatidylinositol 3-kinase signaling in cancer cells. *Mol. Cancer Ther.* 7, 915–922. doi: 10.1158/1535-7163.mct-07-2060
- Sigel, M. M., Wellham, L. L., Lichter, W., Dudeck, L. E., Gargus, J. L., and Lucas, A. H. (1970). "Anticellular and antitumor activity of extracts from tropical marine invertebrates," in *Food-Drugs from the Sea Proceedings 1969*, ed H. W. Youngken Jr. (Washington, DC: Marine Technology Society), 281–294.
- Siller, G., Gebauer, K., Welburn, P., Katsamas, J., and Ogbourne, S. M. (2009). PEP005 (ingenol mebutate) gel, a novel agent for the treatment of actinic keratosis: results of a randomized, double-blind, vehicle-controlled, multicentre, phase IIa study. *Australas. J. Dermatol.* 50, 16–22. doi: 10.1111/j.1440-0960.2008.00497.x
- Su, D.-S., Meng, D., Bertinato, P., Balog, A., Sorensen, E. J., Danishefsky, S. J., et al. (1997). Total synthesis of (-)-epothilone B: an extension of the suzuki coupling method and insights into structure-activity relationships of the epothilones. *Angew. Chem. Int. Ed. Engl.* 36, 757–759. doi: 10.1002/anie.199707571
- Sundar, S., Jha, T. K., Thakur, C. P., Sinha, P. K., and Bhattacharya, S. K. (2007). Injectable paromomycin for visceral leishmaniasis in India. *N. Engl. J. Med.* 356, 2571–2581. doi: 10.1056/NEJMoa066536
- Swindells, D. C. N., White, P. S., and Findlay, J. A. (1978). The X-ray crystal structure of rapamycin, C51H79NO13. *Can. J. Chem.* 56, 2491–2492. doi: 10.1139/v78-407
- Swinney, D. C., and Anthony, J. (2011). How were new medicines discovered? *Nat. Rev. Drug Discov.* 10, 507–519. doi: 10.1038/nrd3480
- Tamma, A., Misset, J. L., Riofrio, M., Guzman, C., Brain, E., Lopez Lazaro, L., et al. (2001). Phase I and pharmacokinetic study of ecteinascidin-743, a new marine compound, administered as a 24-hour continuous infusion in patients with solid tumors. *J. Clin. Oncol.* 19, 1256–1265.
- Taft, F., Brünjes, M., Floss, H. G., Czempinski, N., Grond, S., Sasse, F., et al. (2008). Highly active ansamitocin derivatives: mutasynthesis using an AHBA-blocked mutant. *Chembiochem* 9, 1057–1060. doi: 10.1002/cbic.200700742
- Takebayashi, Y., Pourquier, P., Yoshida, A., Kohlhagen, G., and Pommier, Y. (1999). Poisoning of human DNA topoisomerase I by ecteinascidin 743, an anticancer drug that selectively alkylates DNA in the minor groove. *Proc. Natl. Acad. Sci. U.S.A.* 96, 7196–7201. doi: 10.1073/pnas.96.13.7196
- Takebayashi, Y., Pourquier, P., Zimonjic, D. B., Nakayama, K., Emmert, S., Ueda, T., et al. (2001). Antiproliferative activity of ecteinascidin 743 is dependent upon transcription-coupled nucleotide-excision repair. *Nat. Med.* 7, 961–966. doi: 10.1038/91008
- Tang, R., Faussat, A.-M., Majdak, P., Marzac, C., Dubrulle, S., Marjanovic, Z., et al. (2006). Semisynthetic homoharringtonine induces apoptosis via inhibition of protein synthesis and triggers rapid myeloid cell leukemia-1 down-regulation in myeloid leukemia cells. *Mol. Cancer Ther.* 5, 723–731. doi: 10.1158/1535-7163.mct-05-0164
- Thaler, F., and Mercurio, C. (2014). Towards selective inhibition of histone deacetylase isoforms: what has been achieved, where we are and what will be next. *ChemMedChem* 9, 523–536. doi: 10.1002/cmdc.201300413
- Thuau, F., Ribeiro, N., Nebigil, C. G., and Désaubry, L. (2013). Prohibitin ligands in cell death and survival: mode of action and therapeutic potential. *Chem. Biol.* 20, 316–331. doi: 10.1016/j.chembiol.2013.02.006
- Ueda, H., Nakajima, H., Hori, Y., Goto, T., and Okuhara, M. (1994). Action of FR901228, a novel antitumor bicyclic depsipeptide produced by *Chromobacterium violaceum* no. 968, on Ha-ras transformed NIH3T3 cells. *Biosci. Biotechnol. Biochem.* 58, 1579–1583.
- Uemura, D., Takahashi, K., Yamamoto, T., Katayama, C., Tanaka, J., Okumura, Y., et al. (1985). Norhalichondrin A: an antitumor polyether macrolide from a marine sponge. *J. Am. Chem. Soc.* 107, 4796–4798. doi: 10.1021/ja00302a042

- Vandermolén, K. M., McCulloch, W., Pearce, C. J., and Oberlies, N. H. (2011). Romidepsin (Istodax, NSC 630176, FR901228, FK228, depsipeptide): a natural product recently approved for cutaneous T-cell lymphoma. *J. Antibiot. (Tokyo)* 64, 525–531. doi: 10.1038/ja.2011.35
- Vasaitis, T. S., and Njar, V. C. O. (2010). Novel, potent anti-androgens of therapeutic potential: recent advances and promising developments. *Future Med. Chem.* 2, 667–680. doi: 10.4155/fmc.10.14
- Vezina, C., Kudelski, A., and Sehgal, S. N. (1975). Rapamycin (AY 22,989), a new antifungal antibiotic. I. Taxonomy of the producing streptomycete and isolation of the active principle. *J. Antibiot. (Tokyo)* 28, 721–726.
- Villalona-Calero, M. A., Eckhardt, S. G., Weiss, G., Hidalgo, M., Beijnen, J. H., Van Kesteren, C., et al. (2002). A phase I and pharmacokinetic study of ecteinascidin-743 on a daily x 5 schedule in patients with solid malignancies. *Clin. Cancer Res.* 8, 75–85.
- Vlahov, I. R., and Leamon, C. P. (2012). Engineering folate-drug conjugates to target cancer: from chemistry to clinic. *Bioconjug. Chem.* 23, 1357–1369. doi: 10.1021/bc2005522
- Von Hoff, D. D. (1998). There are no bad anticancer agents, only bad clinical trial designs—twenty-first Richard and Hinda Rosenthal Foundation Award Lecture. *Clin. Cancer Res.* 4, 1079–1086.
- Vrignaud, P., Sémiond, D., Lejeune, P., Bouchard, H., Calvet, L., Combeau, C., et al. (2013). Preclinical antitumor activity of cabazitaxel, a semisynthetic taxane active in taxane-resistant tumors. *Clin. Cancer Res.* 19, 2973–2983. doi: 10.1158/1078-0432.ccr-12-3146
- Wang, A. Z., Langer, R., and Farokhzad, O. C. (2012). Nanoparticle delivery of cancer drugs. *Annu. Rev. Med.* 63, 185–198. doi: 10.1146/annurev-med-040210-162544
- Watson, C. J. E., Friend, P. J., Jamieson, N. V., Frick, T. W., Alexander, G., Gimson, A. E., et al. (1999). Sirolimus: a potent new immunosuppressant for liver transplantation. *Transplantation* 67, 505–509. doi: 10.1097/00007890-199902270-00002
- Weedon, D., and Chick, J. (1976). Home treatment of basal cell carcinoma. *Med. J. Aust.* 1, 928.
- Xu, Z. (2011). Modernization: one step at a time. *Nature* 480, S90–S92. doi: 10.1038/480S90a
- Yadav, V. G., De Mey, M., Giaw Lim, C., Kumaran Ajikumar, P., and Stephanopoulos, G. (2012). The future of metabolic engineering and synthetic biology: towards a systematic practice. *Metab. Eng.* 14, 233–241. doi: 10.1016/j.ymben.2012.02.001
- Yang, J., Chen, H., Vlahov, I. R., Cheng, J.-X., and Low, P. S. (2006). Evaluation of disulfide reduction during receptor-mediated endocytosis by using FRET imaging. *Proc. Natl. Acad. Sci. U.S.A.* 103, 13872–13877. doi: 10.1073/pnas.0601455103
- Yang, Z., He, Y., Vourloumis, D., Vallberg, H., and Nicolaou, K. C. (1997). Total synthesis of epothilone A: the olefin metathesis approach. *Angew. Chem. Int. Ed. Engl.* 36, 166–168. doi: 10.1002/anie.199701661
- Zard, S. Z. (2012). Some aspects of the chemistry of nitro compounds. *Helv. Chim. Acta* 95, 1730–1757. doi: 10.1002/hlca.201200324
- Zewail-Foote, M., and Hurley, L. H. (1999). Ecteinascidin 743: a minor groove alkylator that bends DNA toward the major groove. *J. Med. Chem.* 42, 2493–2497. doi: 10.1021/jm990241l
- Zewail-Foote, M., Li, V.-S., Kohn, H., Bearss, D., Guzman, M., and Hurley, L. H. (2001). The inefficiency of incisions of ecteinascidin 743–DNA adducts by the UvrABC nuclease and the unique structural feature of the DNA adducts can be used to explain the repair-dependent toxicities of this antitumor agent. *Chem. Biol.* 8, 1033–1049. doi: 10.1016/S1074-5521(01)00071-0
- Zheng, S., Chan, C., Furuuchi, T., Wright, B. J. D., Zhou, B., Guo, J., et al. (2006). Stereospecific formal total synthesis of ecteinascidin 743. *Angew. Chem. Int. Ed. Engl.* 45, 1754–1759. doi: 10.1002/anie.200503983

Conflict of Interest Statement: The authors declare that the research was conducted in the absence of any commercial or financial relationships that could be construed as a potential conflict of interest.

Received: 06 March 2014; accepted: 04 April 2014; published online: 01 May 2014.

Citation: Basmadjian C, Zhao Q, Bentouhami E, Djehal A, Nebigil CG, Johnson RA, Serova M, de Gramont A, Faivre S, Raymond E and Désaubry LG (2014) Cancer wars: natural products strike back. *Front. Chem.* 2:20. doi: 10.3389/fchem.2014.00020

This article was submitted to Medicinal and Pharmaceutical Chemistry, a section of the journal *Frontiers in Chemistry*.

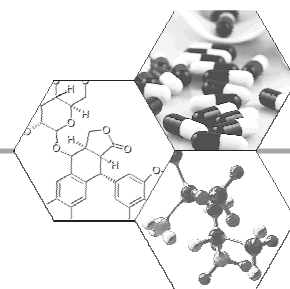
Copyright © 2014 Basmadjian, Zhao, Bentouhami, Djehal, Nebigil, Johnson, Serova, de Gramont, Faivre, Raymond and Désaubry. This is an open-access article distributed under the terms of the Creative Commons Attribution License (CC BY). The use, distribution or reproduction in other forums is permitted, provided the original author(s) or licensor are credited and that the original publication in this journal is cited, in accordance with accepted academic practice. No use, distribution or reproduction is permitted which does not comply with these terms.

PUBLICATION N°2

Flavaglines: potent anticancer drugs
that target prohibitins and the eIF4 helicase.

Basmadjian C, Thuaud F, Ribeiro N, Désaubry L. *Future Med. Chem.* **2013**, 5, 2185-2197

Copyright ©2013 holded by Future Science Ltd and its licensors



Flavaglines: potent anticancer drugs that target prohibitins and the helicase eIF4A

Flavaglines are complex natural products that are found in several medicinal plants of Southeast Asia in the genus *Aglaia*; these compounds have shown exceptional anticancer and cytoprotective activities. This review describes the significance of flavaglines as a new class of pharmacological agents and presents recent developments in their synthesis, structure–activity relationships, identification of their molecular targets and modes of action. Flavaglines display a unique profile of anticancer activities that are mediated by two classes of unrelated proteins: prohibitins and the translation initiation factor eIF4A. The identification of these molecular targets is expected to accelerate advancement toward clinical studies. The selectivity of cytotoxicity towards cancer cells has been shown to be due to an inhibition of the transcription factor HSFI and an upregulation of the tumor suppressor TXNIP. In addition, flavaglines display potent anti-inflammatory, cardioprotective and neuroprotective activities; however, the mechanisms underlying these activities are yet to be elucidated.

Discovery & pharmacological activities

Flavaglines, also called rocaglamides or rocaglates, are a family of cyclopenta[*b*]benzofurans that are found exclusively in plants of the genus *Aglaia* (Meliaceae). These plants are used in traditional medicine to treat asthma and inflammatory skin diseases [1]. Rocaglamide (**1**; **FIGURE 1**) was first isolated in 1992 by King and colleagues based on its potent antileukemic activity [2]. Thus far, more than 100 other natural flavaglines have been identified, including silvestrol (**9**) which has the peculiarity to be substituted by a complex pseudo-sugar [3,4]. These compounds have attracted the attention of biologists due to their wide profile of biological activities including insecticidal, antifungal, anti-inflammatory, neuroprotective, cardioprotective and, in particular, anticancer activities. They have also fascinated synthetic chemists because of the challenge presented by the complexity of their highly strained and functionalized structure [3,4].

The most intriguing feature of flavaglines is the selective cytotoxicity toward cancer cells. Indeed, as far as we know, all cancer cell lines and transformed cell lines are sensitive to this cytotoxicity, while primary cultures of noncancerous cells are not affected [4]. Only silvestrol, which is a very particular flavagline, has been shown to be toxic to several normal hematopoietic cells [5]. Such toxicity was not observed with other flavaglines such as rocaglamide and its derivatives [6–8]. On the other hand, flavaglines promote the survival of neurons and cardiac cells when these cells are exposed to various stressors. These unique

features cannot be explained using our current understanding of flavagline biochemistry. It seems that these compounds target a feature that is consubstantial to the very nature of cancer.

The chemistry and pharmacology of flavaglines has been the object of several reviews [3,4,9,10]. Over the last year, the pharmacological investigation of the flavaglines greatly increased, in particular with the identification of their molecular targets. The purpose of this article is to highlight the most recent advances related to these exciting anticancer agents, with a special emphasis on their mode of action.

Syntheses

Following Trost's total synthesis of rocaglamide (**1**) in 1990 [11], more than ten different synthetic approaches have been developed, attesting to the fascination with these highly compact, functionalized heterocycles. Flavagline synthesis remains a challenge as the compounds have two contiguous quaternary chiral centers and *cis* aryl groups on adjacent carbons of a strained cyclopentane ring. Since most of these efforts have already been reviewed, we will discuss only the most recent developments in this field [3,4,12].

Magnus successfully achieved Nazarov cyclization of dienone (**17**) to an intermediate (**18**) by the use of acetyl bromide and obtained a yield of 81% (**FIGURE 2**) [13]. Compound **18**, which encompasses the critical features of flavaglines, was transformed in six steps into dehydroflavagline (**19**), which has been shown to yield methyl rocaglate in two steps by Trost [11].

**Christine Basmadjian,
Frédéric Thuaud, Nigel
Ribeiro & Laurent
Désaubry***

Therapeutic Innovation Laboratory
(UMR 7200), CNRS/University of
Strasbourg, Faculty of Pharmacy, 67401
Illkirch Cedex, France
*Author for correspondence:
Tel.: +33 368 854 141
Fax: +33 368 854 320
E-mail: desaubry@unistra.fr

**FUTURE
SCIENCE** part of
fsg

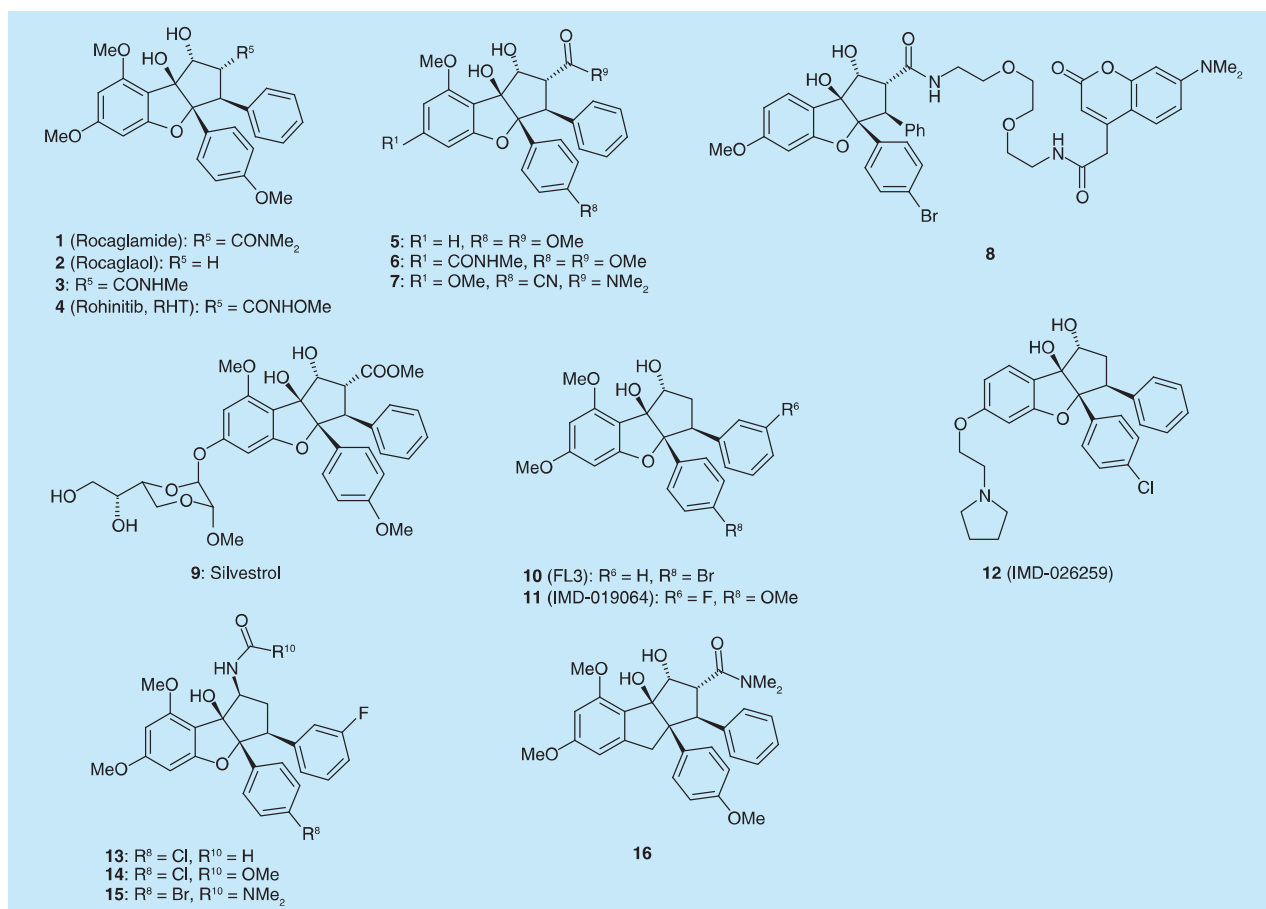


Figure 1. Representative flavaglines (1–15) and carbaisostere (16).

Key Terms

Prohibitins: Scaffold proteins that perform different functions depending on their post-translational modifications, which are under the control of many signaling pathways. These modifications dictate the localization of prohibitins in the cytoplasm, mitochondria, nucleus, endoplasmic reticulum and plasma membrane. Prohibitins exist as two isoforms, which have been involved in the etiology of cancers, inflammatory and metabolic diseases. They are also deeply involved in the promotion of survival against many stresses.

eIF4A: Subunit of the heterotrimeric eIF4F complex involved in the recruitment of mRNA to ribosomes. It functions as a helicase to unwind double-stranded RNA during the initiation of protein synthesis.

Recently, Porco and colleagues improved their biomimetic [3+2] photocycloaddition between 3-hydroxyflavones and cinnamate dipolarophiles to obtain an intermediate that leads to a flavagline by an acyloin rearrangement (FIGURE 3) [14]. To induce chirality, these authors used a chiral catalyst (TADDOL), which complexes hydroxyflavone in such a way that it promotes the [3+2] cycloaddition in an enantioselective manner.

Another significant improvement of this methodology was provided by Tremblay and colleagues, who used flow chemistry to produce tens of grams of photoadducts over the course of only a few hours [15].

Molecular targets of flavaglines & their mechanism of action

In 2012, Li-Weber and colleagues used affinity chromatography and identified **prohibitins** (PHBs) as the molecular targets of flavaglines [16]. PHBs are scaffold proteins that exist as two

isoforms, PHB1 and PHB2 [17]. Both proteins interact with each other and with numerous other proteins in several cellular compartments. PHB function is regulated through post-translational modifications induced by the signaling of Akt, CamK IV, PKC- δ , and by insulin, IGF1, EGF, TGF- β , and IgM receptors. These modifications modulate the affinity of PHBs for specific lipids and control their intracellular localization. In mitochondria, PHBs regulate respiration, protein metabolism, and possibly, resistance to oxidative stress. In the nucleus, PHBs interact with several transcription factors, histone deacetylases, histone methyltransferases, transcriptional corepressors and minichromosome maintenance proteins to regulate transcription and DNA synthesis. In the cytoplasm, PHBs regulate the activity of many signaling proteins such as the kinases c-Raf, Akt and MLK2, the phosphatase Shp1/2, the chaperones Hsp70 and mortalin/Grp75, the phospholipase C γ 2, and the magnesium channel TRPM6 [17].

The role of PHBs in the etiology of cancer is complex. On one hand, they exhibit antitumorigenic effects by activating the tumor suppressors p53, Rb, p107 and p130, and inhibiting DNA replication; however, on the other hand, they may also enhance tumorigenesis by promoting the activation of c-RAF, the survival of prostate cancer cells, as well as the resistance to taxoids [17].

Li-Weber and colleagues demonstrated that the binding of flavaglines to PHBs blocks their heterodimerization with the kinase c-Raf [16]. However, this protein–protein interaction is necessary for Ras to phosphorylate c-Raf (**FIGURE 4**). Consequently, flavaglines inhibit Ras-c-Raf-MEK-ERK signaling, which is critical for the survival of many cancer cell types.

Indeed, this pathway is overactivated in many human cancers, and represents an important

target in oncology [18]. Whether flavaglines modulate the interaction of PHBs with other partner proteins is currently under investigation.

While the synthesis of many proteins requires a minimal amount of **eIF4A**, a subset of mRNA coding for proteins that are particularly involved in cell progression, resistance to apoptosis, and angiogenesis is highly dependent upon eIF4A for translation. Flavaglines have been known for many years to inhibit cap-dependent translation, and in particular the production of CDK4, CDK6, cyclins D1 and D3, cdc25A, Bcl-2, survivin, Mcl-1, the PIM1/2 kinases, c-Myc, VEGF, MMP9 and MUC1-C [16,19–23].

Although these studies suggest that inhibition of cap-dependent translation is an important component of the anticancer mechanism of flavaglines, the significance of the depletion

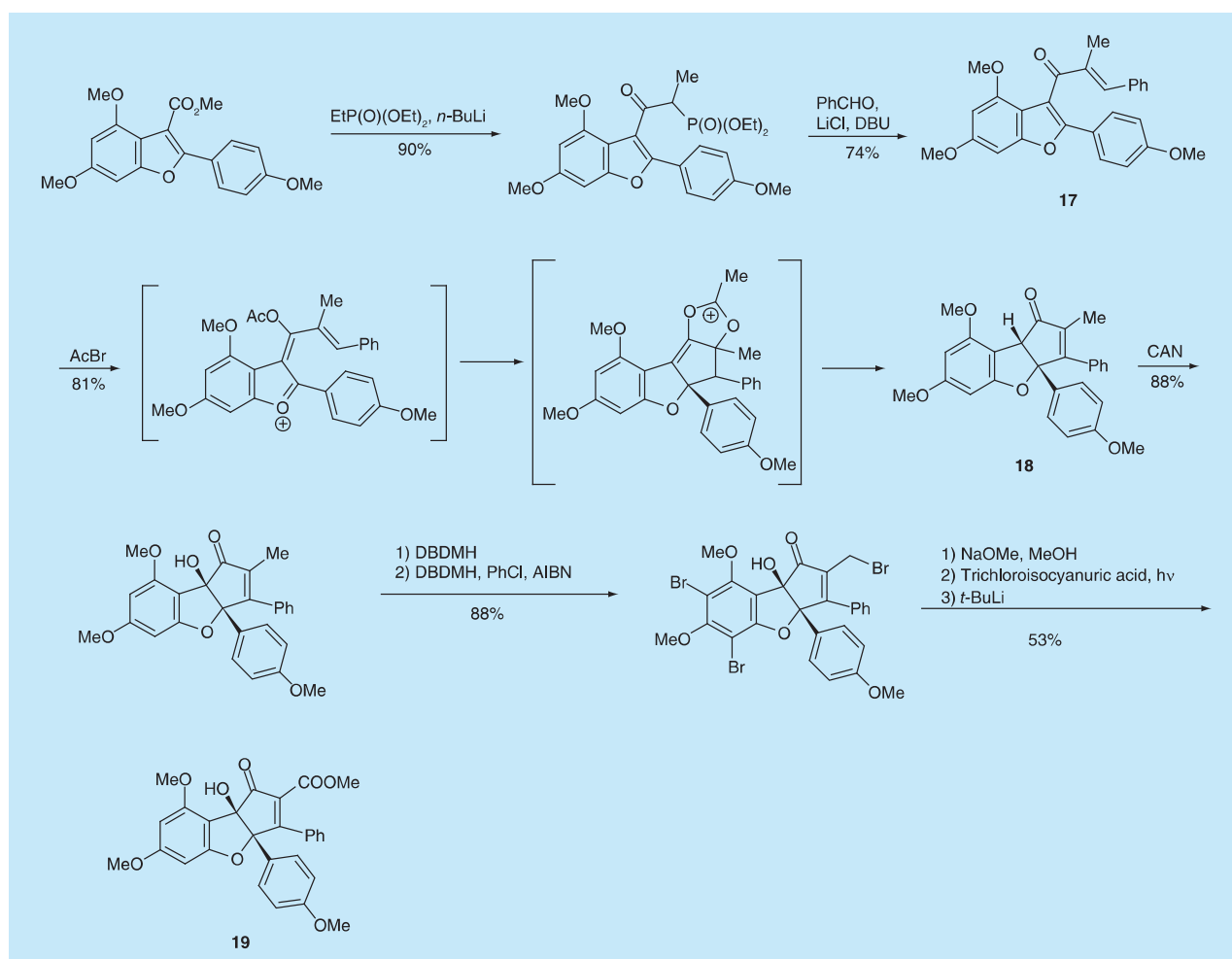


Figure 2. Magnus' synthesis of flavaglines based on Nazarov cyclization.

Adapted with permission from [13] © American Chemical Society (2012).

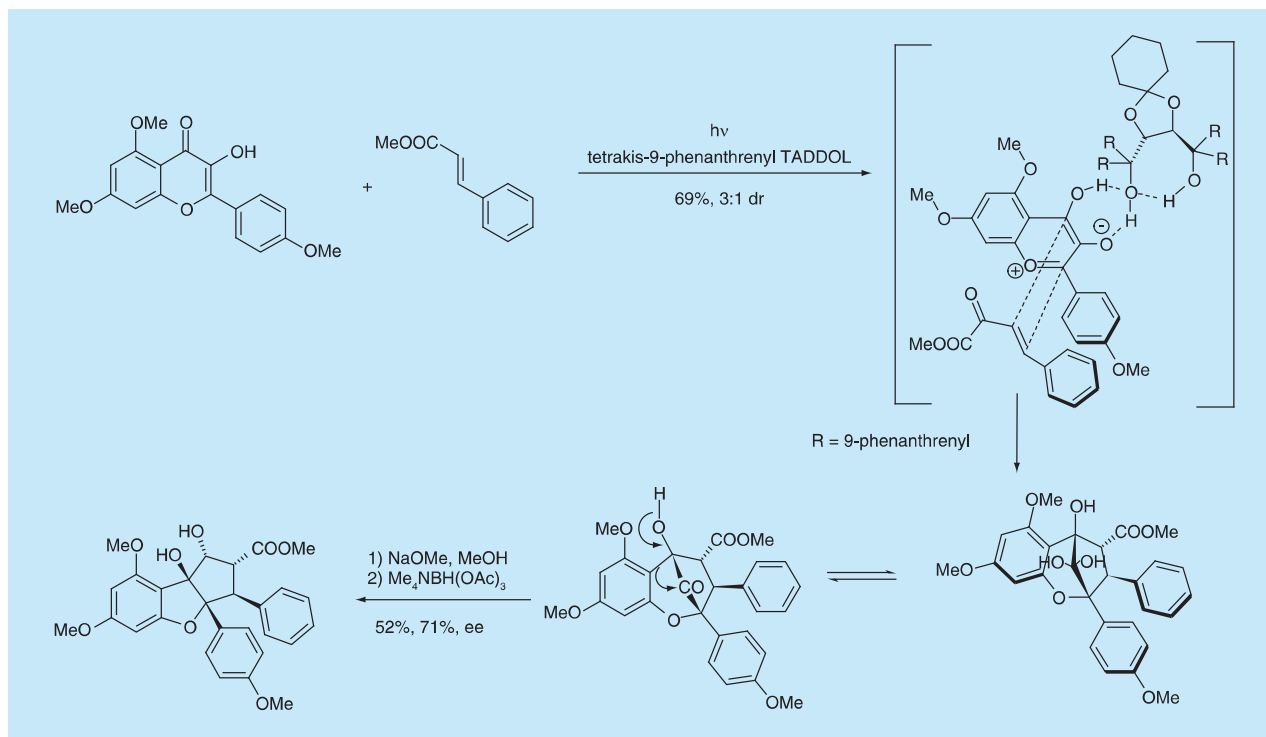


Figure 3. Porco's enantioselective biomimetic synthesis.

dr: Diastereomeric ratio; ee: Enantiomeric excess; TADDOL: Tetraaryl-1,3-dioxolane-4,5-dimethanol. Adapted with permission from [14] © American Chemical Society (2012).

of each of these proteins remains unclear. Indeed, Lindqvist recently demonstrated that silvestrol-induced reduction in Mcl-1 does not significantly contribute to the induction of apoptosis in immortalized fibroblasts and normal B lymphoid cells [5]. The depletion of another anti-apoptotic protein, Bcl-2, is also not essential to the cytotoxicity of silvestrol in B-cell malignancy mantle cell lymphoma [24], chronic lymphocytic leukemia or acute lymphoblastic leukemia [25]. Both Mcl-1 and Bcl-2 are known to enhance cell survival by inhibiting apoptosis.

In 2009, Pelletier and colleagues found that flavaglines enhance the binding of mRNA to the helicase eIF4A, which blocks the recycling of this translation factor and therefore inhibits cap-dependent translation [20]. In 2013, Rizzacasa and colleagues used affinity chromatography to demonstrate that a biotinylated episilvestrol physically interacts with eIF4A [26]. Shortly after this report, Sadlish and colleagues independently confirmed this interaction with eIF4A [27]. Using chemogenomic profiling, they identified eIF4A as the primary target of flavaglines in yeast. By mutagenesis,

they defined residues that are critical for binding to flavaglines. Interestingly, all of these residues are located close to one another in proximity to the mRNA binding site. *In silico* modeling provided a model to explain how the binding of flavaglines to eIF4A enhances interaction with mRNAs. This stabilization of the interaction of eIF4A with mRNAs prevents the recycling of eIF4A and consequently results in an inhibition of translation that opposes the survival of cancer cells. Subsequently, Whitesell and colleagues reported in *Science* how translational inhibition selectively affects the proliferation and survival of cancer cells [28]. Previously, these authors had demonstrated that the transcriptional factor **HSF1** controls the metabolic reprogramming, survival and proliferation of cancer cells, in addition to the transcription of genes in response to temperature stress, namely the heat-shock response. They now demonstrated that inhibition of protein synthesis blocks HSF1, which acts as a sensor of mRNA translation to coordinate protein synthesis with transcription in cancer cells. These authors screened more than 300,000 compounds for inhibition of HSF1 signaling and identified rocaglamide (**1**) as the

Key Term

HSF1: Transcription factor that controls expression of genes involved in the metabolic reprogramming, survival and proliferation of cancer cells, in addition to the transcription of genes induced by temperature stress.

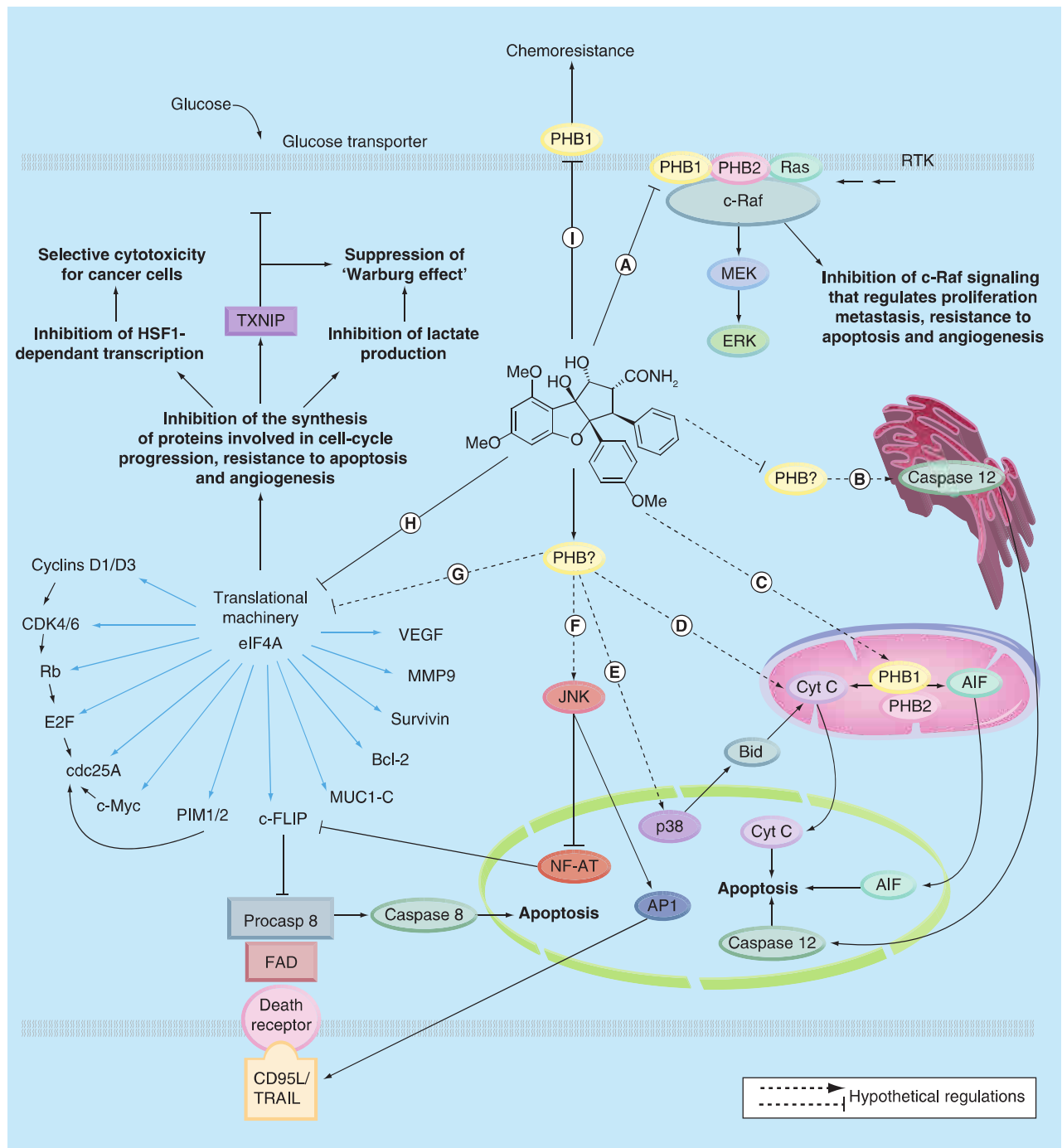


Figure 4. Anticancer mechanisms of flavaglines. (A) Inhibition of the activation of c-Raf by Ras. (B,C) Translocation of caspase-12 and AIF to the nucleus to induce apoptosis. (D) Translocation of cytochrome C to induce the intrinsic apoptotic pathway. (E) Activation of p38-mediated transcription of the pro-apoptotic Bcl-2 family. (F) Activation of JNK, which promotes the transcription of the pro-apoptotic proteins CD95 ligand and c-FLIP. (G) Hypothetical inhibition of the translational machinery through an action on prohibitins. (H) Inhibition of eIF4A leading to a downregulation of proteins involved in cell-cycle progression, resistance to apoptosis and angiogenesis. This inhibition of protein synthesis leads to a reduced activity of transcription factor HSF1 and an upregulation of the tumor suppressor TXNIP. TXNIP blocks glucose uptake and consequently prevents the 'Warburg effect'. (I) Hypothetical inhibition of the chemoresistance mediated by prohibitin 1 at the surface of cancer cells. Adapted with permission from [17] © Elsevier (2013).

Key Terms

TXNIP: Tumor suppressor that inhibits the antioxidant thioredoxins and regulates metabolism through suppression of lipogenesis and glucose uptake.

Aneuploidy: Abnormal number of chromosomes.

most potent and selective hit (IC_{50} ~50 nM). Further assays were performed with other flavaglines, and among those, rohinittib (**4**) displayed the highest potency (IC_{50} ~20 nM). Interestingly, rohinittib substantially blocked the transcription of all HSF1-regulated genes in several cancer cell lines. Importantly, this effect was much less pronounced in proliferating non-tumorigenic cells.

In cancer cells, rohinittib reversed the ‘Warburg effect’, a metabolic shift that is manifested by a high rate of glycolysis and an increased production of lactic acid. Indeed, rohinittib inhibited both glucose uptake and lactate production in a panel of cancer cells, through an upregulation of the thioredoxin-interacting protein **TXNIP**. TXNIP is a tumor suppressor that inhibits thioredoxin. It is also a key regulator of cellular energy status that blocks glucose uptake. Importantly, rohinittib promoted transcription of TXNIP to prevent the ‘Warburg effect’.

One of the features of flavaglines, perhaps the most interesting, is the high selectivity of the cytotoxicity toward cancer and immortalized cells versus normal cells. Whitesell and collaborators demonstrated that wild-type mouse embryonic fibroblasts (MEFs) were less sensitive to rohinittib cytotoxicity than *Nf1* null mutant MEFs [28], which overexpress HSF1 due to the inactivation of tumor suppressor *Nf1*. These *Nf1*^{-/-} MEFs represent a model of premalignant cells with early-stage oncogenic lesions.

Aneuploidy, a characteristic of cancer cells, induces a proteotoxic stress that is alleviated by HSF1 signaling. Whitesell, Lindquist and collaborators demonstrated that trisomic MEFs were much more sensitive to rohinittib than wild-type MEFs [28], through an inactivation of HSF1 signaling. Importantly, patient-derived colon cancer cell lines with high chromosomal instability were particularly sensitive to rohinittib.

Both PHBs and the cellular translation machinery represent emerging targets in oncology [17,29]. Indeed, the dysregulation of both of these targets has been established to be involved in the etiology of cancers. In addition, PHBs and eIF4A are overexpressed in many types of cancers. PHB1 is now being considered as a biomarker of malignant tumors with poor prognosis [30,31].

Unanswered questions regarding anticancer mechanisms

When Li-Weber and colleagues knocked-down PHB1 or PHB2 with siRNA, they observed an

inhibition of cap-dependent translation and an arrest of cell cycle progression via a depletion of cyclin D3, CDK4, CDK6 and cdc25A, mimicking the effects of flavaglines [16]. These effects may be explained by an inhibition of the Ras-c-Raf-MEK-ERK-MnK1 pathway that activates the translation initiation factor eIF-4E. An alternative explanation could be that PHBs may also interact with a component of the transcriptional machinery to control protein synthesis, and that flavaglines may modulate this interaction. While PHBs are known to regulate mitochondrial translation, an interaction with the cytoplasmic transcriptional machinery is currently hypothetical.

Flavaglines trigger apoptosis in cancer cells through several mechanisms involving cytochrome C [8,32,33], AIF [34], caspase 12 [34] and the MAP kinases JNK and p38 [7,8]. We do not know yet whether these effects are subsequent to an action on PHB1, PHB2 or eIF4A. In the course of their medicinal chemistry studies, Tremblay and colleagues identified flavaglines (such as compound **5**) that display a strong *in vitro* cytotoxicity without inhibiting cap-dependent translation [15]. These data suggest that in some cell types, cytotoxicity may be caused by an action on PHBs rather than on eIF4A.

Another intriguing question is related to the observation that a fluorescent probe (**8**) accumulates in the endoplasmic reticulum (ER) of HeLa cells, suggesting two scenarios [34]. This probe may preferentially bind to PHBs when they are located in the ER, or it may selectively target eIF4A. It has also not been considered whether it is an action on eIF4A or PHBs that triggers the ER stress that is responsible for the activation of caspase-12 in the ER [34]. Regarding this issue, another question that needs to be examined concerns the effects of flavaglines on the rerouting of PHBs in subcellular compartments, and how it affects PHBs signaling.

Preclinical development of flavaglines for the treatment of cancer

In a 1998 study involving BC1 breast tumor implantation in athymic mice, Pezzuto and colleagues reported that after 3 weeks of flavagline treatment, no further delay of tumor growth was observed because of development of treatment resistance in the mice [35]. At that time, research was focused on cytotoxic agents that eradicated tumors, and the study of flavaglines was interrupted until the appearance of

targeted therapies, when the approach toward the development of anticancer drugs drastically changed [36]. Indeed, resistance to a treatment in a mouse model of cancer is not uncommon, even for drugs that are presently used in the clinic. Currently, this phenomenon is not considered sufficient reason to prevent clinical development of a promising anticancer drug.

Pelletier and colleagues showed that silvestrol suppresses human tumor growth in MDA-MB-231 breast cancer xenografts [20]. The impressive antitumor efficacy may be explained by the requirement for eIF4A signaling in these cancer cells, where it is constitutively activated. This *in vivo* anticancer activity was further substantiated by several complementary studies, which suggest that flavaglines may find an optimal use in association with another anticancer drug to potentiate their activity and prevent resistance (TABLE 1) [2,4,7,20,22,24,25,28,37–40,101]. Importantly, in all of these preclinical studies, flavaglines did not show any sign of toxicity in mice.

The flavagline that has been studied the most *in vivo* for its anticancer potential is silvestrol (TABLE 1). However, this compound has recently been found to be sensitive to P-glycoprotein-mediated multidrug resistance [41]. Fortunately, flavaglines that are not substituted at position 2 with an ester or an amide are insensitive to multidrug resistance and retain excellent cytotoxicity (FIGURE 5) [34,42,43].

Several academic institutions and, to our knowledge, only two pharmaceutical companies, IMD Natural Solutions (Dortmund, Germany) and Infinity Pharmaceuticals (MA, USA), have explored the *in vivo* efficacy of flavaglines in preclinical models of cancers. None of these compounds have reached clinical trials as of yet.

Cytoprotective activities

Beyond their anticancer effect, flavaglines have been shown to display potent anti-inflammatory and neuroprotective activities [6,44]. At nanomolar concentrations, they induce a strong immunosuppression via inactivation of the nuclear factor of activated T-cells, subsequent to an activation of the MAP kinases JNK and p38, although the precise mechanism is undefined [6]. At higher concentrations, flavaglines also inhibit NF- κ B signaling, which is also involved in inflammation [1]. Interestingly, Sanders and colleagues very recently demonstrated that PHBs interact with the cell receptor CD86 to

promote NF- κ B activation [45]. It is therefore tempting to speculate that the inhibition of NF- κ B signaling by flavaglines is mediated by an action on PHBs.

The synthetic flavagline IMD-019064, which also inhibits NF- κ B signaling, was found to inhibit the release of pro-inflammatory mediators from microglia, astrocytes and endothelial cells [44]. This compound also protects dopaminergic neurons in models of Parkinson's disease and traumatic brain injury. Subsequent studies from our group led to the identification of compound **15**, which was shown *in vitro* to protect neurons from various forms of stress with greater efficacy than IMD-019064 [43]. The German pharmaceutical company IMD Natural Solutions is currently examining IMD-026259 (**12**; FIGURE 1) in a preclinical trial for the treatment of Parkinson's disease [201]. Many analogs of this compound have been synthesized, but biological data have not been disclosed for the majority [102]. Therefore, structure–activity relationship (SAR) data are unknown, and the exact contribution of the pyrrolidinoethyl moiety remains obscure.

The authors' group found that flavaglines not only protect neurons in models of Parkinson's disease, but also against the neurotoxicity induced by the anticancer drug cisplatin [43]. These findings inspired examination of whether flavaglines could protect other organs from the iatrogenicity of cancer chemotherapies, and in particular, that of the anthracyclines. Indeed, anthracyclines, such as doxorubicin, are among the most widely used anticancer medicines, in spite of their pronounced cardiotoxicity that may lead to dilated cardiomyopathy and congestive heart failure [46]. We were pleased to find that the synthetic flavagline FL3 (**10**; FIGURE 1), which displays strong anticancer activities [34], also protects cardiomyocytes against various stressors, including anthracycline cardiotoxicity and serum starvation [47]. Interestingly, the mechanism of these two stresses are very different: doxorubicin induces oxidative stress, while serum starvation blocks growth factor signaling that is necessary for cell survival, mimicking an important component of myocardial ischemia. *In vivo*, FL3 greatly reduced mortality and alleviated both cardiac apoptosis and fibrosis in a mouse model of acute cardiotoxicity induced by doxorubicin [47]. These data indicate that flavaglines may not only circumvent resistance to cancer chemotherapies, but also attenuate the iatrogenic effect of these treatments.

A preliminary investigation into the mechanism of these cardioprotective effects showed a potential role for the small heat-shock protein Hsp27. FL3 strongly induced the phosphorylation of this chaperone protein, which is a key factor in the resistance of cardiomyocytes to many types of stress [48]. Exactly how flavaglines activate

Hsp27 is currently under investigation. Taking into account the importance of the damaging effects of cancer treatments, the discovery of a new class of cytoprotective agents is of paramount importance in the clinic, and further studies to examine this therapeutic potential are warranted.

Table 1. *In vivo* activity in murine cancer models.

Compound	Murine model of cancer	Observed effects	Doses	Ref.
Rocaglamide (1) 3	P388 lymphocytic leukemia	Increase in lifetime: T/C of 156%	1 mg/kg	[2]
	RMA T lymphoma	Potential of the effects of concanavalin A (otherwise inactive) to significantly inhibit tumor progression	2.5 mg/kg i.p. three times a week for 2 weeks	[7]
Rohinitib (4) 5	M091 human myeloid leukemia cells	Inhibition of tumor growth and suppression of glucose uptake	1 mg/kg i.p. 4 consecutive days a week for 3 weeks	[28]
7	Eμ-Myc/(myr)Akt lymphoma cells	Potential of the effects of doxorubicin (otherwise inactive): increase in lifetime by 9 days	0.2 mg/kg i.p. daily for 5 days	[37]
	RPMI-8226 myeloma	Absence of significant effect	0.2 mg/kg i.p., 5 days/week for 3 weeks equals maximum tolerated dose	[38]
Silvestrol (9)	L3.6pl pancreatic cancer and RPMI-8226 myeloma	Absence of significant effect	0.2 mg/kg i.p., 5 days/week equals maximum tolerated dose	[38]
Silvestrol (9)	Eμ-Myc/(myr)Akt lymphoma	Potential of the effects of doxorubicin (otherwise inactive): increase in lifetime by 7 days (used in monotherapy, silvestrol did not display any significant effect)	0.2 mg/kg i.p. daily for 5 days	[37]
Silvestrol (9)	P388 leukemia	Increase in lifespan corresponding to a T/C of 150%	2.5 mg/kg i.p. for 5 days	[39]
Silvestrol (9)	PC3 prostate cancer	Reduction of the mean tumor weight by 60%	3 mg/kg i.p., three times per week for 3 weeks	[101]
Silvestrol (9)	Pten ⁺ /Eμ-Myc lymphoma	Potential of the effects of doxorubicin: increase in lifetime by 5 days compared with doxorubicin alone (silvestrol alone was inactive)	0.2 mg/kg i.p. daily for 5 days	[41]
Silvestrol (9)	Eμ-Myc/eIF4E lymphoma	Potential of the effects of doxorubicin: increase in lifetime by 16 days compared with doxorubicin alone (silvestrol alone was inactive)	0.2 mg/kg i.p. daily for 5 days	[40]
Silvestrol (9)	Eμ-Tcl-1 chronic lymphocytic leukemia	Significant reduction in B-cell number	1.5 mg/kg i.p. daily for 5 days	[25]
Silvestrol (9)	697 B-ALL acute lymphoblastic leukemia	Increase in lifetime by more than 2 weeks	1.5 mg/kg i.p. every other day	[25]
Silvestrol (9)	MDA-MB-231 breast cancer	Considerable suppression of tumor growth after more than 75 days	0.5 mg/kg i.p. daily for 8 consecutive days	[20]
Silvestrol (9)	PC-3 prostate cancer	Considerable suppression of tumor growth after more than 50 days	0.5 mg/kg i.p. daily for 8 consecutive days	[20]
Silvestrol (9)	MV4-11 acute myeloid leukemia	Increase in lifetime by more than 1 month. Impressively, 30% were still alive 74 days after engraftment (all vehicle-treated mice were dead 31 days after engraftment)	1.5 mg/kg i.p. every other day for 3 weeks	[40]
Silvestrol (9)	Eμ-Myc/Tsc2 ^{-/-} /PIM2 lymphoma	Potential of the effects of rapamycin: increase in lifetime by 6 days compared with rapamycin alone	0.2 mg/kg i.p. daily for 7 days	[22]
Silvestrol (9)	Mantle cell lymphoma	Increase in lifetime by 2 weeks	1.5 mg/kg i.p. every other day	[24]
13	3LL lung carcinoma	Significant suppression of tumor growth	25 mg/kg i.p. twice a week for 17 days	[41]

i.p.: Intraperitoneal administration; *T/C*: Treated versus control. Adapted with permission from [4] © Elsevier (2012).

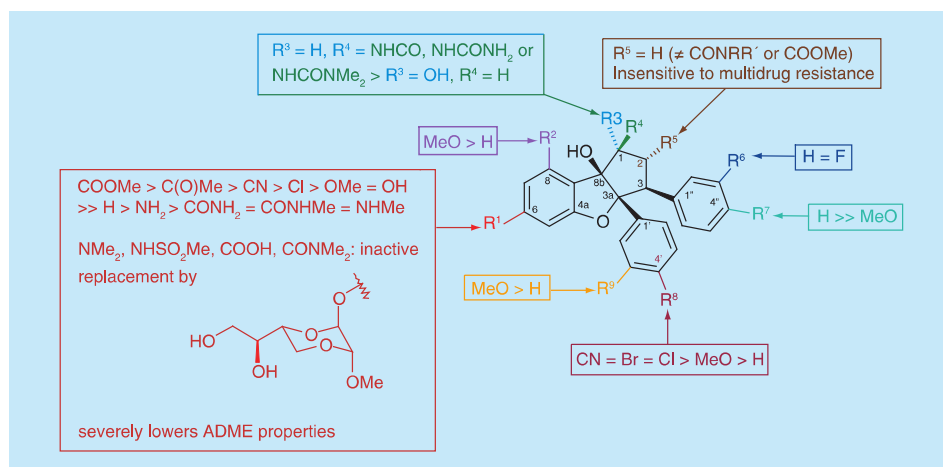


Figure 5. Key structure–activity relationships findings related to flavagline antiproliferative activity.

ADME: Absorption, distribution, metabolism and excretion. Adapted with permission from [4] © Elsevier (2012).

It seems paradoxical that flavaglines promote the death of cancer cells and the survival of normal cells. It is without doubt their most puzzling feature. The recent implication of PHBs, eIF4 and HSF1 provides some clues. It seems that PHBs fulfill different functions in cancer cells than in normal cells [17]. In the former, the migration of PHB1 outside the nucleus induces apoptosis, whereas in the latter, the opposite is true, leading to the promotion of survival [49]. An involvement of eIF4A in cytoprotection is also conceivable. Indeed, another natural product that inhibits eIF4, pateamine A, displays potent anticancer, immunosuppressive and cytoprotective effects in models of cachexia induced by IFN γ , TNF α or adenocarcinoma tumors [50–52]. One way to delineate the relative contributions of PHBs and eIF4A in these effects would be to identify cytoprotective flavaglines that do not bind to PHBs or eIF4A.

SAR studies

Since the release of the preceding reviews, three articles published in the *Journal of Medicinal Chemistry* from John Porco's laboratory, Martin Tremblay's group at Infinity Pharmaceuticals and our own laboratory, have revealed critical SAR data regarding the anticancer and cytoprotective activities of flavaglines [37,38,43]. Tremblay and colleagues explored the anticancer properties of several silvestrol derivatives and concluded that this class of flavaglines, substituted by a pseudo-sugar, display poor absorption, distribution, metabolism and excretion properties that severely

limit their development toward clinical applications [38]. These authors displayed the first SAR studies describing the influence of substituents at position 6 on cytotoxicity, and also on the inhibition of cap-dependent translation. They demonstrated for the first time that a substitution at the 6-position by an electron-withdrawing group ($R^1 = \text{OOMe}, \text{C(O)Me}, \text{CN}, \text{Cl}$; **FIGURE 5**) significantly improves antiproliferative activity. While the inhibition of cap-dependent translation was globally correlated with antiproliferative activity, there were some exceptions. For instance, compounds **5** and **6** displayed similar *in vitro* cytotoxicity: **6** effectively inhibited cap-dependent translation, but **5** did not. These data suggest that the antiproliferative effect of compound **5** does not involve eIF4A, but another target, possibly PHBs. These authors also reported for the first time that the replacement of the 4'-methoxy in natural flavaglines with a cyano group ($R^8 = \text{CN}$) significantly improved *in vitro* cytotoxicity.

Neither silvestrol, nor synthetic flavagline (**7**), display a significant inhibition of the growth of myeloma RPMI-8226 xenografts in NOD/SCID mice at their maximum tolerated doses administered (0.2 mg/kg intraperitoneally) for 3 weeks (administered daily \times 5 days \times 3 weeks). The authors postulated that the therapeutic window of these compounds is too narrow, probably due to inhibition of the synthesis of proteins essential for the viability of non-cancerous cells. Unfortunately, the *in vivo* anticancer activity of compound **5** was not reported. It would have been very interesting to know whether this compound

that does not inhibit translation was able to block tumor growth *in vivo*.

Porco and colleagues synthesized several rocaglamide hydroxamates and found that compound **4** inhibits cap-dependent translation and synergizes with doxorubicin in E μ -Myc(Myr) Akt lymphoma tumors in mice, with an efficacy similar to silvestrol [37]. Our group also refined the effect of substituents at positions 1, 4', and 4'' for *in vitro* cytotoxicity, and examined for the first time the structural requirements for cardioprotection and neuroprotection [43]. We did not find any difference in the relative order of activity for neuroprotection and cardioprotection, but identified slight differences in the SAR for cardioprotection and cytotoxicity in cancer cells. Overall, each of the cardioprotective flavaglines was also cytotoxic in cancer cells and *vice versa*. We observed some variation only in the ranking of activities. For instance, compound **13** (FIGURE 1) was found to be more cytotoxic, but less cytoprotective than compound **14**. Although we do not currently have any experimental evidence, it is tempting to hypothesize that this difference in biological activity is due to an action of compound **13** on both eIF4A and PHBs, and that compound **14** affects only PHBs. This question is currently under investigation.

Future perspective

Flavaglines display a unique profile of pharmacological activities and the recent identification of their molecular targets is a key element for further development toward clinical investigation. The most important outstanding issue is probably to define the clinical context in which they could be used. Related to this issue is the selectivity of the cytotoxicity for cancer cells (and why this is true for all cancer cells). A key step to develop flavaglines as anticancer agents will be to perform standard preclinical toxicology assays.

Regarding their application in oncology, it will be important to determine why, in some models, these compounds are either totally ineffective or may delay tumor growth in mice by only a few weeks. The appearance of resistance to treatment does not preclude further development, but it is certainly a phenomenon that needs to be understood. Another important task will be to deconvolute the precise nature of flavagline actions on eIF4A, PHB1 and PHB2 with regard to their anticancer and iatrogenic effects. It has been demonstrated that PHBs may be overexpressed or mutated in some human tumors. Whether these tumors are particularly

sensitive to flavagline treatment is another point to be examined.

The mechanisms of immunosuppression, cardioprotection and neuroprotection are also poorly understood. Examination of these pharmacological effects may unravel novel signaling pathways and lead to a better understanding of the physiology and pathophysiology of the cardiac, nervous and immune systems. Additionally, such knowledge will greatly facilitate the preclinical, and possibly the clinical, development of flavaglines. Currently, the pharmaceutical company IMD Natural Solutions is intensively investigating the potential of their lead compound, IMD-026259, in the treatment of Parkinson's disease [201].

PHBs have been described to form heterodimers with more than 50 proteins [17]. Among those, only c-Raf was shown to have its interaction with PHBs blocked [16]. Whether flavaglines may modulate interactions with other molecular partners remains to be determined. Such studies may lead to new therapeutic applications, and also help to understand their iatrogenic effects.

The structural requirements of flavaglines for their interactions with eIF4A, PHB1 and PHB2 are almost completely unexplored. The examination of these requirements should provide selective drugs with enhanced pharmacological properties. A first step in this direction was recently provided by Sadlish *et al.*, who proposed the first *in silico* modeling of the interaction of silvestrol with the eIF4A-mRNA complex [27]. A model of interactions with PHBs is also anticipated. The construction of such a model is hindered by the current absence of solid data regarding the 3D structure of PHBs. We expect that these modeling studies will not only provide drugs that are selective for each of these three targets, but they should also facilitate scaffold hopping, which is critical for the clinical development of flavaglines. Indeed, it is highly unlikely that a pharmaceutical company will invest in the clinical development of such compounds without obtaining intellectual property regarding their structure. Up to now, all pharmacologically active flavaglines derivatives have had the same cyclopenta[*b*]benzofurans skeleton. Only one isostere had been described by Novartis scientists (**16**; FIGURE 1), but it is currently lacking biological data. However, because this compound was not protected by a patent, it is likely that it does not exhibit significant biological activity. From an industrial point of view, developing a flavagline analog with a novel structure is probably a prerequisite for clinical development.

Acknowledgements

The authors would like to thank our friend and mentor RA Johnson for useful discussions.

Financial & competing interest disclosure

The authors are grateful to the 'Association pour la Recherche sur le Cancer' (grant numbers 3940 and SFI20111204054), the 'Agence nationale de la recherche' (grant number ANR-11-EMMA-021), and the 'Fondation pour la Recherche Médicale' for generous financial support.

We also thank AAREC Folia Research (C Basmadjian), ARC (N Ribeiro) and MNESR (F Thnaud) for fellowships. L Désaubry is an employee of CNRS and is affiliated with the University of Strasbourg, both of which have a financial interest in flavaglines. The authors have no other relevant affiliations or financial involvement with any organization or entity with a financial interest in or financial conflict with the subject matter or materials discussed in the manuscript apart from those disclosed. No writing assistance was utilized in the production of this manuscript.

Executive summary

Flavaglines may potentiate the efficacy of cancer chemotherapies & alleviate their adverse effects

- Flavaglines delay tumor growth in several mouse models of cancer when used alone, but their most exciting anticancer properties likely lie in their ability to reverse the resistance to established chemotherapeutic agents in mice.
- Flavaglines protect neurons and cardiomyocytes from the adverse effects of cisplatin and doxorubicin, respectively.
- Flavagline safety needs to be assessed prior to clinical developments.

Flavaglines target eIF4A & prohibitins

- Recently, flavaglines were shown to target two families of unrelated proteins: prohibitins and the translation initiation factor eIF4A.
- Both prohibitins and eIF4A are emerging targets in oncology.

The inhibition of HSF1 signaling is involved in the selectivity of the cytotoxicity of flavagline for cancer

- The inhibition of eIF4A by flavaglines suppresses the transcriptional activity of HSF1, upregulates the tumor suppressor TXNIP and reverses the Warburg effect in cancer cells.

Flavaglines display pronounced anti-inflammatory, neuroprotective & cardioprotective activities

- Flavaglines were shown to have potent anti-inflammatory activities, and also to protect neurons and cardiomyocytes against various stressors.
- The synthetic flavagline IMD-026259 is currently under intensive investigation by a pharmaceutical company for the treatment of Parkinson's disease.

References

Papers of special note have been highlighted as:

■ of interest

■ of considerable interest

- Baumann B, Bohnstengel F, Siegmund D *et al.* Rocaglamide derivatives are potent inhibitors of NF- κ B activation in T-cells. *J. Biol. Chem.* 277(47), 44791–44800 (2002).
- King ML, Chiang CC, Ling HC, Fujita E, Ochiai M, McPhail AT. x-ray crystal structure of rocaglamide, a novel antileukemic 1H-cyclopenta[*b*]benzofuran from *Aglaiia elliptifolia*. *Chem. Commun.* 20(1982), 1150–1151 (1992).
- Ebada SS, Lajkiewicz N, Porco JA Jr, Li-Weber M, Proksch P. Chemistry and biology of rocaglamides (= flavaglines) and related derivatives from *Aglaiia* species (Meliaceae). *Prog. Chem. Org. Nat. Prod.* 94, 1–58 (2011).
- Ribeiro N, Thnaud F, Nebigil C, Désaubry L. Recent advances in the biology and chemistry of the flavaglines. *Bioorg. Med. Chem.* 20(6), 1857–1864 (2012).
- Lindqvist LM, Vikstrom I, Chambers JM *et al.* Translation inhibitors induce cell death by multiple mechanisms and Mcl-1 reduction is only a minor contributor. *Cell. Death. Dis.* 3, e409 (2012).
- Proksch P, Giaisi M, Treiber MK *et al.* Rocaglamide derivatives are immunosuppressive phytochemicals that target NF-AT activity in T cells. *J. Immunol.* 174(11), 7075–7084 (2005).
- Zhu JY, Giaisi M, Kohler R *et al.* Rocaglamide sensitizes leukemic T cells to activation-induced cell death by differential regulation of CD95L and c-FLIP expression. *Cell Death Differ.* 16(9), 1289–1299 (2009).
- Zhu JY, Lavrik IN, Mahlknecht U *et al.* The traditional Chinese herbal compound rocaglamide preferentially induces apoptosis in leukemia cells by modulation of mitogen-activated protein kinase activities. *Int. J. Cancer* 121(8), 1839–1846 (2007).
- Kim S, Salim AA, Swanson SM, Kinghorn AD. Potential of cyclopenta[*b*]benzofurans from *Aglaiia* species in cancer chemotherapy. *Anticancer. Agents Med. Chem.* 6(4), 319–345 (2006).
- Proksch P, Edrada R, Ebel R, Bohnstengel F, Nugroho B. Chemistry and biological activity of rocaglamide derivatives and related compounds in *Aglaiia* species (Meliaceae). *Curr. Org. Chem.* 5, 923–938 (2001).
- Trost BM, Greenspan PD, Yang BV, Saulnier MG. An unusual oxidative cyclization. A synthesis and absolute stereochemical assignment of (-)-rocaglamide. *J. Am. Chem. Soc.* 112(24), 9022–9024 (1990).
- Malona JA, Cariou K, Spencer WT III, Frontier AJ. Total synthesis of (\pm)-rocaglamide via oxidation-initiated nazarov cyclization. *J. Org. Chem.* 77(4), 1891–1908 (2012).
- Magnus P, Freund WA, Moorhead EJ, Rainey T. Formal synthesis of (\pm)-methyl rocaglate using an unprecedented acetyl bromide mediated nazarov reaction. *J. Am. Chem. Soc.* 134(14), 6140–6142 (2012).
- Lajkiewicz NJ, Roche SP, Gerard B, Porco JA. Enantioselective photocycloaddition of 3-hydroxyflavones: total syntheses and absolute configuration assignments of (+)-ponapensin and (+)-elliptifoline. *J. Am. Chem. Soc.* 134(31), 13108–13113 (2012).
- Liu T, Nair SJ, Lescarbeau A *et al.* Synthetic silvestrol analogues as potent and selective protein synthesis inhibitors. *J. Med. Chem.* 55(20), 8859–8878 (2012).

- 16 Polier G, Neumann J, Thuaud F *et al.* The natural anticancer compounds rocaglamides inhibit the RAF-MEK-ERK pathway by targeting prohibitin 1 and 2. *Chem. Biol.* 19(9), 1093–1104 (2012).
- **Identification of prohibitins as a molecular target of flavaglines.**
- 17 Thuaud F, Ribeiro N, Nebigil CG, Désaubry L. Prohibitin ligands in cell death and survival: mode of action and therapeutic potential. *Chem. Biol.* 20(3), 316–331 (2013).
- **Comprehensive overview of the physiological and physiopathological roles of prohibitins, including a description of prohibitins ligands.**
- 18 Matallanas D, Birtwistle M, Romano D *et al.* RAF family kinases: old dogs have learned new tricks. *Genes Cancer* 2(3), 232–260 (2011).
- 19 Bordeleau ME, Robert F, Gerard B *et al.* Therapeutic suppression of translation initiation modulates chemosensitivity in a mouse lymphoma model. *J. Clin. Invest.* 118(7), 2651–2660 (2008).
- **Demonstration that flavaglines inhibit eIF4A.**
- 20 Cencic R, Carrier M, Galicia-Vazquez G *et al.* Antitumor activity and mechanism of action of the cyclopenta[b]benzofuran, silvestrol. *PLoS ONE* 4(4), e5223 (2009).
- 21 Nasr Z, Robert F, Porco JA Jr., Muller WJ, Pelletier J. eIF4F suppression in breast cancer affects maintenance and progression. *Oncogene* 32(7), 861–871 (2012).
- 22 Schatz JH, Oricchio E, Wolfe AL *et al.* Targeting cap-dependent translation blocks converging survival signals by AKT and PIM kinases in lymphoma. *J. Exp. Med.* 208(9), 1799–1807 (2011).
- 23 Jin C, Rajabi H, Rodrigo CM, Porco JA Jr., Kufe D. Targeting the eIF4A RNA helicase blocks translation of the MUC1-C oncoprotein. *Oncogene* 32(17), 2179–2188 (2012).
- 24 Alinari L, Prince CJ, Edwards RB *et al.* Dual targeting of the cyclin/Rb/E2F and mitochondrial pathways in mantle cell lymphoma with the translation inhibitor silvestrol. *Clin. Cancer Res.* 18(17), 4600–4611 (2012).
- 25 Lucas DM, Edwards RB, Lozanski G *et al.* The novel plant-derived agent silvestrol has B-cell selective activity in chronic lymphocytic leukemia and acute lymphoblastic leukemia *in vitro* and *in vivo*. *Blood* 113(19), 4656–4666 (2009).
- 26 Chambers JM, Lindqvist LM, Webb A, Huang DCS, Savage GP, Rizzacasa MA. Synthesis of biotinylated Episilvestrol: highly selective targeting of the translation factors eIF4A1/II. *Org. Lett.* 15(6), 1406–1409 (2013).
- **Identification of eIF4A as a molecular target of flavaglines.**
- 27 Sadlish H, Galicia-Vazquez G, Paris CG *et al.* Evidence for a functionally relevant rocaglamide binding site on the eIF4A-RNA Complex. *ACS Chem. Biol.* 8(7), 1519–1527 (2013).
- **Confirmation that eIF4A is a molecular target of flavaglines.**
- 28 Santagata S, Mendillo ML, Tang YC *et al.* Tight coordination of protein translation and HSF1 activation supports the anabolic malignant state. *Science* 341(6143), 1238303 (2013).
- **Demonstration that the inhibition of HSF1 signaling is involved in the selectivity of the cytotoxicity of flavaglines for cancer.**
- 29 Ruggero D. Translational control in cancer etiology. *Cold Spring Harb. Perspect. Biol.* 5(2) (2013).
- 30 Guo F, Hiroshima K, Wu D *et al.* Prohibitin and its rapidly emerging role as a biomarker of systemic malignancies-reply. *Hum. Pathol.* 44(4), 679–680 (2013).
- 31 Kapoor S. Prohibitin and its rapidly emerging role as a biomarker of systemic malignancies. *Hum. Pathol.* 44(4), 678–679 (2013).
- 32 Barnhart KF, Christianson DR, Hanley PW *et al.* A peptidomimetic targeting white fat causes weight loss and improved insulin resistance in obese monkeys. *Sci. Transl. Med.* 3(108), 108ra112 (2011).
- 33 Mi Q, Su BN, Chai H *et al.* Rocaglaol induces apoptosis and cell cycle arrest in LNCaP cells. *Anticancer Res.* 26(2A), 947–952 (2006).
- 34 Thuaud F, Bernard Y, Turkeri G *et al.* Synthetic analogue of Rocaglaol displays a potent and selective cytotoxicity in cancer cells: involvement of apoptosis inducing factor and Caspase-12. *J. Med. Chem.* 52(16), 5176–5187 (2009).
- **First demonstration of a cardioprotective activity of flavaglines.**
- 35 Lee SK, Cui B, Mehta RR, Kinghorn AD, Pezzuto JM. Cytostatic mechanism and antitumor potential of novel 1H-cyclopenta[b]benzofuran lignans isolated from *Aglaia elliptica*. *Chem. Biol. Interact.* 115(3), 215–228 (1998).
- 36 Gutierrez ME, Kummar S, Giaccone G. Next generation oncology drug development: opportunities and challenges. *Nat. Rev. Clin. Oncol.* 6(5), 259–265 (2009).
- 37 Rodrigo CM, Cencic R, Roche SP, Pelletier J, Porco JA. Synthesis of rocaglamide hydroxamates and related compounds as eukaryotic translation inhibitors: synthetic and biological studies. *J. Med. Chem.* 55(1), 558–562 (2012).
- 38 Liu T, Nair SJ, Lescarbeau A *et al.* Synthetic silvestrol analogues as potent and selective protein synthesis inhibitors. *J. Med. Chem.* 55(20), 8859–8878 (2012).
- 39 Hwang BY, Su BN, Chai H *et al.* Silvestrol and episilvestrol, potential anticancer rocaglate derivatives from *Aglaia silvestris*. *J. Org. Chem.* 69(10), 3350–3358 (2004).
- 40 Alachkar H, Santhanam R, Harb JG *et al.* Silvestrol exhibits significant *in vivo* and *in vitro* antileukemic activities and inhibits FLT3 and miR-155 expressions in acute myeloid leukemia. *J. Hematol. Oncol.* 6, 21 (2013).
- 41 Gupta SV, Sass EJ, Davis ME *et al.* Resistance to the translation initiation inhibitor silvestrol is mediated by ABCB1/P-glycoprotein overexpression in acute lymphoblastic leukemia cells. *AAPS J.* 13(3), 357–364 (2011).
- 42 Thuaud F, Ribeiro N, Gaiddon C, Cresteil T, Désaubry L. Novel flavaglines displaying improved cytotoxicity. *J. Med. Chem.* 54, 411–415 (2011).
- 43 Ribeiro N, Thuaud F, Bernard Y *et al.* Flavaglines as potent anticancer and cytoprotective agents. *J. Med. Chem.* 55, 10064–10073 (2012).
- **First structure–activity relationship data of flavaglines for cardio- and neuro-protection.**
- 44 Fahrig T, Gerlach I, Horvath E. A synthetic derivative of the natural product rocaglaol is a potent inhibitor of cytokine-mediated signaling and shows neuroprotective activity *in vitro* and in animal models of Parkinson's disease and traumatic brain injury. *Mol. Pharmacol.* 67(5), 1544–1555 (2005).
- **First demonstration of a neuroprotective activity of flavaglines.**
- 45 Lucas CR, Cordero-Nieves HM, Erbe RS *et al.* Prohibitins and the cytoplasmic domain of CD86 cooperate to mediate CD86 signaling in B lymphocytes. *J. Immunol.* 190(2), 723–736 (2013).
- 46 Minotti G, Menna P, Salvatorelli E, Cairo G, Gianni L. Anthracyclines: molecular advances and pharmacologic developments in antitumor activity and cardiotoxicity. *Pharmacol. Rev.* 56(2), 185–229 (2004).

- 47 Bernard Y, Ribeiro N, Thuaud F *et al.* Flavaglines alleviate doxorubicin cardiotoxicity: implication of Hsp27. *PLoS ONE* 6, e25302 (2011).
- **First demonstration of a cardioprotective activity of flavaglines.**
- 48 Kostenko S, Moens U. Heat shock protein 27 phosphorylation: kinases, phosphatases, functions and pathology. *Cell. Mol. Life Sci.* 66, 3289–3307 (2009).
- 49 Fusaro G, Dasgupta P, Rastogi S, Joshi B, Chellappan S. Prohibitin induces the transcriptional activity of p53 and is exported from the nucleus upon apoptotic signaling. *J. Biol. Chem.* 278(48), 47853–47861 (2003).
- 50 Di Marco S, Cammas A, Lian XJ *et al.* The translation inhibitor pateamine A prevents cachexia-induced muscle wasting in mice. *Nat. Commun.* 3, 896 (2012).
- 51 Lindqvist L, Pelletier J. Inhibitors of translation initiation as cancer therapeutics. *Future Med. Chem.* 1(9), 1709–1722 (2009).
- 52 Romo D, Choi NS, Li S, Buchler I, Shi Z, Liu JO. Evidence for separate binding and scaffolding domains in the immunosuppressive and antitumor marine natural product, pateamine a: design, synthesis, and activity studies leading to a potent simplified derivative. *J. Am. Chem. Soc.* 126(34), 10582–10588 (2004).
- **Patents**
- 101 Baiocchi RA, Patton JT Jr, Lucas DM, Kinghorn D, Grever M: WO2013016658 (2013).
- 102 Wabnitz P, Gehling M, Henkel T, Schmitz ML: WO2010063471 A1 (2010).
- **Website**
- 201 IMD-026259: an innovative drug for disease-modifying treatment of Parkinson's disease. www.michaeljfox.org/foundation/grant-detail.php?grant_id=1020

Synthesis and pharmacology of flavaglines

Basadjian, C., Zhao, Q., De Gramont, A., Serova, M., Raymond, E., Vagner, S., Robert, C., Nebigil, C. G., Désaubry, L., Bioactive Natural Products: Chemistry & Biology, Brahmachari, G., Ed. John Wiley & Sons, **2015**.

Copyright © 2015 by John Wiley & Sons, Inc.

7

Bioactive Flavaglines: Synthesis and Pharmacology

Christine Basmadjian, Qian Zhao, Armand de Gramont, Maria Serova, Sandrine Faivre, Eric Raymond, Stephan Vagner, Caroline Robert, Canan G. Nebigil, and Laurent Désaubry

7.1

Introduction

A recent survey of the first-in-class medicines approved over the last decades indicates that a quarter of them are derivatives of natural products [1]. This report clearly demonstrates the importance of these compounds in the development of new drugs. Indeed, natural compounds display certain notable advantages compared to synthetic drugs [2]. Firstly, natural products are secondary metabolites that were selected through evolution to act as chemical weapons or signaling molecules, with the ability to reach their receptor in the targeted organism. As such, they often have the ability to cross biological membranes. Many of these are suspected to be substrates of membrane transporters. This is an important issue, because natural compounds that are identified on the basis of *in vitro* pharmacological assays are often also active *in vivo*. Secondly, natural products, in general, have more chiral centers, more varied ring systems, a higher ratio of C_{sp^3}/C_{sp^2} , less nitrogen, and more oxygen atoms than synthetic drugs. This structural complexity provides excellent opportunities to explore new areas of chemical space and to generate original and therefore patentable compounds.

Although natural products had traditionally been invaluable as a source of medicines, the development of new natural compounds in oncology was interrupted for over 10 years with the advent of targeted therapies [2]. After the approval of Topotecan in 1996, the development of other natural products essentially came to a stop because of the nearly exclusive focus on targeted therapies by the pharmaceutical industries. However, because targeted therapies did not fulfill all their expectations, natural product derivatives returned to front stage. This is evident from the approval of 14 of these compounds between 2007

and 2013 for use in oncology [2]. Since the initial report of rocaglamide (**1**) by King and collaborators in 1992 [3], there has been growing interest from chemists and biologists in this unique class of cyclopenta[*b*]benzofurans called *flavaglines* (or sometimes, *rocaglamides* or *rocaglates*). Figure 7.1 offers a glimpse of certain significant natural and synthetic flavaglines.

The flavaglines are a family of more than 100 cyclopenta[*b*]benzofurans found in Asian plants of the genus *Aglaia* (Meliaceae). These compounds display potent insecticidal, antifungal, anti-inflammatory, neuroprotective, cardioprotective, and above all, anticancer activities. Their most intriguing feature is the selectivity of their cytotoxicity toward cancer cells. Indeed, as far as we know, all cancer cell lines and transformed cell lines are sensitive to this cytotoxicity, while primary cell cultures of noncancerous cells are not affected. This selective cytotoxicity was first described by Marian and collaborators [4]. It has also been observed that flavaglines promote the survival of neurons and cardiac cells toward many types of stresses. This unique feature is not rationalized with our current state of knowledge; it seems that these compounds target a feature that is consubstantial to the nature of the cancer itself.

The chemistry and pharmacology of flavaglines has been the object of several reviews [5–9]. Over the last year, we observed acceleration in the pharmacological investigation of the flavaglines, marked in particular by the identification of their molecular targets. The purpose of this article is to highlight the most recent advances on these exciting anticancer agents, with a special emphasis on their mode of action.

7.2

Biosynthetic Aspects

Along with flavaglines, aglaforbesins **18** and aglains **19** are also characteristic metabolites of the genus *Aglaia* (Scheme 7.1). The term *flavagline* proposed by Harald Greger from the University of Vienna, originally covered these three groups of compounds [10] but over time, it has tended to solely refer to cyclopenta[*b*]benzofurans because of their distinctive pharmacological activities. These three families of secondary metabolites display the same patterns of substitution and stereochemical relationships. Proksch was the first to propose a biosynthetic pathway that begins with the condensation of hydroxyflavone (**14**) with a cinnamic amide (**15**) to afford an aglain (**16**) that may undergo an α -ketol rearrangement to yield a flavagline **17** [11]. Reduction of intermediary ketones, possibly by NADPH, would generate the diols **18**, **19**, and **20**. Aglaforbesins are also probably generated by the same process, but with an addition of the cinnamic amide on the hydroxyflavone that occurs with the opposite orientation.

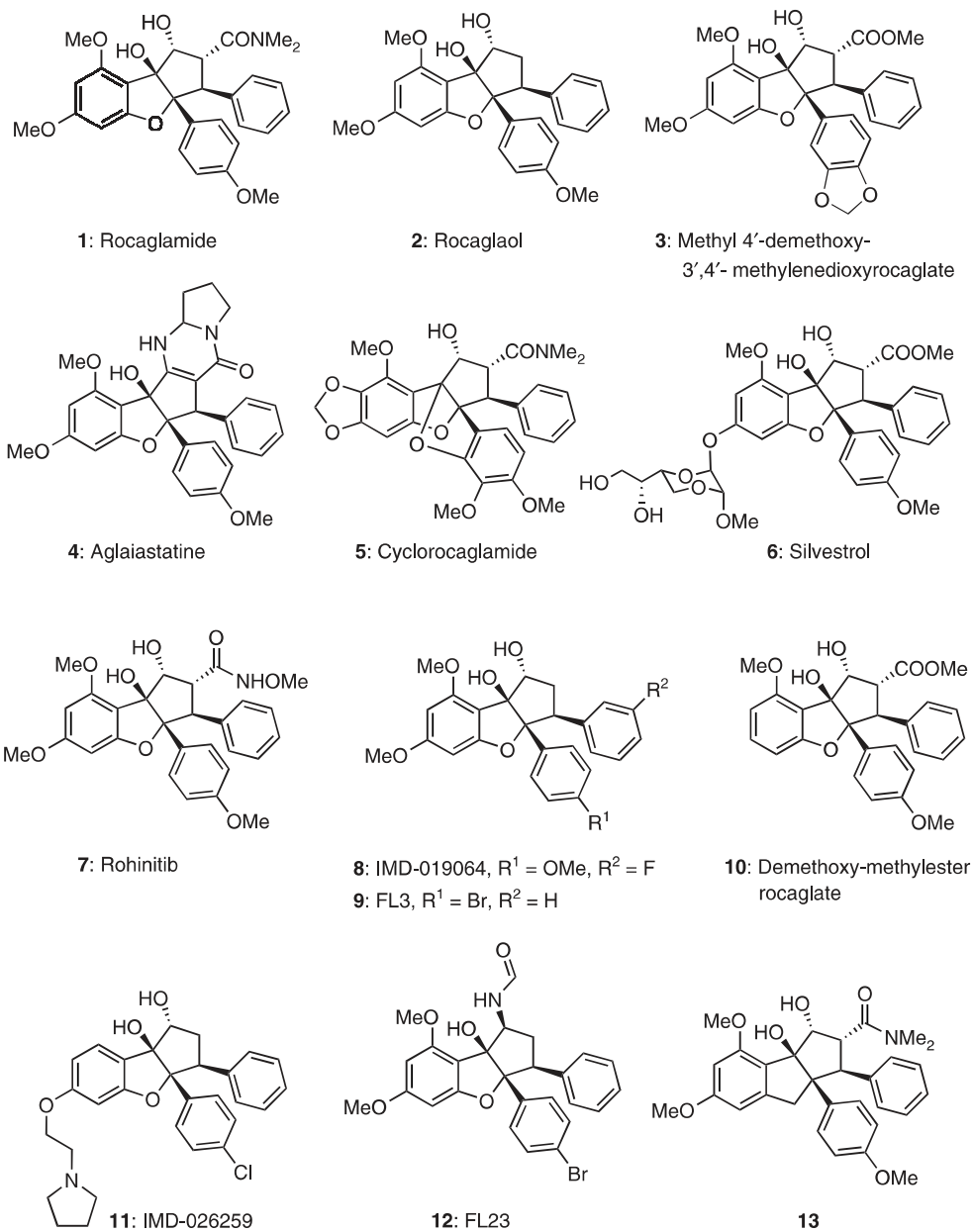
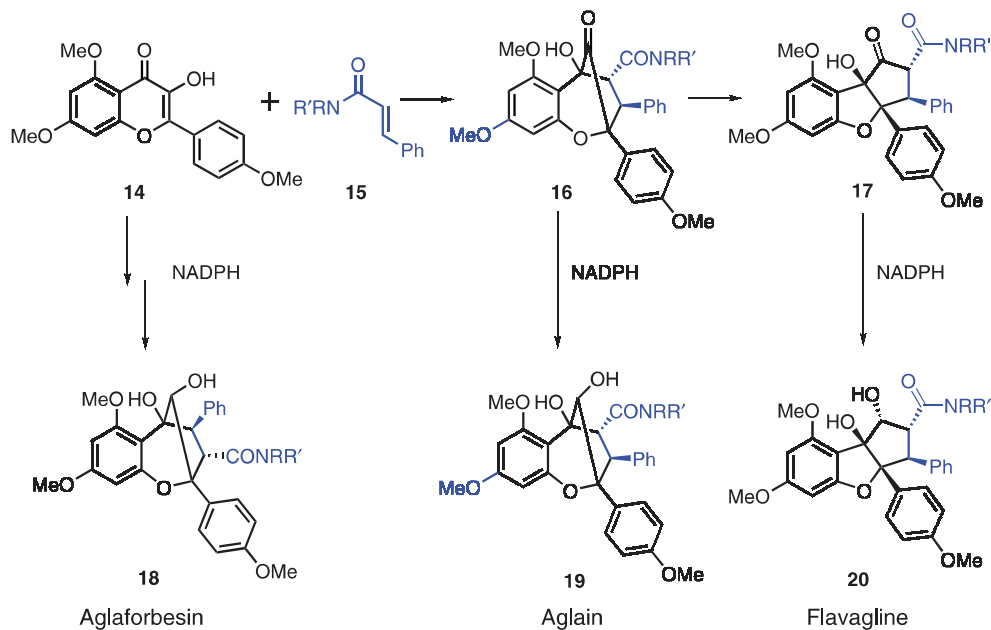


Figure 7.1 Representative natural (1–6) and synthetic (7–13) flavaglines.



Scheme 7.1 Hypothetical biosynthesis of flavaglines and related aglaforbesins and aglains.

7.3

Synthesis of Flavaglines

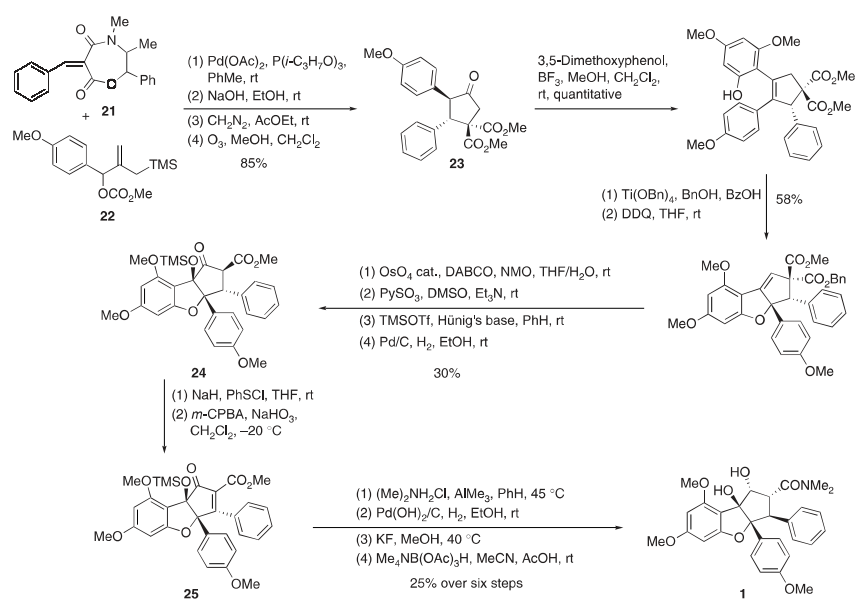
7.3.1

Chemical Syntheses

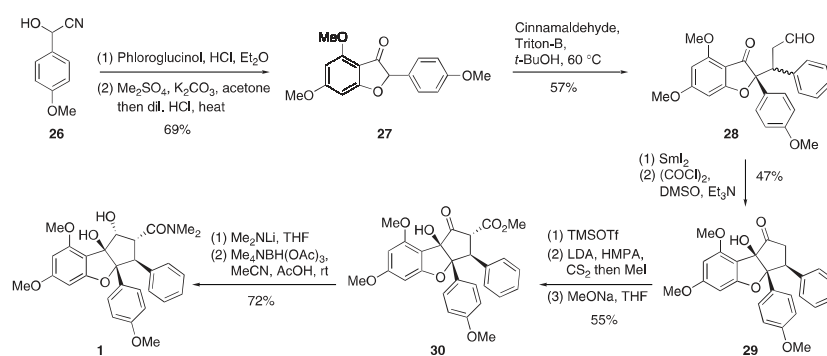
The first total synthesis of a flavagline, rocaglamide (**1**), was described in 1990 by Trost *et al.* [12]. Since then, multiple laboratories were attracted by this challenge due to the complexity of this structure characterized by two contiguous quaternary chiral centers and two adjacent aryl groups in *cis*-orientation on the cyclopentane ring (Scheme 7.2).

Trost's approach relies on the enantioselective [3+2]-cycloaddition of a trimethylenemethane derivatives generated from **22** with the oxazepinedione **21** (Scheme 7.2). Subsequent transformations, including the condensation of 3,5-dimethoxyphenol to cyclopentanone **23**, gave access to the flavaglines' skeleton but with an incorrect configuration compared to the natural product. Six additional steps afforded rocaglamide (**1**) with the desired stereochemistry via a dehydro-intermediate **25**. Despite these long and multiple steps, this synthesis remains the only enantiospecific one to date.

Since Trost's synthesis, more than 10 syntheses of flavaglines have been described. In 1992, Taylor *et al.* developed a racemic synthesis of rocaglamide



Scheme 7.2 Trost's enantioselective synthesis of rocaglamide [12].



Scheme 7.3 Taylor's synthesis of rocaglamide (1) [13].

which was later improved by Dobler's group in 2001 [13, 14]. Taylor's strategy begins with a Hoesch reaction between cyanohydrin **26** and phloroglucinol to afford benzofuranone **27** (Scheme 7.3) [13]. Aldehyde **28**, obtained by a Michael addition, was converted to the cyclopentanone **29** after cyclization and Swern oxidation. Silylation was followed by enolate formation, sequential addition of carbon disulfide and iodomethane, and treatment with sodium methoxide gave β -keto ester **30**, which was converted to rocaglamide (**1**) in the next two steps.

Dobler and colleagues [14] modified the previous strategy using cyanohydrin **31** in an umpolung reaction to generate the cyclopentanone **29** (Scheme 7.4) after deprotection. This ketone was treated with Stiles' reagent to give the ester **30**, which was then transformed into rocaglamide (**1**) in three steps.

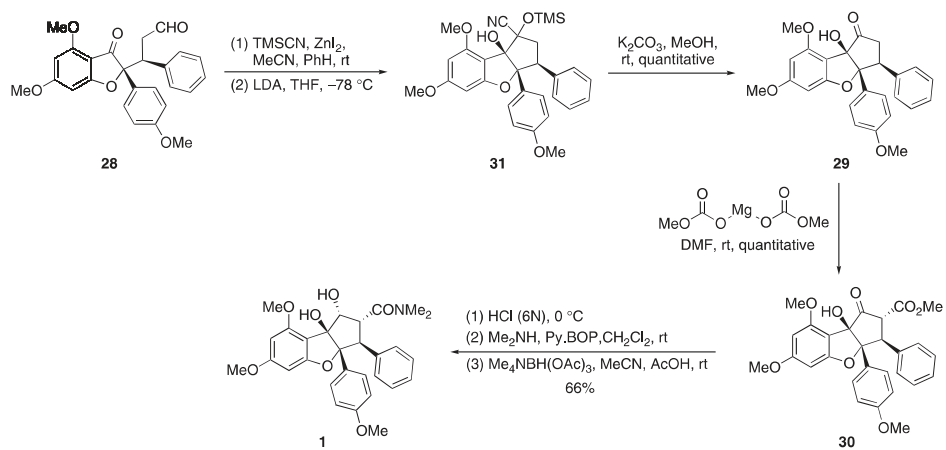
In 2008, Qin and his group [15] further modified Taylor's synthesis by introducing a methoxycarbonyl to the Michael acceptor, therefore circumventing Stiles carboxylation. Condensation of benzofuranone **27** with the dimethyl 2-benzylidenemalonate afforded the adduct **32**, which underwent a pinacol coupling promoted by SmI_2 giving access to **30** (Scheme 7.5).

In 2004, Ragot's group [16] published a synthesis of flavaglines based on an intramolecular hydroxyepoxide opening. Cyclopentenone **35** was obtained in two steps from bromoketone **33** and triphenylphosphorane **34**. Heating β -ketoester **35** in dimethyl sulfoxide (DMSO), followed by α -bromination and elimination of HBr afforded the α -bromo enone **36** (Scheme 7.6). Suzuki reaction with boronate **37** provided didemethoxyrocaglaol **40** upon diastereoselective reduction, epoxydation, and hydrogenation with spontaneous cyclization via intermediate **39**.

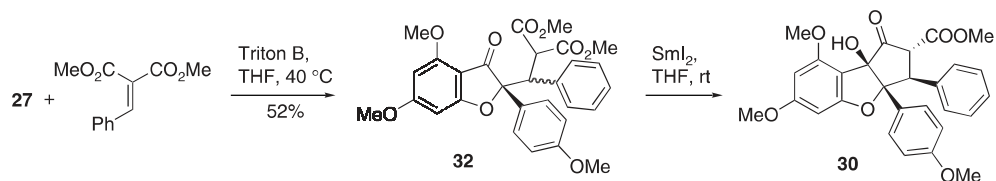
In 2009, Frontier and coworkers [17] established a new synthetic route to flavaglines based on a Nazarov-type reaction. The investigators used the benzofuranone **27** as a starting material, similarly to Taylor and Dobler. Alkylation with vinyl magnesium bromide and cleavage of the resulting alcohol provided the aldehyde **41** (Scheme 7.7). After introduction of the phenylacetylene moiety and protection of the propargylic alcohol, compound **42** was deprotonated with *tert*-butyllithium and quenched with *n*- Bu_3SnCl to afford the key intermediate **43**. The tricyclic skeleton of flavaglines was obtained by a Nazarov-type cyclization from highly reactive allenyl oxide **45** generated *in situ* with *m*-CPBA. The tributylstannyl group was cleaved off during this oxidation-ring closure reaction. The resulting intermediate **46** gave access to ketoester **30** using palladium-mediated carbonylation.

Magnus and his group developed another synthesis of flavaglines also based on a Nazarov reaction. Intermediate **50** was prepared in six steps from the alkyne **48** (Scheme 7.8) [18]. Treatment of compound **50** with SnCl_4 induced its cyclization to afford the cyclopentenone **51**. Subsequent hydrosilylation, palladium-mediated introduction of a carboxymethyl group, and hydroxylation afforded the methyl rocaglate **54**.

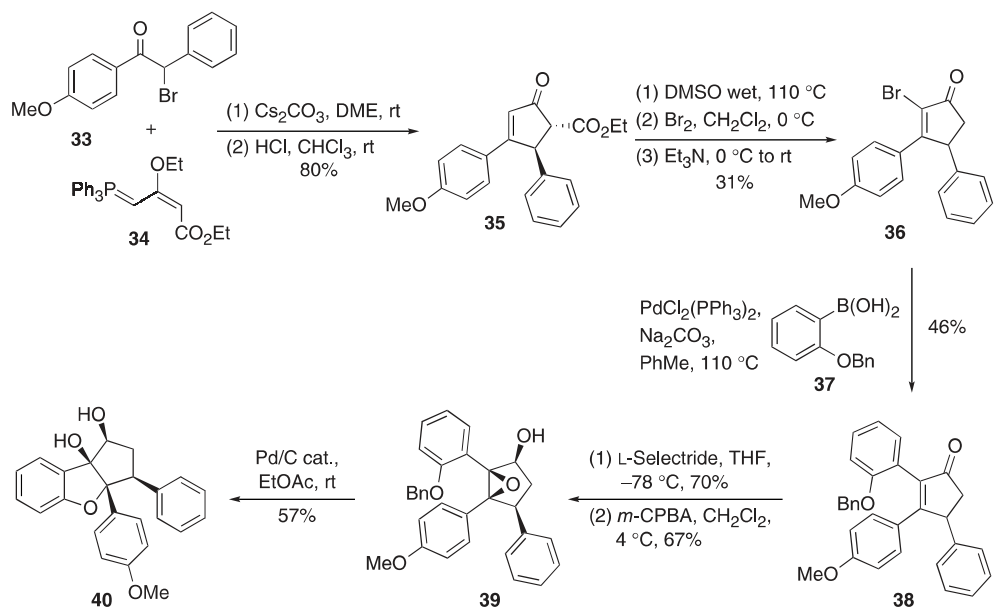
In 2012, Magnus' group [19] improved their synthesis of methyl rocaglate with an unprecedented Nazarov reaction promoted by acetyl bromide. The dienone **56**



Scheme 7.4 Dobler's racemic synthesis of rocaglamide [14].



Scheme 7.5 Qin's synthesis of rocaglamide [15].



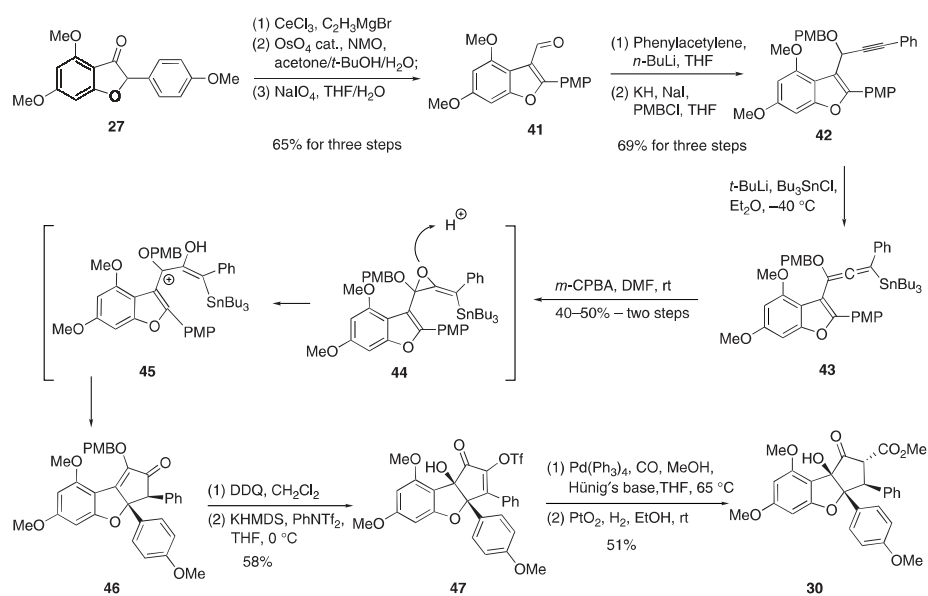
Scheme 7.6 Ragot's synthesis of flavagline skeleton [16].

was converted into the intermediate **57** with 81% yield (Scheme 7.9). Cyclopentenone **58** was then transformed into dehydroflavagline **59** in six steps, which afforded methyl rocaglate in two steps following Trost's strategy.

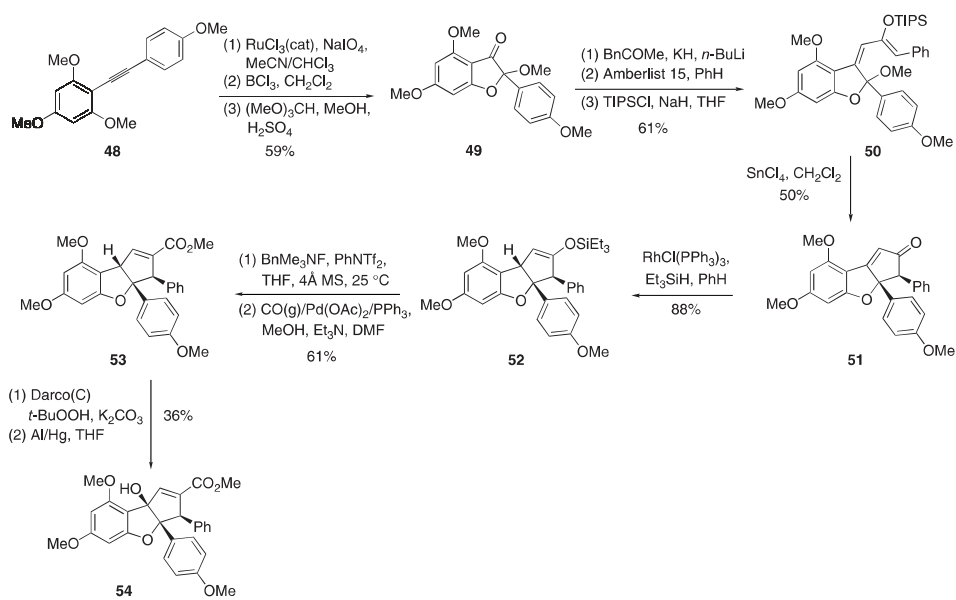
7.3.2

Biomimetic Synthesis of Flavaglines

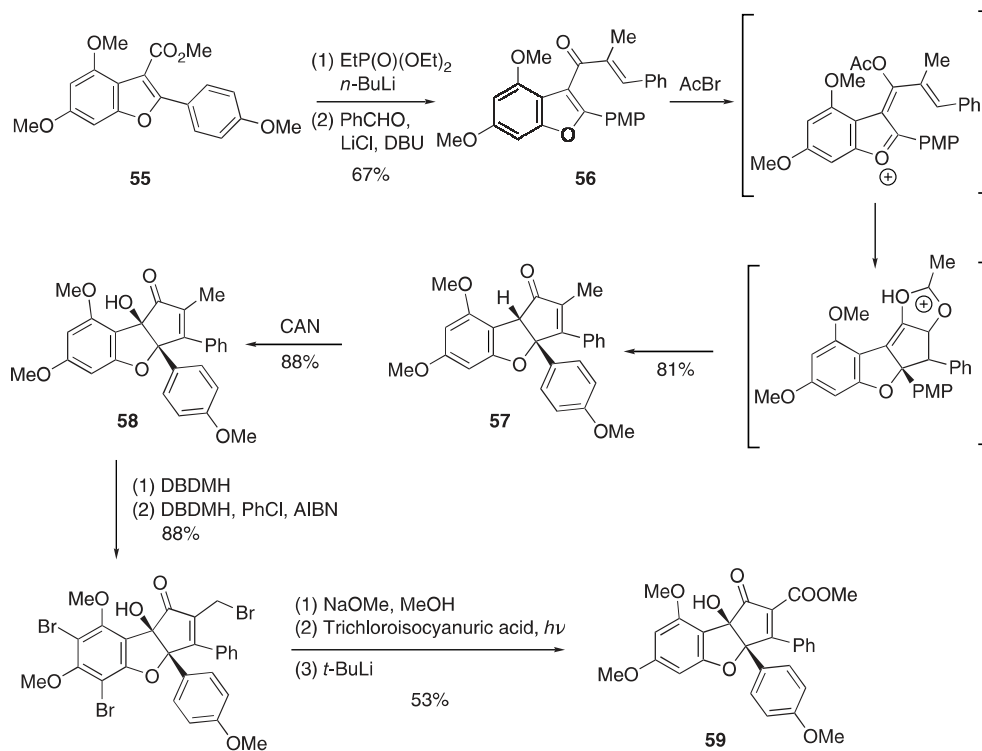
On the basis of Proksch's [6] proposal for biosynthesis (Scheme 7.1), in 2004, Porco reported biomimetic synthesis of flavaglines from 3-hydroxyflavones and cinnamic esters using photochemistry (Scheme 7.10) [20]. Irradiation of **14** with **60** gave the adduct **61** through a [3+2]-cycloaddition reaction. A β -acyloin rearrangement of this intermediate in basic conditions gave the cyclopentanone **62** which upon diastereoselective reduction gave methyl rocaglate **63**. In 2012,



Scheme 7.7 Frontier's synthesis of rocaglamide based on a Nazarov reaction [17].



Scheme 7.8 Magnus' synthesis to access flavaglines [18].



Scheme 7.9 Magnus' synthesis of methyl rocaglate by acetyl bromide-mediated Nazarov reaction [19].

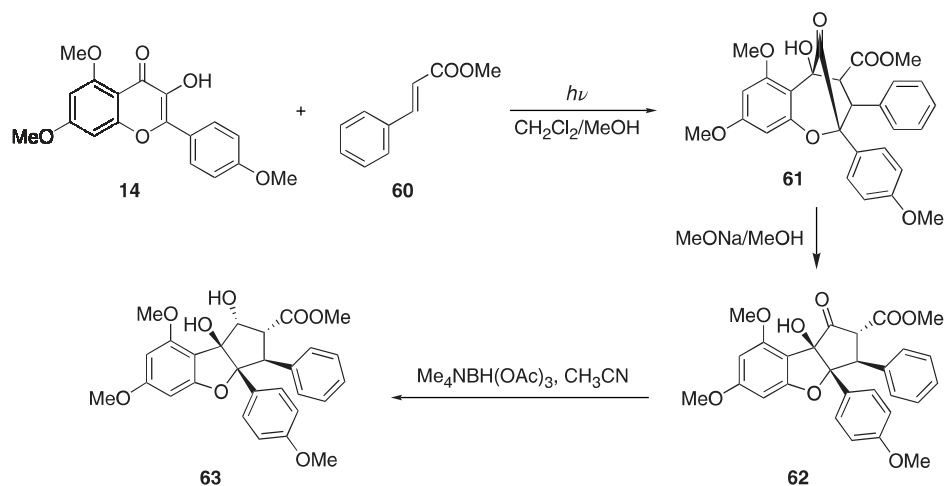
the same group of investigators developed a chiral version of this approach using the TADDOL (α,α,α -tetraaryl-1,3-dioxolane-4,5-dimethanol) derivative to prepare **61** in 69% yield and 85.5 : 14.5 er [21].

7.3.3

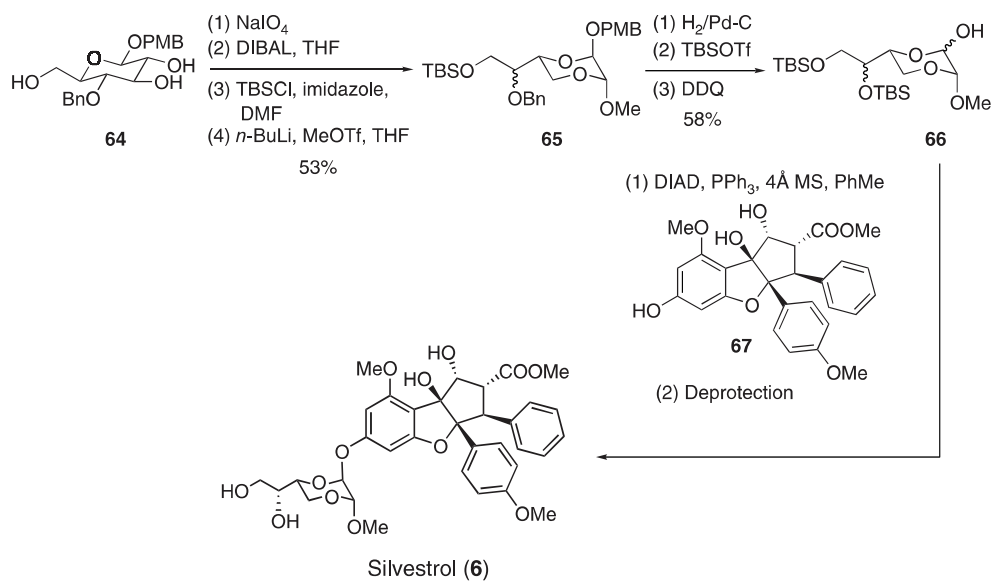
Synthesis of Silvestrol (**6**)

In 2007, in the same issue of *Angewandte Chemie* Porco's and Rizzacasa's groups published a total synthesis of silvestrol (**6**), a flavagline substituted by a pseudo-sugar. Both teams used the [3+2]-photocycloaddition to prepare the cyclopenta[*b*]benzofuran core of the molecules [22, 23]. The main difference between Porco's and Rizzacasa's approaches lies in the synthesis of the 1,4-dioxanyloxy intermediate.

Rizzacasa and collaborators [22] conceived their approach on the basis of the periodic cleavage of *D*-glucose derivative **64** (Scheme 7.11). Reduction of this intermediate with DIBAL, followed by protection with TBSCl, and O-methylation



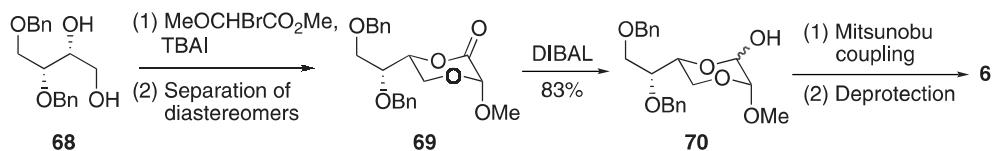
Scheme 7.10 Porco's biomimetic synthesis of rocaglamide [20].



Scheme 7.11 Rizzacasa's synthesis of silvestrol 6 [22].

afforded **65**, which was transformed into lactol **66**. A Mitsunobu reaction with compound **67** and deprotection yielded silvestrol **6**.

On the other hand, Porco and his group [23] condensed diol **68** with 2-bromo-2-methoxy acetate to obtain lactone **69**, which after reduction with DIBAL, yielded the lactol **70** (Scheme 7.12).



Scheme 7.12 Porco's synthesis of silvestrol **6** [23].

7.4

Pharmacological Properties of Flavaglines

7.4.1

Anticancer Activity

Rocaglamide (**1**) was shown to display a potent *in vivo* antileukemic activity right from its discovery [3]. Thereafter, a similar compound, methyl 4'-demethoxy-3',4'-methylenedioxyrocaglate (**3**) was found to delay for 3 weeks the growth of BC1 breast tumor implanted in athymic mice [24]. Because the tumors were not eradicated, flavaglines remained aloof from mainstream research works, which were mainly dedicated at that time to cytotoxic agents. The emergence of targeted therapies in the following decade modified the evaluation of the therapeutic potential of cytostatic agents, which prompted flavaglines to exit from limbo [25]. In many murine cancer models, flavaglines increased lifetime by one to several weeks and potentiated the efficacy of other anticancer agents (Table 7.1). Probably, the most impressive result was observed by Pelletier and colleagues who showed that silvestrol suppresses the growth of xenografted breast tumors addicted to eIF4A (eukaryotic initiation factor-4A) signaling [26]. Additional studies indicated that flavaglines might be particularly beneficial to alleviate the resistance to other chemotherapeutic agents (Table 7.1).

The scaffold proteins prohibitins-1 and 2 (PHB1, PHB2) were identified as molecular targets of flavaglines by Li-Weber and colleagues [39] at the German Cancer Research Center (DKFZ). PHB1 and PHB2 form heterodimers and oligomers with each other and also with numerous other signaling proteins [40]. PHB functions are regulated by the signaling of insulin, IGF1 (insulin-like growth factor), EGF (endothelial growth factor), TGF- β (transforming growth factor), and IgM (immunoglobulin M) receptors and also by the kinases Akt, CamK (calmodulin-dependent protein kinase) IV, and PKC- δ . These posttranslational modifications impact intracellular localization of PHBs by affecting their affinity for specific lipids. PHBs are essential to maintain the structural and functional integrity of mitochondria. In the nucleus, PHBs control DNA synthesis and transcription by interacting with many transcription factors, histone deacetylases, histone methyltransferases, transcriptional corepressors, and minichromosome maintenance (MCM) proteins. In addition, PHBs regulate many cytoplasmic

Table 7.1 *In vivo* activity of flavaglines in murine cancer models.

Compound	Murine model of cancer/ observed effects/(doses)	References
Rocaglamide (1)	P388 lymphocytic leukemia/increase in lifetime: T/C ^a of 156%/(1 mg kg ⁻¹)	[3]
Rocaglamide (1)	AsPC-1 metastatic pancreatic cancer/suppression of tumor growth (T/C of 37%) and significant increase in lifetime/(5 mg kg ⁻¹)	[27]
<i>N</i> -Desmethyl-rocaglamide	RMA T lymphoma/potential of the effects of concanavalin A (otherwise inactive) to significantly inhibit tumor progression/(2.5 mg kg ⁻¹ <i>i.p.</i> three times a week for 2 weeks)	[28]
Rohinitib (7)	M091 human myeloid leukemia cells/inhibition of tumor growth and suppression of glucose uptake/(1 mg kg ⁻¹ <i>i.p.</i> 4 consecutive days a week for 3 weeks)	[29]
10	E μ -Myc/(myr)Akt lymphomacells/potential of the effects of doxorubicin (otherwise inactive): increase in lifetime by 9 days/(0.2 mg kg ⁻¹ <i>i.p.</i> daily for 5 days)	[30]
Silvestrol (6)	L3.6pl pancreatic cancer and RPMI-8226 myeloma/absence of significant effect/(0.2 mg kg ⁻¹ <i>i.p.</i> , 5 days/week)	[31]
Silvestrol (6)	E μ -Myc/(myr)Akt lymphoma/potential of the effects of doxorubicin (otherwise inactive): increase in lifetime by 7 days (used in monotherapy, silvestrol did not display any significant effect)/(0.2 mg kg ⁻¹ <i>i.p.</i> daily for 5 days)	[30]
Silvestrol (6)	P388 leukemia/increase in lifespan corresponding to a T/C of 150%/(2.5 mg kg ⁻¹ <i>i.p.</i> for 5 days)	[32]
Silvestrol (6)	PC3 prostate cancer/reduction of the mean tumor weight by 60%/(3 mg kg ⁻¹ <i>i.p.</i> three times per week for 3 weeks)	[33]
Silvestrol (6)	Pten ⁺ /E μ -Myc lymphoma/potential of the effects of doxorubicin: increase in lifetime by 5 days compared to doxorubicin alone (silvestrol alone was inactive)/(0.2 mg kg ⁻¹ <i>i.p.</i> daily for 5 days)	[34]
Silvestrol (6)	E μ -Myc/eIF4E lymphoma/potential of the effects of doxorubicin: increase in lifetime by 16 days compared to doxorubicin alone (silvestrol alone was inactive)/(0.2 mg kg ⁻¹ <i>i.p.</i> daily for 5 days)	[34]
Silvestrol (6)	E μ - <i>Tcl-1</i> chronic lymphocytic leukemia Significant reduction in B-cell number (1.5 mg kg ⁻¹ <i>i.p.</i> per day for 5 days)	[35]

(continued overleaf)

Table 7.1 (Continued)

Silvestrol (6)	697 B-ALL acute lymphoblastic leukemia Increase in lifetime by more than 2 weeks (1.5 mg kg ⁻¹ <i>i.p.</i> every other day)	[35]
Silvestrol (6)	MDA-MB-231 breast cancer/considerable suppression of tumor growth after more than 75 days/(0.5 mg kg ⁻¹ <i>i.p.</i> daily for 8 consecutive days)	[26]
Silvestrol (6)	PC-3 prostate cancer/considerable suppression of tumor growth after more than 50 days/(0.5 mg kg ⁻¹ <i>i.p.</i> daily for 8 consecutive days)	[26]
Silvestrol (6)	MV4-11 acute myeloid leukemia/increase in lifetime by more than 1 month impressively, 30% were still alive 74 days after engraftment (all vehicle-treated mice were dead 31 days after engraftment)/(1.5 mg kg ⁻¹ <i>i.p.</i> every other day for 3 weeks)	[34]
Silvestrol (6)	E μ -Myc/Tsc2 ^{-/-} /PIM2 lymphoma/potential of the effects of rapamycin: increase in lifetime by 6 days compared to rapamycin alone/(0.2 mg kg ⁻¹ <i>i.p.</i> daily for 7 days)	[36]
Silvestrol (6)	Mantle cell lymphoma/increase in lifetime by 2 weeks/(1.5 mg kg ⁻¹ <i>i.p.</i> every other day)	[37]
FL23 (12)	3LL lung carcinoma/significant suppression of tumor growth/(25 mg kg ⁻¹ <i>i.p.</i> twice a week for 17 days)	[38]

a) T/C: Treated versus control.

Source: Adapted from Ref. [6] with permission of Future Science Ltd.

proteins such as the kinases C-Raf, Akt, and MLK2, the phosphatase Shp1/2, the chaperones Hsp70, and mortalin/Grp75 or the phospholipase C γ 2 [40].

Activation of the kinase C-Raf by Ras requires a direct interaction with PHBs, which can be disrupted by flavaglines (Figure 7.2) [39]. Their anticancer activities could thus be partially explained by the inhibition of Ras-C-Raf-MEK-ERK (extracellular-signal-regulated kinase) signaling, which is constitutively activated in many human cancers [41]. This observation that binding of flavaglines to PHBs prevents their interaction with C-Raf has recently been confirmed by Chen, He, and collaborators in the context of pancreatic ductal adenocarcinoma (PDAC) [27]. In PDAC, constitutive activation of C-Raf is the result of constitutive mKRAS activity, the most common oncogenic mutation in PDAC. The investigators also found that in highly malignant AsPC-1 human PDAC cell lines, PHB1 was over-expressed and mainly localized in the plasma membrane and cytosol, whereas in poorly malignant Capan-2 PDAC cells, PHB1 was poorly expressed and uniformly distributed within the cells. Rocaglamide was found to exert a strong inhibitory effect against ERK1/2 activities in AsPC-1 cells, reducing phosphorylation of the

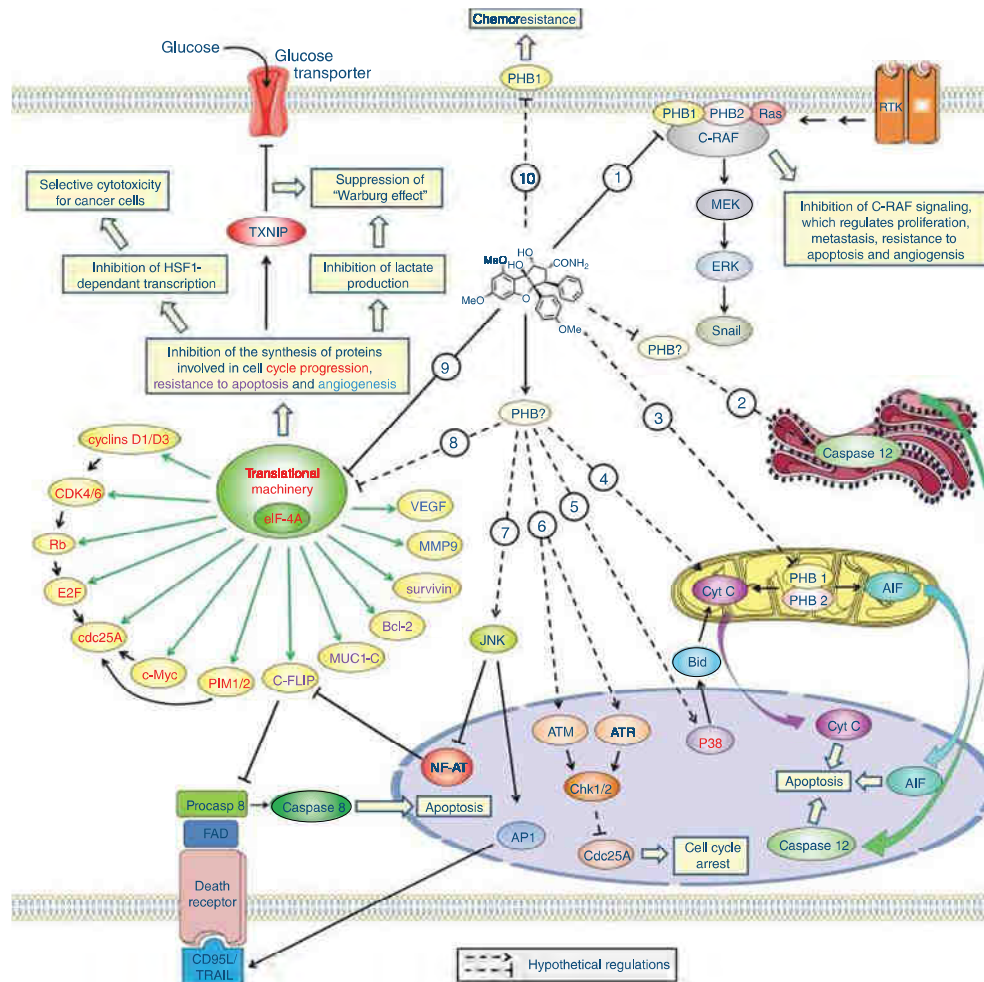


Figure 7.2 Anticancer mechanisms of flavaglines. 1. Inhibition of the Ras-dependent C-Raf activation. 2, 3. Translocation of caspase-12 and AIF to the nucleus to induce apoptosis. 4. Translocation of cytochrome C to the nucleus to induce the intrinsic apoptotic pathway. 5. Activation of p38-mediated transcription of the pro-apoptotic Bcl-2 family. 6. Induction of the ATM/ATR-Chk1/2-Cdc25A pathway leading to cell cycle arrest. 7. Activation of JNK-dependent transcription of the pro-apoptotic proteins CD95 ligand and c-FLIP. 8. Hypothetical PHB-dependent inhibition of the

translational machinery. 9. Inhibition of eIF4A leading to a downregulation of expression of proteins involved in cell cycle progression, resistance to apoptosis and angiogenesis. This inhibition of protein synthesis leads to suppression of the activity of the transcription factor HSF1 and an upregulation of the tumor suppressor TXNIP. TXNIP blocks glucose uptake and consequently prevents the "Warburg effect." 10. Hypothetical inhibition of cell surface PHB1-mediated chemoresistance. (Adapted from Ref. [5] with permission from Elsevier).

transcriptional factor Snail, one of the main promoters of epithelial-mesenchymal transition (EMT). Reversal of the EMT phenotype in these cells was characterized by upregulation of *E*-cadherin and β -catenin and downregulation of vimentin. These *in vitro* effects were also observed *in vivo*. Indeed, rocaglamide prevented the dissemination of cancer cells in the liver and lungs in PDAC-xenografted mice, in addition to significantly inhibiting tumor growth.

The initiation step of protein synthesis is a highly regulated and rate-limiting process that is emerging as a promising target in oncology. Indeed, the synthesis of many factors controlling oncogenesis, angiogenesis, and chemoresistance necessitates the helicase eIF4A. Using affinity chromatography, Rizzacasa and colleagues [42] demonstrated that some flavaglines directly bind to eIF4A. Sadlish and colleagues [43] substantiated this discovery using chemogenomic profiling to validate eIF4A as the main target of flavaglines in yeast. By means of mutagenesis and *in silico* modeling, they identified the binding site of flavaglines and proposed a model to account for the enhancement of eIF4A binding to mRNAs promoted by flavaglines. This action inhibits the recycling of eIF4A leading to an inhibition of cap-dependent translation, which had already been observed by Pelletier and colleagues [26]. Indeed, flavaglines have been reported for several years to inhibit protein synthesis, and in particular the translation of the mRNAs encoding CDK4 (cyclin-dependent kinase), CDK6, cyclins D1 and D3, *cdc25A*, Bcl-2 (B-cell lymphoma 2), survivin, Mcl-1 (myeloid cell leukemia protein 1), the PIM1/2 kinases, *c-Myc*, VEGF (vascular endothelial growth factor), matrix metalloproteinase 9 (MMP9), and MUC1-C [26, 36, 39, 44–46]. It is noteworthy that depletion of the anti-apoptotic proteins Mcl-1 and Bcl-2 was not necessary for the induction of apoptosis by flavaglines in lymphoma cells [47], B-cell malignancy mantle cell lymphoma [37], chronic lymphocytic leukemia, or acute lymphoblastic leukemia [35].

In 2013, Whitesell, Lindquist, and colleagues [29] have reported in *Science* about how the inhibition of protein synthesis selectively impedes the proliferation and survival of cancer cells without affecting normal cells. These authors screened more than 300 000 compounds for the inhibition of the transcriptional factor heat shock factor 1 (HSF1), which is deeply involved in metabolic reprogramming, survival, and proliferation of cancer cells in addition to heat-shock response. Among these compounds, rocaglamide (**1**) was found to be the most potent and selective inhibitor of HSF1 signaling ($IC_{50} \approx 50$ nM). Additional tests with other compounds showed that another flavagline called *rohinitib* (**7**, Figure 7.1) was even more active ($IC_{50} \approx 20$ nM). This molecule inhibited HSF1-dependant transcriptional activity much more effectively in cancer cell lines, than in proliferating nontumorigenic cells. The cascade of events that links the inhibition of protein synthesis to HSF1 signaling remains unknown for the moment. In addition, flavaglines were shown to overturn a metabolic feature in cancer cells called the *Warburg effect*, manifested by an elevated rate of glycolysis and lactic acid production. Rohinitib upregulated the thioredoxin-interacting protein (TXNIP), a tumor suppressor that regulates cellular redox potential and glucose uptake.

This effect on TXNIP leads to a spectacular inhibition of glucose uptake and lactate production in several cancer cell lines.

These authors also showed that wild-type mouse embryonic fibroblasts (MEFs) are less sensitive to rohinib cytotoxicity than mutant MEFs overexpressing HSF1, which are used as a model of premalignant cells with early-stage oncogenic lesions. Cancer cells carry an abnormal number of chromosomes, causing a proteotoxic stress that is attenuated by HSF1 activity. The same authors showed that rohinib is more cytotoxic to trisomic than to wild-type MEFs. Human cancer cell lines with high chromosomal instability were extremely responsive to rohinib. Altogether, these data provide some clues as to decipher why flavaglines are selectively cytotoxic to cancer and immortalized cells without affecting normal cells viability.

It is quite uncommon for structurally complex natural products to target two classes of proteins, even though there are some precedents [2]. Remarkably, both PHBs and eIF4A are over-activated in many malignant tumors and are regarded as promising targets to treat cancers [40, 48].

As far as we know, apoptosis is the only type of cellular death induced by flavaglines in cancer cells. It may occur through the classical intrinsic and extrinsic pathways [22–24] or independently of caspase-3 via the apoptosis-inducing factor (AIF) or caspase-12 [49]. Whether these effects involve PHB1, PHB2, or eIF4A remains unknown. Interestingly, flavagline **10**, developed by Tremblay and coworkers [31] at Infinity Pharmaceuticals, is highly cytotoxic to cancer cells but does not inhibit protein synthesis. This observation indicates that in some cell types, a sole action on PHBs is sufficient to induce apoptosis without involving inhibition of translation.

Several flavaglines have been examined in murine models of cancers. Silvestrol (**6**), which has been the most widely studied, was unfortunately shown to be very susceptible to P-glycoprotein-mediated multidrug resistance [34]. In contrast, compounds that are not substituted at position 2 with an ester or an amide are highly cytotoxic to cancer cells with acquired multidrug resistance (Figure 7.3) [38, 49, 50]. In few murine models of cancer, flavaglines did not display any significant effect [31] but in most instances, they significantly increased lifetime [3, 26, 30, 32, 34–37]. It is noteworthy that in all of these *in vivo* experiments, flavaglines did not show any overt indication of toxicity.

Recently, Li-Weber and collaborators demonstrated that rocaglamide activates the DNA repair pathway (or DNA damage checkpoint) without inducing any significant DNA damage or modifying the redox status of cancer cells. The authors hypothesized that rocaglamide blocks DNA replication promoting the transcription of genes responsive to DNA replication stress. Activation of ATM (ataxia telangiectasia mutated) and ATR (ataxia telangiectasia and Rad3-related) ATM induces ATR Chk1/Chk2 (Chk, checkpoint kinase) phosphorylation, and consequently Cdc25A degradation, which stops the cell cycle at the G1-S transition [50]. Importantly, activation of the ATM/ATR-Chk1/2-Cdc25A pathway that led

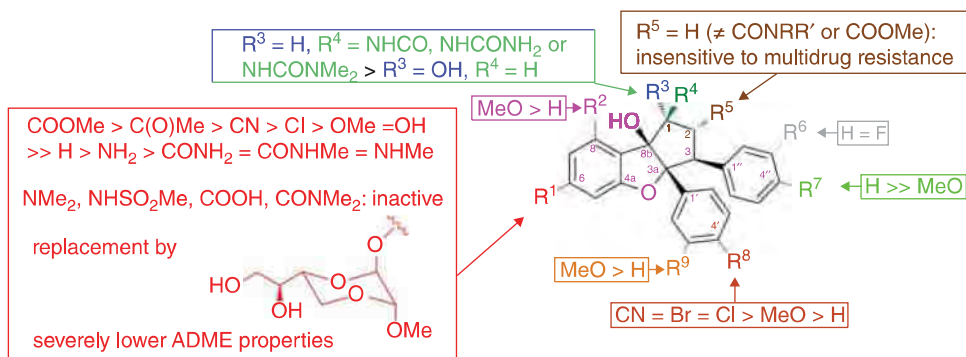


Figure 7.3 Key structure–activity relationship findings related to flavagline antiproliferative activity. (Adapted from Ref. [3] with permission from Elsevier).

to leukemic cell growth inhibition which was not observed in normal proliferating T cells [51]. These findings confirmed the selective cytotoxicity of flavaglines toward malignant cells.

7.4.2

Anti-inflammatory and Immunosuppressant Activities

In addition to their anticancer effect, flavaglines exhibit potent anti-inflammatory properties, which are mediated by activation of the MAP (mitogen-activated protein) kinases, JNK (c-Jun N-terminal kinase), and p38-inhibition of nuclear factor of activated T-cells (NFATs) signaling [52]. At higher doses, flavaglines also block pro-inflammatory NF- κ B (nuclear factor kappa-light-chain-enhancer of activated B cells) signaling, probably through an action on PHBs [53]. Indeed, PHBs are known to be involved in the activation of NF- κ B [54]. Nevertheless, the exact mechanism of action and the molecular target involved in these effects remain undefined.

7.4.3

Cytoprotective Activity

IMD-019064, a flavagline originally developed at Bayer, inhibits the release of pro-inflammatory factors from microglia, astrocytes, and endothelial cells [55]. On the basis of these anti-inflammatory activities, Bayer scientists examined its neuroprotective effects and showed that it protects mice in models of Parkinson's disease and traumatic brain injury. Optimization of this compound yielded IMD-026259 (**11**, Figure 7.1) which is currently undergoing a preclinical trial for the treatment of Parkinson's disease by the company IMD Natural Solutions [56]. Many analogs were patented, but structure–activity relationships (SARs)

data were not revealed. Our own lab also has investigated the neuroprotective activity of flavaglines and identified several derivatives such as FL3 (**9**) and FL23 (**12**) that protect neurons from several stresses more efficiently than IMD-019064 [49]. In the course of our research, we established the first SAR data for neuroprotection. We also showed that flavaglines offer some sort of protection against the neurotoxicity induced by cisplatin, an anticancer medicine [50]. On the basis of these observations, we studied whether flavaglines could protect other tissues from the side effects of anticancer treatments. We focused our attention on anthracyclines such as doxorubicin, which are commonly used anticancer medicines, even though they are highly cardiotoxic [57]. We found that flavaglines protect cardiomyocytes from two totally unrelated types of stress: doxorubicin-induced cardiotoxicity and serum starvation [49]. We also demonstrated that the synthetic flavagline FL3 (**9**, Figure 7.1) greatly lowered mortality induced by doxorubicin [58]. It also reduced cardiac apoptosis and fibrosis. These observations suggest that flavaglines may enhance the efficacy of cancer treatments and at the same time alleviate the cardiac side effects of these treatments. FL3 was shown to induce cytoprotection through a phosphorylative activation of the small heat-shock protein Hsp27, which is a key factor in the resistance of cardiomyocytes to many types of stresses [59]. This observation represents a small piece of the puzzle. Deciphering the mechanisms underlying both cytoprotection in normal cells and cytotoxicity in cancer cells is a fascinating challenge that deserves further in-depth investigation. It is still unclear whether cytoprotection is mediated through PHBs or eIF4A. On one hand, PHBs represent an attractive hypothesis because they display different functions and intracellular localizations in cancer and normal cells [40]. In addition, some flavaglines that do not inhibit protein synthesis display potent neuro- and cardioprotective activities (unpublished data). On the other hand, Jerry Pelletier and colleagues showed that a pretreatment with rohitib protects *in vitro* hair follicle cells against the apoptosis induced by paclitaxel in a model of chemotherapy-induced alopecia (hair loss) [60]. This protection against paclitaxel-induced apoptosis was shown to be due to a transient suppression of translation initiation. Unfortunately, this effect was not translated *in vivo*: rohitib failed to protect mice against cyclophosphamide-induced alopecia.

7.4.4

Antimalarial Activities

Recently Julia Walochnik and collaborators [61] showed that two flavaglines, rocaglamide and aglafoline, display some antimalarial activities that are intermediate between those of artemisinin and quinine. However, these promising results remain to be validated *in vivo* before their antimalarial potential can be examined in detail.

7.5

Structure–Activity Relationships (SARs)

In addition to data that were obtained with natural compounds, a few laboratories have synthesized flavaglines to explore the structural requirements for their anticancer properties. Considering that extensive description of SAR data has recently been reviewed (Figure 7.3), we will disclose only its most striking features [8]. Martin Tremblay and colleagues from Infinity Pharmaceuticals synthesized many derivatives of silvestrol and confirmed that flavaglines substituted by a pseudo-sugar suffer poor ADME (absorption, distribution, metabolism, and excretion) properties that preclude their development as a medicine [31]. This group disclosed for the first time the SAR for both cytotoxicity and inhibition of translation. Interestingly, both of these activities followed the same trends, suggesting that inhibition of cap-dependent translation is a critical component of the mechanism involved in cytotoxicity. However, these authors identified demethoxy-methyl ester rocaglate **10** (Figure 7.1), which displays a strong cytotoxicity without inhibiting translation, suggesting another mechanism of action, probably involving PHBs.

Many flavaglines are sensitive to multidrug resistance mediated by efflux pumps. Our group showed that the deletion of the amide moiety in rocaglamide derivatives leads to rocaglaol analogs that are totally insensitive toward multidrug resistance [49].

The structural requirements for cytoprotection have been disclosed in only one article so far [50]. These SARs are close to those for cytotoxicity in cancer cells, even though some slight differences have been observed in the relative ranking of activity. Direct evaluation of the activity on PHB signaling and inhibition of eIF4A would greatly contribute to better characterize the structural requirements of flavaglines for their various pharmacological activities.

7.6

Concluding Remarks

Flavaglines hold a great potential as a new class of therapeutics, but much basic research is still required before initiation of clinical trials. In oncology, it is crucial to identify why some tumors more responsive to flavagline treatments than others are. This knowledge would greatly optimize the design of clinical assays through the stratification of patients based on predictive biomarkers, such as the overexpression of PHBs, PHB-interacting proteins, or an addiction to eIF4A signaling.

Even though the mode of action of cytoprotection remains poorly understood, it is for the treatment of Parkinson's disease that flavaglines are the closest to reaching clinical trials. Indeed, the German Company IMD Natural Solution is, as far as

we know, the most advanced to initiate a clinical trial for this ailment with IMD-026259 [56].

PHBs are emerging as key regulators of cell metabolism, development, and survival that integrate multiple internal and external signals. More than 50 proteins have been shown to directly interact with PHBs, and this number is constantly growing. Identifying new physiological and pathophysiological functions of PHBs may provide novel therapeutic intervention for additional types of diseases.

Up to now, structures of the disclosed flavaglines analogs remain close to those of the natural compounds. Only the carbaisostere **13** developed by Novartis scientists (Figure 7.1) has been published. The absence of a corresponding patent suggests that it may not be pharmacologically active. However, the cyclopenta[*b*]benzofuran core would likely need to be modified to generate patentable molecules that could advance toward clinical assays.

Abbreviations

ADME	absorption, distribution, metabolism, and excretion
AIF	apoptosis-inducing factor
ATM	ataxia telangiectasia mutated
ATR	ataxia telangiectasia and Rad3-related
Bcl-2	B-cell lymphoma 2
CamK	calmodulin-dependent protein kinase
CDK	cyclin-dependent kinase
Chk	checkpoint kinase
DBDMH	1,3-dibromo-5,5-dimethylhydantoin
eIF4A	eukaryotic initiation factor-4A
EMT	epithelial-mesenchymal transition
ERK	extracellular-signal-regulated kinase
HSF	heat shock factor
IGF	insulin-like growth factor
IgM	immunoglobulin M
JNK	c-Jun N-terminal kinases
MAP	mitogen-activated protein
MCM	minichromosome maintenance
Mcl-1	myeloid cell leukemia protein 1
MEFs	mouse embryonic fibroblasts
NFAT	nuclear factor of activated T-cells
NF- κ B	nuclear factor kappa-light-chain-enhancer of activated B cells
PDAC	pancreatic ductal adenocarcinoma
PHB	prohibitin
SAR	structure–activity relationships
TADDOL	α,α,α -tetraaryl-1,3-dioxolane-4,5-dimethanol

TGF transforming growth factor
 TXNIP thioredoxin-interacting protein
 VEGF vascular endothelial growth factor

References

1. Swinney, D.C. and Anthony, J. (2011) How were new medicines discovered? *Nat. Rev. Drug Discovery*, **10** (7), 507–519.
2. Basmadjian, C., Zhao, Q., Djehal, A., Bentouhami, E., Nebigil, C., Johnson, R., Serova, M., de Gramont, A., Faivre, S., Raymond, E., and Désaubry, L. (2014) Cancer wars: the natural products strike back. *Front. Chem.*, **2**, 20.
3. King, M.L., Chiang, C.C., Ling, H.C., Fujita, E., Ochiai, M., and McPhail, A.T. (1992) X-Ray crystal structure of rocaglamide, a novel antileukemic 1H-cyclopenta[b]benzofuran from *Aglaia elliptifolia*. *Chem. Commun.*, 1150–1151.
4. Hausott, B., Greger, H., and Marian, B. (2004) Flavaglines: a group of efficient growth inhibitors block cell cycle progression and induce apoptosis in colorectal cancer cells. *Int. J. Cancer*, **109** (6), 933–940.
5. Ribeiro, N., Thuaud, F., Nebigil, C., and Désaubry, L. (2012) Recent advances in the biology and chemistry of the flavaglines. *Bioorg. Med. Chem.*, **20** (6), 1857–1864.
6. Proksch, P., Edrada, R., Ebel, R., Bohnenstengel, F., and Nugroho, B. (2001) Chemistry and biological activity of rocaglamide derivatives and related compounds in *Aglaia* species (Meliaceae). *Curr. Org. Chem.*, **5**, 923–938.
7. Kinghorn, A.D., Chin, Y.W., and Swanson, S.M. (2009) Discovery of natural product anticancer agents from biodiverse organisms. *Curr. Opin. Drug Discovery Dev.*, **12** (2), 189–196.
8. Basmadjian, C., Thuaud, F., Ribeiro, N., and Désaubry, L. (2013) Flavaglines: potent anticancer drugs that target prohibitins and the helicase eIF4A. *Future Med. Chem.*, **5** (18), 2185–2197.
9. Ebada, S.S., Lajkiewicz, N., Porco, J.A. Jr., Li-Weber, M., and Proksch, P. (2011) Chemistry and biology of rocaglamides (=flavaglines) and related derivatives from *Aglaia* species (Meliaceae). *Prog. Chem. Org. Nat. Prod.*, **94**, 1–58.
10. Brader, G., Vajrodaya, S., Greger, H., Bacher, M., Kalchhauser, H., and Hofer, O. (1998) Bisamides, lignans, triterpenes, and insecticidal cyclopenta[b]benzofurans from *Aglaia* species. *J. Nat. Prod.*, **61** (12), 1482–1490.
11. Nugroho, B.W., Edrada, R.A., Wray, V., Witte, L., Bringmann, G., Gehling, M., and Proksch, P. (1999) An insecticidal rocaglamide derivatives and related compounds from *Aglaia odorata* (Meliaceae). *Phytochemistry*, **51** (3), 367–376.
12. Trost, B.M., Greenspan, P.D., Yang, B.V., and Saulnier, M.G. (1990) An unusual oxidative cyclization. A synthesis and absolute stereochemical assignment of (-)-rocaglamide. *J. Am. Chem. Soc.*, **112** (24), 9022–9024.
13. Davey, A.E., Schaeffer, M.J., and Taylor, R.J.K. (1992) Synthesis of the novel anti-leukaemic tetrahydrocyclopenta[b]benzofuran, rocaglamide and related synthetic studies. *J. Chem. Soc., Perkin Trans. 1*, (20), 2657–2666.
14. Dobler, M.R., Bruce, I., Cederbaum, F., Cooke, N.G., Diorazio, L.J., Hall, R.G., and Irving, E. (2001) Total synthesis of (±)-rocaglamide and some aryl analogues. *Tetrahedron Lett.*, **42** (47), 8281–8284.
15. Li, H., Fu, B., Wang, M.A., Li, N., Liu, W.J., Xie, Z.Q., Ma, Y.Q., and Qin, Z. (2008) Total synthesis and biological activity of (±)-rocaglamide and its 2,3-di-epi analogue. *Eur. J. Org. Chem.*, (10), 1753–1758.

16. Thede, K., Diedrichs, N., and Ragot, J.P. (2004) Stereoselective synthesis of (\pm)-rocaglaol analogues. *Org. Lett.*, **6** (24), 4595–4597.
17. Malona, J.A., Cariou, K., and Frontier, A.J. (2009) Nazarov cyclization initiated by peracid oxidation: the total synthesis of (\pm)-rocaglamide. *J. Am. Chem. Soc.*, **131** (22), 7560–7561.
18. Magnus, P. and Stent, M.A.H. (2005) Stereospecific synthesis of (\pm)-1,2-anhydro methyl rocaglate. *Org. Lett.*, **7** (18), 3853–3855.
19. Magnus, P., Freund, W.A., Moorhead, E.J., and Rainey, T. (2012) Formal synthesis of (\pm)-methyl rocaglate using an unprecedented acetyl bromide mediated Nazarov reaction. *J. Am. Chem. Soc.*, **134** (14), 6140–6142.
20. Gerard, B., Jones, G., and Porco, J.A. (2004) A biomimetic approach to the rocaglamides employing photogeneration of oxidopyryliums derived from 3-hydroxyflavones. *J. Am. Chem. Soc.*, **126** (42), 13620–13621.
21. Lajkiewicz, N.J., Roche, S.P., Gerard, B., and Porco, J.A. (2012) Enantioselective photocycloaddition of 3-hydroxyflavones: total syntheses and absolute configuration assignments of (+)-ponapensin and (+)-elliptifoline. *J. Am. Chem. Soc.*, **134** (31), 13108–13113.
22. El Sous, M., Khoo, M.L., Holloway, G., Owen, D., Scammells, P.J., and Rizzacasa, M.A. (2007) Total synthesis of (–)-episilvestrol and (–)-silvestrol. *Angew. Chem. Int. Ed.*, **46** (41), 7835–7838.
23. Gerard, B., Cencic, R., Pelletier, J., and Porco, J.A. (2007) Enantioselective synthesis of the complex rocaglate (–)-silvestrol. *Angew. Chem. Int. Ed.*, **46** (41), 7831–7834.
24. Lee, S.K., Cui, B., Mehta, R.R., Kinghorn, A.D., and Pezzuto, J.M. (1998) Cytostatic mechanism and antitumor potential of novel 1H-cyclopenta[b]benzofuran lignans isolated from *Aglaia elliptica*. *Chem. Biol. Interact.*, **115** (3), 215–228.
25. Gutierrez, M.E., Kummar, S., and Giaccone, G. (2009) Next generation oncology drug development: opportunities and challenges. *Nat. Rev. Clin. Oncol.*, **6** (5), 259–265.
26. Cencic, R., Carrier, M., Galicia-Vazquez, G., Bordeleau, M.-E., Sukarieh, R., Bourdeau, A., Brem, B., Teodoro, J.G., Greger, H., Tremblay, M.L., Porco, J.A. Jr., and Pelletier, J. (2009) Antitumor activity and mechanism of action of the cyclopenta[b]benzofuran, silvestrol. *PLoS ONE*, **4** (4), e5223.
27. Luan, Z., He, Y., Alattar, M., Chen, Z., and He, F. (2014) Targeting the prohibitin scaffold-CRAF kinase interaction in RAS-ERK-driven pancreatic ductal adenocarcinoma. *Mol. Cancer*, **13** (1), 38.
28. Zhu, J.Y., Giaisi, M., Kohler, R., Muller, W.W., Muhleisen, A., Proksch, P., Krammer, P.H., and Li-Weber, M. (2009) Rocaglamide sensitizes leukemic T cells to activation-induced cell death by differential regulation of CD95L and c-FLIP expression. *Cell Death Differ.*, **16** (9), 1289–1299.
29. Santagata, S., Mendillo, M.L., Tang, Y.-C., Subramanian, A., Perley, C.C., Roche, S.P., Wong, B., Narayan, R., Kwon, H., Koeva, M., Amon, A., Golub, T.R., Porco, J.A. Jr., Whitesell, L., and Lindquist, S. (2013) Tight coordination of protein translation and HSF1 activation supports the anabolic malignant state. *Science*, **341** (6143), 1238303.
30. Rodrigo, C.M., Cencic, R., Roche, S.P., Pelletier, J., and Porco, J.A. (2012) Synthesis of rocaglamide hydroxamates and related compounds as eukaryotic translation inhibitors: synthetic and biological studies. *J. Med. Chem.*, **55** (1), 558–562.
31. Liu, T., Nair, S.J., Lescarbeau, A., Belani, J., Peluso, S., Conley, J., Tillotson, B., O'Hearn, P., Smith, S., Slocum, K., West, K., Helble, J., Douglas, M., Bahadoor, A., Ali, J., McGovern, K., Fritz, C., Palombella, V.J., Wylie, A., Castro, A.C., and Tremblay, M.R. (2012) Synthetic silvestrol analogues as potent and selective protein synthesis inhibitors. *J. Med. Chem.*, **55** (20), 8859–8878.
32. Hwang, B.Y., Su, B.N., Chai, H., Mi, Q., Kardono, L.B., Afriastini, J.J.,

- Riswan, S., Santarsiero, B.D., Mesecar, A.D., Wild, R., Fairchild, C.R., Vite, G.D., Rose, W.C., Farnsworth, N.R., Cordell, G.A., Pezzuto, J.M., Swanson, S.M., and Kinghorn, A.D. (2004) Silvestrol and episilvestrol, potential anticancer rocaglate derivatives from *Aglaia silvestris*. *J. Org. Chem.*, **69** (10), 3350–3358.
33. Alachkar, H., Santhanam, R., Harb, J.G., Lucas, D.M., Oaks, J.J., Hickey, C.J., Pan, L., Kinghorn, A.D., Caligiuri, M.A., Perrotti, D., Byrd, J.C., Garzon, R., Grever, M.R., and Marcucci, G. (2013) Silvestrol exhibits significant *in vivo* and *in vitro* antileukemic activities and inhibits FLT3 and miR-155 expressions in acute myeloid leukemia. *J. Hematol. Oncol.*, **6**, 21.
34. Gupta, S.V., Sass, E.J., Davis, M.E., Edwards, R.B., Lozanski, G., Heerema, N.A., Lehman, A., Zhang, X., Jarjoura, D., Byrd, J.C., Pan, L., Chan, K.K., Kinghorn, A.D., Phelps, M.A., Grever, M.R., and Lucas, D.M. (2011) Resistance to the translation initiation inhibitor silvestrol is mediated by ABCB1/P-glycoprotein overexpression in acute lymphoblastic leukemia cells. *AAPS J.*, **13** (3), 357–364.
35. Lucas, D.M., Edwards, R.B., Lozanski, G., West, D.A., Shin, J.D., Vargo, M.A., Davis, M.E., Rozewski, D.M., Johnson, A.J., Su, B.-N., Goettl, V.M., Heerema, N.A., Lin, T.S., Lehman, A., Zhang, X., Jarjoura, D., Newman, D.J., Byrd, J.C., Kinghorn, A.D., and Grever, M.R. (2009) The novel plant-derived agent silvestrol has B-cell selective activity in chronic lymphocytic leukemia and acute lymphoblastic leukemia *in vitro* and *in vivo*. *Blood*, **113** (19), 4656–4666.
36. Schatz, J.H., Oricchio, E., Wolfe, A.L., Jiang, M., Linkov, I., Maragulia, J., Shi, W., Zhang, Z., Rajasekhar, V.K., Pagano, N.C., Porco, J.A. Jr., Teruya-Feldstein, J., Rosen, N., Zelenetz, A.D., Pelletier, J., and Wendel, H.G. (2011) Targeting cap-dependent translation blocks converging survival signals by AKT and PIM kinases in lymphoma. *J. Exp. Med.*, **208** (9), 1799–1807.
37. Alinari, L., Prince, C.J., Edwards, R.B., Towns, W.H., Mani, R., Lehman, A., Zhang, X., Jarjoura, D., Pan, L., Kinghorn, A.D., Grever, M.R., Baiocchi, R.A., and Lucas, D.M. (2012) Dual targeting of the cyclin/Rb/E2F and mitochondrial pathways in mantle cell lymphoma with the translation inhibitor silvestrol. *Clin. Cancer Res.*, **18** (17), 4600–4611.
38. Thuaud, F., Ribeiro, N., Gaiddon, C., Cresteil, T., and Désaubry, L. (2011) Novel flavaglines displaying improved cytotoxicity. *J. Med. Chem.*, **54** (1), 411–415.
39. Polier, G., Neumann, J., Thuaud, F., Ribeiro, N., Gelhaus, C., Schmidt, H., Giaisi, M., Koehler, R., Mueller, W.W., Proksch, P., Leippe, M., Janssen, O., Désaubry, L., Krammer, P.H., and Li-Weber, M. (2012) The natural anticancer compounds rocaglamides inhibit the Raf-MEK-ERK pathway by targeting prohibitin 1 and 2. *Chem. Biol.*, **19** (9), 1093–1104.
40. Thuaud, F., Ribeiro, N., Nebigil, C.G., and Désaubry, L. (2013) Prohibitin ligands in cell death and survival: mode of action and therapeutic potential. *Chem. Biol.*, **20** (3), 316–331.
41. Matallanas, D., Birtwistle, M., Romano, D., Zebisch, A., Rauch, J., von Kriegsheim, A., and Kolch, W. (2011) Raf family kinases: old dogs have learned new tricks. *Genes Cancer*, **2** (3), 232–260.
42. Chambers, J.M., Lindqvist, L.M., Webb, A., Huang, D.C.S., Savage, G.P., and Rizzacasa, M.A. (2013) Synthesis of biotinylated episilvestrol: highly selective targeting of the translation factors eIF4A1/II. *Org. Lett.*, **15** (6), 1406–1409.
43. Sadlish, H., Galicia-Vazquez, G., Paris, C.G., Aust, T., Bhullar, B., Chang, L., Helliwell, S.B., Hoepfner, D., Knapp, B., Riedl, R., Roggo, S., Schuierer, S., Studer, C., Porco, J.A. Jr., Pelletier, J., and Movva, N.R. (2013) Evidence for a functionally relevant rocaglamide binding site on the eIF4A-RNA complex. *ACS Chem. Biol.*, **8** (7), 1519–1527.

44. Bordeleau, M.E., Robert, F., Gerard, B., Lindqvist, L., Chen, S.M., Wendel, H.G., Brem, B., Greger, H., Lowe, S.W., Porco, J.A. Jr., and Pelletier, J. (2008) Therapeutic suppression of translation initiation modulates chemosensitivity in a mouse lymphoma model. *J. Clin. Invest.*, **118** (7), 2651–2660.
45. Jin, C., Rajabi, H., Rodrigo, C.M., Porco, J.A. Jr., and Kufe, D. (2013) Targeting the eIF4A RNA helicase blocks translation of the MUC1-C oncoprotein. *Oncogene*, **32** (17), 2179–2188.
46. Nasr, Z., Robert, F., Porco, J.A. Jr., Muller, W.J., and Pelletier, J. (2013) eIF4F suppression in breast cancer affects maintenance and progression. *Oncogene*, **32** (7), 861–871.
47. Lindqvist, L.M., Vikstrom, I., Chambers, J.M., McArthur, K., Ann Anderson, M., Henley, K.J., Happo, L., Cluse, L., Johnstone, R.W., Roberts, A.W., Kile, B.T., Croker, B.A., Burns, C.J., Rizzacasa, M.A., Strasser, A., and Huang, D.C. (2012) Translation inhibitors induce cell death by multiple mechanisms and Mcl-1 reduction is only a minor contributor. *Cell Death Dis.*, **3**, e409.
48. Ruggero, D. (2013) Translational control in cancer etiology. *Cold Spring Harbor Perspect. Biol.*, **5** (2), pii: a012336.
49. Thuaud, F., Bernard, Y., Turkeri, G., Dirr, R., Aubert, G., Cresteil, T., Bague, A., Tomasetto, C., Svitkin, Y., Sonenberg, N., Nebigil, C.G., and Désaubry, L. (2009) Synthetic analogue of rocaglaol displays a potent and selective cytotoxicity in cancer cells: involvement of apoptosis inducing factor and caspase-12. *J. Med. Chem.*, **52** (16), 5176–5187.
50. Ribeiro, N., Thuaud, F., Bernard, Y., Gaidon, C., Cresteil, T., Hild, A., Hirsch, E.C., Michel, P.P., Nebigil, C.G., and Désaubry, L. (2012) Flavaglines as potent anticancer and cytoprotective agents. *J. Med. Chem.*, **55** (22), 10064–10073.
51. Neumann, J., Boerries, M., Kohler, R., Giaisi, M., Krammer, P.H., Busch, H., and Li-Weber, M. (2014) The natural anticancer compound rocaglamide selectively inhibits the G1-S-phase transition in cancer cells through the ATM/ATR-mediated Chk1/2 cell cycle checkpoints. *Int. J. Cancer*, **134** (8), 1991–2002.
52. Proksch, P., Giaisi, M., Treiber, M.K., Palfi, K., Merling, A., Spring, H., Krammer, P.H., and Li-Weber, M. (2005) Rocaglamide derivatives are immunosuppressive phytochemicals that target NF-AT activity in T cells. *J. Immunol.*, **174** (11), 7075–7084.
53. Baumann, B., Bohnenstengel, F., Siegmund, D., Wajant, H., Weber, C., Herr, I., Debatin, K.M., Proksch, P., and Wirth, T. (2002) Rocaglamide derivatives are potent inhibitors of NF-kappa B activation in T-cells. *J. Biol. Chem.*, **277** (47), 44791–44800.
54. Lucas, C.R., Cordero-Nieves, H.M., Erbe, R.S., McAlees, J.W., Bhatia, S., Hodes, R.J., Campbell, K.S., and Sanders, V.M. (2013) Prohibitins and the cytoplasmic domain of CD86 cooperate to mediate CD86 signaling in B lymphocytes. *J. Immunol.*, **190** (2), 723–736.
55. Fahrig, T., Gerlach, I., and Horvath, E. (2005) A synthetic derivative of the natural product rocaglaol is a potent inhibitor of cytokine-mediated signaling and shows neuroprotective activity in vitro and in animal models of Parkinson's disease and traumatic brain injury. *Mol. Pharmacol.*, **67** (5), 1544–1555.
56. The Michael J. Fox Foundation (2012) IMD-026259 – An Innovative Drug for Disease-Modifying Treatment of Parkinson's Disease, https://www.michaeljfox.org/foundation/grant-detail.php?grant_id=1020 (accessed 15 July 2014).
57. Minotti, G., Menna, P., Salvatorelli, E., Cairo, G., and Gianni, L. (2004) Anthracyclines: molecular advances and pharmacologic developments in antitumor activity and cardiotoxicity. *Pharmacol. Rev.*, **56** (2), 185–229.
58. Bernard, Y., Ribeiro, N., Thuaud, F., Turkeri, G., Dirr, R., Boulberdaa, M., Nebigil, C.G., and Désaubry, L. (2011) Flavaglines alleviate doxorubicin cardiotoxicity: implication of Hsp27. *PLoS ONE*, **6** (10), e25302.

59. Kostenko, S. and Moens, U. (2009) Heat shock protein 27 phosphorylation: kinases, phosphatases, functions and pathology. *Cell. Mol. Life Sci.*, **66** (20), 3289–3307.
60. Nasr, Z., Dow, L.E., Paquet, M., Chu, J., Ravindar, K., Somaiah, R., Deslongchamps, P., Porco, J.A. Jr, Lowe, S.W., and Pelletier, J. (2013) Suppression of eukaryotic initiation factor 4E prevents chemotherapy-induced alopecia. *BMC Pharmacol. Toxicol.*, **14**, 58.
61. Astelbauer, F., Gruber, M., Brem, B., Greger, H., Obwallner, A., Wernsdorfer, G., Congpuong, K., Wernsdorfer, W.H., and Walochnik, J. (2012) Activity of selected phytochemicals against *Plasmodium falciparum*. *Acta Trop.*, **123** (2), 96–100.

PUBLICATION N°3

Reprinted from

Exploratory studies toward a synthesis of flavaglines.
A novel access to a highly substituted cyclopentenone intermediate.

Basmadjian C., Zhao Q., Désaubry L. *Tetrahedron lett.* **2015**, 56, 727–730.

Copyright © 2014 with permission from Elsevier



Exploratory studies toward a synthesis of flavaglines. A novel access to a highly substituted cyclopentenone intermediate



Christine Basmadjian, Qian Zhao, Laurent Désaubry*

Laboratory of Therapeutic Innovation (UMR 7200), University of Strasbourg-CNRS, Faculty of Pharmacy, 67401 Illkirch, France

ARTICLE INFO

Article history:

Received 13 September 2014

Revised 14 December 2014

Accepted 16 December 2014

Available online 23 December 2014

Keywords:

Cyclopentenones

Carbocationic rearrangement

Propargyl alcohols

Flavaglines

ABSTRACT

The gold(I)-catalyzed intramolecular siloxycyclization developed by Rhee and collaborators was shown to operate also on alkyl ethers to generate a highly substituted 2-cyclopentenone **8**, extending the application of this reaction. Conversion of **8** to known anticancer natural products following a reported strategy was examined.

© 2014 Elsevier Ltd. All rights reserved.

Isolated from medicinal plants of the genus *Aglaiia*, flavaglines have attracted considerable attention due to their remarkable structural complexity and unique biological activities, which include a strong cytotoxicity that is specific to cancer cells.^{1–5} In the course of our medicinal program aiming at developing flavaglines with enhanced pharmacological properties,^{5,6} we considered to prepare novel flavaglines using a strategy developed by Ragot and coll. at Bayer (Scheme 1).⁷ These authors achieved the synthesis of the flavagline core **3** in three steps from cyclopentenone **1a**, using an intramolecular hydroxy epoxide opening in the key step.

Although the disclosed preparation of unsubstituted cyclopentenone **1a** could be achieved in 4 steps with an overall yield of 14%, the introduction of substituents necessary for the anticancer activity (e.g., R = OMe) was not reported. In order to synthesize pharmacologically active flavaglines, we considered to prepare **1b** by another approach. While symmetrical 3,4-diaryl-cyclopent-2-enones can easily be obtained from α,β -diketones, the synthesis of cyclopentenones substituted by different aryl moieties is more tedious.

At the heart of our approach to prepare **1b** is the Rautenstrauch rearrangement, which is particularly efficient to prepare variously substituted cyclopentenones.⁸ To test the viability of this strategy, we first examined the reactivity of the Rautenstrauch's substrate **7**.

Our attempt of synthesis of ester **7** is depicted in Scheme 2. Perkin condensation of acid **4** and benzaldehyde followed by the

conversion to an acyl chloride and a Sonogashira coupling conveniently afforded ketone **5** as a sole *E* isomer. Condensation with lithiated trimethoxybenzene gave adduct **6** in 71% yield.

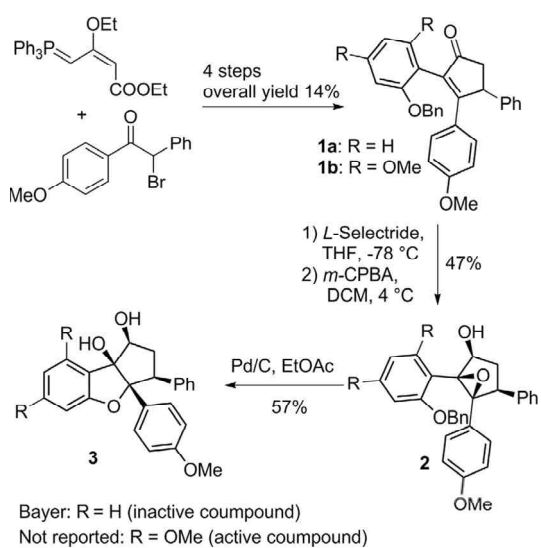
With carbinol **6** in hand, we tested many esterification protocols.⁹ However, all our attempts were unsuccessful due to lack of reactivity or high instability of expected ester **7**.

This failure led us to explore another strategy based on the recently described gold(I)-catalyzed synthesis of highly substituted cyclopentenones by an intramolecular siloxycyclization process developed by Rhee and coll. (Scheme 3).¹⁰ The utility of this approach was validated with the total synthesis of herbertene natural products.¹¹ Although this reaction was described exclusively with tertiary silyl ethers ($R^1 = \text{SiEt}_3$, R^2 and $R^3 \neq \text{H}$), we considered that the phenyl and the trimethoxyphenyl groups of substrate **11** should sufficiently stabilize the carbocationic intermediate to allow the reaction to proceed (Scheme 4). This hypothesis was supported by Toste's report of a related Au(I)-catalyzed carboxyalkoxylation using benzylic ethers as substrates to synthesize indenyl ethers.¹² Thus, the silyl ether was replaced by an ethoxy group due to its easier preparation.

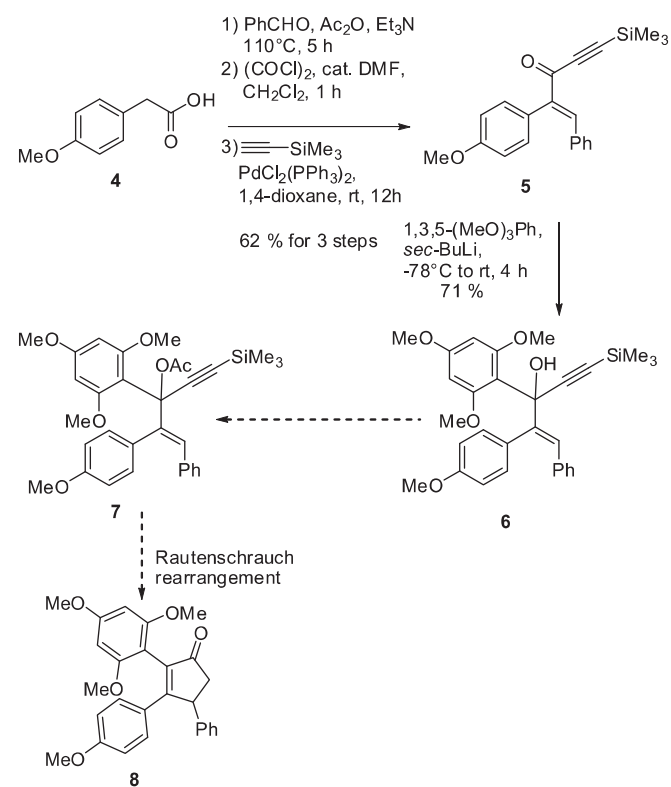
Indeed, the direct molybdenum(VI)-catalyzed transposition and etherification of allylic alcohol **6** at 50 °C afforded a 1:1 mixture of ethers **9** and **10** in a 55% yield.¹³ Gratifyingly, increasing the temperature to 65 °C improved the ratio to 1:3 in favor of the desired ether **10** in a 85% yield. Increasing the temperature further promoted the decomposition of this product. Desilylation provided alkyne **11**, which gratifyingly proved to be a good substrate for the Rhee's annulation reaction. The attempt to perform this reaction on silylated alkyne **10** also afforded **8** (58%).

* Corresponding author. Tel.: +33 036 885 4141; fax: +33 036 885 4320.

E-mail address: desaubry@unistra.fr (L. Désaubry).



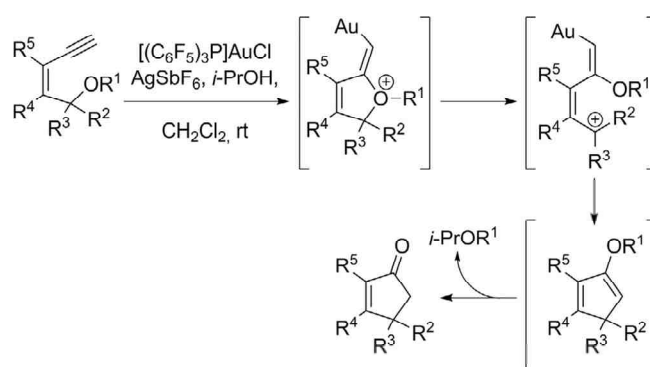
Scheme 1. Bayer synthesis of the flavagline core (the synthesis of pharmacologically active compounds (R = OMe) was not reported with this approach).⁷



Scheme 2. Attempt synthesis of an advanced precursor of flavaglines.

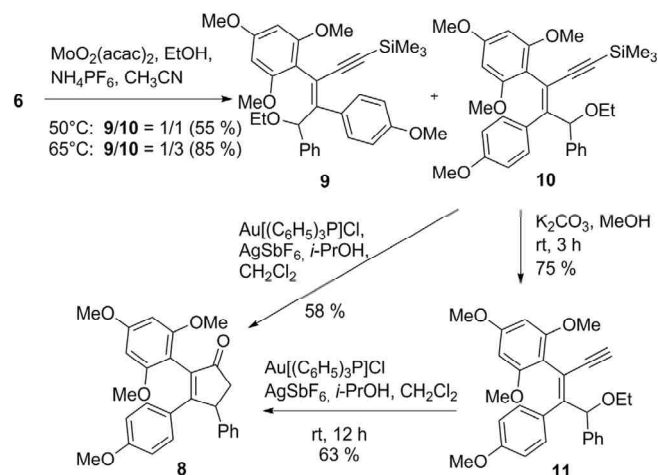
The synthesis of two other cyclopentenones was next examined (Scheme 5). The substrates of the Au-catalyzed cyclization were prepared from acyl chloride **12** through Suzuki coupling, ethynylation, rearrangement and desilylation of the alkyne. Enyne **13** harboring an unsubstituted phenyl afforded the desired cyclopentenone **15** in a satisfactory yield of 50%. Interestingly, introduction of a chlorine atom in the *para* position increased the yield to 75%, probably due to a higher stabilization of the carbocationic intermediate.

Thanks to the assistance of ketone, **8** was selectively monodemethylated upon treatment with BBr₃ in a 75% yield (Scheme 6).

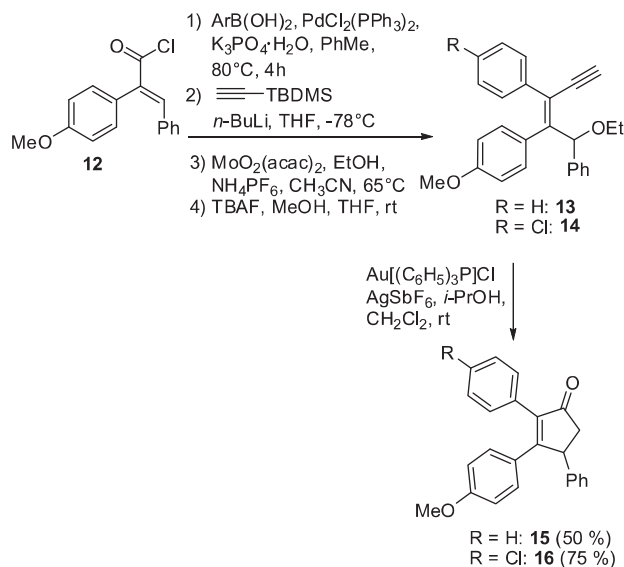


Rhee and coll.: R¹ = SiEt₃; R², R³ ≠ H
Our work: R¹ = Et; R² = 4-MeO-Ph, R³ = H

Scheme 3. Proposed mechanism for the gold(I)-catalyzed cyclopentanone formation developed by Rhee and coll.¹⁰

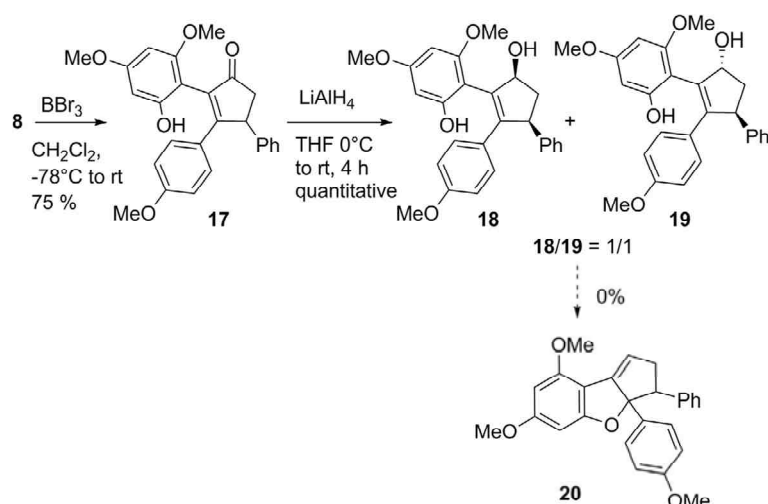


Scheme 4. Synthesis of cyclopentenone **8**.

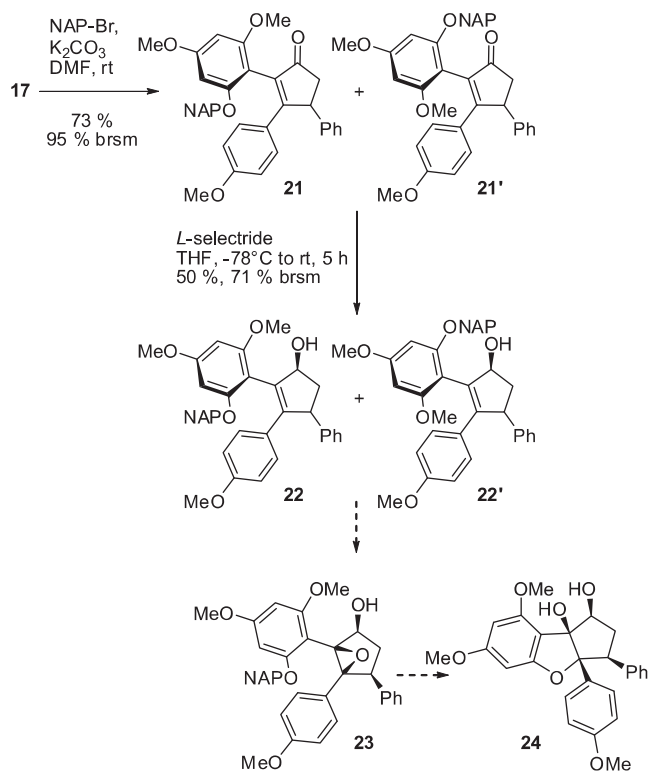


Scheme 5. Synthesis of cyclopentenones **15** and **16**.

Reduction of ketone **17** was not diastereoselective under various conditions (*L*-selectride; Red-Al; NaBH₄; NaBH₄, CeCl₃·7H₂O). In addition, the mixture of **18** and **19** significantly degraded during



Scheme 6. Synthesis of the allylic alcohols **18/19** and attempts to generate the flavagline scaffold.



Scheme 7. Synthesis of the atropoisomeric allylic alcohols **22/22'** and epoxidation attempts to synthesize flavagline **24**.

purification steps. After extensive work, we eventually were able to quantitatively prepare a mixture of **18/19** in a 1/1 ratio using 4 equivalents of LiAlH_4 .

With **18** and **19** in hand, we tried to convert these reactive allylic alcohols into the flavagline precursor **20** using many methods of activation of allylic alcohols ($\text{Pd}[\text{P}(\text{OC}_6\text{H}_5)_3]_4$, Na_2SO_4 ; PPh_3 - AuCl , AgOTf , 4 Å MS; $\text{Bi}(\text{OTf})_3$, KPF_6 , CaSO_4 ; $\text{Ar-B}(\text{OH})_2$; FeCl_3 ; $\text{MoO}_2(\text{acac})_2$, NH_4PF_6 ; Re_2O_7).^{14–18} Unfortunately, all of these assays only generated degradation products. Even though compounds similar to **20** have been described,^{19–23} it is probable that the inherent ring strain of this product and the kinetic lability of the carbocationic intermediate prevent such a cyclization.

At this point, attempts at following Ragot's strategy using a protected phenol were examined (Scheme 7). 2-Naphthylmethyl (NAP) group was selected as the protecting group due to extremely mild conditions involved in its removal by catalytic hydrogenolysis.²⁴ The adduct was obtained as a pair of atropoisomers **21** and **21'**. As far as we know atropoisomerism for 1,2-diaryl cyclopentenes has not been reported hitherto.

Diastereoselective reduction with *l*-selectride afforded alcohols **22** and **22'** with 71% of conversion. Epoxidation of cyclopentenols **21/22'** under various conditions (*m*-CPBA, NaHCO_3 ; $\text{VO}(\text{acac})_2$, *t*- BuO_2H ; H_2O_2 , NaOH ; 4-nitroperbenzoic acid, NaHCO_3) provided none of the desired product probably due to the low reactivity of the sterically hindered alkene and instability of the product. Under Sharpless type conditions (*t*- BuO_2H , $\text{Ti}(\text{Oi-Pr})_4$, 4 Å MS), formation of the ketone was predominant, probably due to ring strain release.

The inability to obtain substrate **23** suggests that the method reported by Bayer scientist is restricted to the synthesis of flavaglines that are not substituted by the functional groups necessary for the pharmacological activity. Indeed, none of the required decorations proposed in this Letter were described in Bayer patents.

Acknowledgments

L.D. was supported by the 'Association pour la Recherche sur le Cancer' (ARC). We are also grateful to AAREC Filia Research and ANRT for fellowships to C.B. and Q.Z. and also Julie Schmitt for technical help.

Supplementary data

Supplementary data (experimental procedures for the synthesis of compounds **5**, **6**, **8**, **10–16**) associated with this article can be found, in the online version, at <http://dx.doi.org/10.1016/j.tetlet.2014.12.093>.

References and notes

- Santagata, S.; Mendillo, M. L.; Tang, Y.; Subramanian, A.; Perley, C. C.; Roche, S. P.; Wong, B.; Narayan, R.; Kwon, H.; Koeva, M.; Amon, A.; Golub, T. R.; Porco, J. A., Jr.; Whitesell, L.; Lindquist, S. *Science* **2013**, *341*, 1238303.
- Wolfe, A. L.; Singh, K.; Zhong, Y.; Drewe, P.; Rajasekhar, V. K.; Sanghvi, V. R.; Mavrakis, K. J.; Jiang, M.; Roderick, J. E.; Van der Meulen, J.; Schatz, J. H.; Rodrigo, C. M.; Zhao, C.; Rondou, P.; de Stanchina, E.; Teruya-Feldstein, J.; Kelliher, M. A.; Speleman, F.; Porco, J. A., Jr.; Pelletier, J.; Rätsch, G.; Wendel, H. G. *Nature* **2014**, *513*, 65–70.

- Boussemart, L.; Malka-Mahieu, H.; Girault, I.; Hemmingsson, O.; Allard, D.; Tomasic, G.; Thomas, M.; Ribeiro, N.; Thuaud, F.; Basmadjian, C.; Mateus, C.; Routier, E.; Kamsu-Kom, N.; Agoussi, S.; Eggermont, A. M.; Désaubry, L.; Robert, C.; Vagner, S. *Nature* **2014**, *513*, 105–109.
- Pan, L.; Woodard, J. L.; Lucas, D. M.; Fuchs, J. R.; Douglas Kinghorn, A. *Nat. Prod. Rep.* **2014**, *31*, 924–939.
- Basmadjian, C.; Thuaud, F.; Ribeiro, N.; Désaubry, L. *Future Med. Chem.* **2013**, *5*, 2185–2197.
- Ribeiro, N.; Thuaud, F.; Bernard, Y.; Gaiddon, C.; Cresteil, T.; Hild, A.; Hirsch, E. C.; Michel, P. P.; Nebigil, C. G.; Désaubry, L. *J. Med. Chem.* **2012**, *55*, 10064–10073.
- Thede, K.; Diedrichs, N.; Ragot, J. P. *Org. Lett.* **2004**, *6*, 4595–4597.
- Shiroodi, R. K.; Gevorgyan, V. *Chem. Soc. Rev.* **2013**, *42*, 4991–5001.
- Attempted esterification methods: Ac₂O, Et₃N/DMAP or DIPEA/P(Bu)₃; AcCl, *n*-BuLi or Et₃N/DMAP; BzCl, *n*-BuLi or NaH; TsNCO, *n*-BuLi; (4-NO₂-Ph)OCHO, *n*-BuLi.
- An, S. E.; Jeong, J.; Baskar, B.; Lee, J.; Seo, J.; Rhee, Y. H. *Chem. Eur. J.* **2009**, *15*, 11837–11841.
- Jeong, J.; Lee, J.; Seo, J.; Rhee, Y. H. *Bull. Korean Chem. Soc.* **2013**, *34*, 303–305.
- Dubé, P.; Toste, D. J. *Am. Chem. Soc.* **2006**, *128*, 12062–12063.
- Yang, H.; Fang, L.; Zhang, M.; Zhu, C. *Eur. J. Org. Chem.* **2009**, *5*, 666–672.
- Kayaki, Y.; Koda, T.; Ikariya, T. *J. Org. Chem.* **2004**, *69*, 2595–2597.
- Aponick, A.; Biannic, B. *Synthesis* **2008**, *20*, 3356–3359.
- Qin, H.; Yamagiwa, N.; Matsunaga, S.; Shibasaki, M. *Angew. Chem., Int. Ed.* **2007**, *46*, 409–413.
- Zheng, H.; Ghanbari, S.; Nakamura, S.; Hall, D. G. *Angew. Chem., Int. Ed.* **2012**, *51*, 6187–6190.
- Guérinot, A.; Serra-Muns, A.; Gnam, C.; Bensoussan, C.; Reymond, S.; Cossy, J. *Org. Lett.* **2010**, *12*, 1808–1811.
- Giese, M. W.; Moser, W. H. *Org. Lett.* **2008**, *10*, 4215–4218.
- Magnus, P.; Stent, M. A. H. *Org. Lett.* **2005**, *7*, 3853–3855.
- Malona, J. A.; Cariou, K.; Frontier, A. J. *J. Am. Chem. Soc.* **2009**, *131*, 7560–7561.
- Malona, J. A.; Cariou, K.; Spencer, W. T. I. I. I.; Frontier, A. J. *J. Org. Chem.* **2012**, *77*, 1891–1908.
- Trost, B. M.; Greenspan, P. D.; Yang, B. V.; Saulnier, M. G. *J. Am. Chem. Soc.* **1990**, *112*, 9022–9024.
- Gaunt, M. J.; Yu, J.; Spencer, J. B. *J. Org. Chem.* **1998**, *63*, 4172–4173.

Revision of the synthesis and pharmacological activity
of a reported translation inhibitor.

Christine Basmadjian, H  l  ne Malka-Mahieu, Laurent D  saubry, *Anticancer Agents in Medicinal Chemistry*, **2015**, *15*, in press

Copyright    2015 Bentham Science

Revision of the Synthesis and Pharmacological Activity of a Reported Translation Inhibitor

Christine Basmadjian^a, H el ene Malka-Mahieu^b, Laurent D esaubry^{*a}

^aLaboratory of Therapeutic Innovation (UMR 7200), University of Strasbourg- CNRS, Faculty of Pharmacy, 67401 Illkirch, France; ^bINSERM U981 and Gustave Roussy, 94805 Villejuif, France.

Abstract: 4EGI-1 is the prototype of a novel class of anticancer agents targeting translation. Patented drug-like analogue **1** was synthesized and examined for inhibition of translation and cytotoxicity in cancer cells. Unexpectedly, **1** was found inactive in both assays.

Keywords: eIF4E, cancer, metastatic melanoma, protein synthesis, thiazoles, mRNA translation.

INTRODUCTION

Translation, i.e. protein synthesis, is strictly regulated by initiation factors that are under the control of several signaling pathways [1]. It is currently established that translation deregulation is deeply involved in oncogenic transformations. The control of the synthesis of proteins involved in cancer cell survival, angiogenesis, transformation, invasion and metastasis is particularly altered in tumors. Consequently, targeting the translational machinery has emerged as a promising approach to treat cancers [2,3]. Along this line of research, Gerhard and coll. performed a high throughput screening to identify 4EGI-1, a small molecule that disrupts the interaction between the initiation factors of translation eIF4E and eIF4G [4]. The most active compound, 4EGI-1 was shown to preferentially affect cancer cells than non-transformed cells. It also blocks the synthesis of proteins involved in the etiology of cancer, such as cyclins D1 and E, C-myc, and Bcl-2 without disturbing the expression of housekeeping proteins.

In order to develop a more drug-like compound and to generate some intellectual property, Hoffmann-La Roche scientists synthesized a series of thiazole derivatives harboring an aryl in place of the hydrazono moiety [5]. Compound **1** was one most active molecule of this series, with an IC₅₀ of 1.4 μ M for the binding to eIF4E.

We recently demonstrated that another type of inhibitors targeting the initiation factors of translation eIF4A overcome

the resistance to anti-BRAF therapies in chemoresistant metastatic melanoma [3]. In the course of this study, we wanted to compare the effects of these compounds to those of **1**.

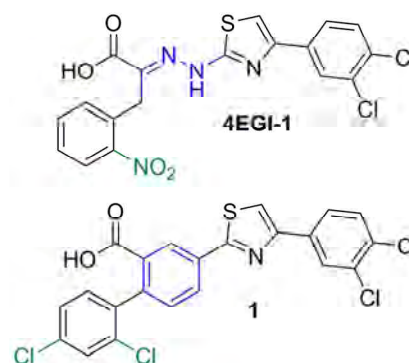


Figure 1. Structure of 4EGI-1 and Hoffmann-La Roche analogue **1**.

MATERIALS AND METHODS

Chemistry

Methyl 2-amino-5-cyanobenzoate (**3**)

Methyl 2-amino-5-bromobenzoate **2** (5 g, 0.022 mol) and copper (I) cyanide (2.34 g, 0.026 mol) were dissolved in *N*-methyl-2-pyrrolidone (25 mL). The reaction mixture was stirred at reflux for 6 hours then cooled at room temperature and added to a solution of FeCl₃ (9 g) and HCl (36%, 2.2 mL) in water (100 mL). After 1h30 at 60 $^{\circ}$ C, the mixture was cooled at room temperature and extracted with EtOAc. The

*Address correspondence to this author at Laboratory of Therapeutic Innovation (UMR 7200), University of Strasbourg-CNRS, Faculty of Pharmacy, 67401 Illkirch, France; Tel/Fax: +33-036-885-4141+33-036-885-4320; E-mails: desaubry@unistra.fr

organic layer was washed with an aqueous solution of NaOH 1 N then with brine, dried over MgSO₄, filtered and concentrated. After trituration in Et₂O, compound **3** was obtained in 90% yield (3.57 g). ¹H RMN (DMSO-*d*₆, 400 MHz) δ 3.82 (s, 3H), 6.87 (d, 1H, J = 8.8 Hz), 7.46 (br, s, 2H), 7.57 - 7.60 (dd, 1H, J = 2.0 and 8.8 Hz), 8.05 (d, 1H, J = 2 Hz) ppm; ¹³C RMN (DMSO-*d*₆, 400 MHz) δ 51.1, 104.2, 109.6, 118.3, 131.7, 135.9, 149.8, 166.10 ppm.

Methyl 2-bromo-5-cyanobenzoate (4)

Copper (II) bromide (3.56 g, 0.017 mol) was suspended in acetonitrile (50 mL). *Tert*-butyl nitrite (2.24 mL, 0.018 mol) was added dropwise at 0°C then, after 5 minutes, **3** was added by portions. After 2 hours at 0°C and 16 hours at room temperature, the reaction mixture was concentrated and acidified with an aqueous solution of HCl 1 N until pH ≈ 2. The product was extracted 3 times with EtOAc and the resulting organic layer was dried over MgSO₄, filtered and concentrated. After filtration over a silica gel pad, compound **4** was obtained in 85% yield (4.1 g). ¹H RMN (DMSO-*d*₆, 400 MHz) δ 3.89 (s, 3H), 7.93 (dd, 1H, J = 2.1 and 8.4 Hz), 7.99 (dd, 1H, J = 0.5 and 8.3 Hz), 8.23 (dd, 1H, J = 0.5 and 2.0 Hz) ppm; ¹³C RMN (DMSO-*d*₆, 400 MHz) δ 52.5, 110.5, 116.8, 125.2, 133.2, 133.6, 134.7, 135.4, 164.3 ppm.

Methyl 2-bromo-5-carbamothioylbenzoate (5)

Phosphorus pentasulfide (3.59 g, 8 mmol) was added to compound **4** (3.88 g, 0.016 mol) in suspension in absolute EtOH (40 mL) under argon atmosphere. 0.5 equivalent of phosphorus pentasulfide were added after 6 hours then every hour until completion of the reaction. After stirring at room temperature for 16 hours and sonication for 1h30, the reaction mixture was diluted with EtOAc, washed 3 times with water and once with a solution of saturated NaHCO₃. The organic layer was dried over MgSO₄, filtered and concentrated. After trituration in CH₂Cl₂, compound **5** was obtained in 81% yield (3.6 g). ¹H RMN (DMSO-*d*₆, 400 MHz) δ 3.90 (s, 3H), 7.82 (d, 1H, J = 8.4 Hz), 7.91 (dd, 1H, J = 2.4 and 8.4 Hz), 8.26 (d, 1H, J = 2.3 Hz), 9.72 (br, s, 1H), 10.10 (br, s, 1H) ppm; ¹³C RMN (DMSO-*d*₆, 400 MHz) δ 52.7, 123.1, 129.7, 130.9, 131.7, 133.6, 165.6, 197.6 ppm.

Methyl 2-bromo-5-[4-(3,4-dichlorophenyl)thiazol-2-yl]benzoate (6)

Compound **5** (3.5 g, 0.013 mol) and 2-bromo-1-(3,4-dichlorophenyl)ethan-1-one (3.46 g, 0.013 mol) were dissolved in absolute EtOH (50 mL) under argon atmosphere. After stirring at 70°C for 16 hours, the reaction mixture was cooled at room temperature and the formed precipitate was filtered to yield compound **6** (5.28 g, 92%). ¹H RMN (DMSO-*d*₆, 400 MHz) δ 3.92 (s, 3H), 7.71 (d, 1H, J = 8.5 Hz), 7.88 (d, 1H, J = 8.4 Hz), 8.03 (dd, 1H, J = 2.0 and 8.4 Hz), 8.08 (dd, 1H, J = 2.3 and 8.3 Hz), 8.29 (d, 1H, J = 2.0 Hz), 8.35 (d, 1H, J = 2.1 Hz), 8.42 (s, 1H) ppm; ¹³C RMN (DMSO-*d*₆, 400 MHz) δ 52.7, 114.4, 123.5, 125.5,

128.4, 129.1, 130.0, 130.8, 132.4, 132.6, 133.0, 133.1, 134.0, 135.1, 154.3, 166.0, 166.1 ppm.

2',4'-Dichloro-4-[4-(3,4-dichlorophenyl)thiazol-2-yl]-[1,1'-biphenyl]-2-carboxylic acid (1)

Compound **6** (500 mg, 1.13 mmol) and (2,4-dichlorophenyl)boronic acid (431 mg, 2.26 mmol) were dissolved in DMF (12 mL) under argon atmosphere. Palladium (0) triphenylphosphine tetrakis (104 mg, 0.09 mmol) and a 3M aqueous solution of K₂CO₃ were added and the resulting mixture was stirred at 100°C for 20 hours. The product was extracted with EtOAc and washed with water. The organic layer was dried over MgSO₄, filtered and concentrated. A chromatography on silica gel (pentane/CH₂Cl₂, 50/50) afforded the ester (422 mg, 73%). ¹H RMN (DMSO-*d*₆, 400 MHz) δ 3.71 (s, 3H), 7.41 (d, 1H, J = 8.3 Hz), 7.51 (d, 1H, J = 8.3 Hz), 7.53 (dd, 1H, J = 2.1 and 8.3 Hz), 7.73 (d, 1H, J = 2.1 Hz), 7.78 (d, 1H, J = 8.4 Hz), 8.08 (dd, 1H, J = 2.0 and 8.4 Hz), 8.33 (d, 1H, J = 2.0 Hz), 8.34 (dd, 1H, J = 1.0 and 1.9 Hz), 8.51, (s, 1H), 8.55 (d, 1H, J = 1.9 Hz) ppm; ¹³C RMN (DMSO-*d*₆, 400 MHz) δ 52.4, 114.4, 125.6, 127.0, 128.4, 128.4, 129.0, 129.7, 130.8, 130.8, 131.1, 132.0, 132.3, 133.1, 133.5, 133.5, 134.1, 134.2, 138.5, 141.0, 154.3, 166.5, 166.6 ppm.

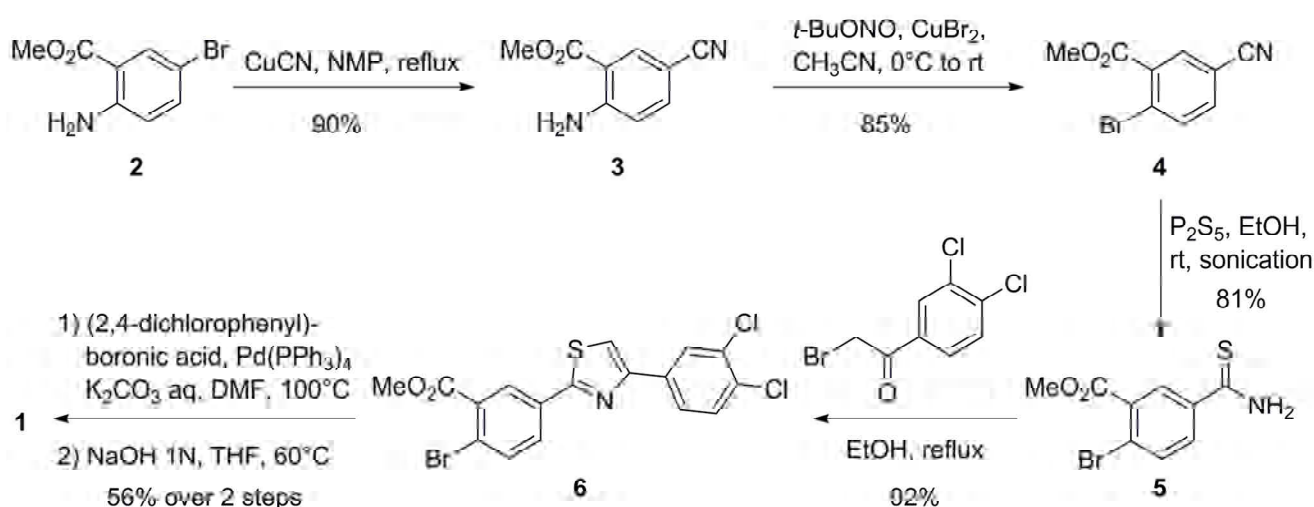
An aqueous solution of NaOH 1N (12 mL) was added to the ester (320 mg, 6.28 mmol) in solution in THF (4 mL). After stirring overnight 24 h at 90°C, the reaction mixture was concentrated, dissolved in water and extracted with EtOAc. The resulting aqueous layer was quenched with a solution HCl 1N until pH < 5, and then extracted with EtOAc. The organic layers were combined, dried over MgSO₄, filtered and concentrated under vacuum to afford compound **1** (241 mg, 77%). The product is further purified by recrystallization in CH₂Cl₂ (**1**, 120 mg, 39 %). ¹H RMN (DMSO-*d*₆, 400 MHz) δ 7.39 (d, 1H, J = 8.3 Hz), 7.45 (d, 1H, J = 7.9 Hz), 7.50 (dd, 1H, J = 2.1 and 8.2 Hz), 7.70 (d, 1H, J = 2.1 Hz), 7.76 (d, 1H, J = 8.4 Hz), 8.08 (d, 1H, J = 2.0 and 8.4 Hz), 8.28 (dd, 1H, J = 2.0 and 8.0 Hz), 8.33 (d, 1H, J = 2.0 Hz), 8.49 (s, 1H), 8.55 (d, 1H, J = 2.0 Hz), 13.15 (br, s, 1H); ¹³C RMN (DMSO-*d*₆, 400 MHz) δ 35.9, 131.6, 131.6, 132.4, 132.7, 133.5, 133.6, 134.6, 135.9, 136.4, 136.8, 137.0, 137.4, 137.5, 137.9, 138.0, 138.1, 139.6, 144.1, 145.5, 158.1, 171.1, 172.1 ppm. BR-MS calculated for C₂₂H₁₁Cl₄NO₂S: 495.2 found: 495.6. Anal. Calcd for C₂₂H₁₁Cl₄NO₂S: C, 53.36; H, 2.24; N, 2.83. Found: C, 53.40; H, 2.35; N, 2.75.

Cap-dependent translation assay

The capacity of **1** to inhibit cap-dependent translation was examined using a bicistronic luciferase reporter construct (pR-HepC-L) using the procedure described in reference 3.

RESULTS AND DISCUSSIONS

The synthesis of **1** was performed by a modification of Hoffmann-La Roche procedure [5]. In our hands, the



Scheme 1. Synthesis of Hoffmann-La Roche analogue **1**.

introduction of a cyanide in the first step following the described procedure afforded the expected adduct in 5% yield (instead of 73%). We eventually found that treating the reaction medium with FeCl₃ and HCl at 60°C improved the yield to 90% [6]. The rest of the synthesis followed the described procedure [7] except for the conversion of cyanide **4** into the amide **5** (which required 2.5 eq of P₂S₅ instead of 0.5 eq). We also add of an extra step of purification after the Suzuki reaction (**5** → **6**) to remove any trace of palladium that could induce an artifactual cytotoxicity during the biological tests.

The capacity of **1** to inhibit cap-dependent translation was examined using a bicistronic luciferase reporter construct (pR-HepC-L)³ (Fig. 2). In this assay, translation of the first (LucR) cistron is cap-dependent, while translation of the (IRES)-driven second (LucF) cistron is cap-independent. The ratio of luciferase activities directly reflects differences in cap-dependent and independent translation. Surprisingly, **1** did not display any inhibition of cap-dependent translation, which is in sharp contrast with the claims of Hoffmann-La Roche patent. This discrepancy might result for the

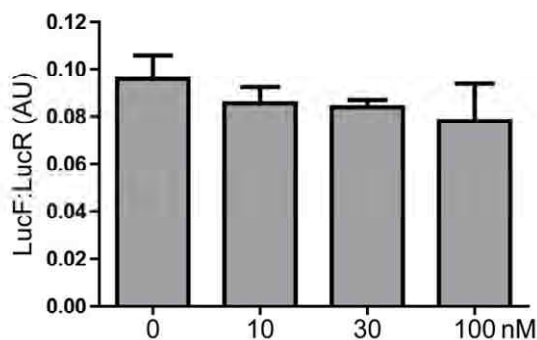


Figure 2. Ratio of LucF to LucR activity (AU, arbitrary units) in pR-HepC-L-transfected A375 cells treated with **1**.

different nature of both tests. Indeed, it is conceivable that compound **1** binds to eIF4E, but without significantly blocking its biochemical function, in contrast to 4EGI-1 [4].

In addition, **1** (1 mM) did not display any significant cytotoxicity in A375, A 2058 and Mel624 cancer cells (survival ≥ 65% at 1 mM).

CONCLUSION

In summary, one of the leading compounds described by Hoffmann-La Roche scientists was synthesized following an improved procedure. In contrast to the claims of the cognate patent, this compound (**1**) did not induce display any significant inhibition of cap-dependent translation or cytotoxicity in cancer cells, which casts doubts upon its value to treat cancers.

CONFLICT OF INTEREST

The authors confirm that this article content has no conflict of interest.

ACKNOWLEDGEMENTS

L.D. was supported by the "Association pour la Recherche sur le Cancer" (ARC). We are also grateful to AAREC Filia Research and ANRT for fellowships to C.B.

REFERENCES

Journal Reference:

- [1] Kong, J.; Lasko, P. Translational control in cellular and developmental processes. *Nat. Rev. Genet.* **2012**, *13*, 383-394.
- [2] Jia, Y.; Polunovsky, V.; Bitterman, P. B.; Wagner, C. R. Cap-dependent translation initiation factor eIF4E: an emerging anticancer drug target. *Med. Res. Rev.* **2012**, *32*, 786-814.
- [3] Boussemaert, L.; Malka-Mahieu, H.; Girault, I.; Allard, D.; Hemmingsson, O.; Tomasic, G.; Thomas, M.; Basmdjian, C.; Ribeiro, N.; Thuaud, F.; Mateus, C.; Routier, E.; Girault, I.; Allard, D.; Hemmingsson, O.; Tomasic, G.; Thomas, M.; Basmdjian, C.; Ribeiro, N.; Thuaud, F.; Mateus, C.; Routier, E.; Kamsu-Kom, N.;

- Agoussi, S.; Eggermont, A. M.; Désaubry, L.; Robert, C.; Vagner, S. eIF4F is a nexus of resistance to anti-BRAF and anti-MEK cancer therapies. *Nature* **2014**, *513*, 105-109.
- [4] Moerke, N. J.; Aktas, H.; Chen, H.; Cantel, S.; Reibarkh, M. Y.; Fahmy, A.; Gross, John D.; Degterev, A.; Yuan, J.; Chorev, M.; Halperin, J. A.; Wagner, G. Small-molecule inhibition of the interaction between the translation initiation factors eIF4E and eIF4G. *Cell* **2007**, *128*, 257-267.
- [5] Gillespie, P. Benzoic acid derivatives as EIF4E inhibitors. WO 2013/041468 A1, 2013.
- [6] Wall, M. J.; Player, M. R.; Patch, R. Joseph; Meegalla, S.; Liu, J. U.; Illig, C. R.; Cheung, W. U.; Chen, J. U.; Asgari, D. U. Quinoline derivatives as inhibitors of C-FMS kinase. WO/2005/009967, 2005.

Patent:

Received:

Revised:

Accepted:

eIF4F is a key and targetable convergence nexus of multiple resistance mechanisms to anti-RAF and anti-MEK cancer therapies.

Boussemart L., Malka-Mahieu H., Girault I., Hemmingsson O., Allard D, Tomasic G., Thomas M., Ribeiro N., Thuaud F., Basmadjian C., Mateus C., Routier E., Kamsu-Kom N., Agoussi S., Eggermont A., Désaubry L., Robert C., Vagner S. *Nature*, **2014**, *513*, 105-109

Copyright © 2014, Rights Managed by Nature Publishing Group

eIF4F is a nexus of resistance to anti-BRAF and anti-MEK cancer therapies

Lise Boussemart^{1,2,3*}, H el ene Malka-Mahieu^{1,2*}, Isabelle Girault^{1*}, Delphine Allard¹, Oskar Hemmingsson^{1†}, Gorana Tomasic⁴, Marina Thomas³, Christine Basmadjian⁵, Nigel Ribeiro⁵, Fr ed eric Thuaud⁵, Christina Mateus³, Emilie Routier³, Nyam Kamsu-Kom¹, Sandrine Agoussi¹, Alexander M. Eggermont^{2,3}, Laurent D esaubry⁵, Caroline Robert^{1,2,3} & St ephan Vagner^{1,2,3†}

In BRAF(V600)-mutant tumours, most mechanisms of resistance to drugs that target the BRAF and/or MEK kinases rely on reactivation of the RAS–RAF–MEK–ERK mitogen-activated protein kinase (MAPK) signal transduction pathway, on activation of the alternative, PI(3)K–AKT–mTOR, pathway (which is ERK independent) or on modulation of the caspase-dependent apoptotic cascade^{1–3}. All three pathways converge to regulate the formation of the eIF4F eukaryotic translation initiation complex, which binds to the 7-methylguanylate cap (m⁷G) at the 5' end of messenger RNA, thereby modulating the translation of specific mRNAs^{4,5}. Here we show that the persistent formation of the eIF4F complex, comprising the eIF4E cap-binding protein, the eIF4G scaffolding protein and the eIF4A RNA helicase, is associated with resistance to anti-BRAF, anti-MEK and anti-BRAF plus anti-MEK drug combinations in BRAF(V600)-mutant melanoma, colon and thyroid cancer cell lines. Resistance to treatment and maintenance of eIF4F complex formation is associated with one of three mechanisms: reactivation of MAPK signalling, persistent ERK-independent phosphorylation of the inhibitory eIF4E-binding protein 4EBP1 or increased pro-apoptotic BCL-2-modifying factor (BMF)-dependent degradation of eIF4G. The development of an *in situ* method to detect the eIF4E–eIF4G interactions shows that eIF4F complex formation is decreased in tumours that respond to anti-BRAF therapy and increased in resistant metastases compared to tumours before treatment. Strikingly, inhibiting the eIF4F complex, either by blocking the eIF4E–eIF4G interaction or by targeting eIF4A, synergizes with inhibiting BRAF(V600) to kill the cancer cells. eIF4F not only appears to be an indicator of both innate and acquired resistance but also is a promising therapeutic target. Combinations of drugs targeting BRAF (and/or MEK) and eIF4F may overcome most of the resistance mechanisms arising in BRAF(V600)-mutant cancers.

A plethora of mechanisms of resistance to BRAF(V600) inhibitors have been described, including mutations of *NRAS*, *MAP2K1* and *PIK3CA*, partial deletion of *PTEN*, expression of *BRAF* splice variants, upregulation of PDGFR β , IGF-1R, EGFR, HER3 and COT and downregulation of BH3-only proteins (which are pro-apoptotic)^{1–3,6}. By activating the MAPK or the PI(3)K pathway or by modulating the caspase-dependent apoptotic cascade, all of these mechanisms converge on eIF4F-dependent mRNA translation.

To investigate the potential role of eIF4F complex formation in the resistance of BRAF(V600) melanoma to anti-BRAF and anti-MEK compounds, we first tested a panel of human melanoma cell lines (Supplementary Table 1) for their sensitivity to vemurafenib. Two BRAF(V600)-mutated cell lines (Mel624 and A2058) were resistant to vemurafenib compared with other cell lines (for example, A375 and Mel888) in both short-term (Extended Data Fig. 1a) and long-term (Extended Data Fig. 1b) proliferation assays. Similarly to the sensitivity pattern observed *in vitro*,

A375 xenografts were more sensitive to vemurafenib than were Mel624 xenografts (Extended Data Fig. 2a). Determination of the half-maximum inhibitory concentration (IC₅₀) (Extended Data Fig. 1a and Supplementary Table 1), together with long-term proliferation assays (Extended Data Fig. 1c), indicated that these two vemurafenib-resistant cell lines (Mel624 and A2058) were also less sensitive to dabrafenib (another BRAF(V600) inhibitor), PD0325901 and trametinib (both MEK inhibitors), the combination of dabrafenib and trametinib, and CGP 57380 (a MNK inhibitor). To determine the status of the eIF4F complex in these various cell lines, we used a cap-binding assay in which synthetic m⁷GTP-Sepharose beads capture eIF4E and its two binding partners, eIF4G and 4EBP1. We observed that vemurafenib treatment increased the amount of eIF4E-bound 4EBP1 and concomitantly decreased the amount of eIF4E-bound eIF4G in the two sensitive cell lines (A375 and Mel888) (Fig. 1a). Incorporation of [³⁵S]methionine and cysteine and profiling of polysomes showed that this decrease in eIF4F complex formation led to a weak decrease (13%) in translation initiation in the acute phase (3 h) of the response to treatment and to a greater decrease (30%) in protein synthesis after 24 h of treatment (Extended Data Fig. 3a, b). As expected from another study⁷, describing mTOR-dependent translation regulation, the analysis of mRNAs that are differentially recruited to heavy polysomes (Supplementary Table 2) showed that the translation of several mRNAs containing 5' terminal oligopyrimidine (TOP) motifs and encoding many ribosomal proteins and translation factors was inhibited during the acute response to vemurafenib treatment (Extended Data Figs 3c, d and 4 and Supplementary Table 2).

Strikingly, the vemurafenib-dependent disruption of the eIF4E–eIF4G complex was not observed in the resistant cell lines (Mel624 and A2058) (Fig. 1a). We further investigated the formation of the eIF4F complex using a proximity ligation assay procedure (Extended Data Fig. 5), and we observed that vemurafenib induced a decrease in eIF4E–eIF4G interaction and an increase in eIF4E–4EBP1 complex formation in vemurafenib-sensitive cell lines (A375 and Mel888) that was not observed in the resistant cell lines (Mel624 and A2058) (Fig. 1b and Extended data Fig. 6a, b). *In vivo* experiments in mice were consistent with these findings, as we also found fewer eIF4E–eIF4G interactions, compared with eIF4E–4EBP1 interactions, in vemurafenib-treated A375 xenografts (sensitive) than in vemurafenib-treated Mel624 xenografts (resistant) (Extended Data Fig. 2b, c). The same correlation between sensitivity to the drugs and the level of activation of the eIF4F complex was observed with dabrafenib, trametinib and combinations of both drugs (Extended Data Fig. 7a, b), extending our observation to anti-MEK agents and anti-BRAF plus anti-MEK combinations⁸.

In parallel, we generated a melanoma cell line with acquired resistance to vemurafenib (Supplementary Table 1) by exposing the Malme-3M cell line, which has the BRAF(V600) mutation, to incremental increases

¹Inserm UMR981, Villejuif F-94805, France. ²Universit e Paris-Sud XI, Kremlin-Bic etre F-94276, France. ³Gustave Roussy, Dermato-Oncology, Villejuif F-94805, France. ⁴Gustave Roussy, Pathology Department, Villejuif F-94805, France. ⁵CNRS-Strasbourg University, UMR7200, Illkirch F-67400, France. [†]Present addresses: Department of Surgical and Perioperative Sciences, Ume a University, Ume a SE-90187, Sweden (O.H.); CNRS UMR3348, Institut Curie, Orsay F-91405, France (S.V.).

*These authors contributed equally to this work.

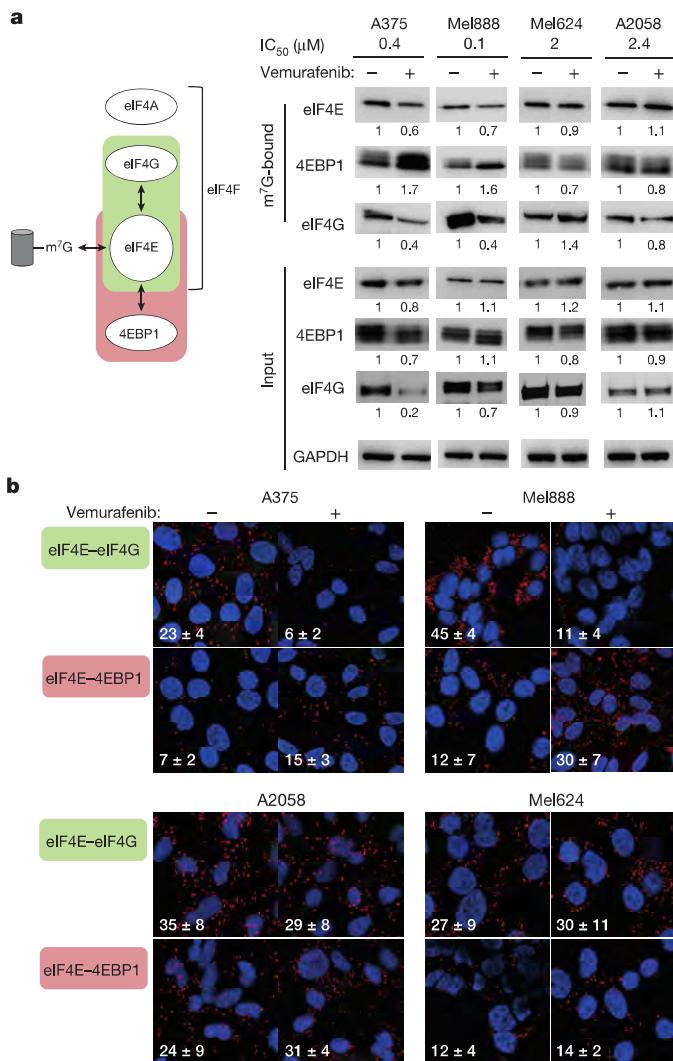


Figure 1 | The formation of the eIF4F translation initiation complex is associated with resistance to BRAF inhibitors. **a**, eIF4F complex formation, as determined using the cap-binding assay in vemurafenib-treated or untreated tumour cell lines. Eluates from beads (m⁷G-bound) and total extracts (input) were analysed by western blotting. The half-maximum inhibitory concentration (IC₅₀) for vemurafenib is indicated (see also Supplementary Table 1). **b**, eIF4E-eIF4G or eIF4E-4EBP1 interactions detected by proximity ligation assay (PLA) in vemurafenib-treated or untreated cell lines. The interactions were visualized as red spots. The white numbers indicate the mean ± s.d. ($n = 3$).

in vemurafenib concentration over 2 months. Again, vemurafenib induced a decrease in eIF4E-eIF4G interactions and an increase in eIF4E-4EBP1 complex formation in vemurafenib-sensitive Malme-3M cells but not in vemurafenib-resistant Malme-3M (R-Malme-3M) cells (Extended Data Fig. 8a). Finally, this paradigm was not limited to melanoma cell lines: we observed the maintenance of the eIF4F complex in two other cell lines: the colon cancer cell line HT-29, in which resistance is associated with an activating PI(3)K(P449T) mutation⁹ and *EGFR* overexpression¹⁰, and the papillary thyroid cancer cell line BCPAP, in which resistance is linked to *HER3* overexpression¹¹ (Extended Data Fig. 8b).

We next addressed the mechanisms underlying the differences in the sensitivity to vemurafenib in the above-mentioned melanoma cell lines. We observed that R-Malme-3M exhibited a higher ERK phosphorylation level than the sensitive Malme-3M cell line (Fig. 2a). The sustained phosphorylation of ERK was associated with a vemurafenib-dependent increase in BRAF-CRAF dimerization, revealing a mechanism of resistance linked to reactivation of the MAPK pathway (Fig. 2b). Vemurafenib

treatment inhibited ERK phosphorylation in all of the other cell lines tested, including the vemurafenib-resistant cell lines Mel624 and A2058 (Fig. 2c), showing that the differential sensitivity to vemurafenib in these cell lines cannot be explained by the reactivation of the MAPK pathway. The expression and phosphorylation of the main translation initiation factors remained unchanged in vemurafenib-resistant cell lines, except for eIF4G and eIF4B, for which vemurafenib-dependent dephosphorylation was observed (Fig. 2c). However, these dephosphorylations also occurred in vemurafenib-sensitive cell lines and therefore were not correlated with vemurafenib resistance. 4EBP1 was dephosphorylated in the vemurafenib-treated sensitive cell line Mel888 and to a lesser extent in A375. This dephosphorylation is linked to AKT dephosphorylation (Fig. 2c), which does not occur in resistant cell lines. The amounts of eIF4G and eIF4B were decreased in the vemurafenib-treated sensitive A375 cell line (Fig. 2c).

To uncover the mechanisms underlying this decrease, we sought to identify the genes whose expression is altered after vemurafenib treatment in A375 cells compared with Mel624 cells, by using microarrays (Supplementary Table 3). As expected from previous studies^{12,13}, vemurafenib led to the inhibition of expression of genes encoding transcription factors associated with ERK-dependent transformation and genes encoding feedback regulators of ERK signalling, such as members of the dual specificity phosphatase (DUSP) and sprouty (SPRY) gene families (Fig. 2d and Supplementary Table 3). These changes were found in both the sensitive and resistant cell lines, reinforcing the finding that the differential sensitivity of these two cell lines to vemurafenib is independent of the MAPK pathway. We focused on a set of 27 genes that were differentially upregulated in A375 cells, including *BMF* (Fig. 2d), a pro-apoptotic gene that had already been shown to be involved in acquired resistance to PLX4720 (ref. 6), a vemurafenib analogue. Of these 27 genes, *BMF* was the only one that, when knocked down (by short interfering RNA (siRNA)-mediated depletion), led to the relative resistance of A375 cells to vemurafenib (Extended Data Fig. 9a, b). Vemurafenib treatment led to a strong increase in the expression of *BMF* in A375 cells but not in Mel624 cells (Fig. 2e). siRNA-mediated depletion of *BMF* led to decreased vemurafenib-dependent eIF4G cleavage (Fig. 2f) and to increased eIF4F complex formation (Fig. 2g), suggesting that *BMF* is involved in the sensitivity to vemurafenib by acting on the cleavage of eIF4G, which, in turn, affects eIF4F complex formation. In favour of this hypothesis, we found that the cleavage of eIF4G (first observed 45 min after treatment) preceded the disruption of eIF4F (first observed 90 min after treatment) (Extended Data Fig. 6c, d). Thus, in addition to reactivation of the MAPK pathway and/or activation of the PI(3)K-AKT-mTOR pathway, the formation of the eIF4F complex is also an indicator of resistance linked to modulation of apoptotic cascades.

To further support the idea that the formation of the eIF4F complex is involved in sensitivity to vemurafenib, we used the small molecule inhibitor 4EGI-1 (4EGI-1), which disrupts eIF4E-eIF4G interaction¹⁴. 4EGI-1 decreased the eIF4E-eIF4G interaction and, in parallel, increased the eIF4E-4EBP1 interaction in all cell lines tested (Extended Data Fig. 5b). Vemurafenib-resistant cell lines were more sensitive to 4EGI-1 than were vemurafenib-sensitive cell lines (Fig. 3a), suggesting a direct role of the eIF4F complex in proliferation. To examine whether resistance can be reversed by disrupting the eIF4F complex, we explored the effect of the combination of vemurafenib and 4EGI-1 on Mel624 cells and found a clear synergistic effect of these compounds (Fig. 3b). Thus, the formation of the eIF4F complex is directly involved in sensitivity to vemurafenib. Targeting translation may therefore be a strategy to overcome resistance to anti-BRAF and/or anti-MEK compounds. Silvestrol, a naturally occurring member of the flavagline family of compounds, inhibits cap-dependent translation by targeting eIF4A¹⁵⁻¹⁷. However, silvestrol displays poor ADME (absorption, distribution, metabolism and excretion) characteristics and is sensitive to P-glycoprotein-mediated multidrug resistance, which severely hampers its use in *in vivo* studies^{18,19}.

To circumvent this problem, we chose to evaluate a series of synthetic flavagline derivatives (Supplementary Notes) for their capacity

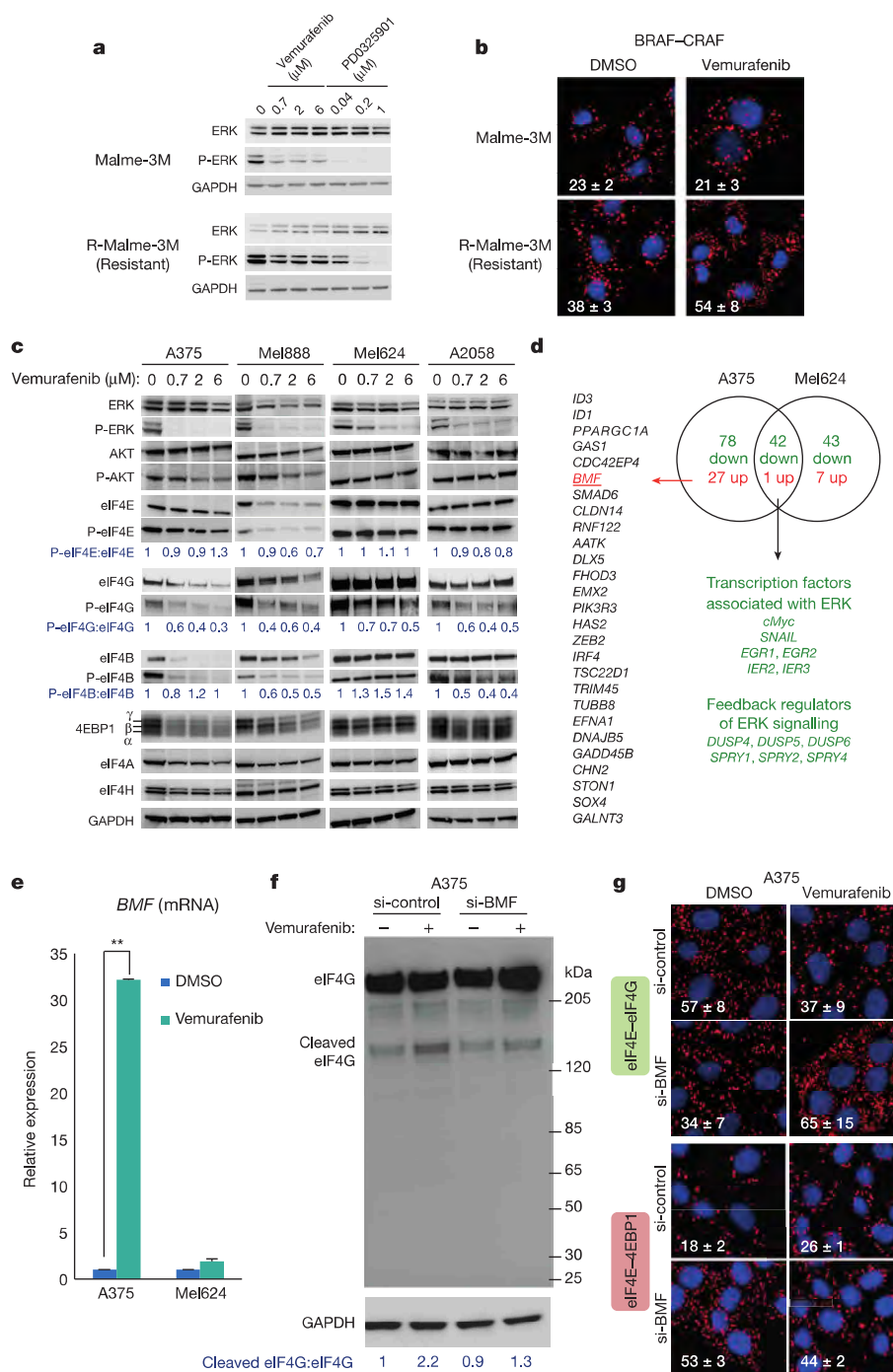


Figure 2 | Identification of mechanisms of resistance associated with persistent eIF4F formation. **a, c**, Western blot analysis with antibodies specific for phosphorylated (P-) or total proteins as indicated. **b**, BRAF-CRAF interaction detected by PLA. The white numbers indicate the mean \pm s.d. ($n = 3$). **d**, Venn diagram showing the overlap of differentially expressed genes in several vemurafenib-treated cell lines. The list of genes on the left represents the 27 genes whose expression was upregulated by vemurafenib in A375 cells but not in Mel624 cells. *EGR*, early growth response; *IER*, immediate early

response. **e**, Expression of *BMF* mRNA (as determined by quantitative reverse transcription PCR (qRT-PCR)) in vemurafenib-treated A375 cells compared with dimethylsulphoxide (DMSO) controls. The data are presented as the mean \pm s.d. ($n = 3$), and differences were assessed with Student's *t*-test (**, $P < 0.01$). **f**, Western blotting analysis of vemurafenib treatment on *BMF*-depleted A375 cells. si-BMF, *BMF*-directed siRNA; si-control, control siRNA. **g**, eIF4E-eIF4G and eIF4E-4EBP1 interactions detected by PLA. The white numbers are the mean \pm s.d. ($n = 3$).

to inhibit the eIF4F complex, by using a bicistronic luciferase reporter construct (pR-HepC-L) (Fig. 3c). In this assay, translation of the first (LucR) cistron is eIF4F-dependent, while translation of the hepatitis C virus internal ribosome entry site (IRES)-driven second (LucF) cistron is eIF4F-independent. Differential translation of both cistrons, as measured by the ratio of luciferase activities, directly reflects differences in eIF4F activity. Treatment of pR-HepC-L-transfected A375 cells with

silvestrol and several flavaglines (for example, FL3, FL14, FL23 or FL36) led to an increase in the LucF:LucR ratio (Fig. 3d), indicating that those drugs target eIF4F in a specific manner. A structure-function relationship study allowed us to define the best translation inhibitors (Fig. 3e). The ability to inhibit eIF4F-dependent translation correlated with the ability to inhibit cell proliferation (Fig. 3f). Finally, we found that combining vemurafenib and an eIF4A inhibitor, such as FL3, silvestrol or

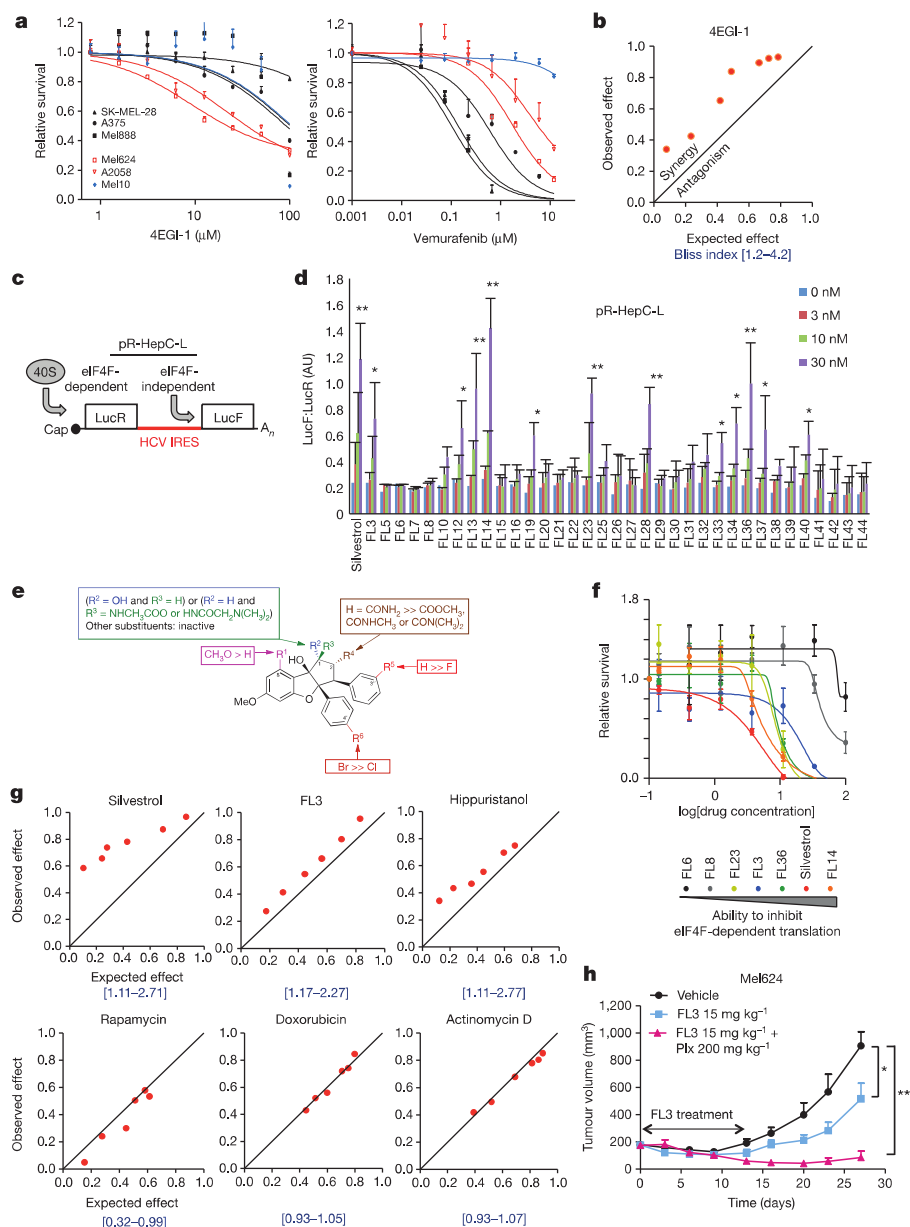


Figure 3 | Flavaglines target eIF4F and synergize with vemurafenib. **a, f**, Cell proliferation assays. The data are presented as the mean \pm s.d. ($n = 4$). Survival is shown relative to DMSO controls. (The ability to inhibit eIF4F-dependent translation is derived from **d**.) **b, g**, Isobologram of the effect of the combination of vemurafenib plus the indicated drugs on Mel624 cells. The Bliss index is shown in square brackets. **c**, Schematic of the mRNA produced from the pR-HepC-L vector. HCV IRES, hepatitis C virus internal ribosome entry site. **d**, Ratio of LucF to LucR activity (AU, arbitrary units) in pR-HepC-L-transfected A375 cells treated with flavaglines. The data are presented as the mean \pm s.d. ($n = 4$), and differences were assessed with Student's *t*-test (*, $P < 0.05$; **, $P < 0.01$). **e**, Structure–function relationships of the flavaglines. **h**, Growth of Mel624 xenografts in mice. The data are presented as mean tumour volume + s.e.m. ($n = 6$ mice per group); one-sided Mann–Whitney test, *, $P < 0.05$; ** $P < 0.01$.

hippuristanol⁸, had a synergistic effect on the proliferation of Mel624 cells (Fig. 3g). Interestingly, this synergy was not observed with other chemotherapeutics such as doxorubicin (which intercalates into duplex DNA), actinomycin D (which inhibits RNA synthesis) or rapamycin (which targets mTORC1) (Fig. 3g). Rapamycin is expected to dephosphorylate 4EBP1 and should disrupt the eIF4F complex, which, in turn, should lead to a synergistic effect of vemurafenib and rapamycin. However, we found that rapamycin did not lead to 4EBP1 dephosphorylation in Mel624 cells, explaining the lack of synergy (Extended Data Fig. 9c). Xenograft experiments were then performed with FL3, which was chosen from the flavaglines because of its ability to overcome multidrug resistance and its activity *in vivo*²⁰. The combination of FL3 plus PLX4720 (Plx) given at a moderate dose of 200 mg per kg body weight led to a strong reduction in Mel624 tumour growth (Fig. 3h). The cooperative action of FL3 and Plx was shown by using a low dose of Plx (90 mg per kg body weight), at which no effect on Mel624 tumour growth was observed with Plx alone (Extended Data Fig. 2d).

To evaluate the clinical relevance of the eIF4F complex in patients, we investigated its presence in 16 biopsy specimens (before and during anti-BRAF therapy) from 7 patients with metastatic melanoma (Supplementary

Table 4). Interestingly, sequencing of the tumours that were progressing revealed an acquired PI(3)K(Q546R) mutation in a metastasis from patient 6 (Supplementary Table 5) close to a recently described activating mutation (E545G) in PI(3)K that is associated with acquired resistance². We observed a decrease in eIF4F complex formation (as measured by the ratio of the eIF4E–eIF4G complex to the eIF4E–4EBP1 complex) in three out of four biopsy samples of responding tumours (Fig. 4 and Extended Data Fig. 10) compared with biopsy samples taken before therapy (baseline). By contrast, in all resistant tumours that were progressing under therapy, we found a clear increase in eIF4F complex formation compared with the baseline biopsy samples (Fig. 4 and Extended Data Fig. 10). Interestingly, patient 4 had two metastases with an early mixed response to vemurafenib treatment: one metastasis responding to treatment (meta. 1), and the other resisting treatment (meta. 2). While an increase in eIF4F was found in the resistant metastasis, no change was observed in the responding metastasis (Fig. 4b). Thus, a direct correlation was found between the response to treatment and the formation of eIF4F complexes, illustrating the *in vivo* association between sensitivity to anti-BRAF therapy and inhibition of the eIF4F complex. We found that the increase in eIF4F complex formation was

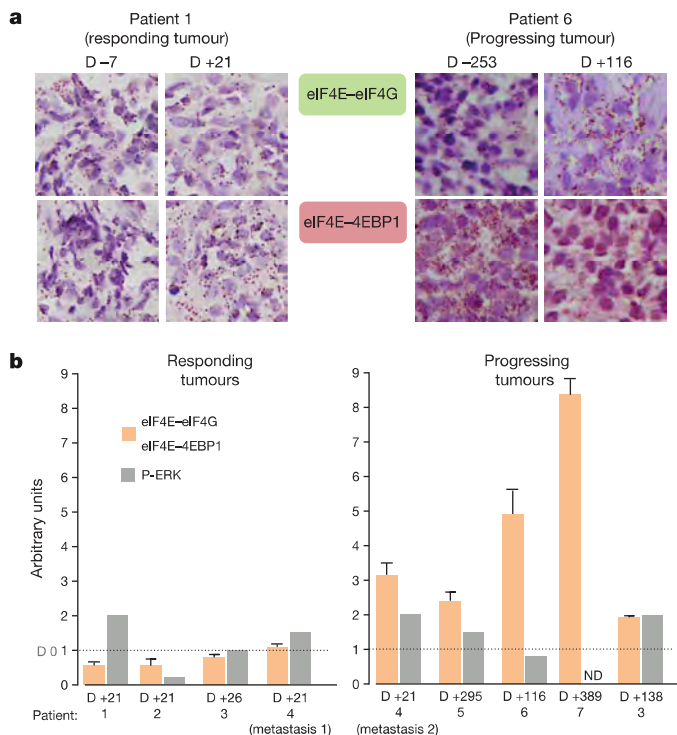


Figure 4 | Formation of the eIF4F complex in patients. **a**, eIF4E-eIF4G and eIF4E-4EBP1 interactions detected by PLA in samples from the indicated patients at the indicated times. The number corresponds to the day (D) of biopsy before (–) or after (+) treatment. Each brown spot represents an interaction. **b**, PLA quantification showing the ratio between the eIF4E-eIF4G interactions per 100 nuclei and the eIF4E-4EBP1 interactions per 100 nuclei, normalized to the same ratio before treatment (D 0) (mean \pm s.d.). Phosphorylated ERK (P-ERK) immunoreactivity was assessed semiquantitatively (grey bars).

more significantly associated with resistance than was the ERK phosphorylation level, which is conventionally investigated to explore resistance (Fig. 4b). This finding confirmed our *in vitro* data showing that the formation of the eIF4F complex was associated with resistance to vemurafenib in both ERK-dependent and ERK-independent resistance mechanisms. Using emerging technologies, such as ribosome profiling²¹, to examine the translation landscape of anti-BRAF and/or anti-MEK-sensitive and -resistant tumour cell lines should pave the way for an in-depth understanding of the contribution of genes that are regulated at the translational level in resistance mechanisms to targeted cancer therapies.

Online Content Methods, along with any additional Extended Data display items and Source Data, are available in the online version of the paper; references unique to these sections appear only in the online paper.

Received 19 December 2013; accepted 10 June 2014.

Published online 27 July 2014.

- Lito, P., Rosen, N. & Solit, D. B. Tumor adaptation and resistance to RAF inhibitors. *Nature Med.* **19**, 1401–1409 (2013).
- Shi, H. *et al.* Acquired resistance and clonal evolution in melanoma during BRAF inhibitor therapy. *Cancer Discov.* **4**, 80 (2014).
- Tentori, L., Lacial, P. M. & Graziani, G. Challenging resistance mechanisms to therapies for metastatic melanoma. *Trends Pharmacol. Sci.* **34**, 656–666 (2013).

- Blagden, S. P. & Willis, A. E. The biological and therapeutic relevance of mRNA translation in cancer. *Nature Rev. Clin. Oncol.* **8**, 280–291 (2011).
- Silvera, D., Formenti, S. C. & Schneider, R. J. Translational control in cancer. *Nature Rev. Cancer* **10**, 254–266 (2010).
- Shao, Y. & Aplin, A. E. BH3-only protein silencing contributes to acquired resistance to PLX4720 in human melanoma. *Cell Death Differ.* **19**, 2029–2039 (2012).
- Thoreen, C. C. *et al.* A unifying model for mTORC1-mediated regulation of mRNA translation. *Nature* **485**, 109–113 (2012).
- Cencic, R., Galicia-Vazquez, G. & Pelletier, J. Inhibitors of translation targeting eukaryotic translation initiation factor 4A. *Methods Enzymol.* **511**, 437–461 (2012).
- Oikonomou, E., Koc, M., Sourkova, V., Andera, L. & Pintzas, A. Selective BRAFV600E inhibitor PLX4720, requires TRAIL assistance to overcome oncogenic PIK3CA resistance. *PLoS ONE* **6**, e21632 (2011).
- Prahallad, A. *et al.* Unresponsiveness of colon cancer to BRAF(V600E) inhibition through feedback activation of EGFR. *Nature* **483**, 100–103 (2012).
- Montero-Conde, C. *et al.* Relief of feedback inhibition of *HER3* transcription by RAF and MEK inhibitors attenuates their antitumor effects in *BRAF*-mutant thyroid carcinomas. *Cancer Discov.* **3**, 520–533 (2013).
- Packer, L. M., East, P., Reis-Filho, J. S. & Marais, R. Identification of direct transcriptional targets of *v600E*BRAF/MEK signalling in melanoma. *Pigment Cell Melanoma Res.* **22**, 785–798 (2009).
- Pratlas, C. A. *et al.* *v600E*BRAF is associated with disabled feedback inhibition of RAF-MEK signaling and elevated transcriptional output of the pathway. *Proc. Natl Acad. Sci. USA* **106**, 4519–4524 (2009).
- Moerke, N. J. *et al.* Small-molecule inhibition of the interaction between the translation initiation factors eIF4E and eIF4G. *Cell* **128**, 257–267 (2007).
- Bordeleau, M. E. *et al.* Therapeutic suppression of translation initiation modulates chemosensitivity in a mouse lymphoma model. *J. Clin. Invest.* **118**, 2651–2660 (2008).
- Cencic, R. *et al.* Synergistic effect of inhibiting translation initiation in combination with cytotoxic agents in acute myelogenous leukemia cells. *Leuk. Res.* **34**, 535–541 (2010).
- Sadlish, H. *et al.* Evidence for a functionally relevant rocaglamide binding site on the eIF4A-RNA complex. *ACS Chem. Biol.* **8**, 1519–1527 (2013).
- Gupta, S. V. *et al.* Resistance to the translation initiation inhibitor silvestrol is mediated by ABCB1/P-glycoprotein overexpression in acute lymphoblastic leukemia cells. *AAPS J.* **13**, 357–364 (2011).
- Liu, T. *et al.* Synthetic silvestrol analogues as potent and selective protein synthesis inhibitors. *J. Med. Chem.* **55**, 8859–8878 (2012).
- Thuaud, F. *et al.* Synthetic analogue of rocaglamide displays a potent and selective cytotoxicity in cancer cells: involvement of apoptosis inducing factor and caspase-12. *J. Med. Chem.* **52**, 5176–5187 (2009).
- Ingolia, N. T., Brar, G. A., Rouskin, S., McGeachy, A. M. & Weissman, J. S. The ribosome profiling strategy for monitoring translation *in vivo* by deep sequencing of ribosome-protected mRNA fragments. *Nature Protocols* **7**, 1534–1550 (2012).

Supplementary Information is available in the online version of the paper.

Acknowledgements The authors thank J. Tanaka for providing hippuristanol. We thank the following Gustave Roussy platforms: Imaging and Cytometry Platform IRCIV (S. Salome-Desmoulez), Module de Développement en Pathologie, SIRIC SOCRATE (J. Adam), Translational Research Laboratory and Biobank (M. Breckler and L. Lacroix), Plateforme d'évaluation Préclinique (P. Gonin and K. Ser-le Roux), Genomic Core Facility (N. Pata-Merci) and Bioinformatic Core Facility (G. Meurice). We also thank V. Camara-Clayette for help with ³⁵S experiments, S. Roy for patient data collection and L. Saint Ange for text editing. C.R. and S.V.'s team was supported by Institut National du Cancer (INCA), Association pour la Recherche sur le Cancer (ARC) and Ligue contre le Cancer via an Integrated Research Action Program Melanoma (PAIR Melanome), Cancéropôle Ile de France and Ensemble Contre le Mélanome. L.D. was supported by the Association pour la Recherche sur le Cancer (ARC). We also thank the ARC and AAREC Filia Research for fellowships to N.R. and C.B. O.H. was supported by the Wenner-Gren Foundation and the Swedish Society of Medicine.

Author Contributions L.B., H.M.-M., I.G., D.A., O.H., G.T., C.B., N.R., F.T., N.K.-K., S.A. and L.D. designed and performed experiments and analysed the data. C.M., E.R., M.T. and A.M.E. provided clinical samples and gave advice. S.V. and C.R. supervised all research, wrote the manuscript and are joint senior authors.

Author Information Microarray data have been deposited in the ArrayExpress database under accession number E-MTAB-2607. Reprints and permissions information is available at www.nature.com/reprints. Readers are welcome to comment on the online version of the paper. The authors declare competing financial interests: details are available in the online version of the paper. Correspondence and requests for materials should be addressed to C.R. (caroline.robert@gustaveroussy.fr) or S.V. (stephan.vagner@inserm.fr).

METHODS

Cell lines and reagents. The A375, Mel888, A2058, SK-MEL-28, SK-MEL-5 and Malme-3M melanoma cell lines used in this study were purchased from the ATCC. The Mel624 and Mel10 cell lines were a gift from G. Lizee and L. Zitvogel, respectively. The BCPAP thyroid cancer cell line, HT-29 colorectal cancer cell line and MDA-MB-468 breast cancer cell line were gifts from C. Dupuy, S. Chouaib, and C. Nahmias, respectively. Cancer cell lines were maintained at 37 °C and 5% CO₂ in a humidified atmosphere and grown in RPMI 1640, MEM or DMEM growth media supplemented with 10% FBS, 2 mM glutamine, 50 U ml⁻¹ penicillin and 50 mg ml⁻¹ streptomycin (Gibco). The Malme-3M cells were grown in IMDM supplemented with 20% FBS. All cell lines were regularly verified to be mycoplasma-free using a PCR-based test (Biovalley). Genomic DNA was isolated using Genomic-Tips kits (QIAGEN), and the mutational status of *BRAF* (exons 11 and 15) and *NRAS* (exons 2 and 3), and other hotspot genes listed in Supplementary Table 1, was determined by direct sequencing of PCR amplification products.

Cells were treated with BRAF inhibitors (vemurafenib and dabrafenib), MEK inhibitors (trametinib and PD0325901), a MNK inhibitor (CGP 57380), an eIF4E-eIF4G interaction inhibitor (4EGI-1), eIF4A inhibitors (flavaglines and hippuristanol), rapamycin, doxorubicin or actinomycin D. All drugs were dissolved in dimethylsulphoxide (DMSO) for *in vitro* studies. Trametinib and dabrafenib were obtained from GlaxoSmithKline, and PLX4720 was obtained from Plexikon, without any financial support.

Proliferation analysis and Bliss index. Cell proliferation was measured using WST-1 reagent (Roche Applied Science). Melanoma cells were plated (5,000 cells per well) in 96-well tissue culture plates. After 24 h, the cells were treated with drugs or DMSO at the indicated concentrations, in triplicate. WST-1 reagent was added to the wells and incubated at 37 °C for 2 h before and after the treatment period of 48 h. The plates were then read at 450 nm on a Victor³ Multilabel Counter model 1420 (Perkin Elmer). Cell proliferation is expressed as percentage of the absorbance compared with mock-treated cells.

To evaluate the effect of vemurafenib in combination with other drugs, we compared the observed and expected responses obtained from combination treatment. The Loewe additivity model was used to predict the combined effect of each drug. The expected effect (E_{exp}) of the combination was estimated from each separate drug effect:

$$E_{exp} = E_{drug1} + E_{drug2} - (E_{drug1} \times E_{drug2}).$$

The observed:expected ratio was calculated according to the Bliss method. In this model, the excess above the predicted Bliss index represents the synergistic effect of the combination treatment. The Bliss index was calculated as the observed:expected ratio, where an index of 1, <0 or >1 indicates additive, antagonistic or synergistic effects, respectively.

Mel624 cells were treated for 48 h before the WST-1 assay with 6 mM 4EGI-1 or 8 nM FL3 and variable doses of vemurafenib, ranging from 25 nM to 12 μM.

Isobolograms represent the correlation between the observed and the expected effects of the combination of two drugs. The upper left region of the figure represents increasing degrees of synergy.

Clonogenic assays. For clonogenic assays, cells were plated at low density (1 × 10³ cells per well in 6-well tissue culture plates) in fresh media. After 24 h, cells were treated with drugs or DMSO at the indicated concentrations, in duplicate. After 14 days, cells were stained with 0.5% (w/v) crystal violet in 70% ethanol, and the number of colonies was counted.

Western blot analysis. Western blot analysis was performed on cell extracts of the indicated cell lines treated for 24 h (Fig. 2a, c) or 3 h (Fig. 2f) with the indicated concentrations of vemurafenib or PD0325901. Immunoblots were performed from whole cell lysate prepared using RIPA Buffer (Cell Signaling Technology) supplemented with dithiothreitol (DTT), phenylmethylsulphonyl fluoride (Sigma), and fresh protease and phosphatase inhibitors (Roche). Cell lysates were quantified for protein content using a bicinchoninic acid (BCA) protein assay kit (Thermo). Protein samples were resolved on NuPAGE 12% Bis-Tris gels with MOPS buffer or 3–8% Tris acetate gels with Tris acetate buffer (Life Technologies) and then transferred to 0.45-μm nitrocellulose membrane (Bio-Rad). After saturation in Tris-buffered saline buffer supplemented with 5% powdered milk, the membranes were incubated with antibodies (diluted at 1:1,000) overnight at 4 °C. Antibodies specific for the following proteins were purchased from Cell Signaling Technology: eIF4G (raised in rabbits, catalogue no. 2498), 4EBP1 (rabbit, clone 53H11, 9644), 4EBP1 phospho-S65 (rabbit, 9451L), eIF4E (rabbit, clone C46H6, 2067), eIF4A1 (rabbit, 2490), eIF4B (rabbit, 3592), eIF4B phospho-S422 (rabbit, 3591), eIF4G phospho-S1108 (rabbit, 2441), eIF4H (rabbit, clone D85F2, 3469), AKT (rabbit, 9272), AKT phospho-S473 (rabbit, clone D9E, 4060), ERK1/2 (rabbit, 9102) and ERK1/2 phospho-T202/Y204 (rabbit, clone 20G11, 4376). The antibody specific for eIF4E phospho-S209 (rabbit, clone EP2151Y, ab76256) was purchased from

Abcam. The antibody specific for GAPDH (mouse, clone 6C5, MAB374) was purchased from Millipore. The antibody specific for β-actin (rabbit, A5060) was purchased from Sigma. Horseradish peroxidase (HRP)-conjugated secondary antibodies were purchased from Sigma. Quantification of the bands was done with ImageJ. In most cases (except Fig. 2f), the displayed images were cropped to focus on the protein of interest.

In Fig. 2f, full-length eIF4G is observed at an apparent molecular weight of 220 kDa. The p120 and p150 fragments represent products from a single caspase-3 cleavage event in the amino-terminal and carboxy-terminal halves of eIF4G, respectively. **Cap-binding assay.** eIF4F complex formation using the cap-binding assay was assessed in vemurafenib-treated (6 μM, 24 h) or untreated melanoma cell lines (A375, Mel888, Mel624 and A2058) (Fig. 1a). Cells were washed in cold PBS and lysed by three cycles of freezing at -80 °C and thawing on ice. Protein lysate (50 μg) was diluted in 200 μl 150 mM KCl, 50 mM HEPES, pH 7.5, 2 mM DTT, 0.2% Tween 20 and protease inhibitor cocktail. Lysates were incubated for 3 h with m⁷GTP-Sepharose 4B reconstituted beads (GE Healthcare, Amersham). Eluates and total cell lysates were used for immunoblotting.

Metabolic labelling. A375 cells were plated at 2.5 × 10⁵ cells in 6-well plates and incubated for 24 h. Cells were then treated with vemurafenib (3 or 24 h) or with 100 μg ml⁻¹ cycloheximide (15 min). After washing with methionine/cysteine-free DMEM (Gibco) supplemented with 10% dialysed FBS, cells were incubated with 11 μCi μl⁻¹ EasyTag EXPRESS³⁵S Protein Labeling Mix (PerkinElmer) in the presence of drugs in methionine/cysteine-free DMEM for 30 min. After washing with PBS, the cells were harvested in RIPA Buffer. The lysates were centrifuged at 12,000 r.p.m. (4 °C) and spotted onto Whatman 3MM filter paper. The proteins were precipitated with cold 10% trichloroacetic acid (TCA) solution for 15 min followed by 5% TCA solution for 10 min. The filters were then washed with 95% ethanol and air dried. The radioactivity was measured by scintillation counting and normalized to protein content.

Proximity ligation assay. Interactions between eIF4E and eIF4G (eIF4E-eIF4G) or eIF4E and 4EBP1 (eIF4E-4EBP1) were detected by *in situ* proximity ligation assay (PLA) in melanoma cell lines treated with 6 μM vemurafenib or untreated (Fig. 1b, 24 h treatment; Fig. 2g, 3 h treatment). The BRAF-CRAF interaction was detected by PLA in the Malme-3M melanoma cell line and its vemurafenib-resistant counterpart (R-Malme-3M) after treatment with vemurafenib (6 μM, 24 h) or no treatment (Fig. 2b). PLAs were performed on both fixed, permeabilized cells and on melanoma tissue sections. Following dewaxing and rehydration of tissue sections, antigen retrieval was performed by heating the slides for 30 min at 95 °C in Tris-EDTA buffer, pH 9. From this point, the tissue sections and the fixed, permeabilized cells were treated identically, and the PLA protocol was followed according to the manufacturers' instructions (Olink Bioscience), with incubation of the primary antibodies at 4 °C overnight. After blocking, the antibodies were used at the following concentrations: for eIF4E (mouse, clone A-10, catalogue number SC-271480, Santa Cruz Biotechnology, 1:200); for eIF4G (rabbit, 2498; Cell Signaling Technology, 1:200); for 4EBP1 (rabbit, clone 53H11, 9644, Cell Signaling Technology, 1:200). PLA minus and PLA plus probes (containing the secondary antibodies conjugated to oligonucleotides) were added and incubated for 1 h at 37 °C. More oligonucleotides were then added and allowed to hybridize to the PLA probes. Ligase was used to join the two hybridized oligonucleotides into a closed circle. The DNA was then amplified (with rolling circle amplification), and detection of the amplicons was carried out using the Brightfield detection kit for chromogenic development or using the Far Red detection kit for fluorescence. Cell nuclei were stained with 4',6-diamidino-2-phenylindole (DAPI). The sections were mounted with Olink Mounting Medium. The first results were visualized by confocal microscopy (Leica SPE), and the analysis was supported by Volocity software. To improve the sensitivity of the fluorescence detection, we next used a scanner (Olympus VS120) (magnification 20×; 2-ms exposure for the DAPI channel and 300-ms exposure for the Cy5 channel; 1 pixel = 0.32 μm), and the number of PLA signals per cell was counted (more than three fields) by semi-automated image analysis (ImageJ and OlyVIA).

Polysomal fractionation and microarray experiment. Sucrose density gradient centrifugation was used to separate the subpolysomal and the polysomal ribosome fractions. Fifteen minutes before collection, cells were incubated at 37 °C with 100 μg ml⁻¹ cycloheximide added to the culture medium. Next, cells were washed, scraped into ice-cold PBS supplemented with 100 μg ml⁻¹ cycloheximide, centrifuged at 3,000 r.p.m. for 5 min and then collected into 400 μl of LSB buffer (20 mM Tris, pH 7.4, 100 mM NaCl, 3 mM MgCl₂, 0.5 M sucrose, 2.4% Triton X-100, 1 mM DTT, 100 U ml⁻¹ RNasin and 100 μg ml⁻¹ cycloheximide). After homogenization, 400 μl LSB buffer supplemented with 0.2% Triton X-100 and 0.25 M sucrose was added. Samples were centrifuged at 12,000g for 10 min at 4 °C. The resultant supernatant was adjusted to 5 M NaCl and 1 M MgCl₂. The lysates were loaded onto a 15–50% sucrose density gradient and centrifuged in an SW41 rotor at 38,000 r.p.m. for 2 h at 4 °C. Polysomal fractions were monitored and collected using a gradient fractionation system (Isco). Total RNA was extracted from the four heaviest fractions

and the input samples using the TRIzol–chloroform method. Microarray experiments were performed in quadruplicate using Human Gene Expression 8×60 K arrays (Agilent). Microarray data are available in the ArrayExpress database under accession number E-MTAB-2607.

For quantitative reverse transcription PCR (qRT–PCR) experiments, total RNA was extracted by the TRIzol–chloroform method from 300 µl of each fraction (1–16). cDNA was prepared using SuperScript III Reverse Transcriptase (Invitrogen) with random hexamer primers according to the manufacturer's instructions. The same volume of cDNA from each fraction was used to perform qPCR experiments.

RNA extraction and qPCR. Total RNA was extracted using the TRIzol–chloroform extraction method. Samples were digested with DNase I (Turbo DNA free, Ambion). The quality of RNAs was assessed using a Bioanalyzer instrument (Agilent) and then quantified using a NanoDrop 1000 instrument (Thermo Scientific). cDNA was prepared using SuperScript III Reverse Transcriptase with random hexamer primers according to the manufacturer's instructions. Transcript abundance was determined by qPCR using SYBR Green PCR Master Mix (Applied Biosystems) with the primers indicated in Supplementary Table 7. Data were analysed by the threshold cycle (Ct) comparative method and normalized to the *TBP* gene. Relative expression of *BMF* mRNA (as determined by qRT–PCR) was assessed in vemurafenib-treated (6 µM for 3 h) or control cell lines (Fig. 2e).

RNA interference. Cells were transfected with 20 nM of each siRNA using Lipofectamine RNAiMAX Reagent (Life Technologies) following the supplier's instructions. siRNAs were purchased from Thermo Scientific (ON-TARGETplus SMARTpool technology). The sequences of the siRNAs are shown in Supplementary Table 6.

Dual luciferase reporter assays. Dual luciferase assays were conducted in A375 cells transfected with 50 ng pR–HepC–L bicistronic vector in 96-well plates using Lipofectamine 2000 reagent (Life Technologies) and treated for 16 h with three concentrations of each of the indicated flavaglines (formulae in Supplementary Notes). The lysates were prepared in triplicate with the Dual-Luciferase Reporter Assay System (Promega), and 12 µl firefly and *Renilla* bioluminescence lysates were measured with the GloMax 96 Microplate Luminometer (Promega) ($n = 3$).

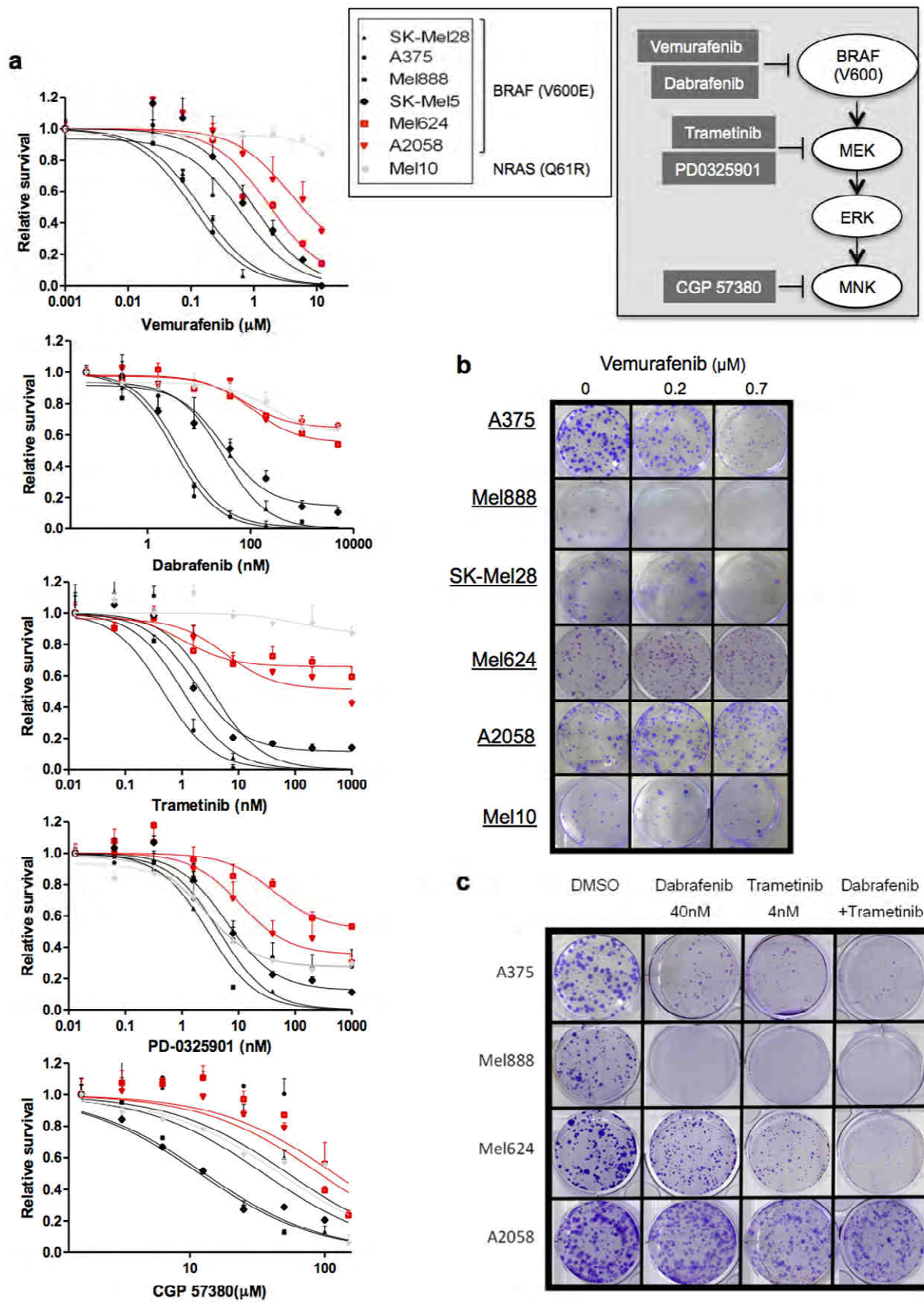
Mouse xenograft study. Animals were housed under pathogen-free conditions with food and water *ad libitum*. Experiments were performed in accordance with the CCAC

guidelines and approved by the ethical committee of the Plateforme d'évaluation Préclinique of Gustave Roussy. Animals were allocated to experimental groups so that the groups had similar mean tumour volumes at day 0 of treatment. The investigator was not blinded to the group allocation or when assessing the outcome. Female Swiss nude (athymic) mice were purchased from the animal facility of Gustave Roussy. At the age of 6–8 weeks, they were injected subcutaneously in the right flank with 5×10^6 A375 cells in 200 µl PBS or 5×10^6 Mel624 cells in 200 µl PBS and 50% Matrigel (BD Biosciences). When tumours reached an average volume of 100–300 mm³, mice were fed with the control rodent diet or 90 (low dose), 200 (medium dose) or 417 (high dose) mg of the vemurafenib analogue PLX4720 (Plexixikon) per kg body weight. FL3 (15 mg per kg body weight) was injected intraperitoneally each day for 13 days. FL3 was dissolved in DMSO to make a 27.5 mg ml⁻¹ stock solution and then diluted in PBS containing 5% Kolliphor (Sigma) just before injection. Tumour growth was monitored twice a week in two dimensions using a digital caliper. Tumour volumes were calculated with the ellipsoid volume formula $L \times w^2 \times 0.5$, where L is length and w is width.

Clinical samples. Patients with metastatic melanoma harbouring a BRAF(V600) mutation were treated with a BRAF inhibitor, vemurafenib or dabrafenib. Patients had received appropriate information and signed an informed consent form authorizing tumour biopsies and molecular studies in the context of an institutional CRB-approved protocol (MSN-08-027). Tumours were biopsied before treatment, at various time points after treatment initiation, as well as on progression.

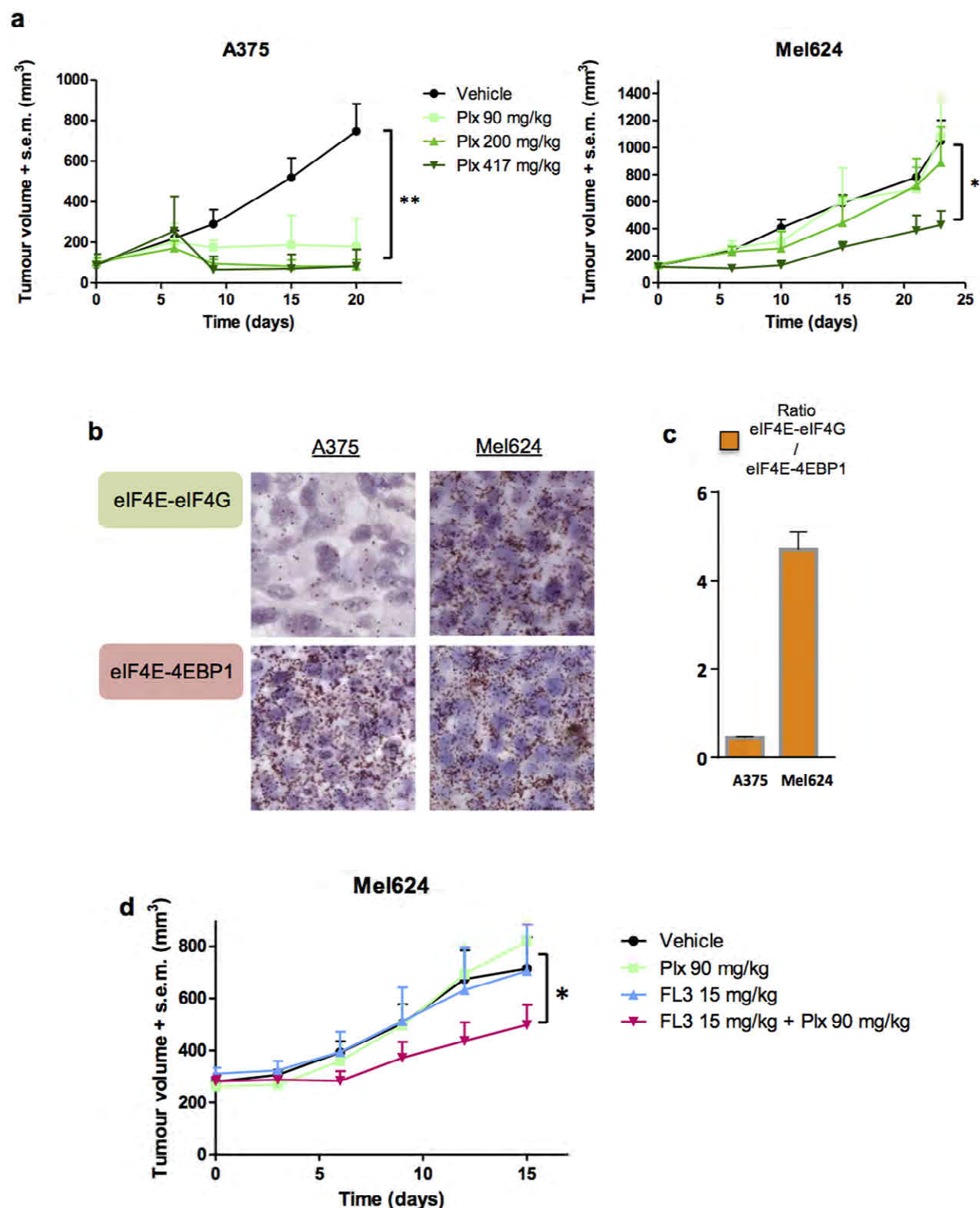
Notably, patient 4 had a mixed response 21 days after initiation of anti-BRAF treatment (metastasis 1 was responding while metastasis was growing). Patient 3 had a biopsy performed at day 26 during clinical response and at day 138 when relapsing.

Immunohistochemistry. Deparaffinized tissue sections were treated with Antigen Retrieval Solution (made from citrate buffer, pH 6.0, concentrated 10×, T0050 Diapath). Tissue sections were then incubated with Peroxidase Blocking Solution (S2023, Dako) for 15 min and Protein Block (X0909, Dako) for 20 min. Primary antibody specific for phospho-T202/Y204 ERK1/2 (rabbit, clone 20G11, 4376, Cell Signaling Technology) was applied, and the slides were incubated overnight at 4 °C. Signals were visualized using rabbit HRP-conjugated secondary antibody (K4003, Dako) and a haematoxylin (MHS32, Sigma) counterstain.



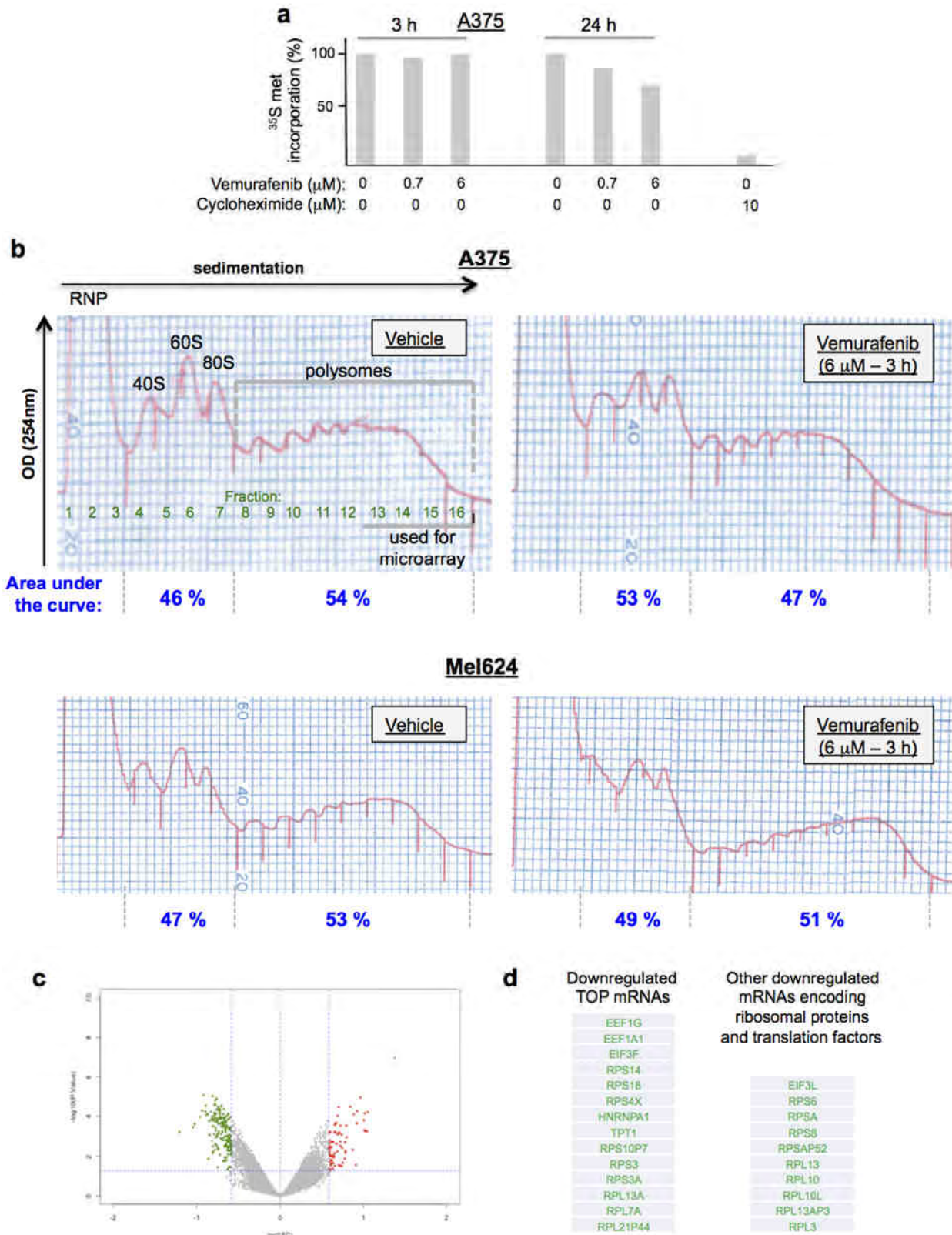
Extended Data Figure 1 | Sensitivity of melanoma cell lines to anti-BRAF, anti-MEK or anti-MNK inhibitors. a, Short-term growth-inhibition assay of the indicated cell lines (SK-MEL-28, A375, Mel888, SK-MEL-5, A2058, Mel624 and Mel10) treated with increasing concentrations of vemurafenib, dabrafenib, PD0325901, trametinib and CGP 57380 for 48 h. The Mel10 cell line does not have a mutated *BRAF* gene and was used as a control

vemurafenib-insensitive cell line. Cell viability was determined using the WST-1 cell proliferation assay. The data are presented as the mean \pm s.d. ($n = 3$). b, c, Long-term colony formation assay of the indicated cell lines. Cells were grown in the absence or presence of vemurafenib (b) or dabrafenib and trametinib (c) at the indicated concentrations for 2 weeks. For each cell line, all dishes were fixed at the same time, stained and photographed.



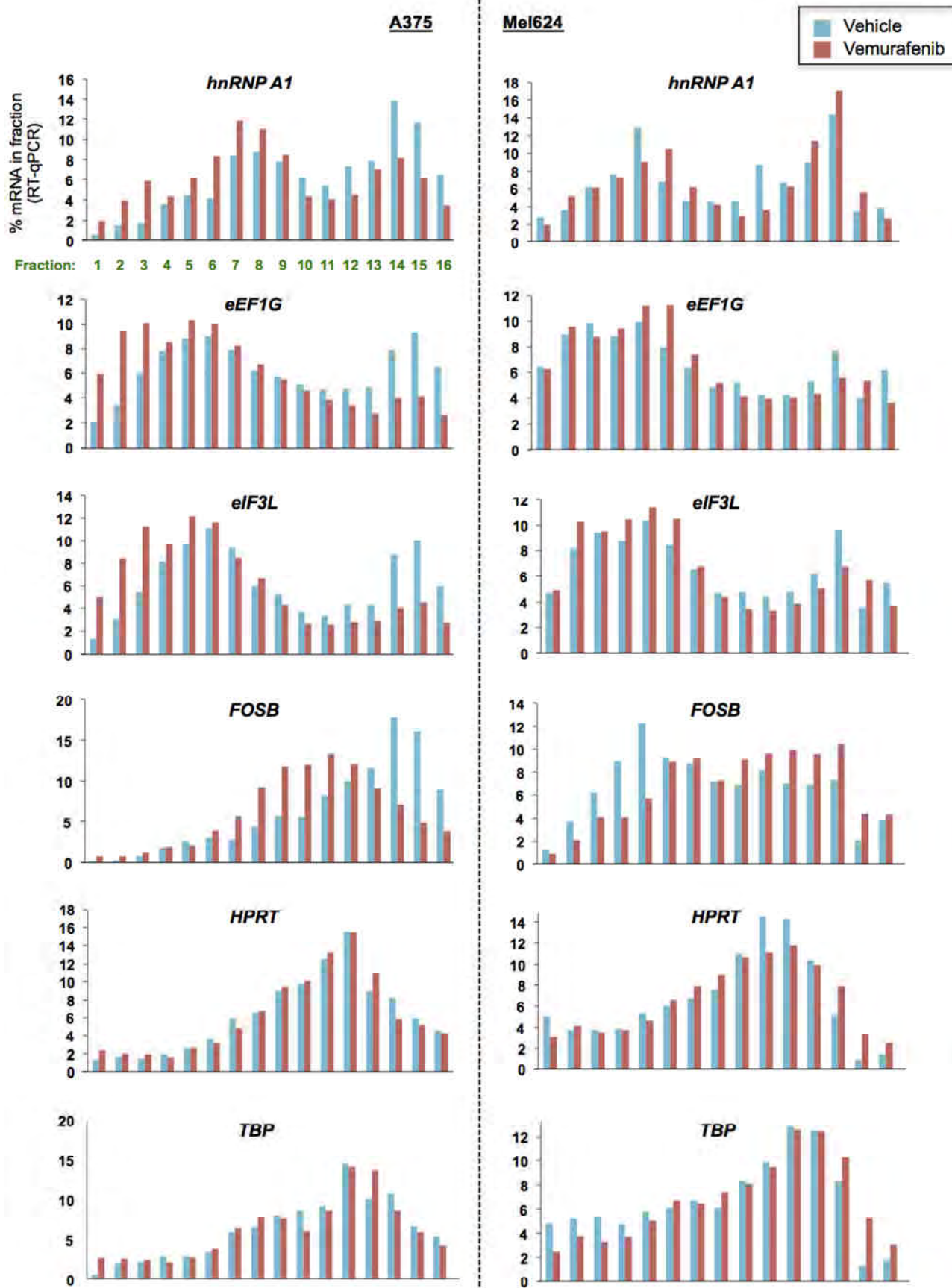
Extended Data Figure 2 | Xenograft study. **a**, Growth of A375 and Mel624 cells as tumour xenografts in nude mice treated with vehicle or increasing concentrations of PLX4720 (Plx). Mean tumour volumes + s.e.m. are shown (vehicle and 200 mg Plx per kg body weight groups of A375- and Mel624-xenografted mice comprised 4 mice; 90 mg and 417 mg Plx per kg body weight groups of A375-xenografted mice comprised 3 mice; 90 mg and 417 mg Plx per kg body weight groups of Mel624-xenografted mice comprised 5 mice). Significance was determined by one-sided Mann–Whitney U test (*, $P < 0.05$; ** $P < 0.01$). **b**, Interactions between eIF4E and eIF4G (eIF4E–eIF4G) or eIF4E and 4EBP1 (eIF4E–4EBP1) detected by *in situ* proximity ligation assay (PLA) in paraffin-embedded tissue sections of A375 and Mel624 xenografts from Plx-treated mice. The interactions were visualized as brown spots.

c, Quantification of the PLA showing the ratio between the number of purple spots corresponding to the eIF4E–eIF4G interaction per 100 nuclei and the number of purple spots corresponding to the eIF4E–4EBP1 interaction per 100 nuclei, normalized to the same ratio before treatment. Error bars, s.d. **d**, Growth of Mel624 cells as tumour xenografts in nude mice treated with vehicle, a low dose of Plx alone, FL3 alone or a combination of Plx and FL3. FL3 treatment was stopped after 13 days. The data are presented as the mean + s.e.m. (Vehicle, 15 mg FL3 per kg body weight, and 90 mg Plx per kg body weight plus 15 mg FL3 per kg body weight groups comprised 6 mice; 90 mg Plx per kg body weight group comprised 3 mice.) Significance was determined by one-sided Mann–Whitney U test (*, $P < 0.05$).



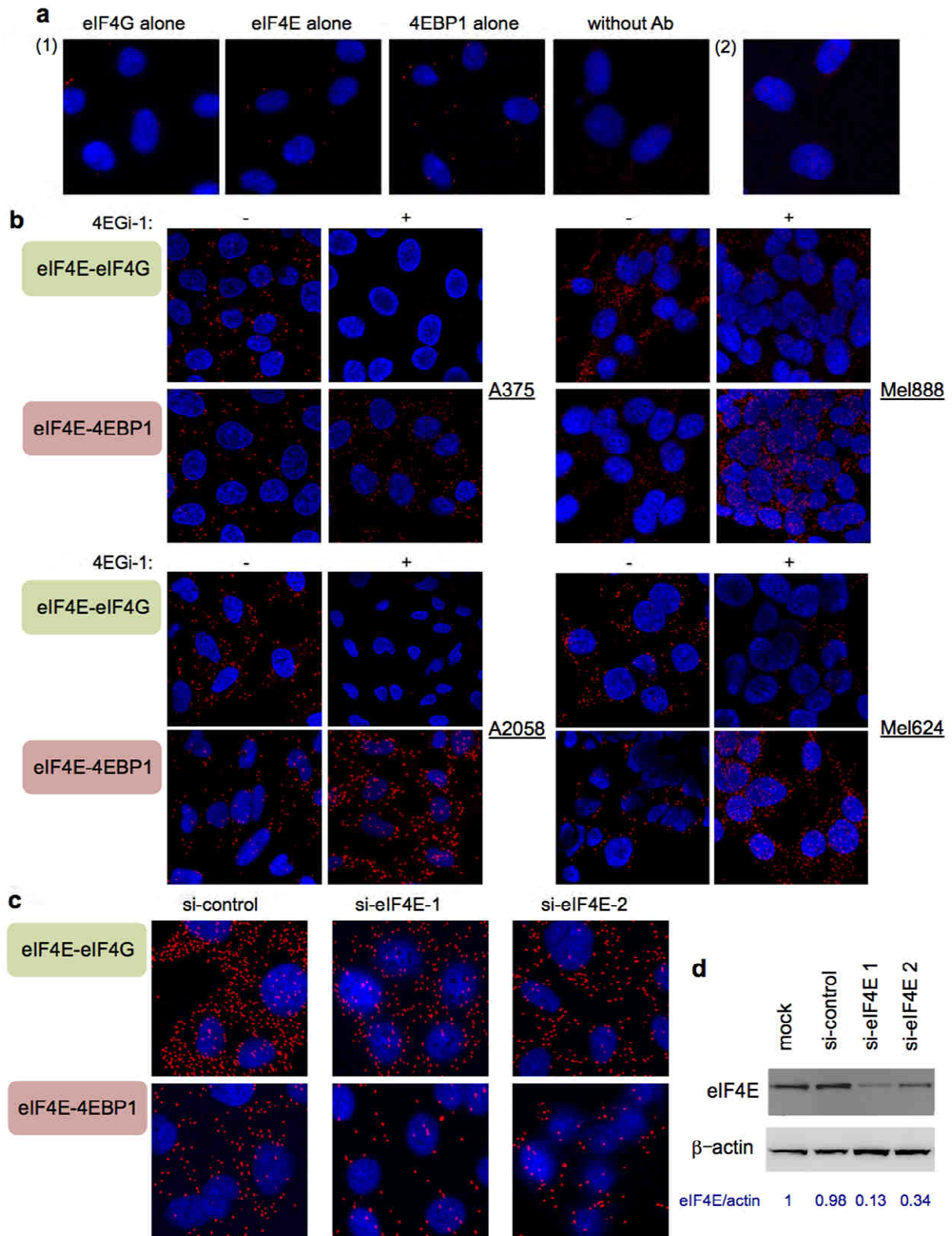
Extended Data Figure 3 | Protein synthesis rates and polysome profiles.
a, Protein synthesis rates were determined in A375 cells treated for the indicated times (3 or 24 h) with vehicle (dimethylsulphoxide (DMSO)) or 0.7 or 6 μM vemurafenib or for 15 min with 10 μM cycloheximide. Cells were then pulsed for 30 min with [³⁵S]Cys/Met, and the incorporation of ³⁵S into proteins was quantified and normalized to the total protein amount. The data are presented as the mean (*n* = 2). **b**, Polysome profiles of A375 and Mel624 cells treated with DMSO or 6 μM vemurafenib for 3 h. The area under the curve was

measured with ImageJ software. OD, optical density; RNP, ribonucleoparticle.
c, Volcano plot showing a subset of 251 mRNAs that were differentially translated between vemurafenib-treated and untreated A375 cells. Of these 251 mRNAs, 73 were overexpressed (red), and 178 were underexpressed (green).
d, A table showing some of the genes that encode mRNAs whose translation is inhibited by vemurafenib in A375 cells (see also Supplementary Table 2). These mRNAs belong to the TOP mRNA class, the members of which contain a TOP motif and/or encode translation factors and ribosomal proteins.



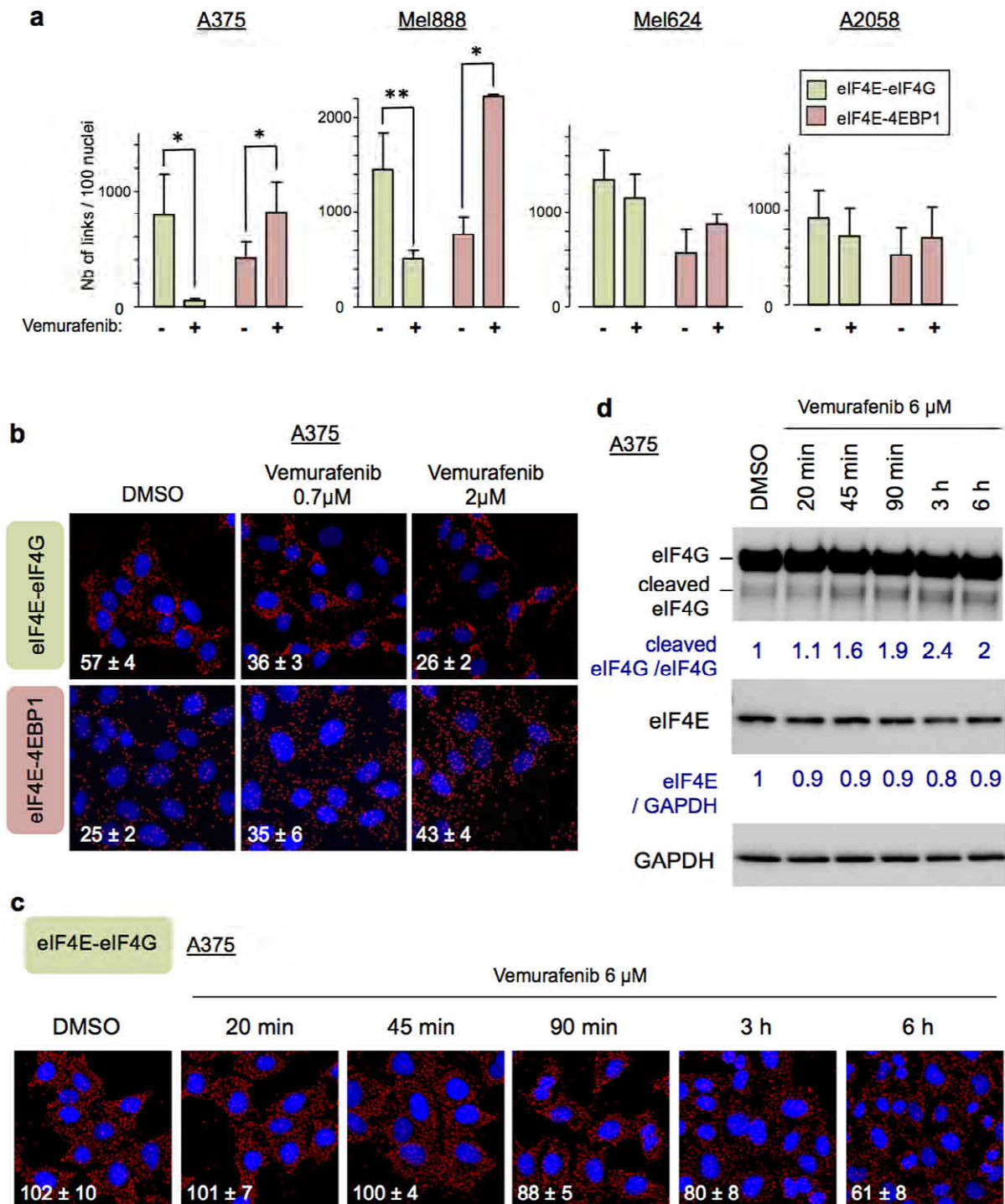
Extended Data Figure 4 | Translation of selected mRNAs in vemurafenib-treated melanoma cell lines. The abundance of *EEF1G*, *HNRNPA1*, *EIF3L*, *FOSB*, *TBP* (control) and *HPRT* (control) transcripts in fractions from

Extended Data Fig. 3b were quantified by quantitative reverse transcription PCR (qRT-PCR). The percentage of each mRNA in each fraction was calculated.



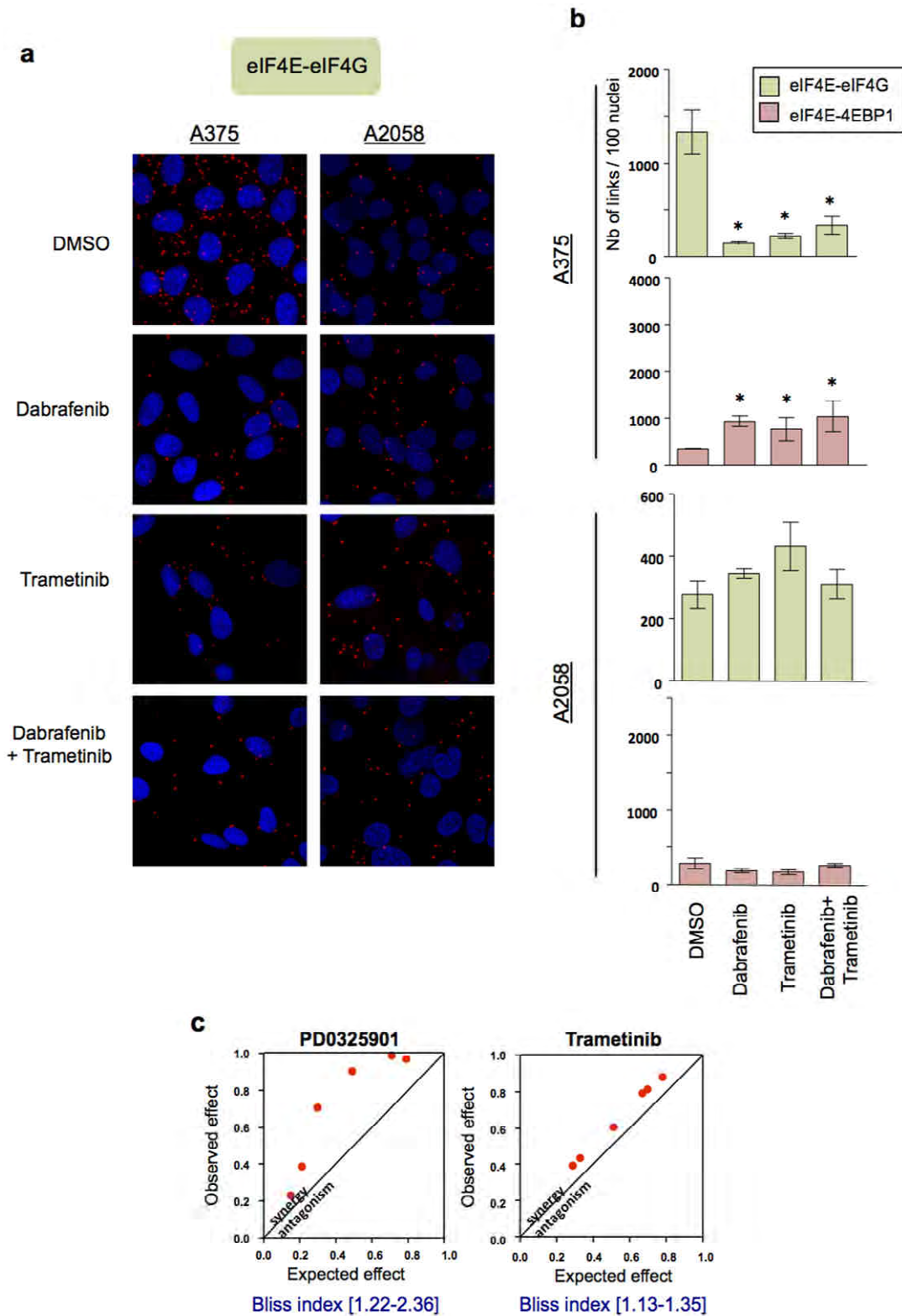
Extended Data Figure 5 | Formation of the eIF4F complex using a PLA procedure. **a**, The specificity of the PLA was evaluated by omitting one of the two primary antibodies or the two primary antibodies and by omitting the minus and plus PLA probes. **b**, The interactions between eIF4E and eIF4G (eIF4E-eIF4G) and eIF4E and 4EBP1 (eIF4E-4EBP1) detected by *in situ* PLA in the indicated cell lines treated for 24 h with the small molecule inhibitor 4EGI-1, which disrupts eIF4E-eIF4G interaction¹⁴. The interactions were

visualized as red fluorescent spots. Cell nuclei were stained with 4',6-diamidino-2-phenylindole (DAPI) (blue). **c**, The interactions between eIF4E and eIF4G (eIF4E-eIF4G) or eIF4E and 4EBP1 (eIF4E-4EBP1) detected by *in situ* PLA in siRNA-mediated eIF4E-depleted A375 cells. The interactions were visualized as red fluorescent spots. The cell nuclei were stained with DAPI (blue). **d**, Western blot analysis with antibodies specific for eIF4E and β-actin, to evaluate siRNA-mediated depletion of eIF4E.



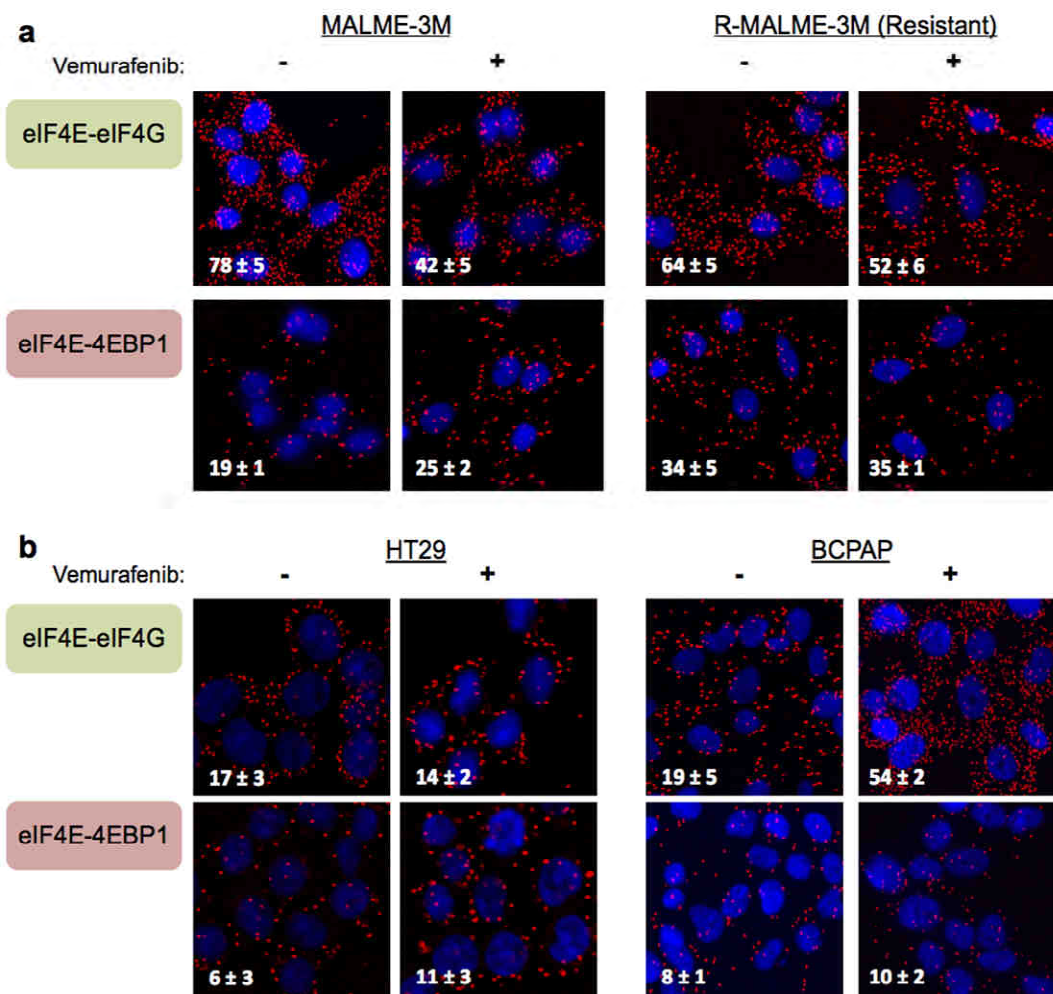
Extended Data Figure 6 | Formation of the eIF4F complex in vemurafenib-treated melanoma cell lines and analysis of eIF4G cleavage. **a**, Quantification of the PLA showing the number of red spots (corresponding to eIF4E-eIF4G or eIF4E-4EBP1 interactions) per 100 nuclei (quantified with Velocity software). The data are presented as the mean \pm s.d. ($n = 3$). Significance was determined by Mann-Whitney U test (*, $P < 0.05$; **, $P < 0.01$). **b**, The interactions between eIF4E and eIF4G (eIF4E-eIF4G) or eIF4E and 4EBP1 (eIF4E-4EBP1) detected by *in situ* PLA in A375 cells treated for 24 h with vemurafenib at the indicated concentrations. The interactions were visualized as red fluorescent spots. The cells were counterstained with DAPI (blue). White

numbers correspond to means, and error bars are derived from three replicates. **c**, Time course of the interactions between eIF4E and eIF4G (eIF4E-eIF4G) detected by *in situ* PLA in response to the treatment of A375 cells with 6 μ M vemurafenib. The interactions were visualized as red fluorescent spots at the indicated times. **d**, A375 cells were treated (or not treated) with 6 μ M vemurafenib and collected at the indicated times for western blot analysis with antibodies specific for eIF4G, eIF4E and GAPDH. The cleaved eIF4G:full-length eIF4G density ratio and the eIF4E:GAPDH density ratio (indicated in blue for each time point) were quantified by densitometric scanning of the blots followed by ImageJ analysis.



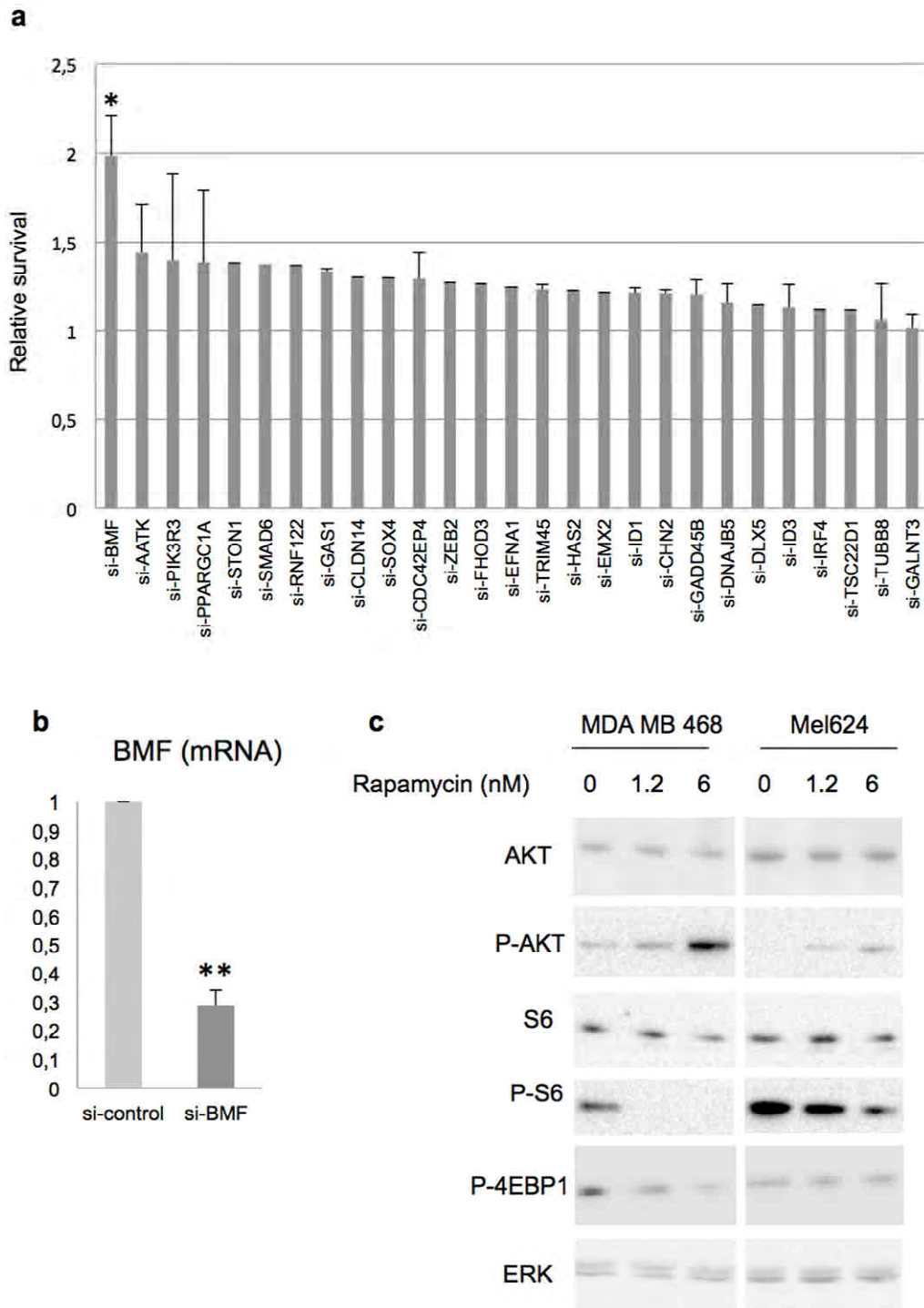
Extended Data Figure 7 | Formation of the eIF4F complex in anti-BRAF and anti-MEK treated melanoma cell lines and analysis of the synergistic effect of FL3 and anti-MEK compounds. **a**, The interactions between eIF4E and eIF4G (eIF4E-eIF4G) detected by *in situ* PLA in A375 and A2058 cell lines treated for 24 h with dabrafenib, trametinib or a combination of dabrafenib and trametinib. The interactions were visualized as red fluorescent spots with confocal microscopy (Leica SPE). Cell nuclei were stained with DAPI (blue). **b**, Quantification of the PLA results showing the number of red spots (corresponding to the eIF4E-eIF4G or eIF4E-4EBP1 interactions) per 100 nuclei calculated with Volocity software. The data are presented as the

mean \pm s.d. ($n = 3$). Significance was determined by the Mann-Whitney U test (*, $P < 0.05$; **, $P < 0.01$). **c**, Isobolograms showing the correlation between the observed and expected effects of the combination of MEK inhibitors (such as PD0325901 or trametinib) and FL3 on the Mel624 cell line. The upper left region of the figure represents increasing degrees of synergy. The minimum and maximum Bliss index values are shown as an interval within square brackets under each isobologram. The Bliss index was calculated as the ratio observed:expected, where 1, <0 or >1 indicate additive, antagonistic or synergistic effects, respectively.



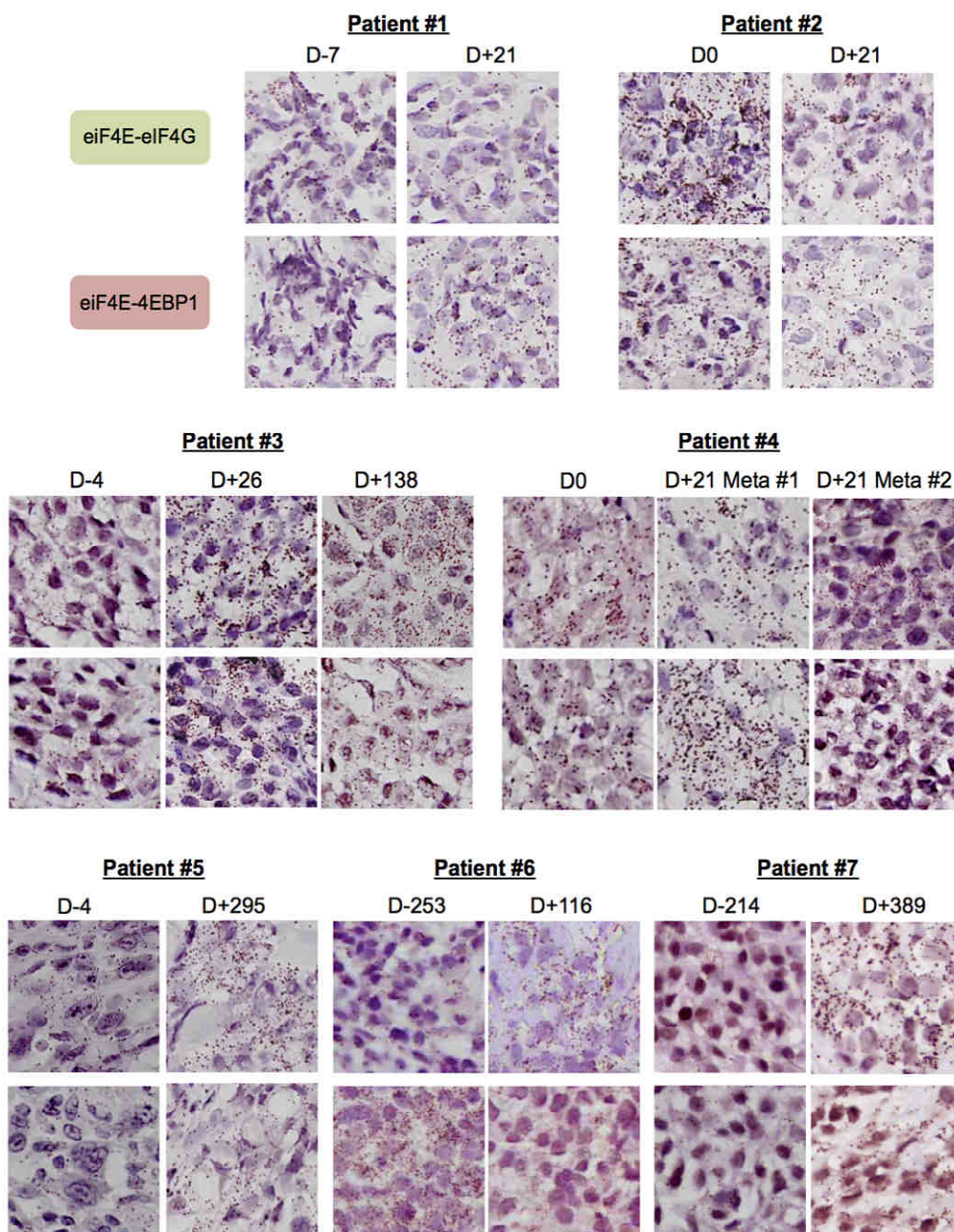
Extended Data Figure 8 | Formation of the eIF4F complex in various vemurafenib-treated cell lines. **a**, The eIF4E-eIF4G and eIF4E-4EBP1 interactions detected by *in situ* PLA in the Malme-3M melanoma cell line and its vemurafenib-resistant counterpart (R-Malme-3M) after treatment with 6 μ M vemurafenib (24 h) or no treatment. The interactions were visualized as red fluorescent spots. Cell nuclei were stained with DAPI (blue). White

numbers correspond to the mean \pm s.d. derived from three replicates quantified with ImageJ. **b**, The eIF4E-eIF4G and eIF4E-4EBP1 interactions detected by *in situ* PLA in the HT-29 colon cancer cell line and the BCPAP thyroid cancer cell line treated with 6 μ M vemurafenib (24 h) or untreated. The interactions were visualized as red fluorescent spots. Cell nuclei were stained with DAPI (blue).



Extended Data Figure 9 | Involvement of BMF in relative resistance to vemurafenib and analysis of rapamycin effects on AKT, S6 and 4EBP1 phosphorylation. **a**, Relative proliferation of A375 cells after siRNA-mediated depletion of 27 mRNAs associated with the result in Fig. 2d. The data are presented as the mean \pm s.d. ($n = 3$). Significance was determined by Student's t -test (*, $P < 0.05$). **b**, Relative expression of *BMF* mRNA (as determined by

qRT-PCR) after siRNA-mediated depletion of *BMF* (si-BMF) in A375 cells. Data are presented as the mean \pm s.d. ($n = 3$). Significance was determined by Student's t -test (**, $P < 0.01$). **c**, Western blot analysis with antibodies specific for phosphorylated (P-) and/or total AKT, S6, 4EBP1 and ERK1/2 (ERK) on cell extracts of the MDA-MB-468 breast cancer and Mel624 melanoma cell lines treated for 24 h with the indicated concentrations of rapamycin.



Extended Data Figure 10 | Formation of the eIF4F complex in each of the tumour samples from seven patients. The eIF4E-eIF4G and eIF4E-4EBP1 interactions detected by *in situ* PLA in tumour samples collected from each

patient (patient 1 to 7), before and during vemurafenib or dabrafenib treatment. Each brown spot represents an interaction.

Assessment of flavaglines
as potential chikungunya virus entry inhibitors.

Wintachai P., Thuaud F., Basmadjian C., Ubol S., Désaubry L., Smith D.R.
Microbiol Immuno. **2015**, *59*, 129-141

Copyright ©2015 The Societies and Wiley Publishing Asia Pty Ltd

ORIGINAL ARTICLE

Assessment of flavaglines as potential chikungunya virus entry inhibitors

Phitchayapak Wintachai¹, Frédéric Thuaud², Christine Basmadjian², Sittiruk Roytrakul³, Sukathida Ubol^{4,5}, Laurent Désaubry² and Duncan R. Smith^{1,5}

¹Institute of Molecular Biosciences, Mahidol University, Nakorn Pathom, Thailand, ²Laboratory of Therapeutic Innovation (UMR7200), CNRS-University of Strasbourg, Illkirch, France, ³National Center for Genetic Engineering and Biotechnology, National Science and Technology Development Agency, Pathumthani, Thailand, ⁴Department of Microbiology, Faculty of Science, Mahidol University, Nakorn Pathom and ⁵Center for Emerging and Neglected Infectious Diseases, Mahidol University, Nakorn Pathom, Thailand

ABSTRACT

Chikungunya virus (CHIKV) is a re-emerging mosquito-borne alphavirus that recently caused large epidemics in islands in, and countries around, the Indian Ocean. There is currently no specific drug for therapeutic treatment or for use as a prophylactic agent against infection and no commercially available vaccine. Prohibitin has been identified as a receptor protein used by chikungunya virus to enter mammalian cells. Recently, synthetic sulfonyl amidines and flavaglines (FLs), a class of naturally occurring plant compounds with potent anti-cancer and cytoprotective and neuroprotective activities, have been shown to interact directly with prohibitin. This study therefore sought to determine whether three prohibitin ligands (sulfonyl amidine 1 m and the flavaglines FL3 and FL23) were able to inhibit CHIKV infection of mammalian Hek293T/17 cells. All three compounds inhibited infection and reduced virus production when cells were treated before infection but not when added after infection. Pretreatment of cells for only 15 minutes prior to infection followed by washing out of the compound resulted in significant inhibition of entry and virus production. These results suggest that further investigation of prohibitin ligands as potential Chikungunya virus entry inhibitors is warranted.

Key words Chikungunya virus, entry inhibitor, flavaglines, sulfonyl amidines.

Chikungunya virus, the cause of CHIKF, is transmitted to humans by the bites of infected *Ae* mosquitos, most commonly *Ae. aegypti* and *Ae. albopictus*; CHIKV-infected patients develop symptoms some 2–4 days (range 1 to 12 days) days after being bitten (1). Clinically, the disease is similar to dengue fever, patients present with a sudden febrile illness with rash, headache, edema of the extremities, gastrointestinal complaints, myalgia, and polyarthralgia (a hallmark of CHIKV infection) that frequently persists for two or more months (1).

Chikungunya virus belongs to the *Alphavirus* genus, family *Togaviridae*. The genome is an 11.8 kb positive sense single stranded RNA with a 5'-methylguanylate cap and a 3'-poly A tail (2). The genome possesses two open reading frames, which encode for four nsPs (nsP1–nsP4), three structural proteins (capsid, E1 and E2) and two proteins of ill-defined function (E3 and 6 K). The CHIKV virion is approximately 70 nm in diameter and contains a nucleocapsid surrounded by a lipid bilayer envelope in which are embedded 80 trimeric spikes composed of 240 heterodimers of the E1 and E2

Correspondence

Duncan R. Smith, Institute of Molecular Biosciences, Mahidol University, Salaya Campus, 25/25 Phuttamonthol Sai 4, Nakorn Pathom 73170, Thailand. Tel +66 2441 9003 7; fax +66 2441 9906; email: duncan.smi@mahidol.ac.th, duncan_r_smith@hotmail.com

Received 12 September 2014; revised 19 December 2014; accepted 21 January 2015.

List of Abbreviations: *Ae.*, Aedes; CC₅₀, 50% cytotoxicity concentration; CHIKF, Chikungunya fever; CHIKV, Chikungunya virus; DMEM, Dulbecco's modified Eagle's medium; E, envelope; ECSA, East Central and South Africa; FL, flavagline; IC₅₀, 50% inhibitory concentration; MTT, 3-(4,5-dimethylthiazol-2-yl)-2,5-diphenyltetrazolium bromide; nsP, nonstructural protein(s); pfu, plaque forming unit; PHB, prohibitin.

glycoproteins (3). The 52 kDa E1 glycoprotein mediates fusion of virus with host cell membrane, whereas the 50 kDa E2 glycoprotein is responsible for receptor binding (2).

Chikungunya fever was first formally described after an outbreak in Tanzania in 1952 (4). The virus was first isolated from the same outbreak (5) and was subsequently shown to be present in several parts of Africa and South and Southeast Asia (6). An outbreak of CHIKF in Kenya in 2004 (7) spread to the Indian Ocean islands of Comoros and Seychelles in 2005 (8) and then to Mauritius and La Reunion (9). Some 266,000 cases of CHIKF were believed to have occurred in La Reunion (10, 11) and outbreaks were subsequently reported in India starting from 2005, and later in Singapore, Malaysia and Thailand and other parts of Southeast Asia (12–14). CHIKV has now been reported in many countries, and has caused particular concern through cases of autochthonous transmission in European countries (15).

A number of cell types, including epithelial, endothelial, fibroblast and monocyte-derived macrophage, are susceptible to CHIKV infection, whereas monocytes, lymphocytes, NK cells and monocyte-derived dendritic cells are reportedly not susceptible to CHIKV infection (16, 17). However, one study has shown CHIKV infection and replication in monocytes (18). The mechanism of entry of the virus remains somewhat unclear. Sourisseau and colleagues proposed that CHIKV entry (into HeLa cells) was via a clathrin-dependent pathway (16); however, Bernard and colleagues proposed that entry was via a clathrin-independent, Eps-15-dependent endocytic pathway (19). Both studies proposed that a cholesterol and pH dependent step is required for infection (19, 16).

In a recent study, PHB1 was identified as a receptor protein for CHIKV entry into mammalian cells (20). PHB1 and its homologue PHB2 are pleiotropic scaffold proteins that act as signaling hubs (21). Multiple heterodimers of PHB1 and PHB2 organize into large,

ring-like structures with diameters of 20–25 nm in the mitochondria (22–24), whereas in the cytoplasm, endoplasmic reticulum, nucleus and plasma membrane PHB forms heterodimers with signaling proteins to regulate many aspect of cell physiology, including mitochondrial biogenesis, survival, metabolism and cell division (25).

Cell surface-expressed PHB has been shown to act as an interacting molecule for the Vi polysaccharide of *Salmonella typhi* (26), whereas PHB expressed on the surfaces of insect cells has been shown to be a receptor for dengue virus (27) and an interacting protein for Cry4B, one of the major insecticidal toxins produced by *Bacillus thuringiensis* (28).

There is currently no specific antiviral treatment or commercially available vaccine to either protect against or treat CHIKV infections, although there are a number of vaccine development programs (29–32). Flavaglines are a family of plant natural products that have potent anticancer and neuro- and cardio-protective properties (33–35); studies have shown that prohibitins are directly interacting targets of this class of molecules (36). The synthetic sulfonyl amidine 1 m, which inhibits bone remodeling, also reportedly binds PHB1 (37). This study therefore sought to determine whether the synthetic flavaglines FL3 and FL23 and sulfonyl amidine 1 m are able to interfere with the CHIKV–prohibitin interaction that occurs at the receptor binding stage of CHIKV infection of mammalian cells.

MATERIAL AND METHODS

Compounds

The structures of flavaglines FL3 ($C_{25}H_{23}BrO_5$; MW: 483.36), FL23 ($C_{26}H_{24}BrNO_5$; MW 510.38) and sulfonyl amidine 1 m ($C_{20}H_{32}N_2O_2S$; MW 364.55) are shown in Figure 1. FL3 and sulfonyl amidine 1 m were synthesized according to described procedures (38, 21). The purity of these compounds was over 95% based on reversed-phase

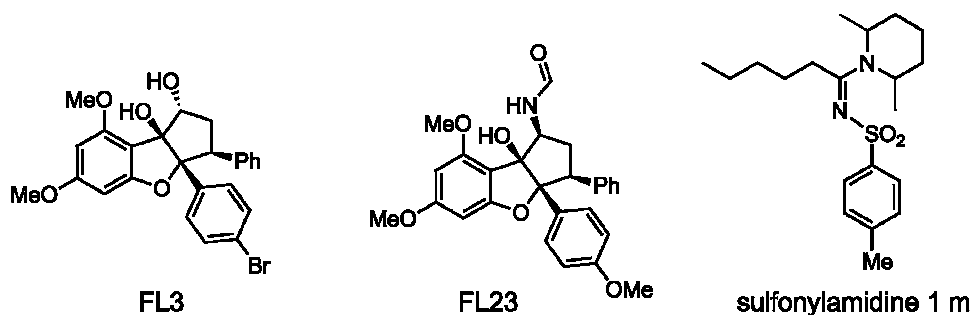


Fig. 1. Structures of flavagline FL3, FL23 and sulfonyl amidine 1 m.

HPLC analyses (Hypersil Gold column 30 1 mm, C18, Thermo Fisher Scientific, Waltham, MA, USA) under the following conditions: flow rate, 0.3 mL/min; buffer A, CH₃CN, buffer B, 0.01% aqueous trifluoroethanoic acid; gradient, 98–10% buffer B over 8 min (detection, $\lambda = 220/254$ nm). The compounds were initially dissolved in DMSO as stock and serially diluted in DMEM for working solutions with a final DMSO concentration of less than 0.1%. Vehicle/DMEM used as a control consisted of DMSO diluted to 0.1% in DMEM.

Cell culture and virus propagation

The human embryonic kidney cell line Hek293T/17 (ATCC Cat No. CRL-11268) was cultured in DMEM supplemented with 10% heat-inactivated FBS and 100 units/mL of penicillin/streptomycin at 37 °C with 5% CO₂, whereas Vero (ATCC Cat No. CCL-81) was cultured with 5% FBS and 100 units/mL of penicillin/streptomycin.

The CHIKV used in this study was a Thai isolate of an ECSA strain with genotype E1:226V ECSA; it was propagated and stock virus produced as described previously (17). Stock titers were determined by standard plaque assays, undertaken essentially as described elsewhere (17, 20).

Immunofluorescence

Immunofluorescence was performed essentially as described previously (39) by incubating Hek293T/17 cells with 20 pfu/cell CHIKV for 1 hr at 4 °C in the presence or absence of various compounds at 100 nM. The cells were subsequently fixed by treatment with pre-cooled 1% paraformaldehyde in PBS for 20 min and then incubated with a 1:100 dilution of a mouse monoclonal anti- alphavirus (3581) antibody (STSC-58088, Santa Cruz Biotechnology, Santa Cruz, CA, USA) and a 1:200 dilution of a goat polyclonal anti- PHB-1 antibody (SC-18196, Santa Cruz Biotechnology) followed by incubation with a 1:150 dilution of an Alexa Fluor 488 labeled donkey anti-mouse IgG antibody (A11029, Invitrogen, Thermo Fisher Scientific, Waltham, MA, USA) and a 1:150 dilution of an Alexa Fluor 568 labeled donkey anti-goat IgG antibody (A11057, Invitrogen, Thermo Fisher Scientific). The cells were visualized under an Olympus FluoView 1000 confocal microscope (Olympus, Shinjuku-ku, Tokyo, Japan) equipped with Olympus FluoView Software v. 1.6. Image analysis and calculation of Pearson correlation coefficients and CIs were carried out as described previously (40).

Cell viability analysis

Cell viability was determined using a Vybrant MTT Cell proliferation assay kit (V13154, Invitrogen, Thermo

Fisher Scientific) according to the manufacturer's recommendations. The percentage cell viability was calculated from the average of eight sample measurements compared with negative control (vehicle/DMEM).

Flow cytometry

Flow cytometry to determine cellular infection with CHIKV was undertaken exactly as described elsewhere (17). The cells were analyzed on a BD FACalibur cytometer (Becton Dickinson, BD Biosciences, San Jose, CA, USA) and data analyzed using CELLQuest™ software.

Analysis of apoptosis

Analysis of induction of apoptosis in response to CHIKV infection was performed exactly as described elsewhere (17). As a positive control, Hek293T/17 cells were treated with 5% DMSO diluted in complete DMEM for 24 hrs. All experiments were undertaken independently in triplicate.

Assay of effect of compounds on CHIKV infection

Hek293T/17 cells were seeded in six well culture plates and grown under standard conditions until the cells reached approximately 90% confluence. The cells were then pre incubated with different concentrations of FL3, FL23 and sulfonyl amidine 1 m finally diluted in DMEM for the times stated, or incubated with the equivalent volume of vehicle/DMEM, after which they were washed and incubated with 10 pfu/cell of CHIKV ECSA genotype (E1:226V) in the absence of the drug. Following infection, cells were washed three times with DMEM, after which they were re-incubated in complete medium containing the compound or the equivalent of vehicle/DMEM. At 20 hrs the cell pellets were analyzed by flow cytometry and the supernatant by standard plaque assay to determine CHIKV titers. In some experiments, compounds were added at designated times after the virus infection step. All experiments were undertaken independently in triplicate, with duplicate plaque assays.

Assay of effect of pulse addition of compounds on CHIKV infection

Hek293T/17 cells were seeded in six wells culture plates and grown under standard conditions until the cells reached approximately 90% confluence. Cells were then pre incubated with different concentrations of FL3, FL23 and sulfonyl amidine 1 m finally diluted in DMEM or incubated with the equivalent volume of vehicle/DMEM for 15 minutes, after which they were washed twice with

DMEM and subsequently incubated with 10 pfu/cell of CHIKV ECSA genotype (E1:226V) in the absence of the drug. Following infection cells were washed three times with DMEM, after which they were re-incubated in complete medium. At 20 hrs the cell pellets were analyzed by flow cytometry and the supernatant analyzed by standard plaque assay to determine CHIKV titers. All experiments were performed independently in triplicate, with duplicate plaque assays.

Assay for virucidal activity

Stock CHIKV ECSA genotype (E1:226V) was incubated directly with different concentrations of FL3, FL23 and sulfonyl amidine 1 m as indicated for 1 hr. The titers of the virus were then directly determined by standard plaque assay. These preparations were also used to infect Hek293T/17 cells that had been cultured in six well plates until they had reached approximately 90% confluence.

Statistical analysis

Viral infection and viral production data were analyzed using the GraphPad Prism program (GraphPad Software). Statistical analysis of significance was undertaken by a paired sample *t*-tests using SPSS (SPSS, Chicago, IL, USA); $P < 0.05$ was considered significant. CC_{50} and IC_{50} values were calculated using freeware ED50plus (v1.0) software (<http://sciencegateway.org/protocols/cellbio/drug/data/ed50v10.xls>).

RESULTS

Colocalization between prohibitin and CHIKV E2 protein

In our previous study identifying PHB as a CHIKV receptor protein, the majority of the analysis was undertaken in CHME-5 (human microglial) cells (20). To investigate the effect of flavaglines on CHIKV entry in this study, we decided to use Hek293T/17 cells because these cells are more suitable for flow cytometry analysis. Our previous study showed that Hek293T/17 cells expressed PHB, which was capable of binding CHIKV (20). We therefore initially confirmed that CHIKV colocalized with PHB on the surfaces of Hek293T/17 cells, as previously shown for CHME-5 cells (20). As shown in Figure 2, we found cell surface expression of PHB and distinct colocalization between PHB and CHIKV.

Evaluation of cytotoxicity, cell death and virucidal activity

We incubated Hek293T/17 cells individually with various concentrations of each compound under

investigation for 24 hrs, after which we assessed cell viability using an MTT assay. We calculated the percentage cell viability from the average of eight replicates and compared it with negative (vehicle/DMEM) and positive (5% DMSO) controls. We found that after 24 hrs incubation, cell viability for FL3, FL23 and sulfonyl amidine 1 m at concentrations of 20 nM or less (0.1, 0.25, 0.5, 1, 5, 10 and 20 nM) was comparable to that of the negative control; however, we saw significant cytotoxicity at values above 20 nM (Supplementary Fig. S1). The compounds showed approximately equal CC_{50} values of 118.77 nM (FL3), 92.18 nM (FL23) and 138.53 nM (sulfonyl amidine 1 m) as calculated from dose response curves (see Supplementary Fig. S2).

To confirm the results of the MTT assay, we cultured Hek293T/17 cells and incubated them with various concentrations of FL3, FL23 and sulfonyl amidine 1 m at 37 °C or mock incubated them with vehicle/DMEM for 1 hr, after which we washed the cells and re-incubated them with the same concentration of drug for a further 24 hrs. We employed this two-step incubation to more closely mimic infection protocols as undertaken at later stages. We found approximately 80% apoptosis induction in cells treated with 5% DMSO as a positive control; however, amounts of apoptosis in cells treated with different concentrations (1, 5, 10 and 20 nM) of the compounds under investigation were comparable to that in negative control (mock) cells treated with vehicle/DMEM (Supplementary Fig. S3).

To evaluate potential virucidal activity, we incubated stock CHIKV directly with each compound separately at different concentrations for 1 hr or with vehicle/DMEM, after which we determined virus titers by standard plaque assays on Vero cells. We observed no direct effect of the compounds on the virus (Supplementary Fig. S4). We repeated the experiment using virus/compound mixtures to infect Hek293T/17 cells and found no significant effect on the ability of the virus to infect into Hek293T/17 cells. Moreover, plaque assay analysis of the highest concentration treatments showed no significant effect on virus production (Supplementary Fig. S4). Combined, these results show that the three compounds tested do not possess anti-CHIKV virucidal activity.

Effect of compounds on CHIKV infection

To determine the effects of the compounds on CHIKV infection, we cultured Hek293T/17 cells and then pre-incubated them with and without FL3, FL23 or sulfonyl amidine 1 m at various concentrations for 1 hr followed by infection with 10 pfu/cells of CHIKV or mock infected in serum-free medium without the compounds

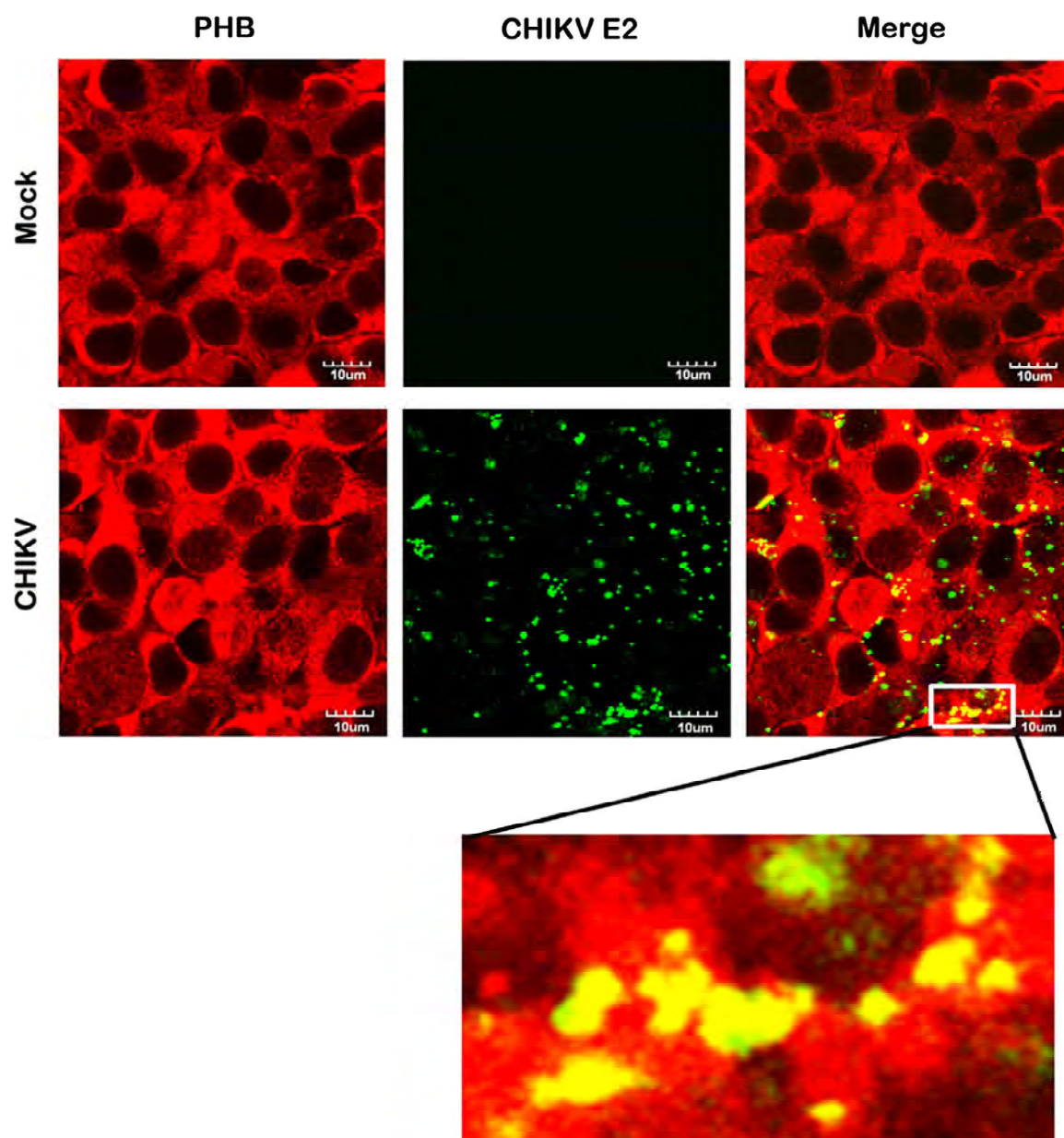


Fig. 2. Colocalization of CHIKV E2 protein with PHB. (a) Hek293T/17 cells were grown on glass slides and incubated with CHIKV or mock incubated and examined for the cell surface colocalization of PHB (red) and CHIKV E2 protein (green). Fluorescent signals were observed using an Olympus Fluoview 1000 confocal microscope. Scale bar for magnification is shown. Representative, non-contrast adjusted, unmerged and merged images are shown.

under investigation. After 2 hr, we removed extracellular virus by washing three times and subsequently incubated the cells in complete medium under standard conditions in the presence of the compounds for 20 hrs, after which we harvested the cells for flow cytometry and collected the supernatant for standard plaque assay. We found a reduction in the percentage of infected cells for all three compounds at concentrations of 10 and 20 nM (Fig. 3a,c,

e), whereas FL3 additionally showed a significant reduction in the percentage of cells infected with CHIKV at 5 nM (Fig. 3a). Similarly, we observed a significant reduction in viral production in cells incubated with 10 and 20 nM of the three compounds (Fig. 3b,d,f and Supplementary Fig. S5), whereas FL23 additionally showed a significant effect on virus production at 1 and 5 nM (Fig. 3d and Supplementary Fig. S5). The

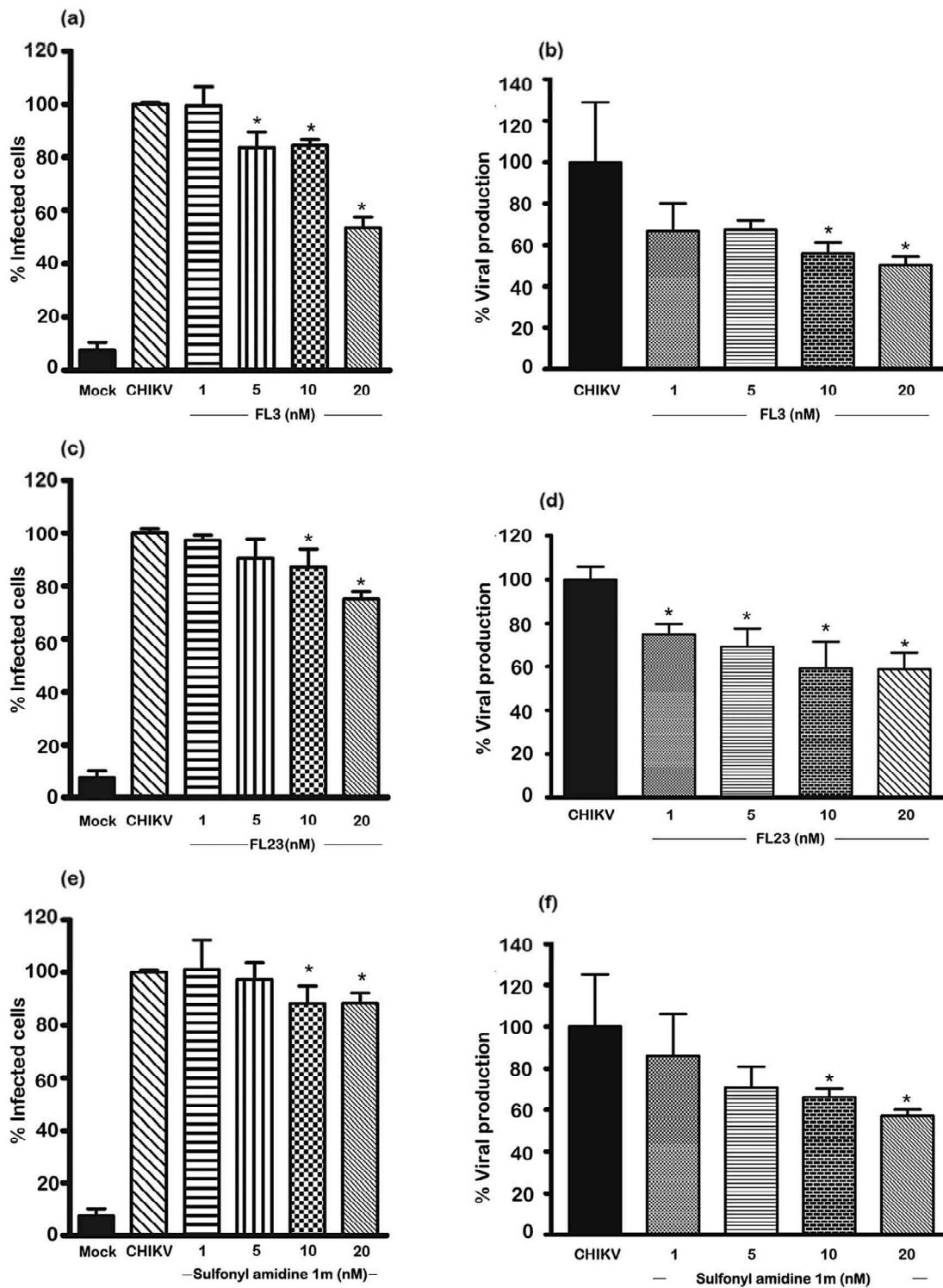


Fig. 3. Effects of various compounds on CHIKV infection of Hek293T/17 cells. Hek293T/17 cells were pre-incubated with vehicle/DMEM (mock and CHIKV) or pre-incubated with (a, b) FL3, (c,d) FL23 or (e,f) sulfonyl amidine 1m for 1 hr before being infected with 10 pfu/cell of CHIKV or being mock infected (Mock). After infection, cells were incubated under standard conditions in the presence or absence of the appropriate drug for 20 hrs before (a, c, e) determination of degree of infection of cells by flow cytometry or (b, d, f) assay of the supernatant for virus titer by standard plaque assay. All experiments were undertaken independently in triplicate with duplicate plaque assays; error bars show SD. *, $P < 0.05$. Mock, pre-incubation with vehicle/DMEM and mock (CHIKV) infection; CHIKV (incubation with vehicle/DMEM and standard infection).

Flavaglines as CHIKV entry inhibitors

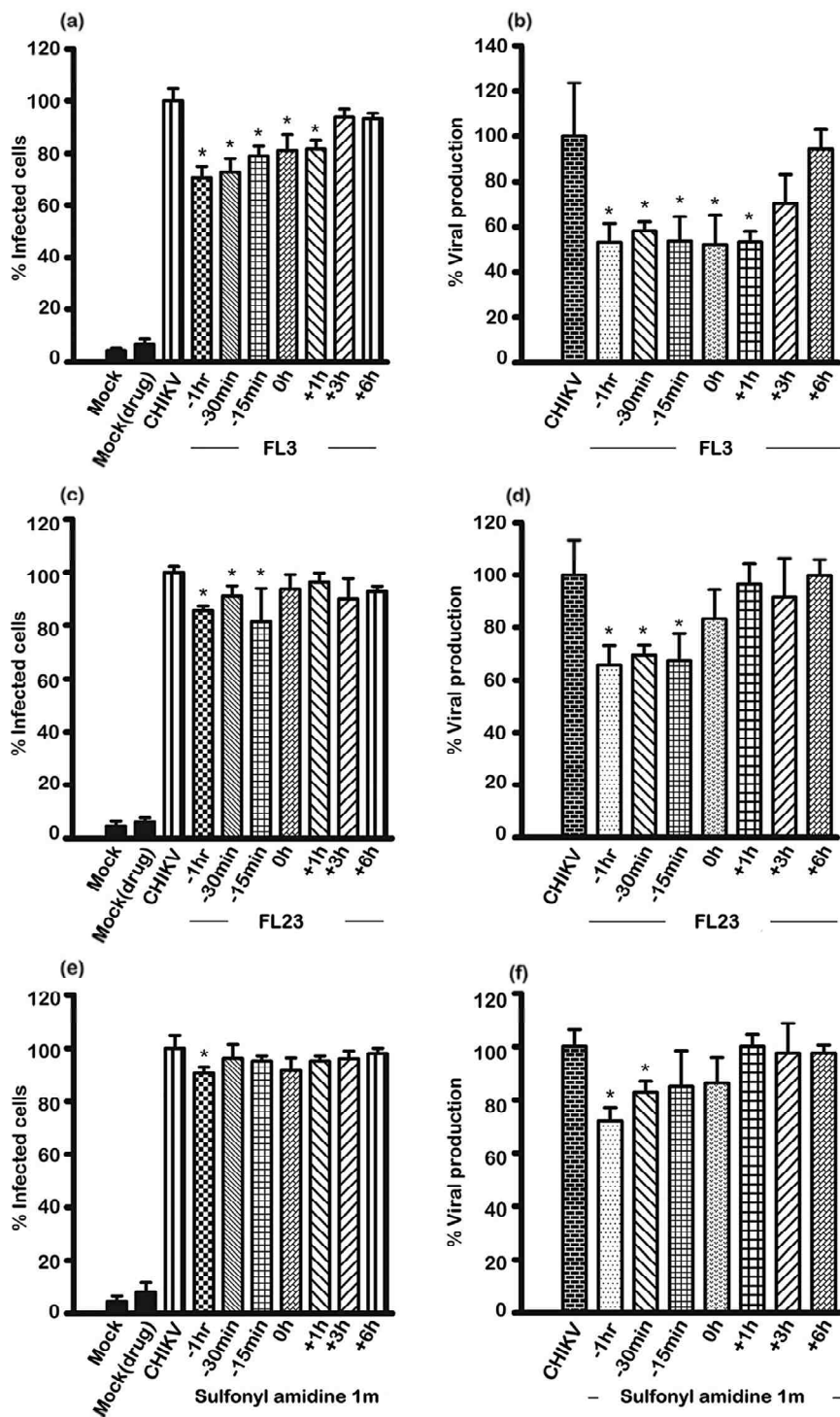


Fig. 4. Time course of effect of flavaglines on CHIKV infection of Hek293T/17 cells. Hek293T/17 cells were mock pre-incubated with vehicle/DMEM or pre-incubated with (a, b) FL3, (c,d) FL23 or (e,f) sulfonyl amidine 1m for the indicated times before being infected with 10 pfu/cell of CHIKV or being mock (Mock) infected, or the compounds were added at the indicated times post-infection. After infection, cells were incubated under standard conditions in the presence or absence of the drug as appropriate for 20 hrs before (a, c, e) determination of degree of infection of cells by flow cytometry or (b, d, f) the supernatant assayed for virus titer by standard plaque assay. Mock, incubation with vehicle/DMEM and mock infection; Mock (drug), incubation with compound and mock infection; CHIKV, incubation with vehicle/DMEM and standard CHIKV infection. All experiments were undertaken independently in triplicate with duplicate plaque assays; error bars show SD. *, $P < 0.05$.

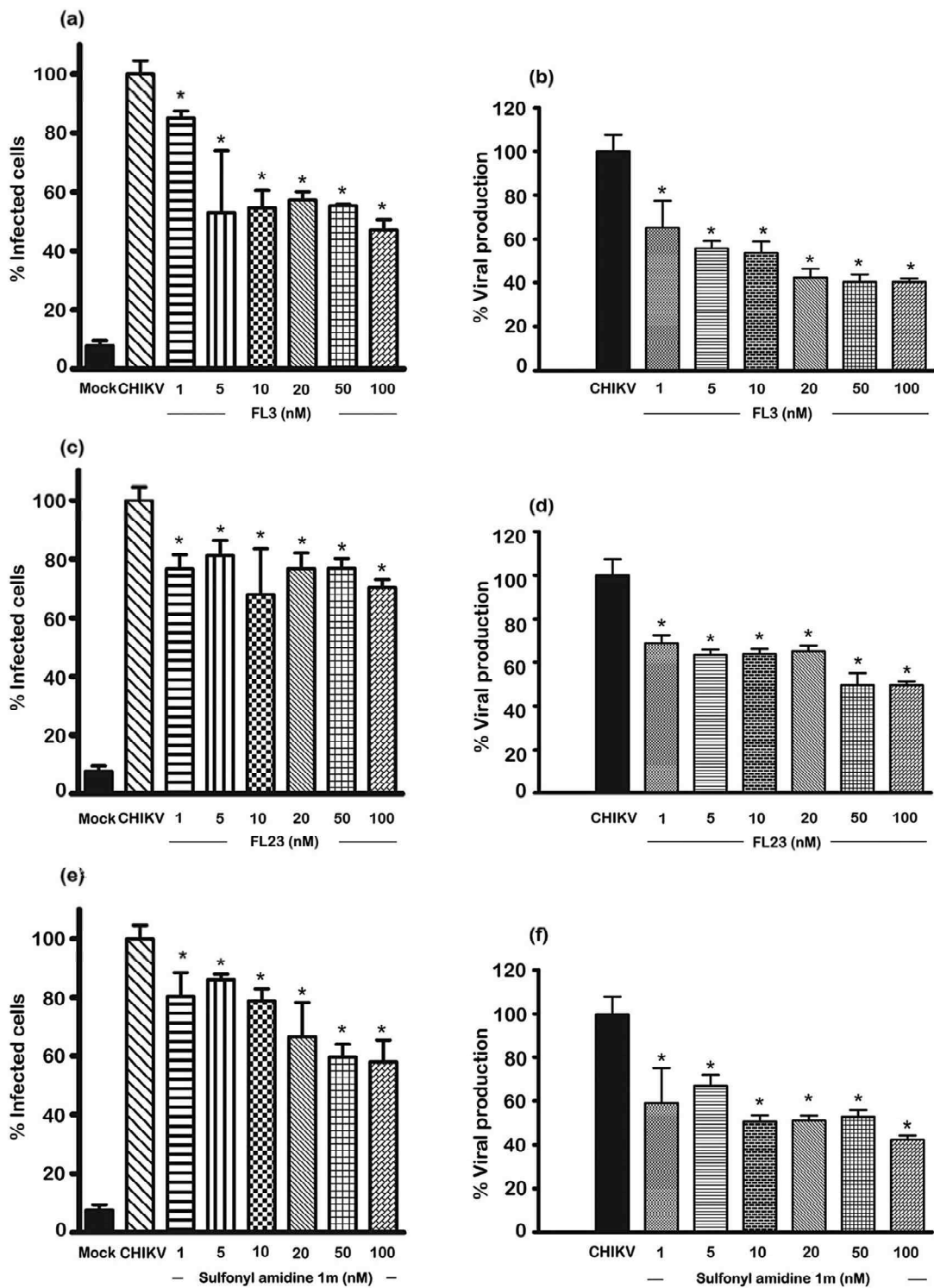


Fig. 5. Effect of pulse pre-treatment of compounds on CHIKV infection of Hek293T/17 cells. Hek293T/17 cells were mock pre-incubated with vehicle/DMEM or pre-incubated with (a, b) FL3, (c,d) FL23 or (e,f) sulfonyl amidine 1m for 15 minutes after which cells were washed twice before being infected with 10 pfu/cell of CHIKV or being mock infected. After infection, cells were incubated under standard conditions for 20 hrs before (a, c, e) determination of degree of infection of cells by flow cytometry or (b, d, f) assay of the supernatant for virus titer by standard plaque assay. All experiments were undertaken independently in triplicate with duplicate plaque assays; error bars show SD. *, $P < 0.05$. Mock, pre-incubation with vehicle/DMEM and mock (CHIKV) infection; CHIKV, (incubation with vehicle/DMEM and standard infection).

maximum effect observed was with 20 nM FL3, which reduced both infection and virus production by nearly 50%, the IC_{50} for this compound was 22.4 nM.

Time course analysis of the effect of compounds on CHIKV infection

To determine whether the compounds were having an effect at the entry step of CHIKV infection, we incubated cells with the highest non-cytotoxic concentrations of the compounds (20 nM) for increasingly shorter times pre-infection, or added them only after infection. We analyzed cells and supernatant at 20 hrs post-infection as in previous experiments.

We found that FL23 and sulfonyl amidine 1 m only had effects on the number of infected cells and the amount of virus production when the cells were pre-incubated with the compounds (Fig. 4). We saw no effect when we added these two compounds post-infection (Fig. 4c–f and Supplemental Fig. S6). FL23 showed some effect when the pre-incubation was as short as 15 minutes pre-infection, whereas sulfonyl amidine 1 m showed an effect on number of cells infected only with pre-incubation for 1 hr pre-infection.

FL3 showed both the largest effect and the greatest range of time points that had an effect. Even incubation with FL3 at 1 hr post-infection had a significant effect on both number of cells infected and amount of virus produced. This may mean that continued inhibition of virus entry was not completely prevented by the washing step and suggests that FL3 may remain associated with PHB for a longer time than either FL23 or sulfonyl amidine 1 m. However, addition of FL3 at 3 hrs post-infection showed no significant effect.

Effect of pulse treatment of compounds on CHIKV infection

The results of the time course experiment are consistent with the action of the compounds occurring at the attachment/entry step of CHIKV infection. To further verify this, we undertook experiments with a short (15 minutes) pulse pre-treatment with wash out of the compound before infection. Because the cell treatment was for a short period, it was possible that we could use higher concentrations of the compounds. To verify this, we treated cells for 15 minutes with different concentrations of the compounds (up to 100 nM), after which we washed the cells twice with DMEM before incubating them under standard conditions for 24 hrs and assessing cell viability as undertaken previously. We found no evident loss of cell viability, even at the highest concentration used (100 nM; Supplemental Fig. 7). We therefore repeated the experiment and infected the cells after washing with

CHIKV and assayed for degree of infection and virus production at 20 hrs post-infection as before. We found a significant reduction in both infection and virus production under all conditions tested (Fig. 5 and Supplementary Fig. S8). Virus output for both FL3 and sulfonyl amidine 1 m was reduced by nearly 60% by pulse treatment at 100 nM as compared with untreated cells.

Effect of compounds on CHIKV receptor binding

Finally, to confirm that the compounds acted by interfering with receptor binding, we repeated the initial colocalization experiment between PHB and CHIKV, this time in the presence or absence of each of the compounds. We found a marked reduction in colocalization between CHIKV and PHB when we incubated the virus with cells in the presence of the compounds at 100 nM, as compared to incubation with no compound (Fig. 6). The high degree of colocalization between CHIKV and PHB (Pearson correlation coefficient 0.85, 95% CI 0.82–0.88) was reduced to a statistically significantly degree in the presence of FL3 (Pearson correlation coefficient 0.22; 95% CI 0.09–0.34; $P < 0.05$) and FL23 (Pearson correlation coefficient 0.63; 95% CI 0.53–0.73; $P < 0.05$) and reduced, although not significantly, in the presence of sulfonyl amidine 1 m (Pearson correlation coefficient 0.72; 95% CI 0.34–1.09) These results confirm that the ligands interfere with the receptor binding of CHIKV.

DISCUSSION

Prohibitin is located in a number of cell compartments, primarily the mitochondria; cell surface expression has also been demonstrated in a number of studies (41, 42, 26, 20, 43, 44). PHB has been shown to interact with a number of different pathogens or pathogen proteins including CHIKV (20), dengue (27), severe acute respiratory syndrome coronavirus (45), HIV (46) and foot-and-mouth disease virus (47).

Prohibitins have been shown to be specific targets for flavaglines (36). Flavaglines are a family of natural products found in plants of the genus *Aglaiia*, family *Meliaceae* (mahogany), of which the first identified molecule was rocaglamide (48). Rocaglamide was first identified based on its potent anti-leukemic activity; since then both natural and synthetic flavaglines have been shown to have potent anti-cancer properties, often in the low nanomolar range (34, 35). Recent studies have suggested that flavaglines, including rocaglamide and silvestrol, are promising candidates for the treatment of leukemia (49). Studies have shown that the anti-cancer

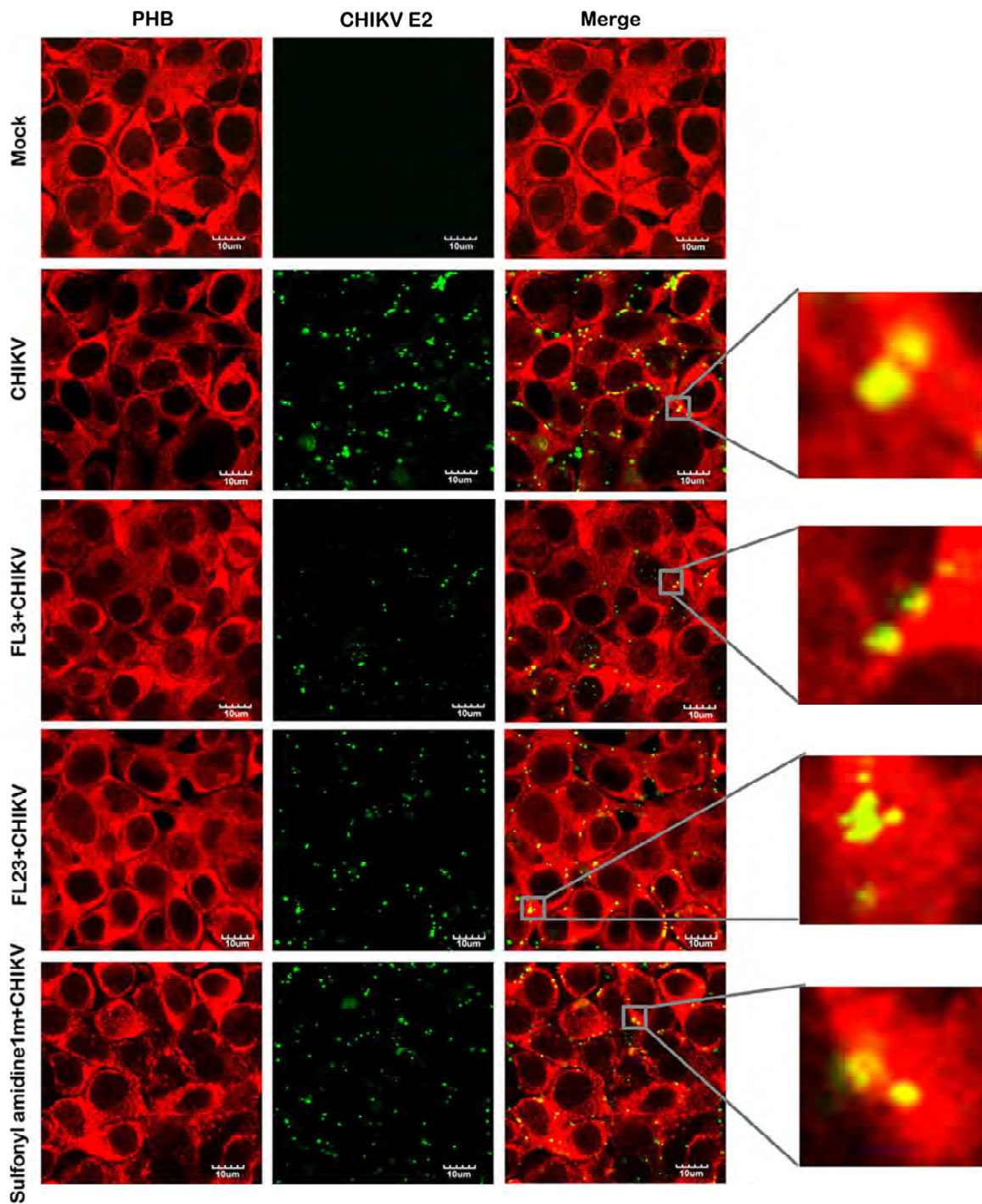


Fig. 6. Colocalization of CHIKV E2 protein with PHB in the presence and absence of test compounds. Hek293T/17 cells were grown on glass slides and incubated with CHIKV or mock incubated in the presence and absence of test compounds at 100 nM and examined for cell surface colocalization of PHB (red) and CHIKV E2 protein (green). Fluorescent signals were observed using an Olympus FluoView 1000 confocal microscope. Scale bar for magnification is shown. Representative, non-contrast adjusted, unmerged and merged images are shown.

action of flavaglines derives, at least in part, from a specific interaction between PHB and flavaglines (36). This study was undertaken to determine whether the interaction between flavaglines and PHB was sufficient to disrupt the interaction between PHB and CHIKV. All of our results are consistent with the compounds acting at the entry stage, possibly by physically interfering with the binding of CHIKV to the PHB receptor. The maximum inhibition observed was approximately 50% of viral entry (seen with pulse treatment of cells with FL3), a degree of inhibition consistent with that seen in previous antibody inhibition experiments (20). The compounds tested showed little effect when added post-entry; while this may suggest that flavaglines have only limited potential utility as prophylactic agents, because natural infections are not synchronous, administration during the course of the disease could have therapeutic effects by preventing new cells from becoming infected. The fact that both antibody inhibition experiments (20) and the compounds tested here showed a maximum effect on entry of about 50% may indicate that CHIKV uses multiple receptor protein to enter susceptible cells.

The compounds tested showed significant cytotoxicity to Hek293T/17 cells under conditions of continuous culture, consistent with the compounds known anti-cancer activities (34, 35). However, no cytotoxicity was observed after exposure to dramatically higher doses when the compounds were administered as short (15 minute) pulses. Importantly, these compounds show no toxicity to normal cells and do not display any evidence of toxicity *in vivo* (33), suggesting that these compounds, or indeed other ligands of PHB, could form the basis of a prophylactic or therapeutic regime in CHIKV outbreaks.

ACKNOWLEDGMENTS

This work was supported by grants from Mahidol University and the Office of the Higher Education Commission under the National Research Universities Initiative, The Thailand Research Fund (IRG5780009) and Mahidol University. P.W. was supported by a Thailand Graduate Institute of Science and Technology (TGIST) PhD scholarship. We also thank AAREC Folia Research (C.B.) and MNESR (F.T.) for fellowships.

DISCLOSURE

The authors have no conflict of interest to disclose.

REFERENCES

- Burt F.J., Rolph M.S., Rulli N.E., Mahalingam S., Heise M.T. (2012) Chikungunya: a re-emerging virus. *Lancet* **379**: 662–71.
- Schwartz O., Albert M.L. (2010) Biology and pathogenesis of chikungunya virus. *Nat Rev Microbiol* **8**: 491–500.
- Voss J.E., Vaney M.C., Duquerois S., Vonnrhein C., Girard-Blanc C., Crublet E., Thompson A., Bricogne G., Rey F.A. (2010) Glycoprotein organization of Chikungunya virus particles revealed by X-ray crystallography. *Nature* **468**: 709–12.
- Robinson M.C. (1955) An epidemic of virus disease in Southern Province, Tanganyika Territory, in 1952–53 I Clinical features *Trans R Soc Trop Med Hyg* **49**: 28–32.
- Ross R.W. (1956) The Newala epidemic. III. The virus: isolation, pathogenic properties and relationship to the epidemic. *J Hyg (Lond)* **54**: 177–91.
- Halstead S.B. (1966) Mosquito-borne haemorrhagic fevers of South and South-East Asia. *Bull World Health Organ* **35**: 3–15.
- Sergon K., Njuguna C., Kalani R., Ofula V., Onyango C., Konongoi L.S., Bedno S., Burke H., Dumilla A.M., Konde J., Njenga M.K., Sang R., Breiman R.F. (2008) Seroprevalence of Chikungunya virus (CHIKV) infection on Lamu Island, Kenya, October 2004. *Am J Trop Med Hyg* **78**: 333–7.
- Sergon K., Yahaya A.A., Brown J., Bedja S.A., Mlindasse M., Agata N., Allaranger Y., Ball M.D., Powers A.M., Ofula V., Onyango C., Konongoi L.S., Sang R., Njenga M.K., Breiman R.F. (2007) Seroprevalence of Chikungunya virus infection on Grande Comore Island, union of the Comoros, 2005. *Am J Trop Med Hyg* **76**: 1189–93.
- Josseran L., Paquet C., Zehgnoun A., Caillere N., Le Tertre A., Solet J.L., Ledrans M. (2006) Chikungunya disease outbreak, Reunion Island. *Emerg Infect Dis* **12**: 1994–5.
- Gerardin P., Guernier V., Perrau J., Fianu A., Le Roux K., Grivard P., Michault A., De Lamballerie X., Flahault A., Favier F. (2008) Estimating Chikungunya prevalence in La Reunion Island outbreak by serosurveys: two methods for two critical times of the epidemic. *BMC Infect Dis* **8**: 99.
- Renault P., Solet J.L., Sissoko D., Ballez dier E., Larrieu S., Filleul L., Lassalle C., Thiria J., Rachou E., De Valk H., Ille D., Ledrans M., Quatresous I., Quenel P., Pierre V. (2007) A major epidemic of chikungunya virus infection on Reunion Island, France, 2005–2006. *Am J Trop Med Hyg* **77**: 727–31.
- Ng L.C., Hapuarachchi H.C. (2010) Tracing the path of Chikungunya virus—evolution and adaptation. *Infect Genet Evol* **10**: 876–85.
- Powers A.M. (2010) Chikungunya. *Clin Lab Med* **30**: 209–19.
- Pulmanausahakul R., Roytrakul S., Auewarakul P., Smith D.R. (2011) Chikungunya in Southeast Asia: understanding the emergence and finding solutions. *Int J Infect Dis* **15**: 671–76.
- Tomasello D., Schlagenhauf P. (2013) Chikungunya and dengue autochthonous cases in Europe 2007–2012. *Travel Med Infect Dis* **5**: 274–84.
- Sourisseau M., Schilte C., Casartelli N., Trouillet C., Guivel-Benhassine F., Rudnicka D., Sol-Foulon N., Le Roux K., Prevost M.C., Fsihi H., Frenkiel M.P., Blanchet F., Afonso P.V., Ceccaldi P.E., Ozden S., Gessain A., Schuffenecker I., Verhasselt B., Zamborlini A., Saib A., Rey F.A., Arenzana-Seisdedos F., Despres P., Michault A., Albert M.L., Schwartz O. (2007) Characterization of reemerging chikungunya virus. *PLoS Pathog* **3**: e89.
- Wikan N., Sakoonwatanyoo P., Ubol S., Yoksan S., Smith D.R. (2012) Chikungunya virus infection of cell lines: analysis of the East, Central and South African lineage. *PLoS ONE* **7**: e31102.
- Her Z., Malleret B., Chan M., Ong E.K., Wong S.C., Kwek D.J., Tolou H., Lin R.T., Tambyah P.A., Renia L., Ng L.F. (2010) Active infection of human blood monocytes by Chikungunya virus triggers an innate immune response. *J Immunol* **184**: 5903–13.

19. Bernard E., Solignat M., Gay B., Chazal N., Higgs S., Devaux C., Briant L. (2010) Endocytosis of chikungunya virus into mammalian cells: role of clathrin and early endosomal compartments. *PLoS ONE* **5**: e11479.
20. Wintachai P., Wikan N., Kuadkitkan A., Jaimipuk T., Ubol S., Pulmanasahakul R., Auewarakul P., Kasinrerak W., Weng W.Y., Panyasrivanit M., Paemanee A., Kittisenachai S., Roytrakul S., Smith D.R. (2012) Identification of prohibitin as a Chikungunya virus receptor protein. *J Med Virol* **84**: 1757–70.
21. Thuaud F., Bernard Y., Turkeri G., Dirr R., Aubert G., Cresteil T., Baguet A., Tomasetto C., Svitkin Y., Sonenberg N., Nebigil C.G., Desaubry L. (2009) Synthetic analogue of rocaglaol displays a potent and selective cytotoxicity in cancer cells: involvement of apoptosis inducing factor and caspase-12. *J Med Chem* **52**: 5176–87.
22. Ikonen E., Fiedler K., Parton R.G., Simons K. (1995) Prohibitin, an antiproliferative protein, is localized to mitochondria. *FEBS Lett* **358**: 273–7.
23. Merkwirth C., Langer T. (2009) Prohibitin function within mitochondria: essential roles for cell proliferation and cristae morphogenesis. *Biochim Biophys Acta* **1793**: 27–32.
24. Nijtmans L.G., De Jong L., Artal Sanz, Coates M., Berden P.J., Back J.A., Muijsers J.W., Van Der Spek A.O., Grivell H. (2000) Prohibitins act as a membrane-bound chaperone for the stabilization of mitochondrial proteins. *Embo J* **19**: 2444–51.
25. Thuaud F., Ribeiro N., Nebigil C.G., Desaubry L. (2013) Prohibitin ligands in cell death and survival: mode of action and therapeutic potential. *Chem Biol* **20**: 316–31.
26. Sharma A., Qadri A. (2004) Vi polysaccharide of Salmonella typhi targets the prohibitin family of molecules in intestinal epithelial cells and suppresses early inflammatory responses. *Proc Natl Acad Sci USA* **101**: 17492–7.
27. Kuadkitkan A., Wikan N., Fongsaran C., Smith D.R. (2010) Identification and characterization of prohibitin as a receptor protein mediating DENV-2 entry into insect cells. *Virology* **406**: 149–61.
28. Kuadkitkan A., Smith D.R., Berry C. (2012) Investigation of the Cry4B-prohibitin interaction in *Aedes aegypti* cells. *Curr Microbiol* **65**: 446–54.
29. Akahata W., Yang Z.Y., Andersen H., Sun S., Holdaway H.A., Kong W.P., Lewis M.G., Higgs S., Rossmann M.G., Rao S., Nabel G.J. (2010) A virus-like particle vaccine for epidemic Chikungunya virus protects nonhuman primates against infection. *Nat Med* **16**: 334–8.
30. Edelman R., Tacket C.O., Wasserman S.S., Bodison S.A., Perry J.G., Mangiafico J.A. (2000) Phase II safety and immunogenicity study of live chikungunya virus vaccine TSI-GSD-218. *Am J Trop Med Hyg* **62**: 681–5.
31. Wang E., Volkova E., Adams A.P., Forrester N., Xiao S.Y., Frolov I., Weaver S.C. (2008) Chimeric alphavirus vaccine candidates for chikungunya. *Vaccine* **26**: 5030–9.
32. Weaver S.C., Osorio J.E., Livengood J.A., Chen R., Stinchcomb D.T. (2012) Chikungunya virus and prospects for a vaccine. *Expert Rev Vaccines* **11**: 1087–101.
33. Bernard Y., Ribeiro N., Thuaud F., Turkeri G., Dirr R., Boulberdaa M., Nebigil C.G., Desaubry L. (2011) Flavaglines alleviate doxorubicin cardiotoxicity: implication of Hsp27. *PLoS ONE* **6**: e25302.
34. Ribeiro N., Thuaud F., Bernard Y., Gaidon C., Cresteil T., Hild A., Hirsch E.C., Michel P.P., Nebigil C.G., Desaubry L. (2012) Flavaglines as potent anticancer and cytoprotective agents. *J Med Chem* **55**: 10064–73.
35. Ribeiro N., Thuaud F., Nebigil C., Desaubry L. (2012) Recent advances in the biology and chemistry of the flavaglines. *Bioorg Med Chem* **20**: 1857–64.
36. Polier G., Neumann J., Thuaud F., Ribeiro N., Gelhaus C., Schmidt H., Giaisi M., Kohler R., Muller W.W., Proksch P., Leippe M., Janssen O., Desaubry L., Krammer P.H., Li-Weber M. (2012) The natural anticancer compounds rocaglamides inhibit the Raf-MEK-ERK pathway by targeting prohibitin 1 and 2. *Chem Biol* **19**: 1093–104.
37. Chang S.Y., Bae S.J., Lee M.Y., Baek S.H., Chang S., Kim S.H. (2011) Chemical affinity matrix-based identification of prohibitin as a binding protein to anti-resorptive sulfonyl amidine compounds. *Bioorg Med Chem Lett* **21**: 727–9.
38. Lee M.Y., Kim M.H., Kim J., Kim S.H., Kim B.T., Jeong I.H., Chang S., Kim S.H., Chang S.Y. (2010) Synthesis and SAR of sulfonyl- and phosphoryl amidine compounds as anti-resorptive agents. *Bioorg Med Chem Lett* **20**: 541–5.
39. Fongsaran C., Jirakanwisal K., Kuadkitkan A., Wikan N., Wintachai P., Thepparit C., Ubol S., Phaonakrop N., Roytrakul S., Smith D.R. (2014) Involvement of ATP synthase beta subunit in chikungunya virus entry into insect cells. *Arch Virol* **159**: 3353–64.
40. Panyasrivanit M., Khakpoor A., Wikan N., Smith D.R. (2009) Co-localization of constituents of the dengue virus translation and replication machinery with amphisomes. *J Gen Virol* **90**: 448–56.
41. Kolonin M.G., Saha P.K., Chan L., Pasqualini R., Arap W. (2004) Reversal of obesity by targeted ablation of adipose tissue. *Nat Med* **10**: 625–32.
42. Patel N., Chatterjee S.K., Vrbanac V., Chung I., Mu C.J., Olsen R.R., Waghorne C., Zetter B.R. (2010) Rescue of paclitaxel sensitivity by repression of Prohibitin1 in drug-resistant cancer cells. *Proc Natl Acad Sci USA* **107**: 2503–8.
43. Yurugi H., Tanida S., Ishida A., Akita K., Toda M., Inoue M., Nakada H. (2012) Expression of prohibitins on the surface of activated T cells. *Biochem Biophys Res Commun* **420**: 275–80.
44. Zhang Y., Wang Y., Xiang Y., Lee W., Zhang Y. (2012) Prohibitins are involved in protease-activated receptor 1-mediated platelet aggregation. *J Thromb Haemost* **10**: 411–8.
45. Cornillez-Ty C.T., Liao L., Yates J.R., 3rd, Kuhn P., Buchmeier M.J. (2009) Severe acute respiratory syndrome coronavirus nonstructural protein 2 interacts with a host protein complex involved in mitochondrial biogenesis and intracellular signaling. *J Virol* **83**: 10314–8.
46. Emerson V., Holtkotte D., Pfeiffer T., Wang I.H., Schnolzer M., Kempf T., Bosch V. (2010) Identification of the cellular prohibitin 1/prohibitin 2 heterodimer as an interaction partner of the C-terminal cytoplasmic domain of the HIV-1 glycoprotein. *J Virol* **84**: 1355–65.
47. Chiu C.F., Peng J.M., Hung S.W., Liang C.M., Liang S.M. (2012) Recombinant viral capsid protein VP1 suppresses migration and invasion of human cervical cancer by modulating phosphorylated prohibitin in lipid rafts. *Cancer Lett* **320**: 205–14.
48. Lu King, Chiang M., Ling C-C., Fujita H-C., Ochiai E., Mcphail M. (1982) X-ray crystal structure of rocaglamide, a novel antileukemic 1H-cyclopenta[b]benzofuran from *Aglaia elliptifolia*. *J Chem Soc Chem Commun* **20**: 1150–1.
49. Callahan K.P., Minhajuddin M., Corbett C., Lagadinou E.D., Rossi R.M., Grose V., Balys M.M., Pan L., Jacob S., Frontier A., Grever M.R., Lucas D.M., Kinghorn A.D., Liesveld J.L., Becker M.W., Jordan C.T. (2014) Flavaglines target primitive leukemia cells and enhance anti-leukemia drug activity. *Leukemia* **28**: 1960–8.

Supporting Information

Additional supporting information may be found in the online version of this article at the publisher's web-site.

Figure S1: Determination of cell viability. Hek293T/17 cells were incubated with different concentrations of (a) DMSO, (b) FL3, (c) FL23 or (d) sulfonyl amidine 1 m for 24 hours before determination of cell viability using the MTT assay. Data is derived from eight replicates; error bars show SD. *, $P < 0.05$; negative, vehicle/DMEM, positive, 5% DMSO.

Figure S2: Dose response curves generated by the ED50plus (v1.0) software used for CC_{50} calculations.

Figure S3: Analysis of apoptosis in response to treatment with flavaglines. Hek293T/17 cells were incubated with different concentrations of (a) FL3, (b) FL23 or (c) sulfonyl amidine 1 m for 24 hours before determination of the amount of apoptosis by annexin V/propidium iodide staining and analysis by flow cytometry. Experiments were undertaken independently in triplicate; error bars show SD. Mock, vehicle/DMEM.

Figure S4: Analysis of virucidal activity of flavaglines. Stock CHIKV was incubated for 1 hr in the presence or absence of various concentrations of FL3, FL23 and

sulfonyl amidine 1 m after which the virus was either (a) directly assayed by standard plaque assay or (b) used to infect Hek293T/17, with the percentage infection being determined at 20 hours by flow cytometry. (c) Virus titers in the supernatants from 20 nM treatments in (b) were assayed by standard plaque assay. Experiments were undertaken independently in triplicate with duplicate plaque assays; error bars show SD. Mock, mock virus incubated with vehicle/DMEM; CHIKV, CHIKV incubated with vehicle/DMEM.

Figure S5: Virus production data from Figure 3 plotted as pfu/mL.

Figure S6: Virus production data from Figure 4 plotted as pfu/mL.

Figure S7: Determination of cell viability after pulse treatment. Hek293T/17 cells were incubated with different concentrations of (a) FL3, (b) FL23 or (c) sulfonyl amidine 1 m for 15 minutes, after which cells were washed and incubated under standard conditions for a further 24 hrs before determination of cell viability using the MTT assay. Data is derived from eight replicates. Negative (vehicle/DMEM) and positive (5% DMSO) controls were run in parallel. Error bar show SD. *, $P < 0.05$.

Figure S8: Virus production data from Figure 5 plotted as pfu/mL.

Flavaglines stimulate transient receptor potential melastatin
type 6 (TRPM6) channel activity.

Blanchard MG., de Baaij J.H.F., Verkaar S.A.J., Lameris A.L., Basmdjian C., Zhao Q.,
Déaubry L., Bindels R.J.M., Hoenderop JG. *Plos One*, **2015**, *10*, e0119028.

RESEARCH ARTICLE

Flavaglines Stimulate Transient Receptor Potential Melastatin Type 6 (TRPM6) Channel Activity

Maxime G. Blanchard¹, Jeroen H. F. de Baaij¹, Sjoerd A. J. Verkaar¹, Anke L. Lameris¹, Christine Basmadjian², Qian Zhao², Laurent Désaubry², René J. M. Bindels¹, Joost G. J. Hoenderop^{1*}

1 Department of Physiology, Radboud Institute for Molecular Life Sciences, Radboud University Medical Center, Nijmegen, The Netherlands, **2** Laboratory of Therapeutic Innovation (UMR7200), CNRS-University of Strasbourg, Faculty of Pharmacy, Illkirch, France

© These authors contributed equally to this work.

* joost.hoenderop@radboudumc.nl



OPEN ACCESS

Citation: Blanchard MG, de Baaij JHF, Verkaar SAJ, Lameris AL, Basmadjian C, Zhao Q, et al. (2015) Flavaglines Stimulate Transient Receptor Potential Melastatin Type 6 (TRPM6) Channel Activity. PLoS ONE 10(3): e0119028. doi:10.1371/journal.pone.0119028

Academic Editor: Stuart E Dryer, University of Houston, UNITED STATES

Received: October 10, 2014

Accepted: January 1, 2015

Published: March 16, 2015

Copyright: © 2015 Blanchard et al. This is an open access article distributed under the terms of the [Creative Commons Attribution License](https://creativecommons.org/licenses/by/4.0/), which permits unrestricted use, distribution, and reproduction in any medium, provided the original author and source are credited.

Data Availability Statement: All relevant data are within the paper.

Funding: This work was supported by grants from the Netherlands Organization for Scientific Research (ZonMW 9120.8026, NWO Vici 016.130.668) and the EURenOmics project from the European Union seventh framework programme (FP7/2007-2013, agreement no. 305608). The authors also thank the Association Nationale Recherche Technologie (ANRT) and the Association d'Aide à la Recherche et à l'Enseignement en Cancérologie (AAREC Filia Research) for fellowships to C. Basmadjian and Q.

Abstract

Magnesium (Mg^{2+}) is essential for enzymatic activity, brain function and muscle contraction. Blood Mg^{2+} concentrations are tightly regulated between 0.7 and 1.1 mM by Mg^{2+} (re)absorption in kidney and intestine. The apical entry of Mg^{2+} in (re)absorbing epithelial cells is mediated by the *transient receptor potential melastatin type 6* (TRPM6) ion channel. Here, flavaglines are described as a novel class of stimulatory compounds for TRPM6 activity. Flavaglines are a group of natural and synthetic compounds that target the ubiquitously expressed prohibitins and thereby affect cellular signaling. By whole-cell patch clamp analyses, it was demonstrated that nanomolar concentrations of flavaglines increases TRPM6 activity by ~2 fold. The stimulatory effects were dependent on the presence of the alpha-kinase domain of TRPM6, but did not require its phosphotransferase activity. Interestingly, it was observed that two natural occurring TRPM6 mutants with impaired insulin-sensitivity, TRPM6-p.Val1393Ile and TRPM6-p.Lys1584Glu, are not sensitive to flavagline stimulation. In conclusion, we have identified flavaglines as potent activators of TRPM6 activity. Our results suggest that flavaglines stimulate TRPM6 via the insulin receptor signaling pathway.

Introduction

Magnesium (Mg^{2+}) is an essential electrolyte for cell growth, protein synthesis and enzymatic activity. Therefore, physiological mechanisms maintain blood Mg^{2+} concentrations within a tightly regulated range (0.7–1.1 mM) [1,2]. The apically expressed *Transient Receptor Potential Melastatin type 6* (TRPM6) channels are the gatekeepers of epithelial Mg^{2+} transport in colon and in the distal convoluted tubule segment (DCT) of the kidney nephron [3]. Loss-of-function mutations of TRPM6 cause intestinal Mg^{2+} malabsorption and renal Mg^{2+} wasting, as evidenced in patients suffering from hypomagnesemia with secondary hypocalcemia (HSH, OMIM #602014) [4,5].

Zhao. The funders had no role in study design, data collection and analysis, decision to publish, or preparation of the manuscript.

Competing Interests: The authors have declared that no competing interests exist.

TRPM6 channels are thought to form tetramers of subunits comprising six transmembrane segments, with a central divalent-selective pore ($\text{Ba}^{2+} > \text{Ni}^{2+} > \text{Mg}^{2+} > \text{Ca}^{2+}$) [3]. Functional channels are inhibited by intracellular Mg^{2+} [3,6] and consequently display a time-dependent increase in currents upon dialysis of cells with a pipette solution containing a strong Mg^{2+} chelator such as ethylenediaminetetraacetic acid (EDTA). Like its close homolog TRPM7, TRPM6 channels comprise an intrinsic intracellular Ser/Thr kinase domain, which has similarities to proteins of the alpha-kinase family [7]. TRPM6 channels undergo autophosphorylation, but the role of the alpha-kinase on channel function and cell physiology is still incompletely understood [6,8–11].

Over the last decade, the epidermal growth factor (EGF) and insulin were shown to stimulate the activity and membrane expression of TRPM6 [12,13]. Two TRPM6 single nucleotide polymorphisms (SNPs: p.Val1393Ile and p.Lys1584Glu) were recently associated with an increased risk of diabetes development in humans [13,14]. Subsequently, it was shown that these mutations prevent a rapid insulin-evoked increase in channel plasma membrane expression [13].

By combined pull down and mass spectrometry studies of the TRPM6 alpha-kinase domain, three interacting proteins have been identified: I) *Methionine sulfoxide reductase B1* (MSRB1) which reduces the sensitivity of TRPM6 to oxidative stress [15], II) *Guanine nucleotide-binding protein subunit beta-2-like 1* (GNB2L1/RACK1) which inhibits TRPM6 activity in an alpha-kinase-dependent manner [16]. III) *Prohibitin 2* or *Repressor protein of Estrogen receptor Activity* (PHB2/REA) which inhibits TRPM6, an effect that is relieved by estrogens [17].

Prohibitins (PHB1 and PHB2) are ubiquitously expressed members of the family of stomatin/prohibitin/flotillin and HflK/C (SPFH) domain containing proteins [18–20]. PHBs are found in the nucleus, cytoplasm and plasma membrane, where they play an important role in cellular differentiation, anti-proliferation and mitochondrial morphogenesis. PHBs modulate the cell cycle progression, regulate transcription and facilitate cell surface signaling [18,19]. Recently, a family of natural compounds named flavaglines was established as high affinity ligand of PHBs [21].

Flavaglines are a family of natural compounds characterized by a cyclopenta[*b*]benzofuran structure [22]. Natural flavaglines and synthetic analogs have been intensively studied, owing to their pleiotropic favorable properties (anti-inflammatory, anticancer, cardioprotective and neuroprotective) [23]. Flavaglines bind PHB1 and PHB2 (with nM affinity) and prevent the CRaf-mediated activation of oncogenic MAPK signaling [21]. Additionally and independently from PHBs, flavaglines inhibit *eukaryotic initiation factor-4A* (eIF4A)-dependent oncogenic protein synthesis [23]. In addition, the binding properties of flavaglines to PHB and/or eIF4A lead to the induction of apoptosis in *apoptosis inducing factor* (AIF) and caspase-12-dependent manners [23,24]. The mechanism of flavaglines neuro- and cardioprotection are likely mediated by their PHB-interacting properties, thereby reducing oxidative stress, deleterious growth factor signaling and release of inflammatory mediators [23].

Given the previously described inhibitory interaction of PHB2 on TRPM6 and the high affinity binding of flavaglines to PHB1 and PHB2, this study aims to identify and characterize the effect of flavaglines on TRPM6 activity.

Materials and Methods

Cell culture

Human embryonic kidney cells (HEK293) were grown at 37°C in DMEM (Biowhittaker Europe, Vervier, Belgium) supplemented with 10% (v/v) fetal calf serum (PAA Laboratories, Linz, Austria), non-essential amino acids and 2 mM L-glutamine in a humidified 5% (v/v) CO₂ atmosphere. Cells were seeded in 12-well plates and subsequently transfected with 1 µg of human NH₂-terminal HA-tagged TRPM6 or empty pCINeo IRES GFP vectors (mock) cDNA using Lipofectamine 2000 (Invitrogen) at 1:3 DNA:Lipofectamine ratio. For patch clamp

experiments, cells were seeded two days after transfection on glass coverslips coated with $50 \mu\text{l}/\text{cm}^2$ of $50 \mu\text{g}/\text{ml}$ fibronectin (Roche, Mannheim, Germany). Two hours later, cells were placed in the recording chamber and selected based on the intensity of the fluorescent reporter.

Electrophysiology

All experiments were undertaken and analyzed using an EPC-9 amplifier and the Patchmaster software (HEKA electronics, Lambrecht, Germany). The sampling interval was set to 200 ms and data was low-pass filtered at 2.9 kHz. Patch clamp pipettes were pulled from thin-walled borosilicate glass (Harvard Apparatus, March-Hugstetten, Germany) and had resistance between 1 and $3 \text{ M}\Omega$ when filled with the pipette solution. Series resistance compensation was set to 75–95% in all experiments. Current densities were obtained by normalizing the current amplitude to the cell capacitance.

Compound synthesis and purity

FL2, FL3 and FL23 were synthesized as previously described [24,25]. Purity of the compounds was >95%, as assessed by reversed-phase high performance liquid chromatography (HPLC) analyses (Hypersil Gold column $30 \times 1 \text{ mm}$, C18, Thermo Scientific) under the following conditions: flow rate: 0.3 mL/min; buffer A: CH_3CN , buffer B: 0.01% aqueous Trifluoroacetic Acid (TFA); gradient: 98–10% (v/v) buffer B over 8 min (detection: $\lambda = 220/254 \text{ nm}$).

Solutions and compound application

The extracellular solution contained (in mM): 150 NaCl, 1 CaCl_2 , 10 HEPES/NaOH pH 7.4. The pipette solution was made of (in mM): 150 NaCl, 10 Na_2EDTA , 10 HEPES/NaOH pH 7.2 [3]. Cells were pre-incubated 15 minutes at 37°C in bath solution containing the compound of interest diluted from a 1000x stock solution or vehicle (0.1% v/v dimethyl sulfoxide (DMSO)).

Immunoblotting

HEK293 cells were lysed for 1 hour at 4°C in TNE lysis buffer containing (in mM): 50 Tris/HCl (pH 8.0), 150 NaCl, 5 EDTA, 1% (v/v) Triton X-100 and protease inhibitors (pepstatin $1 \mu\text{g}/\text{ml}$, PMSF 1 mM, leupeptin $5 \mu\text{g}/\text{ml}$ and aprotinin $5 \mu\text{g}/\text{ml}$). Protein lysates were denatured in Laemmli containing 100 mM dithiothreitol (DTT, 30 minutes, 37°C) and subsequently subjected to SDS-PAGE. Immunoblots were incubated with mouse anti-HA (Roche, high affinity 3F10, 1:5,000), rabbit anti-Akt (Cell signaling, 1:1000) and rabbit anti-ERK1/2 (Cell signaling, 1:1,000) primary antibodies and peroxidase conjugated sheep anti-mouse secondary antibodies (Jackson Immunoresearch, 1:10,000).

Statistical analysis

All results are depicted as mean \pm standard error of the mean (SEM). Statistical analysis was conducted by one-way Student's t-test when comparing two treatment groups or experimental conditions. Difference in means with P values < 0.05 were considered statistically significant and indicated by a star (*).

Curve fitting

Current time-development curves were fitted with a logistic equation: $I = I_0 + ((I_{\text{max}} - I_0) / (1 + (t/t_{1/2})^{-h})^s)$, with I the current density, I_0 the baseline current density, t the time, $t_{1/2}$ the time of half-maximal current density, h the slope and s a parameter. Half-maximal stimulatory

concentration (EC_{50}) was obtained by fitting a Hill equation to the data points: $I = I_0 + (I_{max} - I_0) * (([FL23]^n) / (IC_{50}^n + [FL23]^n))$, with I the current density, I_0 the baseline current density obtained in control conditions, I_{max} the maximal current value and n the Hill equation.

Results

Synthetic flavaglines stimulate TRPM6 activity

HEK293 cells were transfected with the previously described pCINeo-TRPM6-HA-IRES-GFP vector [3]. This construct allows the visual identification of cells expressing TRPM6. Cells were then subjected to whole-cell patch clamp analysis, as previously described [3]. Briefly, currents were elicited by a series of voltage ramps applied at 0.5 Hz from a holding voltage of 0 mV. Due to the dialysis of the cytoplasm with a pipette solution containing EDTA, time-dependent outwardly rectifying currents were observed in response to this ramp protocol (Fig. 1A). In order to assess the effect of flavaglines on TRPM6, cells were first exposed to FL23 (50 nM) [25], a potent analog of the established PHB2 ligand FL3 [21]. This protocol yielded a

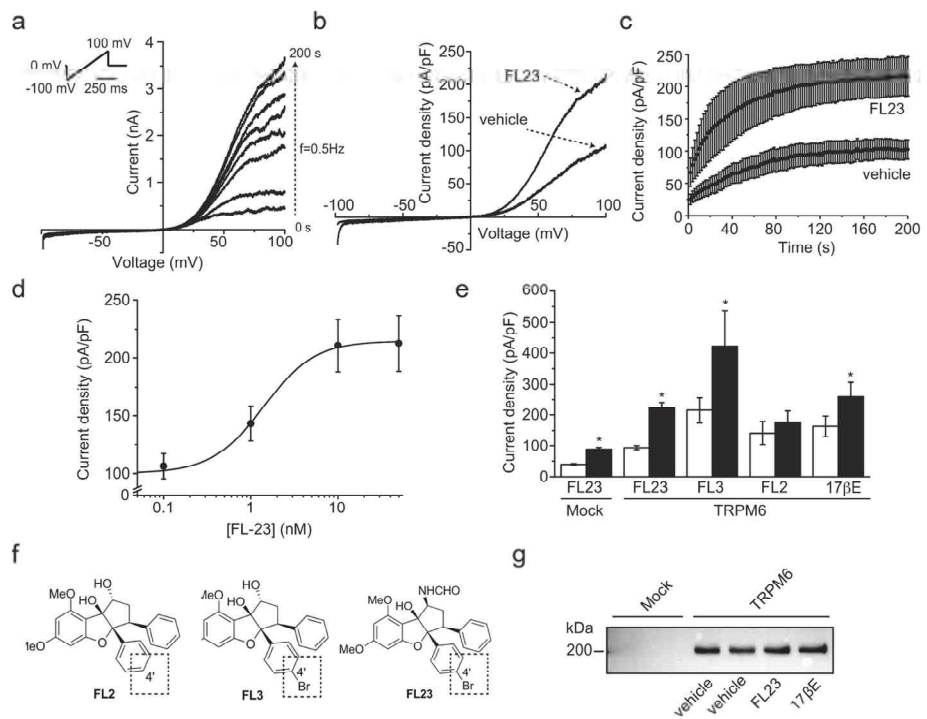


Fig 1. Flavaglines stimulate TRPM6 at nanomolar concentration. **a.** TRPM6 currents were evoked by a series of 500 ms voltage ramp from -100 to +100 mV applied every 2 s (0.5 Hz) from a holding potential of 0 mV (top left inset). A typical set of current-voltage curves obtained from a single cell is shown. **b.** Typical current-voltage curves obtained 200 s after break-in from cells pre-incubated 15 minutes with vehicle or FL23 (50 nM). **c.** The average time-course of TRPM6 current development with ($n = 19$) or without ($n = 19$) FL23 pre-treatment are shown for current values measured at +80 mV. **d.** FL23 increases TRPM6 current density in a concentration-dependent manner ($n \geq 3$ per data points). Line represents the fit of data points with a Hill equation (see [Material and Methods](#)). **e.** Incubation of TRPM6 expressing cells with FL3 (50 nM, $n \geq 10$), FL23 (50 nM, $n \geq 22$) or 17βE (50 nM, $n \geq 9$) significantly increased the average current densities measured at +80 mV 200 s after break-in. Mock-transfected cells showed a similar increase in current density ($n \geq 8$). TRPM6 currents were not sensitive to FL2 ($n \geq 10$). Stars indicate statistically significant difference ($P < 0.05$) between vehicle- (white bar) and compound-treated cells (black bar). **f.** The chemical structures of FL2, FL3 and FL23 are shown. **g.** Cells were pre-incubated with vehicle, FL23 (50 nM) or 17βE (50 nM). Total lysate were subjected to Western blot analysis using an anti-HA primary antibody. FL23 and estradiol (17βE) did not significantly affect the expression of TRPM6. A representative blot of three separate experiments is shown.

doi:10.1371/journal.pone.0119028.g001

significant increase in the current density without affecting the characteristic shape of the current-voltage (IV) curve (Fig. 1B) or the current time-development characteristics (Fig. 1C). The average time-development curves were fitted with a logistic equation (see Material and Methods). This analysis revealed that the time of half-maximal activation ($t_{1/2}$) was not changed between control and FL23-treated cells (control: 48 ± 2 s, FL23: 43 ± 3 s). The rate of current development (the slope h) was increased with FL23 treatment (control: 1.8 ± 0.1 pApF⁻¹s⁻¹, FL23: 3.0 ± 0.2 pApF⁻¹s⁻¹). Pre-incubation of the cells with concentrations of FL23 ranging from 0.01 to 50 nM revealed a concentration-dependent stimulation of TRPM6 activity with an $EC_{50} = 1.4 \pm 0.2$ nM and Hill equation $n = 1.5 \pm 0.3$ (see Material and Methods, Fig. 1D). A similar increase in TRPM6 activity was observed with FL3 (50 nM, Fig. 2A-B). Next, cells were pre-incubated with FL2 (50 nM, Fig. 1F), a flavagline that does not display significant cytotoxicity in cancer cells [24] nor cytoprotection in cardiomyocytes [26]. In contrast to FL3 and FL23, this treatment did not significantly alter the current density of TRPM6-expressing cells (Fig. 2C-D). As previously reported, estradiol (17 β E) significantly stimulated TRPM6 currents (Fig. 1E) [17]. On average, 17 β E, FL3 and FL23 stimulated TRPM6 activity by 1.5 to 2-fold (Fig. 1E). Interestingly, mock-transfected cells demonstrated a similar ~ 2 -fold increase in current density upon FL23 treatment, indicating that TRPM7 is also a likely target of flavaglines action (Fig. 1E). As expected from the short pre-incubation period, the expression of TRPM6 was not influenced by FL23 or 17 β E (Fig. 1G).

The stimulating effects of flavaglines require the intrinsic kinase domain of TRPM6

To assess the involvement of the intrinsic alpha-kinase domain in the flavagline-mediated potentiation of TRPM6 currents, cells were transfected with the previously described kinase-truncated

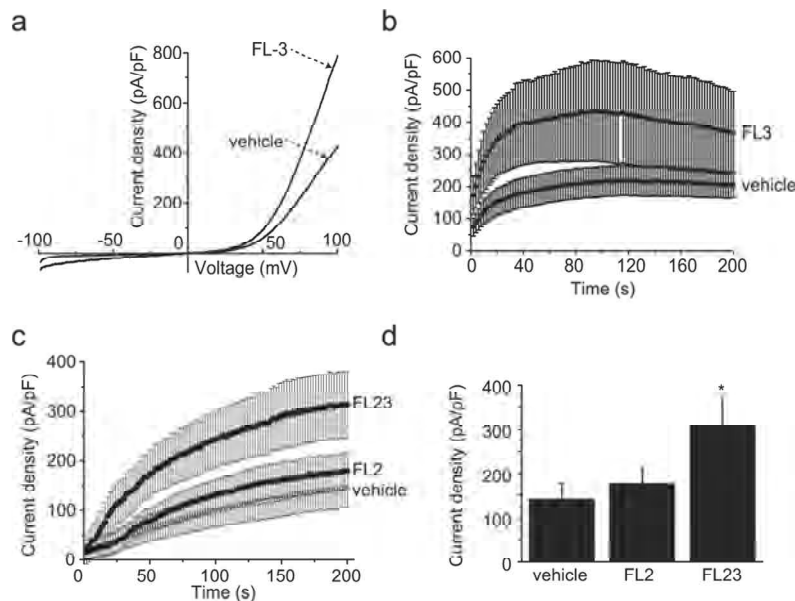


Fig 2. Analogs of FL23 show distinct effects on TRPM6 currents. **a.** Typical current-voltage curves obtained 200 s after break-in are shown for vehicle and FL23 (50 nM) pre-incubated cells. **b.** The average time-course of TRPM6 current development with ($n = 8$) or without ($n = 11$) FL23 (50 nM) is shown for current values measured at +80 mV. **c.** The average time-course of TRPM6 current development with FL2 (50 nM, $n = 12$), vehicle ($n = 10$) or FL23 (50 nM, $n = 10$) pre-treatment is shown for current values measured at +80 mV. **d.** FL2 incubation did not significantly stimulate TRPM6 activity ($n \geq 10$). Stars indicate statistically significant difference ($P < 0.05$) between vehicle and compound-treated cells.

doi:10.1371/journal.pone.0119028.g002

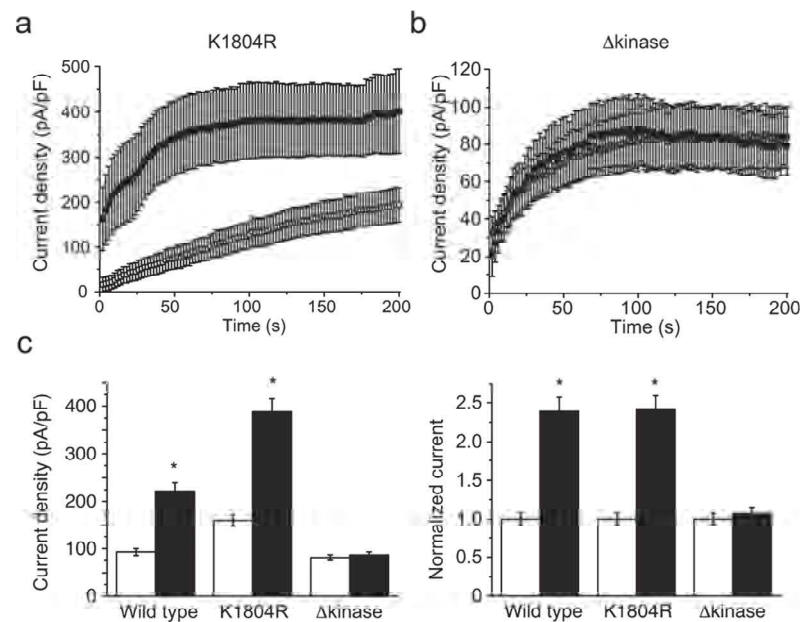


Fig 3. The presence of the intrinsic alpha-kinase domain of the channel but not its activity is required for flavagline-mediated stimulation of TRPM6. **a.** The average time-course of current development of the kinase-inactive channels (TRPM6^{K1804R}) with (n = 7, full symbols) or without (n = 9, empty symbols) FL23 (50 nM) pre-incubation is shown for current values measured at +80 mV. **b.** The average time-course of current development of TRPM6^{L1749X} (Δ kinase) with (n = 8, full symbols) or without (n = 9, empty symbols) FL23 (50 nM) pre-incubation is shown for current values measured at +80 mV. **c.** Pre-incubation of cells with FL23 (50 nM) stimulated wild type (n \geq 22), K1804R (n \geq 9), but not Δ kinase (n \geq 8, p>0.05) channel activity. Right panel shows current values normalized to each control condition. Stars indicate statistically significant difference (P<0.05) between vehicle- (white bar) and compound-treated cells (black bar).

doi:10.1371/journal.pone.0119028.g003

(p.Leu1749*, Δ kinase) or kinase-inactive (p.Lys1804Arg, KI) TRPM6 constructs [9]. While the first construct produces mutant channels lacking the complete kinase domain, the KI construct forms channels without intrinsic alpha-kinase phosphotransferase activity. Both constructs produce functional proteins with apparently normal channel function in the absence of intracellular Mg²⁺. Using an identical pre-incubation protocol, cells expressing the KI mutant demonstrated a FL23-mediated increase in current densities similar to wild type (Fig. 3A and C). In contrast, the Δ kinase mutant failed to respond to this treatment (Fig. 3B-C).

Flavaglines act along a shared pathway with insulin

The intracellular amino acid residues p.Val1393 and p.Lys1584 have been shown to independently confer sensitivity of TRPM6 channels to insulin stimulation, probably by altering the phosphorylation of the neighboring p.Thr1391 and p.Ser1583 residues, respectively [13]. Phosphomimicking mutations of either p.Thr1391Asp or p.Ser1583Asp were shown to be permissive in the insulin-mediated potentiation of TRPM6 [13]. To address whether flavaglines act on TRPM6 in a similar way as insulin, cells expressing either of two naturally occurring insulin-insensitive TRPM6 SNPs (p.Val1393Ile or p.Lys1584Glu) were pre-incubated with FL23 (50 nM). These mutants failed to respond to FL23 (Fig. 4A-B and E).

Following the activation of the insulin receptor, a complex multi-branched signaling cascade is activated. One of these branches involves the activation of *Phosphoinositide 3-kinase* (PI3K), Akt and *Ras-related C3 botulinum toxin substrate 1* (Rac1) [27]. Co-expression of TRPM6 together with the constitutively active (p.Gly12Val) or dominant-negative (p.Thr17Asn)

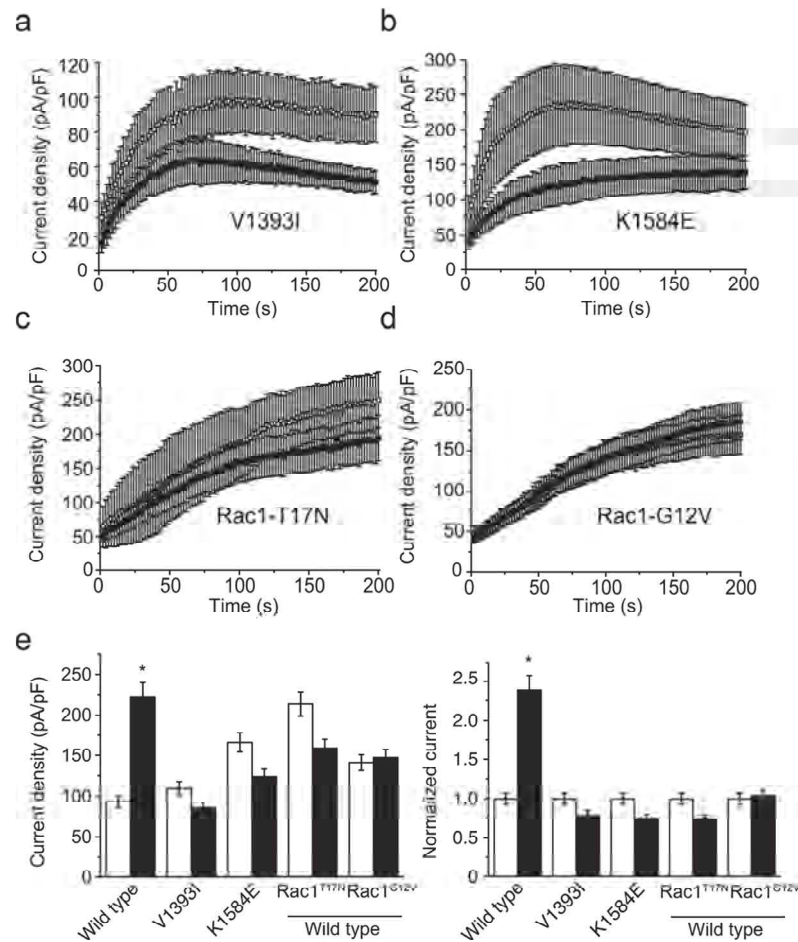


Fig 4. Flavaglines act upon a common pathway with insulin receptor signaling. a-d. The average time-course of current development of cells pre-incubated with (full symbols) or without (empty symbols) FL23 (50 nM) for: (a) TRPM6^{V1393I} (n≥8), (b) TRPM6^{K1584E} (n≥7), (c) wild type TRPM6 together with Rac1^{T17N} (n≥6) and (d) wild type TRPM6 together with Rac1^{G12V} (n≥11). e. FL23 pre-incubation failed to alter currents in cells expressing TRPM6^{V1393I} (n = 11), TRPM6^{K1584E} (n≥8) and cells co-expressing wild type TRPM6 together with Rac1^{T17N} (n = 8) and TRPM6 together with Rac1^{G12V} (n≥14). Right panel shows current values normalized to each control condition. Stars indicate statistically significant difference (P<0.05) between vehicle- (white bar) and compound-treated cells (black bar).

doi:10.1371/journal.pone.0119028.g004

mutants of Rac1 have been shown to respectively allow and prevent the increase of TRPM6 membrane expression by insulin [13]. Here, cells were co-transfected with TRPM6 and either the p.Thr17Asn or p.Gly12Val Rac1 mutants. Both mutants prevented the stimulation of TRPM6 by FL23 (Fig. 4C-D and F).

Flavaglines do not affect Akt phosphorylation

Given the previously described modulation of Akt by PHBs [28], the effects of flavaglines on Akt phosphorylation were examined using the same experimental conditions as were used in the patch clamp experiments. Following 15 minutes of incubation, phosphorylation of Akt was not induced by FL2, FL3 and FL23 (50 nM, Fig. 5). It has been previously demonstrated that flavaglines prevent ERK1/2 phosphorylation in a manner that depends on CRaf [21]. Here,

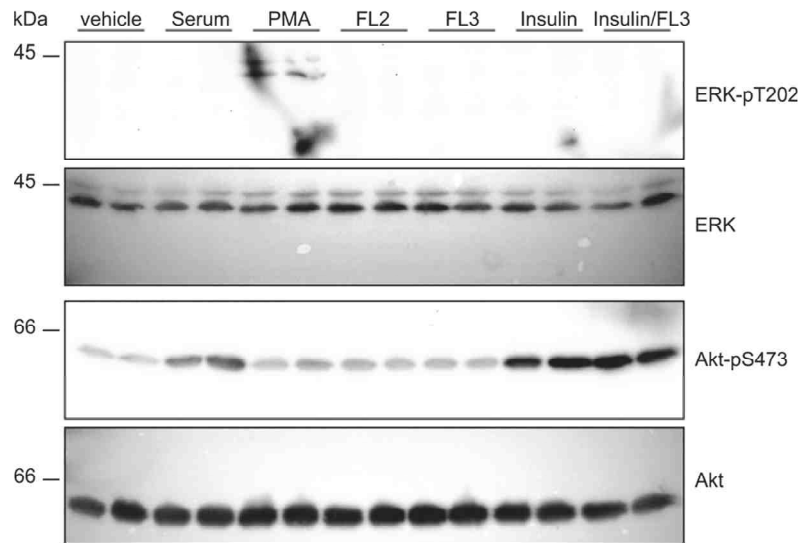


Fig 5. Cellular Akt and ERK signaling is unaffected by FL3. HEK293 cells were incubated with FL2 (50 nM), FL3 (50 nM), PMA (100 nM), insulin (10 nM) or 17βE (50 nM) for 15 minutes. Protein lysates were immediately obtained and immunoblots were performed to detect pERK1/2 and pAkt. PMA and insulin served as positive controls for ERK and Akt phosphorylation, respectively.

doi:10.1371/journal.pone.0119028.g005

basal ERK1/2 phosphorylation was not apparent in control condition and no additional phosphorylation was detected upon flavaglines stimulation (Fig. 5).

Discussion

The present study demonstrates that the activity of the Mg²⁺-permeant TRPM6 channel is stimulated ~2-fold by the flavaglines compounds FL3 and FL23. This is the first report of an exogenous natural compound that stimulates TRPM6 activity.

The activity of TRPM6 and its plasma membrane expression have been shown to be increased upon stimulation with insulin. This effect relied on the PI3K, Akt and Rac1 signaling cascade (Fig. 6). Detailed electrophysiological and total internal reflection fluorescence (TIRF)

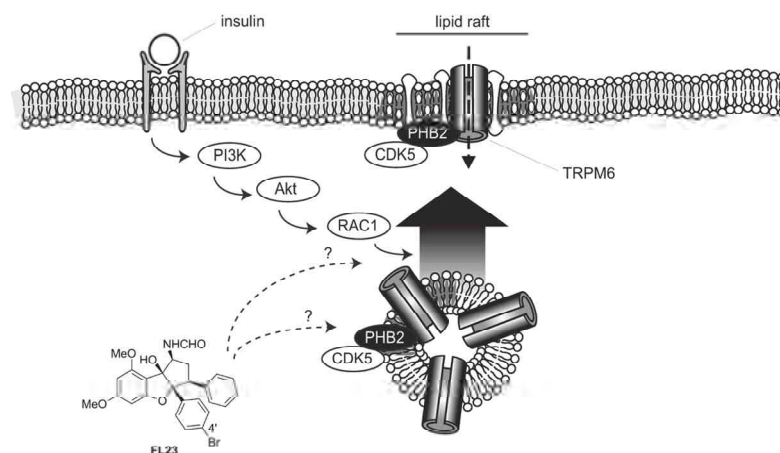


Fig 6. Proposed model of flavaglines action. Flavaglines stimulate TRPM6 activity by acting on downstream effector(s) of the insulin receptor. PHB2 and CDK5, proteins which are known to regulate TRPM6 are localized in lipid rafts.

doi:10.1371/journal.pone.0119028.g006

microscopy analyses have revealed a permissive role for TRPM6-p.Val1393 and TRPM6-p.Lys1584 sites in insulin-evoked insertion of channels in the plasma membrane [13]. Here, it is proposed that flavaglines stimulate TRPM6 by acting along the same pathway (Fig. 6). This hypothesis is based on the following observations: (I) flavaglines increased TRPM6 activity ~ 1.5–2 fold, which is quantitatively similar to the previously described action of insulin on TRPM6 activity [13]; (II) the insulin-insensitive (TRPM6-p.Val1393Ile and TRPM6-Lys1584-Glu) TRPM6 mutants were not potentiated by flavaglines; (III) flavaglines-induced TRPM6 stimulation was absent when overexpressing TRPM6 together with Rac1 mutants; (IV) in concordance with the mechanism of insulin action on TRPM6, flavaglines stimulated the kinase-inactive (TRPM6-p.Lys1804Arg) mutant. Taken together, it is hypothesized that flavaglines act by triggering or relieving a tonic inhibition on one (or more) of the molecular player(s) involved in insulin signaling, effectively promoting the plasma membrane insertion of wild type TRPM6 channels but not of TRPM6 channels containing insulin-insensitive SNP mutants. Our data suggest that the effects of flavagline-stimulation take place downstream of Akt, since no additional Akt phosphorylation was evident upon treatment with FL3. Further experiments investigating the detailed molecular action of flavaglines on the localization and phosphorylation of the known kinases involved in growth-factor stimulation of TRPM6 (PI3K/Akt/Rac1/Cdk5) will be necessary to elucidate the exact molecular targets.

Flavaglines have recently been identified as potent interactors of PHBs [18,19]. Interestingly, PHB1 and PHB2 are enriched in detergent resistant (lipid rafts) fractions of the plasma membrane [18]. Given the previously described action of PHBs as chaperone of Ras-dependent CRaf activation in the plasma membrane [21], a general function of PHBs is to provide spatial constraints necessary for the proper regulation of proteins in specialized regions (eg the lipid rafts) of the plasma membrane. It can be hypothesized that TRPM6 channels transiently or permanently localize together with PHB in the lipid raft fractions of the plasma/vesicular membrane, where channels undergo regulatory phosphorylation. The following facts support this hypothesis: (I) TRPM6 has been shown to establish an inhibitory interaction with PHB2 [17]; (II) TRPM6 requires CDK5 phosphorylation for proper insulin-mediated regulation, CDK5 localizing and being activated in the lipid raft fraction of plasma membrane [29]; (III) the close homolog TRPM7 has been reported to localize in lipid rafts [30], (IV) TRPM6 requires PIP2 for proper function [31], a lipid that is enriched in lipid rafts. Therefore, it is tempting to speculate that PHBs binding to TRPM6 promotes the formation of a macromolecular regulatory complex in the lipid rafts of the plasma membrane. In this perspective, it is interesting to note that the insulin-induced signaling pathway becomes more active when the insulin receptor is expressed in lipid rafts [32–34]. In addition to the inhibitory PHB2-TRPM6 interaction, other TRP channels are modulated by members of the SPFH protein family [20]. Podocin, an SPFH protein similar to prohibitin, regulates the insulin sensitive *transient receptor potential canonical type 6* (TRPC6) ion channel in the kidney [35]. In line with the current hypothesis, it has been proposed that podocin organize TRPC6-lipid complexes in the plasma membrane, thereby modulating channel activity [36]. Altogether, these findings point towards a compartmentalized insulin signaling cascade on/near the lipid rafts in the vesicular/plasma membrane. In this model, expression of TRPM6 and the insulin receptor in the lipid rafts allows for the rapid local regulation of TRPM6 by insulin.

Comparison of structure-function activity between active (FL3, FL23) and inactive (FL2) flavaglines analogs revealed a positive correlation between cytostatic/cytotoxic properties of flavaglines in cancer cell lines and their action on TRPM6 [21,24,25]. While the effects of flavaglines on cellular proliferation and growth factor signaling were evident starting from 2 hours after compound application, the stimulatory effect shown here occurs within 15 minutes. These results suggest that the short-term effects of flavaglines on TRPM6 take place

independently from any translational effect (eg eIF4A-dependent). However, the concurrent structure-function relationship of flavaglines in their TRPM6-stimulatory effects and in their cytotoxic properties suggests that both mechanisms are PHB-dependent. It has previously been shown that PHB2 interacts with TRPM6 and that 17 β E reduces this inhibitory interaction [17]. However, the current results suggest that 17 β E and FL23 only share a partially overlapping mechanism of action. Exogenous PHB2 inhibits TRPM6 in an alpha-kinase phosphotransferase-dependent manner [17]. In contrast, flavaglines stimulated the kinase-inactive TRPM6-p.Lys1804Arg mutant. Moreover, flavaglines induce an increase in endogenous TRPM7 currents, while TRPM7 currents were insensitive to PHB2-mediated inhibition [17]. Further work identifying the major players that are part of the TRPM6-PHB macromolecular complex and its regulation by flavaglines and 17 β E are necessary to further understand the stimulatory but slightly distinct effects of these compounds on the activity of TRPM6.

Evidences suggest that the stimulatory action of flavaglines is not restricted to TRPM6. Here, a stimulatory effect of FL23 was also observed in mock-transfected cells. Given the experimental conditions used in this study, a substantial part of the current in mock-transfected HEK293 cells is carried by endogenous TRPM7 channels [3]. Further experiments investigating the action of flavaglines on other members of the SPFH protein and TRP channel (eg TRPC6) families will be needed to understand the complex mechanism of action of flavaglines.

Reduced TRPM6 channel activity results in a clinically relevant hypomagnesemia due to renal Mg²⁺ wasting. Because insulin and EGF stimulate TRPM6 function, patients with diabetes mellitus type 2 or users of EGFR inhibitors are at risk to develop hypomagnesemia [12,13]. Given that FL3 and FL23 stimulate TRPM6 activity, flavaglines may provide an important therapeutic potential for these patient groups. A preliminary experiment with FL3 (daily i.p. injection 0.1 mg/kg, 7 days,) did not reveal changes in serum or urinary Mg²⁺ concentration in mice (data not shown). In addition to the optimization of treatment duration, the actual dose of FL3 reaching the DCT cells in the kidney where TRPM6 is located may be much lower and challenging to assess. Future experiments assessing the bioavailability of flavaglines should be performed to assess putative magnesiotropic effects *in vivo*. Additionally, given the physiological mechanism of intestinal and/or renal compensation of Mg²⁺ transport, the effects of flavaglines should be assessed in a murine model of hypomagnesemia.

In conclusion, the natural compounds flavaglines stimulate the activity of TRPM6 Mg²⁺ channels at nanomolar concentrations. The effect is rapid (within 15 minutes) and probably relies on a near-plasma membrane mechanism that likely involves PHBs.

Author Contributions

Conceived and designed the experiments: MB JDB SV RB JH. Performed the experiments: MB JDB SV AL. Analyzed the data: MB JDB RB JH. Contributed reagents/materials/analysis tools: CB QZ LD. Wrote the paper: MB JDB LD JH RB.

References

1. de Baaij JH, Groot Koerkamp MJ, Lavrijsen M, van Zeeland F, Meijer H, Holstege FC, et al. Elucidation of the distal convoluted tubule transcriptome identifies new candidate genes involved in renal Mg(2+) handling. *Am J Physiol Renal Physiol*. 2013; 305: F1563–1573. doi: [10.1152/ajprenal.00322.2013](https://doi.org/10.1152/ajprenal.00322.2013) PMID: [24089412](https://pubmed.ncbi.nlm.nih.gov/24089412/)
2. de Baaij JHF, Hoenderop JGJ, Bindels RJM. Regulation of magnesium balance: lessons learned from human genetic disease. *Clinical kidney journal*. 2012; 5: i15–i24.
3. Voets T, Nilius B, Hoefs S, van der Kemp AW, Droogmans G, Bindels RJ, et al. TRPM6 forms the Mg²⁺ influx channel involved in intestinal and renal Mg²⁺ absorption. *J Biol Chem*. 2004; 279: 19–25. PMID: [14576148](https://pubmed.ncbi.nlm.nih.gov/14576148/)

4. Walder RY, Landau D, Meyer P, Shalev H, Tsolia M, Borochowitz Z, et al. Mutation of TRPM6 causes familial hypomagnesemia with secondary hypocalcemia. *Nat Genet.* 2002; 31: 171–174. PMID: [12032570](#)
5. Schlingmann KP, Weber S, Peters M, Niemann Nejsum L, Vitzthum H, Klingel K, et al. Hypomagnesemia with secondary hypocalcemia is caused by mutations in TRPM6, a new member of the TRPM gene family. *Nat Genet.* 2002; 31: 166–170. PMID: [12032568](#)
6. Zhang Z, Yu H, Huang J, Faouzi M, Schmitz C, Penner R, et al. The TRPM6 kinase domain determines the Mg ATP-sensitivity of TRPM7/M6 heteromeric ion channels. *J Biol Chem.* 2014; doi: [10.1074/jbc.M113.512285](#).
7. Ryazanova LV, Dorovkov MV, Ansari A, Ryazanov AG. Characterization of the protein kinase activity of TRPM7/ChaK1, a protein kinase fused to the transient receptor potential ion channel. *J Biol Chem.* 2004; 279: 3708–3716. PMID: [14594813](#)
8. van der Wijst J, Blanchard MG, Woodroof HI, Macartney TJ, Gourlay R, Hoenderop JG, et al. Kinase and channel activity of TRPM6 are co-ordinated by a dimerization motif and pocket interaction. *Biochem J.* 2014; 460: 165–175. doi: [10.1042/BJ20131639](#) PMID: [24650431](#)
9. Thebault S, Cao G, Venselaar H, Xi Q, Bindels RJ, Hoenderop JG. Role of the alpha-kinase domain in transient receptor potential melastatin 6 channel and regulation by intracellular ATP. *J Biol Chem.* 2008; 283: 19999–20007. doi: [10.1074/jbc.M800167200](#) PMID: [18490453](#)
10. Schmitz C, Dorovkov MV, Zhao X, Davenport BJ, Ryazanov AG, Perraud AL. The channel kinases TRPM6 and TRPM7 are functionally nonredundant. *J Biol Chem.* 2005; 280: 37763–37771. PMID: [16150690](#)
11. Brandao K, Deason-Towne F, Zhao X, Perraud AL, Schmitz C. TRPM6 kinase activity regulates TRPM7 trafficking and inhibits cellular growth under hypomagnesian conditions. *Cell Mol Life Sci.* 2014; doi: [10.1007/s00018-014-1647-7](#).
12. Thebault S, Alexander RT, Tiel Groenestege WM, Hoenderop JG, Bindels RJ. EGF increases TRPM6 activity and surface expression. *J Am Soc Nephrol.* 2009; 20: 78–85. doi: [10.1681/ASN.2008030327](#) PMID: [19073827](#)
13. Nair AV, Hoher B, Verkaart S, van Zeeland F, Pfab T, Slowinski T, et al. Loss of insulin-induced activation of TRPM6 magnesium channels results in impaired glucose tolerance during pregnancy. *Proc Natl Acad Sci U S A.* 2012; 109: 11324–11329. doi: [10.1073/pnas.1113811109](#) PMID: [22733750](#)
14. Song Y, Hsu YH, Niu T, Manson JE, Buring JE, Liu S. Common genetic variants of the ion channel transient receptor potential membrane melastatin 6 and 7 (TRPM6 and TRPM7), magnesium intake, and risk of type 2 diabetes in women. *BMC Med Genet.* 2009; 10: 4. doi: [10.1186/1471-2350-10-4](#) PMID: [19149903](#)
15. Cao G, Lee KP, van der Wijst J, de Graaf M, van der Kemp A, Bindels RJ, et al. Methionine sulfoxide reductase B1 (MsrB1) recovers TRPM6 channel activity during oxidative stress. *J Biol Chem.* 2010; 285: 26081–26087. doi: [10.1074/jbc.M110.103655](#) PMID: [20584906](#)
16. Cao G, Thebault S, van der Wijst J, van der Kemp A, Lasonder E, Bindels RJ, et al. RACK1 inhibits TRPM6 activity via phosphorylation of the fused alpha-kinase domain. *Curr Biol.* 2008; 18: 168–176. doi: [10.1016/j.cub.2007.12.058](#) PMID: [18258429](#)
17. Cao G, van der Wijst J, van der Kemp A, van Zeeland F, Bindels RJ, Hoenderop JG. Regulation of the epithelial Mg²⁺ channel TRPM6 by estrogen and the associated repressor protein of estrogen receptor activity (REA). *J Biol Chem.* 2009; 284: 14788–14795. doi: [10.1074/jbc.M808752200](#) PMID: [19329436](#)
18. Chowdhury I, Thompson WE, Thomas K. Prohibitins role in cellular survival through Ras-Raf-MEK-ERK pathway. *J Cell Physiol.* 2014; 229: 998–1004. doi: [10.1002/jcp.24531](#) PMID: [24347342](#)
19. Thuaud F, Ribeiro N, Nebigil CG, Desaubry L. Prohibitin ligands in cell death and survival: mode of action and therapeutic potential. *Chem Biol.* 2013; 20: 316–331. doi: [10.1016/j.chembiol.2013.02.006](#) PMID: [23521790](#)
20. Browman DT, Hoegg MB, Robbins SM. The SPFH domain-containing proteins: more than lipid raft markers. *Trends Cell Biol.* 2007; 17: 394–402. PMID: [17766116](#)
21. Polier G, Neumann J, Thuaud F, Ribeiro N, Gelhaus C, Schmidt H, et al. The natural anticancer compounds rocaglamides inhibit the Raf-MEK-ERK pathway by targeting prohibitin 1 and 2. *Chem Biol.* 2012; 19: 1093–1104. doi: [10.1016/j.chembiol.2012.07.012](#) PMID: [22999878](#)
22. Pan L, Woodard JL, Lucas DM, Fuchs JR, Kinghorn AD. Rocaglamide, silvestrol and structurally related bioactive compounds from *Aglaia* species. *Nat Prod Rep.* 2014; 31: 924–939. doi: [10.1039/c4np00006d](#) PMID: [24788392](#)
23. Basmadjian C, Thuaud F, Ribeiro N, Desaubry L. Flavaglines: potent anticancer drugs that target prohibitins and the helicase eIF4A. *Future Med Chem.* 2013; 5: 2185–2197. doi: [10.4155/fmc.13.177](#) PMID: [24261894](#)

24. Thuaud F, Bernard Y, Türkeri G, Dirr R, Aubert G, Cresteil T, et al. Synthetic analogue of rocaglaol displays a potent and selective cytotoxicity in cancer cells: involvement of apoptosis inducing factor and caspase-12. *Journal of medicinal chemistry*. 2009; 52: 5176–5187. doi: [10.1021/jm900365v](https://doi.org/10.1021/jm900365v) PMID: [19655762](https://pubmed.ncbi.nlm.nih.gov/19655762/)
25. Thuaud F, Ribeiro N, Gaiddon C, Cresteil T, Desaubry L. Novel flavaglines displaying improved cytotoxicity. *J Med Chem*. 2011; 54: 411–415. doi: [10.1021/jm101318b](https://doi.org/10.1021/jm101318b) PMID: [21142180](https://pubmed.ncbi.nlm.nih.gov/21142180/)
26. Bernard Y, Ribeiro N, Thuaud F, Türkeri G, Dirr R, Boulberdaa M, et al. Flavaglines alleviate doxorubicin cardiotoxicity: implication of Hsp27. *PLoS One*. 2011; 6: e25302. doi: [10.1371/journal.pone.0025302](https://doi.org/10.1371/journal.pone.0025302) PMID: [22065986](https://pubmed.ncbi.nlm.nih.gov/22065986/)
27. Bezzerides VJ, Ramsey IS, Kotecha S, Greka A, Clapham DE. Rapid vesicular translocation and insertion of TRP channels. *Nat Cell Biol*. 2004; 6: 709–720. PMID: [15258588](https://pubmed.ncbi.nlm.nih.gov/15258588/)
28. Ande SR, Mishra S. Prohibitin interacts with phosphatidylinositol 3,4,5-triphosphate (PIP3) and modulates insulin signaling. *Biochem Biophys Res Commun*. 2009; 390: 1023–1028. doi: [10.1016/j.bbrc.2009.10.101](https://doi.org/10.1016/j.bbrc.2009.10.101) PMID: [19854158](https://pubmed.ncbi.nlm.nih.gov/19854158/)
29. Okada S, Yamada E, Saito T, Ohshima K, Hashimoto K, Yamada M, et al. CDK5-dependent phosphorylation of the Rho family GTPase TC10(alpha) regulates insulin-stimulated GLUT4 translocation. *J Biol Chem*. 2008; 283: 35455–35463. doi: [10.1074/jbc.M806531200](https://doi.org/10.1074/jbc.M806531200) PMID: [18948252](https://pubmed.ncbi.nlm.nih.gov/18948252/)
30. Yogi A, Callera GE, Tostes R, Touyz RM. Bradykinin regulates calpain and proinflammatory signaling through TRPM7-sensitive pathways in vascular smooth muscle cells. *Am J Physiol Regul Integr Comp Physiol*. 2009; 296: R201–207. doi: [10.1152/ajpregu.90602.2008](https://doi.org/10.1152/ajpregu.90602.2008) PMID: [18799634](https://pubmed.ncbi.nlm.nih.gov/18799634/)
31. Xie J, Sun B, Du J, Yang W, Chen HC, Overton JD, et al. Phosphatidylinositol 4,5-bisphosphate (PIP(2)) controls magnesium gatekeeper TRPM6 activity. *Sci Rep*. 2011; 1: 146. doi: [10.1038/srep00146](https://doi.org/10.1038/srep00146) PMID: [22180838](https://pubmed.ncbi.nlm.nih.gov/22180838/)
32. Cohen AW, Razani B, Wang XB, Combs TP, Williams TM, Scherer PE, et al. Caveolin-1-deficient mice show insulin resistance and defective insulin receptor protein expression in adipose tissue. *Am J Physiol Cell Physiol*. 2003; 285: C222–235. PMID: [12660144](https://pubmed.ncbi.nlm.nih.gov/12660144/)
33. Morino-Koga S, Yano S, Kondo T, Shimauchi Y, Matsuyama S, Okamoto Y, et al. Insulin receptor activation through its accumulation in lipid rafts by mild electrical stress. *J Cell Physiol*. 2013; 228: 439–446. doi: [10.1002/jcp.24149](https://doi.org/10.1002/jcp.24149) PMID: [22740366](https://pubmed.ncbi.nlm.nih.gov/22740366/)
34. Vainio S, Heino S, Mansson JE, Fredman P, Kuismanen E, Vaarala O, et al. Dynamic association of human insulin receptor with lipid rafts in cells lacking caveolae. *EMBO Rep*. 2002; 3: 95–100. PMID: [11751579](https://pubmed.ncbi.nlm.nih.gov/11751579/)
35. Anderson M, Kim EY, Hagmann H, Benzing T, Dryer SE. Opposing effects of podocin on the gating of podocyte TRPC6 channels evoked by membrane stretch or diacylglycerol. *Am J Physiol Cell Physiol*. 2013; 305: C276–289. doi: [10.1152/ajpcell.00095.2013](https://doi.org/10.1152/ajpcell.00095.2013) PMID: [23657570](https://pubmed.ncbi.nlm.nih.gov/23657570/)
36. Huber TB, Schermer B, Benzing T. Podocin organizes ion channel-lipid supercomplexes: implications for mechanosensation at the slit diaphragm. *Nephron Exp Nephrol*. 2007; 106: e27–31. PMID: [17570936](https://pubmed.ncbi.nlm.nih.gov/17570936/)

Novel carbocationic rearrangements of 1-styryl propargyl alcohols

Basmadjian C., Zhang F., Désaubry L., *Beilstein. J. Org. Chem.* **2015**, *11*, 1017–1022.



Novel carbocationic rearrangements of 1-styrylpropargyl alcohols

Christine Basmadjian, Fan Zhang and Laurent Désaubry*

Full Research Paper

Open Access

Address:

Laboratory of Therapeutic Innovation (UMR 7200), University of Strasbourg - CNRS, Faculty of Pharmacy, 67401 Illkirch, France

Email:

Laurent Désaubry* - desaubry@unistra.fr

* Corresponding author

Keywords:

carbocationic rearrangement; cyclopentenones; furans; propargyl alcohols

Beilstein J. Org. Chem. **2015**, *11*, 1017–1022.

doi:10.3762/bjoc.11.114

Received: 10 March 2015

Accepted: 27 May 2015

Published: 15 June 2015

Associate Editor: J. A. Murphy

© 2015 Basmadjian et al; licensee Beilstein-Institut.

License and terms: see end of document.

Abstract

The dehydration and subsequent cyclization reactions of 1-styrylpropargyl alcohols was examined. In the course of these studies, numerous scaffolds were synthesized, including a furan, a cyclopentenone, an acyclic enone and even a naphthalenone. The diversity of these structural motifs lies in novel cascades of reactions originating from a common carbocationic manifold.

Introduction

In the course of our medicinal program on a new class of anti-cancer agents [1-3], we developed a novel synthesis of cyclopentenones substituted by three different aryl groups (Scheme 1) [4]. This approach combines a molybdenum(VI)-catalyzed etherification of allylic alcohol with a gold(I)-catalyzed intramolecular cyclization process [5,6].

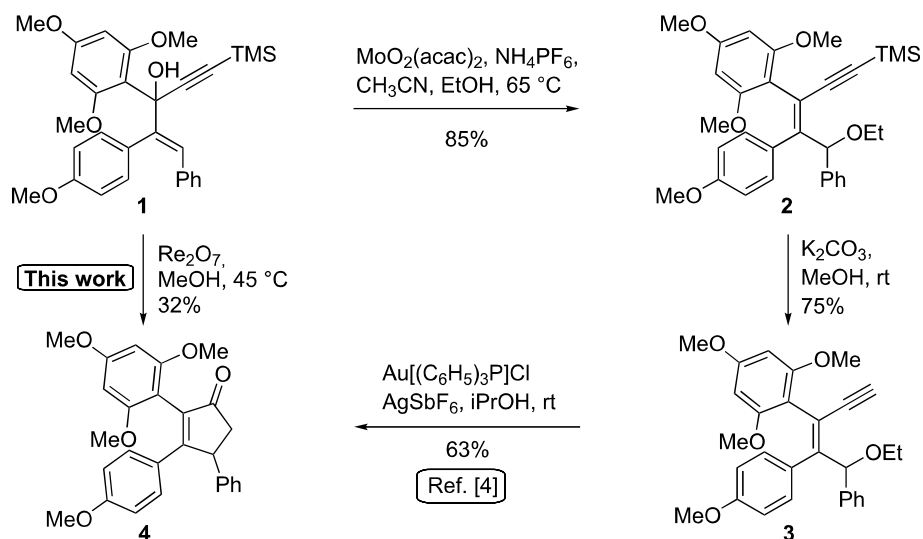
During the optimization process of this synthesis, we examined several catalysts to transform allylic alcohol **1** into ether **2**, including Re_2O_7 , which is described to efficiently catalyze this type of transformation [7]. Unexpectedly, instead of obtaining ether **2**, we observed the formation of cyclopentenone **4** in 32% yield. We noticed that this reaction only occurs when Re_2O_7 is heated at 45 °C for 15 minutes in MeOH prior to the addition of the substrate. As far as we know, this type of reaction has not been described before. It provides a useful

alternative to the Rautenstrauch rearrangement, the main limitation of which lies on the necessity to have the alcohol esterified (Scheme 2) [8]. Indeed, in many cases, this esterification occurs in low yield, or may even be impossible to achieve [4,8,9].

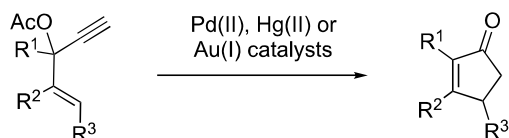
The importance of cyclopentenones as intermediates to the synthesis of bioactive compounds prompted us to explore the synthetic potential of this novel rearrangement of 1-styrylpropargyl alcohols (Table 1). Toward this purpose, a number of other substrates were synthesized from the readily prepared acyl chloride **5** and ketone **6** [4] (Scheme 3).

Results and Discussion

We began our study by applying the reaction conditions developed for alcohol **1** using Re_2O_7 (1.5%), MeOH (8 equiv) at



Scheme 1: Described synthesis of cyclopentenone **4** using a combination of Mo(VI) and Au(I)-catalyzed reactions and serendipitous discovery of a direct conversion of alcohol **1** into **4** [4].

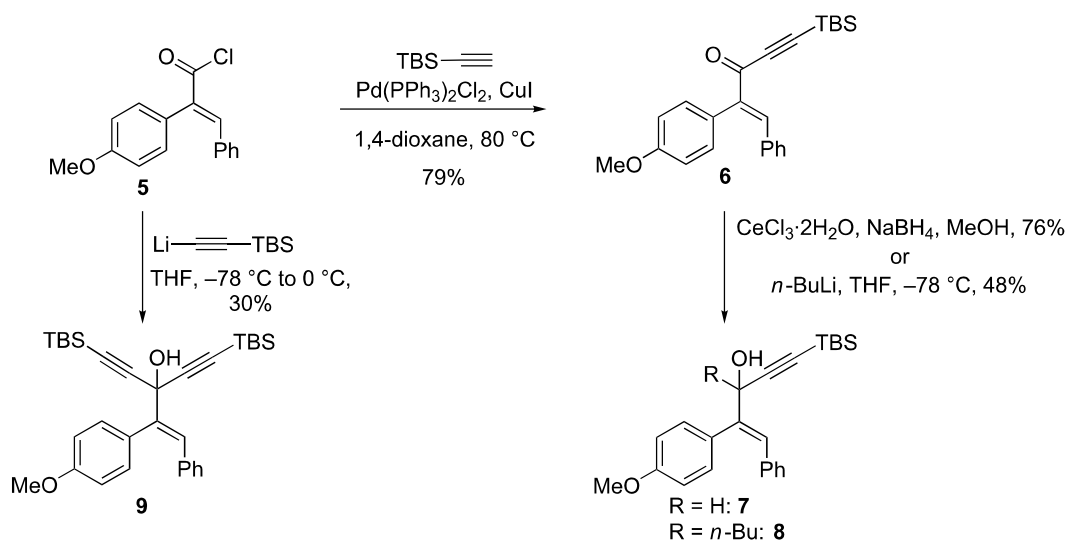


Scheme 2: The Rautenstrauch rearrangement.

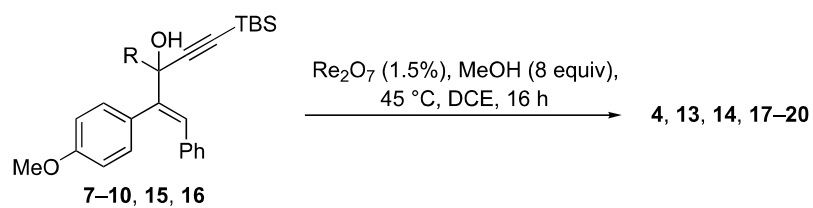
45 °C in DCE (entry 1, Table 1). Gratifyingly, replacing the TMS group by a TBS group improved the yield to 44% (which is superior to the overall yield of the previous three steps syn-

thesis). Along with cyclopentenone **4**, we observed the formation of furan **13** (27% isolated yield).

The proposed mechanism for this reaction is shown in Scheme 4. Both **4** and **13** are expected to arise through the formation of the stabilized carbocation **11** that may evolve through two pathways. This intermediate may either undergo a ring closure due to the nucleophilic character of the silylated alkyne (pathway A) or react with an oxygenated nucleophile, such as the perrhenate anion, to generate the transient intermediate **12** that undergoes an oxo-cyclization to afford an oxonium en route to furan **13** (pathway B). Alternatively, intermediate **12** may

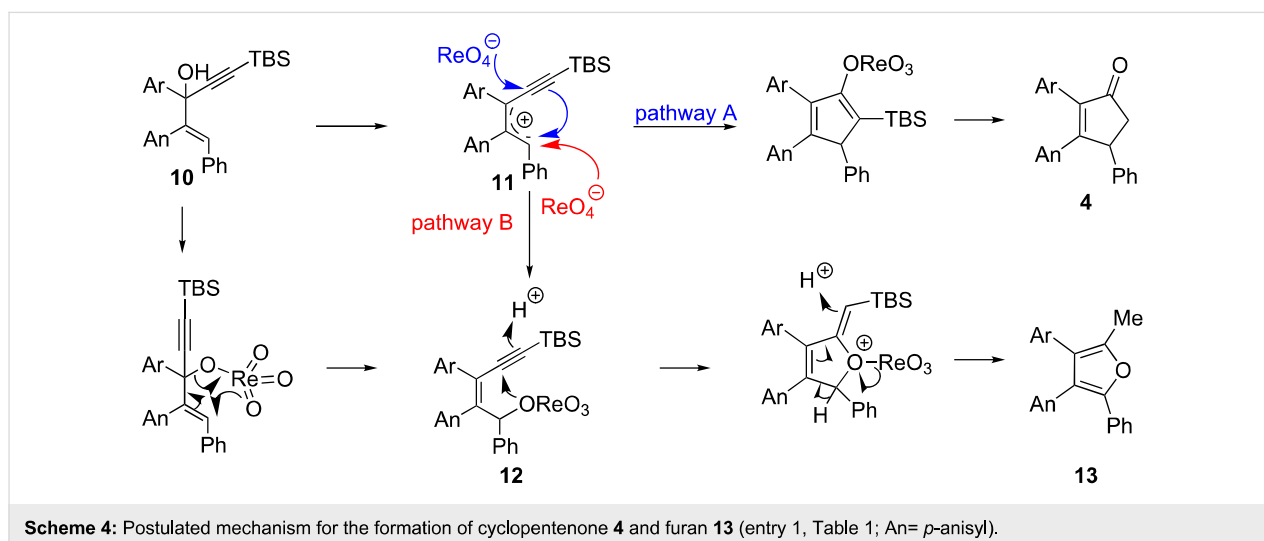


Scheme 3: Synthesis of 1-styrylpropargyl alcohols.

Table 1: Rearrangement of 1-styrylpropargyl alcohols **7–10**, **15**, and **16**.

Entry	R	Isolated products ^a	Yield (%) ^b
1	 10^c	 4	44
		 13	27
2	 15^c	 14	20
3	Ph 16^c	 17	35
4	H 7	 18	54
5	<i>n</i> -Bu 8	 19	47
6	 9	 20	31

^aRe₂O₇ (1.5%), MeOH (8 equiv), 45 °C, DCE, 16 h. ^bIsolated yields. ^cSynthesis described in ref [4]. An = *p*-anisyl.



result from the allylic [1,3]-transposition of a perrhenate ester [10].

Replacement of the highly electron-donating 2,4,6-trimethoxyphenyl group by a 4-chlorophenyl substituent reduced the yield of cyclopentenone formation to 20% (entry 2, Table 1). No furan or other compound could be isolated. As a result, we turned to the examination of substrate **16** [4], whose unsubstituted phenyl ring is even less amenable to stabilize a carbocationic intermediate. Unsurprisingly, we could not detect any cyclopentenone. Instead, we were amazed to isolate the rearranged ketone **17** (entry 3, Table 1). Indeed, 4,4-diarylnaphthalen-1-ones are highly unusual compounds, whose synthesis is rarely described in literature [11]. The structure of **17** was confirmed by NOE and key HMBC correlations (Figure S1, Supporting Information File 1). Although highly speculative and without any experimental support, a putative mechanism for this unprecedented reaction is proposed in Supporting Information File 1 (Scheme S1).

Remarkably, removal of the trimethoxyphenyl group suppressed the formation of cyclopentanone but promoted the formation of furan **18** (54% yield, entry 4, Table 1). Interest-

ingly, substitution of the carbinol part by an *n*-butyl substituent provided an alternate type of product: the acyclic enone was the sole product isolated from the reaction medium (47% yield, entry 5, Table 1). It could be envisioned that this compound results from the rearrangement of an allene oxide (Scheme 5). Interestingly the dipropargylic alcohol **9** afforded the rearranged allylic ether **20** as the only isolated product (entry 6, Table 1).

In order to improve the yields of these reactions and gain insight in the reaction mechanisms, we explored different reaction conditions starting from alcohol **21** (Table 2). 1,2-Dichloroethane and dichloromethane (entries 1 and 2, Table 2) gave better yields (27–31% for **22** and 10–16% for **23**) compared to THF (entry 3, Table 2). In an effort to understand the role of Re_2O_7 , the catalyst was changed to $\text{ReO}_4\text{SiPh}_3$ (entry 5, Table 2) and ReO_4H (entry 6, Table 2). In both cases, the results were similar to those obtained with Re_2O_7 . Removal of methanol from the medium suppressed the formation of **22** (entry 7, Table 2). In this case only furan **23** and rearranged alcohol **25** could be isolated as traces (5%).

To confirm that the reaction is catalyzed by an acid, we changed its nature and tested two Brønsted acids. With $\text{F}_3\text{CSO}_3\text{H}$ (entry

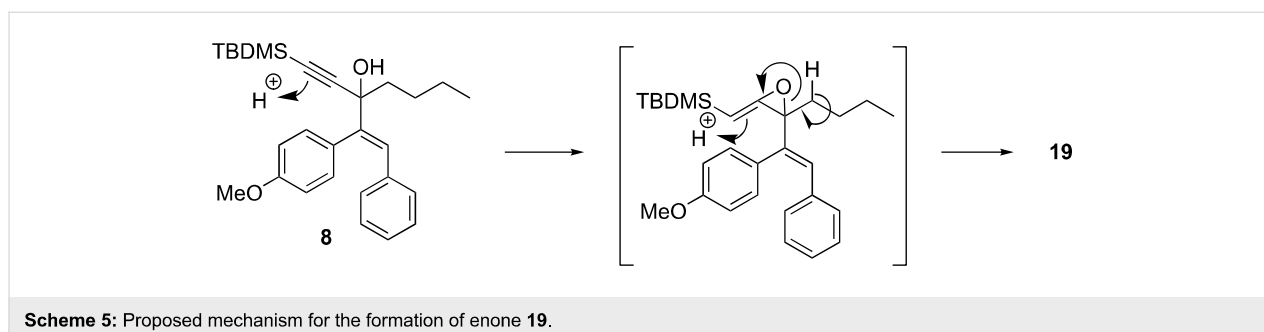
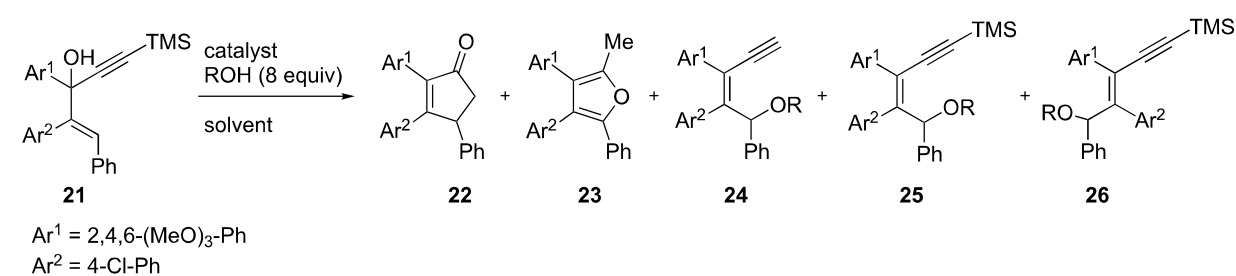


Table 2: Optimization of the acid-catalyzed rearrangements of enynol **21**.

Entry	R	Catalyst	Solvent	T (°C)	22 (%) ^a	23 (%) ^a	24 (%) ^a	25 (%) ^a	26 (%) ^a
1	CH ₃	Re ₂ O ₇	DCE	45	31	16	–	–	–
2	CH ₃	Re ₂ O ₇	CH ₂ Cl ₂	45	27	10	–	–	–
3	CH ₃	Re ₂ O ₇	THF	45	11	9	–	12	–
4	CH ₃	Re ₂ O ₇	THF	rt	12	–	–	4	–
5	CH ₃	ReO ₄ SiPh ₃	DCE	45	28	17	6	–	–
6	CH ₃	ReO ₄ H	DCE	45	30	17	–	–	–
7	–	ReO ₄ H	DCE	45	–	5	–	5 ^b	–
8	CH ₃	F ₃ CSO ₃ H	DCE	45	36	12	–	–	–
9	CH ₃	AcOH	DCE	45	–	–	–	51	47
10 ^c	–	F ₃ CSO ₃ H	DCE	45	–	–	–	–	–
11 ^c	CF ₃ CH ₃	F ₃ CSO ₃ H	DCE	45	–	–	–	–	–
11	CH ₃	F ₃ CSO ₃ H	CH ₃ NO ₂	45	30	–	–	–	–
12 ^c	CH ₃	F ₃ CSO ₃ H	CH ₃ NO ₂	rt	–	–	–	–	–

^aIsolated yields. ^bAn allylic alcohol is generated (**25**, R = H). ^cDegradation of the reaction mixture.

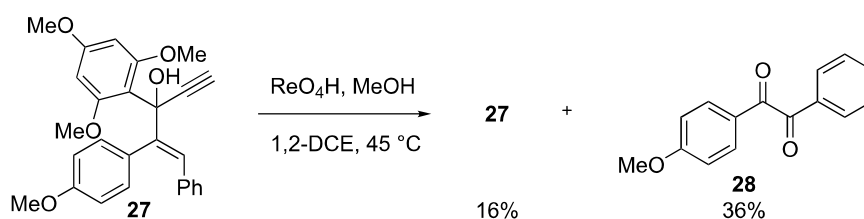
8, Table 2), we obtained comparable yields with 36% of cyclopentenone **22** and 12% of furan **23**. When using a weaker acid such as acetic acid (entry 9, Table 2) only the two acyclic ethers **25** and **26** were isolated. This observation strongly suggests that perrhenic acid is the active reagent generated from Re₂O₇ by methanolysis or hydrolysis with traces of water [12].

When removing methanol or replacing it with trifluoroethanol, the reaction mixture degraded in presence of triflic acid (entries 10 and 11, Table 2). Thus, the presence of methanol seems necessary for the cyclization to occur, perhaps by stabilizing an intermediate. Replacement of dichloroethane by nitromethane slightly decreased the yield of **22**, and suppressed the formation of furan **23**.

To determine whether the protection of the alkyne group was necessary for a rearrangement to take place, the reaction was carried out on compound **27**. In the presence of perrhenic acid, 16% of the starting material was recovered along with 36% of diketone **28** (Scheme 6). No cyclization product was isolated. This observation strengthened the hypothesis that the silyl group stabilizes the carbocation intermediate which seems necessary for the cyclization step.

Conclusion

The discovery of new reaction manifolds often provides a good opportunity to discover novel reactivity in related systems. In this article, we demonstrate the delicate balance among several mechanistic pathways by a minor change of substrate in acid-

**Scheme 6:** Rearrangement of unprotected propargylic carbinol **27**.

catalyzed rearrangements of 1-styrylpropargyl alcohols. Indeed, these compounds may generate a furan (**18**), an enone (**19**), an allylic ether or even a naphthalenone (**17**). The formation of the latter is quite intriguing because it suggests an unprecedented cascade of reactions.

Supporting Information

Supporting Information File 1

Experimental procedures for the synthesis of compounds **7–9**, **13**, **14** and **17–28**.

[<http://www.beilstein-journals.org/bjoc/content/supplementary/1860-5397-11-114-S1.pdf>]

Acknowledgements

L.D. was supported by the "Association pour la Recherche sur le Cancer" (ARC). We are also grateful to AAREC Filia Research and ANRT for fellowships to C.B.

References

- Boussemart, L.; Malka-Mahieu, H.; Girault, I.; Allard, D.; Hemmingsson, O.; Tomasic, G.; Thomas, M.; Basmadjian, C.; Ribeiro, N.; Thuaud, F.; Mateus, C.; Routier, E.; Kamsu-Kom, N.; Agoussi, S.; Eggermont, A. M.; Désaubry, L.; Robert, C.; Vagner, S. *Nature* **2014**, *513*, 105–109. doi:10.1038/nature13572
- Basmadjian, C.; Thuaud, F.; Ribeiro, N.; Désaubry, L. *Future Med. Chem.* **2013**, *5*, 2185–2197. doi:10.4155/fmc.13.177
- Ribeiro, N.; Thuaud, F.; Bernard, Y.; Gaidon, C.; Cresteil, T.; Hild, A.; Hirsch, E. C.; Michel, P. P.; Nebigil, C. G.; Désaubry, L. *J. Med. Chem.* **2012**, *55*, 10064–10073. doi:10.1021/jm301201z
- Basmadjian, C.; Zhao, Q.; Désaubry, L. *Tetrahedron Lett.* **2015**, *56*, 727–730. doi:10.1016/j.tetlet.2014.12.093
- An, S. E.; Jeong, J.; Baskar, B.; Lee, J.; Seo, J.; Rhee, Y. H. *Chem. – Eur. J.* **2009**, *15*, 11837–11841. doi:10.1002/chem.200901824
- Yang, H.; Fang, L.; Zhang, M.; Zhu, C. *Eur. J. Org. Chem.* **2009**, 666–672. doi:10.1002/ejoc.200800976
- Herrmann, A. T.; Saito, T.; Stivala, C. E.; Tom, J.; Zakarian, A. *J. Am. Chem. Soc.* **2010**, *132*, 5962–5963. doi:10.1021/ja101673v
- Shiroodi, R. K.; Gevorgyan, V. *Chem. Soc. Rev.* **2013**, *42*, 4991–5001. doi:10.1039/c3cs35514d
- Caruana, P. A.; Frontier, A. J. *Tetrahedron* **2007**, *63*, 10646–10656. doi:10.1016/j.tet.2007.08.008
- Volchkov, I.; Lee, D. *Chem. Soc. Rev.* **2014**, *43*, 4381–4394. doi:10.1039/c4cs00036f
- Terao, Y.; Kametani, Y.; Wakui, H.; Satoh, T.; Miura, M.; Nomura, M. *Tetrahedron* **2001**, *57*, 5967–5974. doi:10.1016/S0040-4020(01)00555-5
- Bellemin-Laponnaz, S. *ChemCatChem* **2009**, *1*, 357–362. doi:10.1002/cctc.200900206

License and Terms

This is an Open Access article under the terms of the Creative Commons Attribution License (<http://creativecommons.org/licenses/by/2.0>), which permits unrestricted use, distribution, and reproduction in any medium, provided the original work is properly cited.

The license is subject to the *Beilstein Journal of Organic Chemistry* terms and conditions:

(<http://www.beilstein-journals.org/bjoc>)

The definitive version of this article is the electronic one which can be found at:

doi:10.3762/bjoc.11.114

Développement de nouvelles approches pour la synthèse des flavaglines

Résumé

Nous avons développé deux méthodes originales de synthèse de cyclopenténones fonctionnalisées et découvert de nouveaux réarrangements d'alcools 1-styryl propargyliques catalysés par des acides.

Ce travail de thèse a aussi permis de mettre en évidence les limitations d'une méthode de synthèse des flavaglines développée par des chercheurs de la compagnie Bayer. De plus, la resynthèse de certaines flavaglines et la synthèse d'une sonde de fluorescence originale ont permis de mieux caractériser le mode d'action et le potentiel thérapeutique des flavaglines pour leurs effets anticancéreux (notamment dans la résistance aux inhibiteurs de B-RAF), la régulation du canal TRPM6 et l'infection par le virus du Chikungunya.

Mots clefs : flavaglines, cyclopenténones, réarrangements carbocationiques, réaction de Nazarov, eIF4A, prohibitines, cancer, chimiorésistance, TRPM6.

Development of new approaches for the synthesis of flavaglines

Abstract

We have developed two novel methods to prepare functionalized cyclopentenones and also discovered new acid-catalyzed rearrangements of 1-styryl propargylic alcohols.

This work also explored the limitations of a method for the synthesis of flavaglines reported by Bayer researchers. Moreover, the re-synthesis of some flavaglines and the synthesis of an original fluorescence probe allowed some advances in the characterization of the mechanism of action and therapeutic potential of flavaglines for their anti-cancer effects (especially in the resistance to B6RAF inhibitors), the regulation of TRPM6 channel and the infection by Chikungunya virus.

Key words: flavagline, cyclopentenones, carbocationic rearrangements, Nazarov reaction, eIF4A, prohibitins, cancer, chemoresistance, TRPM6.